α-Importome in Germline: Towards Identification Of Novel Roles And Binding Candidates For Importin α Family Members In Mammalian Germ Cell Maturation

Arash Arjomand, BSc (Honours)

A Thesis Submitted for the Degree of Doctorate of Philosophy
February 2013

Department of Biochemistry and Molecular Biology,
Faculty of Medicine, Nursing and Health Sciences,
Monash University

Supervisors:

Professor Kate L Loveland
Dr Yoichi Miyamoto
Professor David A Jans

ERRATA

Table 1.1 legend: "includess" change to "include"

Page 82, 2nd last sentence: "permatids" change to "spermatids"

Page 101, 2nd paragraph, 2nd sentence: "coloumn" change to "column"

ADDENDUM

The first question raised by the examiner is concerned with ***the potential effect of alternative nucleocytoplasmic transport pathways in germ cell maturation***. A large portion of nuclear import and export in every cellular homeostasis, developmental and differentiation context is facilitated by non-classical pathways (Chook and Süel, 2011; Wagstaff and Jans, 2009). Close to 20 members of karyopherin β (both importin and exportin) family members operate in both human and mouse. Very commonly, these receptors have specific cargoes for either nuclear or cytoplasmic transport (Pemberton and Paschal, 2005). The review article by Major and colleagues has summarized the expression of these transport factors in embryonic and post-natal testicular development through examination of their GEO profiles (Major et al., 2011). Although not presented in my thesis, I have preliminary data that shows expression of importin β3 protein (a member of importin β family) in pachytene spermatocytes and round spermatids of adult rat testis. Thus, it is clear that non-classical pathways are likely to exert a substantial effect on regulation, rate and dynamics of nucleocytoplsmic transport in spermatogenesis. Whether there is a balance or competition between these two import pathways in the examined context could not be inferred from the data generated in this study, however, this is a hypothesis worthy of pursuit.

The second concern questioned the choice of importins for expression and interaction analysis. ***Why were importin α1 and α6 not included in stoichiometric and proteomic experiments?*** I draw your attention to Figure 1.13 of the Literature Review chapter of this thesis. The initial hypothesis and experimental plan in this study was built on the basis of several previous observations regarding the differential expression of importin family members in spermatogenesis. The results of *in situ* hybridization (Figure 1.13 A) indicated that importin α1 transcript is detectable in a wide range of testicular germ cell types, while importin α6 appeared to be only detectable in post-meiotic cells. On the other hand, transcript analysis of importin α2, α3 and α4, showed that these family members show overlap in their expression pattern, in that they are detectable before, during and after meiosis. Immunohistochemical detection of importin proteins in rodent testis sections (Figure 1.13 B) revealed further intriguing observations regarding the expression and localization of importins α2, α3 and α4 in germ cells. While importin α3 protein appeared to be localized primarily in the cytoplasm, that of importin α4 appeared confined to the nucleus. Importin α2 protein was uniformly detectable in both cytoplasm and nucleus of spermatocytes; however in spermatids, importin α2 protein appeared strictly cytoplasmic. Based on these observations, the decision was made to primarily focus on these family members. By the same token, availability of appropriate antibodies to distinguish importin α1 and α6 at the time of this work in progress would have encouraged me to include these family members in stoichiometric analysis, at the least.

The next question was regarding the usage of the term importin α5 in the text of this thesis, in particular when referring to the Kamei et al 1999 report. The concern was raised since in mouse nomenclature there is no importin α5 (Figure 1.6). This discrepancy is most pronounced in page 36 (Section 1.1.8.2) of this thesis in relation to both Kamei et al 1999 and Hosokawa et al 2008 reports. Importin α5 in this section refers to mouse importin α1 in both of the above reports. I cannot narrate the source of inaccuracy when dealing with Kamei and colleagues communication. However, Hosokawa and co-workers have used the term importin α5 subsequent to unifying the importin nomenclature with the human designation in the interest of simplicity (see Hosokawa et al 2008 Table 1 and page 866 for the description). Thus, in both cases in this thesis importin α5 refers to importin α1. See Major et al., 2011 review for complete clarification of nomenclature).

The next issue concerned the depiction of stages of seminiferous epithelium in mouse (Figure 1.9). ***Why aren't the A spermatocytes depicted as continuous in the XII stages of the mouse cycle?*** I suspect that the reviewer is referring to A spermatogonia rather than A spermatocytes. Under that provision I acknowledge that the Figure is not entirely precise. Type A spermatogonia are present in every stage of adult mouse testis cross sections. The inaccuracy stems from lack of vigilance at the time of figure preparation which was extracted from a review paper (see Figure 1.9 legend). In that review article, the type A spermatogonia are depicted in intervals for reason/s that I could not infer by examining the article.

Next, ***the choice of α-tubulin for loading control of lysates prepared from spermatocytes and spermatids was questioned.*** The issue was raised based on the reasoning that these two cell types are not similar in size (spermatocytes being ~2.5 times larger than spermatids) and that the α-tubulin requirement per cell volume may vary between the two. This claim was also supported by reference made to a developmental process (axoneme genesis) that occurs during spermatid maturation and may require higher amounts of α-tubulin per cell volume in spermatids than in spermatocytes. I would agree with the differences in the cell size and volume. Based on my records and protein concentration calculations, the same amount of protein is reproducibly extracted from approximately twice as many spermatids compared to spermatocytes. This is only an issue if the cellular requirement of α-tubulin is indeed different between the two cell types (as asserted by the reviewer's comment). I have attempted to reconcile some facts and suppositions that may resolve or minimize some opinion differences. Firstly, close to same amount of extra α-tubulin in spermatids that is required for axoneme growth may be necessary to maintain the structure of distinctly larger spermatocytes. It should also be noted that my experiments examined very early spermatids in which axoneme growth is not overly prominent. Furthermore, if the cellular ratio of α-tubulin in spermatids is higher than in spermatocytes (e.g. 2:1), then in similar amount of total lysate (e.g. 40 ug), one would expect to observe a difference of similar magnitude (i.e. 2:1) in signal produced by α-tubulin between spermatids and spermatocytes. Data presented in Figure 3.2 and Figure 3.4 however, do not show a difference in α-tubulin amount between lysates prepared from different sources. This issue could also be inspected by examination of other housekeeping markers in these two lysates. However, the transition to haploid status in developing sperm cells is accompanied by a robust transcriptional switch that complicates normalisation. In response to the final remark of the reviewer regarding the assumed higher α-tubulin ratio per cell volume in spermatids and its implications in the interpretation of the data, I would acknowledge that such scenario could conceivably change the equation and mean that levels of importins are equal in spermatocytes and spermatids or even higher in spermatids (depending on the magnitude of difference in α-tubulin levels between these two cell types). However, based on my calculations (above), I suggest the estimates provided in my thesis are appropriate.

The ***reasoning behind the utilization of an importin α2-ED mutant but not an α4 mutant, and the signal selection process between the wild type and mutant importin α2 mass spec data was also questioned by the reviewer***. The process for selection of signals between wild type and mutant importin α2 included annotation of a signal (absent in GST control) to either wild type or mutant importin α2 only, or to both (if the signal was detectable in both). The importin α2-ED mutant has reduced NLS binding capacity (see page 87 for details and reference). Its inclusion in the screening was based on the following rationale. Firstly, we predicted that the NLS binding deficiency imparted by this mutation on importin α2 would enable us to identify proteins that bind to other domains of importin α (e.g. IBB or C-terminal domain), outside the conventional NLS binding groove. The logic behind this was that if the binding capacity of a protein (i.e. importin α) in binding to a certain category of its targets (i.e. NLS cargo) is compromised, then interaction with other potential binding proteins may become manifest. Also, in contrast to the reviewer's expectation that few if any cargoes with strong NLS would bind to this mutant, we had postulated that only nuclear cargo with exceptionally high putative NLS scores would bind to this mutant isoform of importin α2. Our rational was that only if affinity of a cargo NLS for the binding site in importin α protein is high enough, would it overcome the barrier placed by reduced NLS affinity as a result of this mutation. Neither of the above hypotheses was verified to our satisfaction based on the low number of binding candidates identified for importin α2-ED mutant in two proteomic analyses. Perhaps these mutations create unknown changes on importin α2 protein structure or domain organization. This is not verified yet and could be subject to further study. Since the crystal structure of importin α4 has not been addressed yet, it may be futile to create an ED mutant equivalent of this isoform for importin α4, as in many cases the selection of appropriate residues for mutation incorporation is subject to knowledge of the protein's structure.

The last question addressed ***the possible experimental approaches that would substantiate the view that interaction of importin α with Mtmr4 serves a novel role in regulation of membrane genesis and trafficking***. Perhaps co-localization of importin α (α4 in this instance) with Mtmr4 is the most important issue to be addressed before proceeding. I have preliminary data that shows such co-localization in internal membrane bound vesicles (of unknown nature) in HeLa cells. Subsequent to validation of localization, examining the effect of mutations in putative NLS of Mtmr4 could be informative. Mtmr3, the closest family member of Mtmr4 which shares substrate specificity, FYVE and coiled-coil domain with Mtmr4 (Section 5.6, page 113) is diffusely cytoplasmic and devoid of a putative NLS. Thus the Mtmr4 putative NLS may indeed act as an endosomal targeting motif which is recognized by importin α as a transport factor. This becomes more likely since no consensus endosomal targeting motif has been delineated yet. If an NLS mutant Mtmr4 is displaced from endocytic vesicles, then it could be argued that importin α is involved in its targeting. Furthermore, depletion of importin α from a cell (through RNAi studies, for instance) will cause aberrant phenotypes on endocytic vesicle formation/trafficking or Mtmr4 localization should importin α be involved in these processes.

References:

Chook, Y.M., and Süel, K.E. (2011). Nuclear import by karyopherin-βs: Recognition and inhibition. Biochimica et Biophysica Acta (BBA) - Molecular Cell Research *1813*, 1593-1606.

Major, A.T., Whiley, P.A.F., and Loveland, K.L. (2011). Expression of nucleocytoplasmic transport machinery: Clues to regulation of spermatogenic development. Biochimica et Biophysica Acta (BBA) - Molecular Cell Research *1813*, 1668-1688.

Pemberton, L.F., and Paschal, B.M. (2005). Mechanisms of Receptor-Mediated Nuclear Import and Nuclear Export. Traffic *6*, 187-198.

Wagstaff, K.M., and Jans, D.A. (2009). Importins and Beyond: Non-Conventional Nuclear Transport Mechanisms. Traffic *10*, 1188-1198.

Copyright Notices

Notice 1

Notice 2

Table of contents

Monash University
Monash Research Graduate School
Declaration of the thesis based or partially based on conjointly published or unpublished work

General Declaration

In accordance with Monash University Doctorate Regulation 17/Doctor of Philosophy and Master of Philosophy (MPhil) regulations the following declarations are made:

I hereby declare that this thesis contains no material which has been accepted for the award of any other degree or diploma at any university or equivalent institution and that to the best of my knowledge and belief, this thesis contains no material previously published or written by another person, except where due reference is made in the text of the thesis.

This thesis includes three unpublished results chapters. The core theme of this thesis is concerned with the function of nucleocytoplasmic transport machinery in mammalian spermatogenesis. The ideas, development and writing of all the chapters in the thesis were the principle responsibility of myself, the candidate, working within the Department of Biochemistry and Molecular Biology at Monash University under the supervision of Professor Kate Loveland, Dr Yoichi Miyamoto and Professor David Jans.

In the case of Chapter 4, my contribution included designing and executing every step of the work, except the mass spectrometry analysis. By the same token, I took part in signal selection for mass spectrometry analysis which was performed by Dr Mark Baker in the University of Newcastle.

My contributions to the paper that is attached to this thesis were cloning of mouse SSX2IP gene into a mammalian expression vector, cloning of the SSX2IP putative nuclear localization signal into the bacterial expression vector, and purity determination of elutriated testicular cell fractions.

Signed …….
Date …….

Abstract

Importin α family proteins are the cargo receptor component of the classical nuclear import machinery in eukaryotic cells. In the cytoplasm importin αs bind to cargo proteins through amino acid motifs known as nuclear localization signals (NLSs) and thereby mediate association with the nuclear import transporter, importin β1. This trimeric complex then enters the nucleus through interactions of importin β1 with components of the nuclear pore complex, and nuclear cargo is delivered into the nucleus to perform its function. During evolution, importin α genes have increased in number with increasing organismal complexity. Thus, 7 and 6 importin α family members have been identified in human and mouse, respectively, while lower eukaryotes contain 3 importin α family members and yeast has only 1. Despite sharing a high level of conservation in sequence, structure and function, these family members have acquired non-redundant roles in developmental systems. The functional specialization imparted to importin α proteins is, in part, effected by regulated spatial and temporal expression of individual family members as well as through their acquired cargo binding specificity.

Adult spermatogenesis is a unique maturation process in which spermatogonial stem cells produce spermatozoa through highly regulated cell division and differentiation events. We hypothesized that importin α family members serve distinct functions in spermatogenesis, predicting initially that their roles in nucleocytoplasmic transport would require them to recognize distinct cargo subsets at key germline differentiation steps. We also proposed that based on known differences in their transcription patterns individual importin α proteins would exist in different proportions and levels at distinct steps of spermatogenesis. The purpose of the research conducted as part of this thesis was to first delineate the protein levels and deduce the relative stoichiometry of three importin α family members, (α2, α3 and α4) in addition to importin β1 in testicular germ cells of two sequential developmental stages, pachytene spermatocytes and round spermatids, through quantitative Western blot analyses. The second aim was to define the germline "α-importome" through identification of interacting partners for importin α family members in pachytene spermatocytes and round spermatids by means of recombinant protein pull-down and mass spectrometric

analysis. The third aim of this thesis was to validate the interaction of importin α with a newly identified candidate binding partner, Mtmr4, a protein with known cytoplasmic localization.

The results of the protein detection analyses supported our hypothesis that importin αs serve distinct and dynamic roles in spermatogenesis as reflected by regulated protein synthesis. Amongst the importin α family members examined, importin α2 had the highest variation in total concentration between spermatocytes and spermatids, followed by importin α3, with both α2 and α3 present at higher levels in spermatocytes than in spermatids. In contrast, the concentration of importin α4 and importin β1 did not differ between these two cell types. Comparison of the protein levels in these germ cell lysates to that in a lysate of total adult rat testis demonstrated that importin α family members have distinctly higher levels in the germ cell isolates than in the total testis, while the difference in importin β1 protein levels between isolated germ cells and total adult testis was marginal. Amongst the examined importin α family members, the most abundant was importin α2 followed by importin α3 and α4. Intriguingly however, these analyses revealed that importin αs are collectively more abundant than importin β1. This is the first study in which the differential production of importin proteins in a developmental context has been examined quantitatively, and the outcomes demonstrate that nucleocytoplasmic transport and other importin-mediated functions are potentially governed by processes that specify and modulate intracellular levels of specific importin proteins during development.

The recombinant protein pull-down and mass spectrometry analyses led to identification of numerous binding candidates for importin α2 and α4 from spermatocyte and spermatids. Noticeably, the majority of candidates identified by the different importin αs or from each cell type were distinct. Several bioinformatics analyses of the candidate binding partners supported the hypothesis that importin αs serve distinct functions in each stage of spermatogenesis. Computational analysis aimed at discerning potential nuclear localization motifs verified that, within the list of all identified candidates, there is a clear enrichment in the proportion of proteins containing a putative NLS. However the level of this enrichment was not uniform

between candidate cohorts identified by different importins from spermatocytes and spermatids. Specifically, the protein lists generated by importin α4 from spermatocytes and importin α2 from spermatids contained the highest proportion of candidates with a putative nuclear localization signal (52% each), followed by cohorts of candidates identified by importin α2 in spermatocytes and α4 in spermatids (39% and 30%, respectively). Bioinformatics examination of the molecular pathways represented by different importin α binding candidates showed that importin α2 binding candidate in spermatocytes are predicted to be involved in processes concerning RNA stability and differentiation, while importin α4 binding candidates in spermatocytes enriched many terms related to protein trafficking. The candidate binding partners for both importin α2 and α4 in spermatids, enriched many terms related to chromosomal and nuclear dynamics. These results align with the few recently published studies of a similar nature, which also give insight into the potential diversity in importin α family members function.

The final body of work presented in this thesis is concerned with characterization of a putative interaction between importin α and Mtmr4, a known cytoplasmic protein. Mtmr4 was identified as a binding candidate of importin α4 from spermatocytes lysate in a previous study. One of the Mtmr4 family members (Mtmr2) has essential roles in spermatogenesis. Thus we aimed to accumulate evidence on the authenticity of Mtmr4 interaction with importin α in the context of spermatogenesis. Northern blot analysis showed that Mtmr4 transcript is present in a wide range of tissues; *in situ* hybridization on testis sections showed that this transcript is most readily detectable in pachytene spermatocytes in which importin α4 transcript and protein are present. Subsequently a putative nuclear localization signal was identified within the amino acid sequence of Mtmr4 which was shown to interact with both recombinant importin α2 and α4 *in vitro*. Pull-down and immunoprecipitation experiments provided further support for authenticity of the interaction between importin α and Mtmr4. Interestingly Mtmr4 was more readily detected in the pull-down product of an importin α2 truncate with higher NLS binding capacity and was barely detectable in the pull-down product of an importin α2 mutant, defective in NLS binding activity; this observation suggests that interaction of Mtmr4 and importin α occurs in NLS binding region of importin α. Further experimental approaches devised in this thesis

could verify the functional nature of this intriguing interaction between importin α family members and Mtmr4, once appropriate reagents become available.

Overall the results of this study have shed light on the importance of regulated synthesis and levels of individual importin α family members in developmental processes such as spermatogenesis. Many novel binding candidates for importin α family members have been identified in testicular germ cells which indicate that importin α proteins serve a broad spectrum of roles relating to cellular metabolism, potentially linked to a molecular scaffolding capacity. Advances made in characterizing the previously indicated interaction between importin α and Mtmr4 provide a clear demonstration that importin α proteins have significant interactions with proteins that are predominantly cytoplasmic. The potential for importins to mediate new germline-specific and general cellular metabolic roles is supported by the findings of this thesis.

Declaration

I hereby declare that this thesis contains no material which has been accepted for the award of any other degree or diploma at any University or equivalent institute and that, to the best of my knowledge and belief, this thesis contains no material previously published or written by another person, except where due reference is made in the text of this thesis.

Arash Arjomand Date

Department of Biochemistry and Molecular Biology
Faculty of Medicine, Nursing and Health sciences
Monash University
Melbourne, Victoria, Australia

Acknowledgments

First and foremost, I want to thank Professor Kate Loveland for giving me the opportunity to pursue my academic career in her research laboratory. Besides that, thank you for refusing to give me the second best chance of producing my best in every aspect of my work. Thanks for inciting that scientific curiosity and critical thinking in me at every opportunity. I also want to thank my co-supervisors Dr Yoichi Miyamoto and Professor David Jans. Yoichi, thank you for the knowledge and many other qualities that you have imparted on me throughout this work. I am a better scientist for that and appreciate all your effort. David, thank you for your comments, questions and overall directions for this PhD project.

I am also very thankful to Dr Mark Baker for his hospitality during my stay in Newcastle and his generosity in time, knowledge and expertise of mass spectrometry which made a major part of this thesis possible. I want to also acknowledge both Dr Peter Boag and Dr Lynne Mayne for being part of my progress review panel; this may have not been possible without your contributions. Thanks to Mitchell lab members, Dr Jenny Dyson, Dr David Sheffield and Micka Bertucci for providing me with valuable information and reagents for Mtmr4 work.

A special thanks to all the “Lovelanders”, past and present, for being just who you are. In the past five years I could have not wished to have better colleagues than you, all nice, fun and inspiring. Fair to say that you were all like a second family to me. One day I am going to miss the P*****h colony that I established and maintained in this lab.

To all of you amazing students and staff members in Biochem; it’s you that makes this place so special. Big thanks to all Jans, Mitchell Lackman and Tiganis lab members with whom I developed friendships over the past several years. Im hoping our friendship goes well beyond the Biochem days. Some names cannot be missed in this acknowledgment for many good and memorable reasons. Chin, Sarah, Sibil, Gillaume and Andy, you were always there for me and I knew I could turn to you for support anytime and not be disappointed, so thank you. Damitha and Damon, my great friends outside the lab, you two have most definitely done your share of keeping

me moving with your “philosophical interpretation” of every situation relating to this thesis, thank you for all that time and effort and more.

The “Balcony” and the “Duck pond”, and “everyone” associated with these hot spots get a special mention for reasons beyond the scope of this text.

Last but not least, I will extend my outmost gratitude to my family that has always been there for me. Thanks to both my uncles and aunty and two great cousins, Emilia and Ellena, who have always been supportive and more than helpful over years. To my brothers, Amir, Eghan and Iman with his little family, Khatereh and Iliya, and my only sister Anisa: Thank you for putting up with me and the entire burden that I was in the recent years. My dearest parents, you know that without your love, support and belief, I could have not come close to this. I have lots of doubts that in my life time, I could remotely compensate for one minute of your sacrifice, worries and efforts from the moments I opened my eyes to this world till now and well into the future. Although it is clear that you have no fertility defects (see above) I dedicate this thesis to you.

Papers published during course of candidature

Miyamoto, Y., Baker, M.A., Whiley, P.A., Arjomand, A., Ludeman, J., Wong, C., Jans, D.A, and Loveland, K.L. (2013). Towards delineation of a developmental α-importome in the mammalian male germline. Biochemica et Biophysica Acta (BBA)-Molecular Cell Research 1833, 731-742.

List of abbreviations

aa	amino acid
A_{al}	type A aligned spermatogonia
ACRBP	acrosomal binding protein
ADAR	adenosine deaminase acting on RN
APC	allophycocyanin
A_{pr}	type A paired spermatogonia
APS	ammonium perfulfate
A_s	type A single spermatogonia
Bp	base pair
BSA	bovine serum albumin
BTB	blood-testis barrier
c.elegans	caenorhabditis elegans
CaMKIV	Ca^{2+}/calmodulin-dependent protein kinase type IV
cDNA	complementary DNA
ChIP	chromatin immunoprecipitation
CMT	charcot-marie-tooth disease
cNLS	classical nuclear localization signal
CNS	central nervous system
Cos-7	African green monkey kidney cells
D. melanogaster	drosophila melanogaster
DENN	differentially expressed in neoplastic versus normal cells
DEPC	di-ethyl pyro-carbonate
dH_2O	distilled water
DIF	deionized Formamide
DIG	digoxigenin
DMEM	Dulbecco's modified eagle medium
DNA	deoxyribonucleic acid
dNTP	deoxyribonucleotide triphosphate
dpp	day post-partum
EDTA	ethylenediaminetetraacetic acid
ELISA	enzyme-linked immunosorbent assay
ES	embryonic stem (cell)
FCS	fetal calf serum

FG	phenylalanin-glycine
FYVE	Fab, YOTB, Vac1, EEA1
GEO	gene expression omnibus
GFP	green fluorescent protein
GST	glutathione-S-transferase
HIV	human immunodeficiency virus
HMG	high mobility group
HPLC	high pressure liquid chromatography
Imp	importin
IPC8	infected cell protein 8
IPTG	isopropyl β-D-1-thiogalactopyranoside
ISH	*in situ* hybridization
kb	kilo base
kd	dissociation constant
kDa	kilo Dalton
KO	knock-out
LB	Luria Bertani
LIF	leukaemia inhibitory factor
M	molarity
MD	mega Dalton
ml	milliliter
M.musculus	mus musculus
MQ	MilliQ grade water
MS/MS	tandem mass spectrometry
ng	nanograms
NLS	nuclear localization signal
nmol	nanomolar
NPC	nuclear pore complex
NTF2	nuclear transport factor 2
PAE	porcine aortic endothelial
PLZF	promyelocytic leukemia zinc finger
pmole	picomole
PtdIns(3)P	phosphatidylinositol-3phosphate
PtdIns(3,4)P2	phosphatidylinositol-3,4 biphosphate
PtdIns(3,4,5)P3	phosphatidylinositol-3,4,5 triphosphate

PtdIns(3,5)P2	phosphatidylinositol-3,5 biphosphate
PtdIns(4)P	phosphatidylinositol-4 phosphate
PtdIns(4,5)P2	phosphatidylinositol-4,5 biphosphate
PtdIns(5)P	phosphatidylinositol-5 phosphate
RanBP	Ran binding protein
RanGDP	Ran bound to guanidine nucleotide biphosphate
RanGTP	Ran bound to guanidine nucleotide triphosphate
RCC1	regulator of chromosome condensation 1
RCF	relative centrifugal force
RNA	ribonucleic acid
RNAi	RNA interference
rpm	round per minute
RT	reverse transcription
SBTI	soybean trypsin inhibitor
S.cerevisiae	saccharomyces cerevisiae
SDS	sodium dodecyl sulphate
SRY	sex determining region Y
STAT	signal transducer and activator of transcription
TAE	tris acetate EDTA
T-ag	SV 40 large tumor antigen
T-ag-NLS	nuclear localization of SV 40 large tumor antigen
TBS	tris buffered saline
TEMED	tetraethylmethylenediamine
TGFβ	transforming growth factor β
tRNA	transfer RNA
UTR	untraslated region
V	volt
w/v	weight per volume
WGA	wheat germ agglutinin
WT	wild type
α	alpha
β	beta
γ	gamma
κ	kappa
μ	micro

18 S	ribosomal RNA subunit 18
28 S	ribosomal RNA subunit 28

Chapter 1-
Literature review

CHAPTER 1 LITERATURE REVIEW

1.1 Nucleocytoplasmic transport

1.1.1 Overview: The need for regulated nucleocytoplasmic transport

The most prominent feature that distinguishes eukaryotic and prokaryotic cells is the presence of a nuclear membrane in eukaryotes. The nuclear membrane is a double lipid envelope that surrounds the nuclear content and separates it from the cytoplasm and its organelles. The only time during the cell cycle at which nuclear content is exposed to the cytoplasm is when the nuclear membrane breaks down at the onset of mitosis. At any other cell cycle stage, nuclear content is kept confined within this membrane. This evolutionary feature of eukaryotic cells leads to a segregation of genetic material from the rest of the cell.

The separation of genome and cytoplasm in a eukaryotic cell necessitates a mechanism of communication between the two compartments. Two examples of this requirement are for access of transcription factors to the nucleus and for export of transcribed mRNA from the nucleus into the cytoplasm. Pioneering studies demonstrating translocation into the nucleus of proteins included radioactive labelling of individual cytoplasmic and nuclear proteins from *Xenopus laevis* (*X. laevis*) oocytes followed by their microinjection into the cytoplasm of a recipient oocyte. Auto-radioactive imaging and Western blotting analysis of protein location within the recipient cells showed that nuclear proteins entered into, and accumulated within the nucleus, while cytoplasmic proteins did not (Bonner, 1975). This observation implied that nuclear proteins have an inherent ability to enter the nucleus and demonstrated the existence of a pathway across the nuclear envelope. The following sections discuss the specialized and stringently regulated route by which the exchange of materials between the cytoplasm and nucleus is facilitated.

1.1.1.1 The route to the nucleus

The nuclear envelope is perforated throughout by numerous aqueous channels called nuclear pore complexes (NPCs) which connect the cytoplasmic and nucleoplasmic sides of the membrane. Early observations indicated that a major role was played by the NPCs in transport of large molecules across the nuclear membrane. In these studies, the nuclear uptake of nucleoplasmin-coated gold particles was examined in an *in vitro* assay (Newmeyer et al., 1986b). Nucleoplasmin is the most abundant *X. laevis* oocyte nuclear protein (discussed further in Section 1.1.3.1). Electron microscopic examination revealed that the labelled nucleoplasmin was present both on the cytoplasmic side of the NPC and within the channel connecting the cytoplasm and nucleus after microinjection of *X. laevis* oocytes (Newmeyer et al., 1986b). A similar result was obtained by incubation of labelled nucleoplasmin in an *in vitro* import assay containing *X. laevis* egg extract and rat liver nuclei (Newmeyer and Forbes, 1988; Richardson et al., 1988). Concurrent with the above discoveries, an inhibitor of protein nuclear import was identified. The lectin, wheat germ agglutinin (WGA), is a protein of ~18 kDa with binding specificity to N-acetyl-glucosamine-containing oligosaccharides (Nagata and Burger, 1974). It was demonstrated that WGA blocked nuclear import of fluorescently labelled nucleoplasmin, by binding to the glycoproteins of the NPC, validating identification of the NPC as the sole gateway across the nuclear envelope (Finlay et al., 1987).

1.1.2 Nuclear pore complex (NPC)

The nuclear pore complex (NPC) is one of the largest macromolecular assemblies in a eukaryotic cell, with a rather conserved overall structure and composition throughout evolution (DeGrasse et al., 2009; Yang et al., 1998). The yeast NPC is ~40 MDa in size and that of vertebrates such as rat is ~60 MDa. Given this large molecular size, it was suspected that such a complex is made up of hundreds of subunits. However, proteomic analysis on enriched NPCs have identified only 30 distinct polypeptides called nucleoporins (Nups) in multiple copies that make up the NPC in both yeast and vertebrates (Cronshaw et al., 2002; Rout et al., 2000). The classification of Nups

based on their amino acid sequence composition, localization within the pore complex, and functional attributes is discussed further in Section 1.1.2.1.

1.1.2.1 Structure and composition of the NPC

Different electron microscopic approaches have unequivocally shown that the NPC has a doughnut shape with an eight-fold rotational symmetry around a central channel that connects the cytoplasm to the nucleus. A ring structure covers both the cytoplasmic and nuclear ends of the central channel (Akey and Radermacher, 1993; Beck et al., 2004; Stoffler et al., 1999)-(reviewed in Elad et al., 2009). One prominent feature of the NPC is the filamentous extensions on both cytoplasmic and nuclear sides of the pore. There exist eight filaments on the cytoplasmic ring that protrude into the cytoplasm and eight nuclear filaments that are joined by a ring structure to produce what is termed a nuclear basket at the nucleoplasmic side of the pore complex. These structures have been found in *X. laevis* (Akey and Radermacher, 1993; Jarnik and Aebi, 1991), *Saccharomyces cerevisiae* (*S. cerevisiae*) (Fahrenkrog et al., 1998) and *Dictyostelium discoideum* (Beck et al., 2004). Figure 1.1 shows a schematic diagram of the major domains of a NPC.

The 30 individual Nups interact with each other in several subcomplexes which collectively create the complete NPC. A comprehensive list of Nup interaction networks, stoichiometry of individual Nups/pore complex and their predicted position is presented by Alber and colleagues (Alber et al., 2007). In general, Nups are classified into four groups based on their localization and function in the pore; these are the transmembrane, core, linker, and FG Nups (reviewed in Fernandez-Martinez and Rout, 2009). The first three classes serve structural functions by creating a scaffold within the pore complex (core and linker Nups), and tethering it to the nuclear envelope (transmembrane Nups). For example, the yeast Nup53 (a core Nup) has been shown to be physically linked to the inner nuclear membrane protein network, nuclear lamina, through direct association with lamin B (Hawryluk-Gara et al., 2005). The fourth class of Nups (FG Nups) is characterized by degenerate FG (phenylalanine and glycine) repeats and is involved in nucleocytoplasmic transport.

Figure 1.1 Schematic diagram of the nuclear pore complex (NPC)

The overall structure of a single NPC is depicted as connecting the nuclear and cytoplasmic compartments through nuclear envelope. The central channel perforates the nuclear envelope where the outer and inner nuclear membranes fuse, creating a passage for bidirectional transport of molecules. The channel is surrounded by structural nucleoporins. Cytoplasmic filaments emanate from the cytoplasmic side of the pore, and the nuclear basket is composed of nuclear filaments that extend into the nucleoplasm and are joined by a distal ring (Image adapted from Hoelz et al., 2011).

Cytoplasm

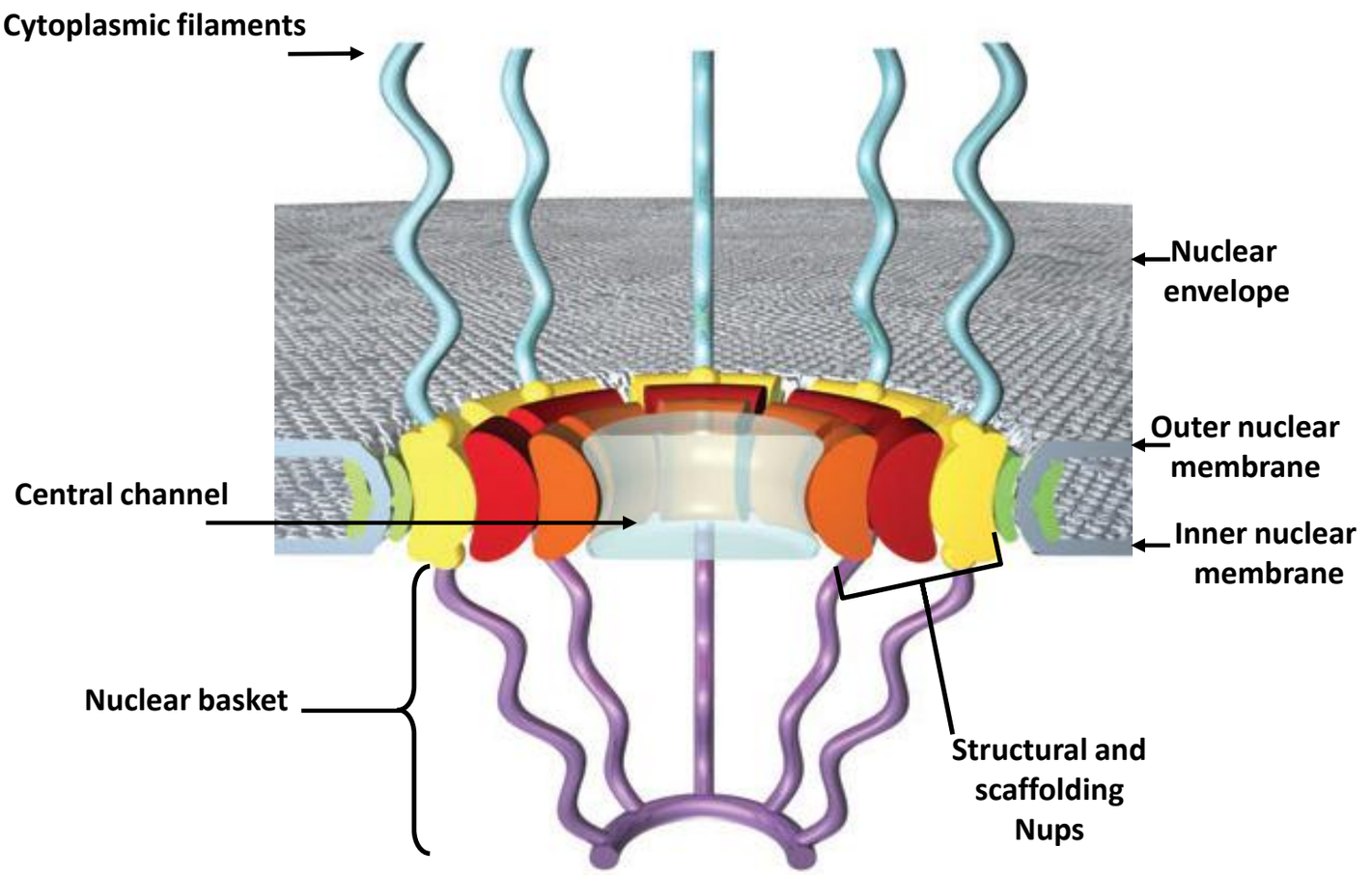

Nucleoplasm

Based on their function in nucleocytoplasmic trafficking, the FG Nups are discussed further in Section 1.1.4.3.

Immunoelectron microscopy has revealed the distinct and overlapping localization of individual Nups in the NPC. In yeast, the majority of Nups (e.g. Nup 49 and Nup57) are either distributed symmetrically on both nuclear and cytoplasmic sides of the pore or concentrated within the channel (e.g. Nup170). On the other hand, some Nups are restricted to either the cytoplasmic (e.g. Nup159 and Nup42) or nuclear (e.g. Nup1 and Nup60) side (Rout et al., 2000). This asymmetric distribution implies there are distinct roles for Nups during the translocation of molecules from one side of the pore to the other.

1.1.2.2 The NPC is dynamic

Visualization of NPCs in an intact nucleus shows they are distributed throughout the nuclear envelope. The individual pore complexes are associated with the inner membrane protein network of the nucleus (discussed in Section 1.1.2.1), and as a result are stably tethered to the nuclear envelope (Daigle et al., 2001). Detection of NPC components by both confocal fluorescence and electron microscopy gauges the density of the pores in a range of cultured mammalian cells to be ~4/μm^2 (Daigle et al., 2001; Kubitscheck et al., 1996). On the other hand, the isolated nuclear envelopes of *X. laevis* oocytes are shown to contain up to ~30 NPCs/μm^2 (Höppener et al., 2005).

The number and density of NPC/nuclear envelope varies depending on the metabolic state of the cells. Winey and colleagues created three dimensional images of yeast nuclei from sections of individual cells, then measured the volume of the nucleus and counted the number of NPCs/nucleus in different stages of the cell cycle. The result showed that both volume (i.e. surface area) of the nucleus and number of NPCs increased from G_1 to S phase and in early M phase cells, with an ensuing decline in late anaphase cells. Despite the parallel fluctuation in the number of NPCs and volume (surface area) of the nucleus, there was a significant increase in the density of NPC/surface area in S phase cells (Winey et al., 1997). More recent analysis in mammalian cells has further implicated the physiological state of the cell in

determining the appearance and disappearance of NPCs. Immunofluorescent detection of Nups in HeLa cells identified large (30 μm^2) pore-free subdomains or "islands" on the nuclear envelope. In this study, ~90% of the HeLa cells in G1 phase were shown to contain such islands. The percentage of the cells containing the islands decreased to 50% in early S phase and 26% in mid-late S phase, dropping even further to 9% and 6% in G2 and late G2-prophase cells respectively. The decrease in occurrence of islands was also shown to be concurrent with an increase in the NPC density from ~4 to ~6/μm^2 in G1 and G2 phase respectively (Maeshima et al., 2006). Such observations implicate the NPC as functionally important to major cellular processes, such as proliferation and gene expression (discussed further in Section 1.1.2.4).

1.1.2.3 Permeability and transit rate through the NPC

Molecules smaller than 30 kDa in molecular mass and 5 nm in diameter can passively diffuse across the NPC with increasingly slower rates at the upper limit of the size range (Gorlich and Kutay, 1999; Paine, 1975). Larger molecules of up to 10 MDa need an active transport mechanism (discussed in Section 1.1.4) to access the nuclear side of the NPC. Microinjection of gold particles of various sizes into *X. laevis* oocytes has shown that the NPC can mediate transport of molecules of up to 39 nm in diameter, with a rate inversely correlated to the size of the particle (Pante and Kann, 2002). The NPC is able to accommodate translocation of a large amount of proteins with high speed across the nuclear envelope. Ribbeck and Gorlich determined the average volume of the nucleus in the HeLa cell to be ~1130μm^3 and the number of the NPCs to be ~2700/nuclear envelope. Subsequently, by measuring the accumulation of a fluorescently labelled pentameric nucleoplasmin (mol.wt. ~620 kDa) in timed intervals they established an approximate mass flow rate of 17 MDa/NPC/sec (Ribbeck and Gorlich, 2001). More advanced fluorescent microscopic techniques that allow tracking of a single molecule estimate the translocation capacity of NPC to be as high as 1000 molecules/sec/NPC for 2 GFP molecules fused to T-antigen nuclear localization signal (T-ag-NLS), a fusion protein of ~50 kDa (T-ag-NLS will be discussed in Section 1.1.3.1)-(Yang et al., 2004).

1.1.2.4 Association of the NPC with chromatin

The NPC is known to have a more complex role in gene expression than facilitating only nuclear import and export (Reviewed in Capelson and Hetzer, 2009). In this section an overview of the NPC function in regulating gene expression through direct interaction with chromosomes is presented.

The results of several studies pointed towards a direct association between NPCs and chromosomes. For example, interaction of NPCs with chromosome regions that are active in gene expression have been documented by means of chromatin immunoprecipitation (ChIP) (Casolari et al., 2004) and fluorescent co-localization of yeast NPCs with chromatins (Taddei et al., 2006). Using another technique called chromatin endogenous cleavage (ChEC) (Schmid et al., 2004), Schmid and colleagues provided evidence for direct interaction of NPC proteins with transcriptionally active regions of chromatin in yeast. In this approach Nup2 of *S. cerevisiae* was fused with the *Micrococcal* nuclease (MN) to create a Nup2-MN fusion protein in living cells. Through its MN moiety, Nup2-MN introduced double stranded DNA breaks that were mapped to the site of interaction between chromosomes and Nup2-MN. Only following activation of the GAL locus in exponentially growing yeast cells by galactose supplement, was strong cleavage of the GAL locus near GAL1 and GAL10 promoters observed, indicating that the GAL locus had come in close proximity to Nup2-MN fusion proteins in the NPC (Schmid et al., 2006).

In a more recent study, Kalverda et al, refined the chromatin interacting components of the NPC to the level of individual Nups (Kalverda et al., 2010). The interaction of Nup62, Nup50 and Nup98 with the chromosomes of embryonic *Drosophila melanogaster* (*D. melanogaster*) cells was investigated by inducing the methylation of chromatins upon expression of *Escherichia coli* (*E.coli*) Dam-methylase fused Nups. The methylated chromosomal regions were then identified by cDNA microarray. This analysis identified a host of loci, the majority of which corresponded to genes involved in development. In addition, the chromosome regions identified, corresponded to transcriptionally active genes in *D. melanogaster* embryonic cells. Furthermore Nup50 was found in decondensed chromatin regions of polytene

chromosomes and shown to co-localize with serine 2-phosphorylated RNA polymerase II after immunostaining of *D. melanogaster* salivary glands, demonstrating its association with transcriptionally active genes (Kalverda et al., 2010).

In summary, NPCs interact with chromosomes and their appearance is spatially and temporally regulated during the cell cycle (Section 1.1.2.2) These observations indicate that gene expression and NPCs exert regulatory effects on one another in developmental contexts such as proliferation and during the cell cycle.

1.1.3 Nuclear localization signals (NLSs)

Many cases of protein trafficking to the correct subcellular compartment, including the nucleus, are dependent on localization signal sequences. Most nuclear proteins possess a signal that directs their nuclear entry. A nuclear localization signal (NLS) is recognized by nuclear import receptors, which facilitate the translocation of proteins across the NPC. Examples of nuclear import receptors are importin α and importin β1 which bind nuclear cargo in the cytoplasm and translocate it into the nucleus. The recognition of NLS by nuclear import receptors and the mechanism of cargo translocation across the pore complex are addressed in Section 1.1.4.

1.1.3.1 The T-antigen and nucleoplasmin NLSs

The first cargo protein sequence implicated in nuclear protein import was a stretch of basic amino acid residues within the DNA binding domain of the large tumor antigen of simian virus 40 (SV40 T-ag). The SV40 T-ag is a nuclear protein, required in transforming ability of the virus in cultured cells, and the key basic polypeptide sequence identified was ^{127}KKKRK^{131}. Using mixed oligonucleotide mutagenesis, Kalderon et al, demonstrated the importance of this peptide, and in particular the lysine at the position 128, for nuclear localization of the protein in transfected Vero cells (Kalderon et al., 1984). The mutant proteins failed to accumulate in the nucleus, while retaining the transforming activity of the wild type protein. To verify the

authenticity of the identified peptide as a nuclear localization signal, Goldfarb and co-workers made a fusion of the peptide and bovine serum albumin (BSA), a large cytoplasmic protein, followed by radiolabelling and microinjection into the *X. laevis* oocyte cytoplasm. The large SV40 T-ag peptide caused the nuclear accumulation of BSA, and the authors concluded that this basic polypeptide has the activity of a nuclear localization signal or NLS (Goldfarb et al., 1986). This peptide sequence is referred to hereafter as T-ag-NLS.

Another well characterized nuclear localization signal is that of nucleoplasmin. The sequence that directs the nuclear localization of nucleoplasmin shares similarity to the T-ag-NLS in amino acid composition (i.e. it is rich in basic residues), but differs in sequence length. Nucleoplasmin is the most abundant protein in the nucleus of the *X. laevis* oocyte, and it is involved in chromatin organization and nucleosome assembly (Frehlick et al., 2007). The protein is a pentamer of five subunits, each of which contains a tail domain. Digestion of nucleoplasmin by trypsin leads to the separation of exposed tails from the pentameric core of the protein. Dingwall and colleagues obtained the pentameric core region of nucleoplasmin by trypsin digestion, and generated the radiolabelled nucleoplasmin core which was then injected into the *X. laevis* oocyte cytoplasm. Analysis of protein localization by nucleocytoplasmic fractionation and autoradiographic studies revealed that the core subunits of nucleoplsmin failed to migrate into the nucleus. These early observations implicated the tail regions of nucleoplasmin in enabling nuclear entry of the protein (Dingwall et al., 1982). The tail domain of nucleoplasmin consists of 50 amino acid residues and contains 4 potential NLSs characterized by a stretch of 5 to 7 basic residues resembling that of SV40 T-ag-NLS. Fusion of this region of the nucleoplasmin tail to the cytoplasmic chicken muscle pyruvate kinase conferred nuclear localization to the pyruvate kinase protein upon transfection of Vero cells. Further truncation of this region identified a stretch of 14 residues that were necessary but not sufficient for nuclear targeting, in that it required three residues on either side to be capable of importing pyruvate kinase into the nucleus (Dingwall et al., 1988). The amino acid sequence of the nucleoplasmin NLS was further characterized in a subsequent study to identify the region of nucleoplasmin that was necessary and sufficient to confer nuclear localization. This region of nucleoplasmin is composed of 16 amino acids

with two clusters of basic motifs separated by a spacer of 10 residues, encoding ^{155}KRPAATKKAGQAKKKK^{170} (basic motifs underlined). The interdependence of the two basic clusters in acting as an NLS was demonstrated in mutagenesis experiments in which the combination of K^{155} and K^{170} mutations abrogated the nuclear accumulation of a heterologous fusion protein (pyruvate kinase fused to the nucleoplasmin NLS), while each mutation on its own did not have such effect (Robbins et al., 1991). The T-ag-NLS and the nucleoplasmin NLS are the best characterized classical NLSs (cNLS), which fall into two categories. T-ag-NLS is a "monopartite" NLS, since it contains one stretch of basic residues. The NLS of nucleoplasmin is a "bipartite" NLS because it is composed of two stretches of basic residues that are separated by a linker sequence.

1.1.3.2 Current understanding of classical NLSs (cNLS)

In general it is agreed that a peptide sequence must meet several criteria in order to be classified as a cNLS. The first of these is being necessary and sufficient for *in vivo* nuclear transport of the protein possessing the peptide. Second, a cNLS must be able to interact with nuclear import receptors. The classical nuclear import receptor is a heterodimer of importin α and importin β1 (importin α/β1) in which the cNLS recognition is provided by importin α and nuclear translocation is facilitated by importin β1 (discussed further in Section 1.1.4). Finally, a cNLS must have the ability to direct a heterologous non-nuclear protein into the nucleus. Many cNLSs of both monopartite and bipartite types have been identified to date, with the prominent hallmark of enrichment in basic residues. Since their discovery, significant advances in understanding cNLSs have been made. These advances expanded the definition of sequence and nuclear import ability of a cNLS.

Alanine scanning experiments have provided insights about the importance of individual amino acids in a cNLS. In this approach, every non-alanine residue in an NLS is mutated to alanine, followed by measuring the affinity of the mutant NLS for binding specific nuclear import receptors and determining its ability to direct nuclear accumulation. This approach was applied by Hodel and colleagues to study the NLSs of T-ag and c-myc (a proto-oncogene with a defined NLS sequence of PAAKRVKLD (Dang and Lee, 1988)) to establish the significance of each amino acid in binding to

the yeast importin α. Their studies defined a consensus for a monopartite cNLS with a core sequence of K(K/R)X(K/R) (where X could be any residue) (Hodel et al., 2001). In case of bipartite cNLSs, the consensus sequence has remained less clearly defined due to the higher variability in basic residue composition and the presence of linker sequences of varying length. The classical bipartite NLS (i.e. nucleoplasmin NLS) is composed of a short basic motif (^{155}KR^{156}) followed by a linker of 10 residues and a longer basic motif (^{167}KKKK^{170}). An example of varied bipartite NLS is found in MH1 domain of SMAD4 (Xiao et al., 2003), a transcription factor regulated by TGF-β signalling (Ross and Hill, 2008). Through truncation and alanine scanning, the critical residues responsible for nuclear import of Smad4 were shown to be K^{45}, K^{46}, K^{48} and R^{81} in the HM1 domain of Smad4. Notably, the linker sequence between the first basic cluster and the second basic residue is of significantly longer length compared to that of nucleoplasmin. Furthermore, the order of basic motifs in the Smad4 NLS resembles an inverted bipartite NLS in that the longer cluster of basic residues occurs before the single R^{81} residue in the primary sequence of the protein (Xiao et al., 2003).

The functionality of the linker sequence in a bipartite NLS has also been the subject of several studies. The linker sequence of the nucleoplasmin NLS has been shown to tolerate an increase in length of up to 12 amino acid residues with no adverse effect on the nuclear import of pyruvate kinase fused with the nucleoplasmin NLS (Robbins et al., 1991). Consistent with these observations, additional nuclear proteins with bipartite NLSs containing longer linker sequence have been identified, such as DNA topoisomerase II from *Aspergillus terreus* with a 15 residue linker sequence (Kim et al., 2002) and Ty1 integrase of *S. cerevisiae* with a linker of 29 residues (Lange et al., 2010). In addition to demonstrating that Ty1 has a long linker sequence in its bipartite NLS, Lange and colleagues also provided functional evidence regarding the importance of amino acid composition within the linker. They used an obligate bipartite NLS reporter system (KR 10aa K<u>T</u>KRKV-2xGFP (Hodel et al., 2001)) in which the NLS of T-ag is mutated at the second K to <u>T</u>, and is connected to the first basic motif (KR) of the nucleoplasmin bipartite NLS at the N-terminus. The mutation of the T-ag-NLS abrogates its monopartite NLS function, but the presence of the KR of nucleoplasmin NLS imparts a bipartite NLS identity to the entire sequence. By

increasing the length of the linker sequence, the authors found that this NLS is functional with the linker of up to a maximum of 20 amino acid, as evident by reduced nuclear accumulation of the reporter molecule, NLS-2xGFP, with linkers of more than 20 amino acids in *S. cerevisiae*. Replacement of the long linkers with that of the Ty1 NLS linker, which contains 29 residues, restored the nuclear accumulation of NLS-2xGFP, demonstrating the sequence-dependence of a functional linker in a bipartite NLS (Lange et al., 2010).

Since a cNLS does not comply with a stringent consensus, several methods have been developed to predict the presence of a putative cNLS in proteins. Cokol and colleagues developed a program for cNLS prediction (PredictNLS) based on sequence identity of a query protein with existing annotated NLSs in protein data bases such as SWISS-PROT (Cokol et al., 2000). In a more recent study, Kosugi et al, serially mutated all of the amino acids of three known yeast NLSs to find contribution of each residue to the activity of an NLS (Kosugi et al., 2009). The activity was then determined *in vivo* by measuring the nuclear accumulation of mutant NLS proteins and placed in an arbitrary scale of 1 to 10, with lowest and highest nuclear accumulation respectively. Based on the obtained results regarding the contribution of individual residues to activity of an NLS, these authors developed a computer algorithm (cNLS Mapper) for prediction of putative cNLSs (Kosugi et al., 2009)

An important feature that imparts functionality to a NLS is its ability to be recognized by cellular nuclear import receptors. Therefore the affinity of a NLS for such receptors is a major determinant of its capacity to confer nuclear localization. Enzyme-linked immunosorbent assay (ELISA) experiments, coupled with *in vivo* and *in vitro* nuclear import analyses, have shown a direct correlation between the affinity of an NLS for a receptor and its ability to mediate nuclear import. Efthymiadis et al, compared the capacity for the NLS of T-ag and of human retinoblastoma (RB) (bipartite KR 11aa linker KKLR (Zacksenhaus et al., 1993)), in directing the nuclear accumulation of a β-galactosidase fusion protein, with their respective affinities for nuclear import receptors. ELISA analyses showed that the K_d of the T-ag-NLS for mouse importin α is ~6 times lower than that of the RB NLS. *In vivo* nuclear import of the fusion proteins in rat hepatoma cell lines illustrated that the T-ag-NLS, which

was shown to have higher affinity for importin α compared to NLS of RB, can also mediate the nuclear accumulation of a fusion protein to a higher rate and a final extent (Efthymiadis et al., 1997). The result of this observation has been supported by further studies in which the affinity of an NLS for import receptors shows direct correlation with its ability to mediate nuclear import in yeast (Hodel et al., 2006) and in rat hepatoma cell lines (Hubner et al., 1997).

1.1.3.3 Regulation of NLSs through post-translational modifications

Biological molecules are routinely modified *in vivo* to attain a fully functional state, with phosphorylation being the best studied example of a modification that can act as a molecular switch, rendering a protein active or inactive. Concerning nuclear import, post-translational modification of amino acid residues within, or in vicinity of, an NLS is known to modulate the activity of NLSs. Such modulations influence the affinity of an NLS for nuclear import receptors and subsequently determining the efficiency of nuclear import in both positive (i.e. enhancement) and negative (i.e. reduction) ways.

The original indication that phosphorylation modulates nuclear import came from the observation that the N-terminal flanking region of T-ag-NLS enhances the nuclear accumulation rate of a fusion protein. In these experiments the T-ag-NLS with flanking sequences on either side of the core NLS (^{127}KKKRK^{131}) were fused with β-galactosidase, followed by microinjection into rat hepatoma cells. Localization of the fusion proteins revealed that inclusion of the 14 residues upstream of T-ag-NLS (111-125) significantly increased the rate of fusion protein nuclear uptake (Rihs and Peters, 1989). There exist 5 phosphorylation sites in the upstream region of the T-ag-NLS, Ser^{111}, Ser^{112}, Ser^{120}, Ser^{123}, and Thr^{124} (Scheidtmann et al., 1982). A recombinant β-galactosidase protein fused to a T-ag-NLS harbouring mutations to either mimic or abrogate phosphorylation in these sites revealed that casein kinase II (CK-II) dependent phosphorylation of Ser^{111} and Ser^{112} sites lead to an enhanced nuclear import rate (Rihs et al., 1991), while p34^{cdc2} dependent phosphorylation of Thr^{124} reduced the rate (Jans et al., 1991). The enhanced import rate of the fusion proteins containing the CK-II kinase sites (Ser^{111} and Ser^{112}) was subsequently shown to be

due to the increased affinity of the T-ag-NLS for a mouse nuclear import receptor, importin α (Hubner et al., 1997).

The *Epstein-Barr virus* antigen 1 (EBNA-1) provides another example of the regulatory effect of phosphorylation on an NLS activity. EBNA-1 is a nuclear protein essential for replication of the *Epstein-Barr virus* plasmid DNA (Leight and Sugden, 2000). The NLS of EBNA-1 (^{379}KRPRSPSS^{386}: EBNA-1 NLS) contains three phosphorylation sites, at serines 383, 385, and 386. HeLa cells microinjected with EBNA-1 NLS-BSA fusion proteins, in which the NLS contained mutations to either mimic or abrogate serine phosphorylation, showed opposite effects of phosphorylation on different serine residues. The results of these studies demonstrated that Ser^{385} is essential for nuclear import of EBNA-1 and its phosphorylation accelerates the rate of import; Ser^{386} on the other hand, is not essential for nuclear import, but its phosphorylation leads to a decrease in rate of nuclear import (Kitamura et al., 2006).

Further examples of enhancing and inhibitory effects of phosphorylation on NLS activity have been reported for DNA polymerase phosphoprotein (ppUL44) of human *Cytomegalovirus* (Alvisi et al., 2005) and bovine *Papillomavirus* type 1 E1 protein (Bian et al., 2007), and this has been the subject of a recent review (Nardozzi et al., 2010). Thus post-translational modifications exert regulation on nuclear transport processes by modulating the NLS activity. Such modulations can have significant impact on cell fate through altered nucleocytoplasmic transport under conditions in which NLSs are modified.

1.1.3.4 Masking and unmasking of NLSs

In addition to post-translational modifications such as phosphorylation, masking and unmasking of an NLS through interacting molecules is known to modulate NLS's activity. In this process, the NLS of a nuclear cargo protein is "masked" by a binding protein which is removed upon signal stimulation, leading to its unmasking. One of the best characterized examples of NLS masking is that of the nuclear factor-kappa B (NF-κB) transcription factor. NF-κB is composed of two subunits that heterodimerize and upon cellular stress induced by cytokines, the dimer translocates into the nucleus

to regulate the expression of several genes involved in the immune response (Hay et al., 1999). The cytoplasmic retention of NF-κB involves occlusion of its NLS by a factor known as inhibitor of NF-κB (IκB). *In vitro* interaction studies using wild type or truncated NF-κB lacking its NLS showed that IκB interacts with the NLS region of NF-κB. Over-expressed NF-κB in COS-7 cells accumulates in the nucleus, while co-expression with IκB leads to cytoplasmic retention of NF-κB; that the cytoplasmic retention of NF-κB is through NLS masking by IκB was demonstrated by the observation that fusion of T-ag-NLS to the N-terminus of NF-κB rescued the cytoplasmic retention and led to nuclear localization of NF-κB upon co-expression with IκB (Beg et al., 1992). Treatment of a variety of cell lines with inducers of NF-κB activity results in phosphorylation-mediated proteolytic loss of IκB and a concurrent accumulation of NF-κB inside the nucleus (Beg et al., 1993; Henkel et al., 1993), demonstrating that removal of IκB leads to unmasking of the NF-κB NLS.

Another case of an NLS that is potentially masked by a heterologous protein is found in BRCA1. This protein exerts tumor suppression activity through its role in DNA repair and maintenance of genome stability (Thompson, 2010). Wild type BRCA1 is localized in the nucleus of normal cells but its localization is cytoplasmic in breast cancer cell lines (Lee et al., 1999). The putative mask of BRCA1 NLS was identified through yeast two hybrid screening of human B lymphocytes (Chen et al., 1996). The identified BRCA1-interacting protein, BRAP2, was shown to interact with the NLS of BRCA1 protein, localize predominantly in the cytoplasm, and bind specifically and strongly to other NLSs such as T-ag-NLS and to the bipartite NLS of mitosin (Li et al., 1998). Although the functionality of BRAP2 in masking the BRCA1 NLS has not been verified, its cytoplasmic localization and NLS binding specificity is indicative of a role in preventing nuclear accumulation of an NLS bearing cargo.

An interesting example of intermolecular NLS masking has recently been reported for the HIV-1 regulatory protein (HIV-1 Rev) which is imported into the nucleus by several importin β family members, including importin β1 (Truant and Cullen, 1999) and transportin (Arnold et al., 2006). Human I-mfa domain-containing protein (HIC) was identified as the cellular factor that masks the HIV-1 Rev NLS, through its ability to prevent nuclear accumulation of Rev in COS-7 cells upon co-expression, and its

specific binding to the Rev NLS (Gu et al., 2011). Intriguingly, HIC was shown to only interfere with importin β1-mediated nuclear import of Rev in 293, COS-7, and CEM cells, but not in HeLa, THP-1, and U937 cells, where transportin is the dominant nuclear import receptor for Rev. These observations suggest that, in a given cellular context, the balance and competition between different import receptors can be a determinant of a cargo import rate. Further examples of NLS masking and unmasking through both interactions with heterologous proteins and conformational status of an NLS bearing molecule has been discussed in several reviews (Jans et al., 2000; Poon and Jans, 2005).

1.1.3.5 Nonclassical NLSs

NLSs that do not meet every criteria of a cNLS are referred to as nonclassical NLSs, and these contribute to the nuclear accumulation of a wide range of cargoes. An example of a nonclassical NLS is that of the signal transducers and activators of transcription (STATs) family member, STAT1. In response to interferon-γ (IFN-γ) stimulation, cytoplasmic STAT1 is phosphorylated and translocates into the nucleus (Shuai et al., 1993b). The NLS and the mechanism of STAT1 nuclear translocation, however, differ from cNLSs in several ways. Firstly, the region of binding between STAT1 and its nuclear import receptor, importin α5, is distinct from the binding site of cNLSs. Sekimoto et al showed that STAT1 binds to the C-terminus region of importin α5, while a cNLS binds to the central region of importin α (Sekimoto et al., 1997). (The binding sites of importin α proteins for cNLSs will be discussed in details in Section 1.1.4.3) Secondly, IFN-γ-induced nuclear accumulation of STAT1 is dependent on dimerization of STAT1. A STAT1 mutant which is unable to dimerize (Y701A (Shuai et al., 1993a)) cannot enter the nucleus after IFN-γ stimulation due to the lack of interaction of monomeric STAT1 with importin α5 (Fagerlund et al., 2002). Furthermore, the domain essential for this dimer-specific NLS (amino acids 376-472) is only functional in the context of STAT1 protein, since the region fails to mediate accumulation of a GST-GFP fusion protein in the nucleus of transfected HeLa cells (Meyer et al., 2002).

Some proteins can enter the nucleus with no discernible NLS, and their nuclear entry is independent of known nuclear import receptors. One example is E7 of *high risk human papillomavirus type 16* (HPV16 E7). Fusion of different regions of this 98 amino acid protein to GST narrowed the nuclear import activity of the protein to the N-terminal amino acids, 1-37 (Knapp et al., 2009). In contrast to a cNLS however, this region does not contain a consensus cNLS enriched by basic motifs; the nuclear accumulation of full length HPV16 E7 was also shown to be independent of any known nuclear import receptor (Angeline et al., 2003; Knapp et al., 2009).

An emerging signal involved in nuclear import of proteins is composed of a Ser-Pro-Ser (SPS) motif that acts as an NLS upon phosphorylation. Erk2 is a member of a signalling molecule family that translocates into the nucleus after extracellular stimulation (Yoon and Seger, 2006). Accumulation of Erk2 into the nucleus is dependent on phosphorylation of ^{244}Ser-Pro-Ser^{246} (^{244}SPS^{246}) and mediated by a nuclear transport factor, importin 7. Although the SPS motif is able to translocate a β-galactosidase fusion protein into the nucleus both *in vivo* and *in vitro*, the sequence of this motif does not resemble or fit with any previously known consensus sequence of a cNLS (Chuderland et al., 2008). This novel nuclear localization signal has also been identified in other signal-activated transcription factors including early growth response-1 (Egr-1) (Chen et al., 2011) which is known to contain a bipartite cNLS (Gashler et al., 1993). Thus, discovery of a growing number of nonclassical NLSs, some of which occur in proteins possessing a cNLS (e.g. Egr-1) indicates the complexity of nuclear transport regulation.

1.1.4 The classical nuclear import pathway

An NLS on its own is not capable of conferring nuclear entry to a nuclear protein possessing it. cNLSs are recognized by specific transport receptors that facilitate the nuclear uptake of these cargo molecules. The classical nuclear import receptors are importin α (imp α) and importin β1 (imp β1) of the importin β superfamily which form a heterodimer (importin α/β1). In this heterodimer, importin α binds to the cNLS and importin β1 translocates the trimeric complex into the nucleus. Importin αs comprise a family of proteins with seven members identified to date in humans, and

six members in mouse (Section 1.1.6). Several terms have been used to refer to nuclear import receptors. The nomenclature of importin β1 and importin α family members has been recently reconciled (Major et al., 2011; Miyamoto et al., 2012a) and the term importin will be used in this review and subsequent chapters for the purpose of clarity. Figure 1.2 summarizes the components of classical nuclear import pathway for a cNLS bearing cargo molecule, including the import complex dissociation, cargo release and return of importin α and importin β1 to the cytoplasm that are discussed in subsequent sections. Importin β1 is known to bind and translocate a cNLS cargo into the nucleus without utilizing importin α (Jans et al., 2000). Importin β1-mediated nuclear import of an cNLS-bearing cargo is also considered a classical import pathway, since the translocation of cargo across the NPC, and release of cargo inside the nucleus resembles that of a trimeric import complex. The following section describes the classical nuclear import receptors and the mechanisms by which they bind and translocate cargo into the nucleus.

1.1.4.1 Discovery of facilitated nuclear import mediators

Classical nuclear import of proteins can be separated into two distinct steps. These include the signal-dependent and energy-independent localization of the nuclear proteins on the nuclear envelope, followed by their energy-dependent translocation across the NPC (Gorlich and Kutay, 1999). When injected into the cytoplasm of Vero cells at 37°C, purified *X. laevis* nucleoplasmin accumulates in the nucleus within one minute; however, the injected nucleoplasmin is arrested on the nuclear membrane at 20°C or when intracellular ATP is depleted by a combination of sodium azide and deoxyglucose treatment. This effect is reversible and can be rescued by incubation of injected cells at 37°C (Richardson et al., 1988). The dependence of nuclear import on a signal sequence and energy expenditure is consistent with the notion of an active and receptor-mediated process. Adam and colleagues developed an *in vitro* nuclear transport assay which led to the identification of cytosolic factors that mediate protein nuclear entry. In this system, cells are treated with digitonin, a weak nonionic detergent which perforates the plasma membrane while leaving the internal membrane structures, including the nuclear envelope, intact. Perforation of the plasma membrane leads to depletion of cytoplasmic content from the permeabilized cells. When

Figure 1.2 Translocation of import complex, cargo release and recycling of importins

In the cytoplasm a cNLS bearing cargo (NLS cargo) is recognized by importin α/β1 heterodimer, leading to the formation of a nuclear import complex. Importin α (Impα) binds the cNLS and importin β1 (Imp β1) translocates the import complex across the NPC. After an import complex has reached the nucleoplasmic side of the NPC, Ran-GTP induces the dissociation of import complex by binding to importin β1. Removal of importin β1 leads to complete dissociation of import complex and release of NLS bearing cargo inside the nucleoplasm. Importin β1 bound to Ran-GTP crosses the pore back to the cytoplasm. Importin α binds to its export factor, CAS, in complex with Ran-GTP and is subsequently recycled to the cytoplasm for another round of import.

Cytoplasm

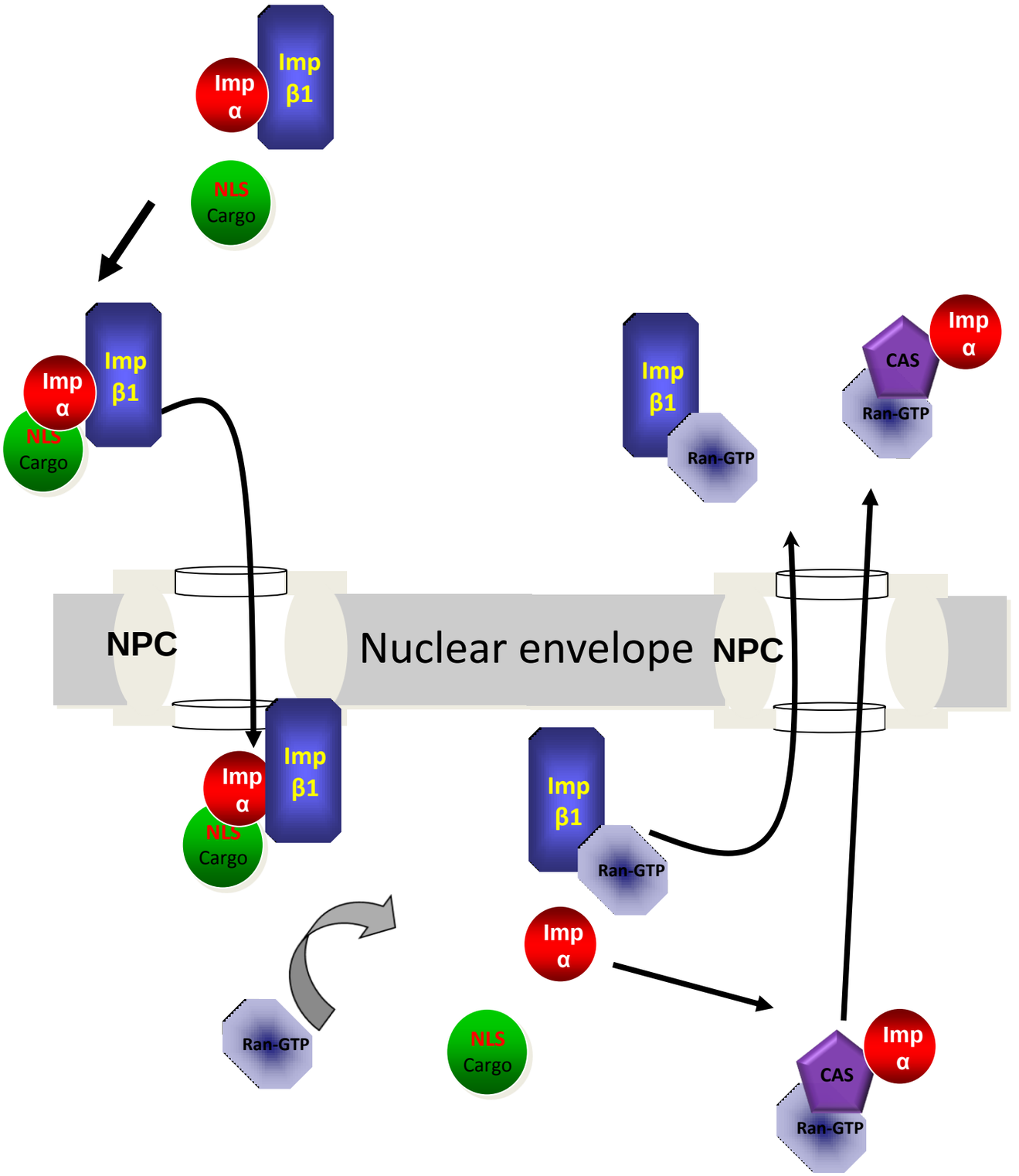

Nucleus

allophycocyanin (APC, a fluorescent tag) fused to the T-ag-NLS (APC-T-ag-NLS) was introduced to the permeabilized cells, no nuclear accumulation of the fusion protein was observed. However, addition of exogenous cytosol from rabbit reticulocytes resulted in fusion protein nuclear accumulation, implicating the cytosolic factors in mediation of nuclear import (Adam et al., 1990). Moore and Blobel, resolved the *X. laevis* oocyte cytosol into several fractions using ion exchange chromatography and showed that two of these fractions (fraction A and fraction B) possess activities that are required for nuclear import of an NLS-bearing conjugate molecule in an *in vitro* nuclear import assay (Moore and Blobel, 1992). They observed that addition of fraction A to the permeabilized buffalo rat liver (BRL) cells allows accumulation of the NLS cargo on the nuclear membrane; the translocation step of the NLS cargo into the nucleus required the addition of fraction B, demonstrating that the two fractions contain independent activities for mediating nuclear import.

1.1.4.2 The importin α/β1 heterodimer

Several laboratories further resolved the fraction A of cytosol from a variety of cell types, and by using *in vitro* nuclear import assays identified two cytoplasmic factors as nuclear import receptors (Adam and Adam, 1994; Görlich et al., 1995; Radu et al., 1995a). In these studies two proteins of 56 and 97 kDa were identified as being responsible for the first step of nuclear import, that is accumulation of an NLS-bearing cargo on the nuclear envelope. The two identified proteins were able to support accumulation of APC-T-ag-NLS on the nuclear envelope of permeabilized MDBK cells without the addition of exogenous cytosol (Adam and Adam, 1994). Based on the nuclear import function of these proteins, the 56 kDa protein was named importin α (imp α) and the 97 kDa protein was named importin β1 (imp β1). Together they make a stable nuclear import complex (impα/impβ1/NLS cargo) in the cytoplasm prior to nuclear envelope binding and nuclear accumulation (Imamoto et al., 1995). Subsequent studies using recombinant importins, revealed that only importin α can directly bind to an NLS-bearing molecule, initially T-ag-NLS fused to human serum albumin (HSA) (Moroianu et al., 1995b). Importin β1 on the other hand, was shown to be essential for docking of the import complex on the nuclear envelope and

subsequent translocation, through direct interactions with components of NPC, including both nuclear and cytoplasmic nucleoporins from rat liver nuclei (Moroianu et al., 1995a; Moroianu et al., 1995b). Based on these observations, the following mechanism for nuclear import of a karyophilic protein was suggested. A karyophilic protein is recognized by importin α/β1 heterodimer in the cytoplasm, through direct binding with importin α. The complex docks on the nuclear envelope and subsequently is translocated across NPC through interactions of importin β1 with nucleoporins.

1.1.4.3 NLS cargo recognition and transport by the importin α/β1 heterodimer

As mentioned in section 1.1.4.2, the NLS recognition and binding ability of importin α/β1 heterodimer is conferred by importin α. Rexach and Blobel showed that yeast importin α can bind the T-ag-NLS fused to Glutathione S-transferase (GST) (T-ag-NLS-GST) in an *in vitro* solution binding assay, and that importin β1 cannot; importantly the binding of importin α to T-ag-NLS-GST was enhanced in the presence of importin β1, indicating that the importin α/β1 heterodimer has higher affinity for the T-ag-NLS cargo than importin α alone (Rexach and Blobel, 1995). These observations were confirmed by ELISA-based binding experiments which showed that mouse importin α and β1 have a synergistic effect in a heterodimeric form with regard to binding both monopartite (T-ag) and bipartite (retinoblastoma protein) NLSs (Efthymiadis et al., 1997; Hu and Jans, 1999; Hubner et al., 1997). This cooperative effect has been attributed to the function of the N-terminal domain of importin α which can bind to both importin β1 and the NLS binding region of importin α. The N-terminal residues 23-49 of importin α fused with HSA was shown to bind to both a truncated importin α which lacked the N-terminal 49 residues, and importin β1 *in vitro* (Moroianu et al., 1996a). These observations implied that the N-terminal domain of importin α can function as an autoinhibitory domain which competes with an autologous NLS in the absence of importin β1. The structural analysis of full length importin α has provided conclusive evidence that the N-terminus of importin α is bound to the NLS binding region of the protein when importin β1 is not bound to importin α (Kobe, 1999). Therefore, binding of importin β1 to importin α blocks activity of the autoinhibitory N-terminal domain of importin α

which provides an explanation for the higher affinity of importin α/β1 heterodimer for an NLS than that of importin α alone.

The NLS binding region of importin α is made up of 10 ARM repeats (discussed in Section 1.1.6) that provide two binding sites designated as major and minor binding grooves. Crystallographic analysis of yeast and mouse importin α bound to monopartite (T-ag) and bipartite (nucleoplasmin) NLSs showed that the short (^{155}KR^{156}) and long (^{167}KKKK^{170}) basic motifs of a bipartite NLS bound to the minor and major NLS binding grooves of importin α, respectively (Fontes et al., 2000), while the monopartite NLS preferentially bound to the major NLS binding groove of importin α (Conti et al., 1998; Fontes et al., 2000). These observations have been supported by additional *in vitro* interaction and *in vivo* functional studies which showed mutations in major NLS binding sites of yeast importin α abrogate the binding of both monopartite and bipartite NLSs, while mutations in the minor NLS binding sites of importin α only affect the bipartite NLS binding to the importin α (Leung et al., 2003).

Docking of the importin α/β1/NLS cargo complex on the NPC and subsequent translocation through the pore is initiated by the interaction of importin β1 with nucleoporins. Blot overlay studies implicated the FG repeat-containing nucleoporins as the site of docking for import complexes. In these experiments, enriched NPCs were isolated from rat liver then separated by SDS-PAGE and transferred to a nitrocellulose membrane. The membrane was then incubated with a T-ag-NLS conjugated to HSA (NLS-HSA) in the presence of cytosolic extracts and subsequently probed with anti-HSA antibody. Using this approach, the proteins of the NPC that interacted with NLS-HSA (i.e. import complex) were identified to be nucleoporins from both the cytoplasmic (e.g. Nup358 and Nup214) and nuclear (Nup153 and Nup198) sides of the NPC. Interestingly, all of these nucleoporins contained FG repeats in their primary amino acid sequence (Moroianu et al., 1995b; Radu et al., 1995b). Further observations regarding the interaction of importin β1 with FG repeat containing nucleoporins led to the proposal of an affinity gradient across the NPC, with importin β1 having increasing affinity for the FG nucleoporins as the import complex moves towards the nuclear side of the pore complex. Shah and colleagues

provided evidence for preferential binding of importin α/β1/NLS cargo to nucleoporins in an *in vivo* system. In this study, *X. laevis* egg extract was used to recapitulate the *in vivo* environment, since it contains all the components and subcomplexes that are necessary for assembly of a functional NPC (Laskey and Leno, 1990). The NLS-HSA conjugate was incubated with *X. laevis* egg extract followed by immunoprecipitation with anti-HSA antibody. The bound proteins were then analysed by Western blotting with antibodies to several nucleoporins. Quantitative measurements revealed that ~20-40% of the total Nup153 (a nuclear basket Nup), but only 10% of Nup358 (a cytoplasmic filament associated Nup) bound to the import complex (Shah et al., 1998). The authors interpreted these data as being suggestive of differential affinity of nucleoporins for an import complex.

In a subsequent study, designed to compare the affinity of importin β1 for a cytoplasmic nucleoporin (Nup358), the central pore channel nucleoporin complex (Nup62, Nup58, and Nup54) and a nucleoplasmic basket nucleoporin (Nup153) of *X. laevis* oocyte (all FG nups), differential affinity of these FG containing nucleoporins for importin β1 was measured by an *in vitro* solid binding assay. Consistent with the proposed affinity gradient model, the affinity of importin β1 was lowest for cytoplasmic Nup358, and highest for the nuclear Nup153. In addition, all of the Nup62 complex nucleoporins had intermediate affinity for importin β1 (Ben-Efraim and Gerace, 2001). The increasing affinity gradient of nucleoporins for an import complex (importin α/β1/NLS cargo) from cytoplasmic to the nuclear end of the pore complex has also been documented in *S. cerevisiae* by *in vitro* binding assays and *in vivo* genetic manipulations (Pyhtila and Rexach, 2003).

1.1.4.4 Import complex dissociation in the nucleus and import receptors return to the cytoplasm

Once the import complex reaches the nucleoplasmic side of the pore complex, karyophilic cargo release is essential to prevent the futile cycle of import reaction. In addition, import receptors (i.e. imp α and imp β1) need to cross the nuclear envelope back to the cytoplasm for next round of import. Cargo release into the nucleoplasm is the outcome of import complex dissociation, initiated by binding of a small guanine

nucleotide binding protein (G protein) Ran, to importin β1. Ran was identified in an *in vitro* nuclear import assay as a constituent of the cytosolic factors that is essential for the translocation step of an NLS bearing molecule into the nucleus (Melchior et al., 1993; Moore and Blobel, 1993). Like other G proteins, Ran exists in two conformational states; these proteins are either in the GDP-bound form due to an induced or intrinsic GTPase activity, or in a GTP-bound form as a result of a nucleotide exchange factor that replaces the GDP with GTP (Bourne et al., 1991). Addition of Ran-GTP to yeast importin α/β1 in complex with either immobilized FG repeat region of Nup1 and Nup2, or to immobilized T-ag-NLS *in vitro*, led to the dissociation of importin α from the FG repeats and both importins from T-ag-NLS, while Ran-GDP had no effect (Rexach and Blobel, 1995). Incubation of *X. laevis* oocyte cytosol with a GTPase-defective Ran (Ran Q69L), which is present only in GTP-bound form, inhibits the formation of importin α/β1 heterodimers. Furthermore, importin β1 lacking the Ran binding domain can translocate an import complex into the nucleus but is unable to release the cargo into the nucleoplasm (Gorlich et al., 1996b), demonstrating the importance of Ran-GTP binding to importin β1 for cargo release. Further examples of the accelerating effect of Ran-GTP on NLS-cargo dissociation from an import complex or Nups has been documented by *in vitro* interaction analysis (Ben-Efraim and Gerace, 2001; Gilchrist et al., 2002). This effect is due to mutually exclusive binding of Ran and importin α to importin β1 (Gorlich et al., 1996b), with Ran-GTP having higher affinity for importin β1 (Moroianu et al., 1996b). Therefore binding of Ran-GTP to importin β1 and removal of importin β1 from the import complex leads to the subsequent dissociation of NLS-cargo from importin α caused by the low affinity of binding between importin α and NLS cargo in the absence of importin β1 (discussed in Section 1.1.4.3). Partitioning of Ran in GTP or GDP-bound form, which ensures the correct directionality of nuclear transport, is discussed in Section 1.1.5. More recent studies have revealed the role of a Nup in import complex dissociation inside the nucleus. Npap60 (also known as Nup50) is a mobile Nup that shuttles between the nucleus and cytoplasm but is predominantly localized within the nucleoplasm. This Nup promotes the release of a cNLS bearing cargo from importin α in the nuclear side of NPC both *in vitro* and *in vivo* (Matsuura and Stewart, 2005).

After completion of import and cargo release inside the nucleus, both importin α and importin β1 are recycled back into the cytoplasm to take part in the next round of import. Importin α requires a dedicated export receptor for cytoplasmic recycling since it is unable to interact with NPC components. Nuclear Ran-GTP was shown to be essential for recycling of importin α to the cytoplasm since depletion of Ran-GTP by microinjection of Ran-GAP1 into the nucleus of *X. laevis* oocyte resulted in nuclear accumulation of importin α (Gorlich et al., 1997). Ran-GAP1 induces the GTPase activity of Ran, rendering it GDP bound and its distribution and function is discussed in Section 1.1.5. Immobilized Ran-GTP incubated with *X. laevis* oocyte cytosol was shown to form a trimeric complex with importin α and a previously described protein known as cellular apoptosis susceptibility (CAS) (Kutay et al., 1997). That CAS is the nuclear export receptor for importin α was shown in a nuclear import assay using CAS-depleted cytosol. Importin α accumulated in the nucleus when added cytosol was devoid of CAS, while addition of recombinant CAS to the import reaction led to complete disappearance of importin α from nucleus (Kutay et al., 1997). The yeast CAS homologue (Cse1p) has also been identified in *S. cerevisiae*; it interacts with importin α in presence of Ran-GTP and its deletion leads to accumulation of importin α inside the nucleus (Hood and Silver, 1998; Solsbacher et al., 1998).

No export factor for cytoplasmic recycling of importin β1 has been identified; return of importin β1 to the cytoplasm is understood to be an inherent feature of importin β1 due to its capacity to interact with nucleoporins of the NPC. Similar to importin α export, nuclear Ran-GTP is required for cytoplasmic recycling of importin β1 since depletion of nuclear Ran-GTP by microinjection of Ran-GAP1 resulted in significant inhibition of importin β1 nuclear export (Izaurralde et al., 1997). Hieda and colleagues developed a monoclonal antibody to human Ran that recognizes the C-terminus of Ran only when Ran is in complex with importin β1 or with the export factor of importin α, CAS. This antibody was microinjected into the cytoplasm or the nucleus of BHK21 cells, followed by 30 minutes incubation at 37°C and immunofluorescent detection of the antibody's localization. Antibody injected into the nucleus was exported into the cytoplasm, and antibody injected into the cytoplasm remained cytoplasmic (Hieda et al., 1999). Based on the earlier characterization of the

antibody in binding to Ran only when in complex with importin β1 or CAS, the authors speculated that export of the antibody to the cytoplasm occurred through binding to Ran-importin β1 or Ran-CAS complex. Contradicting these observations, a Ran-independent pathway for export of importin β1 from the nucleus has also been demonstrated. Kose and co-workers showed that depletion of nuclear Ran-GTP does not completely abrogate importin β1 nuclear export, and that a mutant of importin β1 lacking the Ran binding domain is exported from nucleus to the cytoplasm of BHK21 cells (Kose et al., 1999). Thus, binding of Ran to importin β1 may serve as a nuclear export mechanism for Ran, rather than an absolute requirement for importin β1 recycling to the cytoplasm.

1.1.5 The Ran gradient and directionality of nuclear transport

Since import receptors have the contrasting need to both bind and release cargo, the correct compartment in which cargo loading and unloading takes place is crucial. Partitioning of Ran between the cytoplasmic and nuclear compartments is the major determinant of nucleocytoplasmic transport direction. A Ran concentration gradient exists across the nuclear envelope, with Ran-GTP and Ran-GDP being concentrated in the nucleoplasm and cytoplasm respectively. The partitioning of Ran in GTP and GDP forms is due to the activity of GTP hydrolysing proteins in the cytoplasm and a nucleotide exchange factor of Ran in the nucleus (Pemberton and Paschal, 2005). Ran guanine exchange factor (Ran GEF), known as RCC1, is a chromatin-bound protein, and it converts Ran-GDP to Ran-GTP inside the nucleus (Bischoff and Ponstingl, 1991), to generate the high concentration of Ran-GTP in the nucleoplasm which is essential for import complex dissociation and cargo release. Nuclear Ran-GTP is transported to the cytoplasm as a part of the export complexes as discussed in Section 1.1.4.4. In the cytoplasm, GTP hydrolysis results in conversion of Ran-GTP to Ran-GDP. Cytoplasmic Ran-GAP1 induces the weak intrinsic GTPase activity of Ran (Bischoff et al., 1994), while another Ran binding protein, RanBP1, assists Ran-GAP1 in GTP hydrolysis of Ran (Bischoff et al., 1995). Both Ran-GAP1 and RanBP1 are strictly cytoplasmic proteins (Matunis et al., 1996; Richards et al., 1996), which means cytoplasmic Ran is only in the GDP-bound form and does not interfere with the formation of an import complex. The nuclear pool of Ran is constantly

Figure1.3 Overview of the classical nucleocytoplasmic transport pathway

A. Import complex translocation across the NPC

In the cytoplasm, a nuclear cargo, possessing a cNLS is recognized by a heterodimer of importin α/β1 to form an import complex. Importin α provides the NLS recognition, while importin β1 carries out translocation of the import complex through the NPC. Ran-GDP is imported into the nucleus by its import factor, NTF2. In the nucleoplasm it is converted to RanGTP by the chromatin bound protein, RCC1, leading to a high concentration of Ran-GTP in the nucleus.

B. Import complex dissociation and return of importin α and β1 to the cytoplasm

Upon translocation of the import complex across the nuclear pore, Ran-GTP stimulates the complex dissociation by binding and removing importin β1 and release of cargo within the nucleus. Ran-GTP bound importin β1 is capable of leaving the nucleus, but importin α requires its export receptor, CAS, which binds to importin α in presence of Ran-GTP and mediates its cytoplasmic export.

C. Release of importin α and β1 in the cytoplasm. Completion of an import cycle

Dissociation of export complexes in the cytoplasm is essential for completion of an import cycle. This is triggered by Ran GTPase activating proteins, RanGAP1 and RanBP1 which hydrolyse Ran-GTP to Ran-GDP. Low affinity of Ran-GDP for the importins leads to their release in the cytoplasm. After export complex dissociation, importin α and β1 are ready for another import cycle round.

A. Import complex translocation across the nuclear pore complex

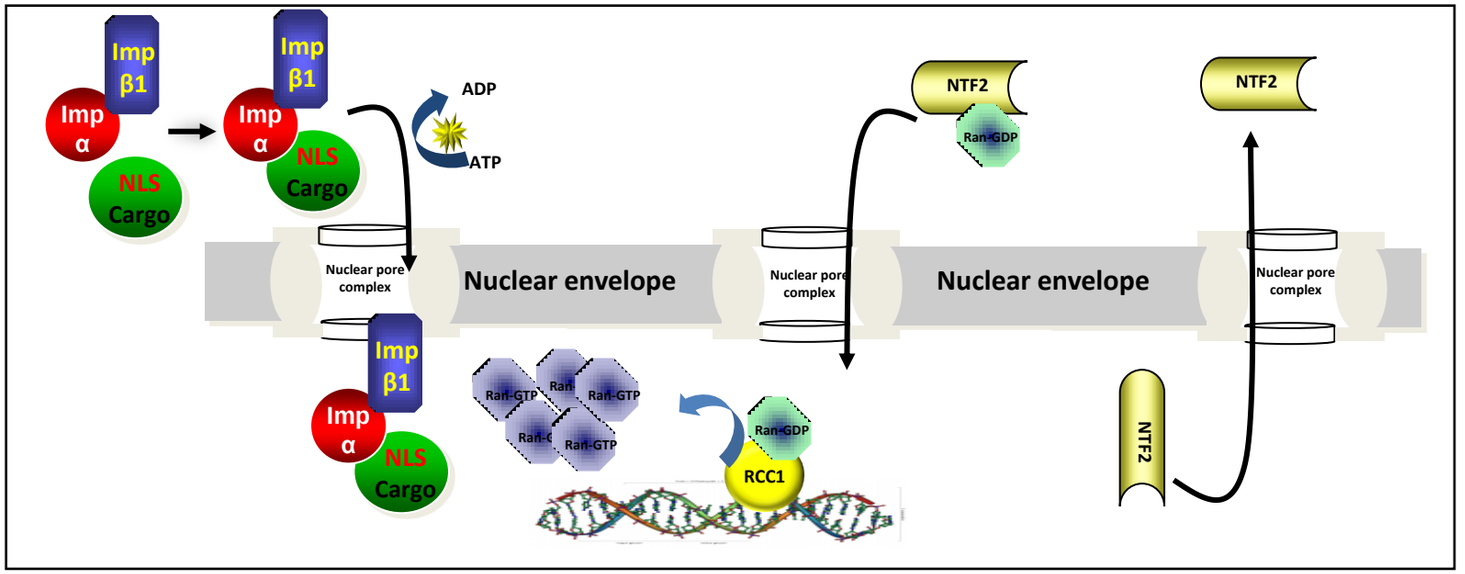

B. Import complex dissociation and return of importin α and β1 to the cytoplasm

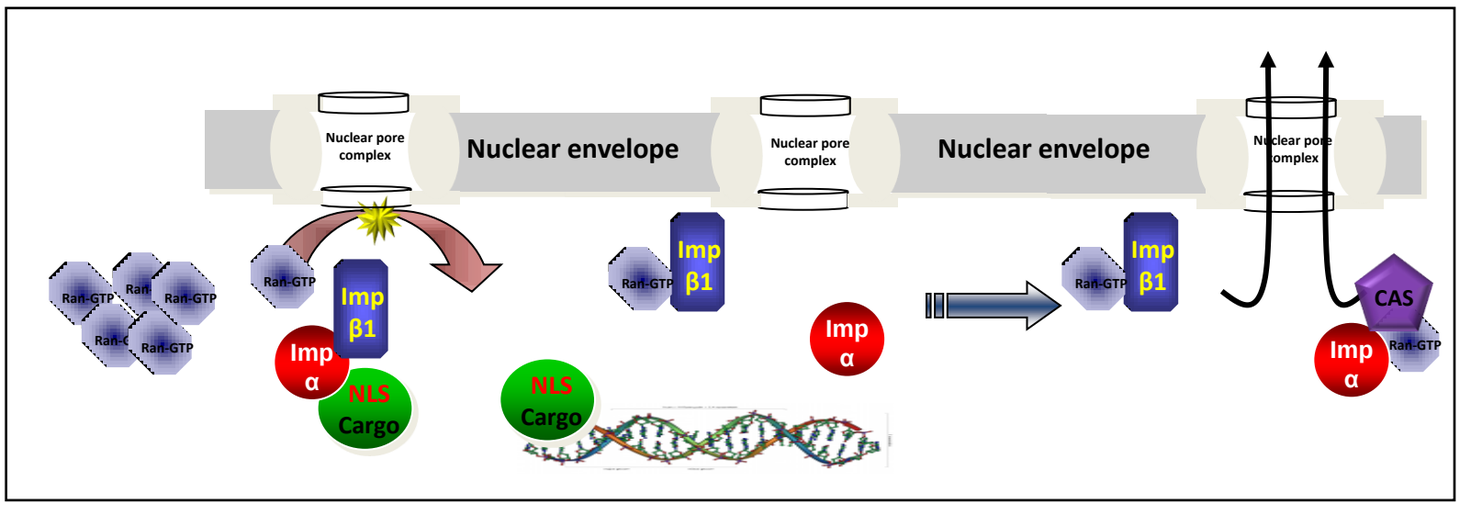

C. Release of importin α and β1 in the cytoplasm. Completion of an import cycle

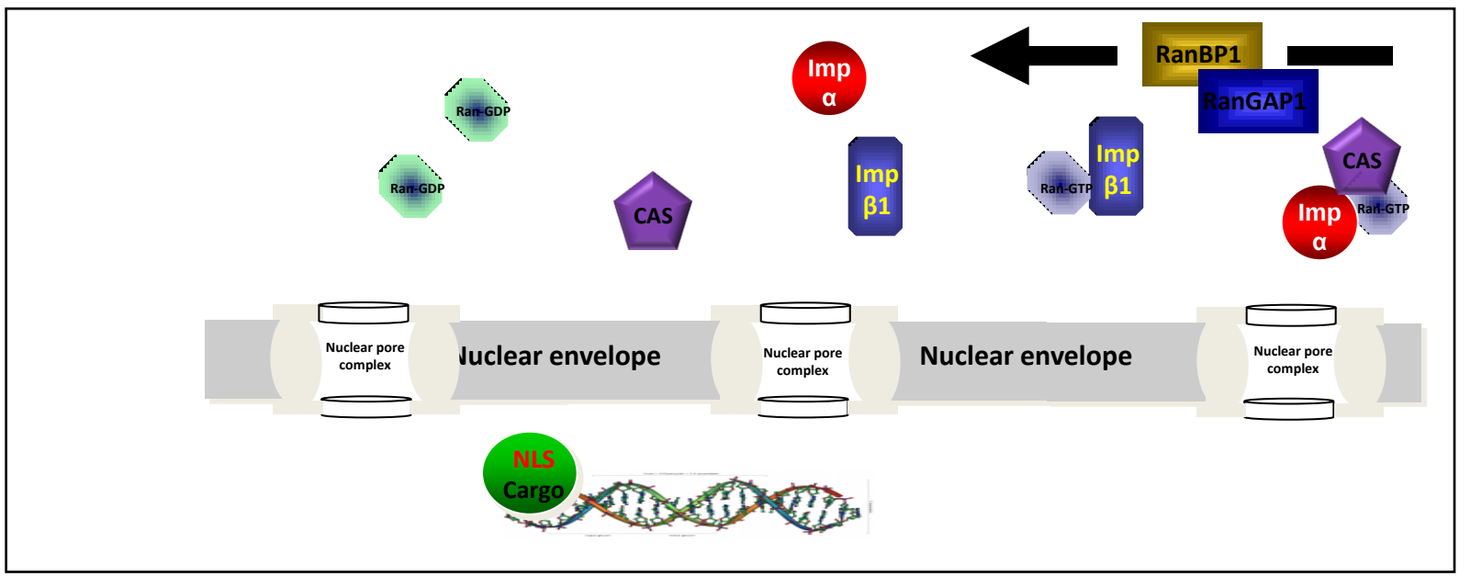

replenished by a dedicated Ran nuclear import receptor known as nuclear transport factor 2 (NTF2) (Smith et al., 1998). Therefore the Ran concentration gradient contributes to the direction of nucleocytoplasmic transport by ensuring that import complexes are formed only in the cytoplasm and are dissociated in the nucleus. Figure 1.3 summarizes the classical nuclear import pathway.

1.1.6 Domain organization and evolution of importin α

Importin α is composed of three distinct domains that collectively contribute to its function (Figure 1.4). These domains include an N-terminal importin β-binding (IBB) domain which mediates the interaction of importin α and importin β1, a central NLS-binding region involved in recognition and binding of cNLSs, and a C-terminal CAS-binding region that mediates the export of importin α from the nucleus through its interaction with CAS.

Deletion mutagenesis coupled with *in vitro* interaction and nuclear import assays showed that the N-terminal amino acids 21-51 of human importin α1 can bind to importin β1 in a manner similar to wild type importin α, and it is able to direct a β-galactosidase fusion protein to the nucleus (Weis et al., 1996). These observations were confirmed by Gorlich et al, who showed that the N-terminus of importin α is highly conserved across several species including *X. laevis*, *S. cerevisiae*, and *D. melanogaster*, both structurally and in binding to importin β1 (Gorlich et al., 1996a). The conservation of IBB domains and their functional attributes have recently been reviewed (Lott and Cingolani, 2011). Along with binding to importin β1 and acting as an autoinhibitory segment (discussed in Section 1.1.4.3), the IBB domain of importin α and other NLS adaptor molecules are thought to also contribute to the translocation of an import complex through the NPC by modulating the affinity of importin β1 for central channel FG nucleoporins (Lott et al., 2010).

As described in Section 1.1.4.4, importin α is exported from the nucleus by its export receptor, CAS. Yeast two-hybrid analysis of truncated importin α identified the conserved acidic C-terminus of importin α as the CAS-binding domain. The functionality of the C-terminus in binding CAS and mediating nuclear export of

Figure 1.4 Domain organization of importin α

A. Importin α is composed of three major functional domains. A schematic diagram of mouse importin α is presented on the left. The N-terminus of importin α is rich in acidic residues and is the site of importin α interaction with importin β1, and hence is known as the importin β1 binding (IBB) domain. The C-terminus of importin α is the region of interaction with the nuclear export receptor, CAS (Goldfarb et al., 2004). The core of importin α is made up of 10 tandem Arm repeats of 40 amino acids with low sequence but high structural conservation. The sequence of the fifth Arm repeat is shown which correspond to residues 242-282 of mouse importin α2. On the right, the ribbon diagram of mouse importin α2 is depicted with a vertical superhelical axis, in which the IBB domain is in magenta and each Arm repeat is represented in different colours (Kobe, 1999).

B. The schematic presentation of yeast importin α Arm repeats and position of cNLS binding sites. Stacking of 10 tandem repeats creates a concave groove (Tree-dimensional diagram below) in which two cNLS binding sites have been delineated. The major cNLS binding site is located between the second and fourth Arm repeats and includes residues 121-247; the minor cNLS binding site is located between the seventh and eighth Arm repeats and includes residues 331-417. The ribbon diagram below shows the three dimensional structure of Arm repeats with a superhelical horizontal axis in which each Arm repeat is coloured differently (Conti et al., 1998).

C. Crystal structure of mouse importin α2 bound to T-ag-NLS (left) and nucleoplasmin NLS (right). The structure of importin α is shown by ribbon, and both NLSs in ball-and-stick diagrams (Fontes et al., 2000). T-ag-NLS can bind to both NLS binding sites of importin α, but preferentially binds to the major groove due to presence of more contact sites (Conti et al., 1998; Fontes et al., 2000). The two basic motifs of nucleoplasmin NLS require both binding sites of importin α, with the short basic motif (KR) and long basic motif (KKKK) occupying the minor and major NLS binding sites respectively, while the linker region does not make extensive contact with importin α (Fontes et al., 2000).

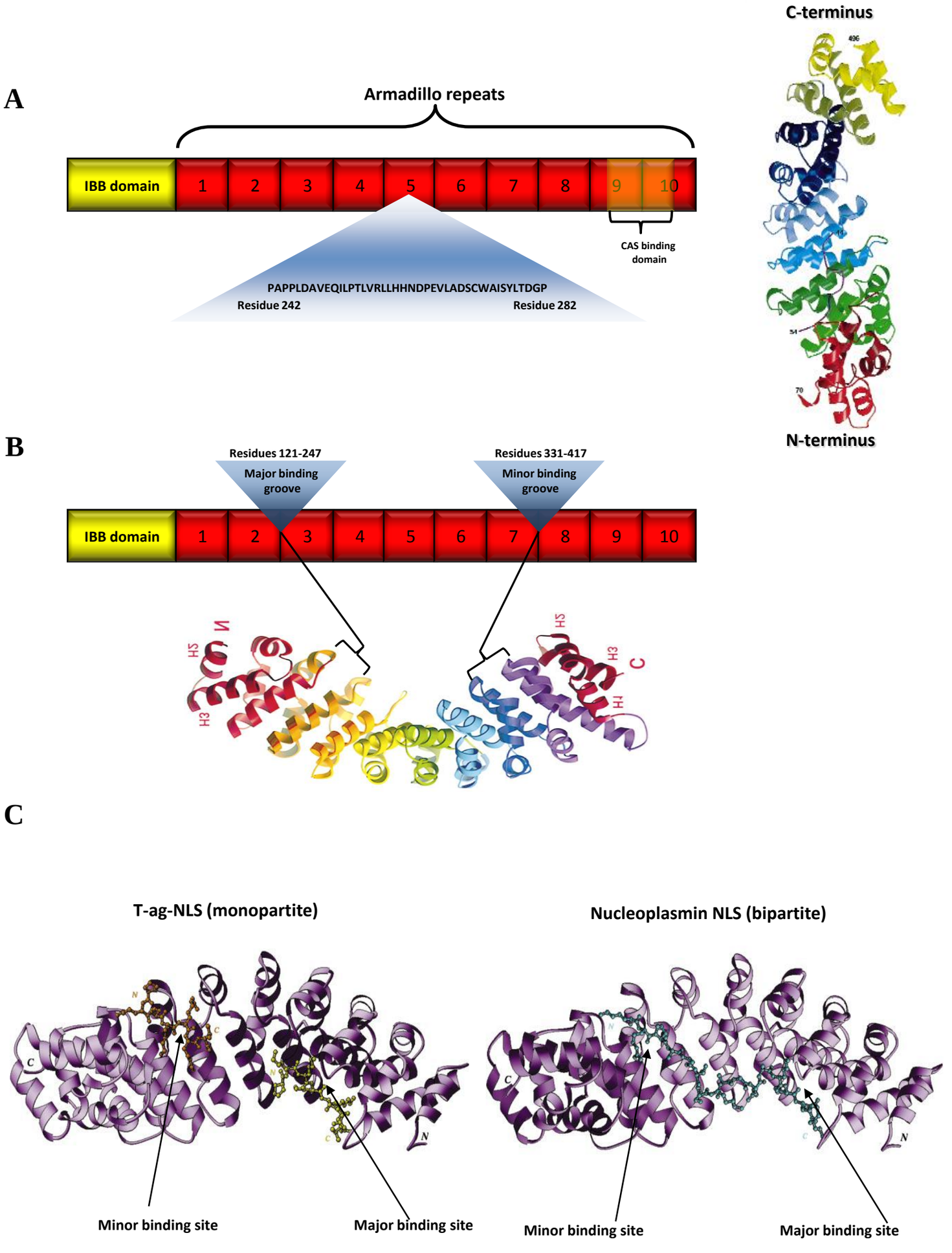
A
Armadillo repeats
IBB domain
1
2
3
4
5
6
7
8
9
10
CAS binding domain
PAPPLDAVEQILPTLVRLLHHNDPEVLADSCWAISYLTDGP
Residue 242
Residue 282
C-terminus
N-terminus
B
Residues 121-247
Major binding groove
Residues 331-417
Minor binding groove
IBB domain
1
2
3
4
5
6
7
8
9
10
H5
H3
N
H5
H3
C
H1
C
T-ag-NLS (monopartite)
Nucleoplasmin NLS (bipartite)
Minor binding site
Major binding site
Minor binding site
Major binding site

importin α was demonstrated by observation of nuclear export defects in yeast importin α mutants that were either lacking the C-terminal domain altogether, or harbouring mutations that inhibited interaction with CAS (Herold et al., 1998).

The central region of importin α is composed of 10 degenerate repeats of 40 amino acids (Goldfarb et al., 2004; Yano et al., 1992) known as Arm repeats. The structural and functional characteristics of Arm repeats are described in Section 1.1.6.1. The involvement of importin α Arm repeats in cNLS binding was delineated through truncation studies (Cortes et al., 1994; Herold et al., 1998), and by crystal structure analysis of importin α bound to both monopartite and bipartite cNLSs (Conti and Kuriyan, 2000; Fontes et al., 2000). Sequence alignment of mouse and yeast importin α proteins has shown that the most structurally conserved residues of the protein occur in the Arm repeat region of importin α (Kobe, 1999). Each Arm repeat is composed of 3 helices (H1, H2, and H3) that form a concave-shaped groove upon tertiary folding, with a hydrophobic core and a surface enriched by solvent-exposed residues (Conti et al., 1998; Kobe, 1999). Figure 1.4, A, shows the schematic and structure of full-length mouse importin α. The crystal structure of importin α bound to T-ag-NLS has revealed two binding sites on the surface groove of importin α. These binding sites correspond to residues 121-247 between the second and fourth Arm domains (major groove) and 331-417 between the seventh and eighth Arm domains (minor groove) (Conti et al., 1998; Figure 1.4, B). A monopartite NLS, such as T-ag-NLS, binds preferentially to the major binding site (Conti et al., 1998), while the bipartite nucleoplasmin NLS binds to both minor and major binding sites of importin α with the short basic motif occupying the minor, and the large basic motif binding to the major binding groove (Fontes et al., 2000; Figure 1.4, C).

Sequence alignment of importin α proteins shows the high level of similarity and conservation of the three specialized domains between the homologues across species including human, mouse and frog (Malik et al., 1997), with noticeably higher conservation in the central Arm repeats of the protein. Alignment of all mouse importin α homologues and an example of orthologue conservation between mouse and human is presented in Figure 1.5. There exist multiple homologues of importin α in higher eukaryotes which have evolved from a common ancestor in yeast. The *S.*

Figure 1.5 Evolutionary conservation of importin α family members

A. Alignment of all mouse importin α family members using Jalview 2.5 software ("Jalview version 2-a multiple sequence alignment editor and analysis workbench". Waterhouse, A.M., Procter, J. B., Martin, D.M.A, Clamp, M. and Barton, G.J. (2009) Bioinformatics doi:10.1093/ bioinformatics/btp033). The accession numbers are those used in Major et al, 2011. Blue colouring indicates the conservation of residues based on amino acid identity with a minimum of three identical residues being required for the consensus. Thus, dark, intermediate and light blue indicates the residues that are identical in all, in at least 4 and in 3 family members, respectively. The regions of highest conservation between family members is located in the central Arm repeats (red boxes) while the C-terminus shows the lowest identity (green box).

B. Alignment of mouse importin α3 and its human homolog, importin α4, as above. The alignment score of the two proteins is 99% which illustrates the high level of conservation in importin α family members during evolution.

A

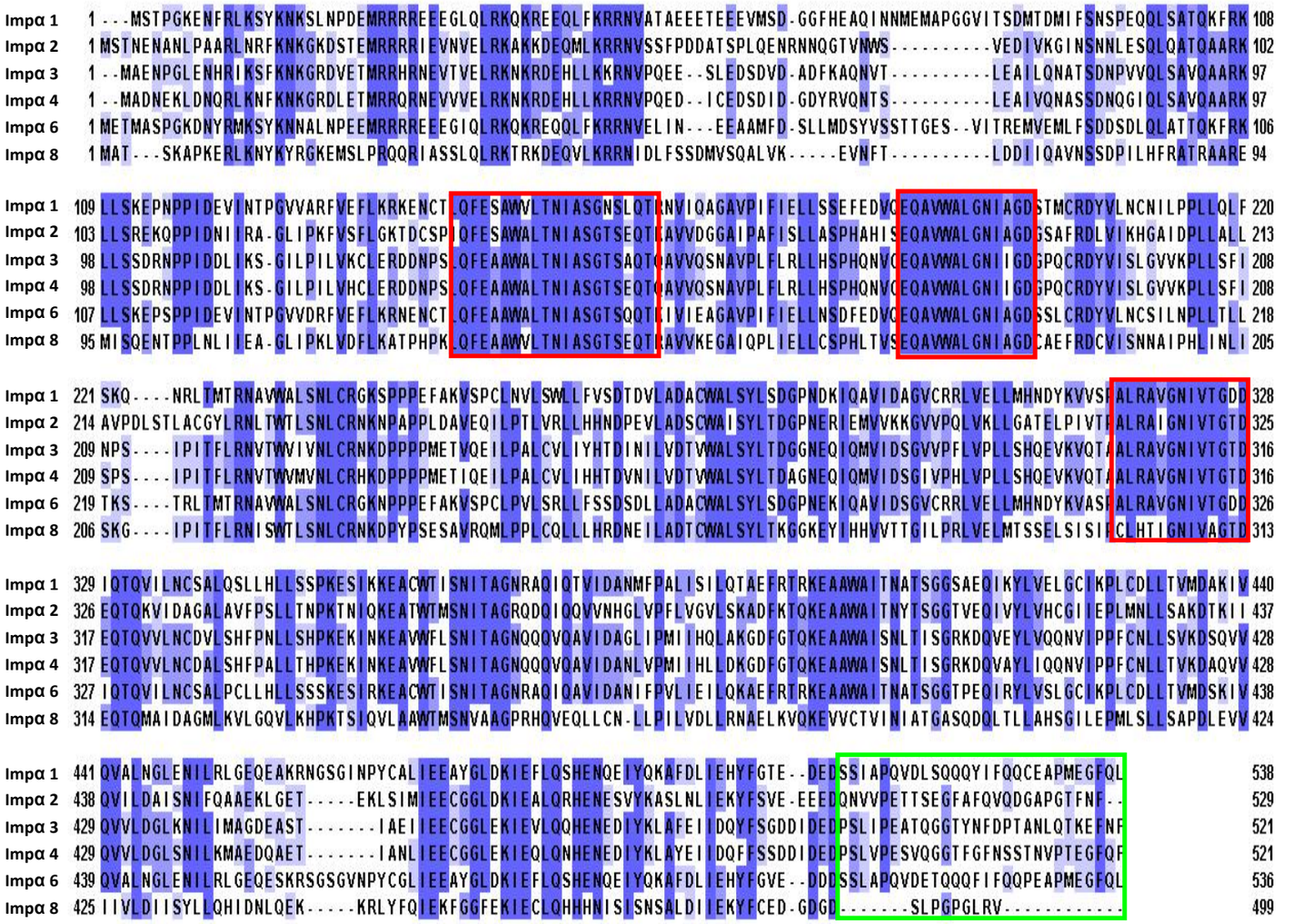

B

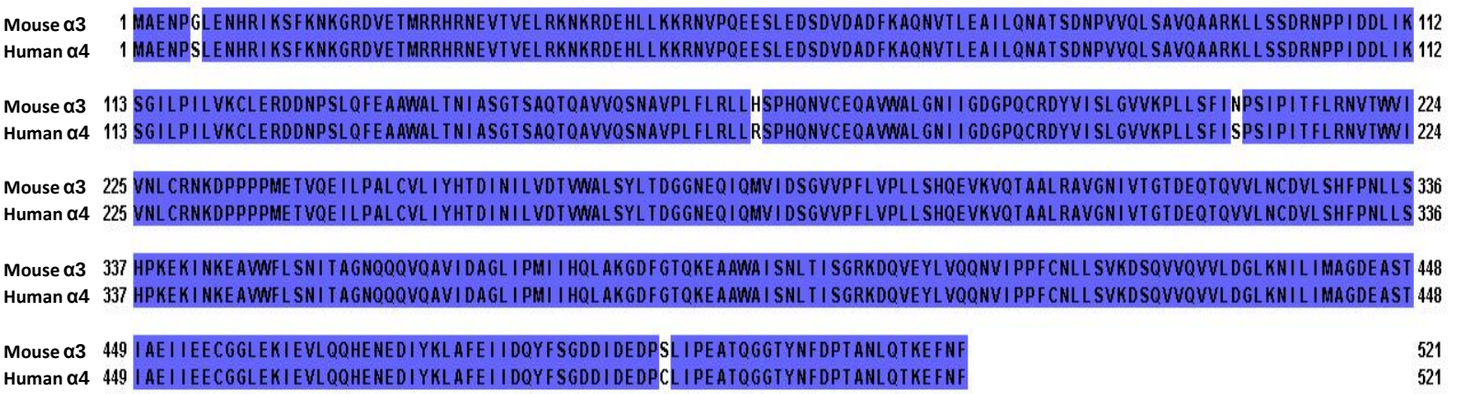

cerevisiae genome encodes only 1 importin α, and *D. melanogaster* contains 3 (Goldfarb et al., 2004; Hogarth et al., 2005), while 6 and 7 family members have been identified in *Mus musculus* (*M. musculus*) and *Homo sapiens* (*H. sapiens*), respectively, to date (Hu et al., 2010; Rother et al., 2011)-(Reviewed in Miyamoto et al., 2012a). The diversification of importin α family during evolution strongly suggests that the family members have evolved to serve increasingly complex developmental processes. The mouse importin α family members have been classified into three distinct sub-groups known as α (S) α (P), and α (Q) based on amino acid identity (Hogarth et al., 2005; Tsuji et al., 1997). According to this classification there exists up to 80% identity within each subgroup and ~50% identity between the groups. The classification of mouse importin α family members is represented in Figure 1.6.

1.1.6.1 Armadillo (Arm) repeats

The first Arm domain was identified in the product of the *D. melanogaster* gene, *armadillo*, which is required for segmentation during development (Riggleman et al., 1989). The Arm domains are composed of 10 tandem repeats of 40 amino acids, each containing three α helices (Coates, 2003; Huber et al., 1997). Although not conserved at the sequence level, Arm repeats are highly conserved structurally by having a right handed superhelix of helices upon tertiary folding which creates a suitable surface for extensive protein-protein interactions. Three-dimensional structures of several Arm domain containing proteins with distinct functions have been resolved. The results have highlighted the structural conservation between members of this protein family despite lack of high amino acid sequence identity (Tewari et al., 2010). An example of such structural conservation between β-catenin, and importin α is illustrated in Figure 1.7.

The Arm repeat containing proteins have been identified throughout the eukaryotic evolution (Coates, 2003), with members having diverse cellular roles. The prototypical Arm domain protein is β-catenin which has two distinct and well-defined roles in cellular homeostasis. β-catenin is involved in cell-cell adhesion through association with cytoskeletal elements and transmembrane cadherins (Nelson, 2008). It is also a key downstream effector of Wnt signalling. Upon binding of a Wnt ligand

Figure 1.6 Classification of mouse importin α family of proteins

The mouse importin α family members are classified into three sub-groups based on their amino acid sequence identity. These sub-groups are α (Q) which includes importin α3 and α4, α (S) including importin α1 and α6, and α (P) which includes importin α2 and the recently identified importin α8 (Rother et al., 2011). The percentage identity within each group is 47%, 80% and 85% for (αP), α (S), and α (Q), respectively; the value in the arrows between sub-groups indicate the lowest percentage identity among the different groups.

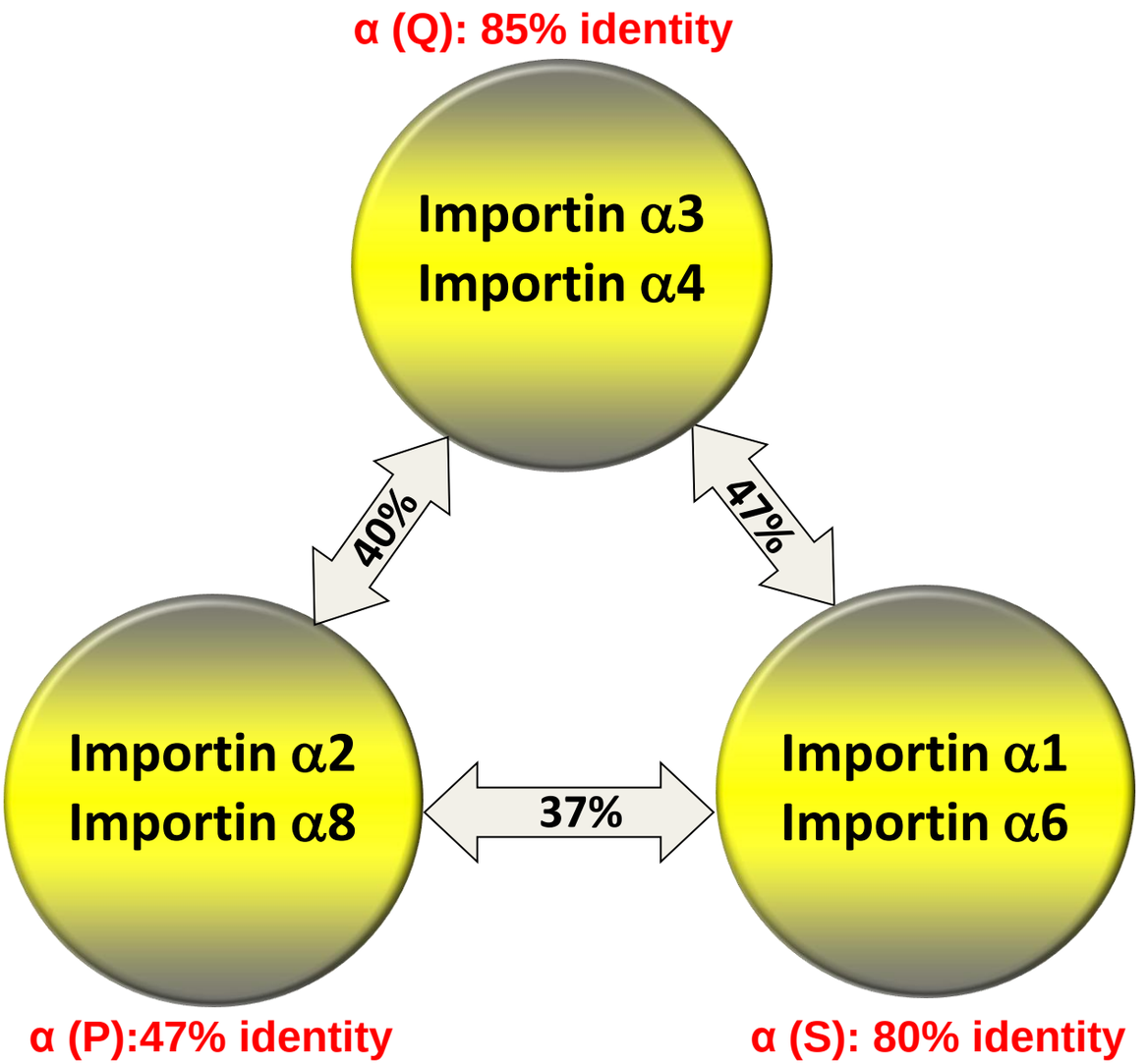
α (Q): 85% identity
Importin α3
Importin α4
40%
47%
Importin α2
Importin α8
37%
Importin α1
Importin α6
α (P):47% identity
α (S): 80% identity

to its receptor, β-catenin translocates into the nucleus and modulates the activity of T-cell factor transcription factor (Behrens, 2000). The importin α family of Arm domain proteins contribute to the nucleocytoplasmic transport of proteins which requires flexible, yet specific and tightly regulated protein-protein interactions. The only other Arm repeat containing protein apart from importin α in yeast is Vac8p, which has high amino acid similarity to importin α, and β-catenin (Fleckenstein et al., 1998; Wang et al., 1998). Vac8p is engaged in regulation of intracellular membrane homeostasis in several ways, each through interaction with different binding partners. These roles include homotypic vacuole fusion (Wang et al., 2001), cytoplasm to vacuole targeting of proteins such as aminopeptidase I (Scott et al., 2000), formation of nucleus-vacuole junctions (Pan et al., 2000), and processes relating to vacuole inheritance (Wang et al., 1998) in yeast. Further examples of Arm repeat proteins in eukaryotes, and their species-specific cellular roles have been reviewed by Coates, and Tewari (Coates, 2003; Tewari et al., 2010). Taken together, Arm repeats are structurally similar, functionally diverse, and are found in a wide range of eukaryotic proteins. Thus, occurrence of such domain in a protein may indicate functional versatility imparted by multiple interaction opportunities and sub-cellular localizations.

1.1.7 Non-classical events concerning import and importins

1.1.7.1 Non-classical nucleocytoplasmic transport

Several cases of protein nuclear accumulation have been uncovered in which the mechanism of nuclear entry does not resemble that of classical nucleocytoplasmic transport pathway in one or several ways. As described above, classical nuclear import relies on cNLSs, and a cNLS receptor such as importin α, a transporter such as importin β1, and the Ran gradient across the nuclear envelope.

β-catenin is a downstream effecter of Wnt signalling in developmental processes and homeostasis through its nuclear accumulation in response to Wnt ligands (MacDonald et al., 2009). Nuclear accumulation of β-catenin is unusual in that it does not require any transport factors in permeabilized cells and is insensitive to high concentration of

Figure 1.7 Arm repeats adopt similar structure despite low sequence identity

A. Alignment of full length human β-catenin (Genbank accession number: CAA79497.1) and mouse importin α2 (NP_001013796.2) amino acid sequence. The alignment was performed using Jalview 2.5 software. The blue colour indicates the amino acids identical between two sequences. Based on the ClustalW alignment, there is 13% identity between human β-catenin and mouse importin α2.

B. The three-dimensional structure of human β-catenin (left) and 10 Arm repeats of mouse importin α2 (right). Each Arm repeat in both proteins is depicted by a different colour ribbon. Despite low sequence identity (13%, above) the structure of proteins are strikingly conserved (Image adapted from Tewari et al., 2010).

A

```
β-catenin    1 MATQADLMELDMAMEPDRKAAVSHWQQQSYLDSGIHSGATTTAPSLSGKGNPEEEDVDTSQVLYEWEQGFSQSFTQEQVADIDGQYAMTRAQRVRAAMFPETLDEGMQIPST 112
Imp-α2       1 ------------MSTNENANLPAARLNRFKNKGKDS------------------------------------------------------------TEMRRRRIEVNVE 37

β-catenin  113 QFDAAHPTNVQRLAEPSQMLKHAVVNLINYQDDAELATRAIPELTKLLNDEDQVVVNKAAVMVHQLSKKEASRHAIMRSPQMVSAIVRTMQNTNDVETARCTAGTLHNLSHH 224
Imp-α2      38 LRKAKKDEQMLKRRNVSSFPDDATSPLQENRNNQGTVNWSVEDIVKGINSNN---------LESQLQATQAARKLLSR----------------------------EK 108

β-catenin  225 REGLLAIFKSGGIPALVKMLG-SPVDSVLFYAITTLHNLLLHQEGAKMAVRLAGGLQKMVALLNKTNVKFLAITTDCLQILAYGNQESKLIILASGGPQALVNIMRTYTYEK 335
Imp-α2     109 QPPIDNIIRAGLIPKFVSFLGKTDCSPIQFESAWALTNIASGTSEQTKAVVDGGAIPAFISLLASPHAHISEQAVWALGNIAGDGSAFRDLVIKHG--------------- 204

β-catenin  336 LLWTTSRVLKVLSVCSSNKPAIVEAGGMQALGLHLTDPSQRLVQNCLWTLRNLSDAATKQEGMEGLLGTLVQLLGSDDINVVTCAAGILSNLTCNNYKNKMMVCQVGGIEAL 447
Imp-α2     205 ------AIDPLLALLAVPDLSTLACGYLRNLTWTLSN-----------LCRNKNPAPPLDAVEQILPTLVRLLHHNDPEVLADSCWAISYLTDGPNERIEMVVKKGVVPQL 298

β-catenin  448 VRTVLRAGDREDITEPAICALRHLTSRHQEAEMAQNAVRLHYGLPVVVKLLHPPSHWPLIKATVGLIRNLALCPANHAPLREQGAIPRLVQLLVRAHQDTQRRTSMGGTQQQ 559
Imp-α2     299 VK--LLGATELPIVTPALRAIGNIVTGTDEQTQKVIDAG---ALAVFPSLLTNPKTNIQKEATWTMSNITAGRQDQIQQVVNHGLVPFLVGVLSKADFKTQKEAAWAITN-- 403

β-catenin  560 FVEGVRMEEIVEGCTGALHILARDVHNRIVIRGLNTIPLFVQLLYSPIENIQRVAAGVLCELAQDKEAAEAIEAEGATAPLTELLHSRNEGVATYAAAVLFRMSEDKPQDYK 671
Imp-α2     404 YTSGGTVEQIVY-------LVHCGIIEPLMNLLSAKDTKIIQVILDAISNIFQAAE----KLGETEKLSIMIEECGGLDKIEALQRHENESVY----------------- 485

β-catenin  672 KRLSVELTSSLFRTEPMAWNETADLGLDIGAQGEPLGYRQDDPSYRSFHSGGYGQDALGMDPMMEHEMGGHHPGADYPVDGLPDLGHAQDLMDGLPPGDSNQLAWFDTDL  781
Imp-α2     486 -KASLNLIEKYFSVE-----EEEDQNVVPETTSEGFAFQVQDGAPGTFNF-------------------------------------------------------  529
```

B

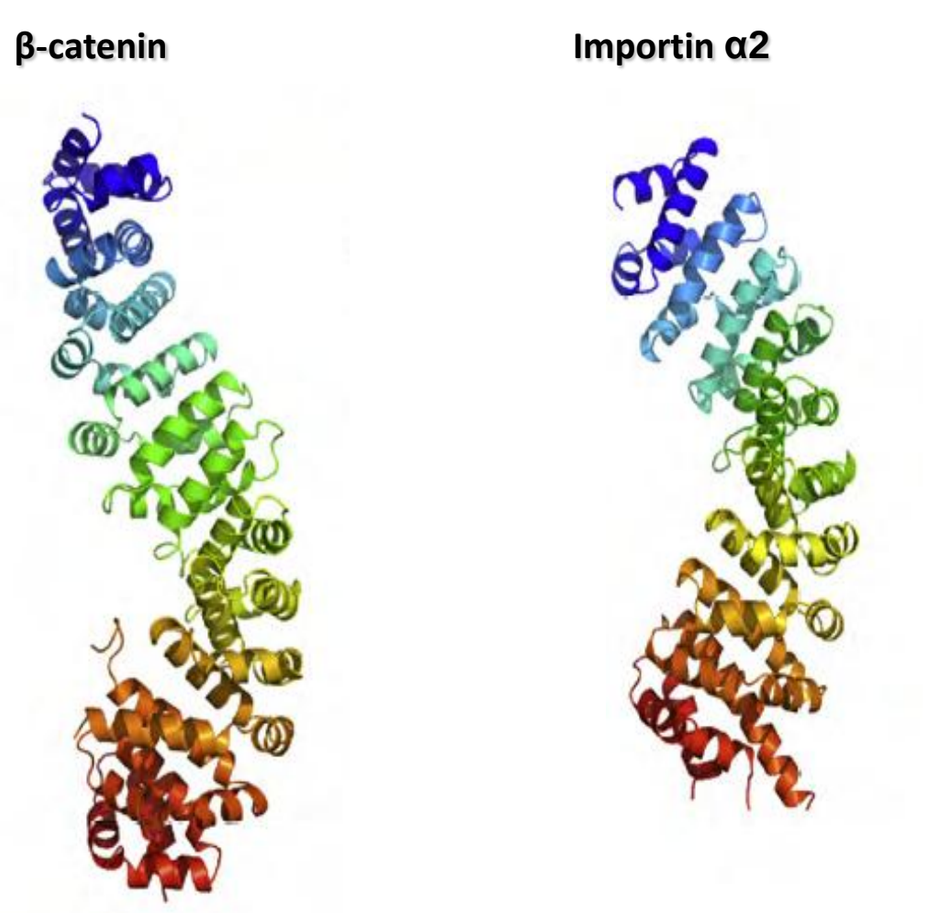

cytoplasmic Ran-GTP (Yokoya et al., 1999); the nuclear transport of β-catenin was shown to be adversely affected however, under several conditions including WGA treatment, incubation of living cells on ice, and excess importin β1, (Yokoya et al., 1999), demonstrating the facilitated nature of its translocation across the NPC. The exact mechanism of β-catenin translocation across the NPC is unknown, but it is thought to be through direct interaction of β-catenin with components of the pore complex since β-catenin interacts with FG repeats of yeast Nup1 *in- vitro* (Fagotto et al., 1998)-(Reviewed in Zhong and Fang, 2012). A very similar principle of nuclear accumulation has been reported for extracellular signal-regulated kinase 2 (ERK2), which can enter the nucleus without the aid of transport factors and independent of an energy source (Whitehurst et al., 2002).

Importin β1-independent nuclear accumulation of importin α has been demonstrated both *in vivo* and in permeabilized HeLa cells. A variant of mouse importin α2 devoid of the importin β1 binding domain (importin α2-ΔIBB) accumulated both in the nucleus of HeLa cells in culture upon overexpression and in the nucleus of permeabilized cells (Miyamoto et al., 2002; Miyamoto et al., 2004). The importin β1-independent nuclear accumulation of importin α is known to facilitate the nuclear transport of cargo proteins. Ca^{2+}/calmodulin-dependent protein kinase type IV (CaMK IV) interacts with importin α but not importin β1 both *in vitro* and *in vivo*, and is transported into the nucleus of permeabilized BHK cells when importin α or its ΔIBB mutant is the only exogenously supplied factor (Kotera et al., 2005). Furthermore, cytoplasmic microinjection of importin α ΔIBB resulted in nuclear accumulation of CaMK IV in NIH3T3 cells in culture, while under the same conditions, nuclear import of T-ag-NLS fusion protein (GST-T-ag-NLS-GFP) was inhibited (Kotera et al., 2005).

Nuclear import of SRY (sex determining region of the Y chromosome) is also mediated in part by a non-conventional pathway. SRY belongs to the HMG (high-mobility group) proteins and contains two NLSs (n-NLS and c-NLS) flanking its HMG domain (Smith and Koopman, 2004). The c-NLS of SRY is recognized by importin β1 and imported into the nucleus through the classical import pathway (Forwood et al., 2001). The n-NLS of SRY, however, is bound and imported into the nucleus by the Ca^{2+} binding protein, calmodulin (CaM). Exogenously expressed SRY,

harbouring XY sex reversing mutations in either the n-NLS or c-NLS in TM4 testicular cells, showed a significant loss of nuclear accumulation in all mutant proteins. When the transfected cells were treated with CDZ (calmidazolium chloride), an inhibitor of CaM activity, a further reduction in nuclear accumulation was observed only in c-NLS (β1 binding NLS) mutant proteins, demonstrating that n-NLS and c-NLS mediate the nuclear import of SRY through independent pathways (Kaur et al., 2010). That the n-NLS is the target of CaM was shown by *in vitro* interaction studies where n-NLS mutants of SRY had diminished affinity for CaM, but bound to importin β1 similar to the wild type protein. Kaur and colleagues also demonstrated the CaM dependent nuclear import is conserved for other HMG containing proteins such as SOX2, SOX9, and SOX10 (Kaur et al., 2010), a phenomenon that has also been reported in yeast for Nhp6Ap protein (Hanover et al., 2007).

1.1.7.2 Non-transport functions of importins

Although mediation of protein nuclear import is the best understood function of importins, few other cellular processes have been shown to be regulated by both importin α and importin β1. These non-transport functions include regulation of microtubule assembly, membrane formation and protein degradation. In this section an overview of such activities is presented.

One of the non-transport functions of importin α is mediation of cell cycle progression. At the onset of M phase, the nuclear envelope and microtubule filaments break down. The segregation of duplicated chromosomes during the M phase is assisted in part by the newly assembled mitotic spindle (Cassimeris and Skibbens, 2003). Ran-GTP is essential for initiation of spindle formation (Wilde and Zheng, 1999; Zhang et al., 1999); it mediates release of the microtubule nucleation factor, TPX2, which is otherwise kept inactive by importin α. Gruss and colleagues demonstrated that addition of excess importin α1 to an M phase *X. laevis* egg extract prevented microtubule assembly even when non-hydrolysable Ran-GTP (Ran Q69L) was present (Gruss et al., 2001), indicating that importin α withholds the microtubule nucleation factor. This factor was identified by ion exchange chromatography to be a microtubule associated protein known as TPX2 (Wittmann et al., 2000), which could

restore microtubule assembly when added in excess to the M phase *X. laevis* egg extract, but was inactive in the presence of excess importin α (Gruss et al., 2001). The direct role of importin α in regulating the nucleation activity of TPX2 was demonstrated by observation that TPX2 mutants, defective in binding to importin α, can induce spindle formation in M phase egg extract in presence of excess importin α; microtubule nucleation activity of wild type TPX2 or mutants that could bind importin α, however, is inhibited by importin α (Schatz et al., 2003). Therefore when the nuclear envelope breaks down at M phase, the high concentration of Ran-GTP in the vicinity of chromosomes (discussed in Section 1.1.5) is sufficient to release TPX2 from importin α, leading to subsequent nucleation and formation of spindles.

Importin α has also been shown to regulate nuclear envelope formation. Knock down of importin α2 (IMA-2) in *Caenorhabditis elegans* (*C. elegans*) resulted in defective nuclear envelope formation during embryonic development (Askjaer et al., 2002). Subsequently, the direct role of *X. laevis* importin α1 in nuclear envelope assembly was demonstrated *in vitro*. Removal of importin α1 from interphase *X. laevis* egg extract by either immunodepletion or addition of excess BSA-NLS (T-ag-NLS fused to BSA) significantly inhibited formation of the nuclear envelope in an *in vitro* nuclear reconstitution reaction (Hachet et al., 2004). A fraction of importin α1 is observed to be associated with membranes, and this membrane-associated importin α1 is essential for formation of the nuclear envelope *in vitro* (Hachet et al., 2004). Although involvement of other factors could not be excluded, these observations clearly implicate importin α in membrane fusion processes.

Importin β1 is also known to exert regulatory effects on formation of both the nuclear envelope and NPCs. Ran-coated sepharose bead system is sufficient for formation of nuclear envelope by *X. laevis* egg extracts in the absence of exogenous DNA (Hetzer et al., 2000). Cytosolic extract depleted of Ran-GTP binding proteins was shown to be deficient in formation of a nuclear envelope around Ran coated beads, an effect that could be reversed by addition of importin β1 alone (Zhang et al., 2002a). Importin β1 mutants defective in binding FG nucleoporins (β1 I178D) or Ran (β1 45-462) were unable to induce nuclear envelope formation (Zhang et al., 2002a). From these observations, the authors inferred that the enhancing effect of importin β1 is through

recruitment of FG nucleoporins to Ran, followed by their release upon Ran binding to importin β1 which allows nucleoporins to take part in formation of a functional nuclear envelope. In other studies, addition of excess importin β1 to an *in vitro* nuclear reconstitution reaction, severely blocked the formation of nuclear envelope, an effect which could be rescued by excess Ran-GTP (Ran Q69L) (Harel et al., 2003). In contrast to Zhang et al observations (discussed above) however, Ran binding-deficient importin β1 (β1 45-462) did not interfere with nuclear envelope assembly, but the assembled envelope was devoid of any NPCs, as evident by nuclear exclusion of an 18 kDa dextran and the absence of nucleoporins upon immunodetection (Harel et al., 2003). Although the exact function of importin β1 in nuclear envelope assembly is not clear, it appears to be similar to the nucleocytoplasmic transport function of importin β1, through interactions with the Ran system and nucleoporins. Further examples of non-transport functions of importins in major cellular processes such as progression of mitosis and protein degradation have been demonstrated by genetic manipulation of yeast (Loeb et al., 1995; Tabb et al., 2000), a phenomenon which could be due to an arrest of general nucleocytoplasmic transport, since the yeast genome encodes only one importin α (discussed in Section 1.1.6).

1.1.8 The relevance of nucleocytoplasmic transport to development

1.1.8.1 The NLS binding specificity of importin α

Given the high conservation and sequence identity between importin α family members (discussed in Section 1.1.6), one would expect redundancy in binding to NLS cargos. However, importin α family members do possess NLS binding specificity, which along with their differential tissue expression pattern (discussed in Section 1.1.8.2) contributes to their functionality in regulating developmental processes.

Nadler and colleagues reported the NLS binding specificity of different importin αs by immobilizing a wide range of NLSs on sepharose resins, followed by addition of cytosolic extracts from RAJI and JURKAT human cell lines (Nadler et al., 1997). These two cell lines were selected for this analysis since they both showed the highest

expression of importin α1 and α4 proteins across several human lymphocyte and leukocyte cell lines. The bound fractions were analysed by Western blotting using specific antibodies to human importin α1 and importin α4. While most of the tested NLSs bound to both importin αs to a similar extent in the RAJI cell extract, clear differences in NLS binding were found in JURKAT cytosolic extracts (Nadler et al., 1997). For example, the interaction of NF-κB-NLS with importin α4 was weak in comparison to T-ag-NLS, and almost non-detectable for importin α1 in JURKAT extracts. On the other hand, infected-cell protein 8 (IPC8) NLS bound only to importin α1 but not to importin α4. Furthermore, in absence of cytosolic extracts, importin α1 bound to different NLSs selectively, with T-ag and HIV 1422 NLSs showing strong binding, while IPC8 and NF-κB NLSs showed weak and non-detectable binding to importin α1, respectively (Nadler et al., 1997). Further examples of early observations regarding NLS binding and transport specificity by importin α family members include the selective binding of DNA helicase Q1 by human importin α3 (Miyamoto et al., 1997) and STAT 1 NLS by human importin α5 but not importin α1 (Sekimoto et al., 1997).

The NLSs of adenosine deaminases acting on RNA (ADARs) family members are also differentially recognized by different importin αs. ADARs shuttle between nuclear and cytoplasmic compartments and their best understood function is deamination of single adenosines in pre-mRNA (Schaub and Keller, 2002). Using the N-terminus of ADAR3, which contains a putative NLS (^{23}KRRRRRRSKRKDK^{35}) as a bait, human importin α1 was identified as a novel interacting partner of ADAR3 by yeast two-hybrid screening of a human lung cDNA library (Maas and Gommans, 2009). Fusion of the ADAR3 N-terminus to EGFP conferred nuclear localization to the heterologous molecule in transfected HEK 293 cells. Examination of other human importin α family members demonstrated the specificity of importin α1 binding to ADAR3 N-terminal, since both importin α4 and importin α5 failed to interact with this region. ADAR2, a closely related family member of ADAR3 contains a putative NLS in its N-terminus which differs from that of ADAR3. When interaction of ADAR2 N-terminus with different importin αs was examined by yeast two-hybrid analysis, completely opposite pattern of interactions were observed; ADAR2 N-terminus strongly bound to importin α4 and importin α5 but not to importin α1 (Maas

and Gommans, 2009). Since nuclear import of ADAR proteins is crucial for their mRNA editing role, differential binding to importin αs may be a regulatory mechanism of their function. *In vitro* interaction and *in vivo* nuclear accumulation studies have shown that the recognition of the p53 bipartite NLS (KRALSNNTSSSPQPKKK) is primarily mediated by human importin α3 (Marchenko et al., 2010), and that the nuclear import of STAT3 in contrast to STAT1 which is dependent on importin α5 (Sekimoto et al., 1997) is carried out by human importin α3 (Liu et al., 2005). Further examples of NLS binding and transport specificity by importin α family members have been documented for *papillomavirus* E1 (Bian et al., 2007) and *papillomavirus* E2 proteins (Bian and Wilson, 2010).

In addition to the NLS binding specificity of each importin α, competition between NLSs for a given importin α exerts further regulation on nucleocytoplasmic transport outcomes. In one study, a comparison was made between fluorescein-labelled constructs encoding a human RNA-binding protein, hnRNP K, the stimulator of Rous sarcoma virus promoter, P/CAF, and RCC1 as import substrates in *in vitro* nuclear transport assays. Both hnRNP K, and P/CAF were transported into the nucleus by all human importin αs, by *X. laevis* importin α2 and by the yeast importin α to a similar extent. Efficient nuclear import of RCC1, on the other hand, was shown to be preferentially affected by human importin α3 (Kohler et al., 1999). When nucleoplasmin was added to the import reactions, striking changes to the nuclear accumulation of these substrates were observed. For example, importin α5 and α1 mediated nuclear import of P/CAF was completely abolished in the presence of nucleoplasmin, while importin α3 mediated accumulation of P/CAF was not affected. In the case of hnRNP K, only human importin α4 and *X. laevis* importin α2 mediated nuclear accumulation was inhibited by nucleoplasmin. Nucleoplasmin did not inhibit nuclear accumulation of RCC1 by its only transport receptor importin α3 (Kohler et al., 1999). These observations provided evidence that with each cellular environment, selectivity of importin α family members for different NLS bearing cargos, along with competition between cargos for binding to importin α regulates the rate and final extent of nuclear import of a certain cargo molecule.

1.1.8.2 Tissue-specific expression patterns of importin α

In addition to possessing NLS binding specificity, importin α family members also exhibit distinct expression profiles, indicating that synthesis of each is regulated in a cell-specific manner. The expression and subcellular localization of family members have been shown to differ between tissues, cell types of the same tissue, in response to developmental cues, and according to disease state. This section contains a summary of importin α expression patterns across different tissues and cell types. In Section 1.1.8.3, changes in expression and subcellular localization of importin α in different physiological conditions will be discussed.

Early observations regarding the expression patterns of importin α by Northern blot analysis demonstrated that the mouse importin α1 transcript is widely expressed across 9 examined mouse tissues, with cerebellum having slightly higher and uterus slightly lower levels than other tissues. Importin α2 on the other hand, although being ubiquitously expressed, was present in considerably higher levels in spleen, thymus and heart (Prieve et al., 1996). Northern blot analysis of human importin α7 across several tissues also demonstrated that this family member is widely expressed; however, no transcript of importin α7 was detected in thymus (Kohler et al., 1999). Examination of protein levels by Western blotting, using antibodies to 5 importin α family members and importin β1 revealed further differences. For example, spleen and liver both contained the lowest levels of both importin β1 and all tested importin αs. Importin α3 had higher expression in ovary and lung compared to other examined tissues, while importin α5 was not detected at all in brain (Kohler et al., 1999). These studies conducted using whole tissues provided indication that cell-specific profiles would be informative.

Importin α is also expressed differentially between various cell lines and when comparing cell types of a given tissue. Measurement of the amount of importin αs and β1 protein by Western blotting in several human cell lines showed that importin α1 has the highest protein level compared to other family members in every examined cell line. Furthermore, importin α1 was the only family member that had considerably higher amounts than importin β1 in human JURKAT and ECV cells, an observation that suggests importin β1-independent roles for importin α1 (Koehler et al., 2002).

Kamei and colleagues developed antibodies to importin β1 and to 3 mouse importin αs, each representing one subgroup (αQ, αS and αP; Section 1.1.6) of the family to examine their distribution in several mouse tissues. Importin β1 protein was detected in every adult mouse tissue examined by Western blotting, consistent with its role in translocating the import complex into the nucleus, while, importin α family members showed distinct expression patterns across tissues (Kamei et al., 1999). Importin α2 (αP) was the most widely distributed importin protein in mouse tissues but was not detectable in whole brain. Importin α5 and α6 (αS) were readily detected in brain lysates, had very low expression in the testis, and were absent from every other examined tissue. Importin α3 and α4 (αQ) appeared to be most abundant in testis, with low expression in brain. Remarkably, testis was the only tissue out of the examined 9 in which all of the importin α family members were detected (Kamei et al., 1999). Examination of importin α proteins in adult mouse testis by immunohistochemistry indicated that family members are expressed differentially in testicular cells. The primary site of importin α3 and α4 (αQ) expression was shown to be Leydig cells, while importin α2 (αP) was predominantly detected in primary spermatocytes; importin α5 and α6 (αS) however, were detected in all cell types of the seminiferous tubules and Leydig cells (Kamei et al., 1999). Hosokawa et al reported regional specific expression of importin α transcripts in the mouse central nervous system (CNS), using *in situ* hybridization to show that all five known importin α sub-types are present in the adult mouse CNS. Specific brain regions, including the brain stem, hypothalamus and septum, appear completely devoid of importin α1 mRNA; this also had the lowest expression in other parts of the brain compared to other importin αs. Importin α3 and α5 were shown to have the strongest signals and potentially highest transcript levels throughout the CNS (Hosokawa et al., 2008). Further examples of differential expression of importin αs include studies at the mRNA level in mouse tissues (Tsuji et al., 1997) and at the protein level in human cell lines (Nadler et al., 1997). In the next section, spatio/temporal expression of importin α family members in response to a range of conditions will be presented, with a focus on the developmental processes associated with such changes.

1.1.8.3 Regulated nucleocytoplasmic transport in development

Several studies have shown that the synthesis and localization of importin α family members changes during development, in disease, and in response to environmental cues such as stress. In this section some examples of regulated importin α expression with a focus on developmental contexts are presented.

Stress is one of the physiological conditions that have been shown to affect importin α distribution. Under a variety of stress conditions, including UV radiation, H_2O_2 exposure, and heat shock, importin α reversibly accumulates in the nucleus of cultured mammalian cells (Furuta et al., 2004; Miyamoto et al., 2004). Nuclear accumulation of importin α2 in stressed cells caused a decrease in nuclear import rate of a GST-NLS-GFP reporter molecule, reflecting down-regulation of general nucleocytoplasmic transport. This nuclear accumulation response has been documented in further studies (Kodiha et al., 2008a; Kodiha et al., 2008b) and is thought to be caused by collapse in the Ran gradient across the nuclear envelope (Ran gradient was discussed in Section 1.1.5) (Miyamoto et al., 2004) and retention of importin α in the nucleus of stressed cells through interactions with nucleoporins (Kodiha et al., 2008b). The nuclear retention of importin α is thought to be a strategy used by stressed cells to reduce energy expenditure through down-regulation of nucleocytoplasmic transport (Yasuda et al., 2006). A novel function has been attributed to the nuclear retained importin α; Yasuda and colleagues demonstrated that importin α2 is retained in the nucleus of stressed HeLa cells through interaction with chromatin since it could be released by DNase I treatment, but not RNase. Furthermore they showed that importin α2 binds to the promoter region of *serine/threonine kinase 35*(*STK35*) leading to its up-regulation under stress, and that *STK35* up-regulation promotes non-apoptotic cell death (Yasuda et al., 2012).

Cell proliferation and differentiation require changes in production of specific importin αs. Expression analysis of all known human importin αs in cultured human fibroblast (HaCaT) and HeLa cell lines by quantitative measurement of protein bands showed that inhibition of proliferation by serum starvation leads to a selective, cell-type specific and reversible decrease in levels of importin α family members (Koehler

et al., 2002). All of the importin α family members were down-regulated in HeLa cells after serum starvation for 72 hours, with importin α1, and α7 showing the most drastic drop in expression by, ~40% and 60%, respectively. In contrast, serum starvation of HaCaT cells for 48 hours (the time limit of starvation before cells died) led to reduction of only importin α1 protein to ~50% compared to untreated cells. Serum supplementation to the starved HeLa cells resulted in steady increase in the protein level of all importin α family members, of which importin α1 and α7 showed the most stark increase in the course of 24 hours (Koehler et al., 2002). These observations implied that importins play distinct and cell-specific roles during proliferation. In line with this notion, knockdown of importin α3, α5, and α7 in HeLa cells by siRNA transfection led to a significant decrease in cell proliferation, while that of importin α1 and α4 had minor and no affect, respectively (Quensel et al., 2004).

Considering the central roles of importin α in cellular homeostasis, one would predict that induction of major cellular events such as differentiation is accompanied by changes in the repertoire of family members. This hypothesis was examined using cultured rat pancreatic cells (AR42J) which have the potential to differentiate either towards a neuroendocrine fate following activin A treatment, or to an acinar phenotype through dexamethasone exposure. The expression of importin α4 protein was increased to ~4x and 2x by dexamethasone and activin A treatments respectively, while importin α3 was up-regulated ~2x only in response to dexamethasone; the expression of other importin α family members was unchanged by either treatment (Koehler et al., 2002). That regulated expression of importin αs in response to transformation cues is pathway-specific was demonstrated by the observation that differentiation of promyelocytic HL60 cell lines towards a macrophage or a neutrophilic phenotype led to reduction in protein levels of importins α1, α4 and α7 after 72 hours, while the level of importin α5 was unchanged and that of importin α3 declined after an initial (24 hours) transient up-regulation (Koehler et al., 2002). Regulated expression of importin αs has also been demonstrated in human peripheral blood lymphocytes, where activation by lipopolysaccharide, concanavalin A, and phorbol myristic acid leads to significant increases in the amount of both cytoplasmic and nuclear importin α1 and α4, as measured by Western blot 2 hours post-treatment (Nadler et al., 1997).

In vivo examination of embryonic and post-natal maturation coupled with *in vitro* studies of cell cultures have further strengthened the understanding of how regulated nucleocytoplasmic transport governs development and differentiation. Three importin αs (importin α1, α2 and α3) are encoded by *D. melanogaster* genome (Miyamoto et al., 2012a). Examination of *D. melanogaster* importin α2 in different stages of embryonic development and adult flies revealed fluctuations in expression of the gene in the course of development. Northern blot analysis showed high expression of the *importin α2* transcript in embryos of up to 4 hours old, with a decline to barely detectable levels between 4 to 24 hours. Transcript levels increased again at the onset of second larvae stage, persisted to the pupal stage and were highest, in adult flies. Interestingly, *importin α2* total mRNA levels were higher in females than male whole flies (Kussel and Frasch, 1995). Protein levels were positively correlated for importin α2 in embryos and larvae stage flies. In adult flies, however, high importin α2 protein was detected in females corresponding to high levels of mRNA, while male flies were devoid of any detectable importin α2 protein despite measurement of abundant mRNA (Kussel and Frasch, 1995). Furthermore immunofluorescent detection of importin α2 in blastoderm embryos revealed that the protein is strictly cytoplasmic during interphase, but accumulates in the nucleus early in prophase before the nuclear envelope breaks down (Kussel and Frasch, 1995). Collectively, the temporal expression and altered subcellular localization of importin α2 during *in vivo* maturation of *D. melanogaster*, implies that stage- and subcellular compartment-specific roles are served by members of nucleocytoplasmic transport receptors in development.

Knock-down of *importin α3* in *D. melanogaster* causes embryonic lethality, since homozygous mutant offspring do not survive past the second larval stage. Ectopic expression of both importin α1 and α2 under the control of Gal4 driver in germline resulted in prolonged survival of importin α3-deficient flies to the early third larval stage, while survival to pigmented pharate adult stage required expression of importin α3 (Mason et al., 2003). Thus, limited rescue of importin α3 deficiency by importin α1 and α2 during early development indicates partial redundancy between importin α family members. Further examples of spatially and temporally regulated expression of

importin α family members in *D. melanogaster* embryonic development and adult life have been demonstrated by *in vivo* localization and expression studies (Fang et al., 2001; Máthé et al., 2000). Altogether, these observations indicate that each importin α has a distinct set of cellular functions that vary between cellular contexts.

Importin α orthologues in *C. elegans* are also differentially expressed during development. All identified importin αs (*IMA-1*, *IMA-2* and *IMA3*) are highly expressed in adult worm at mRNA level, but clear differences exist in embryonic development. *IMA-3* and *IMA-2* are persistently expressed during embryonic development with *IMA-3* being expressed at much higher levels. On the other hand, *IMA-1* is very weakly detectable in early embryos, completely absent from larval stages 1 to 3 and switched on again at larval stage 4 (Geles and Adam, 2001); since spermatogenesis begins during the fourth larval stage in *C. elegans* (Reviewed in Miyamoto et al., 2012a), *IMA-1* may have specific roles in male germ cell development. Both *D. melanogaster* and *C. elegans* have provided valuable insights on the specific role of the importin α family members in processes such as germ cell maturation. In section 1.2.6 an overview of the current knowledge regarding the specific contribution of distinct importin α family members in spermatogenic processes is presented.

Importin α8 is the most recently identified family member, first identified in mouse, with predominant expression in oocytes, zygotes and two-cell stage embryos (Hu et al., 2010). Knock-out of importin α8 led to gender-specific abnormalities in embryonic and adult development. These defects include reduced female foetal survival and adult fertility in both heterozygous and homozygous mice, compared to the wild type littermates. In contrast, importin α8-deficient male mice had a lower rate of foetal deaths and their fertility was unaffected (Hu et al., 2010). Similar observations on organ- and gender-specific roles of importin α include the expression pattern of the only identified importin α in *Pagrus major* (*P. major*), a species of marine teleost fish. Analysis of transcript expression by Northern blot and reverse transcriptase PCR showed that this gene is only expressed in ovaries and testes across 18 examined tissues. Absence of this importin α family member in all other examined organs indicates the presence of other un-identified family members in the genome of

P. major. During sexual maturation, however, measured by use of a gonadosomatic index, the importin α transcript level increased relative to that of β-actin, only in males and remains constant in female fish (Gen et al., 2008).

Studies using mouse embryonic stem (ES) cells have revealed an important case of selective importin α expression in cellular differentiation. Prompted by observations that importin α5 and α1 exhibit the highest and lowest expression levels relative to other importin α family members in adult mouse brain, respectively (discussed in Section 1.1.8.2), Yasuhara et al hypothesized that importin α family members undergo subtype switching during neural differentiation. Several lines of evidence supported this hypothesis in different ways (Yasuhara et al., 2007). Firstly, induction of neural differentiation by retinoic acid treatment induced the simultaneous expression of importin α5 and neural markers, including Nestin, and MAP2; this outcome was concurrent with reduction in expression of importin α1 and ES cell markers, such as Oct3/4 and Nanog. Furthermore, ectopic expression of importin α5 or knock-down of importin α1 by RNAi vector expression in ES cells resulted in neural differentiation, as indicated by the onset of Nestin synthesis. *In vitro* nuclear transport assays provided evidence that importin α1 and α5 are involved in nuclear import of specific transcription factors in ES cells and their differentiated cells respectively, and the authors concluded that subtype switching of importin α is required for correct neural differentiation (Yasuhara et al., 2007). This view has been challenged by Shmidt et al who reported that importin α5-deficient mice showed no abnormalities in any examined tissue including brain. This observation was proposed to indicate that induced redundancy by other importin α family members occurs during embryonic development, supported by the detection of increased importin α4 expression in the brains of importin α5-deficient mice (Shmidt et al., 2007). The role of nuclear transport machinery in development, differentiation and transformation has been the subject of several recent reviews (Major et al., 2011; Okada et al., 2008; Yasuhara et al., 2009). These highlight the accumulating evidence which shows that importin α family members display distinct expression profiles and serve different functions during major developmental events such as embryogenesis and cell fate determination. Based on the most widely studied function of this protein family, it is conceivable that the primary effect of regulated importin α expression is alteration in general

nucleocytoplasmic transport; nonetheless, non-transport functions of importin α family members can also be affected.

1.2 Spermatogenesis

1.2.1 Overall structure and function of the mammalian testis

Spermatogenesis, the production of male gametes, takes place in the mammalian testis. The process is an orderly and tightly regulated series of events during which spermatogonial stem cells differentiate and maturate into highly specialized spermatozoa. Adult spermatogenesis includes proliferation, meiotic division, and extensive transformation of germ cells, supported by somatic cells of the testis and hormonal regulation. In the adult mouse, the time required for a spermatogonial stem cell to progress through each stage and form spermatozoa is 42 days. In this section an overview of the adult testis structure and progression of spermatogenesis is presented, with the aim of highlighting the extensive transformation and differentiation steps that are involved.

The mammalian testis is enclosed by a fibrous capsule known as the tunica albuginea, and it is composed of two main functional compartments (Figure 1.8, A). The two compartments of the testis are the interstitium and the seminiferous tubule. Interstitium compartment is populated with blood vessels, Leydig cells and macrophages. The highly convoluted seminiferous tubules are enclosed by a layer of peritubular myoid cells and are the site of germ cell development (Figure 1.8, B). Inside the seminiferous tubules, the most undifferentiated germ cells, spermatogonial stem cells and spermatogonia, are in contact with the basement membrane which lines the periphery of each tubule. As these cells divide and differentiate, they move towards the lumen of the seminiferous tubule, into which mature spermatozoa are ultimately released. Throughout the maturation process, germ cells are in contact with the somatic Sertoli cells which provide nourishment and hormonal regulation for spermatogenesis (de Kretser, 1995; Figure 1.8, C). Sertoli cells also create the blood-testis barrier (BTB) that divides the seminiferous epithelium into the basal and the adluminal compartments. This barrier is formed by intracellular junctions between the Sertoli cells and regulates the passage of germ cells from the basement membrane towards the lumen during their differentiation (Lie et al., 2009).

Figure 1.8 Overall structure of the mammalian testis

A. The testis is encapsulated within the tunica albuginea. Spermatozoa produced within the epithelia of the seminiferous tubules move to the epididymis via the efferent ducts. Spermatozoa are stored in the epididymis and eventually leave the testis through the vas deferens.

B. Representation of the interstitial and epithelial compartments of the testis, illustrated as cross-sections of two seminiferous tubules. The Sertoli cells (each bordered by red lines) create the epithelial compartment with their cytoplasm (yellow) spanning from the basement membrane to the lumen of the tubule. A layer of peritubular myoid cells covers each tubule. Germ cells of varying developmental stages are depicted by green colour circles, with the mature spermatozoa being released into the lumen. The interstitial compartment is populated mainly by Leydig cells and macrophages.

C. Enlarged view of Sertoli-germ cell positioning within the seminiferous tubule. As shown in the diagram, all germ cells are in contact with the supporting Sertoli cells. Spermatogonial stem cells and spermatogonia are in contact with the basement membrane; upon division and differentiation they lose contact with the basement membrane and move towards the lumen where the mature spermatozoa are released. Tight junctions are the site of contact between the Sertoli cells and create the blood-testis barrier (Lie et al., 2009), which regulates the passage of developing germ cells from the basal toward the adluminal compartment (Image adapted from Cooke and Saunders, 2002).

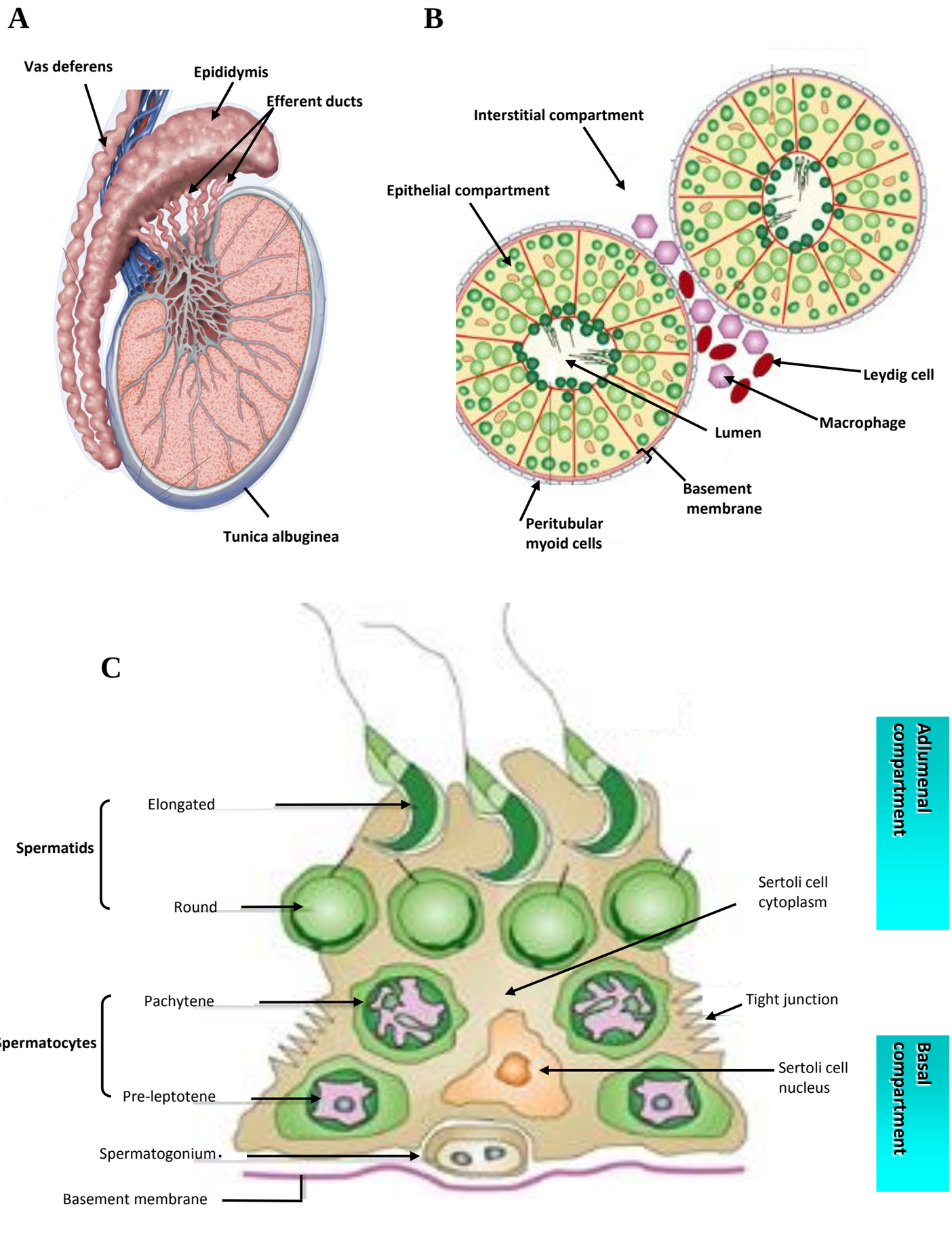
A
Vas deferens
Epididymis
Efferent ducts
Tunica albuginea
B
Interstitial compartment
Epithelial compartment
Leydig cell
Macrophage
Lumen
Basement membrane
Peritubular myoid cells
C
Spermatids
Elongated
Round
Spermatocytes
Pachytene
Pre-leptotene
Spermatogonium
Basement membrane
Sertoli cell cytoplasm
Tight junction
Sertoli cell nucleus
Adlumenal compartment
Basal compartment

1.2.2 The adult seminiferous epithelium

The progression of germ cell maturation from spermatogonial stem cells to spermatozoa in the adult seminiferous tubule is divided into three main stages. In broad terms, the first of these is a proliferative phase in which spermatogonial stem cells divide to produce either a cell committed to differentiation or additional stem cells. In the second phase, spermatocytes go through two meiotic divisions to produce haploid spermatids. The last phase of adult spermatogenesis is the extensive transformation of spermatids into highly specialized spermatozoa through the process of spermiogenesis, which includes widespread cytoplasmic and nuclear remodelling events (Russell et al., 1999). Several types of spermatogonia, spermatocytes and spermatids at different developmental steps are discernible in testis. In seminiferous tubule cross sections the germ cells of different developmental steps appear in unique patterns in relation to each other, known as the stages of the seminiferous epithelium. Thus, each stage is characterized by a specific subset of germ cells that are consistently positioned in a well-defined association. The time required for all of the cellular associations to appear sequentially in a given area of the tubule is defined as the cycle of the seminiferous tubule (Hermo et al., 2009b). The number of stages in the cycle differs between species; for example, the seminiferous epithelium of the adult rat contains 14 stages (de Kretser, 1995) while mouse and human have 12 and 6 stages, respectively (Hermo et al., 2009a). All 12 stages that comprise a cycle of the seminiferous epithelium in mouse are shown in Figure 1.9.

1.2.3 Spermatogonia and the proliferative phase of spermatogenesis

Spermatogonial stem cells are the foundation for the continuous nature of spermatogenesis throughout adult life. When these cells divide, the daughter cells can take on two alternative fates; they either commit to differentiation into spermatozoa or remain as stem cells to maintain the continuing supply of germ cells (Caires et al., 2010). The spermatogonial stem cells are located within a niche created by the tubule basement membrane and which includes the Sertoli and peritubular myoid cells (Dadoune, 2007). Sertoli cells are directly involved in regulation of spermatogonial

Figure 1.9 Stages of the seminiferous epithelium in mouse

Schematic representation of the cellular associations that define all 12 stages of the mouse seminiferous epithelium. The number of each stage is depicted by Roman numerals at the bottom, with the cells present in each stage aligned vertically. Development of germ cells can be followed from the bottom row, left to right, with arrows indicating the next cell type in the scheme of development and differentiation that appears after the rightmost cell in each row. The cell types shown are type A spermatogonia (A), intermediate spermatogonia (In), type B spermatogonia (B), spermatocytes at preleptotene (Ll), leptotene (L), zygotene (Z), pachytene (P), diakinesis (D), and meiotic (Mi) stages of development. Spermatids are the primary determinant of the stages of seminiferous tubules based on their numerous developmental steps and are broadly classified as round (1-8) and elongate (9-16) to reflect their nuclear morphology (Image adapted from Hess and Franca, 2009).

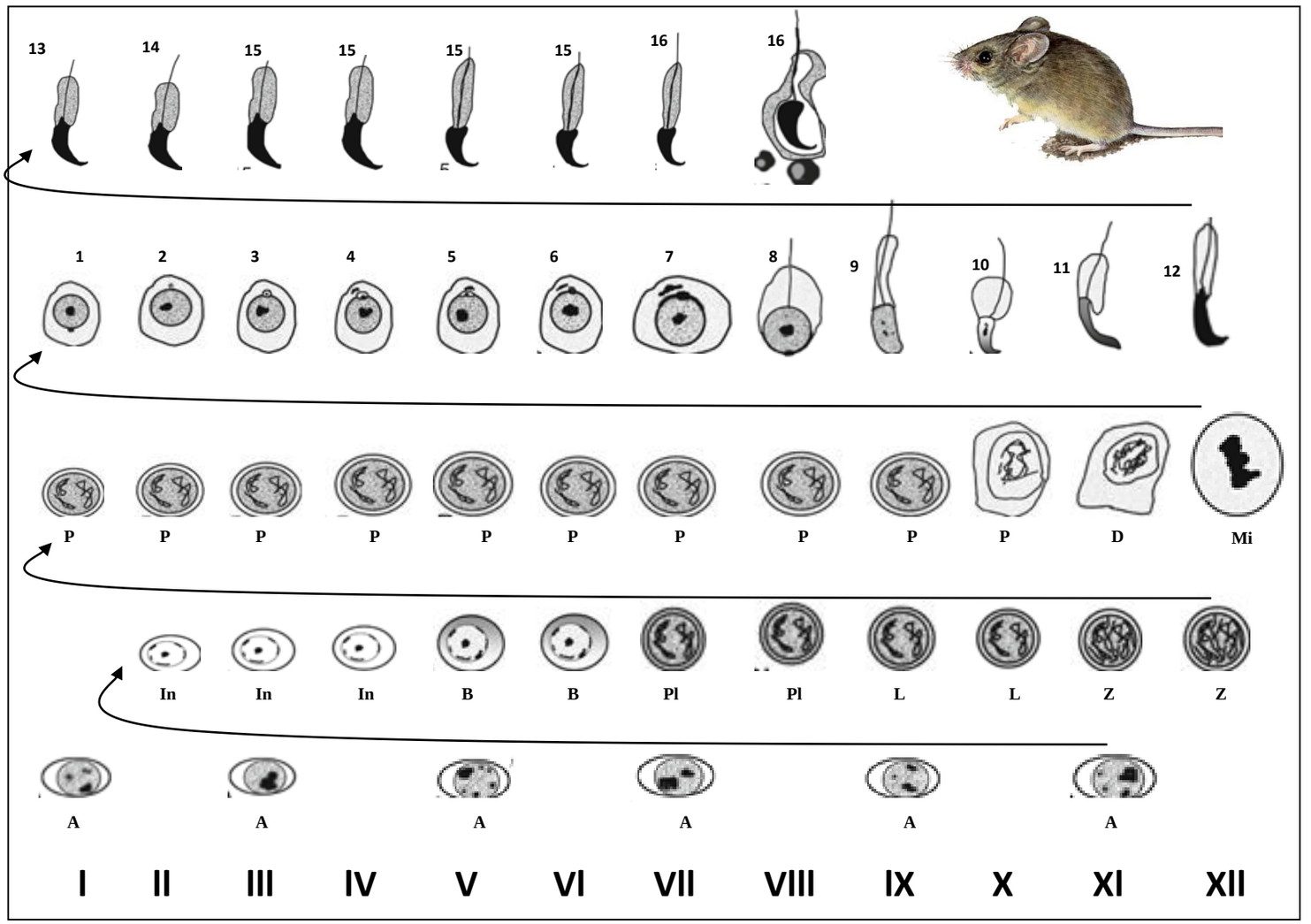
13
14
15
15
15
15
16
16
1
2
3
4
5
6
7
8
9
10
11
12
P
P
P
P
P
P
P
P
P
P
D
Mi
In
In
In
B
B
Pl
Pl
L
L
Z
Z
A
A
A
A
A
A
I
II
III
IV
V
VI
VII
VIII
IX
X
XI
XII

stem cell self-renewal and proliferation by producing growth factors such as glial cell line-derived neurotrophic factor (Meng et al., 2000) and stem cell factor (Hermo et al., 2009a); the activity of Sertoli cells in turn is affected by neighbouring peritubular myoid cells and diffusible interstitial-derived factors (de Rooij, 2009). Evidence for involvement of the interstitial compartment and vasculature in creating a functional stem cell niche in the testis was obtained by observations that the most primitive spermatogonial cells are located in areas of the tubules which are in contact with the interstitial compartment, but not with the other surrounding tubules (Chiarini-Garcia et al., 2001; Chiarini-Garcia et al., 2003; Ogawa et al., 2005). Generally, spermatogonia are classified as type A, intermediate and type B in rodents, with further subdivisions within the type A class. The spermatogonial A_{single} (A_s) cell is considered the spermatogonial stem cell in the adult testis (de Rooij, 2001). Division of A_s spermatogonia for the purpose of proliferation and differentiation is an atypical cell division in which the cytokinesis is incomplete; as a result, the daughter cells, known as A_{paired} (A_{pr}), are connected to each other through intracellular bridges (Huckins, 1978). From this point onwards, these cytoplasmic bridges persist between the progeny of A_{pr} spermatogonia and subsequent germ cells until mature spermatozoa are released into the seminiferous tubule lumen. In rodents, A_{pr} spermatogonia continue to divide, producing clones of 4, 8, 16 and rarely 32 $A_{aligned}$ (A_{al}) spermatogonia, which are the most mature undifferentiated spermatogonial cells in the adult testis. A_{al} spermatogonia differentiate into the A1 type which will give rise sequentially to A2-A4, intermediate and type B spermatogonia through further mitotic divisions (de Rooij, 2001; de Rooij and Russell, 2000). A prominent feature by which different spermatogonia are distinguished is the organization of their heterochromatin; the presence of increasing amounts of heterochromatin within the nucleus, at the periphery of the nuclear envelope is characteristic of differentiating spermatogonia (Russell et al., 1999). Division of type B spermatogonia is the last step of proliferative phase in that the progeny of these cells are spermatocytes that carry out meiosis. Figure 1.10 summarizes the mitotic divisions and differentiation of spermatogonia in the proliferative phase of spermatogenesis.

Figure 1.10 Proliferative phase of adult spermatogenesis

When a spermatogonial stem cell (A_s) divides, the resulting daughter cells are either stem cells which maintain the stem cell pool of the testis, or two daughter cells (A_{pr}) that are connected through an intercellular bridge and are committed to differentiate. Every cell division in this proliferative phase is a stage-specific event, and takes place in the basal compartment of the seminiferous epithelium (Rooij et al., 1989). Division of A_{pr} spermatogonia ultimately produces chains of 4 to 32 connected A_{al} spermatogonia that are considered the most mature undifferentiated spermatogonial cells in the adult testis. At stage VII of the seminiferous epithelium in mouse, all A_{al} spermatogonia differentiate into the type A1 spermatogonia which undergo further mitotic divisions to produce A2-A4, intermediate and type B spermatogonia (de Rooij and Russell, 2000).

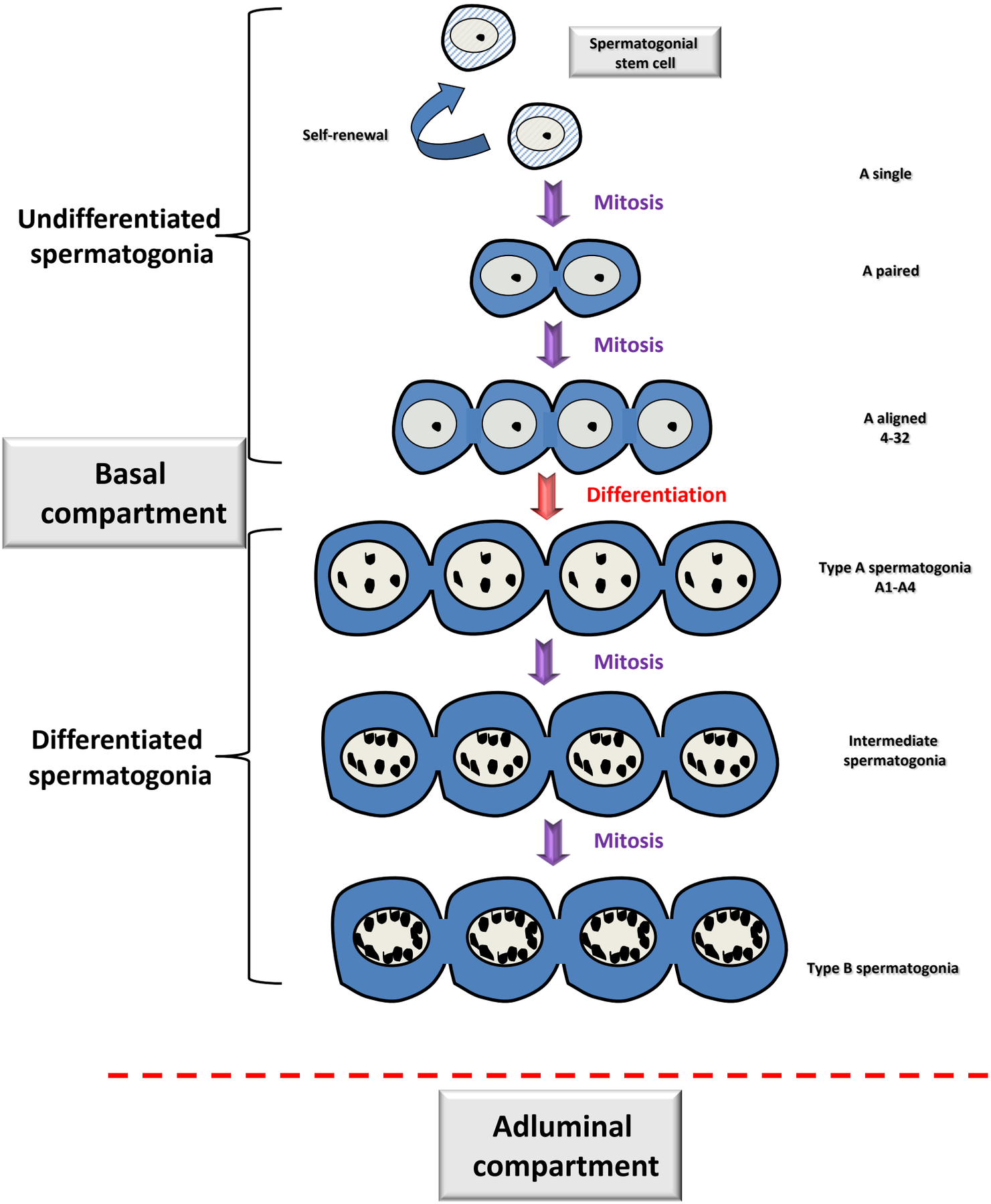
Spermatogonial stem cell
Self-renewal
A single
Mitosis
Undifferentiated spermatogonia
A paired
Mitosis
A aligned 4-32
Basal compartment
Differentiation
Type A spermatogonia A1-A4
Mitosis
Intermediate spermatogonia
Differentiated spermatogonia
Mitosis
Type B spermatogonia
Adluminal compartment

1.2.4 The meiotic phase of spermatogenesis

Significant events that occur during spermatocyte maturation and meiotic division include homologous recombination and chromosome segregation. Some of the major cellular machineries and proteins that contribute to these processes are summarized in Table 1.1. In this section an overview of spermatocyte maturation and meiotic divisions is presented.

The two types of spermatocytes are primary and secondary spermatocytes that undergo two meiotic divisions, meiosis I (MI) and meiosis II (MII); all meiotic steps take about 13 days in mice (Hess and Franca, 2009; Nebel et al., 1961). The most immature spermatocytes are known as preleptotene spermatocytes. These are diploid cells and duplicate the genetic material for the last time in the course of the germ cell development (Russell et al., 1999) and become tetraploid cells. Meiosis I consists of prophase, metaphase, anaphase and telophase. Prophase of meiosis I occupies 90% of the time required for meiosis and is further sub-divided into the leptotene, zygotene, pachytene, and diplotene stages; each of these is defined by morphological changes, primarily in the cell and nuclear size (Russell and Frank, 1978), and include unique molecular events concerning the nucleus and chromosome behaviour (Figure 1.11). In brief, these are chromosome condensation, pairing through synapsis, crossing over and initiation of chromosome segregation which occur in leptotene, zygotene, pachytene, and diplotene spermatocytes, respectively (Hermo et al., 2009a). Prophase is followed in turn by metaphase which features meiotic spindle assembly and nuclear envelope break-down, anaphase, when chromosomes segregate to the opposite poles of the dividing cell, and telophase in which a new nuclear envelope forms and the first meiotic division is completed. The resulting daughter cells are secondary spermatocytes with a haploid chromosome number; each chromosome, however, is consist of two sister chromatids (Kerr et al., 2006). Meiosis of secondary spermatocytes (MII) takes only a few hours and includes the separation of sister chromatids to opposite poles of the dividing cell (Hermo et al., 2009a). Thus, a single diploid spermatocyte produces four haploid spermatids through two meiotic divisions.

Table 1.1 Major molecular machinery in meiosis

The Table includess Major molecular processes that contribute to progression of meiotic cell division, and protiens with well-characterized roles in each process. Phenotypes caused by lack of function for each protein based on the information available in literature cited in the table are listed.

Bibliography for Table 1.1

Baudat, F., Manova, K., Yuen, J.P., Jasin, M., and Keeney, S. (2000). Chromosome Synapsis Defects and Sexually Dimorphic Meiotic Progression in Mice Lacking Spo11. Molecular Cell *6*, 989-998.

Cobb, J., and Handel, M.A. (1998). Dynamics of meiotic prophase I during spermatogenesis: from pairing to division. Seminars in Cell & Developmental Biology *9*, 445-450.

Cole, F., Keeney, S., and Jasin, M. (2010). Evolutionary conservation of meiotic DSB proteins: more than just Spo11. Genes & Development *24*, 1201-1207.

Firooznia, A., Revenkova, E., and Jessberger, R. (2005). From the XXVII North American Testis Workshop: The Function of SMC and Other Cohesin Proteins in Meiosis. J Androl *26*, 1-10.

Kumar, R., Bourbon, H.-M., and de Massy, B. (2010). Functional conservation of Mei4 for meiotic DNA double-strand break formation from yeasts to mice. Genes & Development *24*, 1266-1280.

Losada, A., and Hirano, T. (2005). Dynamic molecular linkers of the genome: the first decade of SMC proteins. Genes & Development *19*, 1269-1287.

Sanderson, M.L., Hassold, T.J., and Carrell, D.T. (2008). Proteins Involved in Meiotic Recombination: A Role in Male Infertility? Systems Biology in Reproductive Medicine *54*, 57-74.

Sehorn, M.G., Sigurdsson, S., Bussen, W., Unger, V.M., and Sung, P. (2004). Human meiotic recombinase Dmc1 promotes ATP-dependent homologous DNA strand exchange. Nature *429*, 433-437.

Shinohara, A., and Shinohara, M. (2004). Roles of RecA homologues Rad51 and Dmc1 during meiotic recombination. Cytogent Genome research *107*, 201-207.

Svetlanov, A., and Cohen, P.E. (2004). Mismatch repair proteins, meiosis, and mice: understanding the complexities of mammalian meiosis. Experimental Cell Research *296*, 71-79.

Table 1.1 Major molecular machinery in meiosis

Process	Protein	Known function	Phenotype	Reference
Double strand DNA break (DSB)	Spo11	DSB formation	Arrest in mouse spermatogenesis due to spermatocyte apoptosis. Defects in DSB formation	(Baudat et al., 2000; Sanderson et al., 2008)
	MEI4	DSB formation	Arrest in mouse spermatogenesis due to spermatocyte apoptosis	(Cole et al., 2010; Kumar et al., 2010)
Synapsis	SCP1	Constituent of central element of the synaptonemal complex	Male and female mouse infertility. Inability to repair DSB and complete synapsis	(Sanderson et al., 2008)
	SCP2 and SCP3	Constituents of lateral element of the synaptonemal complex	Infertility in mouse due to arrest in spermatogenic process at zygotene stage	(Sanderson et al., 2008)
Strand exchange	Rad51	Strand invasion in homologous recombination	Embryonic lethal	(Cobb and Handel, 1998; Sanderson et al., 2008)
	Dmc1	Strand invasion in homologous recombination	Meiotic arrest in mouse at Zygotene/pachytene stage due to failure in synapsis	(Sehorn et al., 2004; Shinohara and Shinohara, 2004)
Mismatch repair	MSH4 and MSH5	Processing of homologous recombination specific structures known as Holliday junction	Loss of Holliday junctions (MSH4) and formation of abnormal synaptonemal complex (MSH5). Infertility in both male and female mice	(Sanderson et al., 2008; Svetlanov and Cohen, 2004)
Chromosomal maintenance	SMC1 and SMC3	Constituents of cohesin complex which holds the sister chromatids together	Male infertility due to arrest in mid-pachytene stage in mice (SMC1,β isoform) and increased aneuploidy in zebra fish as a result of knock down (SMC3)	(Firooznia et al., 2005; Sanderson et al., 2008)
	SMC2 and SMC4	Constituent of the condensing complex which is essential for chromosome condensation and segregation	Chromosomal bridges are formed in metaphase of mitosis as a result of knock down in *C. elegans*	(Losada and Hirano, 2005; Sanderson et al., 2008)

RNA synthetic activity fluctuates throughout spermatocyte maturation. Autoradiographic studies have shown that the rate of RNA synthesis decreases from preleptotene to mid-pachytene, increases from mid-pachytene up to the late pachytene stage, then continuously decreases towards the end of the prophase and ceases in metaphase and anaphase (Monesi, 1965; Williams and Smith, 1996). These fluctuations in the rate of gene expression coincide with a dynamic cellular environment that changes from a program of cell growth to that of cell division. Another important event during spermatocyte maturation is the movement of preleptotene and leptotene spermatocytes from the basal to the adluminal compartment of the interstitium. This process involves extensive cell contact dynamics, leading to disappearance and reappearance of junctions between the Sertoli and germ cells as spermatocytes move through the blood-testis barrier (Wong et al., 2005). Meiosis is subsequently completed in the adluminal compartment of the seminiferous epithelium, an environment devoid of immune cells; this environment is suitable for meiotic and haploid germ cells that appear in the body for the first time after maturation of the immune system (Fijak and Meinhardt, 2006).

1.2.5 Spermiogenesis

Spermiogenesis is the development of mature spermatozoa from round spermatids, a process that includes extensive morphological changes but requires no cell division. Four major processes that take place during the course of spermiogenesis are nuclear remodelling, acrosome formation, flagellum development and elimination of cytoplasm (Figure 1.12).

Throughout spermiogenesis, the nucleus elongates and moves from the centre of the cell towards the plasma membrane (Russell et al., 1999) concurrent with condensation of the nucleus as a result of compact DNA packaging (Ward and Coffey, 1991). Morphological remodelling of the spermatid nucleus is accompanied by two important molecular events. As spermiogenesis proceeds, somatic histones are replaced sequentially, first by transition proteins and then by testis-specific protamines, which facilitate the condensed packaging of the sperm genome (Dadoune, 2003). Secondly, transcription is initially down-regulated and eventually shut down at

Figure 1.11 Overview of meiosis

The diagram depicts the major processes and cellular machineries involved in male gamete meiotic division. In mammals two meiotic divisions, MI and MII, produce four haploid spermatids from a diploid primary spermatocyte. Each of the two meiotic divisions is composed of prophase, metaphase, anaphase and telophase with prophase being further sub-divided into leptotene, zygotene, pachytene, and diplotene stages (Alberts et al., 2002; Nebel et al., 1961).

Initiation of meiotic prophase is indicated by presence of leptotene spermatocytes which cross the blood-testis barrier (BTB) and enter the adluminal compartment of the seminiferous tubule. At zygotene, homologous chromosomes align along a meiotic-specific macromolecular structure known as the synaptonemal complex. Crossing-over between the homologous chromosomes takes place at pachytene which is the longest stage of meiosis; this involves homology search, double strand DNA break and repair, each requiring a set of specialized proteins (Inagaki et al., 2010). At diplotene, paired chromosomes separate along their length except at crossing-over sites known as chiasmata; separation of paired chromosomes is in part supported by break-down of the synaptonemal complex at the end of prophase of meiosis I (Cobb and Handel, 1998). At metaphase, the nuclear envelope is dismantled and the meiotic spindle attaches to the homologous chromosomes at points known as kinetochores. Shortening of the spindle filaments in anaphase leads to chromosome segregation to the cell poles. Meiosis I is completed in telophase by formation of a new nuclear envelope around segregated chromosomes and cytokinesis. Meiosis II follows rapidly, taking just few hours and producing haploid round spermatids (Alberts et al., 2002).

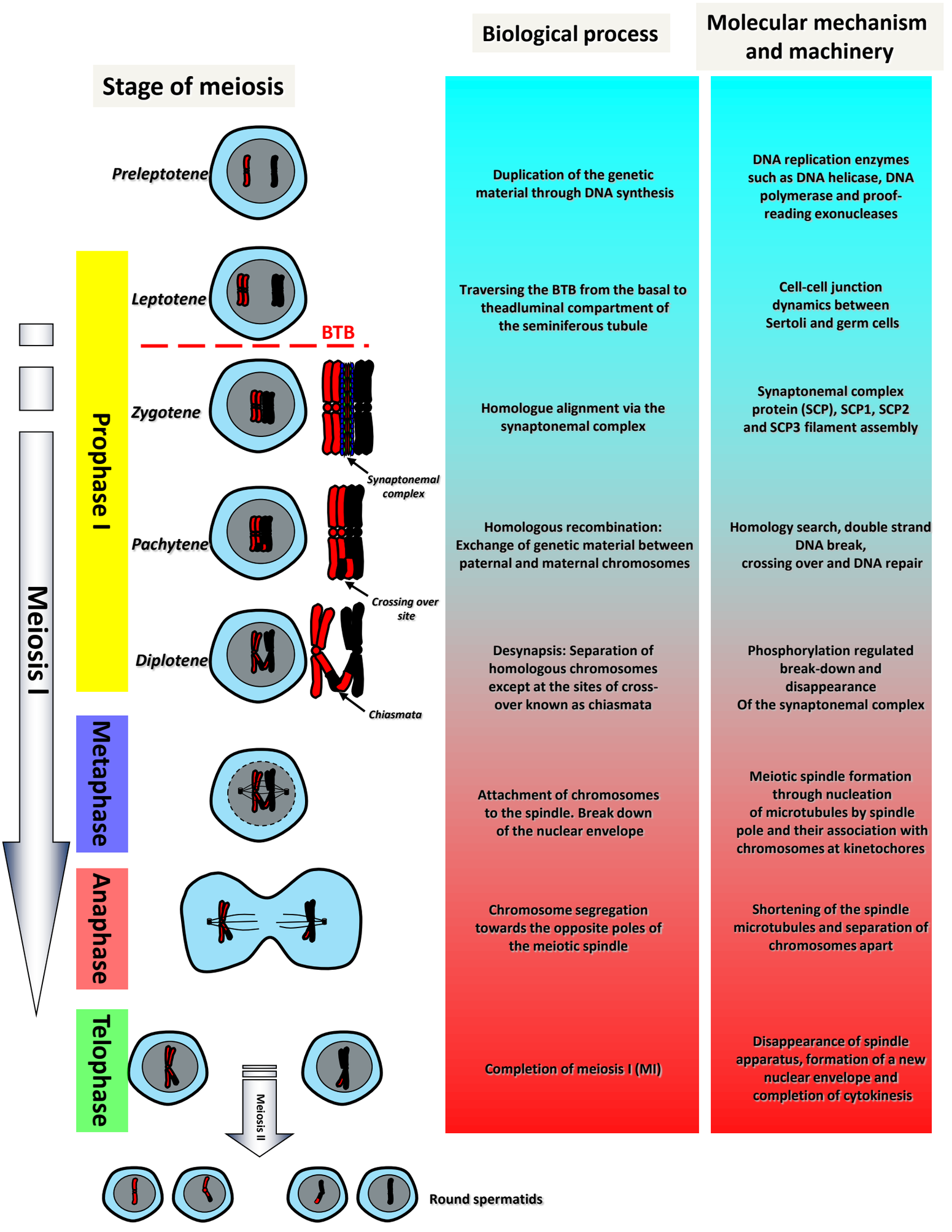
Stage of meiosis
Biological process
Molecular mechanism and machinery
Preleptotene
Duplication of the genetic material through DNA synthesis
DNA replication enzymes such as DNA helicase, DNA polymerase and proof-reading exonucleases
Leptotene
Traversing the BTB from the basal to theadluminal compartment of the seminiferous tubule
Cell-cell junction dynamics between Sertoli and germ cells
BTB
Zygotene
Homologue alignment via the synaptonemal complex
Synaptonemal complex protein (SCP), SCP1, SCP2 and SCP3 filament assembly
Synaptonemal complex
Pachytene
Homologous recombination: Exchange of genetic material between paternal and maternal chromosomes
Homology search, double strand DNA break, crossing over and DNA repair
Crossing over site
Diplotene
Desynapsis: Separation of homologous chromosomes except at the sites of cross-over known as chiasmata
Phosphorylation regulated break-down and disappearance Of the synaptonemal complex
Chiasmata
Prophase I
Meiosis I
Metaphase
Attachment of chromosomes to the spindle. Break down of the nuclear envelope
Meiotic spindle formation through nucleation of microtubules by spindle pole and their association with chromosomes at kinetochores
Anaphase
Chromosome segregation towards the opposite poles of the meiotic spindle
Shortening of the spindle microtubules and separation of chromosomes apart
Telophase
Completion of meiosis I (MI)
Disappearance of spindle apparatus, formation of a new nuclear envelope and completion of cytokinesis
Meiosis II
Round spermatids

mid-spermiogenesis (Hecht, 1998); as a result, a pool of transcribed mRNA is stored in a dormant form within ribonucleoproteins and is subsequently translated in a timely manner depending on requirements of maturating spermatids (Hecht, 1995; Steger, 2001).

The Golgi apparatus is involved in biogenesis of a membranous structure on the surface of the spermatid nucleus that is opposed to the plasma membrane; this membranous structure is known as acrosome, and its developmental steps are major morphological determinants to the process of spermatid maturation (Russell et al., 1999). Vesicles originating from the Golgi complex coalesce on the surface of the nuclear envelope to form the acrosomal cap; the cap is constantly supplied with vesicles from the Golgi and spreads over the nuclear membrane (Kerr et al., 2006). Concordant to formation of the acrosome, the centriole pair initiates formation of a flagellum that indents the nucleus and eventually develops into the sperm tail spatially opposite to the anterior acrosome; the middle piece of tail is enriched in mitochondria and imparts motility to the spermatozoon (de Kretser and Kerr, 1994). Towards the end of spermiogenesis, the bulk of cytoplasm is shed from spermatids in the form of the residual body when mature spermatozoa are released into the lumen during spermiation; the residual body contains remnants of organelles that are not required for sperm function, and it is taken up by Sertoli cells through phagocytosis (Russell et al., 1999). The outcome of spermiogenesis is formation of a highly specialized cell, equipped with unique organelles such as flagellum and acrosome which collectively facilitate the sperm's primary function, transmission of genetic material through fertilization of egg.

1.2.6 Regulated nucleocytoplasmic transport in gametogenesis

Gametogenesis provides an ideal model system to study the function of an evolutionary conserved, yet diversified family of proteins, such as importin α in development and differentiation. Spermatogenesis bears similarity between different phyla of animal kingdom, in that it includes proliferative, meiotic and differentiation phases in the course of gamete development. In this section an overview of the current

Figure 1.12 Overview of spermiogenesis

Selected steps of rat spermiogenesis are shown, emphasizing the key processes and molecular events that underlie spermatid maturation. The number of morphologically distinct spermatids that define the steps of spermiogenesis varies between species but the overall differentiation steps share remarkable similarity in mammals.

Early in spermiogenesis, acrosome formation from the Golgi complex occurs through fusion of small vesicles which coalesce on the nuclear membrane. As spermiogenesis proceeds, the acrosome spreads and eventually covers approximately one third of the spermatid nucleus (Hermo et al., 2009b; Ramalho-Santos et al., 2002). The centriole pair initiates flagellum formation at the pole of the nucleus opposite to the acrosome (Hermo et al., 2009c). At mid-spermiogenesis, several events contribute to spermatid nuclear remodelling. Although there is extensive temporal overlap between these events, for the purpose of clarity they are described separately in this text and figure. The somatic histones are initially replaced by transition proteins, which in turn are exchanged for highly basic testis-specific protamines (Steger, 1999). Concurrent with histone replacement, transcription is down-regulated as a result of chromatin condensation and tight DNA packaging (Hecht, 1998). At the last stages of spermiogenesis, the majority of elongated spermatids cytoplasm is removed and phagocytosed by Sertoli cells enabling mature spermatozoa to be released into the lumen of the seminiferous tubule at spermiation (Russell et al., 1999).

Organelle formation

Acrosome and flagellum development

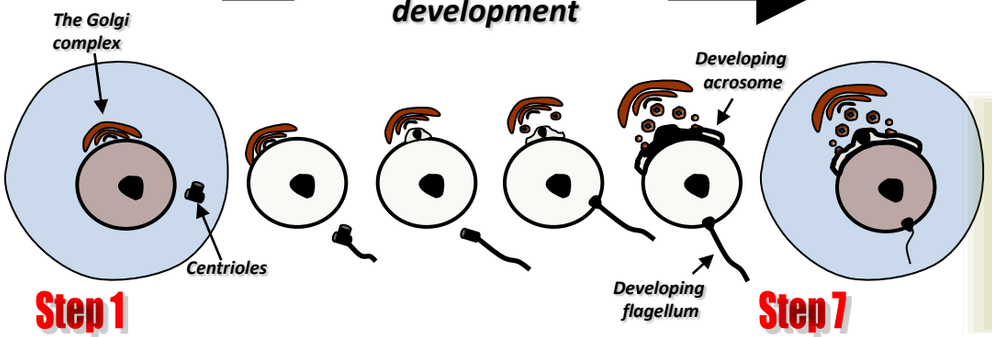

Initiation of the acrosome and flagellum biogenesis by the Golgi complex and centrioles, respectively. The development of both organelles is ongoing until late spermiogenesis.

Nuclear changes

Chromatin remodelling

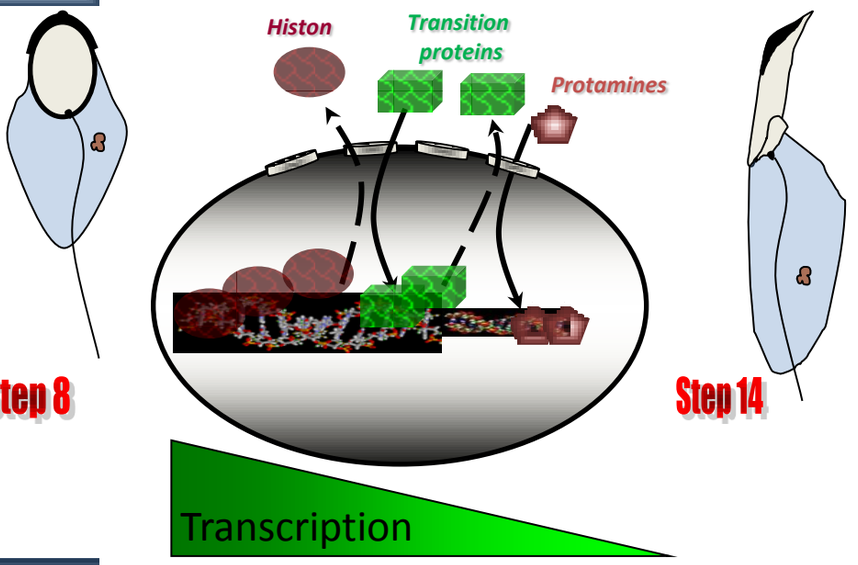

Replacement of the histones with testis-specific transition proteins and protamines, resulting in chromatin condensation. Concurrent with genome compaction, the nucleus shrinks in size and elongates continually until the latest stages of spermiogenesis. Transcription is gradually down-regulated.

Sperm release

Spermiation

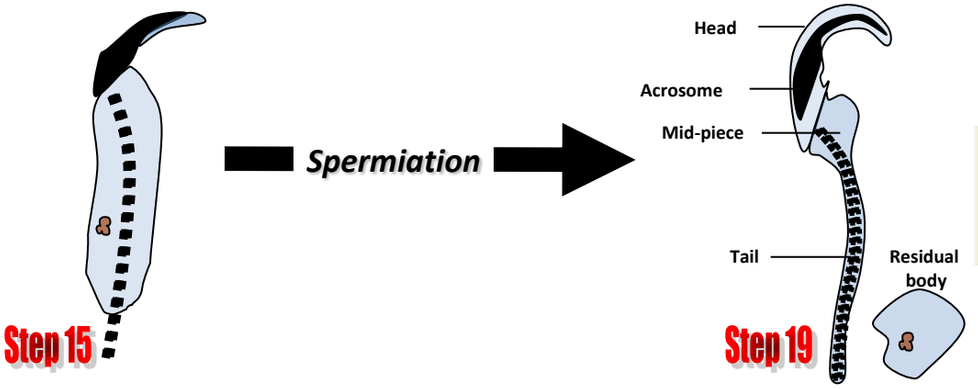

Removal of the residual body and release of the sperm into the lumen of seminiferous tubule.

knowledge regarding the expression and function of importin α family members in gametogenesis, with a focus on spermatogenesis is presented.

Importin α proteins in *C. elegans* serve gender-specific roles in gametogenesis. Of the three importin αs (IMA-1, IMA2, and IMA3) in adult worms, only IMA-3 is expressed in both germline and somatic tissues, while IMA-1 and IMA-2 are restricted to the germline (Geles and Adam, 2001; Geles et al., 2002). RNAi studies on hermaphrodite worms have demonstrated that reduction in the level of IMA-3 abrogates progression of oogenesis, but not spermatogenesis, by causing an arrest in pachytene stage. The defective germ cells had abnormal chromatin morphology, suggestive of impaired chromosome condensation or synapsis (Geles and Adam, 2001). Based on these observations the role of IMA-3 in oogenesis cannot be compensated for by IMA-1 and IMA-2; thus IMA-3 in *C. elegans* may have specific functions in progression of oogenesis.

The *D. melanogaster* genome also encodes three importin α family members, *importin α1*, *importin α2* and *importin α3*. Examination of protein expression by immunofluorescent microscopy revealed distinct spatio/temporal expression pattern for different family members at different stages of spermatogenesis (Giarrè et al., 2002). Importin α2 had strong expression in the cytoplasm of proliferating spermatogonia, with an ensuing decline in the pre-meiotic G phase. During both meiosis I and meiosis II, expression of importin α2 increased again and its subcellular localization switched from the cytoplasm to the nucleus; in post-meiotic germ cells, expression of importin α2 became undetectable. Neither importin α1 nor importin α3 were highly expressed in mitotically dividing spermatogonial cells; however the expression of both importin α1 and α3 was initiated at pre-meiotic G phase, peaked during meiosis I and II and extended into the post-meiotic spermatogenic differentiation (Giarrè et al., 2002). Knock-out of importin α2 led to reduced fertility in males and complete sterility in female flies (Gorjánácz et al., 2002; Mason et al., 2002). In males, reduced fertility was caused by failure in sperm individualization at the end of spermatogenesis, leading to a very low number of motile sperm. Female infertility was caused by the occlusion of the intercellular passages between the nurse cells and developing oocytes known as the ring canals. Transgenic over-expression of

importin α1, α2 or α3 led to a significant increase in fertility in 60% of males, while rescue of female fertility was only possible by ectopic expression of importin α2 (Mason et al., 2002). Given the partial NLS binding redundancy between importin αs (Section 1.1.8.1), and the rescue of spermatogenesis by ectopic expression of the two other family members in importin α2 null flies, defective oogenesis may not be the direct consequence of a failure in nuclear protein import. This observation implies that importin α2 may have acquired paralog-specific roles in *D. melanogaster* oogenesis (Goldfarb et al., 2004).

Expression of *importin α* family members is also regulated in mammalian spermatogenesis. Hogarth et al, detected the transcripts of all known *importin αs* in the adult mouse testis by Northern blot; *in-situ* hybridization showed that each family member was detectable in specific cell types of the adult testis (Figure 1.13 a; Hogarth et al., 2006). *Importin α1* transcripts were observed in spermatogonia, spermatocytes and spermatids, while its closest family member, *importin α6*, was only detected in round spermatids. *Importin α3* was detectable in spermatogonia and spermatocytes, while *importin α4* mRNA was only detectable in spermatocytes. *Importin α2* was first visible in spermatocytes and the signal persisted into round spermatids (Hogarth et al., 2006). Protein detection by immunohistochemistry validated the cell type specific expression and showed the differential subcellular localization of family members in developing germ cells (Figure 1.13b). Importin α3 protein was readily detectable in the cytoplasm of spermatogonia, spermatocytes and spermatids up to the elongating stage. Both the cell type expression and subcellular localization of importin α4 differed from importin α3; it was detected in spermatocytes and round spermatids only, with a visible signal confined to the nucleus (Hogarth et al., 2007). Immunohistochemical analysis of the adult rat testis sections showed that the expression and subcellular localization of importin α3 and α4 are conserved between rat and mouse, and revealed that the rat importin α2 is found in both cytoplasm and nucleus of spermatocytes but only in the cytoplasm of round and elongating spermatids (Figure 1.13, b; Miyamoto et al., 2013). Such differential expression and subcellular localization of importin α family members and other components of the nucleocytoplasmic transport machinery has also been uncovered in adult human testis (Whiley et al., 2011). These expression patterns indicate that importin α family

Figure 1.13 Regulated expression of importin α family members in rodent spermatogenesis

Cell-specific expression patterns of *importin α* family members mRNA (A) and protein (B) in spermatogenesis. A; Spermatogenic cell types from spermatogonia to elongating spermatid; the solid bars at the bottom panel correspond to the cell types in which mRNA of each *importin α* is detected. Figure adapted from Hogarth et al, 2006. B; The protein expression and subcellular localization of importin α family members are shown by brown colouring for the mouse importin α3 and α4 and the rat importin α2.

A. mRNA studies

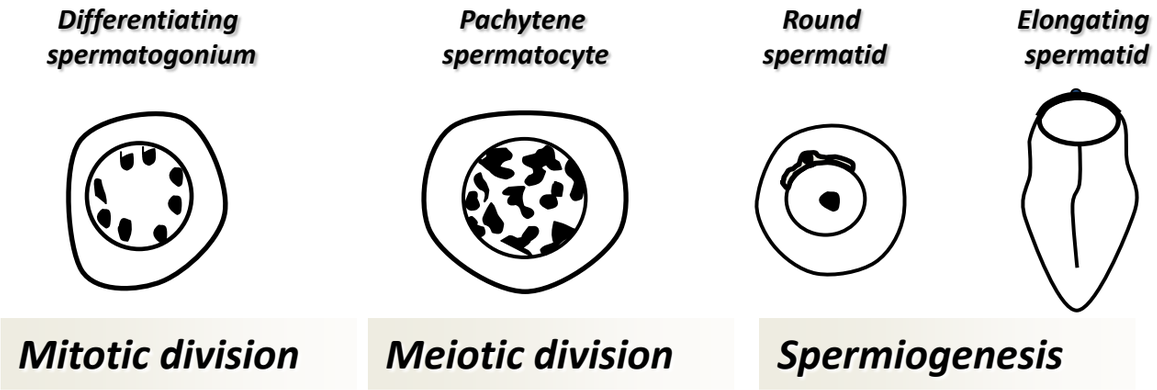

Importin α expression in the adult mouse testis

B. Protein studies

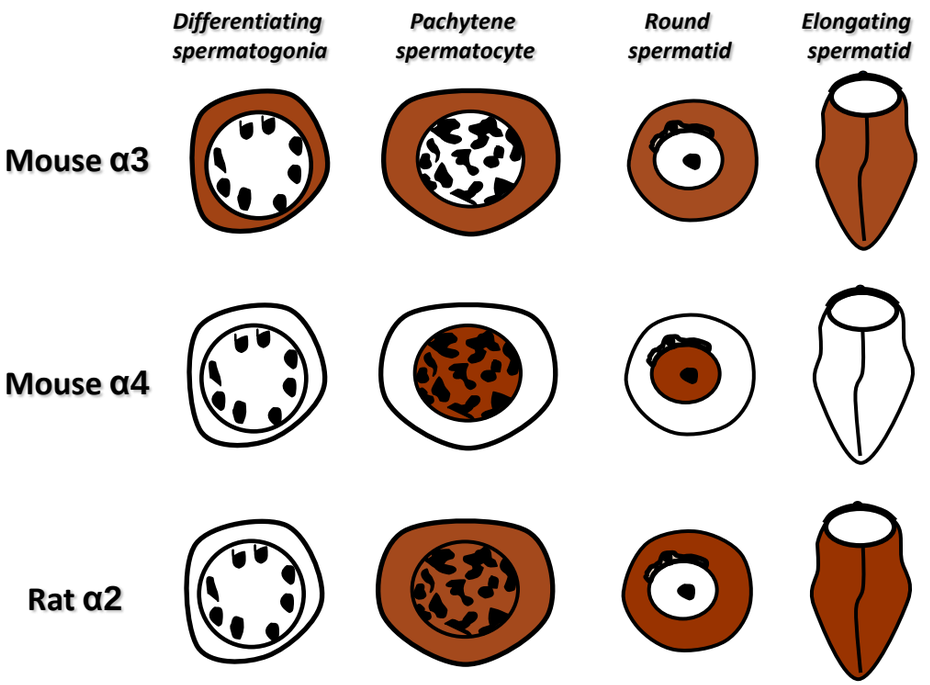

members may serve distinct functions in developmental systems such as spermatogenesis. A potential species-specific expression pattern for importin β1 in mammalian spermatogenesis has been suggested by immunohistochemical detection of the protein in adult mouse and human testis. Importin β1 was readily detected in spermatids of human testis (Whiley et al., 2011) but not that of mouse (Loveland et al., 2006). If confirmed, this phenomenon raises questions about the mechanism of the nucleocytoplasmic transport in murine spermatogenesis, and in particular post-meiotic haploid germ cells. However, this view is not consistent with the results of a proteomic analysis, in which high levels of importin β1 was detected in the post-meiotic spermatids, isolated from the adult mouse testis (Guo et al., 2010). Thus, further examination of importin β1 expression pattern in the testis is required for a better understanding of the nature of nucleocytoplasmic transport in spermatogenesis.

1.3 Hypothesis and aims

The summary of the literature presented above indicates that importin αs serve distinct roles in developmental processes. Based on previously documented differential expression of importin family members in testes we hypothesized that:

1. Importin α family members and importin β1 are differentially expressed at protein level in pachytene spermatocytes and round spermatids of adult murine testis.
2. Importin α family members mediate diverse and distinct cellular processes through selective binding to cargoes in spermatocytes and spermatids.

Thus the specific aims of this study were to:

1. Delineate the protein levels of several importin family members (α2, α3, α4 and β1) in highly enriched fractions of spermatocytes and spermatids, obtained from adult rat testes.
2. Define the germline "α-importome" through identification of binding partners of importin α family members in spermatocytes and spermatids, and thereby elucidate functional differences between importin α family members in these testicular cell types.
3. Assess the previously reported potential interaction between importin α4 and Mtmr4, a cytoplasmic protein with a predicted role in endosomal biology.

Each experimental aim is designed in a separate Chapter which includes a brief discussion of the outcomes. A full discussion in which the body of work is considered together is presented in a final chapter, the General Discussion. The outcomes of the experiments presented in this thesis were intended to provide a unique description of dynamic importin function during development. In addition the unbiased screening approach used to define a germline "α-importome" was intended to examine the emerging understanding that importin α proteins serve many roles in addition to nucleocytoplasmic transport.

Chapter 2-
Materials and methods

CHAPTER 2 MATERIALS AND METHODS

2.1 Animals and tissues

Wild type adult rats (Sprague Dawley outbreeds, 60-90 days old) were obtained from Monash Animal Services, Melbourne, Australia. The animals were killed in carbon dioxide (CO_2) and cervical dislocation followed by dissection of the tissues. All investigations conformed to the NHMRC/CSRIO/AAC Code of Practice for the Care and Use of Animals for experimental purposes and were approved by the Monash University Standing Committee on Ethics in Animal Experimentation.

2.2 Germ cell isolation

The protocol employed here to isolate highly enriched populations of germ cells from adult rat testes is based on the method that was originated by Meistrich and colleagues (Meistrich et al., 1981) and optimized by Loveland and co-workers (Loveland et al., 1993) for use in Beckman JE5.0 elutriator.

2.2.1 Adult rat testes dissociation

In each experiment, four testes from two wild type adult rats were dissected followed by removal of the tunica and blood vessels. The tubules were placed in 3 ml of DMEM media (Gibco, New York, USA), chopped with sterile scissors in a petri dish and suspended to a volume of 40 ml DMEM media containing 140 units/ml of collagenase type IV (Sigma, Aldrich) in a 50 ml falcon tube. The tube was shaken horizontally at 32°C in a water bath for 20 minutes at 120 cycles/minute to disperse the tubules. Next, the tubules were allowed to settle at the bottom by standing the tube in a vertical position for 4 minutes; medium containing the interstitial cells was removed by aspiration of the supernatant and discarded. The tubules were resuspended in 40 ml of DMEM, allowed to settle again, followed by removal of the supernatant. To dissociate the tubules and obtain a single cell suspension, the tubules were suspended in 40 ml of DMEM containing 200 units/ml of trypsin from bovine

pancreas (Sigma, Aldrich) and 120 units/ml of DNase I (Sigma, Aldrich) and agitated at 32°C in a water bath for 30 minutes at 120 cycles/minute. Fetal calf serum (FCS) (Quantum Scientific, Queensland, Australia) and soybean trypsin inhibitor (SBTI) (Gibco, New York, USA) were added to the media to 0.8% and 0.1% final concentrations, respectively. The cell suspension was filtered through a 70 µM filter (BD BioSciences, Erembodegem, Belgium) and pelleted with centrifugation at 4000 rpm (Eppendorf, A-4-81 rotor) for 10 minutes. The cell pellet was resuspended in 50 ml of PBS (0.13M NaCl, 0.002M KCl, 0.01M Na_2HPO_4, 0.0017M KH_2PO_4, pH 7.4) containing 5% BSA, 0.025% SBTI, 120 units/ml DNase I and 5 mM naphthol disulfonic acid.

2.2.2 Centrifugal elutriation

The testicular cell suspension was resolved into several fractions based on cell size by centrifugal elutriation. An elutriation chamber (Beckman Instruments, Palo Alto, CA) embedded in a Beckman elutriation rotor (Beckman JE 5.0) was loaded with the cell suspension through a pump (Masterflex, Cole Parmer, Chicago, IL). Upon loading of the cells into the chamber, the flowthrough from the outlet chamber was progressively collected in six fractions with the size of the cells that exit through the outlet regulated by adjusting the pump flow rate and the centrifuge rotor speed. Fraction 1 (F1) was collected as 180 ml at 3000 rpm and the pump flow rate of 13.5 ml/min. The next three fractions, (F2, F3, and F3') were all collected as 150 ml volume at 3000 rpm at flow rates of 23.4 ml/min, 31.5 ml/min, and 40.7 ml/min, respectively. After collection of F3', the centrifuge rotor speed was reduced to 2000 rpm and the last two fractions (F4, and F5) were collected at this speed, both in 150 ml volume; F4 fraction was collected at the flow rate of 30.2 ml/min and F5 at 51ml/min. Table 2.1 summarizes the parameters that were used in elutriation and the cellular composition of each fraction.

Fractions 3' and 5 containing round spermatids and pachytene spermatocytes were divided into 3 x 50 ml in conical tubes and centrifuged at 1500 rpm (Eppendorf, A-4-81 rotor) for 10 minutes. The supernatant was removed and each cell pellet was resuspended in 10 ml of phosphate buffered saline (PBS). Cells from the same

fractions were combined and centrifuged again as above. The supernatant was removed and the cells were resuspended in 10 ml of PBS and counted using a haemocytometer.

Table 2.1 Parameters used in elutriation

Fraction	Speed of rotor (rpm)	Flow rate of the pump (ml/min)	Volume Collected (ml)	Cellular composition
1	3000	13.5	180	Mixture of cells
2	3000	23.4	150	Mixture of cells
3	3000	31.5	150	Moderately pure spermatids
3'	3000	40.7	150	Highly pure spermatids
4	2000	30.2	150	Mixture of cells
5	2000	51	150	Highly pure spermatocytes

2.2.3 Percoll density gradient

Percoll (Amersham Biosciences, Germany) was diluted to 90% in Ca^{2+} and Mg^{2+}-free PBS (0.13 M NaCl, 0.002 M KCl, 0.01 M Na_2HPO_4, 0.0017 M KH_2PO_4, pH 7.4, 1 mM $MgCl_2$ 10 µg/ml DNase I) by resuspending 45 ml of the Percoll in 5 ml of 10 x PBS. Four concentrations of Percoll were prepared in PBS as indicated in Table 2.2. Linear Percoll gradients were made with increasing concentration from the top to the bottom of a 50 ml polypropylene conical tube. For the spermatocyte fraction a gradient of 25%-37% was prepared, and for the spermatid fraction, a gradient of 23%-33% Percoll was prepared.

Table 2.2 Percoll dilutions used in gradient making

Percoll concentration	90% Percoll in PBS	0% Percoll (1xPBS)
23%	6ml	17.4ml
25%	6.5ml	16.9ml
33%	8.6ml	14.8ml
37%	9.6ml	13.8ml

Cell suspensions obtained by elutriation were centrifuged at 435 x g (Eppendorf, A-4-81 rotor) for 10 minutes and each cell pellet gently resuspended in 3 ml of PBS. To facilitate loading of the cell suspension on top of the Percoll gradient, the cell suspension was mixed with 3 ml of the Percoll of the denser concentration for that cell type (i.e. 33% Percoll for spermatids, and 37% Percoll for spermatocytes). Subsequently the cell suspension was loaded gently on the Percoll gradient and centrifuged (Beckman J6M/E, W/JS_4.2 rotor) at 4000 rpm for 30 minutes. The unit of acceleration was set at 1 and that of deceleration was set at 0 to avoid disturbance to the gradient during the spin. At the end of the centrifugation, the gradient containing round spermatids (F3') typically produced only one major visible band of cells that was removed by aspiration in a 7.5 ml volume. The gradient containing pachytene spermatocytes (F5) typically produced two visible bands. Both of the cell bands were taken by aspiration. Subsequent microscopic examination revealed that the lower band contained the pure population of pachytene spermatocytes and that the upper band was composed of different cell types; therefore the cells from the upper band were not used in any experiment. PBS was added to each cell population to a 40 ml final volume, followed by centrifugation at 435 x g (Eppendorf, A-4-81 rotor) for 15 minutes to pellet the cells. The supernatant was removed and the cell pellet was resuspended in a 5 ml final volume of PBS. Cells were counted using a haemocytometer. Approximately 1 $x10^6$ cells from each fraction were taken for purity determination (see Section 2.2.4), and the rest of the cells were pelleted by centrifugation at 500 x g (Sigma, 222/E), snap frozen on dry ice and stored at -80°C for later use.

2.2.4 Haematoxylin staining of isolated cells for purity estimation

Approximately $1x10^6$ cells from each fraction obtained by Percoll density gradient purification were pelleted by centrifugation at 500 x g (Sigma, 222/E) and resuspended in 0.5-1.0 ml of Bouin's fixative (75% picric acid, 10% formaldehyde, 5% glacial acetic acid) for 30 minutes. After fixation the cells were centrifuged at 500 x g (Sigma, 222/E) for 5 minutes and washed in 70% ethanol to remove the residual Bouin's fixative solution, followed by a wash in sterile MQ water. Subsequently, the cells were suspended in 2% agar (dissolved in MQ water) and pelleted at 12000 x g

(Sigma, 222/E) for 5 minutes. The cell pellet was embedded in paraffin, followed by sectioning of the pellet and Haematoxylin staining in the Monash University Histology Facility. The stained sections were viewed under bright field microscope at 400x magnification. Based on the chromatin morphology, cells were either identified as spermatocytes or spermatids, or counted as impurities. Cells in which the nuclear morphology was not clear were omitted from the counting. In total, 470 cells in sections prepared from a representative spermatocyte fraction and 435 cells in sections prepared from a spermatid fraction were counted in several fields of view. The percentage purity was determined by dividing the number of spermatocytes and spermatids over the total number of counted cells in the respective fractions. As an additional approach for purity estimation Western blot analyses was performed using lysates of cell pellets as described in Section 2.4.

2.3 Recombinant protein purification

2.3.1 General bacterial transformation

For each experiment, 50 µl of $CaCl_2$ competent bacteria was transformed as follows. The competent cells were taken out of the -80°C freezer and thawed on ice for 5 minutes. Between 1 to 5 µg of the plasmid DNA was delivered into the tube containing the bacteria and mixed by gentle tapping. The transformation mix was incubated on ice for 30 minutes followed by a heat-shock of 42°C for 30 seconds in a heat block. After the heat-shock, the bacteria were placed back on ice for 2 minutes. To recover the cells from the heat-shock, bacteria were inoculated in 1ml of Luria broth (LB) media and incubated at 37°C with shaking at 220 cycles/minute for 1 hour. Subsequently, the cells were pelleted by centrifugation at 700 x g (Sigma, 222/E) for 3 minutes, supernatant was removed and the pellet was resuspended in 100 µl of LB and spread on the LB agar plates containing ampicillin at a final concentration of 100 µg/ml (LB_{amp}). Plates were incubated at 37°C for between 12 and 16 hours to allow the growth of the transformed bacterial colonies.

2.3.2 Bacterial culture for protein purification

A single colony from an LB_{amp} agar plate was used to inoculate 2ml of liquid LB_{amp} and incubated at 37°C with rotational shaking at 220 cycles/minute for 7 hours. After this incubation, 1 ml portions of the starter culture were used to inoculate 2 x 20 ml of $LB_{amp,}$ and these were incubated at 37°C with rotational shaking at 220 cycles/minute for 12 hours. Subsequently, both cultures were combined to inoculate 500 ml of LB_{amp} and incubated as before for 4 hours. At this point the temperature of the incubator was reduced to 20°C, a temperature suitable for the induction of protein expression. After 1 hour of temperature equilibration, protein expression was induced by addition of Isopropyl β-D-1-thiogalactopyranoside (IPTG) (Sigma) to a final concentration of between 0.1mM to 1mM, depending on the vector and bacterial host strain. Table 2.3 summarizes the vectors, bacterial strains, and parameters that were used for protein purification in this study. After induction, the cultures were incubated at 20°C with rotational shaking at 220 cycles/minute for between 12 to 16 hours.

Table 2.3 Tools used for recombinant protein purification

Plasmid name	Fusion protein	Bacterial host strain	Selection marker	[IPTG]	Source
pGEX6P2/ PTAC 58	GST-mouse Importin α2	Rosetta	Ampicillin	1mM	Miyamoto et al, 2012
pGEX2T/PTAC 58 ED	GST- mouse Importin α2 mutant in NLS binding region	Rosetta	Ampicillin	1mM	Dr. Miyamoto Monash University
pGEX6P1/Qip2	GST- mouse Importin α3	Rosetta	Ampicillin	0.1mM	Miyamoto et al, 2012
pGEX6P1/Qip1	GST-mouse Importin α4	Rosetta	Ampicillin	0.1mM	Miyamoto et al, 2012
pGEX2T	GST	BL21	Ampicillin	1mM	Amersham Bioscience, UK
pGEX2T-T-ag-NLS-GFP	GST-T ag-NLS-GFP	BL21	Ampicillin	1mM	Dr. Miyamoto Monash University
pGEX2T-R-NLS-GFP	GST-T ag-R-NLS-GFP	BL21	Ampicillin	1mM	Made in this study
pGEX2T-Mtmr4-NLS	GST-Mtmr4-NLS-GFP	BL21	Ampicillin	1mM	Made in this study
pGEX2T-Mtmr4-M-NLS	GST-Mtmr4-M-NLS-GFP	Rosetta	Ampicillin	1mM	Made in this study

2.3.3 Purification of affinity tagged proteins

The induced cultures were centrifuged at 4225 RCF (Sorvall Evolution, SLA 3000 rotor) for 10 minutes at 4°C to collect the cells. The supernatant was removed and the cell pellet resuspended in 50 ml of ice-cold 0.9% NaCl. The cell suspension was centrifuged at 1521 RCF (Sorvall Evolution, SLA 3000 rotor), the supernatant removed and the cell pellet was resuspended in 25 ml of ice-cold lysis buffer (50 mM Tris-HCl, pH 8.3, 500 mM NaCl, 1 mM EDTA, 2 mM DTT, and 0.2 mM PMSF), with 1 µl/ml of protease inhibitor cocktail type III (Calbiochem, Darmstadt, Germany). The cell suspension was frozen in dry ice for 15 minutes and thawed in a 25°C water bath; the freeze and thaw cycle was repeated three times to burst the cells. To enhance the yield of proteins with low expression efficiency, 0.5 mg of lysozyme (Thermo Fisher Scientific, Australia) was added to the cell suspension and mixed thoroughly by gentle agitation followed by incubation on ice for 30 minutes. To completely break open the cellular membranes, the lysates were sonicated 5 x 30 seconds in a Soniprep 150_{plus} (MSE, United Kingdom) at amplitude 10; the lysates were kept on ice throughout the sonication procedure, and 30 second intervals were included in between each sonication to avoid overheating of the samples. Cellular debris was pelleted by centrifugation at 26892 RCF (Sorvall Evolution, SS34 rotor), and supernatant containing the proteins was removed by aspiration. For each cell lysate, 1 ml of glutathione sepharose beads (GSH) (GE Healthcare, Sweden) was suspended in 700 µl of lysis buffer and pelleted by centrifugation at 73 RCF (Sigma, 222/E) for 1 minute followed by removal of buffer. This was repeated five times to equilibrate the beads in lysis buffer. The equilibrated beads were added to the bacterial lysate and incubated at 4°C with gentle rotation for between 8 to 12 hours to immobilize the recombinant proteins on the beads. At the end of the immobilization, the beads were collected by centrifugation at 200 RCF (Eppendorf, A-4-81 rotor). To remove the unbound and weakly bound material, beads were washed by resuspension in lysis buffer and pelleted as described above five times. At the end of the last wash, beads were resuspended in 10 ml of the elution buffer (50 mM Tris-HCl pH 8.3, 100 mM NaCl, 1 mM EDTA, 2 mM DTT) without glutathione, and loaded on a capped poly-prep chromatography column (Bio-Rad Laboratories, California, USA). The elution buffer was allowed to flow through the column by removing the cap to equilibrate the

filter. To elute the recombinant proteins from the beads, 10 ml of the elution buffer with 20 mM reduced glutathione (Sigma Aldrich) was loaded onto the column and allowed to flow through the filter. The flow-through containing the recombinant protein was collected and then used in dialysis buffer exchange and concentrating procedures (Section 2.3.5).

2.3.4 Removal of the affinity tag

Where removal of the affinity tag at the end of the purification process was required, the thrombin cleavage site, positioned between the GST fusion tag and the multiple cloning site of the pGEX vectors, was utilized. At the end of the immobilization step, the GSH beads were collected by centrifugation at 200 RCF (Eppendorf, A-4-81 rotor) for 1 minute. Subsequently the beads were washed in thrombin cleavage buffer (50 mM Tris HCl pH 8, 150 mM NaCl, 2.5 mM $CaCl_2$), with 1 µl/ml of protease inhibitor cocktail type III, by resuspending the beads in 10 ml of the buffer and centrifugation for 1 minute, as above. The washes were repeated 5 times to remove the unbound or weakly bound material and to equilibrate the beads in the thrombin cleavage buffer. After equilibration, 80 units of thrombin (Sigma Aldrich) per ml of the beads was added to the beads and incubated at room temperature with slow rotation. The progress of the cleavage reaction was measured by assessing the protein concentration in the solution at 30 minute intervals by measuring the absorbance of 280 nm UV light by the protein solution, or in the case of a fluorescently tagged protein by visual monitoring of the release of the fluorescent tag (e.g. GFP) into the solution from the beads. At the completion of cleavage, the beads containing the GST tag were pelleted by centrifugation at 73 RCF (Sigma, 222/E) for 1 minute, and supernatant containing the released recombinant protein was removed by aspiration. The obtained recombinant proteins were proceeded to dialysis buffer exchange and concentrating procedures.

2.3.5 Dialysis buffer exchange and concentrating

An Amicon Ultra centrifugal filtered column (Millipore, Ireland) with a semi-permeable membrane was used for the buffer exchange. Prior to protein loading, the membrane in the column was pre-wetted with sterile MQ water. The obtained

recombinant proteins were loaded in the column and centrifuged at 1800 x g (Ependorf, A-4-81 rotor) at 4°C until most of the solution passed through the filter. Subsequently, 4 ml of the dialysis buffer (20 mM Hepes-NaOH pH 7.3, 100 mM CH_3COOK, 2 mM DTT, and 1 µl/ml protease inhibitors) was loaded in the filter and centrifuged until 3.5 ml of the buffer passed through the filter; this buffer exchange was repeated 4 times. The final product was aspirated from the column by pipette and divided into 200 µl aliquots and was snap frozen on dry ice before being stored in a -80°C freezer.

2.3.6 Concentration measurement of recombinant proteins

To assess the concentration of recombinant proteins, 10-fold serial dilutions of each protein was made in dialysis buffer. The diluted proteins were then separated by SDS-PAGE alongside a range of BSA concentrations of 0.3 to 8 µg/µl standard. The gels were subsequently stained with coomassie blue dye (Section 2.5.2) and scanned using the Odyssey® (LI-COR Biosciences, Lincoln, Nebraska, USA) infrared detection system (v3.0). Using the "analyse" function of the Odyssey, a standard curve was generated based on the signal intensities of the known amount of BSA standard bands. Subsequently, the signal intensities of the recombinant proteins were compared with the BSA standard curve to estimate the concentration of each recombinant protein.

2.4 General SDS-PAGE and Western blotting

The BioRad gel casting and electrophoresis system (BioRad, NSW, Australia) was used to separate the protein samples on 12% polyacrylamide gels. The resolving gel (1.5 M Tris Base, pH 8.8, 0.1% SDS, 12% acrylamide, 0.05% ammonium persulphate, 0.05% TEMED) was prepared and poured between the gel casting plates. After pouring, the gel was covered by 2 ml of isopropyl alcohol and allowed to set for 45 minutes, after which isopropyl alcohol was removed and plates were rinsed with MQ water. The stacking gel (0.5% M Tris Base, pH 6.8, 0.1% SDS, 4% acrylamide, 0.5% ammonium persulphate, 0.5% TEMED) was poured on top of the resolving gel and combs were inserted in between the plates; the stacking gel was allowed to set at room

temperature for 45 minutes followed by removal of the comb from the gel. The gels were placed in BioRad protein running tanks filled with running buffer (0.5 M Tris Base pH 3.8, 0.4 M glycine, and 0.1% SDS). The protein samples were prepared by resuspending the proteins in an equal volume of 2 x protein loading buffer (10% glycerol, 2% SDS, 100 mM Tris, pH 6.8, 0.2% bromophenol blue, 0.715 M β-mercaptoethanol) and heating at 95°C for 5 minutes, followed by a pulse spin. Protein samples were loaded on the wells of the gel and run at 30 mA constant current for 60 minutes or until the loading dye front reached the bottom of the gel. The Page Ruler protein ladder (Fermentas, Australia) was loaded into each gel for assessment of protein band sizes.

For Western blot analysis, proteins were transferred onto a hybond nitrocellulose membrane (Amersham, Bioscience, UK). Prior to setting up the transfer apparatus, the membrane, blotting papers, sponges and the gel were soaked in cold transfer buffer (25 mM Tris, 192 mM glycine, and 10% methanol). The transfer cassette was assembled by placing the components in the following order: two layers of sponges, two layers of blotting papers, gel, membrane, two layers of blotting papers, and two layers of sponges. The cassette was placed in the tank filled with cold transfer buffer and transferred at 4°C for 1 hour at 100 V.

At the completion of the transfer, the membrane was soaked in PBS for 5 minutes and placed in blocking solution (5% non-fat milk in PBS) for 1 hour at room temperature with gentle shaking. After blocking, the membrane was incubated with the primary antibody (Table 2.4), diluted in blocking solution at 4°C for 12 hours. This was followed by 4 x 5 minutes washes in PBS. The membrane was then incubated with the secondary antibody (Table 2.5) diluted in blocking solution containing 0.1% Tween-20 and 0.01% SDS for 1 hour at room temperature in a light restricted container. The membrane was then washed 5 x 5 minutes in PBS and scanned by Odyssey fluorescent detection system.

Table 2.4 Primary antibodies used in this study

Target	Antibody	Dilution	Supplier	Host
Importin α2	Importin α2 (C-20)	1:1000	Santa Cruz Biotechnology, Inc, CA, USA	Goat
Importin α3	KPNA3	1:1000	Abcam, Cambridge, UK	Goat
Importin α4	KPNA4	1:1000	Abcam	Goat
GST	GST	1:1000	GE Healthcare, Buckinghamshire, UK	Goat
GFP	GFP	1:1000	Roche, Mannheim, Germany	Mouse
Importin β1	Impβ1 (H-300)	1:1000	Santa Cruz Biotechnology, Inc	Rabbit
PLZF	PLZF (H-300)	1:500	Santa Cruz Biotechnology, Inc	Rabbit
Synaptonemal complex protein 3	SCP3	1:500	Abcam	Rabbit
Acrosome binding potein	ACRBP	1:100000	Gift from O'Brian laboratory, Monash University	Goat
Mtmr4	Mtmr4 (C1)	1:150	Gift from Mitchell's laboratory, Monash University	Mouse
HA	HA tag	1:1000	COVANCE	Mouse

Table 2.5 Secondary antibodies used in this study

Antibody	Dilution	Host	Species reactivity	Supplier
Alexa fluor® 448	1:10,000	Goat	Mouse	Invitrogen, Oregon, USA
Alexa fluor® 448	1:10,000	Goat	Rabbit	Invitrogen
Alexa fluor® 546	1:10,000	Rabbit	Goat	Invitrogen
Alexa fluor® 546	1:10,000	Goat	Rabbit	Invitrogen
Alexa fluor® 546	1:10,000	Rabbit	Mouse	Invitrogen

2.5 Staining of SDS polyacrylamide gel

2.5.1 Silver staining

After electrophoresis, the gels were washed in MQ water for 30 minutes followed by incubation in 0.025% sodium thiosulphate (Sigma, Aldrich) for 1 minute in order to increase the sensitivity of proteins for staining. Subsequently gels were washed in three changes of MQ water, 20 seconds each, followed by incubation in cold (4˚C) 0.1% silver nitrate solution (0.1% $AgNO_3$(GFS chemicals, US), 0.02% formaldehyde (Sigma, Aldrich) in MQ water) for 20 minutes. Next, the gels were washed in three changes of MQ water for 20 seconds each. Developer solution (3% Na_2CO_3 (Celtic

chemicals, UK), 0.05% formaldehyde in MQ water) was added to the gels and colour development was monitored continuously, upon which the reaction was terminated by rinsing the gels in MQ water and incubating in 5% acetic acid (Merck, Australia) for 5 minutes.

2.5.2 Coomassie blue staining

After electrophoresis, gels were placed in fixative solution (20% methanol (v/v), 7.5% acetic acid (v/v) in MQ) for 20 minutes, followed by incubation in staining solution (0.25% Coomassie Brilliant Blue-R250 (Sigma, Aldrich) (w/v), 50% methanol (v/v), 5% acetic acid (v/v) in MQ) for 1 hour. The excess stain was removed from the gels by incubation in destain solution (5% methanol (v/v), 7% acetic acid (v/v) in MQ) with gentle shaking overnight.

2.6 T-ag reverse NLS (T-ag-R-NLS) cloning into the bacterial expression vector

The oligonucleotides listed in Table 2.6 were purchased (Sigma, Aldrich) and were hybridized to create a cDNA encoding the T-ag-NLS in reverse (i.e. T-ag-R-NLS), based on the amino acid sequence encoded by cDNA of simian virus 40, with the GenBank accession number of AAB59924.1. The hybridization product was used to replace the wild type T-ag-NLS from a pGEX-2T bacterial expression vector.

Table 2.6 The oligonucleotides used in cloning of T-ag-R-NLS

Oligonucleotide	Sequence 5' to 3'	Concentration
T-ag-R-NLS-F	GATCCCCGGATGAAGTTAAACGGAAAAAAAAACCGCCC	250 pmol/µl
T-ag-R-NLS-R	GGGCGGTTTTTTTTTCCGTTTAACTTCATCCGGG	250 pmol/µl

For hybridization, 20 µl of each oligonucleotide was placed in 10 µl of 5 x STE buffer (1M Tris HCl Ph 8, 0.5M EDTA, 100 mM NaCl) and mixed by gentle pipetting. The reaction mix was placed on a thermal cycle of decreasing temperatures from 95°C to 25°C, with 5°C intervals of 5 minutes duration. The sequence of the oligonucleotides incorporated a *BamHI* restriction site overhang at the 5' end and a *SmaI* restriction

site blunt end at the 3' end of the hybridization product. One µl of the hybridization product was ligated into a *BamHI* and *SmaI* digested pGEX2T/T-ag-NLS-GFP vector backbone using a Takara ligation kit (TAKARA Bio Inc., Shiga, Japan), following the suppliers recommendation. Five µl of the ligation product was transformed into the competent *E.coli*, DH5α strain, followed by screening of the resulting colonies by plasmid isolation (Qiagen, Victoria, Australia) and restriction digest with *EcoRI* and *HindIII* restriction enzymes. Constructs that were linearized by this double digestion were selected for verification, since successful cloning of the T-ag-R-NLS into the vector leads to removal of the *HindIII* restriction site from the vector (Figure 2.1). Authenticity of the positive constructs was verified by DNA sequencing (Section 2.15).

2.7 In vitro solution binding assay

For each binding assay, 30 µl of GSH Sepharose beads (GE Healthcare) was equilibrated in transport buffer (20 mM HEPES NaOH pH 7.3, 110 mM CH_3COOK, 2 mM CH_3COO_2Mg, 5 mM CH3COONa, 0.5 mM EGTA pH 7.3, 2 mM DTT, 1 µl/ml protease inhibitor cocktail) as described in Section 2.3.3. To reduce nonspecific binding, 0.1% (v/v) of NP40 detergent was included in the transport buffer. After equilibration of the beads, 100 picomoles (pmol) of both the bait (GST-fused) and the target protein were added to the beads to a final volume of 100 µl in transport buffer and incubated at 4°C for 1 hour with slow rotation. Subsequently, the beads were pelleted by centrifugation at 73 x g (Sigma, 222/E) and supernatant was taken by aspiration. The unbound and weakly bound materials were removed from the beads by washing them in transport buffer as described in Section 2.3.3. To elute the bound proteins, the beads were resuspended in 35 µl of 2 x protein sample buffer (10% glycerol, 2% SDS, 100 mM Tris, pH 6.8, 0.2% bromophenol blue, 0.715 M β-mercaptoethanol) and were heated to 95°C for 5 minutes. The beads were pelleted by centrifugation as above and the supernatant containing the eluted proteins was removed by aspiration. A fraction of the eluate was run on a 12% acrylamide gel followed by coomassie blue staining or Western blot analysis.

Figure 2.1 Cloning of the T-ag-R-NLS into the bacterial expression vector

A. Plasmid DNA pGEX2T encoding the T-ag nuclear localization signal (T-ag NLS) fused with a C-terminal GFP tag, was digested sequentially with *SmaI* and *BamHI* restriction enzymes. The double digest of the plasmid led to release of the insert (T-ag-NLS) and removal of *HindIII* restriction site from the vector.

B. cDNA encoding the T-ag-NLS in reverse (T-ag-R-NLS) was created by hybridization of two oligonucleotides (Table 2.6) which incorporated a *BamHI* restriction site overhang and a *SmaI* restriction site blunt end in the hybridization product. The cDNA was ligated into the *BamHI* and *SmaI* digested vector backbone.

A. Vector backbone preparation

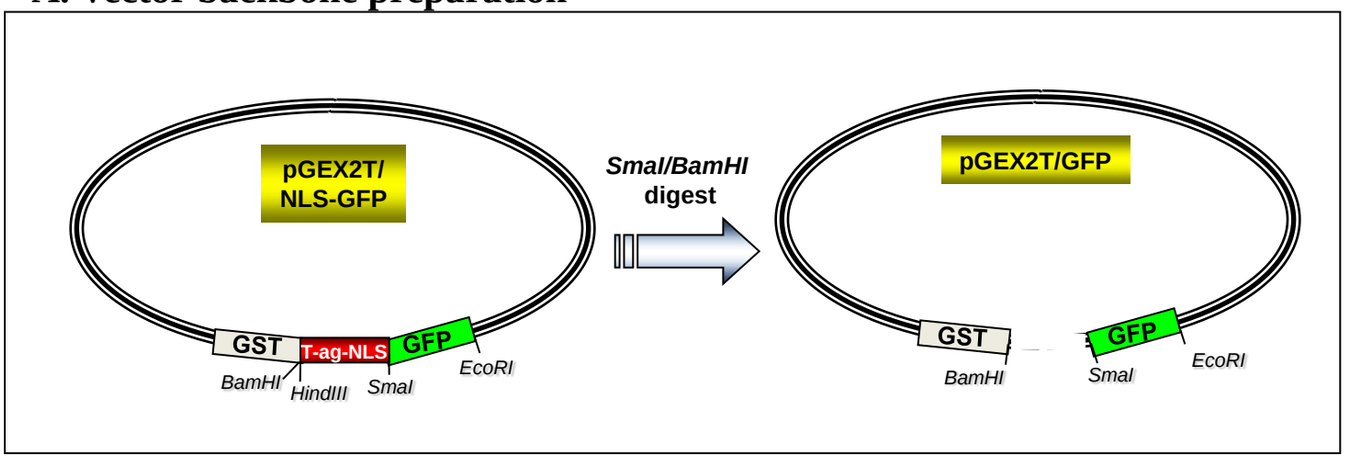

B. Insert ligation

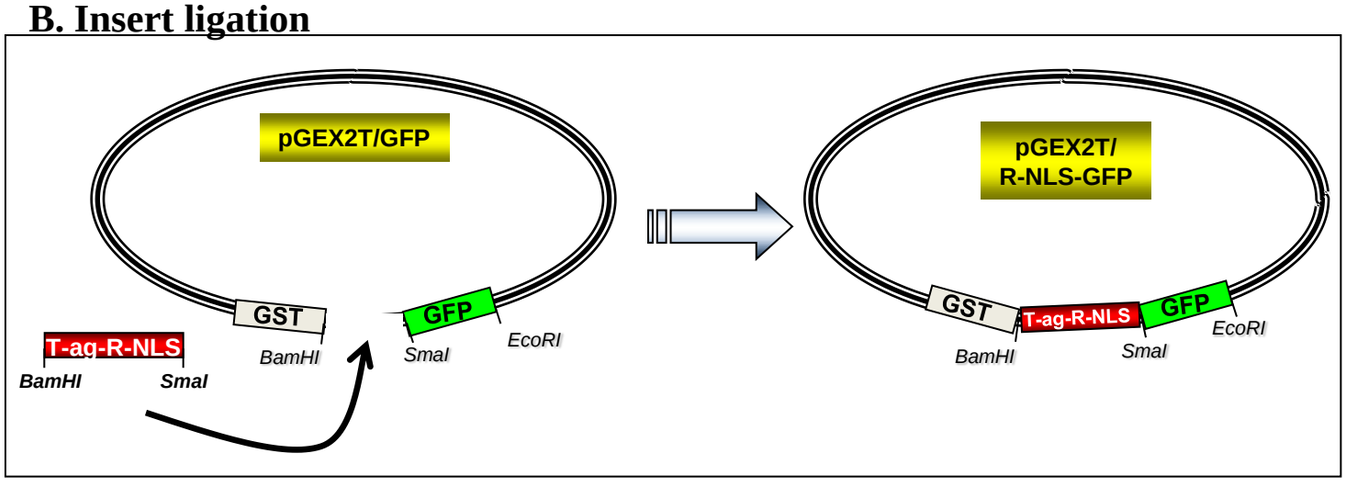

2.8 Importin α pull-down from spermatocytes and spermatids

In each experiment, 100 pmol of recombinant GST-fused protein was used as bait for pull-down from $5x10^6$ spermatocytes or spermatids. The entire procedure was performed on ice or in a 4°C room to prevent protein degradation. The cells were resuspended in 750µl of transport buffer and homogenized by passage through 27 and 30 gauge needles, followed by sonication at amplitude 6 (Soniprep 150_{plus}) for 2 x 30 seconds, with 30 second intervals on ice to avoid lysate overheating. After sonication, the lysates were incubated on ice for 10 minutes. The cell debris was subsequently pelleted by centrifugation at 14000 x g (Sigma, 222/E) for 15 minutes and the supernatant was promptly removed by aspiration. The lysates were incubated with 500 µl of equilibrated GSH sepharose beads for 1 hour with slow rotation to clear the proteins that bind non-specifically to the beads. Subsequently the lysates were removed from the beads and divided equally into four fractions, to each of which was added 50 µl of freshly equilibrated beads and 100 pmol of each of the recombinant importin α proteins or GST alone. The reactions were incubated at 4°C for 1 hour with slow rotation. At the end of this period, the beads were pelleted and the supernatant removed. Beads were washed 5 x in 200 µl of 25mM $NaHCO^{3-}$ (Sigma, Australia) to remove the unbound and weakly bound proteins. After the final wash, the supernatant was discarded and the residual volume of the supernatant was removed by a rolled-up kimwipe tissue paper. Protein complexes were eluted by resuspending the beads in 30 µl of 30 mM Glutathione (Sigma, Australia) and incubation at room temperature for 20 minutes with gentle agitation every 5 minutes. Subsequently the beads were pelleted as above and supernatant containing the eluted proteins were taken by aspiration.

2.9 Methanol chloroform precipitation

The eluent from the importin α affinity purification was taken and 370 µl of MQ grade water was added. To this same tube, 400 µl of methanol and 200 µl of chloroform were added and the sample was vigorously vortexed. Following centrifugation (13000 x g, 2 min), a two phase separation occurred. The upper phase

was removed with care taken to avoid disturbing the interphase which contained the precipitated protein pellet. An additional 300 µl of methanol was added and the sample was gently inverted to allow mixing of the phases. The sample was then centrifuged (13000 x g, 15 min) to pellet the protein, after which the entire supernatant was discarded. The tube was allowed to dry at room temperature until no visible moisture was apparent.

2.10 Trypsin digestion of the protein

The protein pellets obtained from the methanol/chloroform precipitation were resuspended in 50 mM ammonium bicarbonate and 1M urea and then 800 ng of trypsin (Promega, Annandale, NSW, Australia) was added. The sample was left shaking overnight at 37^{o}C (650 rpm). The resulting fraction was then centrifuged (13000 xg, 30 min) and the supernatant containing the peptides was placed into a glass vial (Waters, NSW, Australia). The sample was then acidified by the addition of 1 µl 0.5% (v/v) trifluoroacetic acid.

2.11 Liquid chromatography coupled to mass spectrometry

For all experiments, an Ultimate3000 (Dionex, Castle Hill, Sydney) equipped with a ternary low pressure mixing gradient pump (LPG-3600) with a membrane degasser unit (SRD-3600), a temperature controlled pulled-loop autosampler (WPS-3000T) and a temperature controlled column oven with flow manager (FLM-3100) were used. The liquid chromatography experiments were performed using the "pre-concentration" set-up under the following conditions: Nanotrap: AcclaimPepMap, 75 µm ID x 3 mm, 3 µm, 100 Å, Mobile phase A consisted of 0.1% formic acid (FA), whilst mobile phase B contained 80% acetonitrile with 0.1% FA. A Nano-column C18 PepMap100, 75 µm ID x 150 mm, 3 µm, was used. The sample was loaded using a 5 ul/min isocratic gradient. The peptides were eluted with a 2-40% B gradient over 40 min. The oven temperature was set to 35^{o}C. The sample was measured with the "Enhanced Scan Mode" at 8100 m/z per second (which allows mono-isotopic resolution up to four charge stages) polarity positive, Scan Range from m/z 100-3000,

5 spectra averaged and rolling average of 2. The density view of the generated mass spectra was examined in Profile Analysis 4.1 software (Bruker Daltonik GmbH, Bremen, Germany) to select specific signals present in each importin pull-down assay, but absent from the GST control pull down samples for further analysis.

For the collision induced dissociation and electron transfer dissociation (CID/ETD) experiments an amaZon ETD Ion Trap (Bruker Daltonics GmbH, Bremen, Germany) equipped with an online-nano-sprayer spraying from a 0.090 mm o.d. and 0.02 mm i.d. fused silica capillary was used. Fine tuning using the smart parameter setting option (SPS) for 950 *m/z*, compound stability 60% and trap drive level at 100% in normal mode resulted in the following mass spectrometric parameters: dry gas temperature, 180 °C; dry gas, 4.0 L min-1; nebulizer gas, 0.4 bar; electrospray voltage, 4500 V; high-voltage end-plate offset, -200 V; capillary exit, 140 V; trap drive: 57.4; funnel 1 in:100V out 35V and funnel2 in: 12V out 3.3V; ICC target, 500000; maximum accumulation time, 50 ms.

The ETD reaction time was set to 100 ms using a reactant ion charge control of 500000 allowing a maximum accumulation time for the reactant ion of 20 ms. The "Smart Decomposition" was set to "auto". Acquired ETD/CID spectra were processed in Data Analysis 4.1; deconvoluted spectra were further analyzed with BioTools 3.2 software (Bruker Daltonics GmbH, Bremen, Germany) and submitted to Mascot database search (Mascot 2.2.04, Swissprot Rodent database (533049 sequences; release date 11/2011); peptide mass tolerance +/- 0.3 Da, fragment mass tolerance +/- 0.4 Da; enzyme specificity trypsin with 2 missed cleavages considered. The following modifications have been used: Deamidated (NQ), Oxidation (M), Phosphorylation (STY) were set to variable. To exclude false positive identifications, peptides with Mascot scores below 20 were immediately rejected. Then, every spectrum containing the identified protein sequences was manually validated in BioTools (Bruker Daktronics, Bremen, Germany) on a residue-by residue basis using the raw data to ensure accurate and correct annotation.

2.12 RNA extraction

RNA from adult mouse testis was extracted with RNeasy® Mini Kit (QIAGEN) following the supplier's recommendations. All the steps were performed on ice or at 4°C unless otherwise specified. In brief, up to 30 mg of tissue was resuspended in 600 µl of buffer RTL and homogenized by passing the tissue suspension through needles of 25, 27, and 30 gauge sequentially, three times each. To this homogenate, equal volume of freshly prepared 70% ethanol was added and the lysate was mixed by pipetting four times. The lysate was then loaded on an RNeasy Mini spin column and centrifuged for 15 seconds at 10000 x g, and flowthrough was discarded. Subsequently, 700 µl of buffer RW1 was added to the column and spun as above and flowthrough was discarded. The column was washed by addition of 500 µl of buffer RPE and centrifugation as above followed by disposal of flowthrough. To elute the RNA, the column was placed in a fresh collection tube and 40 µl of RNase-free MQ water was added directly to the spin column membrane followed by centrifugation for 1 minute at 10000 x g. the eluate was snap frozen for later use in cDNA synthesis.

2.13 cDNA synthesis

cDNA was synthesized from total adult mouse testis RNA using the *SuperScript III* kit (Invitrogen) following the suppliers recommendations. For each reaction 400 ng of RNA was placed in a master mix containing 2 µl of 10 mM dNTPs (Fisher Biotec), 2 µl of 0.5 µg/ul of Oligo dT (Sigma) and DEPC treated water to a final volume of 26 µl. The reaction was incubated at 65°C for 5 minutes followed by cooling on ice for 1 minute. Subsequently, 4 µl of 5 x first strand buffer, 2 µl of 0.1 M dithiothreitol (DTT), 2 µl of RNase inhibitor, and 1 µl of *SuperScript III* (200U/µl) was added to each reaction followed by incubation at 50°C for 30 minutes. *SuperScript III* enzyme was then inactivated by incubation of the reaction at 70°C for 15 minutes. The obtained cDNA was divided into 5 µl aliquots, snap frozen on dry ice and stored in -80°C for later use. In parallel experiments, a reaction was set in which no *SuperScript III* was included, as a negative control.

2.14 Polymerase chain reaction (PCR)

In each reaction 1µl of cDNA was placed in a master mix containing 2ul of 10 x PCR buffer (Fisher Biotech, Australia), 1.5 µl of 10 mM dNTPs (Promega, Madison), 1µl of 50 mM $MgSo_4$ (Fisher Biotech, Australia), 1.5 µl of 10 µM forward and reverse primers, 2 µl of 0.5 U/µl *Taq* DNA polymerase and sterile MQ water to 20 µl final volume. The reactions were placed on a thermocycler (Thermo Fisher Scientific) with the following cycle conditions: initial denaturation at 94°C for 3 minutes followed by 35 cycles of denaturation at 94 °C for 30 seconds, annealing at 55°C for 30 seconds, amplification at 72°C for 1 minute, and final extension at 72°C for 7 minutes.

2.15 DNA fragment ligation into pGEM-T-easy cloning vector, construct screening and sequencing

pGEM-T-easy system (Promega) was used as cloning vehicle of the amplified fragments. All reagents were supplied as part of the cloning kit by Promega. For each ligation reaction 3 µl of a PCR amplified DNA fragment was placed in a master mix containing 5 µl of 2 x ligation buffer, 1 µl of pGEM-T-easy vector and 1 µl of T4 DNA ligase, followed by incubation at 16°C for 16 hours. Subsequently, 4 µl of the ligation reaction was transformed into *E.Coli* DH5α strain as describe in Section 2.3.1 and grown on a selective (50 µg/ml ampicillin) agar plate. Plasmid DNA was extracted from several colonies using the QIAGEN Mini kit following supplier's recommendations. The obtained plasmid DNA was digested with *EcoRI* restriction enzyme which cuts at 5' and 3' end of the multiple cloning site leading to drop-out of the inserts lacking the *EcoRI* restriction site. Plasmids that produced the expected band pattern upon *EcoRI* restriction digest were sequenced to validate the integrity of the construct. For each sequencing reaction 350 ng of the plasmid DNA was added to a master mix containing 1 ul of the 10 µM pBluescript (pBS) forward primer (5'caggaaacagctatgaccatgat3') designed to a region upstream of the multiple cloning site, 4.5 µl of BigDye terminator buffer (Applied Biosystems) in 20 µl final volume with sterile MQ water. The reactions were placed on a thermocycler (Thermo Fisher Scientific) with the following cycle conditions: initial denaturation at 96°C for 2

minutes followed by 25 cycles of denaturation at 96 °C for 10 seconds, annealing at 50°C for 30 seconds, amplification at 60°C for 4 minute, and final extension at 60°C for 15 minutes. The reaction was precipitated by addition of 1/10 volume of 3 M NaAc (pH 5.2) and 2.5 x volume of absolute ethanol, incubation at room temperature for 45 minutes and centrifugation at 14 x g for 20 minutes. The precipitated DNA was washed with 70% ethanol followed by centrifugation at 14 x g for 5 minutes. The pellet was dried at 65°C for 5 minutes and sent to the Gandel Charitable Trust Sequencing Facility, Monash Medical Centre, Clayton, for electrophoresis.

2.16 RNA probe generation for Mtmr4

A partial sequence corresponding to the *Mtmr4* mRNA was amplified from an adult mouse testis cDNA using the following gene-specific forward and reverse primers and based on the cDNA sequence in NCBI with the accession number of NP_573478.1.
F: 5’ cacagctgactgtgggagaa3’
R: 5’ aaaatcacaggctccaccac3’

The amplified fragment was ligated into a pGEM-T-easy cloning vector (Promega Corp, Madison, WI) following the manufacturer’s recommendations. The correct construct was identified by bacterial colony screen and plasmid sequencing. The construct was then used as a template in a PCR reaction with the following forward and reverse primers.
pBS-F: 5’caggaaacagctatgaccatgat 3’
pBS-R: 5’ tgtaaaacgacggccagtg 3’.

The PCR reaction was set with 2 ng of plasmid DNA with the following cycles. Denaturation, 94°C, annealing, 55°C, and extension, 72°C, 30 seconds each in 25 cycles. The pBS-F and pBS-R primers amplified the SP6 and T7 RNA polymerase binding sites, flanking the target sequence. The obtained amplicon was subsequently used in an *in vitro* transcription reaction which was performed by DIG RNA labelling kit (Roche) following the suppliers recommendations. SP6 and T7 RNA polymerases were used in separate reactions to generate both antisense (T7) and sense (SP6) probes.

The concentration of RNA probes were measured in a dot blot against a range of DIG-labelled RNA of known concentration.

2.17 Northern blot

All the reagents and buffers used in Northern blot method are listed in Table 2.7. All the steps were performed at room temperature unless otherwise specified. The procedure was performed in containers that were washed with wash buffer and autoclaved prior to use. Total RNA from each tissue was isolated by Trizol® (Invitrogen) following the manufacturer's recommendation. The obtained RNA was resuspended in deionized formamide (DIF) and snap frozen on dry ice.

Up to 30 µg of RNA from each tissue was resuspended in equal volume of 2x RNA loading dye and denatured by heating at 65˚C for 10 minutes prior to loading onto the wells of a 1.2% formaldehyde gel. The RNA was subsequently electrophoresized at 25V for 16 hours in MOPS running buffer. At the completion of electrophoresis, the gel was placed in MQ water for 20 min with gentle shaking to remove excess formaldehyde. The RNA was blotted onto a Hybond XL membrane (Amersham, Buckinghamshire, UK) by capillary transfer, utilizing 20xSSC as transfer buffer at room temperature for 16 hours. Following this, the transfer apparatus was dismantled and the membrane rinsed in 2xSSC prior to fixation at 80˚C for 2 hours. The membrane was subsequently pre-hybridized in Ultrahybe hybridization buffer (Ambion, USA) at 68˚C for 1 hour. Five minutes before the end of pre-hybridization period, 25 ng of RNA probe per ml of hybridization buffer was resuspended in 50 µl of DEPC treated MQ and heated at 95˚C for 5 minutes. The diluted probe was then added to the hybridization buffer and incubated for 16 hours at 68˚C overnight. The following day, the hybridization buffer was discarded and the membrane was washed successively in pre-heated (68˚C) 2xSSC and 0.1xSSC for 2x5 minutes and 2x15 minutes, respectively, at 68˚C. The membranes were subsequently placed in wash buffer for 2 minutes at room temperature, followed by incubation in 1x digoxigenin (DIG) blocking buffer (Roche, Mannheim, Germany) for 30 minutes. At the completion of blocking, anti-DIG antibody (Roche) was added to the membranes at 1:1000 dilution and incubated for another 30 minutes. Antibody was discarded and membranes were washed in wash buffer 2x15 minutes. To detect the hybridization,

CDP-Star substrate (Roche) was added to the membrane and the generated chemiluminescent signal was captured by exposing the membrane to an X-ray film.

2.18 In situ hybridization

Table 2.7 lists all the reagent and components of the buffers used for *in situ* hybridization. The experiment was performed on testis sections (Bouin's fixed and paraffin embedded) on glass slides. All containers and boxes used throughout the experiment were washed in wash solution and rinsed with DEPC treated MQ. The steps were performed at room temperature unless otherwise specified.

Testis sections were dewaxed in two changes of histosol, 5minutes each, followed by rehydration in decreasing ethanol concentration of 100%, 95% and 70% with gentle shaking, 5 minutes each. Rehydration was followed by incubation in 0.2M HCL for 20 minutes with gentle shaking. Subsequently, the slides were washed in two changes of DEPC treated MQ for 5 minute each. Following the second wash, sections were circled with PAP pen and incubated with 100 µl of proteinase K for 30 minutes at 37˚C. The proteinase K reaction was stopped by placing the slides in 0.2% Glycine solution for 10 minutes with gentle shaking. Subsequently, slides were incubated in 0.1M TEA solution for 5 minutes with shaking and then washed in two changes of DEPC treated MQ for 5 minutes each. Sections were then incubated with 150 µl pre-hybridization buffer under cover slip for 2 hours at 55˚C. During the pre-hybridization step, the hybridization solution was prepared by addition of heat denatured (10 min at 95˚C) Herring sperm DNA, and tRNA to the pre-hybridization buffer. Just prior to the hybridization, cRNA probes were added to the hybridization buffer and activated by incubation at 65˚C for 5min. The sections were incubated over night at 55˚C with the hybridization solution under cover slip. The following day, slides were washed successively in 2xSSC, 1xSSC, and 0.1xSSC buffer (pre-warmed to 55˚C) for 15 minutes each with shaking at hybridization temperature (i.e. 55˚C). Slides were subsequently washed in buffer 1 for 5 minutes and then incubated in blocking solution for 30 minutes. For probe detection, 1:1000 dilution of anti-DIG antibody (Roche) in blocking buffer was incubated on each section for 1 hour. Sections were washed in two changes of buffer 1 for 15 minutes each with gentle shaking. After wash, BCIP/NBT reagent (Thermo Scientific) was added to the sections in a light restricted

box and incubated at 4˚C. Sections were examined in short intervals to monitor colour development, upon which the reaction was stopped by rinsing the slides in running tap water for 2 minutes. Sections were then counter-stained with Harris Haematoxylin and mounted on a cover slip by aqueous mounting solution. The mounting solution was allowed to dry out at room temperature overnight. The slides were sealed by nail polish before image taking.

2.19 Cell culture maintenance and transfection

COS-7 and HEK 293 cells were generally maintained in a T-25 flask in DMEM media (Invitrogen) at 37°C in presence of 5% CO2. Cells were passaged when 70% to 90% confluent. To split the cells, media was removed from the flask and cells were rinsed with pre-warmed PBS once. Subsequently 750 µl of 0.1% Trypsin (Invitrogen) was added to each flask and incubated at 37°C for 3 and 5 minutes for HEK 293 and COS-7 cells respectively. The trypsin was inactivated by addition of 5 ml of pre-warmed DMEM to the flasks. Cell suspension was centrifuged for 5 minutes at 200 x g and the supernatant media was discarded. The pellet was resuspended in pre-warmed PBS and centrifuged again as above followed by disposal of supernatant PBS. The cell pellet was resuspended in 5 ml of pre-warmed DMEM. Cell number was counted using a haemocytometer and $2x10^5$ cells were dispensed into 4 ml of DMEM in a fresh T-25 flask. For transfection experiments Effectene transfection kit (QIAGEN) was used following the supplier's recommendations. Generally, $5x10^5$ cells were dispensed in a 60 mm petri dish. 24 hours after this, 1 µg of plasmid DNA was mixed with DNA condensation buffer to a total volume of 150 µl, followed by addition of 8 µl of enhancer solution; the mix was vortexed for 1 second and incubated at room temperature for 5 minutes. Subsequently 25 µl of Effectene solution was added to the reaction followed by pipetting 5 x and incubation at room temperature for 10 minutes. During the above incubation, media was removed from the plated cells, which were then rinsed with pre-warmed PBS followed by addition of 4 ml of fresh DMEM media. Subsequently 1 ml of DMEM was added to the transfection mix and was mixed by pipetting 2 x and added to the cells in a drop-wise manner. The transfection was allowed to proceed between 24 to 30 hours.

Table 2.7 reagents and buffers used for *in situ* hybridization (ISH) and Northern blot (NB)

DEPC treated MQ (NB and ISH)	0.1% DEPC in MQ incubated at room temperature overnight, followed by autoclave
Blocking solution (NB and ISH)	1g blocking powder for nucleic acid hybridization and detection (Roche) in 100ml buffer 1
20X sodium saline citrate (SSC) buffer (NB and ISH)	3M NaCl, 340mM Tri-sodium citrate ($Na_3C_6H_5O_7$)
Buffer 1 (NB and ISH)	0.1M Maleic acid, 0.1M NaCl, pH 7.5
Deionized formamide (DIF) (NB)	500 ml of Formamide (Sigma) incubated and stirred with 25 g of AG® 501-X8(D) Resin (Bio-Rad) overnight and filtered
1.2% formaldehyde gel (NB)	1.2 % (m/v) agarose, 7% (v/v) 40% formaldehyde, 1x MOPS in distilled MQ
MOPS running buffer (NB)	20mM MOPS, 5mM CH_3COONa, 1mM Na_2EDTA, pH7
Wash buffer (NB)	0.03% Tween 20 in Buffer 1
RNA running dye (Blue juice) (NB)	50% (v/v) glycerol, 1 mM EDTA, 0.4% (m/v) bromophenol blue
2x RNA loading dye (NB)	2% (v/v) MOPS, 35% (v/v) formaldehyde, 20% (v/v) blue juice, 1% (v/v) ethidium bromide (10 mg/ml)
Herring sperm DNA (ISH)	Solution prepared by Promega (10mg/ml)
Yeast total RNA (tRNA) (ISH)	5 mg of tRNA powder (Roche) in 1ml of 1x Tris/EDTA buffer
Proteinase K (ISH)	1 mg of proteinase K (Roche) in 1ml of 1x Tris/EDTA buffer
0.1 M TEA solution (ISH)	0.1 M Triethanolamine, 0.25% (v/v) acetic acid in EDPC treated MQ
50X Denhardts solution (ISH)	Ficoll, Polyvinylpyrrolidine, BSA (1% w/v each) in EDPC treated MQ
Wash solution (ISH)	100mM NaOH, 10mM EDTA
Tris/EDTA buffer	50mM EDTA, 100mM Tris, pH8
10x TE buffer	100mM Tris/HCL, 10mM EDTA, pH 7.6
Phosphate buffer	200 mM sodium hydrogen orthophosphate, pH 8
Pre-hybridization buffer	50% (v/v) DIF, 14% (v/v) 20x SSC, 33% (v/v) phosphate buffer, 4% (v/v) denhard's solution

Chapter 3-
Analysis of importin protein levels in germ cell maturation

CHAPTER 3 ANALYSIS OF IMPORTIN PROTEIN LEVELS IN GERM CELL MATURATION

3.1 General introduction

Differential expression of importin α family members in different biological contexts at both mRNA and protein level have been the subject of several studies. Some of the findings that illustrate the restricted expression of importin α family members across tissues, during development or within different cell types of a tissue have been presented in Chapter 1 of this thesis (Section 1.1.8.2). These observations are indicative of discrete roles for importin α family members in various cellular environments. Building on the previously documented differential expression of importin family members in rodent testis (Section 1.2.6), we set out to narrate the expression profile of importin proteins in a quantitative manner in two cell types of adult rat testis. Pachytene spermatocytes and round spermatids are the venue in which meiosis and spermiogenesis take place, respectively. Both processes utilize specialized machinery for progression of events that end in either reductive cell division (meiosis in spermatocyte, Section 1.2.4) or extensive morphological transformation (spermiogenesis in spermatids, Section 1.2.5). Thus, measuring the stoichiometry of importins at protein level in these two cell types could be informative about the cellular roles that each family member is more likely to take part in. Furthermore, we set out to gauge a comparison in the relative levels of importin αs to importin β1 in these two cell types.

3.2 Expression profile of importin mRNAs in murine testis

To begin the analysis of importin expression in testis, the publicly available Gene Expression Omnibus (GEO) datasets in the website maintained by the National Centre for Biotechnology Information (NCBI; http://www.ncbi.nlm.nih.gov) was searched. These datasets contain the results of microarray experiments in which the expression profiles of numerous genes have been documented. Table 3.1 contains the ID number of all the datasets that have been used in this search

The objective was to get an indication of the importin α2, α3, α4, and β1 transcript levels during postnatal mouse testis development and in isolated mouse germ cell types. The timepoints of prime importance in this study are day 14 and 20 testis, in which the pachytene spermatocytes and round spermatids appear for the first time in developing testis, respectively (McCarrey, 1993).

Table 3.1. GDS datasets used in this study. GDS605 and GDS606.

Importin	Postnatal testis development	Isolated germ cells of mouse testis
α2	GDS605: 92790_at	GDS2098: 1415860_at
α3	GDS605: 96010_at	GDS2098: 1450386_at
α4	GDS606: 107588_at	GDS2098: 1417974_at
β1	GDS605: 93111_at	GDS2098: 1448526_at

Figure 3.1 depicts the transcript profile of importins in postnatal testis development from birth to adulthood (left) and in pachytene spermatocytes and round spermatids isolated from adult mouse testis (right). The changing expression levels of each importin during testis development is consistent with this family of proteins being involved in regulation of the dynamic events of spermatogenesis (Figure 3.1, left). Amongst those interrogated here, the *importin α2* and *α3* transcripts exhibit particularly distinct changes in synthesis levels during testis development. The *importin α2* mRNA increases constantly from birth to adulthood. In contrast, *importin α3* transcript fluctuates moderately during the first two postpartum weeks, peaks around day 14, and then declines sharply through to adulthood. *Importin α4* and *importin β1* levels in total testis preparations undergo minor variations across development compared to *importin α2 and α3*; levels of both transcripts increases between day 14 to day 20 followed by a steady decline through adulthood.

The levels of these importins in isolated spermatocytes and spermatids display a noticeable correlation with those recorded in the testis development timecourse (Figure 3.1, right). Firstly, the increase in the transcript of *importin α2* after day 20, when round spermatids appear is consistent with the measurement of higher levels of this transcript in spermatids than in spermatocytes (Figure 3.1, right). On the other

Figure 3.1 Profiles of *importin* mRNA in developing mouse testis and germ cells

Graphs depict the dynamic transcript profiles of four *importins* (*α2*, *α3*, *α4*, and *β1*) across testis development time-course (left) and in isolated pachytene spermatocytes (S'cytes) and round spermatids (S'tids) isolated from adult mouse testis (right). The position of the cell types (see bottom for key) on top left graph correspond to the time point at which these germ cells appear for the first time in the developing mouse testis. Error bars represent the standard deviation of the mean (SDM).

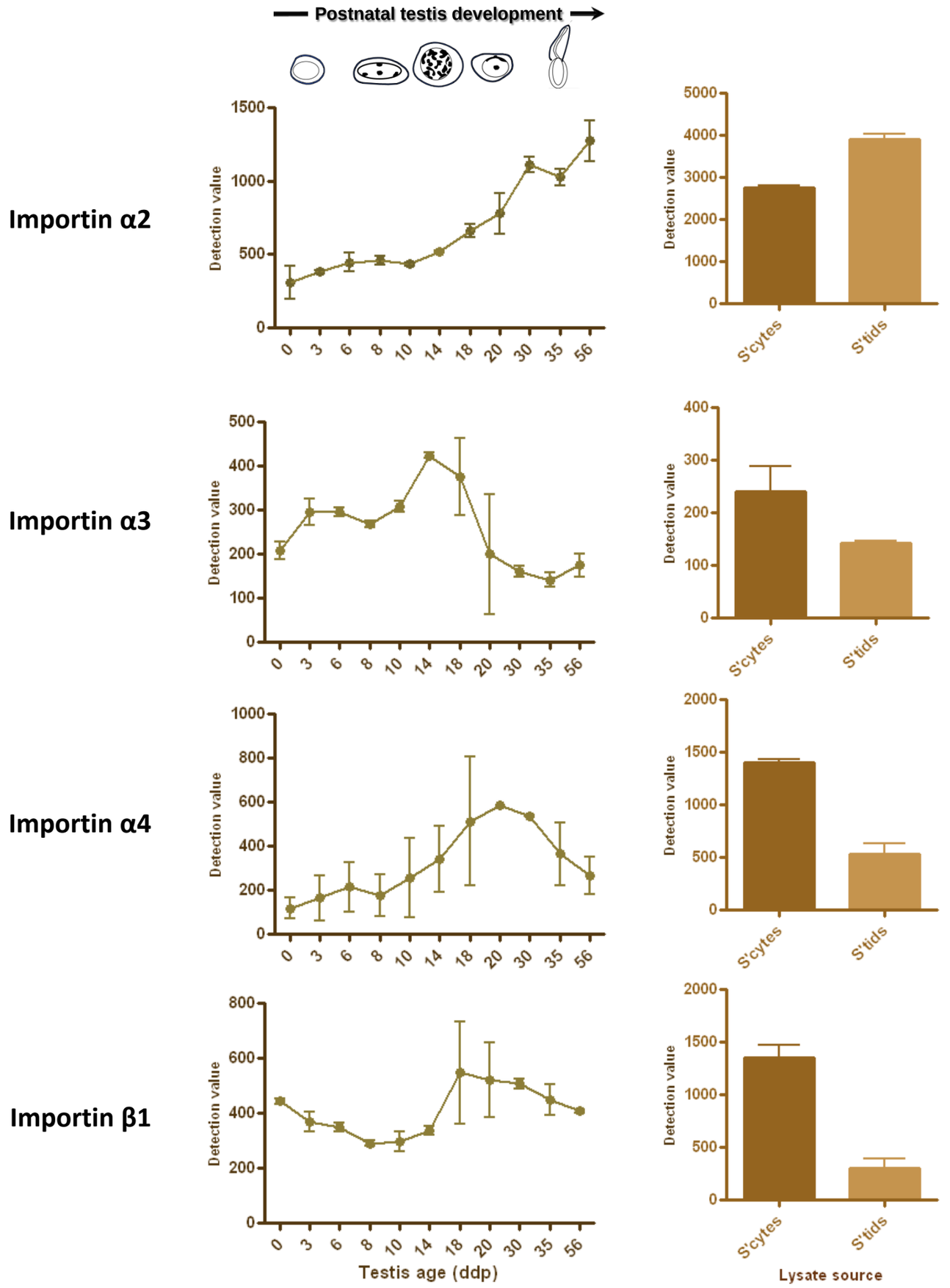
Postnatal testis development
Importin α2
Importin α3
Importin α4
Importin β1
Detection value
Testis age (ddp)
S'cytes
S'tids
Lysate source
Undifferentiated spermatogonia
Differentiated spermatogonia
Pachytene spermatocyte
Round spermatid
Spermatozoon

hand *importin α3, α4* and *β1* transcripts were shown to be lower in spermatids than in spermatocytes, consistent with an overall decrease in mRNA level in testis from day 20 onward. These partial associations are a valuable demonstration that this subset of importins undergoes regulated transcription during testis development and germline maturation; however, they are merely indicative, since a developing testis is increasingly populated by different cell types that contribute to the overall measurement. Furthermore, since the function of genes is exerted through proteins, examination of importin expression at the protein level is of prime importance in understanding the specific roles of this protein family in spermatogenesis. Thus analysis of the importin proteins levels in isolated germ cells of the adult rodent testis was undertaken.

3.3 Germ cell isolation

To obtain highly enriched populations of spermatocytes and spermatids, four adult rat testes were dissociated into single cell suspension by mechanical chopping and enzymatic digestion (Figure 3.2, A, top panel). The cell suspension was resolved into several fractions (1, 2, 3, 3', 4, and 5) based on cell size by centrifugal elutriation. Light microscopic examinations identified fraction 3' as the fraction that predominantly contained round spermatids and fraction 5 as the fraction that predominantly contained pachytene spermatocytes (Figure 3.2, A, middle panels). On average, 3.4×10^7 spermatocytes and 1.1×10^8 spermatids were obtained by each elutriation run. The range of cell number obtained for spermatocytes was between 2.1×10^7 and 4.6×10^7, and for spermatids between 8.1×10^7 and 1.8×10^8 cells. The two fractions containing pachytene spermatocytes (fraction 5) and round spermatids (fraction 3') were further resolved based on the cell density by Percoll density gradients (Figure 3.2, A, bottom panels). On average 1.6×10^7 pachytene spermatocytes and 5.9×10^7 round spermatids were recovered at the end of each Percoll density gradient purification. The range of isolated cell numbers for spermatocytes was 1.3×10^7 to 1.9×10^7, and for spermatids was 4.2×10^7 to 7×10^7 cells.

3.4 Purity determination of isolated germ cells

To determine the purity of the obtained cell populations 1 x 10^6 cells from each fraction were prepared for histological analysis by fixation in Bouin's and were embedded in 2% agar, then sectioned and stained with Haematoxylin to yield differential nuclear staining based on chromatin density and size for cell type identification (Russell et al., 1999) (Figure 3.2, B). Upon microscopic examination, the spermatocyte fraction (Figure 3.2, B, left) was observed to be composed predominantly of cells with a large and dense nucleus as evident by strong and dark staining of the chromatin. In the spermatid fraction (Figure 3.2, B, right), the nucleus appeared smaller, with a less dense chromatin structure. Staining of the acrosome and proacrosomal granules was also considered as distinguishing feature of spermatids. Based on these characteristics of nuclear morphology and cell size, cells in each fraction were assigned as either correct cells for that fraction (i.e. spermatocytes for F5, or spermatids for F3') or impurities; cells in which the ambiguity of nuclear morphology prevented allocation to any of the above categories were counted as unknown. The percentage of purity in each fraction was estimated by dividing the number of cells correctly assigned to the fraction (e.g. spermatocytes in F5) to the total number of the cells counted in that fraction. It should be noted that cells that were assigned as unknown in each cell population were not included in purity determination to avoid inconsistency. Following this method the average percentage purity of spermatocyte fractions was calculated to be ~95% and that of spermatid fractions to be ~90%.

The purity of these cell fractions was also scrutinized by examining the expression of cell-specific markers. Lysates prepared from adult rat testis, spermatocyte and spermatid cell fractions were compared by Western blotting and in each experiment, detection of α-tubulin served as a control for equal loading of protein lysates between lanes (Figure 3.2, C).

Synaptonemal complex protein 3 (SCP3) is a constituent of the lateral element of the synaptonemal complex which facilitates synapsis of homologous chromosomes during meiosis (Sanderson et al., 2008). Distinct signals corresponding to two SCP3

isoforms were detected in total adult rat testis lysate. As expected, the signal intensity was enhanced considerably in lysate of isolated pachytene spermatocytes. The round spermatids lysate yielded a weak but detectable SCP3 signal (Figure 3.2, C left). The presence of SCP3 protein in the lysate of spermatids fraction may arise from cell fraction impurities or from residual SCP3 in spermatids. Proacrosin binding protein (ACRBP) is a haploid germ cell marker, which co-localizes with acrosin in the acrosomal complex (Baba et al., 1994). Spermatids and adult rat testes lysates produced a strong and intermediate signal corresponding to ACRBP, respectively. In spermatocytes lysate however, no signal of ACRBP was observed (Figure 3.2, C, middle), demonstrating the lack of spermatids contamination in the spermatocytes fraction.

The promyelocytic leukemia zinc finger protein (PLZF) is a spermatogonia-specific transcriptional repressor with a molecular mass of ~90 kDa (Costoya et al., 2004). Upon Western blot analysis (Figure 3.2, C, right), a band of 90 kDa was detected in total adult rat testis lysate but absent from both spermatocyte and spermatid lysates. This observation indicates the absence of spermatogonial contamination in the purified post-mitotic cell fractions. Several attempts to check for the presence of a Sertoli cell marker (Sox9) in these lysates failed to produce any signal, even in total adult rat testis (data not shown). Given that Sertoli cells constitute ~3% of an adult testis cellular composition, the levels of this protein may fall below the detection level by Western blotting. Also, the paucity of this cell type in adult testis (i.e. the source of isolated germ cells) eliminates the concerns about disproportionate contamination by Sertoli cells in the purified germ cells.

Taken together, the results of histological and cell-specific protein expression analyses indicate that the obtained cell fractions are of high purity and suitable for examination of expression pattern of genes in spermatocytes and spermatids.

3.5 Recombinant protein purification

Mouse importin α2, α3, α4 and β1 proteins were purified as GST-fusion recombinant proteins, by bacterial expression and affinity purification through the N-terminal GST

Figure 3.2 Germ cell isolation and purity assessment

A. Four testes from two adult rats were dissociated (top panel) and resolved into several fractions based on cell size by centrifugal elutriation (middle panel). Fractions containing pachytene spermatocytes (middle panel, left) and round spermatids (middle panel, right) were further resolved based on cell density on a Percoll gradient (bottom panels).

B. The purified pachytene spermatocytes and round spermatids were fixed in Bouin's fixative, embedded in paraffin followed by sectioning and haematoxylin staining. The images were taken at 400 x magnification. In each image, the green arrow points to an example of a correct cell type for that fraction (i.e. spermatocyte or spermatid), the red arrow points to a cell that has been assigned as an impurity, and the black arrow points to an example of a cell with a nuclear morphology which does not allow accurate assignment of the cell to either of these categories.

C. Forty µg of the lysates from adult rat testis (AdRT), pachytene spermatocytes (S'Cytes) and round spermatids (S'Tids) were separated on a 10% polyacrylamide gel and transferred to a nitrocellulose membrane. The membranes were then probed with antibodies against SCP3 (left), ACRBP (middle), and PLZF (right). Each membrane was subsequently probed with an anti α-tubulin antibody to visualize the equal protein loading in each lane.

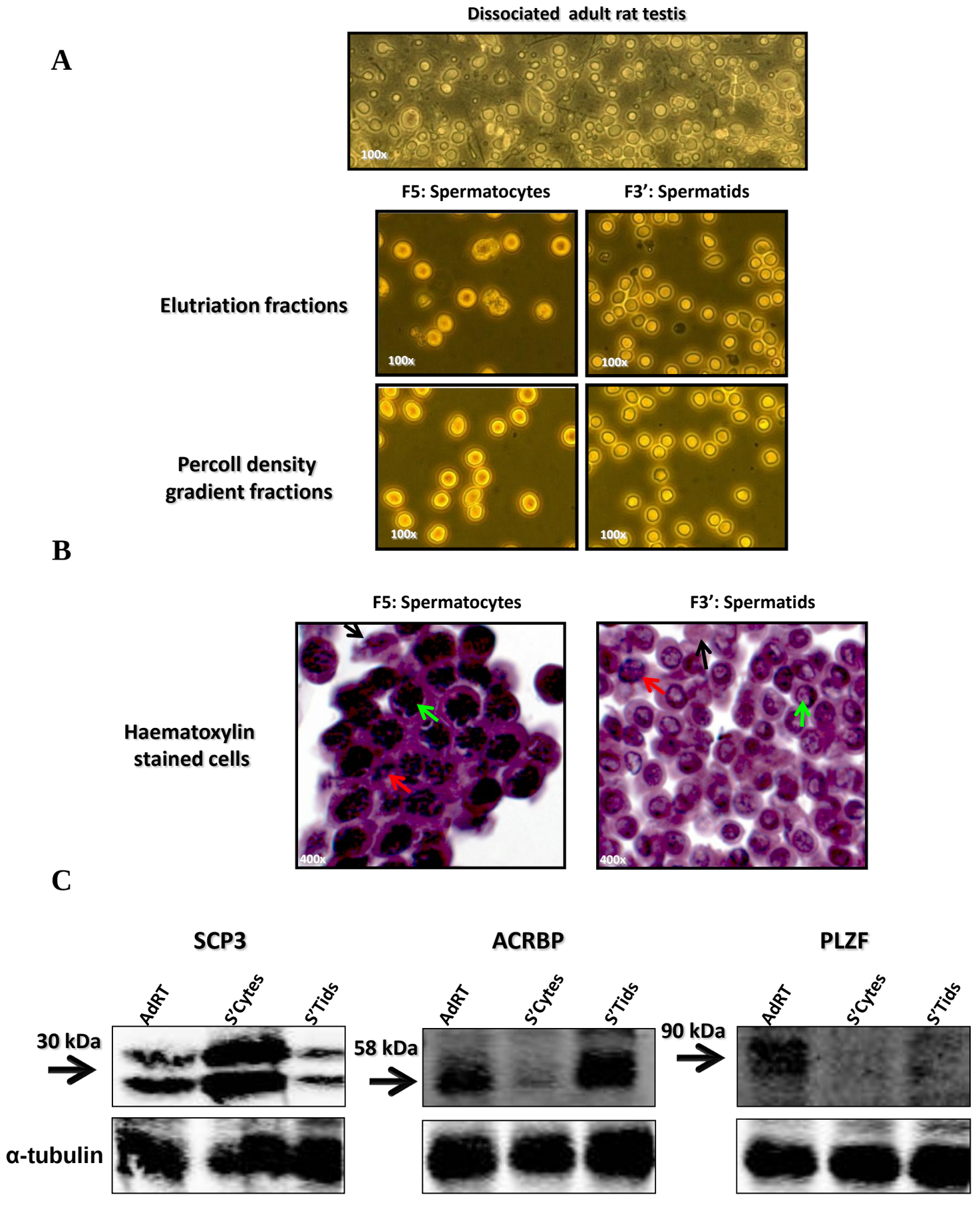
A
Dissociated adult rat testis
100x
F5: Spermatocytes
F3': Spermatids
Elutriation fractions
Percoll density gradient fractions
100x
B
F5: Spermatocytes
F3': Spermatids
Haematoxylin stained cells
400x
C
SCP3
ACRBP
PLZF
AdRT
S'Cytes
S'Tids
30 kDa
58 kDa
90 kDa
α-tubulin

tag. These proteins exhibited differences in the total yield and purity for each protein. A protein quality estimate was obtained by running the proteins on a polyacrylamide gel and staining the gel with coomassie blue followed by scanning of the gel with odyssey; the purity of each recombinant protein was calculated by dividing the signal intensity of the target protein (i.e. protein band of the expected size) to the signal intensity produced from all bands in the sample, Table 3.2. In general, importin α2 and β1 appeared to have both higher yield and integrity. Importin α3 and α4 proteins on the other hand, were of lower concentration and these samples contained multiple bands indicative of degradation. To measure the protein concentration, different volumes of each recombinant importin protein were separated by SDS-PAGE next to a range of BSA concentrations, followed by coomassie blue staining. Scanning of the stained gel by odyssey system produced signal intensities for the BSA concentration gradient bands which allowed the generation of a standard curve through which the measured signal intensities of the target recombinant proteins were converted into the concentration of that protein. This approach for protein concentration measurement was favoured over absorbance reading to avoid the contribution of degraded protein fragments and impurities to the measured concentration of the intact protein.

Figure 3.3 demonstrates the images of the stained gels used in measuring the recombinant importins concentration and purity. The standard procedure included utilization of 1 to 10 µg of BSA and different volumes of recombinant protein. Following this method, the concentration of GST-importin α2 was measured to be 2.91 µg/µl, the concentration of GST-importin α3 was shown to be 0.025 µg/µl and those of GST-importin α4 and GST-importin β1 were 0.11 µg/ µl and 0.82 µg/ µl, respectively.

Table 3.2 Quantity and quality of recombinant proteins

Fusion protein	Molecular mass (kDa)	Concentration (µg/µl)	~% purity
GST-Importin α2	85	2.91	80
GST-Importin α3	85	0.025	5
GST-Importin α4	85	0.11	20
GST-Importin β1	125	0.82	80

Figure 3.3 Recombinant protein concentration and purity measurement

Different volumes of GST fused importin α2 (top left), α3 (top right), α4 (bottom left) and β1 (bottom right) were separated on a 10% SDS-PAGE gel alongside known amounts of BSA. The gels were stained with coomassie blue and scanned using the Odyssey V.3.0. The red arrow points towards the intact GST-fused importin in each gel and the yellow arrow points towards the degraded products or impurities.

GST-importin α2: 2.91 µg/µl

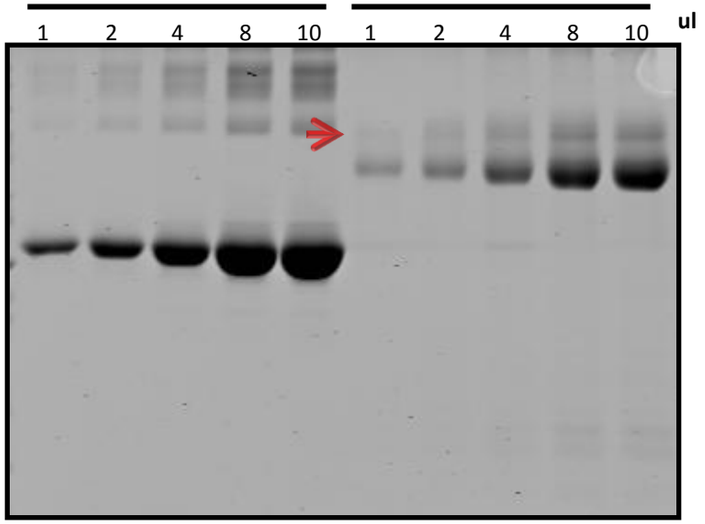

GST-importin α3: 0.025 µg/µl

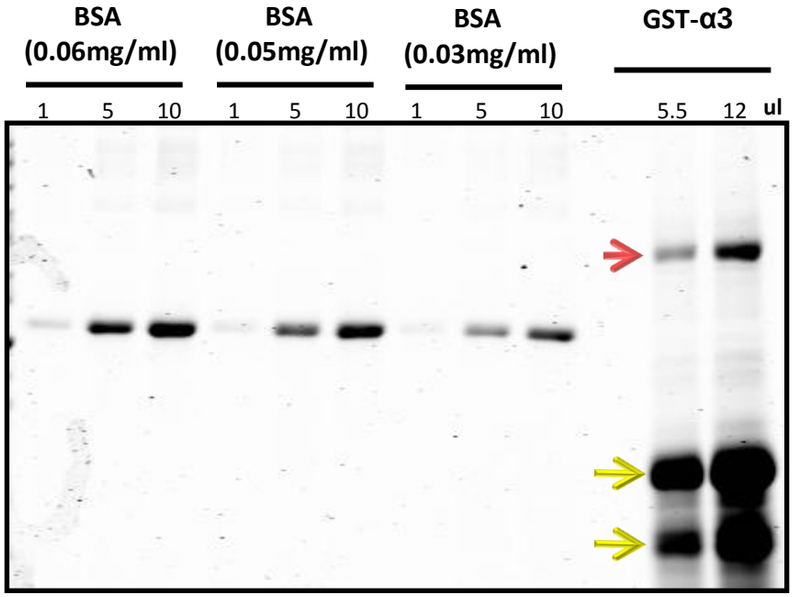

GST-importin α4: 0.11 µg/µl

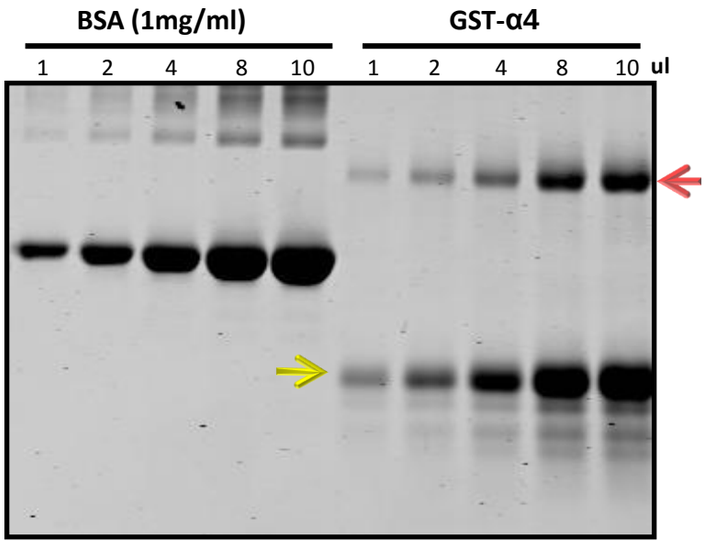

GST-importin β1: 0.82 µg/µl

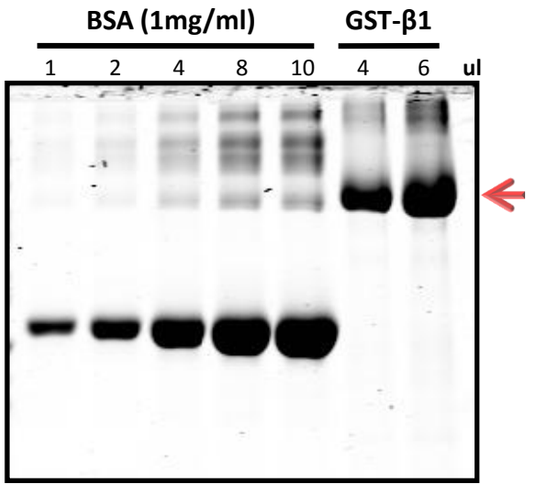

3.6 Measurement of importin levels in germ cells

To begin analysis of the expression profiles of importin proteins in germ cells, Western blot detection of importin α family members (α2, α3, and α4) and importin β1, was performed using specific antibodies to each protein in lysates prepared from three independently isolated populations of spermatocytes and spermatids from adult rat testes, Figure 3.4. Adult rat testis lysate was used as positive and internal control for each importin. For detection of each importin, a range of known amounts of recombinant proteins were run alongside the lysates. By plotting the signal intensities of the recombinant proteins against their concentrations, a standard curve was generated from which, the signal intensities of the endogenous proteins were interpolated to obtain the concentration of the endogenous importins in a given lysate. The obtained concentration of each protein was then converted to ng/mg of lysate (Table 3.3); these conversions are depicted graphically in Figure 3.5. In each experiment, detection of α-tubulin served as a control for equal loading of proteins in each lane, which generally produced consistent values between samples. To account for the variations in loading, the obtained concentrations of the endogenous importins were standardized to the lowest α-tubulin signal in each blot. It should be noted that this adjustment leads to a general, yet uniform reduction in the deduced concentration of each importin. Another prominent issue to be considered in the quantification of concentration of each protein is the differences in the background in lanes loaded with total cellular lysates compared to the lanes loaded with recombinant proteins. In general, the lanes in which endogenous importins were detected from cellular lysates produced a higher background than lanes in which the recombinant proteins were detected. Given that in the quantification method, the background is subtracted from total collected intensity from each band, in general the inferred concentration of an endogenous protein is reduced according to the background relative to that lane.

When the expression of importin α2 was examined, a striking variation in the amount of endogenous protein was evident in lysates prepared from different sources. Spermatocytes lysate consistently produced strong band of importin α2 compared to that of permatids and adult rat testis, both of which produced detectable but weak signals corresponding to the endogenous importin α2 (Figure 3.4, A). Estimation of

the concentration measurement of importin α2 showed that there exists 673 ng of importin α2 in 1 mg of spermatocytes lysate, while the same lysate amount from spermatids and adult rat testis contained 308 and 289 ng of importin α2 respectively (Table 3.3, Figure 3.5, A). Therefore the relative abundance of importin α2 in spermatocytes lysate equates to ~2.1 times that of both spermatids and adult rat testes lysate.

The pattern of importin α3 levels mimicked that of importin α2; however, a smaller magnitude in differences between lysate sources was observed. Importin α3 levels were highest in spermatocytes, intermediate in spermatids and lowest in the adult rat testis lysate (Figure 3.4, B). The concentration of importin α3 in 1 mg of spermatocytes, spermatids and adult rat testis lysates were measured to be 264 ng, 190 ng, and 182 ng, respectively (Table 3.3, Figure 3.5, B). Thus importin α3 levels are lower than importin α2 by ~1.6 fold in adult rat testis and spermatids lysates, and ~2.5 fold in spermatocytes lysate.

The expression pattern of importin α4 differed from both importin α2 and importin α3 in that importin α4 appeared to have the same levels in spermatocytes and spermatids (Figure 3.4, C). The concentration of importin α4 based on the generated standard curve is 90 ng, 172 ng, and 173 ng in 1 mg of adult rat testis, spermatocytes and spermatids lysates, respectively (Table 3.3, Figure 3.5, C). The ratio of importin α4 to importin α3 in adult rat testis and spermatocytes lysate is 1:2 and 1:1.5, respectively; the ratio of these two importin αs in spermatid lysate is ~1:1.1. Importin α4 is also in lower abundance than importin α2 in all of the examined lysates; the molar ratio of importin α4 to importin α2 is ~1:3.2, 1:3.9 and 1:1.7 in adult rat testis, spermatocytes and spermatids lysates, respectively.

When expression of importin β1 was examined in the germ cells, both spermatocytes and spermatids were shown to contain higher amounts of the protein than total adult rat testis lysates, but with a lower magnitude in difference compared to importin αs (Figure 3.4, D). Furthermore, the difference in the expression of importin β1 between spermatocytes and spermatids was a marginal 1:1.06 ratio with spermatocytes containing 332 ng and spermatids containing 354 ng of importin β1 in 1 mg of the

Figure 3.4 Detection of importin protein levels in testicular germ cells

In separate experiments, lysate from adult rat testis, or lysates from 3 independently isolated spermatocytes and spermatids were separated on a 10% SDS-PAGE gel; on each gel a range of known amounts of a recombinant importin protein were also loaded. The proteins were transferred to nitrocellulose membrane and each membrane was probed with antibody to the importin whose recombinant protein was loaded on the gel. In each experiment, detection of α-tubulin served as a loading control for lanes on which cellular lysates were loaded. Negative control included probing the membranes containing lysates of adult rat testis, spermatocytes and spermatids with secondary antibody only (bottom two panels).

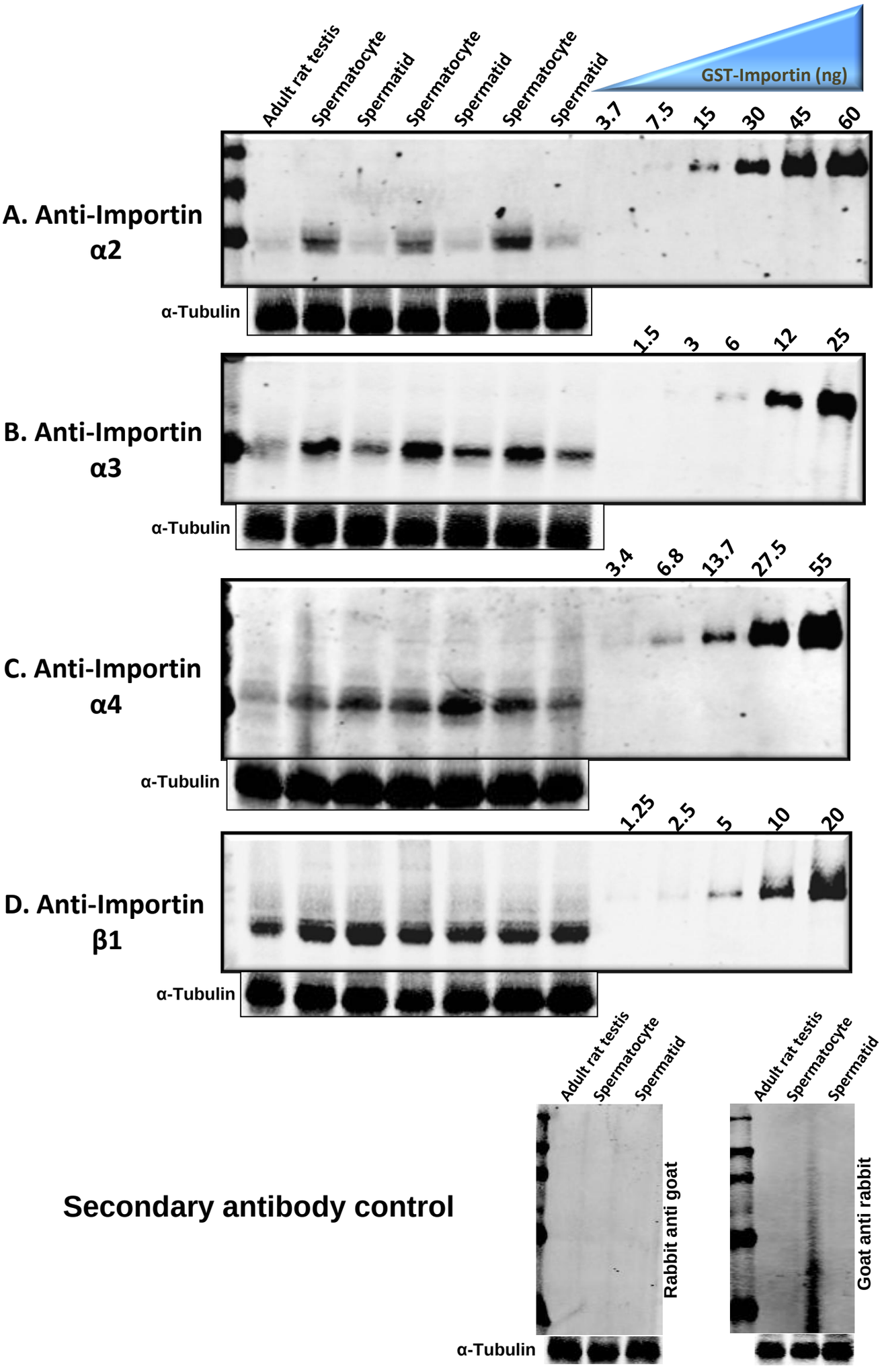
Adult rat testis
Spermatocyte
Spermatid
Spermatocyte
Spermatid
Spermatocyte
Spermatid
GST-Importin (ng)
3.7
7.5
15
30
45
60
A. Anti-Importin α2
α-Tubulin
1.5
3
6
12
25
B. Anti-Importin α3
α-Tubulin
3.4
6.8
13.7
27.5
55
C. Anti-Importin α4
α-Tubulin
1.25
2.5
5
10
20
D. Anti-Importin β1
α-Tubulin
Secondary antibody control
Adult rat testis
Spermatocyte
Spermatid
Rabbit anti goat
α-Tubulin
Adult rat testis
Spermatocyte
Spermatid
Goat anti rabbit

lysates (Table 3.3, Figure 3.5, D). The evident overlap of the error bars in Figure 3.5, D, indicating the standard deviation of the mean (SDM) combined with the negligible difference in the ratio of importin β1 between spermatocytes and spermatids is suggestive of a uniform expression of importin β1 in these two germ cells.

Examination of Figure 3.5 shows that the level of importin α family members between different germ cells have a more noticeable fluctuations than importin β1 levels; this observation suggests that the classical nuclear import in germ cell maturation is primarily governed by cargo receptors (i.e. importin α) rather than transport factor (i.e. importin β1). The estimated concentration of importins in 1 mg of adult rat testis, spermatocytes, and spermatids lysates are graphed in figure 3.6 with the aim of highlighting the abundance of all examined importins in a given lysate. In general, importin α2 appears to be the most abundant of all. Its levels are between ~1.5 to 2 fold higher than both α3 and α4 in every examined lysate. Interestingly importin α2 levels are more than 2 fold higher than importin β1 in spermatocytes lysates (Figure 3.6, B), but noticeably lower than importin β1 in spermatids lysate. Collectively, however, importin α family members appear to outnumber importin β1 to a ratio of 2.5 to 1.

Table 3.3 Concentration of importin proteins (ng/mg) in different testicular lysates

	Adult rat testis	***Spermatocytes***	***Spermatids***
Importin α2	289	673	308
Importin α3	182	264	190
Importin α4	90	172	173
Importin β1	256	332	354

Figure 3.5 Quantification of importin levels in different testicular cell lysates

The graphs show the estimated concentration (ng/mg) of each importin protein in lysates prepared from adult rat testis (AdRT), pachytene spermatocytes (S'cyte) and round spermatids (S'tid)-(Table 3.3). Histograms were generated by GraphPad Prism V.5; the error bars indicate the standard deviation of the mean (SDM) for three biological replicates.

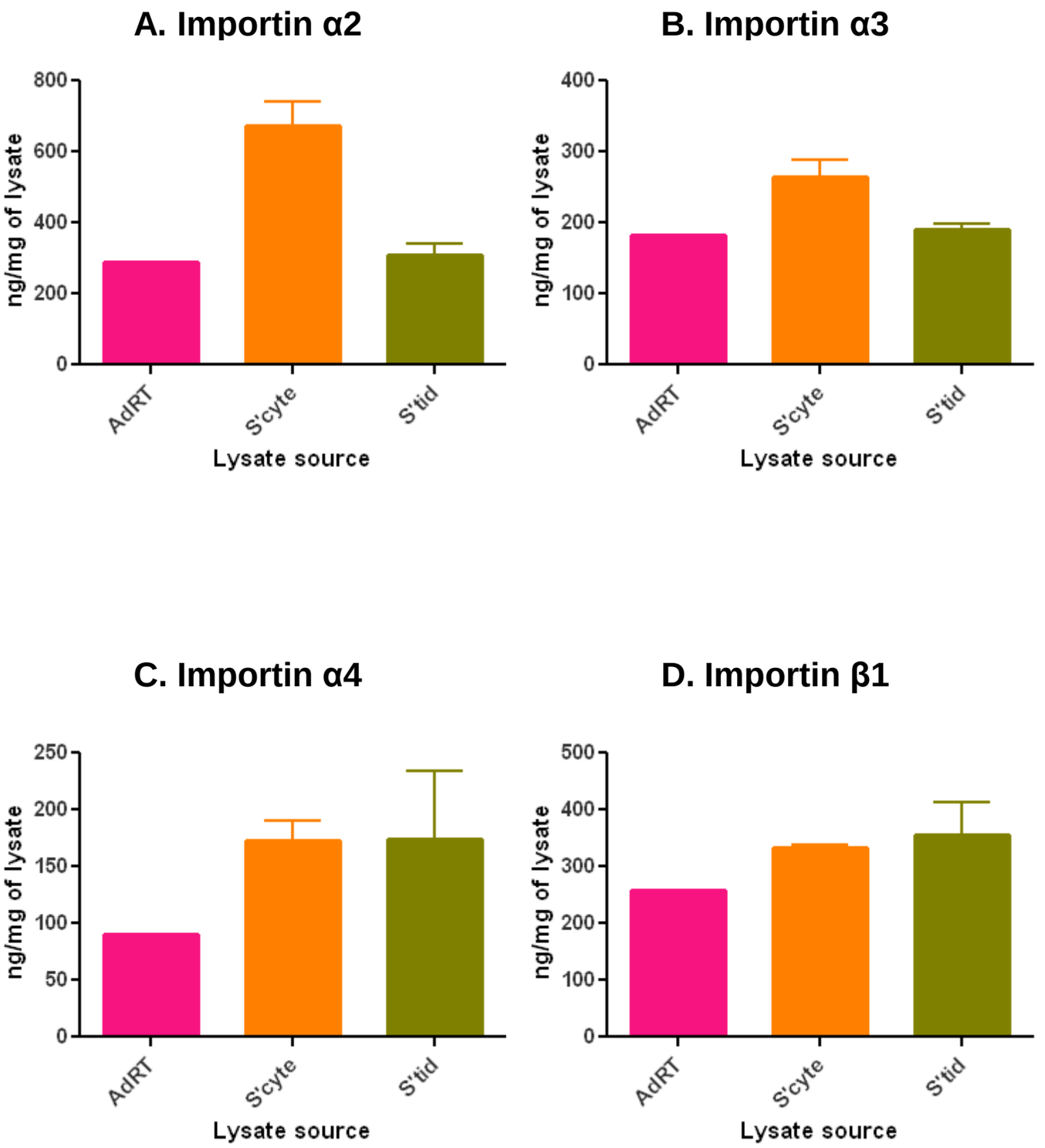
A. Importin α2
ng/mg of lysate
800
600
400
200
0
AdRT
S'cyte
S'tid
Lysate source
B. Importin α3
ng/mg of lysate
400
300
200
100
0
AdRT
S'cyte
S'tid
Lysate source
C. Importin α4
ng/mg of lysate
250
200
150
100
50
0
AdRT
S'cyte
S'tid
Lysate source
D. Importin β1
ng/mg of lysate
500
400
300
200
100
0
AdRT
S'cyte
S'tid
Lysate source

Figure 3.6 Comparison of different importin levels within a testicular lysate

The graphs show the estimated concentration (ng/mg) of importin α2, importin α3, importin α4 and importin β1 in lysates prepared from adult rat testis (top), pachytene spermatocytes (middle) and round spermatids (bottom). The values are those listed in Table 3.3 and the histograms were generated with GraphPad Prism V.5

A. Adult rat testis

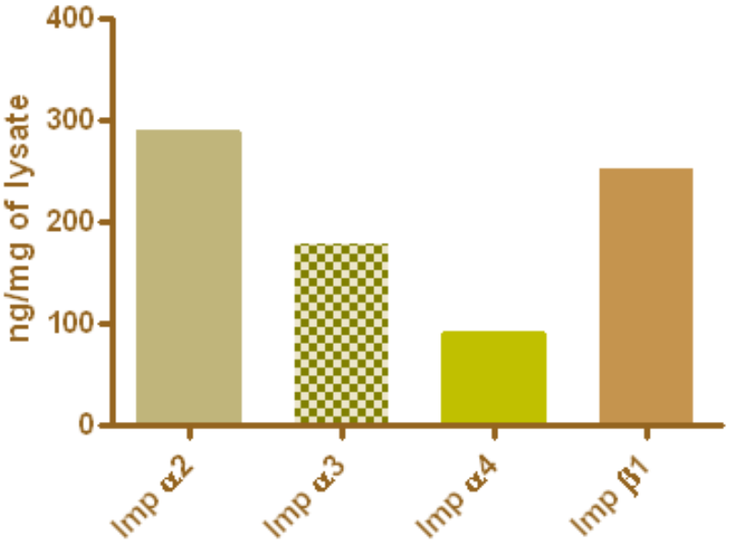

B. Spermatocyte

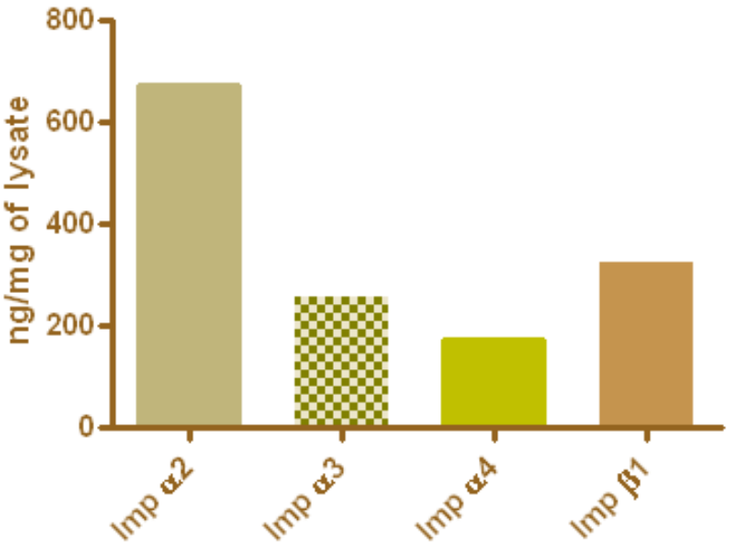

C. Spermatid

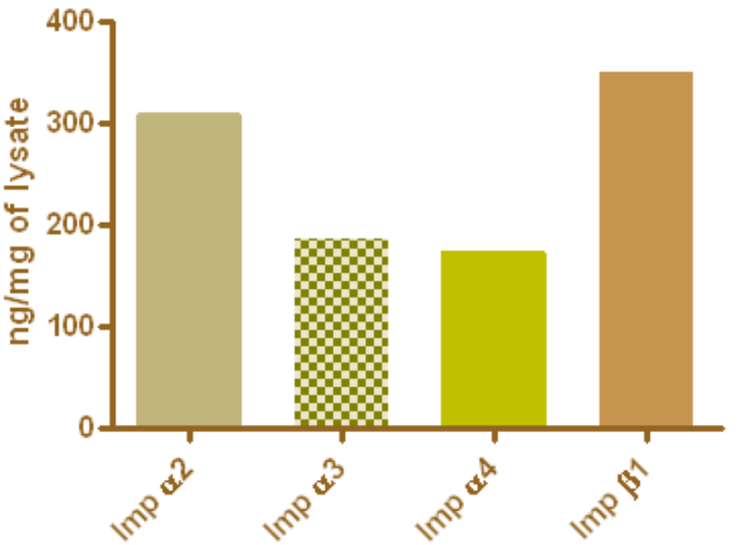

3.7 Concluding remarks

The objective of the work presented in this Chapter was to examine the levels of classical nuclear import receptors during a key cellular transition of spermatogenesis. Pachytene spermatocytes and round spermatids were isolated from adult rat testis by centrifugal elutriation and Percoll density gradient to purity levels of greater than 90%. Western blot detection of importins α2, α3, α4 and β1 in cell lysates, run alongside a range of recombinant proteins of known concentrations, provided evidence for the regulated expression of these proteins in these testicular cells and allowed the estimation of their comparative stoichiometry. Every importin protein examined here, was more abundant in lysates of isolated spermatocytes and spermatids than in a lysate of total adult rat testis. This indicates that importin proteins are involved in major cellular processes specifically relevant to germ cell maturation, such as division and differentiation (discussed further in Chapter 6). Furthermore, individual importin α family members appear to be present at different levels in spermatocytes and spermatids, while importin β1 levels are uniform. Based on the quantity estimations, importin α2 is the most abundant of all importin α family members examined here. Interestingly, importin α family members exist at a higher molar concentration than importin β1 in every testicular lysate examined.

There has been no previous study in which the synthesis level and stoichiometry of several importin proteins in a developmental context had been delineated. Thus, the findings presented in this Chapter offer a significant advance in knowledge towards understanding how regulated expression of nucleocytoplasmic transport machinery components can affect cell fate during development. In order to accumulate further evidence for differential roles of importin α family members in spermatogenesis, we undertook a proteomic approach to identify binding partners for several importin α family members in testicular germ cells.

Chapter 4-
Proteomic analysis of importin α binding partners in germline: α-importome in spermatogenesis

CHAPTER 4 PROTEOMIC ANALYSIS OF IMPORTIN A BINDING PARTNERS IN GERMLINE: A-IMPORTOME IN SPERMATOGENESIS

4.1 General introduction

In recent years, the protein composition of the mammalian testis has come under increasing examination through several proteomic analyses. These have produced repositories of proteins that are present in testicular cell subsets, facilitating a better understanding of the molecular mechanisms that underpin male germ cell maturation. Examples of such studies include the identification of proteins from spermatogonia isolated from immature rats (Com et al., 2003), spermatids isolated from adult mice (Guo et al., 2010) and spermatozoa obtained from both mouse and rat epididymis (Baker et al., 2008a; Baker et al., 2008b). Each of these studies has led to the identification of many testis-specific and novel gene products which are potentially crucial for male fertility, and which could provide potential targets for development of contraceptive products.

An indispensable cellular process that underlies differentiation and transformation is nucleocytoplasmic transport. As described in Section 1.1.5, the importin α family of proteins are mediators of nuclear import through their specific interactions with cNLS motifs in cargo proteins. Supported by the observations regarding the differential expression of importin α family members in pachytene spermatocytes and round spermatids (Chapter 3) we hypothesized that importin α family members serve spermatogenesis through selective cargo binding in germ cells of different developmental stages. Previous attempts have uncovered several binding partners of different importin α family members in spermatogenesis, through yeast two hybrid screening of the adult mouse testis library (Ly-Huynh et al., 2011), and co-immunoprecipitation from germ cells of the adult rat testis (Miyamoto et al., 2013). The aim of this study is to define a comprehensive α-importome by identifying the binding partners of importin α2, α3, and α4 in highly enriched populations of rat pachytene spermatocytes and round spermatids through recombinant protein pull-down of cell lysates and mass spectrometric analysis, as shown in Figure 4.1. The

Figure 4.1 Schematic diagram of pull-down experimental strategy

The figure depicts the experimental scheme applied to identify the binding partners of importin α family members in developing germ cells. The total cellular lysates from spermatocytes and spermatids were incubated with immobilized GST-importin α proteins on GSH sepharose beads. The bound fractions (represented as X and Y) were then eluted followed by trypsin digestion and mass spectrometric analysis for peptide identification.

Isolation of primary spermatocytes and spermatids from adult rat testes

Pachytene spermatocytes

Round spermatids

Total cell lysate

Pull-down of importin α binding proteins in cell lysates with recombinant importin α proteins

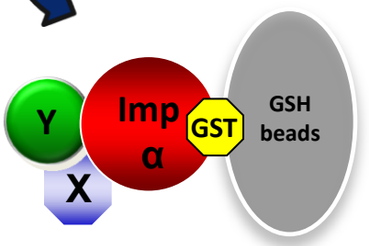

Immobilized importin α on GSH beads

Mass spectrometry analysis for identification of importin α binding candidates

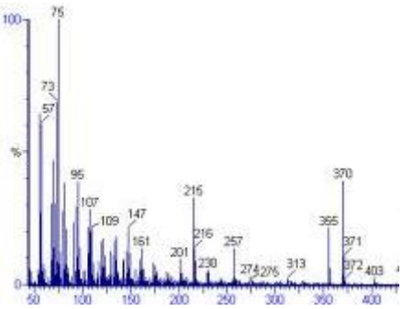

predicted outcome is that distinct proteins would be found to bind each importin, with cargoes of each importin differing between germ cell subtypes.

4.2 Recombinant importin α NLS binding validation

In vitro solution binding assays were performed to validate the cNLS-binding activity of purified recombinant importin α proteins (Figure 4.2, A). In addition to GST-fused importin α2, α3 and α4, a GST-fused mutant form of importin α2 (ED-mutant) which is defective in NLS binding was also included in this assay. This mutant has reduced NLS binding capacity as a result of point mutations in both major and minor NLS binding grooves that converts E_{389} to R and D_{189} to K (Gruss et al., 2001). This mutant of importin α is to be used in the pull-down experiments (Section 4.4). In each experiment, 300 ng of both bait (GST-importin α) and target protein (T-ag-NLS-GFP) was incubated with GSH beads in a final 100 µl volume of transport buffer. To control for the binding specificity of the target proteins to bait proteins (i.e. importin α), either GST alone or no bait was used in two separate and parallel reactions. To control for the binding specificity of importin α proteins to the NLS portion of the target protein, T-ag-R-NLS-GFP, encoding the reverse sequence of the T-ag-NLS fused to GFP (Section 2.5), was used in a parallel reaction. The bound fractions were eluted from the beads, and the eluate was run on an acrylamide gel. The gels were either stained with coomassie blue for detection of bait proteins or transferred to a membrane and probed with anti-GFP antibody for detection of the target proteins.

T-ag-NLS-GFP was pulled-down efficiently by all recombinant importin αs except the importin α2-ED mutant, as evident by strong bands upon immunodetection of the eluate with anti-GFP antibody (Figure 4.2 B). In contrast, T-ag-R-NLS-GFP was detected in the pull-down products as a very faint band. The weak signal corresponding to T-ag-R-NLS-GFP in the pull-down products is not due to the activity of importin α binding, since bands of the same intensity were produced by pull-down of this target with GST only. Thus the capacity of recombinant importin αs to bind NLS cargo is specific.

Figure 4.2 Validation of importin α cNLS binding activity

A. Schematic diagram of the *in vitro* solution binding assay. A recombinant protein was immobilized on GSH beads as bait (in this case, an importin α fusion protein with a GST tag), followed by addition of the target protein. Bound materials were eluted from the beads and the composition of the eluate was examined by SDS-PAGE Western blotting.

B. GST-importin α3 and α4 (top panel) and GST-importin α2 and its ED mutant form (bottom panel) were each immobilized on GSH sepharose beads, followed by addition of the T-ag-NLS-GFP (left) or T-ag-R-NLS-GFP (right). For each reaction, GST only or no bait was immobilized on the beads as negative controls. A fraction of the eluate was run on an acrylamide gel and was either stained with coomassie blue (top row in each panel) for detection of the bait protein or transferred to a nitrocellulose membrane (bottom row in each panel) followed by probing with anti-GFP antibody for detection of the target protein. Asterisks indicate the reactions in which the target has been pulled-down by the bait.

A

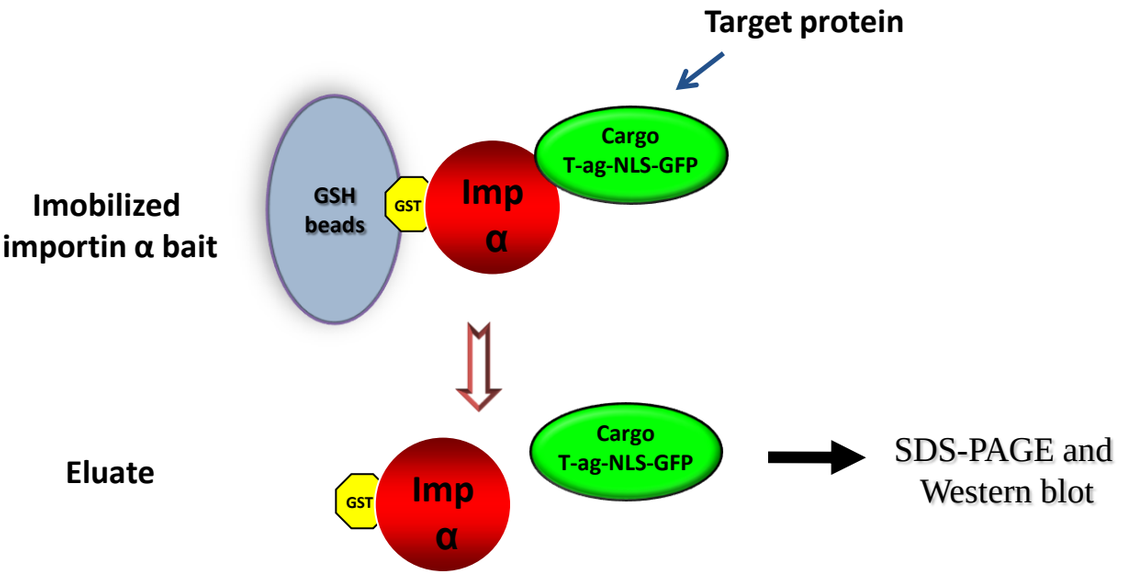
Target protein
Imobilized
importin α bait
GSH
beads
GST
Imp
α
Cargo
T-ag-NLS-GFP
Eluate
GST
Imp
α
Cargo
T-ag-NLS-GFP
SDS-PAGE and
Western blot

B

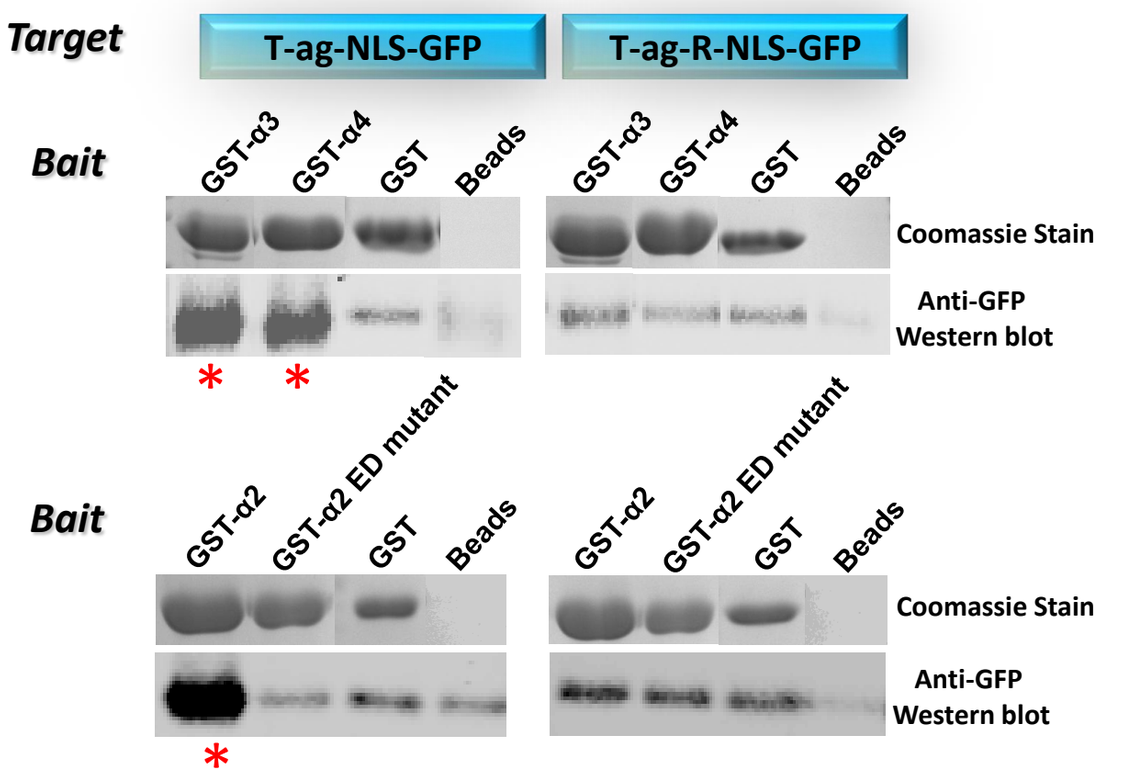
Target
T-ag-NLS-GFP
T-ag-R-NLS-GFP
Bait
GST-α3
GST-α4
GST
Beads
GST-α3
GST-α4
GST
Beads
Coomassie Stain
Anti-GFP
Western blot
*
*
Bait
GST-α2
GST-α2 ED mutant
GST
Beads
GST-α2
GST-α2 ED mutant
GST
Beads
Coomassie Stain
Anti-GFP
Western blot
*

4.3 Optimization of pull-down conditions

To determine the optimal amount of the recombinant proteins to be used in the pull-down experiment, 50, 100, or 200 pmol of GST-importin α2 was digested with trypsin followed by mass spectrometry of the digested products for signal intensity and pattern analysis. A chromatograph view of the results (Figure 4.3, A) showed the similarity in signal pattern produced by digestion of different protein amounts; this indicates the reproducibility of the digest and peptide mass detection. The intensities of the detected peptides, however, differed from each other based on sample input. Fifty pmol of the digested GST-importin α2 produced signals of approximately half the intensity of both 100 and 200 pmol, both of which produced signals of almost equal intensity. These results indicate that 100 pmol of recombinant protein is close to the threshold of saturation in the mass detection system since the signal intensity of 100 pmol is similar to that of 200 pmol. Further analysis to delineate the exact amount of recombinant protein that neither falls overly below, nor exceeds the saturation limit of peptide detection system was not performed due to time and resource constraints. Thus 100 pmol of recombinant proteins was used in each pull-down experiment. Equal loading of proteins in each reaction was demonstrated by silver staining of 10 pmol of each protein in a 10% polyacrylamide gel (Figure 4.3, B)

4.4 Importin α pull-down from isolated germ cells and mass spectrometric identification of binding partners

Binding partners of importin α2, importin α2-ED mutant, and importin α4 from both spermatocytes and spermatids were pulled down by recombinant importin α proteins followed by mass spectrometry analysis to identify the candidate binding proteins. Low concentration and poor quality of recombinant importin α3 (Section 3.5, Table 3.2) prevented the successful analysis of importin α3 along with importin α2 and α4. However, in a previous attempt, the pull-down of importin α3 binding partners from spermatocytes and spermatids followed by mass spectrometric analysis was carried out to completion. The results of that experiment will be discussed in Section 4.11.

Figure 4.3 Optimization of recombinant protein amount for mass spectrometry analysis

A. In separate reactions, 50 pmol, 100 pmol, and 200 pmol of GST-importin α2 were digested with trypsin. The peptides obtained from the trypsin digest were analysed by ion trap mass spectrometry. An extract of the chromatogram produced by detection of peptides in digestion product from three separate reactions is presented. Each peak represents a signal from a detected peptide. The height of each peak is directly correlated to the signal intensity, which is an indication of the peptide abundance.

B. Ten pmol of GST-importin α2, GST-importin α2-ED mutant, GST-importin α4 and GST alone were separated on a 10% polyacrylamide gel followed by silver staining to assess the equivalence of protein loading.

A

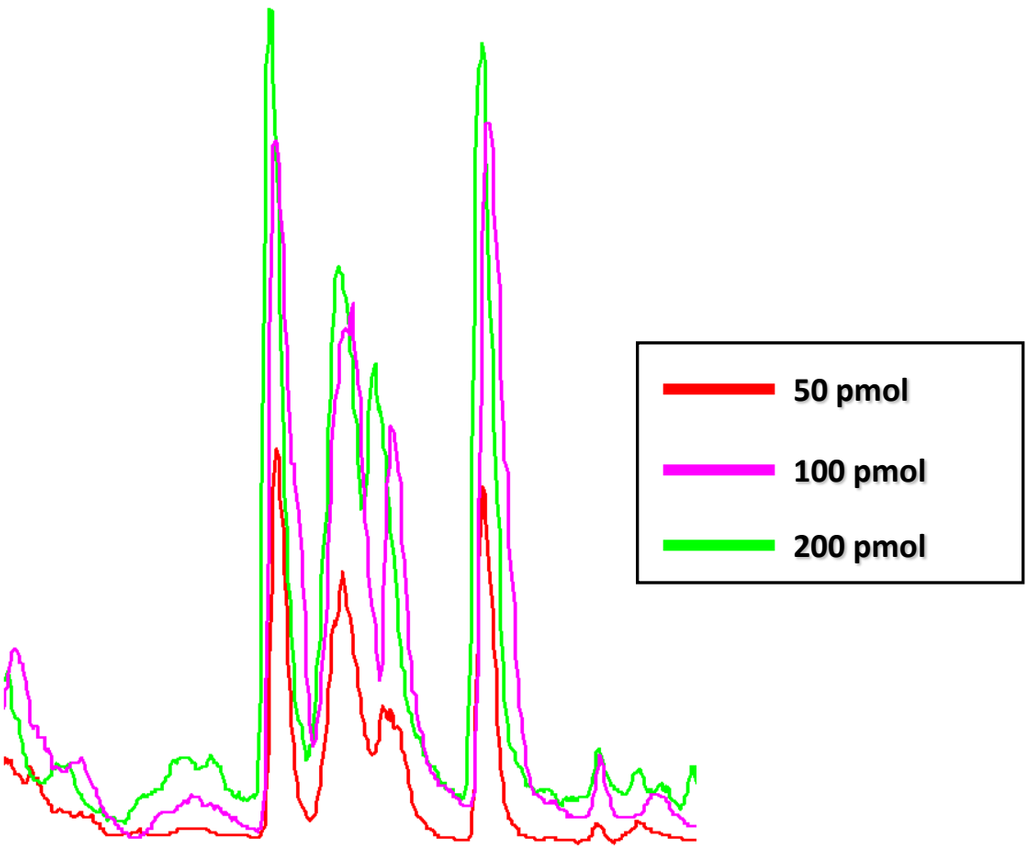
50 pmol
100 pmol
200 pmol

B

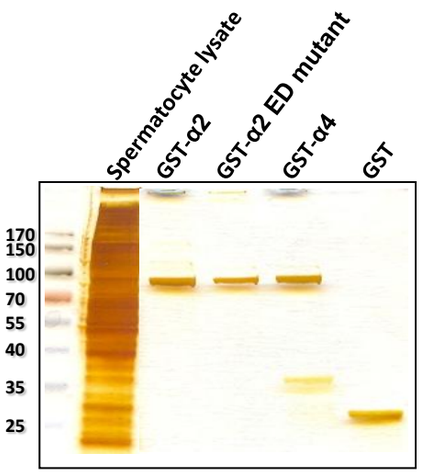
Spermatocyte lysate
GST-α2
GST-α2 ED mutant
GST-α4
GST
170
150
100
70
55
40
35
25

In every pull-down experiment, 100 pmol of each recombinant importin α was immobilized on GSH sepharose beads followed by incubation with protein lysates prepared from $5x10^6$ of either spermatocytes or spermatids isolated from adult rat testes. To control for specificity of binding, immobilized GST on GSH beads was used as a negative control in a parallel reaction. The bound protein complexes were eluted from the beads and digested with trypsin. The resulting peptides were resolved into several fractions by High Pressure Liquid Chromatography (HPLC) to enhance the ionization of less abundant compounds. Subsequently the obtained fractions were vaporized by Electrospray Ionization (ESI) and the ionized peptides were injected into an amaZon ETD Ion Trap. The mass spectra (MS) data were obtained and recorded based on ion retention time in the trap, with the smaller ions being released earlier than larger ions. A density view of the detected ions was generated for each pull-down experiment (Figure 4.4 for spermatocytes and Figure 4.5 for spermatids) in which the position of each signal corresponds to its mass to charge ratio (m/z) (Y axis) and retention time (X axis). The intensity of each signal correlates directly to the abundance of the identified peptide.

As expected, pull-down by GST alone produced fewer signals compared to the pull-downs by GST-importin αs from both spermatocytes and spermatids lysates. However, most of the signals in GST pull-downs were detectable in all of the GST-importin α reactions. The common signals in GST control and GST-importin α pull-downs correspond to the peptide resulting from GST digest or to proteins that bind to GST. Thus, in subsequent steps aimed at inferring the amino acid sequence of the identified peptides, the signals common to importin αs and GST pull-down were not considered for further analysis.

Subsequently, the Profile Analysis program in Data Analysis software (Daltonics, version 4.1) was utilized to select specific signals from the generated density views of all reactions. The program enabled zooming in an area of the view with high resolution and accuracy, allowing the annotation of a signal based on its mass to charge ratio (m/z) and retention time. An example of this discerning signal selection approach is presented in Figure 4.6.

Figure 4.4 Density views of detected peptides in pull-down of spermatocytes lysate

The products of GST and GST-importin α pull-down reactions from spermatocytes lysates were digested with trypsin. The resulting peptides were resolved into several fractions by HPLC prior to ionization and mass detection. Peptides identified by electrospray ionisation and ion trap mass spectrometry are depicted in a density view. Each signal represents an identified ion/peptide with a specific mass to charge ratio (m/z) on the Y axis, and retention time/minute on the X axis.

GST-negative

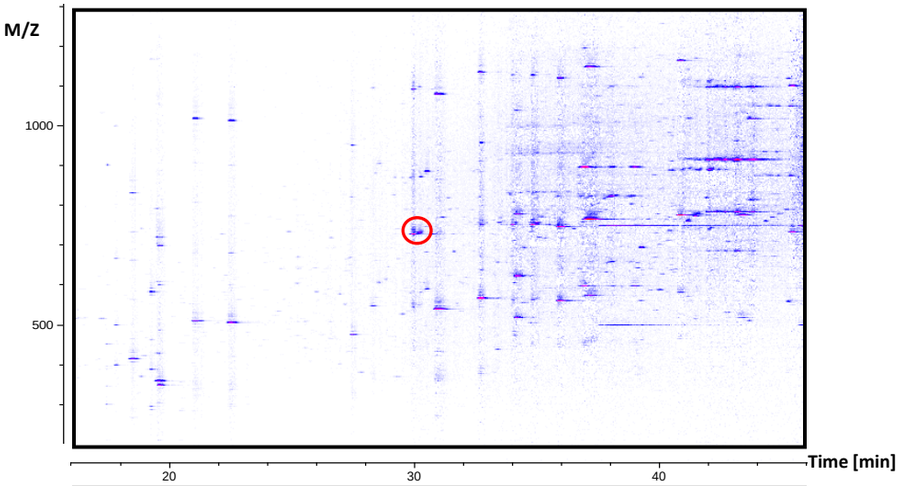

GST-Importin α2

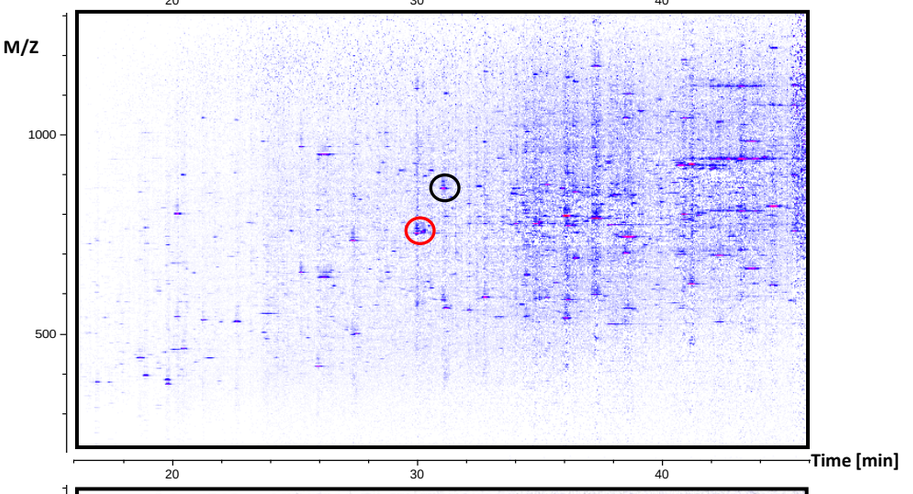

GST-Importin α2
-ED mutant

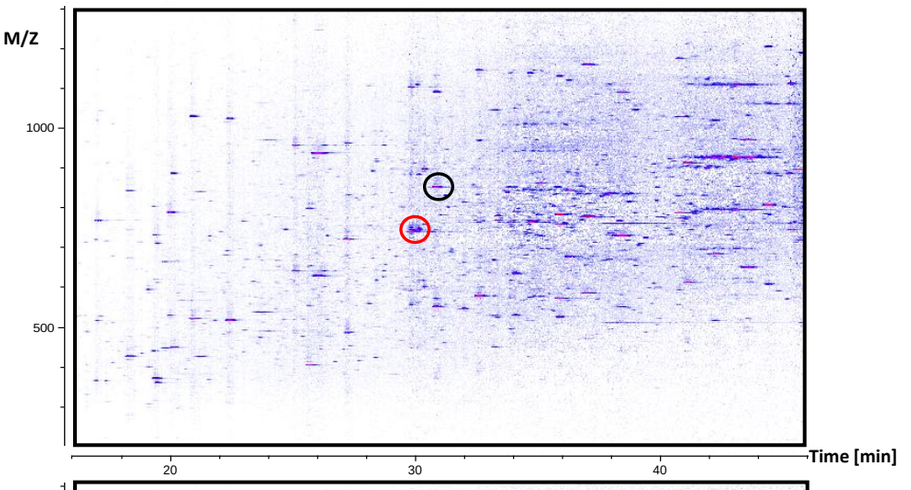

GST-Importin α4

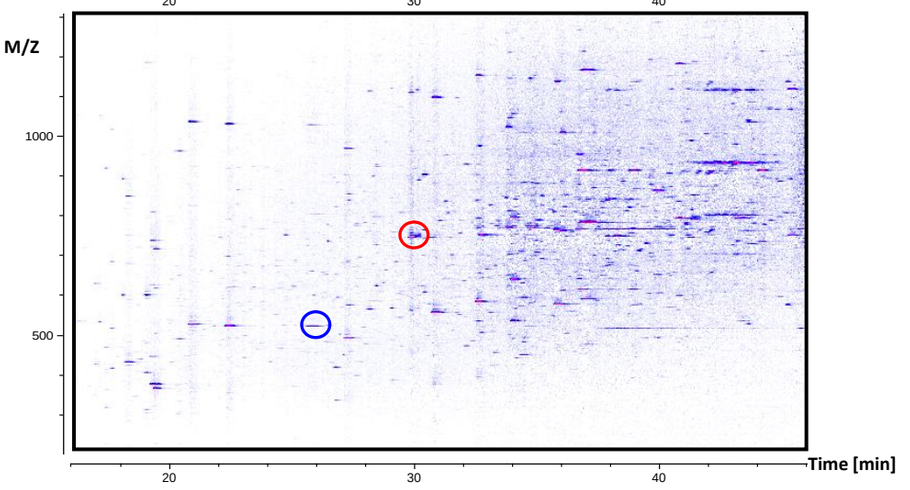

Signal common to all reactions

Signal specific to importin α2 and α2 ED mutant

Signal specific to importin α4

Figure 4.5 Density views of detected peptides in pull-down of spermatids lysate

The products of GST and GST-importin α pull-down reactions from spermatids lysates were digested with trypsin. The resulting peptides were resolved into several fractions by HPLC prior to ionization and mass detection. Peptides identified by electrospray ionisation and ion trap mass spectrometry are depicted in a density view. Each signal represents an identified ion/peptide with a specific mass to charge ratio (m/z) on the Y aies, and retention time/minute on the X- axis.

GST-negative

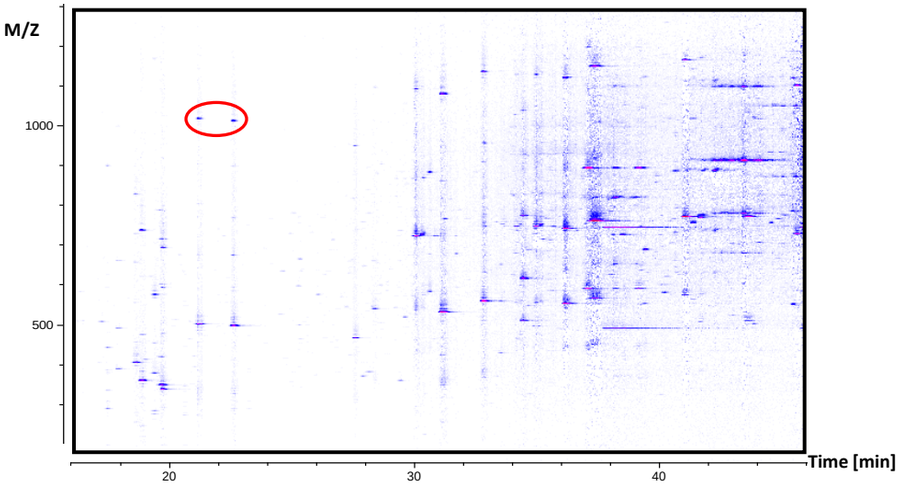

GST-Importin α2

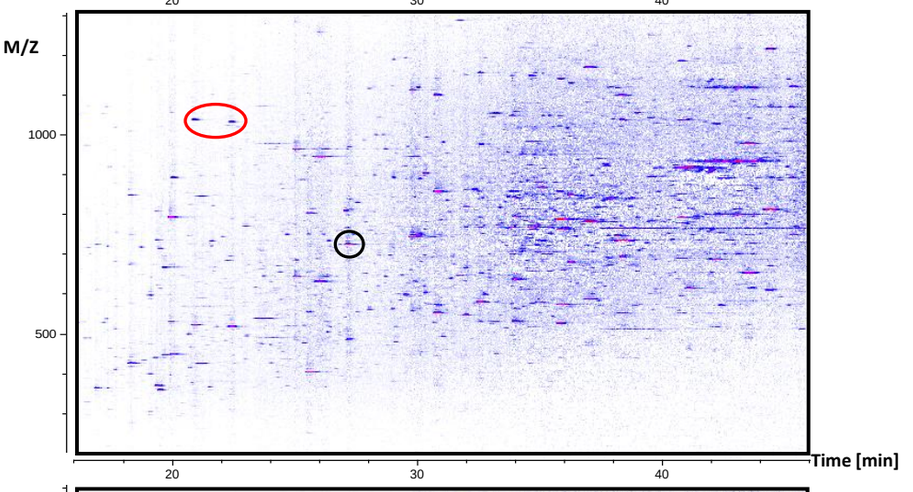

GST-Importin α2
-ED mutant

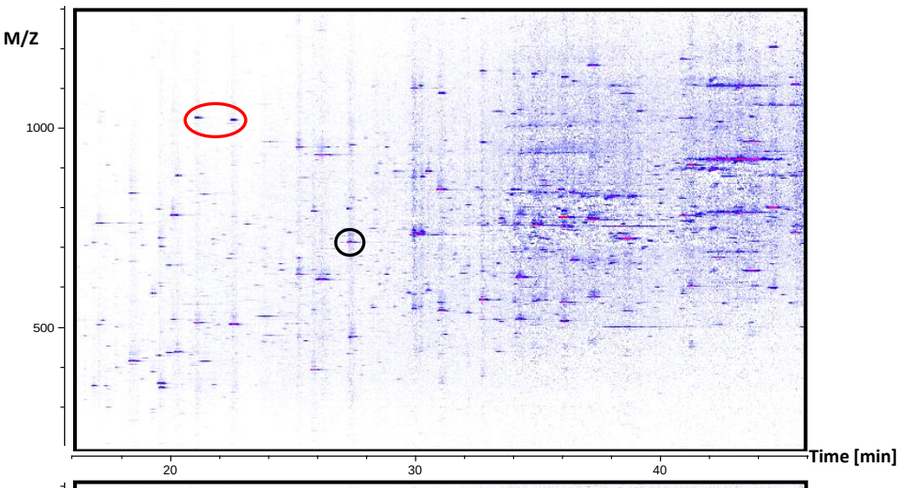

GST-Importin α4

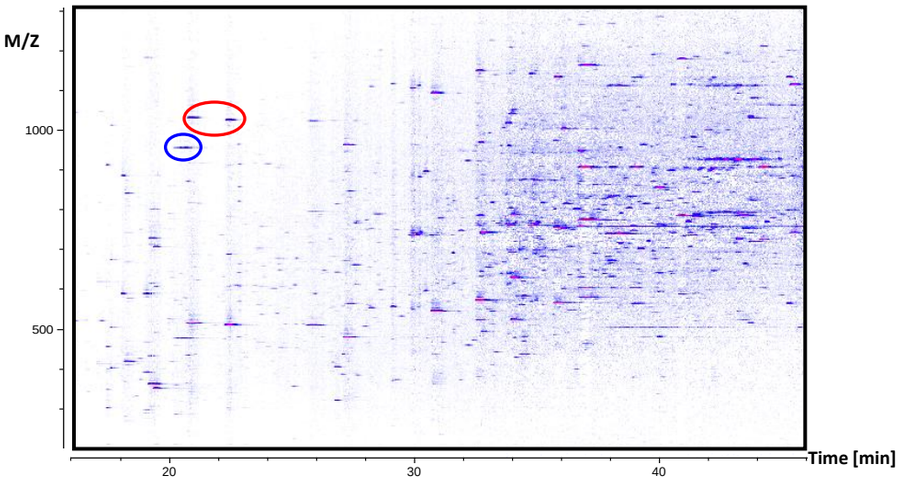

Signal common to all reactions

Signal specific to importin α2 and α2 ED mutant

Signal specific to importin α4

Figure 4.6 Example of signal selection for peptide sequencing

Figure depicts an example of the approach taken to select mass spectrometry (M/S) signals for peptide sequencing, assisted by Profile Analysis program in Data Analysis software. The central panel represents the entire density view from the GST-importin-α2 pull-down from spermatocytes lysate. Areas corresponding to the black square in the central panel are shown in the upper and lower panels. Any signal present in GST pull-down (lower left) was excluded from further analysis base on the reasoning that it would have arisen from peptides produced by trypsin digest of GST, or of proteins that bind to GST. The red circles in two upper views show examples of signals that appeared specifically in the pull-down of GST-importin α2 and of the GST-importin α2-ED mutant. The green circle in the upper left panel and the black circle in the lower right panel are examples of signals that were detected specifically in pull-down of GST-importin α2 and of GST-importin α4, respectively.

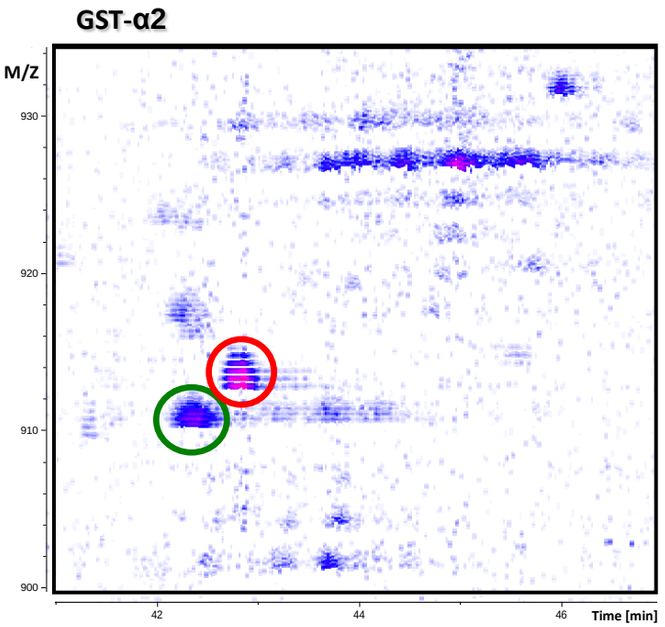
GST-α2
M/Z
930
920
910
900
42
44
46
Time [min]

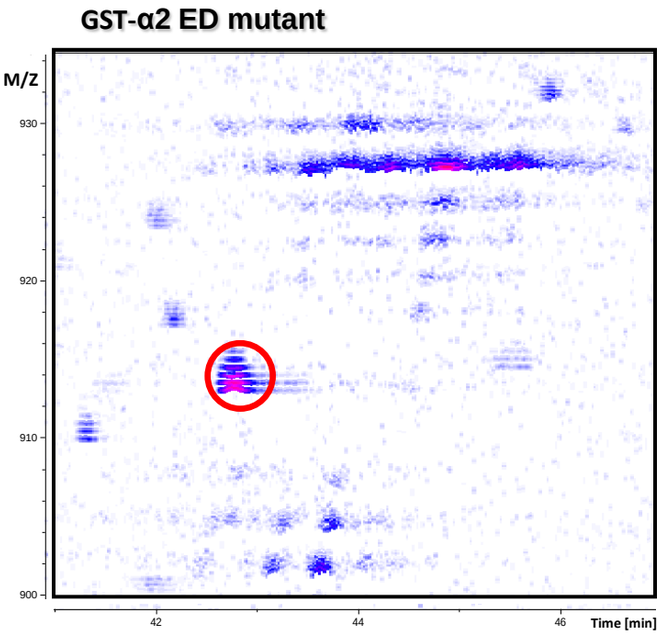
GST-α2 ED mutant
M/Z
930
920
910
900
42
44
46
Time [min]

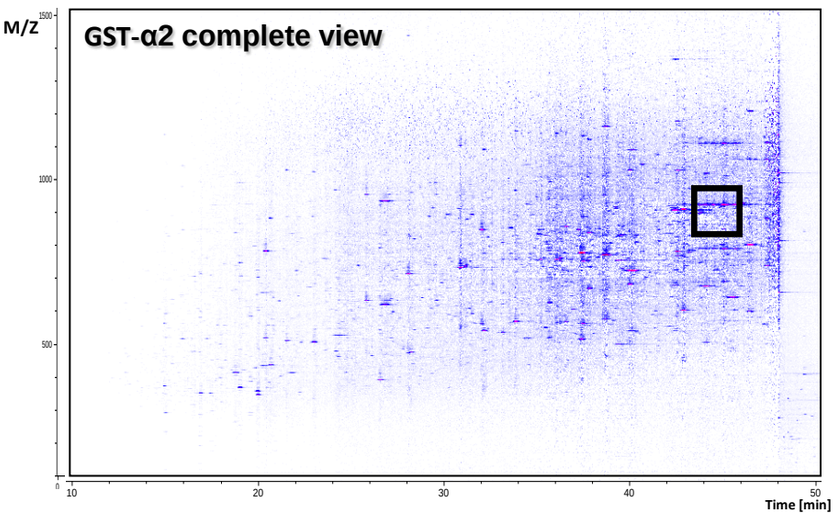
GST-α2 complete view
M/Z
1500
1000
500
0
10
20
30
40
50
Time [min]

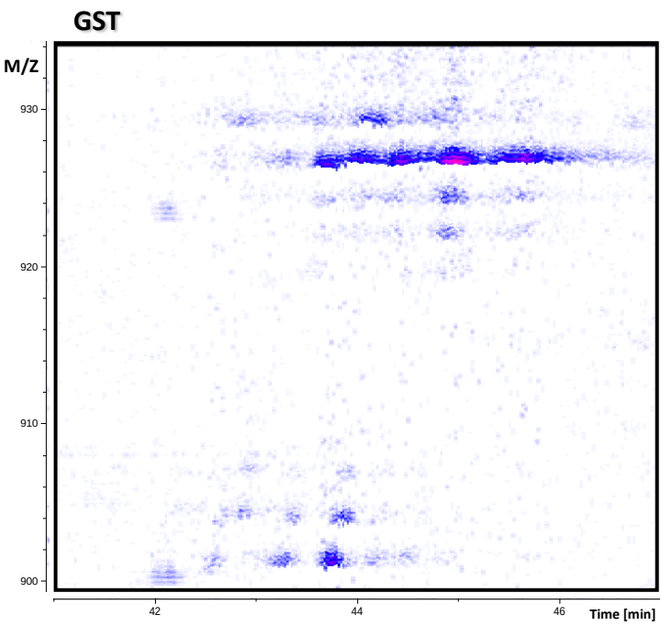
GST
M/Z
930
920
910
900
42
44
46
Time [min]

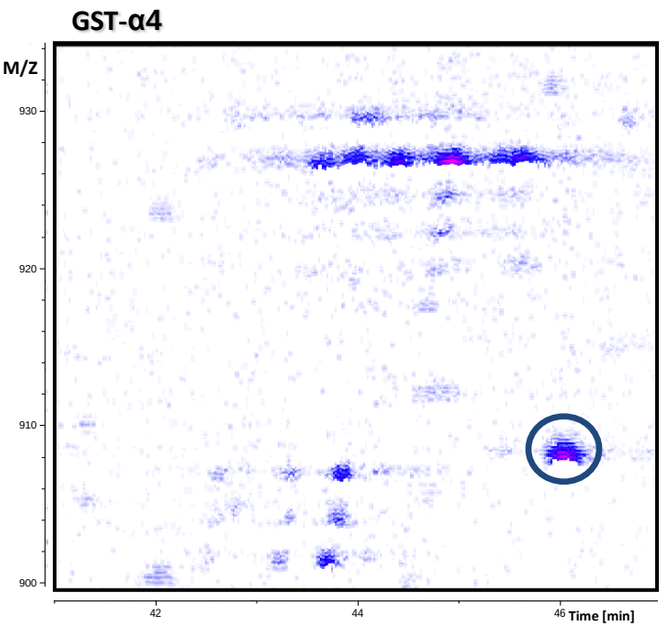
GST-α4
M/Z
930
920
910
900
42
44
46
Time [min]

In total, 382 signals from all reactions were selected for tandem mass spectrometry (MS/MS) in which a target peptide was fragmented on a residue by residue basis caused by collision induced dissociation (CID) force of a nebulizer gas (Nitrogen in this instance). The produced MS/MS spectra was examined manually (by Dr. Mark Baker) to ensure the quality of fragmentation for every reported sequence. Subsequently, the masses of the peptides (generated by MS analysis) and the deduced amino acid sequence of the peptides (generated by MS/MS analysis) were used in combination to search the protein sequence repositories for protein identification.

4.5 Categorization of importin α binding candidates in spermatocytes and spermatids

In total 101 proteins were identified as binding candidates of importin α2, the importin α2-ED mutant and importin α4 in spermatocytes and spermatids of adult rat testis. Amongst all candidates, 39 were identified from spermatocytes, 57 from spermatids, and 5 from both cell lysates. Fifty five of all candidates were found as putative binding partners of importin α2, 41 as candidate binding partners of importin α4 and 5 as candidates of both importin α2 and importin α4.

All of these candidates are listed in Table 4.1 in alphabetical order. The table includes the official full name, official gene symbol, protein and nucleotide accession number obtained from the rat genome database (RGD) and the amino acid sequence of the peptides identified from each candidate, in addition to the amino acid length of each candidate. Among the identified candidates are some of the known binding partners of importin α, including importin β1 (Kpnb1) (Lange et al., 2007) and nucleoporin 50 (Npap60/Nup50) (Lindsay et al., 2002; Matsuura and Stewart, 2005).

In Table 4.2 all of the identified candidates have been classified based on their interaction with specific importin α subtypes and the cell lysate in which the interaction was uncovered. The results of two unbiased computational analyses are also summarized in Table 4.2. Firstly the sequence of each candidate protein was searched for the presence of potential cNLSs using the cNLS Mapper program

Table 4.1. List of imporitn α binding candidates (α-Importome)

All of the identified importin α2, importin α2 ED mutant and importin α4 binding candidates from both spermatocytes and spermatids are listed in alphabetical order. The official full name, symbol, and accession numbers have been extracted from the Rat Genome Database (RGD). The peptide sequence column contains the sequence identified by MS/MS analysis for each candidate. The amino acid length of each candidate (last column) is based on the accession number listed in the Table.

Table 4.1 List of importin α binding candidates (α-Importome)

Official full name	Official symbol	Accession number	Peptide sequence	Protein aa length
Apolipoprotein B	Apob	NP_062160 NM_019287	K.FLVQAEGVQ QSEATAMFK.Y	4506
Ataxin-10	Atxn10	NP_579847 NM_133313	K.EALVTIR.L	475
ATP/GTP binding protein-like 2	Agbl2	XP_001077842 XM_001077842	R.ALCRSLAGNTVY LLTITNPSR.T	861
Baculoviral IAP repeat-containing 2	Birc2	NP_068520 NM_021752	R.AGFYYTGVNDKVK.C	589
Baculoviral IAP repeat-containing 3	Birc3	NP_076477 NM_023987	R.AGFYYTGVNDKVK.C	638
BRF1 homolog, subunit of RNA polymerase III transcription initiation factor IIIB (S. cerevisiae)	Brf1	NP_001100231 NM_001106761	K.QLEQVLSK.K	686
Carbonic anhydrase X like	LOC100364059	XP_002724677 XM_002724631	R.DTITRITYK.N	320
Caspase 4, apoptosis-related cysteine peptidase	Casp4	NP_446188 NM_053736	R.NMEADAVRMSHVEK. D	373
CDC42 binding protein kinase alpha	Cdc42bpa	NP_446109 NM_053657	R.DVLVNGDSK.W	1732
Chromobox homolog 1 (HP1 beta homolog Drosophila)	Cbx1	XP_001081346 XM_001081346	K.GKVEYLLK.W	185
Chromodomain helicase DNA binding protein 7	Chd7	NP_001101376 NM_001107906	R.EAIISEKR.Q	1572
Cyclin G associated kinase	Gak	NP_112292 NM_031030	K.VIQSVANYAK.G	1305
Cytochrome c oxidase II, mitochondrial	mt-Co2	AP_004895 AJ428514	R.VVLPMETPIR.M	227
Cytochrome P450, family 2, subfamily c, polypeptide 7	Cyp2c7	NP_058854 NM_017158	R.TLKAYLIKQK.R	490
Discs, large (Drosophila) homolog-associated protein 2	Dlgap2	NP_446353 NM_053901	R.GGLYNSMDSLDSN KAMNLALETAAAQR.H	1059
Dpy-19-like 1 (C. elegans)	Dpy19l1	NP_001178720 NM_001191791	R.SSPPPLNGASEVAAR.E	746

Official full name	Official symbol	Accession number	Peptide sequence	Protein aa length
ELKS/RAB6-interacting/CAST family member	Erc1	NP_740769 NM_170788	K.ISSMERGLR.D	948
Embryonal Fyn-associated substrate	Efs	NP_001099503 NM_001106033	MAIATSAQLAR.A	561
Epidermal growth factor receptor pathway substrate 15-like 1	Eps15l1	NP_001025092 NM_001029921	R.ALEKEPVPSILPP PLIPPSK.R	878
Eukaryotic translation initiation factor 4A1	Eif4a1	NP_955404 NM_199372	R.DNGPDGMEPEGVIESNW NEIVDSFDDMNLSESLLR.G	406
Fatty acid binding protein 9, testis	Fabp9	NP_074045 NM_022854	K.LVSSENFENYVR.E	132
Fem-1 homolog a (C. elegans)	Fem1a	NP_001020877 NM_001025706	R.AACFDGHLDVVR.Y	654
Ferrochelatase	Fech	NP_001101904 NM_001108434	R.CQSGAAVAATTEKVH HAKTTKPQAQPER.R	422
Fos-like antigen 1	Fosl1	NP_037085 NM_012953	K.IPEEDK.K	275
Galactosidase, beta 1	Glb1	NP_001101662 NM_001108192	K.CGTLQDLYATVDFGTTGNI TR.A	647
General transcription factor IIIC, polypeptide 4	Gtf3c4	NP_001102943 NM_001109473	K.AVKGYFTLR.Q	818
Glutamate receptor, ionotrophic, AMPA 3	Gria3	NP_001106213 NM_001112742	R.ALKMVQVQGMT GNIQFDTYGR.R	888
GNAS complex locus	Gnas	XP_002729310 XM_002729264	K.AAEPASEPR.D	652
Guanine deaminase	Gda	NP_113964 NM_031776	R.FVSEMLQKN YSRVKPIVTPR.F	454
Heterogeneous nuclear ribonucleoproteins A2/B1	Hnrnp A2/B1	NP_001098083 NM_001104613	R.NMGGPYGGGNYGP GGSGGSGGYGGR.S	353
Hyaluronoglucosaminidase 3	Hyal3	NP_997482 NM_207599	R.AALGAAGLTLLR.C	412
Interleukin 12 receptor, beta 2	Il12rb2	NP_001178679 NM_001191750	R.GTLQWEDEG QVVLNQLR.Y	869

Official full name	Official symbol	Accession number	Peptide sequence	Protein aa length
Isoleucyl-tRNA synthetase	Iars	NP_001094042 NM_001100572	R.LKLFLNETQTQEI TEDIPMK.T	1262
Karyopherin (importin) beta 1	Kpnb1	NP_058759 NM_017063	K.SDFDMV DYLNELR.E	875
LanC lantibiotic synthetase component C-like 1 (bacterial)	Lancl1	NP_446175 NM_053723	K.IDPHVPN EMLYGR.I	399
Latant Transforming growth factor beta binding protein 4	Ltbp4	NP_001163807 NM_001170336	R.CCLAQTPRS SHCTRASCR.V	1631
Leucine-rich alpha-2-glycoprotein 1	Lrg1	NP_001009717 NM_001009717	R.SSAALN TLVLR.E	332
LRRGT00108	None found	AAQ91064 None found	K.LEAIPLKSR.T	1102
Matrin 3	Matr3	NP_062022 NM_019149	R.GDTDQASNILAS FGLSAR.D	845
Microtubule-associated protein 1B	Map1b	NP_062090 NM_019217	K.GEAEQSEEEGEE EDKAEDAR.E	2461
Myosin light chain kinase	Mylk	NP_001099344 NM_001105874	K.CVAKNSAGQAE CSCQVTVDDAGTS ENTKAPEMK.S	1961
Ninein-like	Ninl	XP_001060198 XM_001060198	K.SDEDAESPKEPQ NELFEAQGQLR.S	1394
Non-SMC condensin I complex, subunit D2	Ncapd2	XP_001065923 XM_001065923	K.QAIVLTR.E	1393
Nuclear pore associated protein (Nup50)	Npap60	NP_037123 NM_012991	R.NIGFESD SGGAFK.G	467
Nucleophosmin (nucleolar phosphoprotein B23, numatrin)	Npm1	NP_037124 NM_012992	R.MTDQEAI QDLWQWR.K	292
Phosphoglycerate mutase family member 5	Pgam5	NP_001020443 NM_001025272	M.AFRQALQLAAC GLAGGSAAVLFSA VAVGKPR.G	288
POM121 membrane glycoprotein	Pom121	NP_446074 NM_053622	K.VATGTTGR.A	1199
Pregnancy-specific beta 1-glycoprotein	Psgb1	NP_067709 NM_021677	K.EDARMYTLETLN INNKVEK.A	380

Official full name	Official symbol	Accession number	Peptide sequence	Protein aa length
Proprotein convertase subtilisin/kexin type 6	Pcsk6	NP_037131 NM_012999	R.CDENCLS CEGSSR.N	937
Proteasome (prosome, macropain) activator subunit 3	Psme3	NP_001011894 NM_001011894	K.MWVQLLIPR.I	254
Proteasome (prosome, macropain) subunit, alpha type 7	Psma7	NP_001008218 NM_001008217	R.AITVFSPDGHLF QVEYAQEAVK.K	248
Protein kinase N3	Pkn3	NP_001041326 NM_001047861	R.IDFYFDE NPYFENK.V	959
Protein phosphatase 1, regulatory subunit 3A	Ppp1r3a	NP_001102692 NM_001109222	K.AQAVTAYIIK.T	1096
Protocadherin alpha subfamily C, 2	Pcdhac2	NP_958825 NM_201422	K.NDAVSQNEPR. Q	1006
Protocadherin beta 19	Pcdhb19	XP_001056051 XM_001056051	R.ALDRESRAEYNI TISVSDQGTPR.L	802
Protocadherin beta 5	Pcdhb5	NP_001108074 NM_001114602	R.ALDRESRAEYNI TISVSDQGTPR.L	797
Peroxisome proliferator activated receptor gamma coactivator 1-alpha	Ppargc1a	NP_112637 NM_031347	K.SNYADLDTNSD DFDPASTKSK.Y	796
Ral guanine nucleotide dissociation stimulator	Ralgds	NP_062123 NM_019250	R.SKKSTAIVK.R	895
rCG41669-like	LOC100364838	XP_002725991 XM_002725945	K.STFSANVS MNAEYK.E	542
rCG41957-like	LOC100365542	XP_002725514 XM_002725468	K.SFPGTQVYP SWPYLFQK.D	87
Retinoblastoma binding protein 4	Rbbp4	NP_001101382 NM_001107912	K.TVALWDLR.N	425
REV1 homolog (S. cerevisiae). DNA repair protein REV1	Rev1	NP_001101683 NM_001108213	R.SPHRTNSLS PSLHSNTK.I	1119
Rho GTPase activating protein 40	Arhgap40	XP_230802 XM_230802	R.RSQLCDGGLK.T	640
Ribosomal protein L22-like	LOC100360057	XP_002729438 XM_002729392	K.ITVTSEVPFSK.R	128
Ribosomal protein S28	Rps28	NP_001099200 NM_001105730	R.EGDVLT LLESER.E	69
Ring finger protein 170	Rnf170	XP_001061874 XM_001061874	R.RFSGQPR.S	286
Sarcosine dehydrogenase	Sardh	NP_446116 NM_053664	MASLSRVLR.V	919

Official full name	Official symbol	Accession number	Peptide sequence	Protein aa length
Sec1 family domain containing 2	Scfd2	NP_001017499 NM_001017499	R.EIAGARNLLR.Q	684
Secernin 3	Scrn3	NP_001013180 NM_001013162	R.ADTAEKALDVIVDLLEK.Y	304
Seminal vesicle secretory protein 4	Svs4	NP_036794 NM_012662	K.HISRSSGGSNMEGESSYAKK.K	111
Senataxin	Setx	XP_342401 XM_342400	K.QLAKGTLSK.A	2647
Septin 11	Sept11	NP_001100678 NM_001107208	R.NEFLGELQKK.E	432
Serine palmitoyltransferase, long chain base subunit 3	Sptlc3	NP_001099987 NM_001106517	K.YNESMEKVKDTIEK.Y	563
SET domain containing 4	Setd4	NP_001107219 NM_001113747	R.SSLGPYIK.K	439
SET translocation-like 1	Setl1	NP_919334 NM_194353	R.IDFYFDENPYFENK.V	285
Similar to RIKEN cDNA 4930547C10	RGD1309291	XP_002726572 XM_002726526	K.YVQGSGLK.R	664
Similar to RIKEN cDNA D330028D13	LOC500118	NP_001020942 NM_001025771	K.KKVLPMR.L	249
Similar to tropomyosin 1, alpha isoform c	LOC680417	XP_001057085 XM_001057085	R.FHQLLANMKKER.S	1271
Similar to ZK1193.2	LOC687024	XP_001076773 XM_001076773	K.GDDLPQYKNVIIR.K	1704
Sjogren syndrome antigen B	Ssb	NP_112381 NM_031119	K.LDEGWVPLETMIK.F	415
Solute carrier family 7 (anionic amino acid transporter light chain, xc- system), member 11	Slc7a11	NP_001101143 NM_001107673	R.KPVVATISKGGYLQGNMSGR.L	502
Spectrin repeat containing, nuclear envelope 2	Syne2	XP_216738 XM_216738	K.IKKFLGSVENQQGSLSK.L	3832
Splicing factor 3b, subunit 1	Sf3b1	NP_445878 NM_053426	K.AIGPHDVLATLLNNLK.V	1304
ST6 (alpha-N-acetyl-neuraminyl-2,3-beta-galactosyl-1,3)-N-acetylgalactosaminide alpha-2,6-sialyltransferase 1	St6galnac1	NP_001099329 NM_001105859	K.CITCAVVGNGGILNDSR.V	520

Official full name	Official symbol	Accession number	Peptide sequence	Protein aa length
SWI/SNF related, matrix associated, actin dependent regulator of chromatin, subfamily a, member 4	Smarca4	NP_599195 NM_134368	K.AIEEGTLEEIEEEVR.Q	1613
Titin	Ttn	XP_001065955 NM_001065955	R.QQSPSPIRHSPSPVR.H	33295
Topoisomerase (DNA) II alpha	Top2a	NP_071519 NM_022183	K.VFLNGNMLPVK.G	1526
Tripartite motif-containing 28	Trim28	NP_446368 NM_053916	K.LTEDKADVQSIIGLQR.F	835
Tripeptidyl peptidase II	Tpp2	NP_112399 NM_031137	K.FVLHAVQLVK.Q	1249
Tubulin, beta 4B class Ivb	Tubb4b	NP_954525 NM_199094	R.INVYYNEATGGK.Y	445
Tyrosine 3-monooxygenase/tryptophan 5-monooxygenase activation protein, zeta polypeptide	Ywhaz	NP_037143 NM_013011	K.FLIPNASQPESK.V	245
Ubiquitin specific protease 24	Usp24	XP_233260 XM_233260	R.HMISFLLGV SQQNSQIR.R	2617
ULF-250 protein	None found	AAC833369 None found	R.LPQMIK.D	188
WD repeat domain 96	Wdr96	XP_001060079 XM_001060079	R.LKPIIYIYSFPSLTRK.I	1573
Wingless-type MMTV integration site family, member 2B	Wnt2b	NP_001178777 NM_001191848	K.AAGSLGTAGR.V	391
Xin actin-binding repeat containing 1	Xirp1	XP_001077697 XM_001077697	M.ADAQMQ VVHTPTIQMR.T	1822
Y box binding protein 1	Ybx1	NP_113751 NM_031563	R.SVGDGETVEF DVVEGEK.G	322
Y box binding protein 2	Ybx2	XP_001079683 XM_001079683	R.SVGDGETVE FDVVEGEK.G	359
Zinc finger CCCH type, antiviral 1	Zc3hav1	NP_766633 NM_173045	R.NLCKYSHDVL SEQNFQILK.N	776
3'(2'), 5'-bisphosphate nucleotidase 1	Bpnt1	NP_741987 NM_171990	K.EVKHMNSAGVLAALR.N	308

(Kosugi et al., 2009; Section 1.1.3.2). In the output, the motifs are identified as either monopartite or bipartite cNLSs, with a numerical score which is an indication of the likelihood that the motif binds to the importin α NLS binding groove. The sensitivity of the program was regulated to select the potential cNLSs of moderate to high strength by adjusting the cut-off score to 4. Thus any identifiable cNLS with a score of below 4 is not reported in this analysis.

An example of such analysis is shown in Figure 4.7 for Matrin3 which was identified as an importin α2 binding partner in spermatids lysate. As evident in the figure, a given sequence can produce many putative cNLSs of varying scores, partly since a stretch of amino acid sequence can contribute to more than one cNLS. Therefore to simplify the results, only the highest scores of both monopartite and bipartite cNLSs are presented in Table 4.2. The lack of a discernible cNLS motif with score of 4 and above is indicated by "none" in the table. Due to space limitations, the cNLS Mapper output for all of the candidates are not presented as hard copy in this thesis. However, the output of the cNLS Mapper for every candidate is accessible on a compact disc that is attached to this thesis.

The result of the second analysis, also summarized in Table 4.2, is the prediction of protein subcellular localization for all of the identified candidates. To this end, the PSORT II algorithm (Nakai and Horton, 1999) was utilized; this program allocates a given protein to several subcellular locations, with varying probabilities. The allocation is purely based on targeting signals and motifs and the amino acid composition of the protein. The prediction accuracy is partly compromised in this approach due to the potential presence of several competing sorting signals in any one protein. For instance, a protein containing a nuclear localization signal may also contain a mitochondrial targeting sequence with an overriding strength. However, because most proteins localize to more than one compartment under steady state or different physiological conditions, the most rational approach for interpretation of this analysis outcome is to consider a few of the most probable localizations for each protein. Thus, in Table 4.2, the three locations with the highest likelihood (based on PSORT II prediction) for localization of each candidate have been presented along with their respective probabilities.

Table 4.2 Classification of candidates based on importin α and cell type interaction, possession of cNLS and predicted subcellular localization

The importin α- and cell-type specific interaction of each candidate is indicated to demonstrate the sample in which it was detected. The highest scoring of both monopartite (left) and bipartite (right) cNLSs for each candidate as predicted by cNLS Mapper are listed. The cNLS scores above 6 are presented in red colour. The result of PSORT II analyses is summarized with the top 3 locations in which each candidate is likely to localize listed from left to right, and the respective likelihood indicated in the parenthesis.

Table 4.2 Classification of candidates based on importin α and cell type interaction, possession of cNLS and prediction of subcellular localization

	Spermatocyte			Spermatid			NLS prediction (cNLS mapper analysis)		Predicted subcellular localization (PSORT II)		
Gene Symbol	α2	α2 ED	α4	α2	α2 ED	α4	Mono-partite	Bi-partite	% likelihood (Highest)	% likelihood (Second highest)	% likelihood (Third highest)
Casp4				X			4.5	3.2	Nucleus (47%)	Cytoplasm (34%)	Mitochondria (17%)
Pom121				X			8	13.2	Nucleus (47%)	Mitochondria (26%)	Cytoplasm (8%)
Wdr96				X			None	7.5	Nucleus (47%)	Cytoplasm (39%)	Mitochondria (8%)
Scfd2				X			11	5.4	Nucleus (34%)	Cytoplasm (30%)	Mitochondria (8%)
ULF-250				X			4	4	Cytoplasm (43%)	Nucleus (21%)	Extracellular (13%)
RGD1309291				X			5	5.7	Nucleus (73%)	Mitochondria (13%)	Cytoplasm (8%)
Trim28	X			X			None	6.1	Nucleus (60%)	Extracellular (17%)	Mitochondria (13%)
Cdc42bpa			X	X			None	6.3	Nucleus (95%)	Vacuole (4%)	None detected
Eif4a1				X			None	None	Nucleus (39%)	Cytoplasm (26%)	Mitochondria (17%)
Fosl1				X			None	5.2	Nucleus (91%)	Cytoplasm and Mitochondria (4% each)	None detected
Tpp2				X			None	5.7	Cytoplasm (47%)	Nucleus (34%)	Mitochondria (8%)
Kpnb1	X	X	X	X	X	X	None	None	Cytoplasm (43%)	Mitochondria (34%)	Nucleus (13%)
Npm1	X	X	X	X	X		None	9.6	Nucleus (78%)	Mitochondria (13%)	Cytoplasm an d Peroxisome (4% each)
Matr3				X			9	8.9	Nucleus (65%)	Mitochondria (21%)	Cytoplasm (13%)
LOC687024				X			None	None	Nucleus (34%)	Endoplasmic reticulum (30%)	Vacuole (13%)
Glb1				X			None	6.1	Extracellular (33%)	Endoplasmic reticulum and Golgi apparatus (22% each)	Mitochondria (11%)
Setl1				X			6.5	None	Nucleus (73%)	Mitochondria (17%)	Vesicles of secretory system and peroxisome (4% each)

	Spermatocyte			Spermatid			NLS prediction (cNLS mapper analysis)		Predicted subcellular localization (PSORT II)		
Gene Symbol	α2	α2 ED	α4	α2	α2 ED	α4	Mono-partite	Bi-partite	% likelihood (Highest)	% likelihood (Second highest)	% likelihood (Third highest)
Pkn3				X			11	7.5	Cytoplasm (39%)	Mitochondria (26%)	Nucleus (21%)
LOC100365542				X			None	None	Mitochondria (43%)	Cytoplasm (30%)	Nucleus (21%)
Wnt2b				X			None	6.3	Mitochondria (39%)	Cytoplasm (30%)	Endoplasmic reticulum (8%)
Chd7				X			14	12.5	Nucleus (91%)	Vacuole and cytoskeleton (4% each)	None detected
Usp24				X			9	6.5	Nucleus (56%)	Cytoplasm (26%)	Mitochondria (13%)
Pcsk6				X			None	5.2	Nucleus (47%)	Mitochondria (43%)	Cytoplasm and extracellular (4% each)
Sf3b1				X			15	10.1	Endoplasmic reticulum (33%)	Nucleus and vacuole (22% each)	Mitochondria and Golgi apparatus (11% each)
Gda				X			None	None	Mitochondria (47%)	Extracellular and Endoplasmic reticulum (13% each)	Vacuole (8%)
Mylk				X			None	5.6	Nucleus (30%)	Cytoplasm (26%)	Golgi apparatus and Endoplasmic reticulum (13% each)
Fabp9					X		None	5.8	Cytoplasm (52%)	Nucleus (30%)	Mitochondria (13%)
LOC680417					X		None	None	Nucleus (73%)	Cytoplasm and Mitochondria (13% each)	None detected
LOC500118					X		None	4.6	Mitochondria (65%)	Nucleus (34%)	None detected
Ltbp4					X		None	6	Extracellular (55%)	Mitochondria (22%)	Nucleus and vacuole (11% each)

	Spermatocyte			Spermatid			NLS prediction (cNLS mapper analysis)		Predicted subcellular localization (PSORT II)		
Gene Symbol	α2	α2 ED	α4	α2	α2 ED	α4	Mono-partite	Bi-partite	% likelihood (Highest)	% likelihood (Second highest)	% likelihood (Third highest)
Iars					X		7	4.1	Cytoplasm (52%)	Nucleus (34%)	Mitochondria (8%)
Dpy19l1					X		None	4.4	Endoplasmic reticulum (55%)	Mitochondria, Golgi apparatus, Vacuole and vesicle of secretory system (11% each)	None detected
Gria3					X		5.5	4.5	Endoplasmic reticulum (66%)	Mitochondria (33%)	None detected
Hnrnpa2b1					X		5	6.2	Cytoplasm (47%)	Nucleus (39%)	Mitochondria (8%)
Efs					X		None	None	Nucleus (65%)	Mitochondria (17%)	Cytoplasm (13%)
Npap60						X	4	None	Nucleus (82%)	Mitochondria (13%)	Cytoplasm (4.3%)
Tubb4b						X	None	None	Cytoplasm (60%)	Nucleus and Mitochondria (13% each)	Peroxisome, Plasma membrane and vacuole (4% each)
Lancl1						X	None	4.1	Cytoplasm (65%)	Mitochondria (17%)	Nucleus (8%)
Bpnt1						X	None	None	Mitochondria (30%)	Extracellular and cytoplasm (17% each)	Nucleus, Vacuole and Endoplasmic reticulum (8% each)
St6galnac1						X	None	4.4	Endoplasmic reticulum (33%)	Extracellular and Mitochondria (22% each)	Nucleus and Vacuole (11% each)
Ninl						X	None	None	Nucleus (65%)	Cytoplasm (26%)	Peroxisome and Cytoskeleton (4% each)
Hyal3						X	None	4.8	Mitochondria (26%)	Cytoplasm (21%)	Endoplasmic reticulum (17%)

	Spermatocyte			Spermatid			NLS prediction (cNLS mapper analysis)		Predicted subcellular localization (PSORT II)		
Gene Symbol	α2	α2 ED	α4	α2	α2 ED	α4	Mono-partite	Bi-partite	% likelihood (Highest)	% likelihood (Second highest)	% likelihood (Third highest)
Syne2						X	7	6.5	Nucleus (87%)	Cytoplasm, Vacuole and vesicles of secretory system (4.% each)	None detected
Ralgds						X	None	5.2	Nucleus (78%)	Cytoplasm (13%)	Peroxisome and extracellular (4% each)
Cbx1						X	None	10.8	Nucleus (87%)	Mitochondria (13%)	None detected
Xirp1						X	None	5.6	Nucleus (87%)	Cytoplasm (13%)	None detected
Zc3hav1						X	None	None	Nucleus (82%)	Cytoplasm (8%)	Mitochondria and Peroxisome (4% each)
Arhgap40						X	None	5.3	Nucleus (60%)	Mitochondria (17%)	Cytoplasm (13%)
Pcdhac2						X	None	None	Nucleus (34%)	Mitochondria (30%)	Endoplasmic reticulum (21%)
Atxn10						X	None	None	Cytoplasm (52%)	Mitochondria (21%)	Nucleus (13%)
Agbl2						X	4	6.1	Nucleus (73%)	Cytoplasm (21%)	Peroxisome (4%)
LOC100364838						X	None	5.7	Nucleus (69%)	Cytoplasm (13%)	Mitochondria and Peroxisome (4% each)
Rev1						X	5	7.3	Nucleus (69%)	Cytoplasm and Mitochondria (13% each)	Cytoskeleton (4%)
Top2a						X	5	6.4	Nucleus (82%)	Cytoplasm and Mitochondria (8% each)	None detected

	Spermatocyte			Spermatid			NLS prediction (cNLS mapper analysis)		Predicted subcellular localization (PSORT II)		
Gene Symbol	α2	α2 ED	α4	α2	α2 ED	α4	Mono-partite	Bi-partite	% likelihood (Highest)	% likelihood (Second highest)	% likelihood (Third highest)
Slc7a11						X	None	None	Endoplasmic reticulum (77%)	Nucleus and Vesicles of secretory system (11% each)	None detected
Ncapd2						X	None	4.3	Nucleus (47%)	Cytoplasm (43%)	Endoplasmic reticulum and Vesicles of secretory system (4% each)
mt-Co2						X	None	None	Endoplasmic reticulum (55%)	Mitochondria, Golgi apparatus, Vacuole and vesicles of secretory system (11% each)	None detected
Pgam5						X	None	6.3	Endoplasmic reticulum (33%)	Cytoplasm and Extracellular (22% each)	Mitochondria and Vacuole (11% each)
Ppp1r3a						X	None	6.1	Nucleus (34%)	Cytoplasm (26%)	Golgi apparatus (13%)
Svs4						X	7	7.1	Extracellular (55%)	Nucleus (33%)	Mitochondria (11%)
Il12rb2						X	None	4.6	Nucleus and Mitochondria (34% each)	Endoplasmic reticulum (21%)	Cytoplasm and Peroxisome (4% each)
Psme3	X					X	12.5	8	Cytoplasm (47%)	Nucleus (34%)	Mitochondria (13%)
Apob	X						4	7	Nucleus (43%)	Cytoplasm (34%)	Mitochondria (17%)
Psma7	X						None	None	Mitochondria (47%)	Nucleus and Cytoplasm (21% each)	Peroxisome and Vacuole (4% each)
Rps28	X						None	None	Mitochondria (56%)	Nucleus (43%)	None detected
Setx	X						12.5	6.5	Nucleus (69%)	Cytoplasm, Mitochondria, and vesicles of secretory system (8% each)	Plasma membrane (4%)

	Spermatocyte			Spermatid			NLS prediction (cNLS mapper analysis)		Predicted subcellular localization (PSORT II)		
Gene Symbol	α2	α2 ED	α4	α2	α2 ED	α4	Mono-partite	Bi-partite	% likelihood (Highest)	% likelihood (Second highest)	% likelihood (Third highest)
Pcdhb5	X						None	None	Endoplasmic reticulum (44%)	Mitochondria (33%)	Nucleus (22%)
Pcdhb19	X						None	None	Nucleus (30%)	Cytoplasm (26%)	Mitochondria and Golgi apparatus (13% each)
Erc1	X	X					None	6.2	Nucleus (82%)	Cytoplasm (17%)	None detected
LOC100360057	X						None	6.3	Nucleus (47%)	Cytoplasm (30%)	Mitochondria (13%)
Smarca4	X						14	9.7	Nucleus (91%)	Cytoplasm and Cytoskeleton (4% each)	None detected
Ywhaz	X		X				None	None	Nucleus (65%)	Mitochondria (26%)	Cytoplasm (8%)
Psgb1	X						None	None	Mitochondria (43%)	Cytoplasm (39%)	Nucleus (8%)
LOC100364059	X						None	4.4	Nucleus (56%)	Mitochondria (21%)	Cytoplasm (17%)
Brf1	X						5	9.6	Nucleus (73%)	Mitochondria (17%)	Cytoplasm (8%)
Fem1a	X						None	None	Mitochondria (47%)	Cytoplasm (34%)	Nucleus (17%)
Birc2	X						None	4.2	Nucleus (65%)	Cytoplasm (30%)	Mitochondria (4%)
Birc3	X						None	6.2	Nucleus (69%)	Cytoplasm and Mitochondria (13% each)	Peroxisome (4%)
Scrn3	X						None	None	Cytoplasm (60%)	Nucleus (30%)	Mitochondria and vesicles of secretory system (4% each)
Map1b	X						None	5.1	Nucleus (87%)	Cytoplasm, Vacuole, and Cytoskeleton (4% each)	None detected

	Spermatocyte			Spermatid			NLS prediction (cNLS mapper analysis)		Predicted subcellular localization (PSORT II)		
Gene Symbol	α2	α2 ED	α4	α2	α2 ED	α4	Mono-partite	Bi-partite	% likelihood (Highest)	% likelihood (Second highest)	% likelihood (Third highest)
LRRGT00108			X				None	6.3	Nucleus (91%)	Cytoplasm (8.7%)	None detected
Sept11			X				None	4.4	Nucleus (73%)	Cytoplasm (14%)	Mitochondria (8%)
Lrg1			X				None	None	Extracellular (33%)	Mitochondria and Vacuole (22% each)	Golgi apparatus and Endoplasmic reticulum (11% each)
Pcdhac2			X			X	None	None	Nucleus (34%)	Mitochondria (30%)	Endoplasmic reticulum (21%)
Sptlc3			X				None	None	Cytoplasm (56%)	Mitochondria (26%)	Nucleus (8%)
Rbbp4			X				None	None	Cytoplasm (52%)	Nucleus (30%)	Mitochondria (17%)
Cyp2c7			X				None	6.3	Nucleus (39%)	Cytoplasm (21%)	Mitochondria (17%)
Ppargc1a			X				15	4.7	Nucleus (73%)	Cytoplasm (13%)	Mitochondria (4.3%)
Eps15l1			X				12.5	4.8	Nucleus (78%)	Mitochondria (13%)	Cytoplasm (8%)
Gak			X				None	6.7	Nucleus (39%)	Mitochondria (26%)	Cytoplasm (13%)
Setd4			X				4	7.9	Nucleus (60%)	Mitochondria (26%)	Cytoplasm (8.7%)
Dlgap2			X				None	7.2	Nucleus (65%)	Cytoplasm (21%)	Mitochondria and Peroxisome (4% each)
Fech			X				None	4.6	Nucleus (87%)	Cytoplasm (8%)	Mitochondria (4%)
Gtf3c4			X				None	5	Cytoplasm and Mitochondria (30% each)	Golgi apparatus (13%)	Endoplasmic reticulum (8%)
Ttn			X				Many above 6	Many above 6	Sequence too large for analysis	Sequence too large for analysis	Sequence too large for analysis

	Spermatocyte			Spermatid			NLS prediction (cNLS mapper analysis)		Predicted subcellular localization (PSORT II)		
Gene Symbol	α2	α2 ED	α4	α2	α2 ED	α4	Mono-partite	Bi-partite	% likelihood (Highest)	% likelihood (Second highest)	% likelihood (Third highest)
Ybx1	X	X					None	5.2	Nucleus (100%)	None detected	None detected
Ybx2	X	X					None	None	Nucleus (69%)	Cytoplasm (13%)	Many other compartments (4% each)
Sardh	X	X					None	4.7	Mitochondria (95%)	Cytoplasm (4%)	None detected
Ssb	X	X					None	12	Nucleus (91%)	Cytoplasm and cytoskeleton (4% each)	None detected
Gnas (LOC100361691)	X	X					None	None	Nucleus (69%)	Mitochondria (21%)	Cytoplasm (8.7%)
Rnf170	X	X					None	None	Endoplasmic reticulum (55%)	Vacuole (22%)	Golgi apparatus and Mitochondria (11% each)

Figure 4.7 Example of cNLS Mapper analysis output

The amino acid sequence of Matrin3 was submitted to the cNLS Mapper program and the analysis was performed with the cut-off score of 4. In the output, the highlighted sequences in red correspond to the identified cNLSs (Top panel). These NLSs are separated into two categories, monopartite (middle panel) and bipartite (bottom panel), each with a given score. An example of a protein sequence that contributed to two NLSs is indicated in the red box in the bipartite NLS panel.

Matrin 3 protein sequence: NP_062022

Predicted NLSs in query sequence

```
MSKSFQQSSLGRDSQGHGRDLSAAGIGLLAAATQSLSMPASLGRMNQGTA 50
RLASLMNLGMSSSLNQQGAHSALSSASTSSHNLQSIFNIGSRGPLPLSSQ 100
HRGDTDQASNILASFGLSARDLDELSRYPEDKITPENLPQILLQLKRRRT 150
EEGPTLSYGRDGRSATREPPYRVPRDDWEEKRHFRRDSFDDRGPSLNPVL 200
DYDHGSRSQESGYYDRMDYEDDRLRDGERCRDDSFFGETSHNYHKFDSEY 250
ERMGRGPGPLQERSLFEKKRGAPPSSNIEDFHGLLPKGYPHLCSICDLPV 300
HSNKEWSQHINGASHSRRCQLLLEIYPEWNPDNDTGHTMGDPFMLQQSTN 350
PAPGILGPPPPSFHLGGPAVGPRGNLGAGNGNLQGPRHMQKGRVETSRVV 400
HIMDFQRGKNLRYQLLQLVEPFGVISNHLILNKINEAFIEMATTEDAQAA 450
VDYYTTTPALVFGKPVRVHLSQKYKRIKKPEGKPDQKFDQKQELGRVIHL 500
SNLPHSGYSDSAVLKLAEPYGKIKNYILMRMKSQAFIEMETREDAMAMVD 550
HCLKKALWFQGRCVKVDLSEKYKKLVLRIPNRGIDLLKKDKSRKRSYSPD 600
GKESPSDKKSKTDGAQKTENPAEGKEQEEKSGEDGEKDTKDDQTEQEPSM 650
LLESEDELLVDEEEAAALLESGSSVGDETDLANLGDVSSDGKKEPSDKAV 700
KKDASATSKKKLKKVDKIEELDQENEAALENGIKNEENTEPGAESAENAD 750
DPNKDASDNSDGQNDENKEDYTIPDEYRIGPYQPNVPVGIDYVIPKTGFY 800
CKLCSLFYTNEEVAKNTHCSSLPHYQKLKKFLNKLAEERRQKKET      845
```

Predicted monopartite NLS

Pos.	Sequence	Score
141	ILLQLKRRRTE	8
143	LQLKRRRTEE	9

The identified cNLSs and their respective scores

Predicted bipartite NLS

Pos.	Sequence	Score
263	RSLFEKKRGAPPSSNIEDFHGLLPKGYPHLCSI	4.3
530	RMKSQAFIEMETREDAMAMVDHCLKKALW	5.8
590	DKSRKRSYSPDGKESPSDKKSKTD	8.9
590	DKSRKRSYSPDGKESPSDKKSKTDGAQKTENP	5

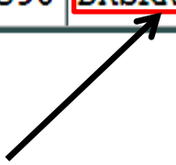

Example of overlapping sequences in different NLSs

4.6 cNLS prediction analysis of importin α binding candidates

The results of cNLS Mapper analysis on candidate importin α binding proteins in spermatocytes and spermatids have been summarized in Figures 4.8 (A) and 4.8 (B). To stratify the analysis results into meaningful outcomes, the following strategy was employed. First, the candidates were divided into several cohorts based on importin α and cell type interactions. The candidates in each cohort were then allocated to one of the three classes based on the putative cNLS score (Table 4.2). These three classes include candidates with a cNLS score of 6 and above (strong; NLS score ≥6), those with cNLS score of between 4 to 6 (moderate; 4≤ NLS score <6) and those with cNLS score of less than 4 (weak; NLS score <4). Subsequently the number of candidates in each class was counted and converted to the percentage constituent of total candidates in that cohort. The charts in Figures 4.8 (A) and 4.8 (B) contain both the number and percentage constituent of each class of cNLS in each cohort.

Figure 4.8 (A) presents categorization of the total list of candidates and also of cohorts composed of each cell type (spermatocytes or spermatids) or each importin α (importin α2 or importin α4). There is a common proportional composition between the cNLS classes for each cohort. In each cohort, 40% to 44% of candidates possess a strong cNLS. The highest variability between cohorts in Figure 4.8 (A) occurs amongst the candidates with moderate cNLS score (4 to 6), with a range of between 18% to 33%. Candidates with weak cNLS scores comprise between 25% to 37% of each cohort (Figure 4.8, A).

Approximately 30% of the proteins encoded by eukaryotic genome are thought to enter the nucleus (Huh et al., 2003; Li et al., 2006; Simpson and Pepperkok, 2003), but not all use the classical import pathway (i.e. Importin α/β1 dimer) for nuclear access (Sorokin et al., 2007). Therefore, presence of a strong cNLS sequence in more than 40% of the identified candidates in this study represents a clear enrichment of potential importin α cargo proteins and an indication of the experimental outcome validity.

Figure 4.8 (A) Classification of importin α binding candidates based on cNLS scores

The proportion and number of candidate proteins falling into each of the three NLS categories is based on the highest cNLS score assigned to them by the cNLS Mapper. The number of candidates corresponding to each percentage value is listed in parenthesis immediately below. Top chart: classification of all identified candidates. Middle charts: classification of all importin α2 (left) and importin α4 (right) candidates. Bottom charts: classification of all candidates identified from spermatocytes (left) and spermatids (right).

Total identified candidates

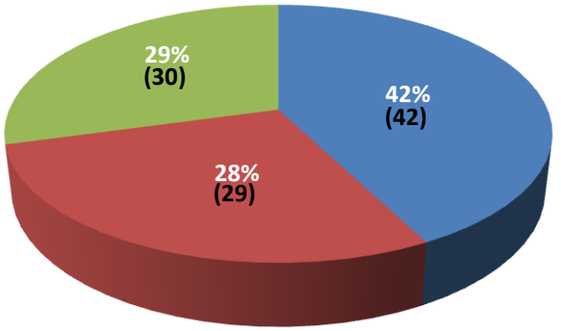

All importin α2 binding candidates

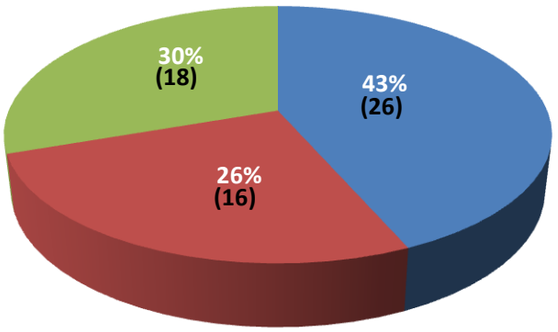

All importin α4 binding candidates

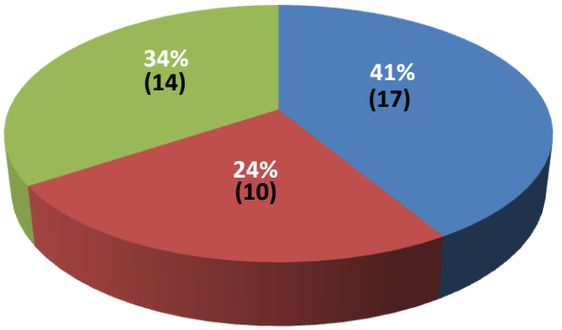

All importin α binding candidates in spermatocytes

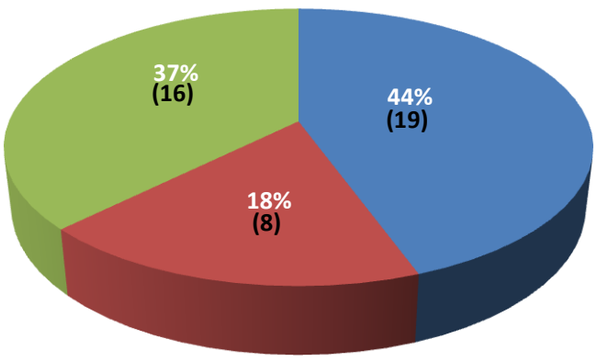

All importin α binding candidates in spermatids

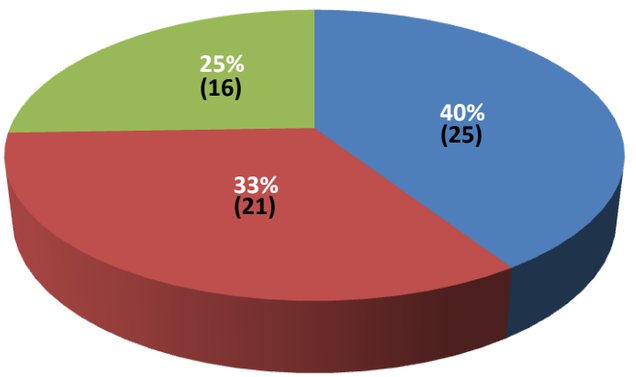

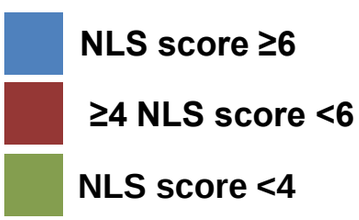

When candidates were classified into groups based on both cell type and the importin α to which they were bound, striking differences in the composition of cNLS scores between the cohorts emerged (Figure 4.8, B). The pull-down with importin α2 produced 28 candidates in spermatocytes and 25 candidates in spermatids. Of the importin α2 binding candidates in spermatocytes, a large proportion, 42%, (12 candidates) contain weak cNLSs while 17% and 39% contained moderate and strong cNLSs, respectively. In contrast, only 20% of the 25 importin α2 binding candidates identified in spermatid lysates contained weak cNLSs, 28% contained moderate cNLS and 52% contained a strong cNLS (Figure 4.8, B, top two charts).

The observation regarding the number and the cNLS motif composition of importin α2 binding candidates in spermatocytes and spermatids is intriguing. The protein expression analysis data (Section 3.6) indicates that importin α2 is much more abundant in spermatocytes than in spermatids. However, a higher proportion of importin α2 candidates in spermatids contain strong putative cNLSs, compared to the candidates identified from the spermatocytes lysate. Thus, down-regulation of importin α2 as germ cells maturate into spermatids may modulate the activity of many proteins by restricting their nuclear access.

The pull-down with importin α4 produced 19 candidates from spermatocytes and 26 candidates from spermatids. Approximately 30% of the importin α4 binding candidates in both spermatocytes and spermatids possessed a weak cNLS. However, the percentage of candidates with cNLSs of moderate and strong scores differed drastically between spermatocytes and spermatids (Figure 4.8, B, bottom two charts). In spermatocytes, 52% of importin α4 binding candidates contained cNLSs with a high score; in contrast this class of cNLS score constituted only 30% of the importin α4 binding candidates in spermatids. The relative paucity of importin α4 candidates with strong cNLSs in spermatids is largely balanced by the class of cNLSs with moderate score. In this class, 38% of importin α4 binding candidates in spermatids contained cNLSs with a moderate score, compared to only 15% of those identified in spermatocytes.

Figure 4.8 (B) Classification of importin α binding candidates based on cNLS scores

The proportion and number of candidate proteins falling into each of three categories is based on the highest cNLS score assigned to them by cNLS Mapper. The number of candidates corresponding to each percentage value is listed in parenthesis immediately below. Top charts: classification of importin α2 binding candidates in spermatocytes (left) and spermatids (right). Bottom charts: classification of importin α4 binding candidates from spermatocytes (left) and spermatids (right).

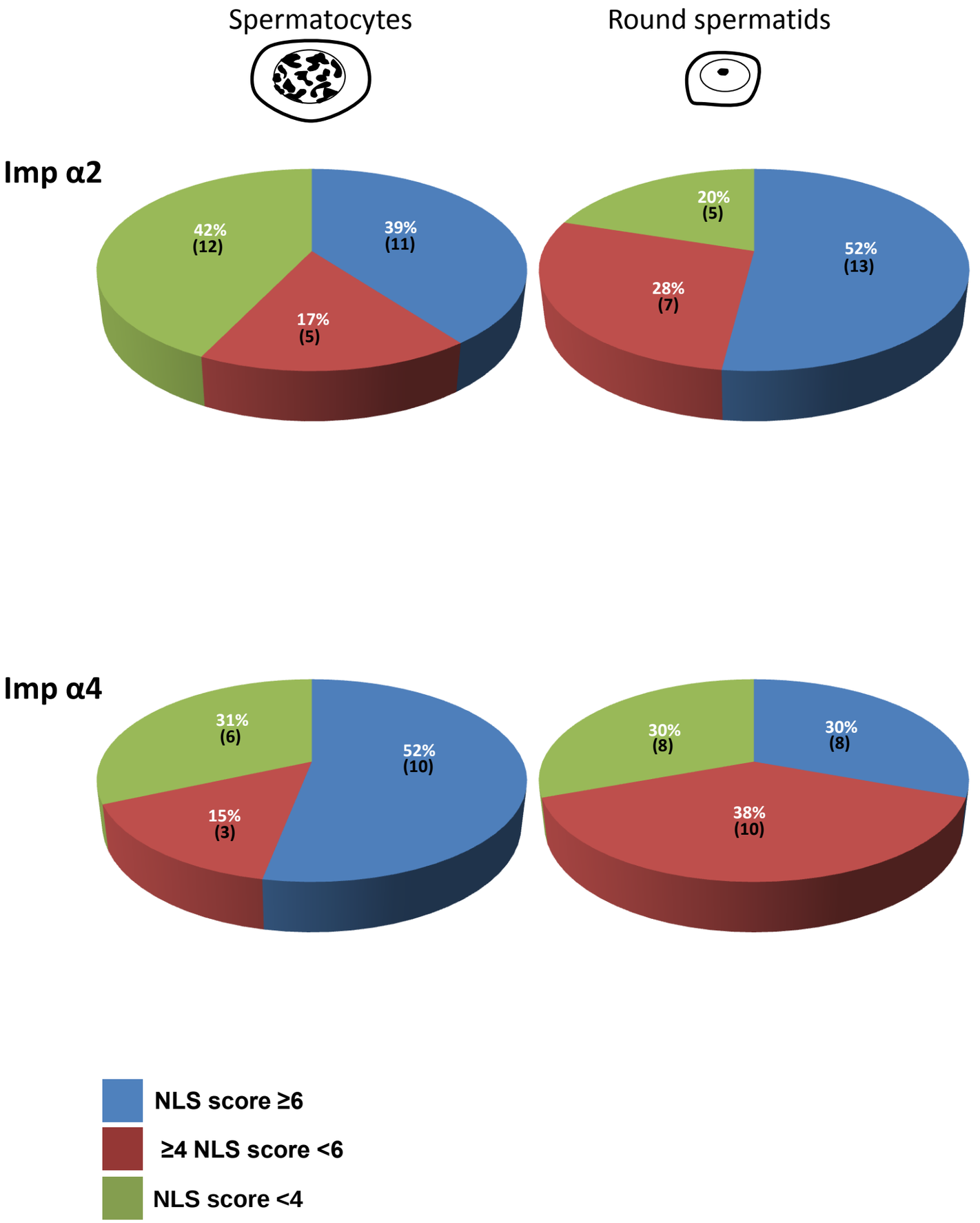
Spermatocytes
Round spermatids
Imp α2
39%
(11)
17%
(5)
42%
(12)
20%
(5)
52%
(13)
28%
(7)
Imp α4
52%
(10)
15%
(3)
31%
(6)
30%
(8)
38%
(10)
30%
(8)
NLS score ≥6
≥4 NLS score <6
NLS score <4

Although the number of importin α4 candidates differs between the two germ cell types, the higher frequency of candidates with strong cNLSs (score ≥6) identified from spermatocytes may indicate a change in the role of importin α4 between spermatocytes and spermatids, from predominantly nuclear transport into other functional associations.

4.7 Examination of the importin α binding candidates based on predicted subcellular localization

The predicted subcellular localization of importin α binding candidates (Table 4.2) is summarized graphically in Figure 4.9. In total, eleven different subcellular and extracellular compartments were identified as the likely (with varying probabilities) sites of localization for the entire list. In Table 4.2 the three most probable compartments in which candidate proteins would be localized are presented in order of the highest to the lowest probability. The candidates were divided into cohorts as described in Section 4.6 to assist interpretation of the analysis. Each candidate in the cohort was then placed in a localization category reflecting the cellular compartment to which the candidate is most likely to localize based on the percentage probability given by PSORT II program. Thus, the data in Figure 4.9 indicate the number of candidates in each cohort with the highest likelihood of localization in the given compartment.

These results revealed that every cohort of candidates followed a strikingly similar pattern of probable localization (Figure 4.9). As expected, the most likely site of localization for the majority of candidates is the nucleus (58% to 65% of candidates). In general, cytoplasm was the second most likely site of localization for candidates of most cohorts. However, the predicted frequency of cytoplasmic localization was only slightly higher than other compartments such mitochondria and endoplasmic reticulum. In particular, of the importin α2 binding candidates identified from spermatocyte lysates, more candidates were allocated to the mitochondrial compartment than to the cytoplasm. In most cohorts, few candidates were predicted to have an extracellular localization (Figure 4.9). PSORT II analysis of the complete list of binding candidates for each importin α (importin α2 and α4) or for each cell type

Figure 4.9 Categorization of candidates based on predicted subcellular localization

Histograms show the predicted localization of candidates in different cohorts based on PSORT II analysis (Table 4.2). The Y axis depicts the number of candidates allocated to each cellular compartment listed on the X axis. The cohorts include importin α2-binding candidates in spermatocytes (top left) and in spermatids (top right) and importin α4-binding candidates in spermatocytes (bottom left) and in spermatids (bottom right).

Spermatocytes

Round spermatids

Importin α2 binding candidates

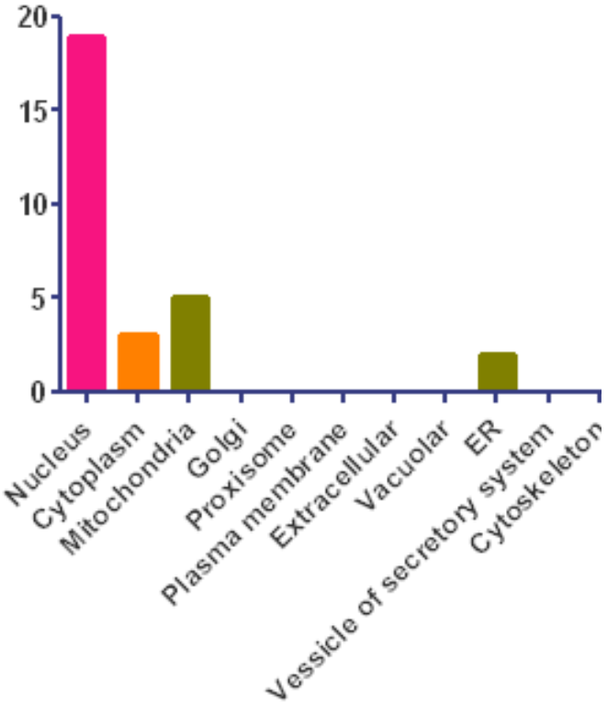

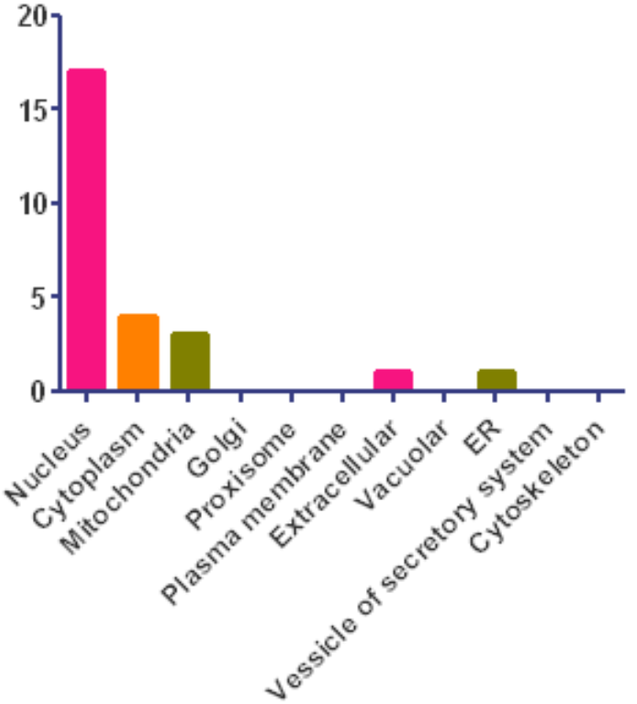

Importin α4 binding candidates

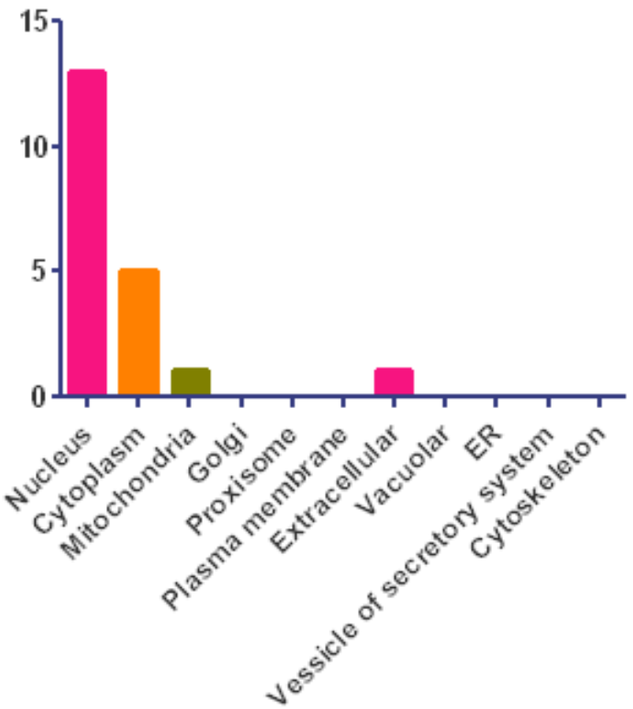

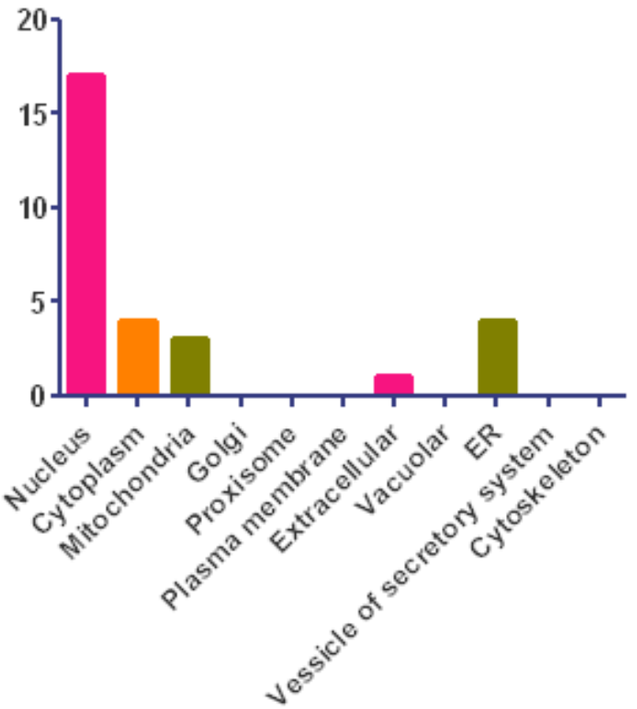

(spermatocytes and spermatids) produced similar results to those presented in Figure 4.9 (not shown); this observation indicates that in general the distribution of importins or their cargoes is similar between spermatocytes and spermatids.

The predicted presence of importin α-binding partners in a rather wide range of localizations is in agreement with the result of several studies in which importin α family members have been localized in different cellular compartments. These studies include the localization of human importin α1 on the plasma membrane of peripheral blood lymphocytes (Andrade et al., 2003), co-localization of human importin α1 with epidermal growth factor receptor (EGFR) on the plasma membrane of MDA-MB-468 cells (Lo et al., 2006), and the discovery of *X. laevis* importin α2 association with intracellular membranes extracted from egg (Hachet et al., 2004).

4.8 Importin α2-ED mutant candidates

In total, 18 candidates were identified as bound to the importin α2-ED mutant in spermatocytes and spermatids. Of these, 9 were not identified by either wild type importin α2 or α4 and thus could potentially be specific binding partners of the importin α2-ED mutant isoform. Given the small list of importin α2-ED mutant specific candidates, the result of an analysis similar to those in Sections 4.6 and 4.7 could be misleading. Thus in this section the results of cNLS Mapper and PSORT II analysis on this small cohort is presented briefly.

The cNLS scores were distributed uniformly between all candidates, with three candidates (i.e. 33%) possessing cNLSs of strong, moderate, and weak scores. Cytoplasm was the predicted site of localization for three candidates in this group while two candidates were predicted to localize in either nucleus or endoplasmic reticulum. The extracellular compartment and mitochondria were predicted to be the primary localization site for one candidate each.

Viewed collectively, there is a lower proportion of proteins in this small cohort of candidates with both predicted nuclear localization and strong cNLS when compared to cohorts identified by wild type importin αs. Despite the limited number of

candidates available for analysis, this observation is in accord with the reduced capacity of the importin α2-ED mutant to bind classical NLSs.

4.9 Bioinformatics interrogation: clues to pathways regulated by the importin α interaction networks

Protein lists generated by proteomic analyses can reveal valuable information regarding the molecular pathways that are most relevant to the context under examination. Here we have uncovered many potential binding partners for a subset of importin α family members in mammalian germ cells at successive stages of differentiation. Thus, extracting biological meanings from this output is of prime importance for understanding the processes in which these protein are involved during spermatogenesis. That importin α2 and importin α4 bound many cargoes distinct from each other that were different between germ cell types provides the initial indication of differential and diverse roles played by this family of proteins.

Given the rather large size of the candidate list in this study, and due to the fact that most proteins take part in more than one functional and interaction network, high computational power is required to reconcile the pathways and processes that are most represented by the candidate proteins. Here we have utilized the WEB-based GEne SeT AnaLysis Toolkit (WebGestalt) program (Zhang et al., 2005) which converts a list of proteins or genes (proteins in this instance) into functional enrichment categories compared to a pre-defined background. The program exploits a knowledgebase composed of many annotation categories, each consisting of a wide range of biological information regarding all genes and proteins in the category. Upon submission of a protein identifier list, WebGestalt allocates each candidate to one or more annotation categories based on the information available in the knowledgebase. The number of candidates that could have been allocated to each category by pure chance is calculated based on the size of the user's list and the number of proteins in the relevant category. Subsequently, the presence of a number of proteins in the list which is higher than that expected by chance is converted to an enrichment factor for each annotation category.

There are three main annotation categories in the output; these are Biological Process, Molecular Function and Cellular Component. The parameters in the program were set to obtain the ten highest enriched terms in each annotation category against the rat genome as the background. The same cohorts of candidates used in the cNLS Mapper prediction and PSORT II classifications (Section 4.6 and 4.7, respectively) were analysed here. The result is presented in Figure 4.10 which provides the enrichment value for the ten highest enriched terms in all three annotation categories. Striking differences in the enriched terms within all annotation categories were observed between the cohorts of candidates (Figure 4.10). Summarized below are some of the most noteworthy patterns produced by binding protein cohorts for different importin αs and cell types, with a focus on the Biological Process category. The analysis is presented in small subsections with headings indicating the relevant cohort.

Cohorts of importin α binding candidates in spermatocytes and spermatids

Regulation of mRNA and RNA stability are the Biological Processes that are most represented by all candidates identified from spermatocytes (enrichment score ~60) (Figure 4.10, A). In contrast, the chromosome condensation term has the highest enrichment score (~80) amongst the spermatid candidates (Figure 4.10, B). The differences between candidates from spermatocytes and spermatids are also evident in the Molecular Function and Cellular Component categories. In cohort of candidates identified from spermatocytes, p53 binding is the most enriched Molecular Function term (score ~100), and nuclear euchromatin (score ~270) is the most enriched Cellular Component term (Figure 4.10, A). In the cohort of candidates identified from spermatid, protein kinase binding and kinase binding are the most enriched terms in the Molecular Function category (scores of 12 and 10 respectively), and condensed chromosome (score 17) is the most enriched term in Cellular Component category (Figure 4.10, B).

Cohorts of importin α2 and importin α4 binding candidates

In the Biological Process category, proteins identified as importin α2 binding candidates produced a significant enrichment score of between 40 to 60 for the two related terms of hindlimb morphogenesis and embryonic hindlimb morphogenesis (Figure 4.10, C), while those of importin α4 produced an enrichment score of similar magnitude (~50) for the chromosome condensation term (Figure 4.10, D). The highest enriched terms within Molecular Function and Cellular Component categories for importin α2 binding candidates are p53 binding (score 48) and nuclear euchromatin (score 180), respectively (Figure 4.10, C), and for importin α4 binding candidates they are histone binding (score 31) and post-synaptic density (score 15, Figure 4.10, D).

The analysis of cohorts of candidates, identified by different importin α subtypes from either spermatocytes or spermatids resolved the annotations further and revealed potentially specific roles for importin αs in these germ cells.

Cohort of importin α2 binding candidates in spermatocytes

Within the Biological Process category, importin α2 binding candidates in spermatocytes produced enrichment factors of ~90 and ~70 for regulation of mRNA stability and embryonic hindlimb morphogenesis, respectively (Figure 4.10, E). These two terms were of highest enrichment in all candidates identified from spermatocytes (score ~60; Figure 4.10 A) and amongst all importin α2 binding candidates (score ~60; Figure 4.10, C), respectively. The relatively higher enrichment score for these terms in candidate importin α2 binding proteins in spermatocytes stems from the smaller list compared to that of the complete importin α2 or spermatocytes candidates. Importantly, neither of these terms were enriched in cohort of importin α2 binding candidates in spermatids (Figure 4.10, F) or in any cohort of importin α4 binding candidates (Figure 4.10, G and H). Thus, importin α2 production in spermatocytes may exert a significant effect on regulation of differentiation (i.e. morphogenesis) and RNA stability.

Cohort of importin α2 binding candidates in spermatids

Many terms pertinent to nuclear or chromatin organization were enriched in Biological Process category (score of up to 30) in the cohort of importin α2 candidates in spermatids (Figure 4.10, F). It should be noted that the results of quantitative Western blots of importin αs, presented in Chapter 3 of this thesis indicated a drastic down-regulation of importin α2 in round spermatids. Many related terms are also enriched in the cohort of importin α4 binding candidates in spermatids (Figure 4.10, H). In view of the apparent down-regulation of importin α2 protein in spermatids (Section 3.6) the nuclear and chromatin dynamics in spermatids may primarily be regulated by importin α4. Transcription coactivator activity with an enrichment score of ~16, and extracellular matrix with score of ~8 are the highest enriched terms in the Molecular Function and Cellular Component categories within the cohort of importin α2 binding candidates in spermatids.

Cohort of importin α4 binding candidates in spermatocytes

Bioinformatics analysis of importin α4 binding candidates in spermatocytes produced the unexpected enrichment factor of ~22 for the mitochondrial organization term within the Biological Process category (Figure 4.10, G). However, terms including protein import, nucleocytoplasmic transport and protein localization in organelle were the highest enriched terms (score 16-20) after mitochondrial organization (Figure 4.10, G). None of these later terms were enriched in the cohort of importin α4 candidates identified from spermatids (Figure 4.10, H). This observation is in agreement with the result of cNLS Mapper analysis in which a higher proportion of importin α4 binding candidates in spermatocytes (52%) contained a strong putative cNLS compared to those in spermatids (30%) (Section 4.6, Figure 4.8 B). Within the Molecular Function and Cellular Component categories, transcription coactivator activity (score 33) and post-synaptic density (score 33) were the most enriched terms in the cohort of importin α4 binding candidates from spermatocytes, respectively (Figure 4.10, G).

Cohort of importin α4 binding candidates in spermatids

As described briefly in preceding section, the cohort of importin α4 binding candidates in spermatids generated many terms related to chromosomal dynamics in the Biological Process and Cellular Component categories (Figure 4.10, H). Of the entire enriched terms in all categories (Figure 4.10), two of the most distinct terms are related to kinase binding. These terms are enriched in the cohort of all spermatid candidates (Figure 4.10, B, score 11) and in the cohort of importin α4 binding candidates in spermatids (Figure 4.10, H, score 11-12). That these terms are not enriched in cohorts of any importin α subtypes in spermatocytes or any cohort generated by importin α2, suggests the intriguing possibility of specific phosphorylation-dependent roles played by importin α4 in post-meiotic germ cells.

Collectively, these analyses results provide evidence for the differential roles of importin α family members in during spermatogenesis.

4.10 Spermatogenic expression profiles of importin α binding candidates

An indispensable part of developmental switches is the regulated spatio/temporal expression of participating factors. In a recent review Major and colleagues have demonstrated the dynamic expression profiles of the nucleocytoplasmic transport machinery in spermatogenesis, including cargo receptors, transport factors, and the components of Ran gradient (Major et al., 2011). Thus it was predicted that putative importin α binding proteins, critical for developmental switches during spermatogenesis, would be synthesized in a manner corresponding to the time in which they are most needed to exert an effect.

To examine the expression pattern of the identified candidates in spermatogenic processes, GEO profile datasets were searched. The objective was to obtain an indication of the expression profiles of candidates in a testis development time-course and in isolated germ cells from mouse testis and compare these with the main

Figure 4.10 Pathway analysis on candidate importin α binding partners

Different cohorts of importin α-binding candidates were submitted to the WebGestalt program with parameters set to identify the top 10 enriched terms in three categories of Biological Process, Molecular Function, and Cellular Component. The graphs depict the enrichment score (Y axis) of the top 10 terms within these categories (X axis).

A

All spermatocyte candidates

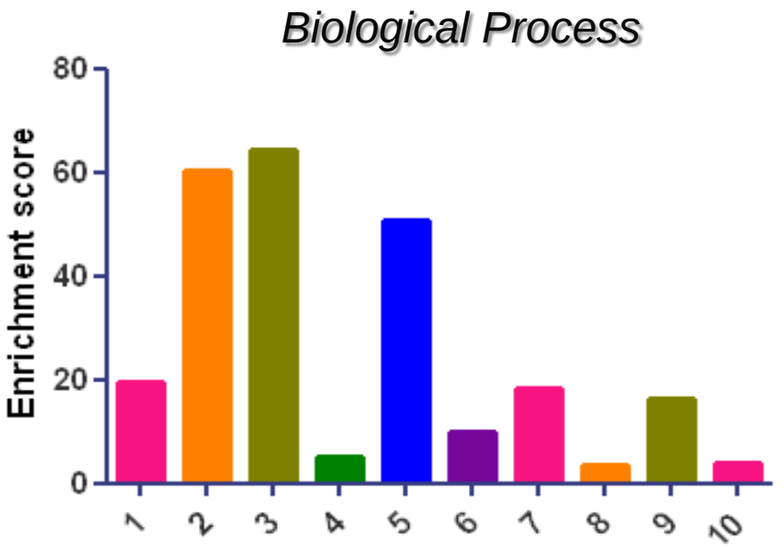

1. Positive regulation of gene-specific transcription
2. Regulation of RNA stability
3. Regulation of mRNA stability
4. Macromolecular complex subunit organization
5. Embryonic hindlimb morphogenesis
6. Posttranscriptional regulation of gene expression
7. Positive regulation of transcription factor activity
8. Macromolecule localization
9. Regulation of ubiquitin-protein ligase activity during mitotic cell cycle
10. Establishment of protein localization

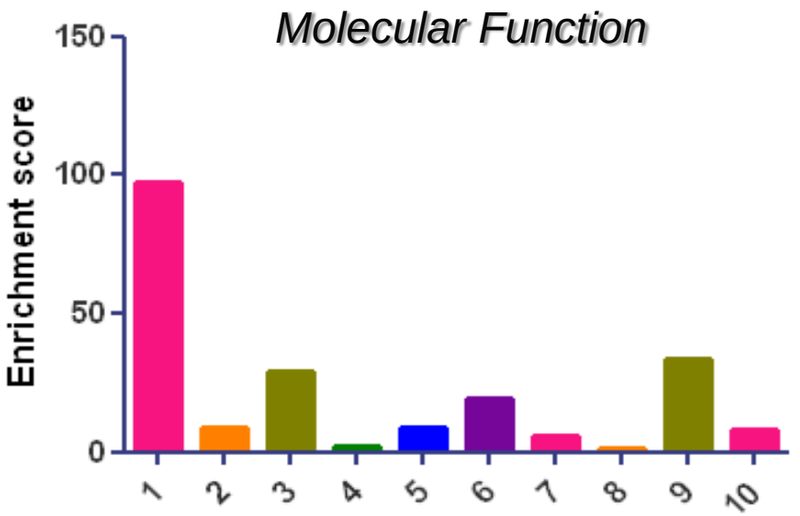

1. p53 binding
2. RNA binding
3. mRNA binding
4. Protein binding
5. Transcription factor binding
6. Transcription coactivator activity
7. Identical protein binding
8. Binding
9. Ribonucleoprotein binding
10. Transcription activator activity

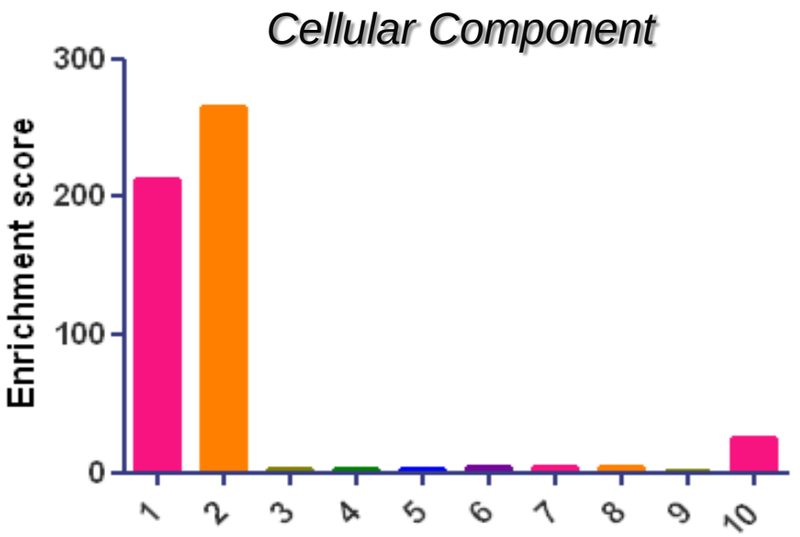

1. Euchromatin
2. Nuclear euchromatin
3. Macromolecular complex
4. Organelle part
5. Intracellular organelle part
6. Intracellular organelle lumen
7. Organelle lumen
8. Membrane-enclosed lumen
9. Intracellular part
10. Heterochromatin

B

All spermatid candidates

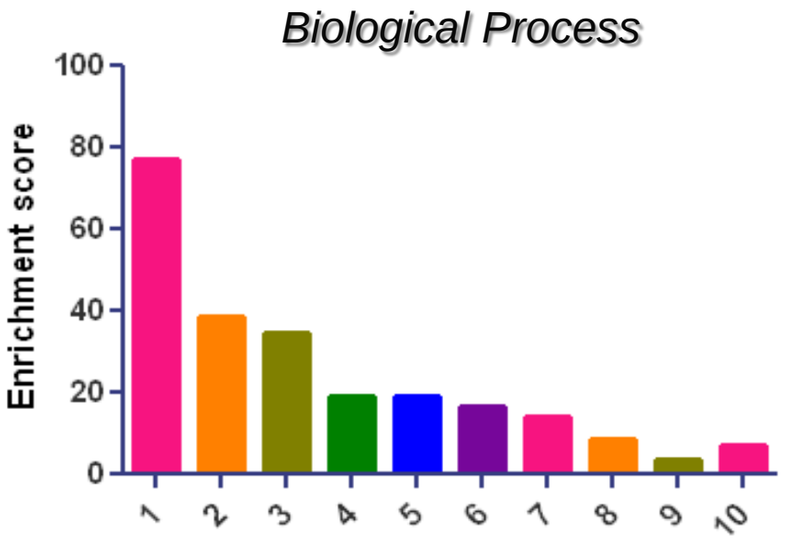

1. Chromosome condensation
2. Nucleus organization
3. Chromosome segregation
4. Protein localization in nucleus
5. DNA packaging
6. DNA conformation change
7. protein localization in organelle
8. Regulation of immune response
9. Organelle organization
10. Response to other organism

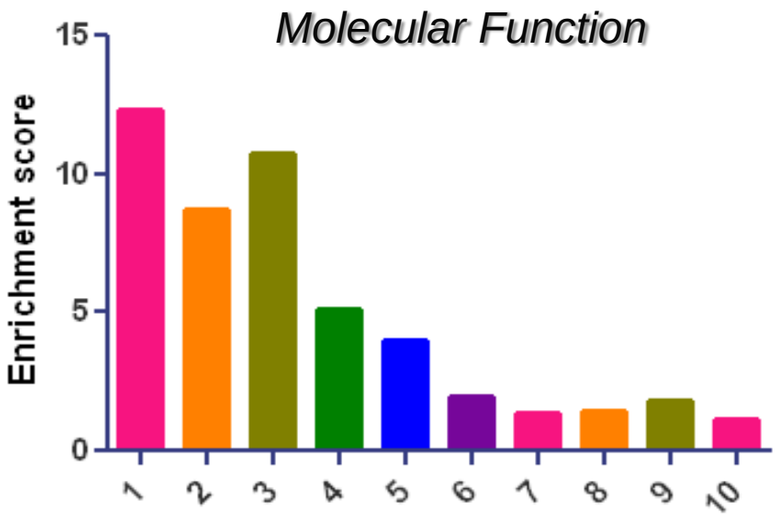

1. Protein kinase binding
2. Actin binding
3. Kinase binding
4. Cytoskeletal protein binding
5. Enzyme binding
6. Hydrolase activity
7. Protein binding
8. Catalytic activity
9. Transferase activity
10. Binding

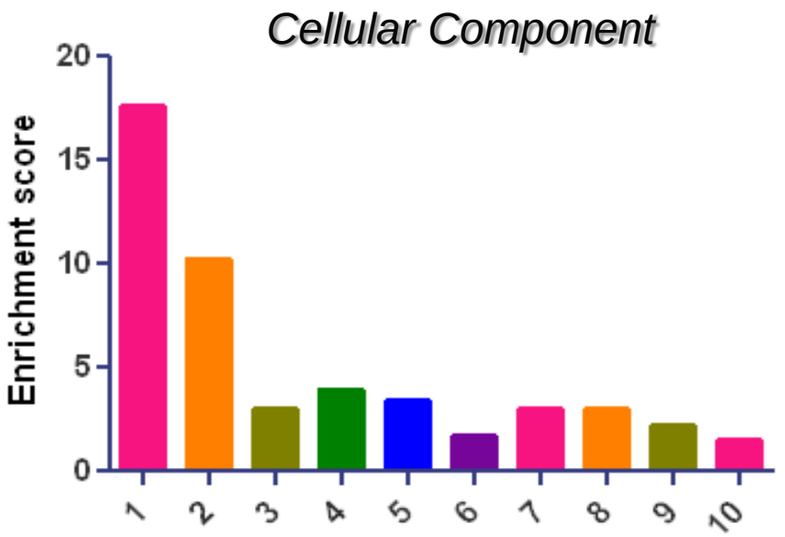

1. Condensed chromosome
2. Nuclear envelope
3. Nuclear part
4. Endomembrane system
5. Nucleolus
6. Nucleus
7. Organelle envelope
8. Envelope
9. Cytosol
10. Cytoplasm

C

All importin α2 binding candidates

Biological Process

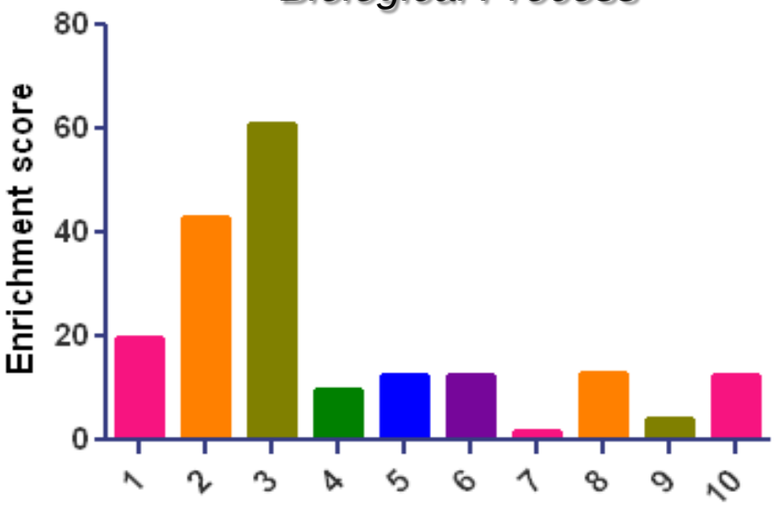

1. Nucleosome organization
2. Hindlimb morphogenesis
3. Embryonic hindlimb morphogenesis
4. mRNA metabolic process
5. Nuclear mRNA splicing, via spliceosome
6. RNA splicing, via transesterification reactions
7. Macromolecule metabolic process
8. Chromatin assembly or disassembly
9. Establishment of localization in cell
10. RNA splicing, via transesterification reactions with bulged adenosine as nucleophile

Molecular Function

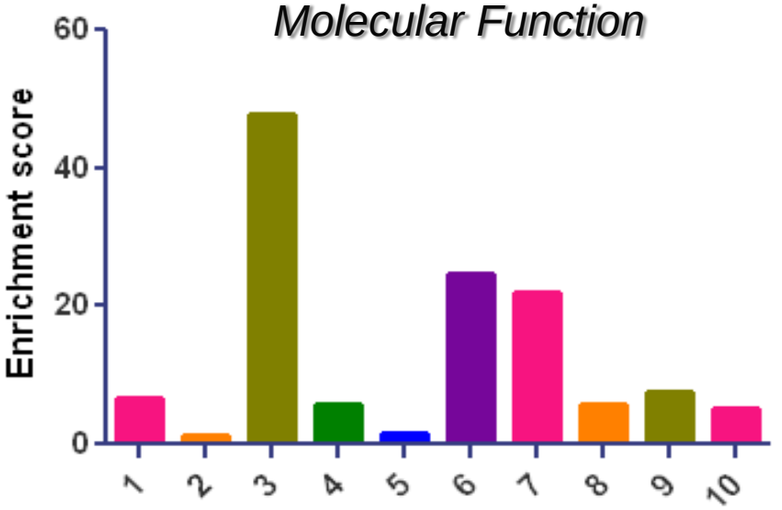

1. RNA binding
2. Binding
3. p53 binding
4. Lipid binding
5. Protein binding
6. Ribonucleoprotein binding
7. Histone binding
8. Transcription activator activity
9. Chromatin binding
10. Transcription factor binding

Cellular Component

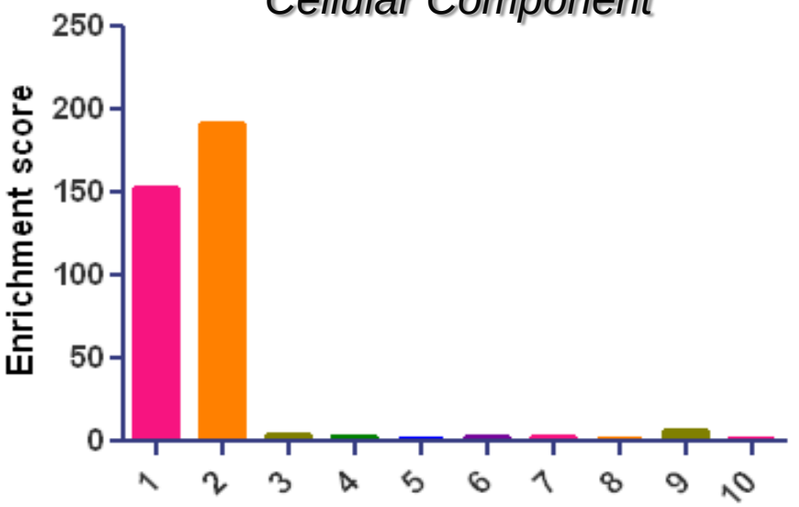

1. Euchromatin
2. Nuclear euchromatin
3. Cell fraction
4. Intracellular organelle lumen
5. Intracellular part
6. Membrane-enclosed lumen
7. Organelle lumen
8. Intracellular
9. Soluble fraction
10. Nucleus

D

All importin α4 binding candidates

Biological Process

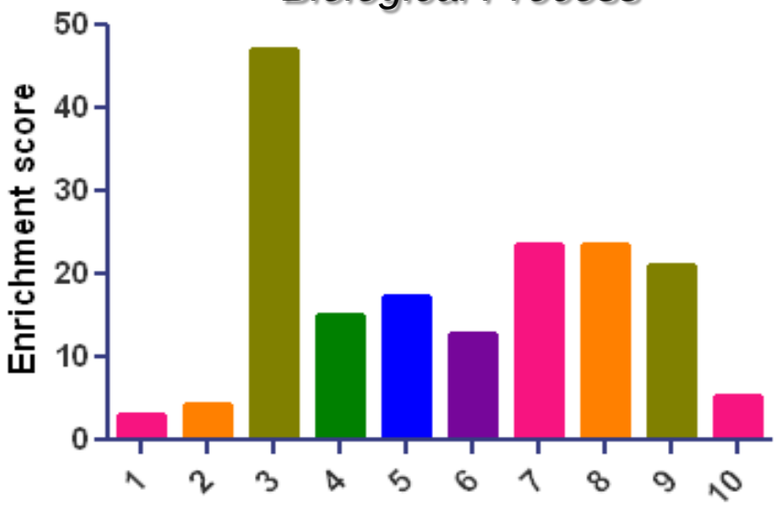

1. Cellular component organization
2. Organelle organization
3. Chromosome condensation
4. DNA conformation change
5. DNA packaging
6. Protein localization in organelle
7. Nucleus organization
8. Response to UV
9. Chromosome segregation
10. Regulation of response to stimulus

Molecular Function

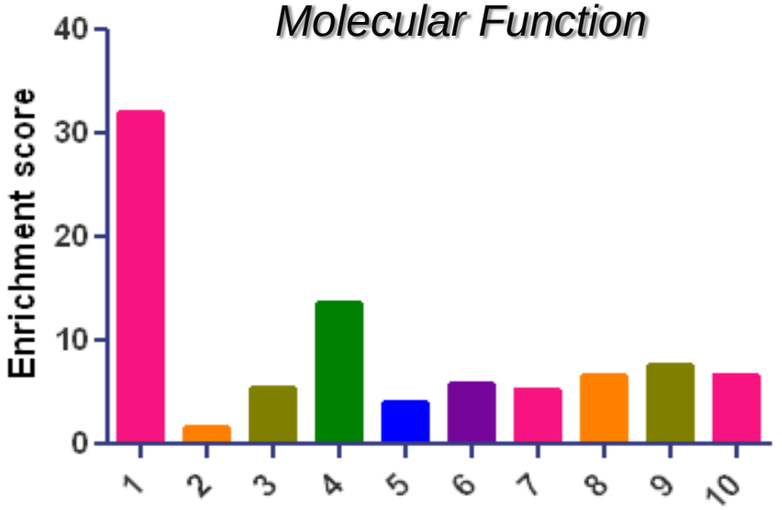

1. Histone binding
2. Protein binding
3. RNA binding
4. Transcription coactivator activity
5. Identical protein binding
6. Transcription factor binding
7. Protein domain specific binding
8. Kinase binding
9. Protein kinase binding
10. Small GTPase regulator activity

Cellular Component

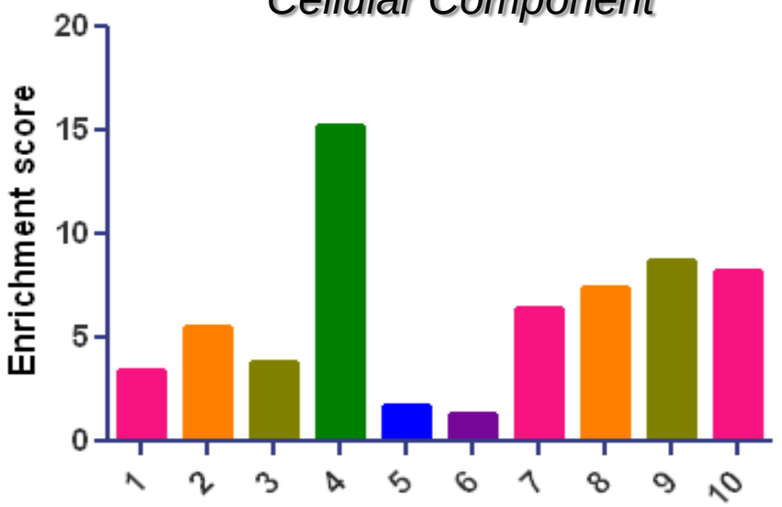

1. Cytoskeleton
2. Cell junction
3. Cytoskeletal part
4. Postsynaptic density
5. Organelle part
6. Intracellular part
7. Nuclear envelope
8. Centrosome
9. Adherens junction
10. Anchoring junction

E

All importin α2 binding candidates in spermatocytes

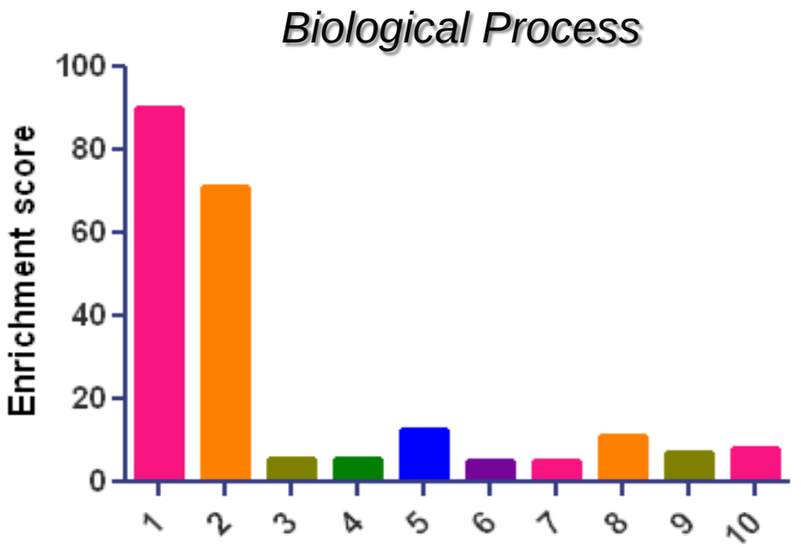

1. Regulation of mRNA stability
2. Embryonic hindlimb morphogenesis
3. Protein localization
4. Establishment of protein localization
5. Nucleocytoplasmic transport
6. Macromolecular complex subunit organization
7. Negative regulation of metabolic process
8. mRNA metabolic process
9. Chordate embryonic development
10. Negative regulation of RNA metabolic process

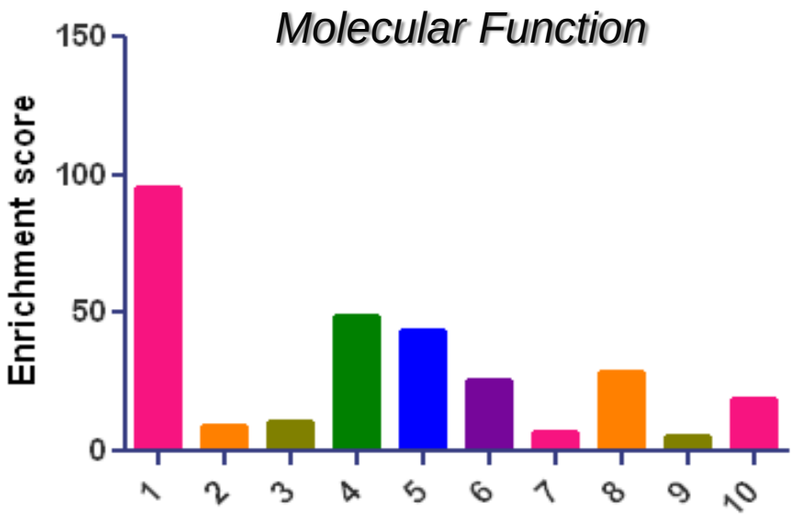

1. p53 binding
2. RNA binding
3. Transcription factor binding
4. Ribonucleoprotein binding
5. Histone binding
6. Protein transporter activity
7. Enzyme binding
8. mRNA binding
9. Identical protein binding
10. Transcription coactivator activity

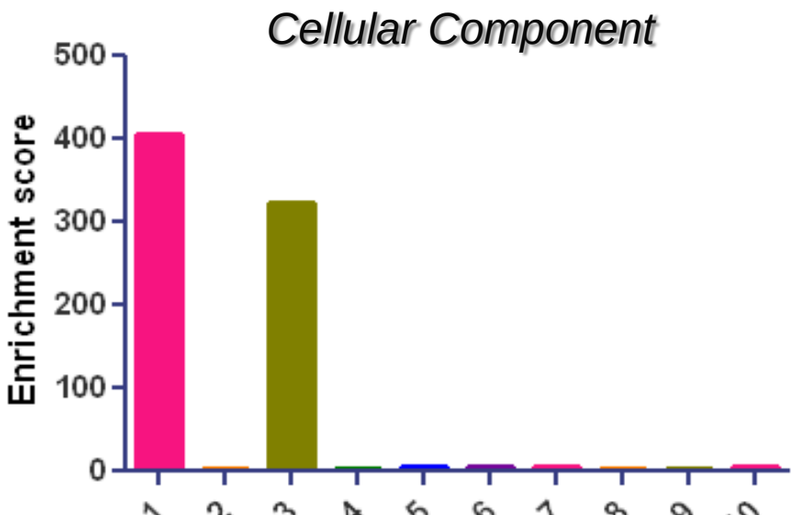

1. Nuclear euchromatin
2. Macromolecular complex
3. Euchromatin
4. Organelle part
5. Intracellular organelle lumen
6. Membrane-enclosed lumen
7. Organelle lumen
8. Intracellular organelle part
9. Nucleus
10. Nuclear part

F

All importin α2 binding candidates in spermatids

Biological Process

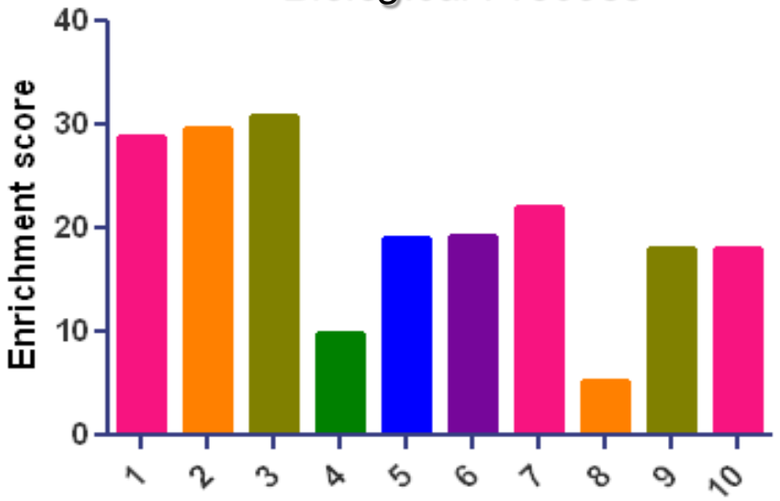

1. Nucleosome organization
2. Chromatin assembly
3. Nucleosome assembly
4. Cellular macromolecular complex assembly
5. Chromatin assembly or disassembly
6. DNA conformation change
7. DNA packaging
8. Establishment of localization in cell
9. RNA splicing, via transesterification reactions
10. Nuclear mRNA splicing, via spliceosome

Molecular Function

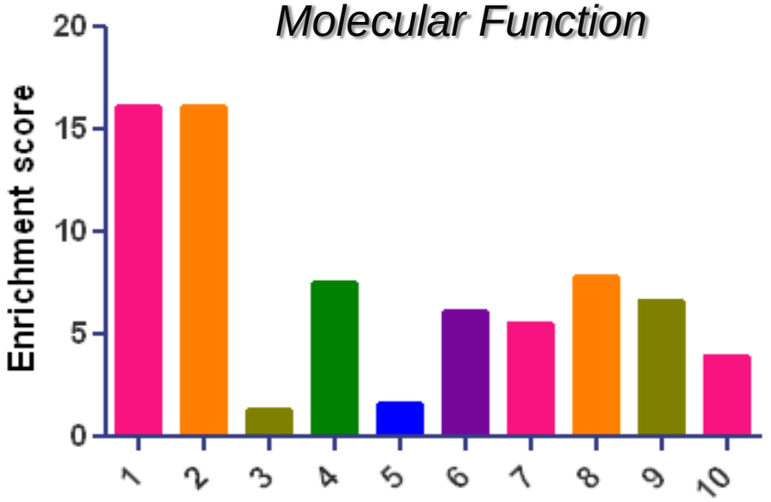

1. Transcription coactivator activity
2. Growth factor binding
3. Binding
4. Transcription activator activity
5. Protein binding
6. Lipid binding
7. Endopeptidase activity
8. Serine-type endopeptidase activity
9. Serine hydrolase activity
10. Peptidase activity, acting on L-amino acid peptides

Cellular Component

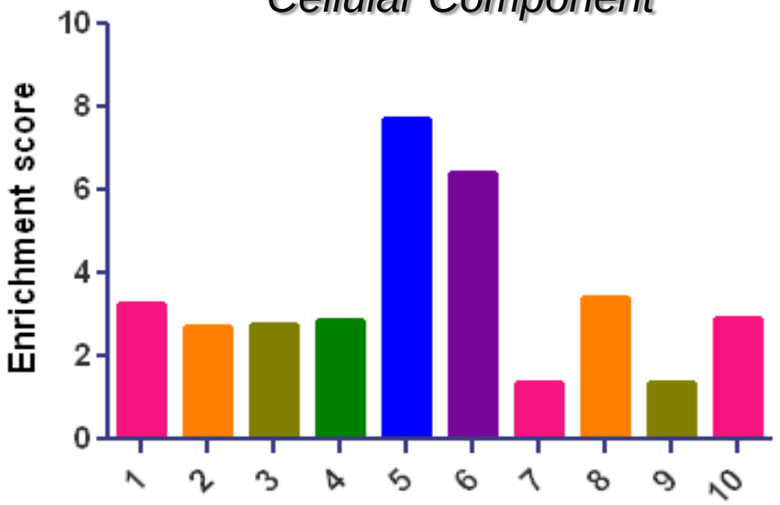

1. Cell fraction
2. Membrane-enclosed lumen
3. Organelle lumen
4. Intracellular organelle lumen
5. Extracellular matrix
6. Soluble fraction
7. Intracellular
8. Cytosol
9. Intracellular part
10. Nuclear lumen

G

All importin α4 binding candidates in spermatocytes

Biological Process

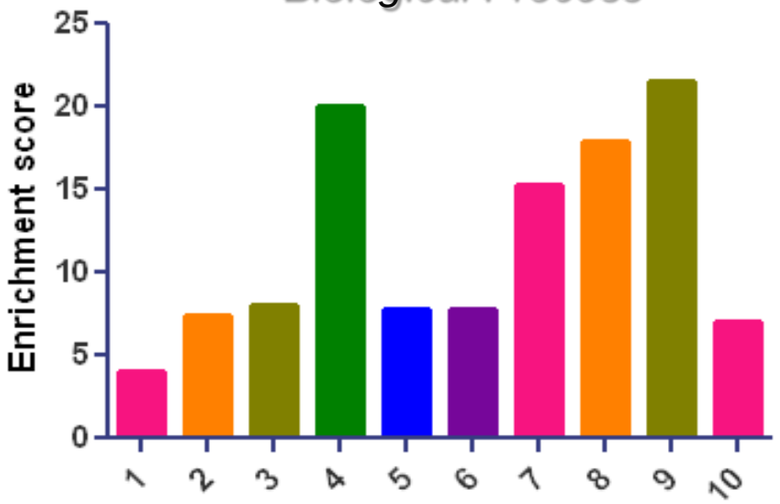

1. Cellular component organization
2. Macromolecular complex subunit organization
3. Macromolecular complex assembly
4. Protein import
5. Protein complex biogenesis
6. Protein complex assembly
7. Nucleocytoplasmic transport
8. Protein localization in organelle
9. Mitochondrion organization
10. Intracellular transport

Molecular Function

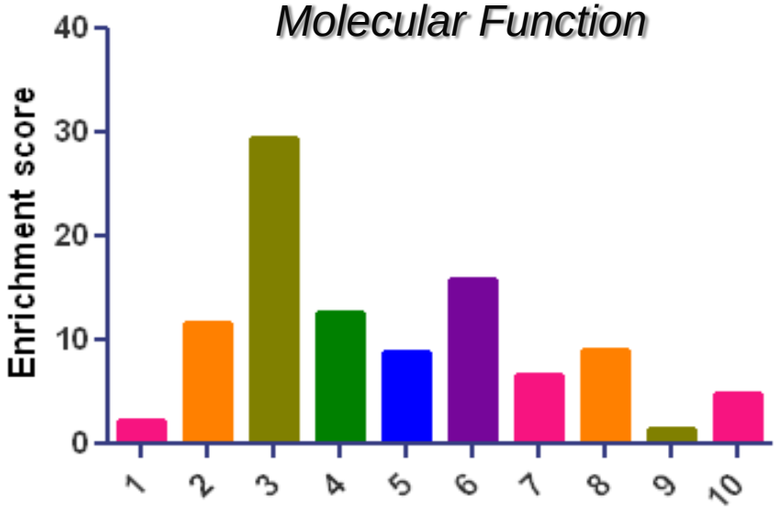

1. Protein binding
2. Protein domain specific binding
3. Transcription coactivator activity
4. Transcription factor binding
5. RNA binding
6. Transcription cofactor activity
7. Identical protein binding
8. Transcription activator activity
9. Binding
10. Kinase activity

Cellular Component

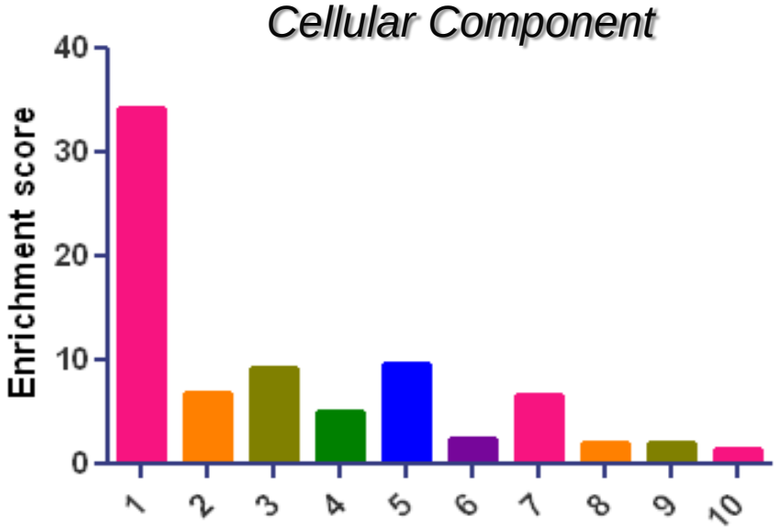

1. Postsynaptic density
2. Cytoskeletal part
3. Cell junction
4. Cytoskeleton
5. Synapse part
6. Plasma membrane
7. Synapse
8. Organelle part
9. Intracellular organelle part
10. Intracellular part

H

All importin α4 binding candidates in spermatids

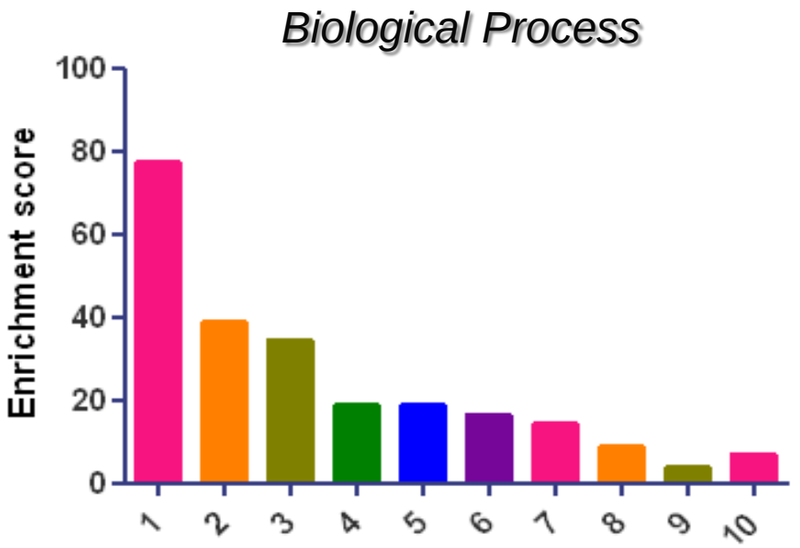

1. Chromosome condensation
2. Nucleus organization
3. Chromosome segregation
4. Protein localization in nucleus
5. DNA packaging
6. DNA conformation change
7. Protein localization in organelle
8. Rgulation of immune response
9. Organelle organization
10. Response to other organism

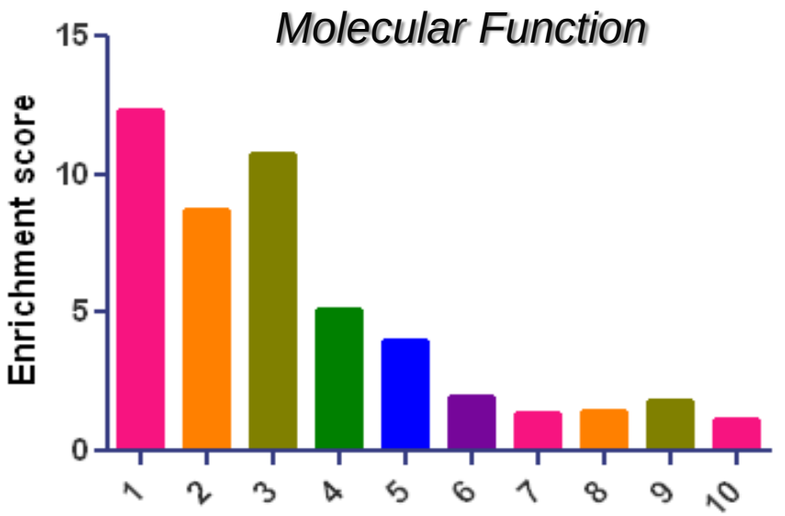

1. Protein kinase binding
2. Actin binding
3. Kinase binding
4. Cytoskeletal protein binding
5. Enzyme binding
6. Hydrolase activity
7. Protein binding
8. Catalytic activity
9. Transferase activity
10. Binding

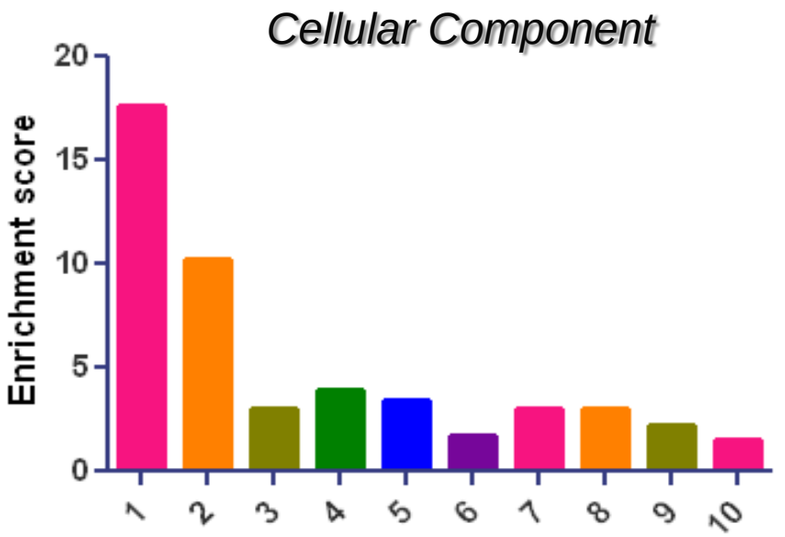

1. Condensed chromosome
2. Nuclear envelope
3. Nuclear part
4. Endomembrane system
5. Nucleolus
6. Nucleus
7. Organelle envelope
8. Envelope
9. Cytosol
10. Cytoplasm

developmental stages of spermatogenesis. Table 4.3 summarizes the GDS datasets from which the expression data were extracted.

GDS file ID	Analysed sample
GDS409	Spermatogenesis and testis development time course
GDS410	Spermatogenesis and testis development time course
GDS605	Spermatogenesis and testis development time course
GDS606	Spermatogenesis and testis development time course
GDS607	Spermatogenesis and testis development time course
GDS2390	Male germ cells
GDS3142	Various adult mouse tissues

Table 4.3 GDS datasets used for expression analysis of candidates

For many candidates, expression data were obtained by several probes within a given dataset or from different datasets. The following rules were applied to select the probe results used for presentation. To narrow down the number of probes, priority was given to the probe sets that produced the most consistent, representative profile for the candidate across all probes. Within these selected probe sets, that which produced the highest detection signal and lowest variation between biological replicates was selected.

This information is presented in Figure 4.11 (testis development timecourse on left and isolated germ cells on right coloumn). The candidates are divided into groups based on the importin α and the cell type from which they were identified, thus the expression profile of some candidates (i.e. those that were identified in more than one pull-down reaction) are presented in more than one group. Furthermore, within each group the candidates are separated into three categories based on their relative expression level (i.e. detection value), corresponding to high, intermediate and low values. This separation is performed to enable the visual discrimination of the fluctuations in expression levels of candidates, which is particularly relevant to those for which low transcript levels were measured. As a result of this adjustment, the mRNA profile of a given candidate in testis development timecourse and in isolated germ cells may not be presented alongside each other.

No detectable expression was found for many (40) candidates in any of GDS datasets in which testis age series or isolated germ cells from testis were examined. To examine the expression of these candidates in the testis, the GDS3142 dataset representing the transcript levels of genes across 22 adult mouse tissues was searched. These findings are presented in Appendix I of this chapter. Of these 40 candidates, 22 had detectable transcript levels in the testis, while no transcript level was detected for 18 due to lack of an mRNA probe in the dataset for these candidates.

The GEO profiles presented in Figure 4.11 are in line with the hypothesis that importin α binding partners have dynamic expression pattern in testis. With a few exceptions (e.g. scfd2 and Tpp2), the transcript levels of all candidates fluctuates in the developing testis and differs between subpopulations of germ cells in the testis.

Figure 4.11 Transcript profiles for importin α binding candidates in the developing mouse testis and in germ cell populations

Graphs show the expression pattern of importin α binding candidate's transcripts in a testis age series (left) and isolated germ cells from testis (right). The candidates have been grouped based on their importin α binding partner and the cell type from which the interaction was identified. Candidates in each group are further divided into subgroups of those with high (top graphs), intermediate (middle graphs) and low (bottom graphs) Affymetrix^{TM} values (Relative Expression).

Expression of importin α2 binding candidates from spermatocytes

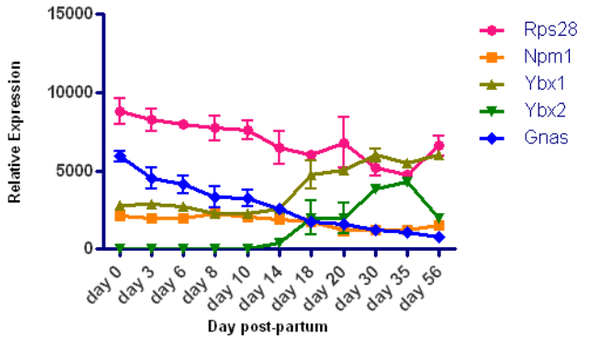

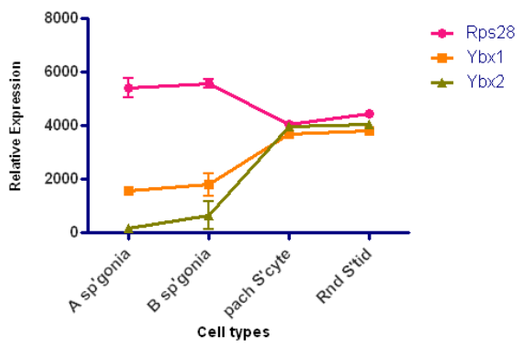

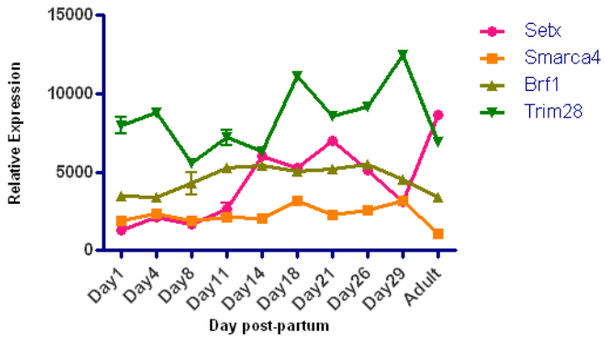

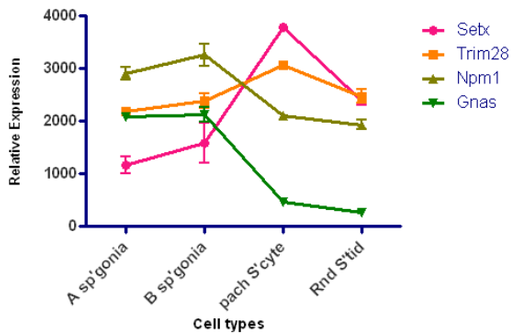

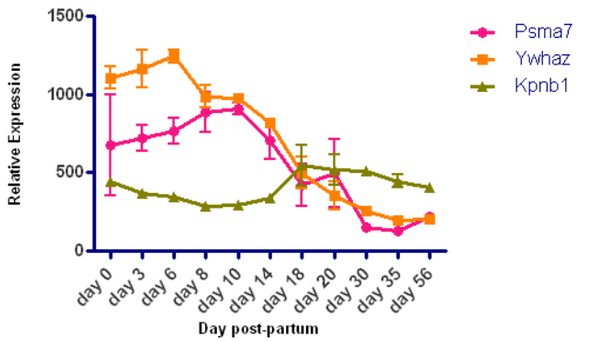

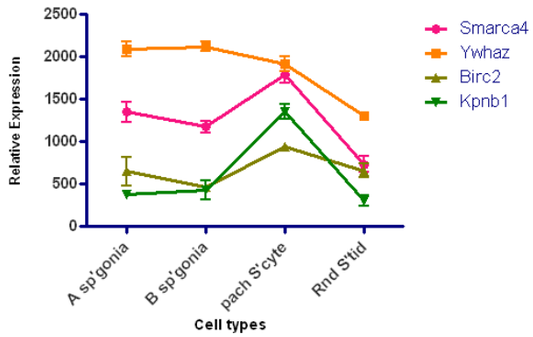

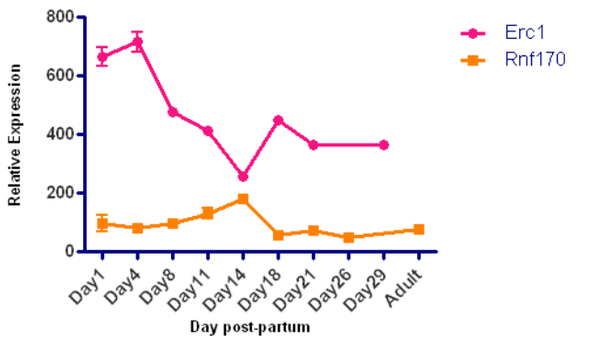

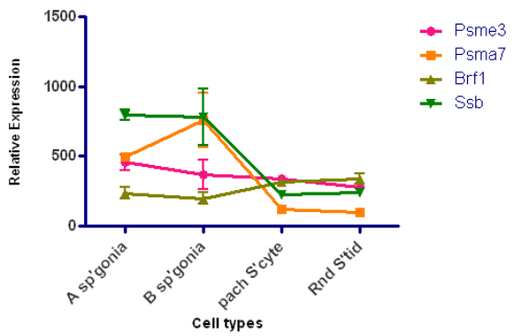

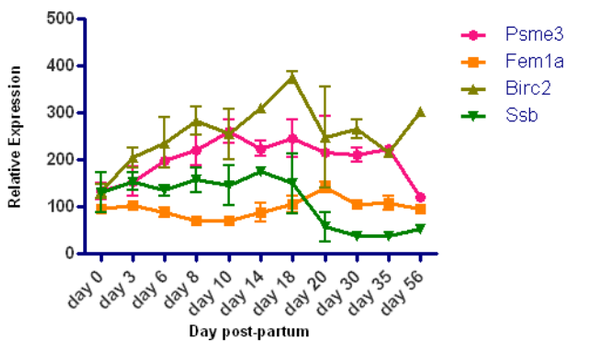

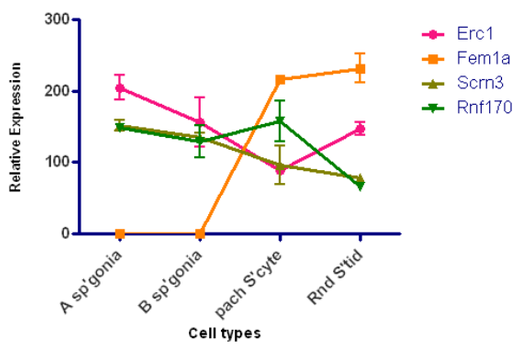

Expression of importin α2 binding candidates from spermatids

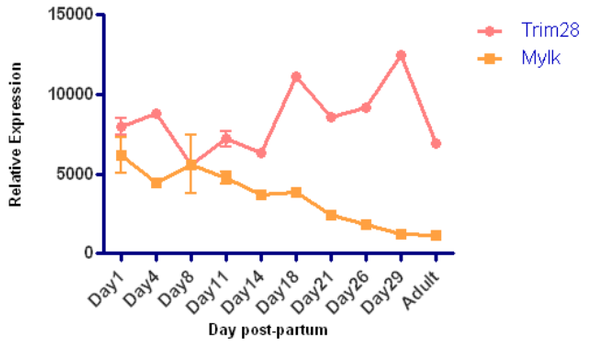

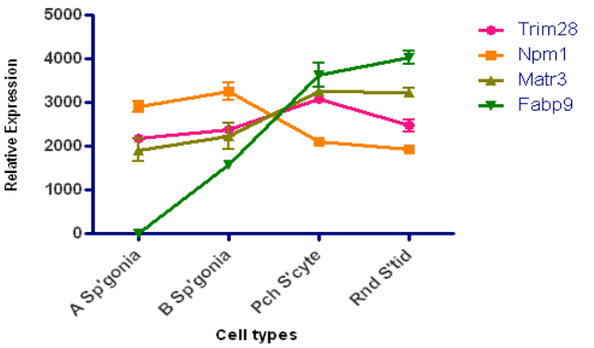

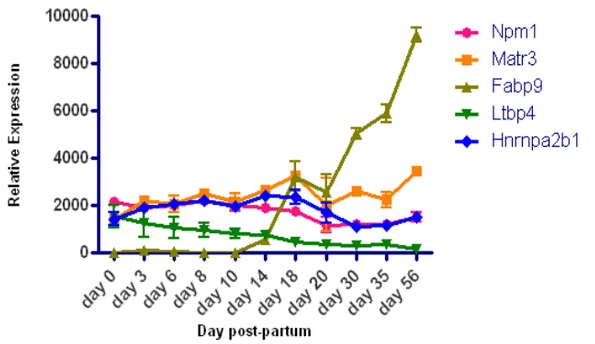

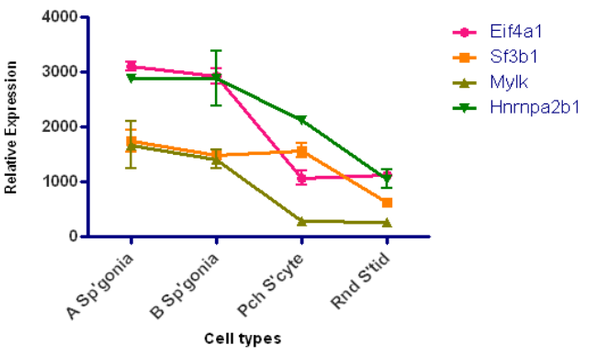

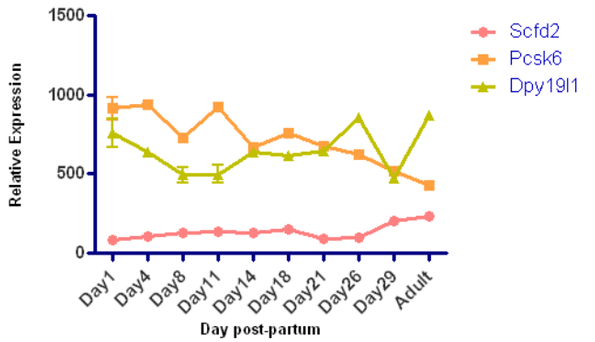

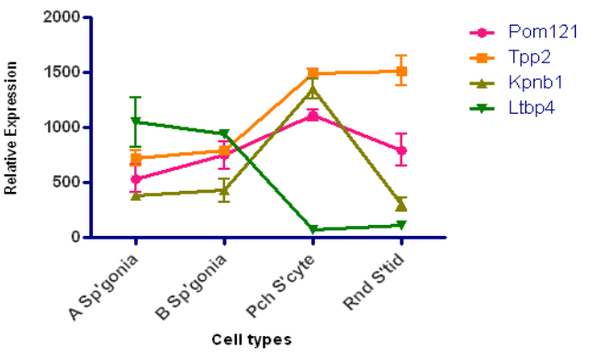

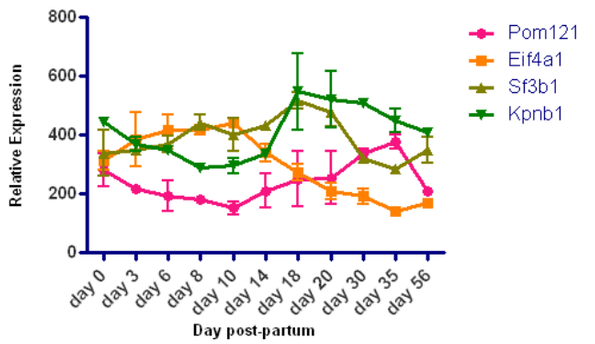

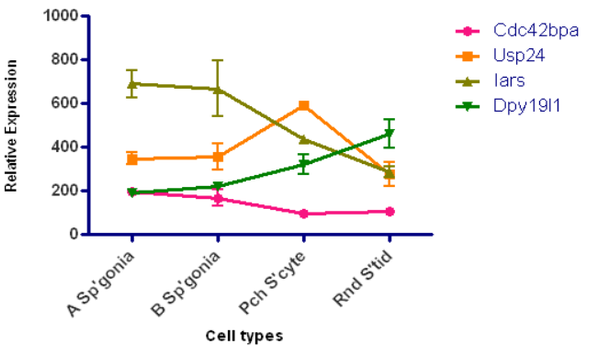

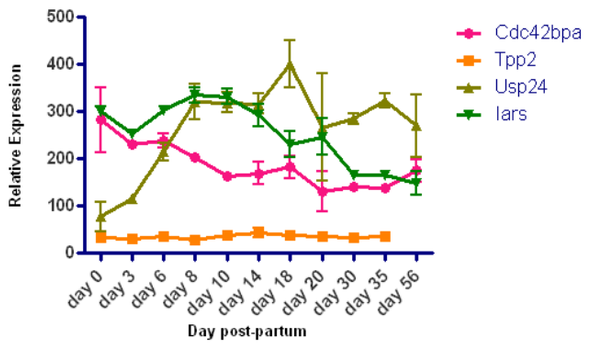

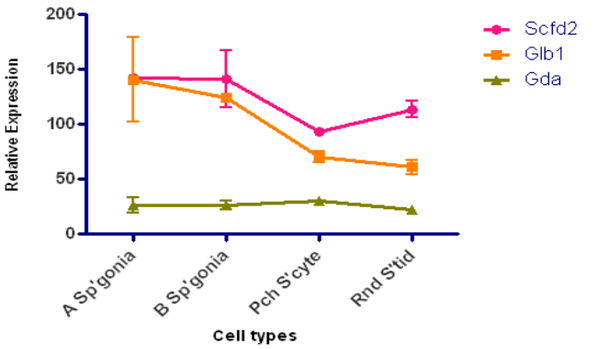

Expression of importin α4 binding candidates from spermatocytes

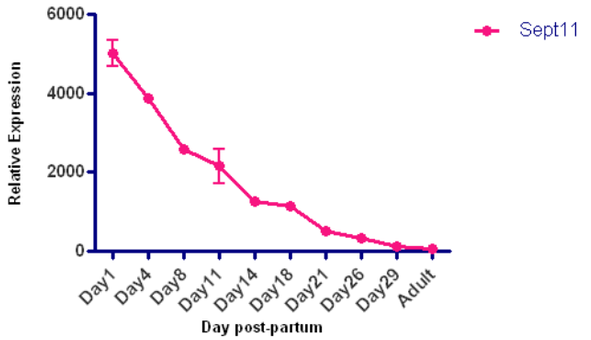

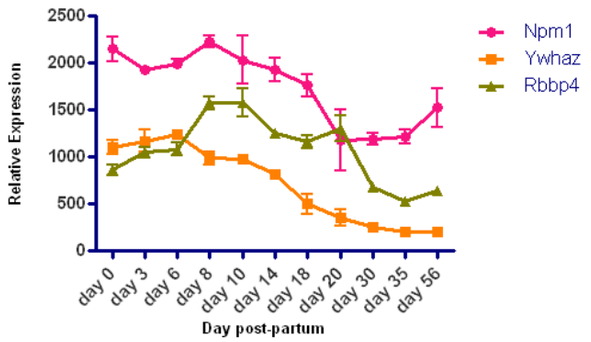

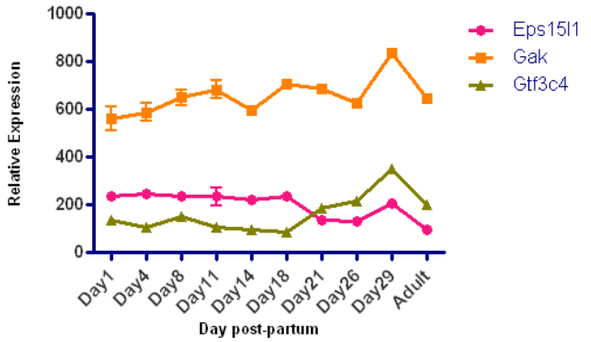

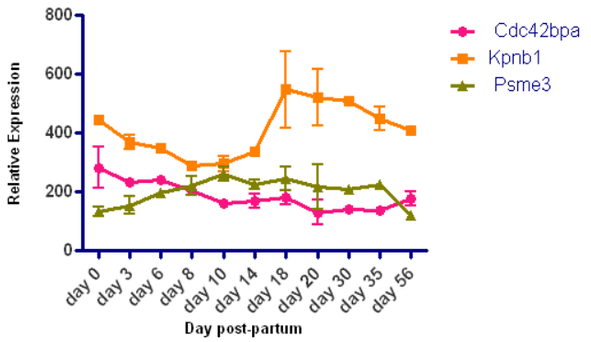

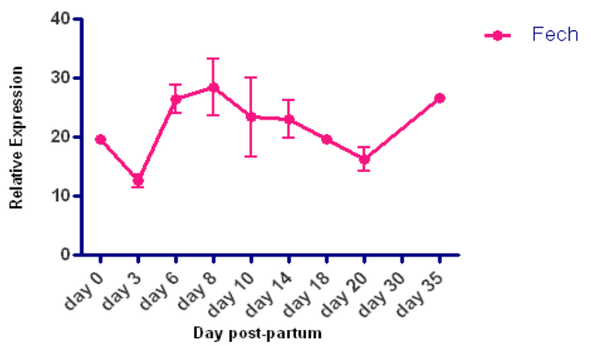

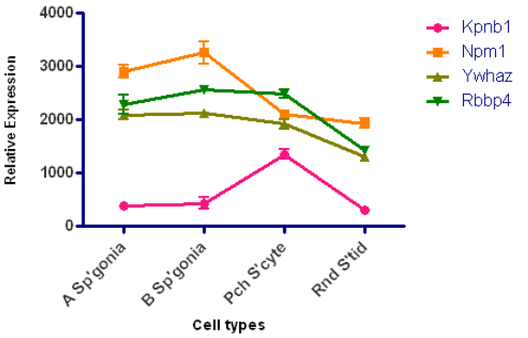

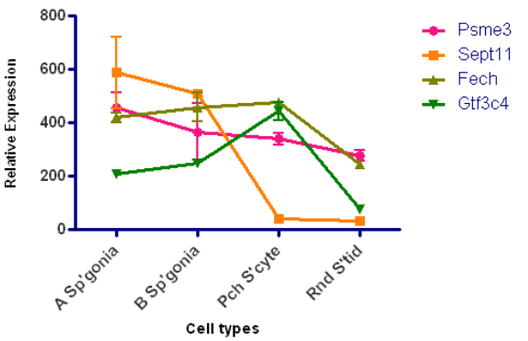

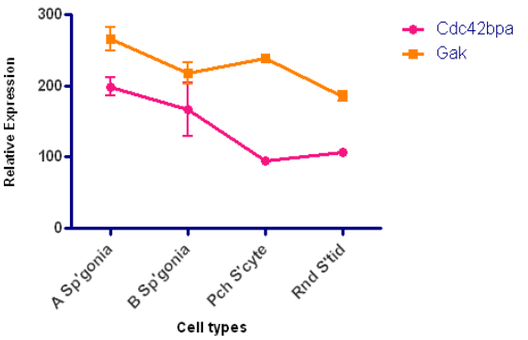

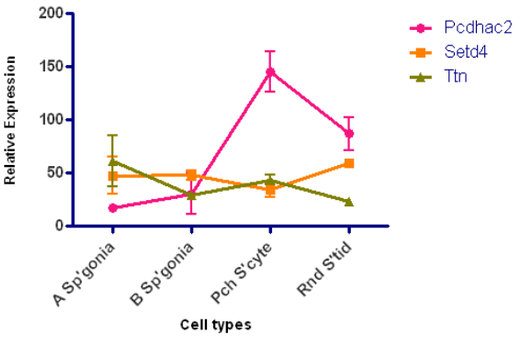

Expression of importin α4 binding candidates from spermatids

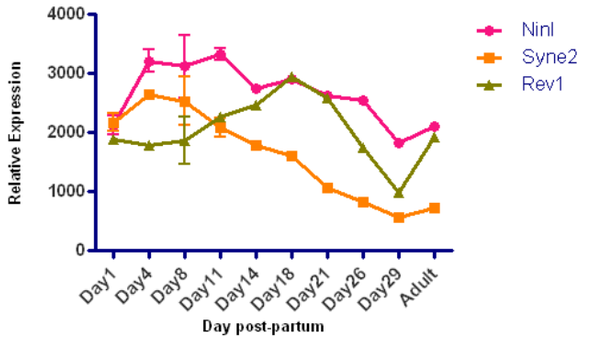

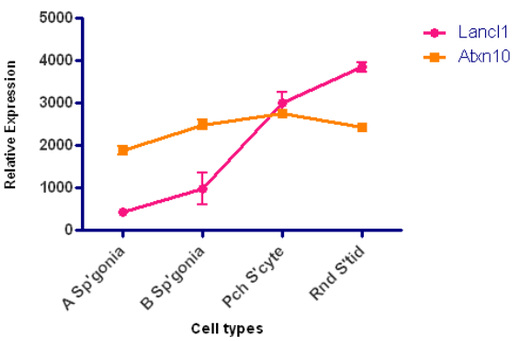

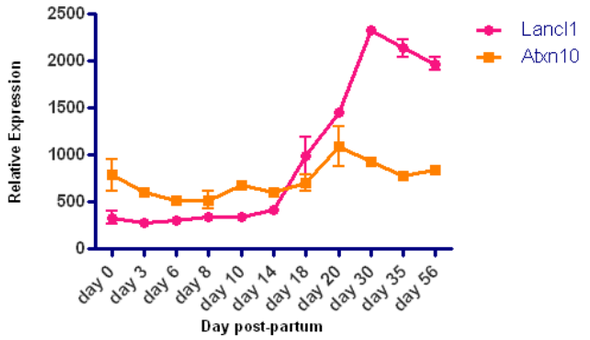

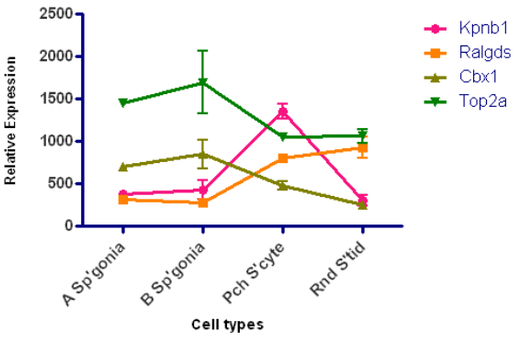

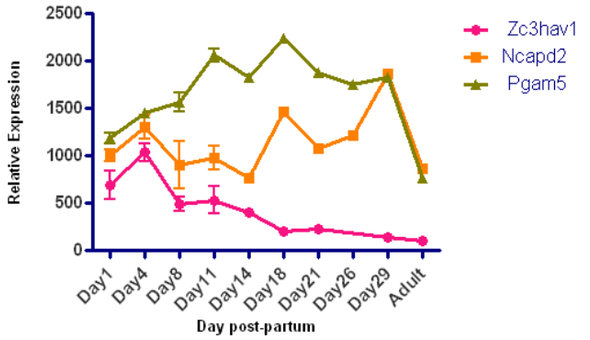

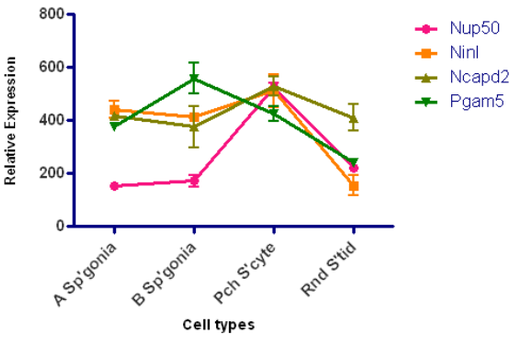

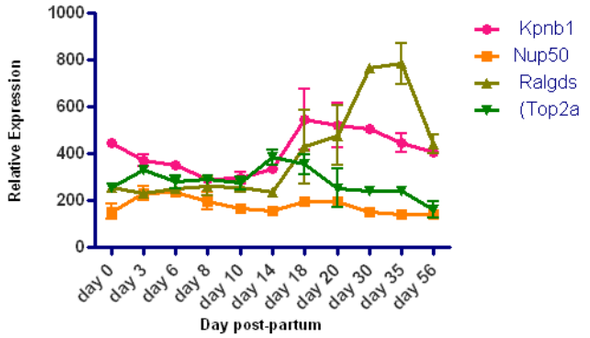

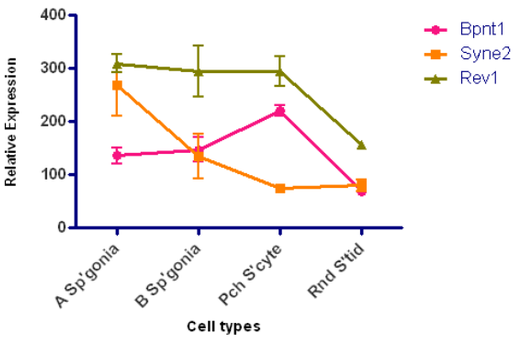

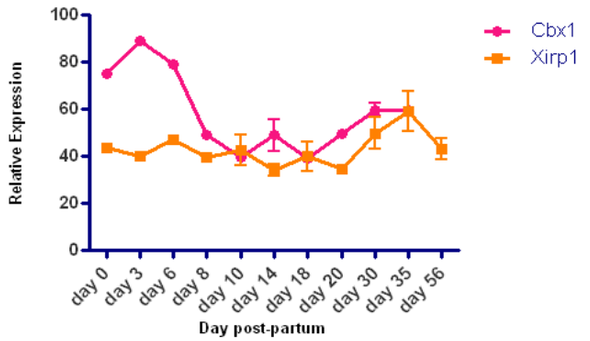

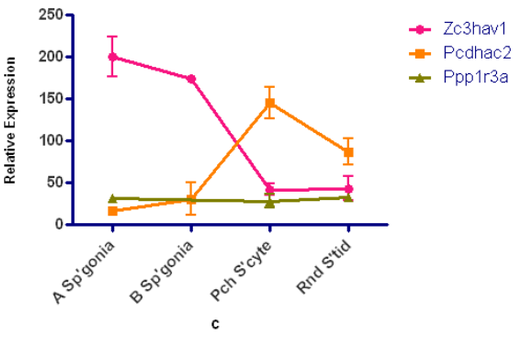

4.11 Results of the first pull-down and mass spectrometry analysis

In the first attempt to identify the binding partners of importins α2, α2-ED mutant, α3 and α4, pulled-down experiments with recombinant proteins from the lysates of spermatocytes and spermatids were performed, generally as described in Section 4.4. These pull-down products were sent to the University of Newcastle for mass spectrometry analysis, which was performed by Dr. Mark Baker as part of a research collaboration. Unfortunately, due to technical complications the samples were not analysed for 6 months. Contrary to the prediction that many binding partners would be identified for each importin α, only 20 candidates were identified from all 8 reactions (Table 4.4). Surprisingly, importin α3 produced only two candidates from the spermatocytes lysate and none from spermatids lysates, while only one candidate for importin α4 was identified from spermatids and none from spermatocytes lysate. Considering the cellular role of importin α proteins and that the binding partners of three family members were pulled-down from two different cell types, the low number of identified candidates was considered indicative of a technical failure. The cause of inadequacy in identifying numerous candidates in this study was narrowed down to factors such as duration of sample processing and unparallel mass spectrometric analysis on different samples. This judgment provoked repetition of the experiment, with prompt and thorough analysis, the result of which was presented in the previous sections of this chapter (Sections 4.4 to 4.10). Thus, this section is concerned with the result of the first pull-down and mass spectrometry analysis.

Of the 20 candidates identified in the initial analysis, there are 4 candidates which were also identified in the second analysis: heterogeneous nuclear ribonucleoprotein A2/B1 (Hnrnpa2b1), nucleophosmin (Npm1), tripartite motif-containing 28 (Trim28) and myosin light chain kinase (Mylk), all of which have both high cNLS scores and predicted or validated nuclear localization (Table 4.4). This observation served as an encouraging indication that the experimental outcome, although not satisfactory, is valid. Given the low number of candidates identified for the different importin α family members and for the two examined cell types, analyses similar to those performed for the second study was deemed misleading. Favourably however, the

small size of the list allowed a reasonably thorough literature search for several attributes of each candidate including experimentally validated subcellular localization, tissue expression, known or inferred function and associated phenotypes in cell lines, tissues or whole organisms. When no experimentally validated subcellular localization was retrieved from the literature for a given candidate, the protein sequence of the candidate was submitted to the PSORT II program (introduced in Section 4.7). Table 4.4 includes the most probable location of these candidates based on PSORT II prediction, in addition to the highest cNLS score given by cNLS Mapper. To compensate for the lack of data on tissue distribution of some candidates, the GDS3142 data set was again searched to get an insight on the transcript expression profiles of these candidates across 22 mouse tissues.

Briefly, 8 and 9 of the candidates in this list possessed a cNLS score of higher than 6 (i.e. strong) and between 4 to 6 (i.e. moderate), respectively; only three of the candidates had motifs that were discerned by cNLS Mapper with a score of less than 4 (i.e. weak). Six of the candidates have been experimentally localized in the nucleus upon detection of endogenous or over expressed proteins, while others have been detected in a wide range of cellular locations in different cell types and under various experimental conditions. Molecular functions attributed to the candidates, and phenotypes associated with defective or loss of function, fall into diverse categories, thus the reader is advised to refer to the table and cited articles therein for further information.

Table 4.4 Candidates identified in the initial pull-down and mass spectrometry experiment

Importin α2, importin α2 ED mutant, importin α3 and importin α4 binding candidates that were identified in the first pull-down and mass spectrometry analysis are listed. The table includes the official gene name and symbol and NCBI accession number, and indicates by which importin α and in which cell type (S'cyte: spermatocytes, S'tid: spermatids) the candidate was identified. The highest NLS score for each candidate is listed. The subcellular localization of candidates (either experimental or predicted by PSORT II, see text) is listed as well as information regarding the expression pattern and function of each candidate. Phenotypes caused by the knock-out or knock-down of the candidates in cell lines, whole-organism or tissues or lack of information regarding any of the above categories for any of the candidates (represented by "-") is presented.

Table 4.4 Candidates identified in the first pull-down and mass spectrometry

Gene name	Symbol/ Accession Number	Imp α and cell type interaction	cNLS score	Subcellular localization	Tissue expression	Known/predicted function	Associated phenotype
Ankyrin repeat, SAM and basic leucine zipper domain containing 1	Asz1 NP_076218.3	α2 S'cyte	7.5	Cytoplasmic in germ cells [1]. Co-localizes with the components of the inter-mitochondrial cement in spermatocytes [2].	Testis and ovary [1].	Evidence for involvement in regulation and stabilization of PIWI family members in male germ cells [2].	Male infertility due to defect in zygotene to pachytene transition [2].
Coiled-coil domain-containing protein 106	Ccdc106 NP_666290	α2 S'cyte	5.1	Human protein is nuclear in transfected HeLa cells [3].	Wide range of human cancer cell lines, including colon, lung and prostate [3].	Shown to inhibit p53 activation [3,4].	—
Heterogeneous nuclear ribonucleoprotein A2/B1	Hnrnpa2b1 NP_058086.2	α2 S'cyte	6	Mostly nuclear and partially cytoplasmic in oligodendrocytes [5].	Highest in brain and testis [5].	Translation inhibition [6]. Activated in mitochondrial stress [7].	—
Mitogen activated protein kinase 6	Mapk6 NP_056621.4	α2 S'cyte	4.3	Spindle localization during oocyte meiosis [8].	Ubiquitous expression. Highest in brain and day 11 developing embryo [9].	Role in chromosome alignment and segregation during oocyte meiosis has been delineated by *in vitro* knock-out studies[8].	Pulmonary hypoplasia and neonatal lethality due to respiration defect [10].
NADH-Cytochrome b5 reductase 3	Cyb5r3 NP_084063.1	α2 S'cyte	3.1	Leading edge of migrating fibroblasts [11] and endosomes [12].	Macrophages [13].	Involvement in phagocytosis [13] and actin polymerization [12].	—
Nucleophosmin 1	Npm1 NP_032748.1	α2 and α3 S'cyte	9.6	Nuclear and nucleolar compartment [14].	Ubiquitous. Highest expression in ES cells based on GEO profile (GDS3142/1432416_a_at).	Inhibition of apoptosis [15] and enhancement of proliferation [16]. Involved in genomic stability by promoting DNA repair [17].	Embryonic lethal [18]. Cytoplasmic mislocalization in 35% of acute myelogenous leukemia patients [19]. Overexpressed in a wide range of carcinomas [17].
Plasminogen activator inhibitor	Serpine1 NP_032897.2	α2 S'cyte	2.9	Cytoplasmic, based on PSORT II prediction.	Highest expression in placenta based on GEO profile (GDS3142/1419149_at).	Protection against extracellular matrix degradation, by inhibition of plasminogen activation [20].	Cardiac fibrosis [21].
Tripartite motif-containing 28	Trim28 NP_035718.2	α2 S'cyte	6.1	Nuclear in NIH 3T3 [22], P19 and F9 EC [23] cell lines.	Highest expression in ES cells, ovary and testis based on GEO profile (GDS3142/1415869_a_at).	Suppression of gene expression through interaction with non-histone chromosomal proteins [23].	Embryonic lethal [24]. Testicular degeneration in testis knock-out mice [25].

Gene name	Symbol/ Accession number	Imp α and cell type interaction	cNLS score	Subcellular localization	Tissue expression	Known/predicted function	Associated phenotype
Voltage dependent L-type Calcium channel subunit alpha 1F	Cacna1f NP_062528.2	α2 S'cyte	8.1	Plasma membrane upon over expression of the human Cacna1f in HEK cells [26].	Highest expression in retina[27]. Detected in human skeletal muscle, spleen and bone marrow but not testis [26].	Tonic neurotransmitter release [28].	Retinal neurotransmission defect (night blindness) [29].
Programmed cell death protein 10	Pdcd10 NP_062719.2	α2 and α2 ED S'tid	3.3	Cytoplasm in HeLa cells [30]. Golgi localization in SaOS2 cells and rat liver cells[31].	Ubiquitous, highest expression in small intestine, ES cells and testis based on GEO profile (GDS3142/1448528).	Induction of apoptosis as a result of overexpression in HeLa cells [30]. Induction of apoptosis and reduction in proliferation as a result of knock-down in malignant T-cell lines [32]. Assembly of Golgi apparatus [31].	Mutated in cerebral cavernous malformation [33]. Embryonic lethality due to defect in angiogenesis[34].
Mitochondrial dicarboxylate carrier	Slc25a10 NP_038798.2	α2 S'tid	5.3	Mitochondrial; based on mass spectrometric analysis of enriched mitochondrial proteins [35].	Very high in white adipose tissue, lower expression in liver and kidney[36].	Transport of dicarboxylates across the mitochondrial membrane in exchange for citrate during fatty acid synthesis [37].	Reduction in citrate transport upon knock-down of Slc25a10 in 3T3 cells [37].
Microtubule associated protein 9	Mtap9 NP_001074699.1	α2 ED S'cyte and S'tid	7	Localizes on the microtubules during interphase and to the mitotic spindle during mitosis [38,39].	High expression in brain and testis [39].	—	Arrest in mitosis progression upon knock-down in U-2 OS cells [38].
Paired amphipathic helix protein Sin3b	Sin3b NP_001106719.1	α2 ED S'cyte	11.2	Cytoplasmic based on PSORT II prediction.	Highest expression in placenta and moderate expression in testis based on GEO profiles (GDS 3142/1434637_x_at).	Transcriptional co-repressor through chromatin modification [40]. Induction of cell cycle exit [40,41].	Knock-out in mouse is embryonic lethal due to differentiation defects [41].
Polymerase I-transcript release factor	Ptrf NP_033012.1	α2 ED S'cyte	5.8	Cytoplasmic side of caveolae [42,43]. Disease causing mutants have been localized in the nucleus [44,45].	Wide expression with variable level; absent in liver and brain, highest in heart and lung [45,46].	Release of mRNA from transcription complex [47]. Formation and stability of caveolae [48]. Membrane damage repair through targeting of accessory proteins (e.g. MG53) [45].	Glucose intolerance. Reduced adipose tissue mass. Increased triglyceride [49].
Voltage dependent P/Q type calcium channel subunit alpha 1A	Cacna1a NP_000059.3	α2 ED S'cyte	8	Endoplasmic reticulum based on PSORT II prediction.	Predominantly expressed in central nervous system [50].	Pore forming subunit of the P/Q-type calcium channel [50]. Neurotransmitter release and dendritic Ca^{2+} transient [28].	Neurological disorders including Tottering [51], and Rocker [52] phenotypes.

Gene name	Symbol/ Accession Number	Imp α and cell type interaction	cNLS score	Subcellular localization	Tissue expression	Known/predicted function	Associated phenotype
beta-1,4-N-acetyl-galactosaminyl transferase 4	B4galnt4 Swiss-prot: Q766D5.1	α2 ED S'tid	5.1	Cytoplasmic based on PSORT II prediction.	Highest expression in ovary, foetal brain and kidney of human [53].	Transfer of N-acetyl-galactosamine to N-Glycans [53].	—
Myosin light chain polypeptide kinase	Mylk NP_647461.3	α2 ED S'tid	5.6	Nuclear based on PSORT II prediction.	High expression in ovary, small intestine and seminal vesicle based on GEO profiles (GDS3142/1425504_at).	Regulation of tight junction protein (ZO-1, Claudin, and occluding) distribution and stability through phosphorylation of Myosin light chain [54,55].	Impairment of gut mobility due to the lack of smooth muscle contraction upon targeted deletion in adult mouse [56]
Kruppel-like factor 10	Klf10 NP_038720.1	α2 ED S'tid	4.6	Endogenous human protein is nuclear in human fetal osteoblastic cells, and cytoplasmic in keratinocytes which accumulates into the nucleus upon H_2O_2 treatment [57].	Wide expression at mRNA level across mouse tissues; low expression in testis and absent from spleen and skeletal muscle [58].	Regulation of transcription through activation [59] and repression [60,61] of target genes. Inhibition of cellular proliferation [62].	Defective osteoblast differentiation [63]. Male specific and age dependent cardiac hypertrophy [64].
Splicing factor proline/ glutamine rich	Sfpq NP_076092	α2 and α3 S'cyte	4	Nuclear speckle localization in HeLa cells [65]. Cytoplasmic and nuclear localization in Sertoli TTE3 cell lines [66].	Ubiquitous, highest expression in thymus, ES cells, and ovary base on GEO profile (GDS3142/1423796). Detected in adult mouse testis by immunofluorescence [66].	Regulation of proliferation and oncogenesis [67,68]. Sister chromatid cohesion and DNA repair [69]. RNA binding and processing [70,71].	—
Iron responsive element binding protein 2	Ireb2 NP_073146.2	α4 S'tid	4.2	Cytoplasmic localization on the punctate membranous structures of unknown nature [72,73].	Human gene is ubiquitously expressed across tissues and cell lines [74].	Regulation of iron homeostasis through binding to the Iron Responsive Element (IRE) of mRNA and modulating the translation of proteins involved in iron uptake and utilization [75].	Progressive neurodegenerative disorders as a result of defective iron metabolism in brain [76].

Bibliography for Table 4.4

1. Yan W, Rajkovic A, Viveiros MM, Burns KH, Eppig JJ, et al. (2002) Identification of Gasz, an Evolutionarily Conserved Gene Expressed Exclusively in Germ Cells and Encoding a Protein with Four Ankyrin Repeats, a Sterile-{alpha} Motif, and a Basic Leucine Zipper. Mol Endocrinol 16: 1168-1184.

2. Ma L, Buchold GM, Greenbaum MP, Roy A, Burns KH, et al. (2009) GASZ Is Essential for Male Meiosis and Suppression of Retrotransposon Expression in the Male Germline. PLoS Genet 5: e1000635.

3. Zhou J, Qiao X, Xiao L, Sun W, Wang L, et al. Identification and characterization of the novel protein CCDC106 that interacts with p53 and promotes its degradation. FEBS Letters 584: 1085-1090.

4. Stelzl U, Worm U, Lalowski M, Haenig C, Brembeck FH, et al. (2005) A Human Protein-Protein Interaction Network: A Resource for Annotating the Proteome. Cell 122: 957-968.

5. Hoek KS, Kidd GJ, Carson JH, Smith R (1998) hnRNP A2 Selectively Binds the Cytoplasmic Transport Sequence of Myelin Basic Protein mRNA Biochemistry 37: 7021-7029.

6. Kosturko LD, Maggipinto MJ, Korza G, Lee JW, Carson JH, et al. (2006) Heterogeneous Nuclear Ribonucleoprotein (hnRNP) E1 Binds to hnRNP A2 and Inhibits Translation of A2 Response Element mRNAs. Mol Biol Cell 17: 3521-3533.

7. Guha M, Tang W, Sondheimer N, Avadhani NG (2010) Role of calcineurin, hnRNPA2 and Akt in mitochondrial respiratory stress-mediated transcription activation of nuclear gene targets. Biochimica et Biophysica Acta (BBA) - Bioenergetics 1797: 1055-1065.

8. Li S, Ou X-H, Wang Z-B, Xiong B, Tong J-S, et al. (2010) ERK3 Is Required for Metaphase-Anaphase Transition in Mouse Oocyte Meiosis. PLoS ONE 5: e13074.

9. Turgeon B, Saba-El-Leil MK, Meloche S (2000) Cloning and characterization of mouse extracellular-signal-regulated protein kinase 3 as a unique gene product of 100 kDa. Biochem J 346: 169-175.

10. Klinger S, Turgeon B, Levesque K, Wood GA, Aagaard-Tillery KM, et al. (2009) Loss of Erk3 function in mice leads to intrauterine growth restriction, pulmonary immaturity, and neonatal lethality. Proceedings of the National Academy of Sciences 106: 16710-16715.

11. Brandt DT, Marion S, Griffiths G, Watanabe T, Kaibuchi K, et al. (2007) Dia1 and IQGAP1 interact in cell migration and phagocytic cup formation. The Journal of Cell Biology 178: 193-200.

12. Fernandez-Borja M, Janssen L, Verwoerd D, Hordijk P, Neefjes J (2005) RhoB regulates endosome transport by promoting actin assembly on endosomal membranes through Dia1. J Cell Sci 118: 2661-2670.

13. Colucci-Guyon E, Niedergang F, Wallar BJ, Peng J, Alberts AS, et al. (2005) A Role for Mammalian Diaphanous-Related Formins in Complement Receptor (CR3)-Mediated Phagocytosis in Macrophages. Current Biology 15: 2007-2012.

14. Spector DL, Ochs RL, Busch H (1984) Silver staining, immunofluorescence, and immunoelectron microscopic localization of nucleolar phosphoproteins B23 and C23. Chromosoma 90: 139-148.

15. Dhar SK, St. Clair DK (2009) Nucleophosmin Blocks Mitochondrial Localization of p53 and Apoptosis. Journal of Biological Chemistry 284: 16409-16418.

16. Li Z, Boone D, Hann SR (2008) Nucleophosmin interacts directly with c-Myc and controls c-Myc-induced hyperproliferation and transformation. Proceedings of the National Academy of Sciences 105: 18794-18799.

17. Grisendi S, Mecucci C, Falini B, Pandolfi PP (2006) Nucleophosmin and cancer. Nat Rev Cancer 6: 493-505.

18. Grisendi S, Bernardi R, Rossi M, Cheng K, Khandker L, et al. (2005) Role of nucleophosmin in embryonic development and tumorigenesis. Nature 437: 147-153.

19. Falini B, Mecucci C, Tiacci E, Alcalay M, Rosati R, et al. (2005) Cytoplasmic Nucleophosmin in Acute Myelogenous Leukemia with a Normal Karyotype. New England Journal of Medicine 352: 254-266.

20. Rerolle J-P, Hertig A, Nguyen G, Sraer J-D, Rondeau EP (2000) Plasminogen activator inhibitor type 1 is a potential target in renal fibrogenesis. Kidney Int 58: 1841-1850.

21. Ghosh AK, Bradham WS, Gleaves LA, De Taeye B, Murphy SB, et al. (2010) Genetic Deficiency of Plasminogen Activator Inhibitor-1 Promotes Cardiac Fibrosis in Aged Mice: Involvement of Constitutive Transforming Growth Factor-beta Signaling and Endothelial-to-Mesenchymal Transition. Circulation 122: 1200-1209.

22. Ryan RF, Schultz DC, Ayyanathan K, Singh PB, Friedman JR, et al. (1999) KAP-1 Corepressor Protein Interacts and Colocalizes with Heterochromatic and Euchromatic HP1 Proteins: a Potential Role for Kruppel-Associated Box-Zinc Finger Proteins in Heterochromatin-Mediated Gene Silencing. Mol Cell Biol 19: 4366-4378.

23. Nielsen AL, Ortiz JA, You J, Oulad-Abdelghani M, Khechumian R, et al. (1999) Interaction with members of the heterochromatin protein 1 (HP1) family and histone deacetylation are differentially involved in transcriptional silencing by members of the TIF1 family. EMBO J 18: 6385-6395.

24. Cammas F, Mark M, Dolle P, Dierich A, Chambon P, et al. (2000) Mice lacking the transcriptional corepressor TIF1beta are defective in early postimplantation development. Development 127: 2955-2963.

25. Weber P, Cammas F, Gerard C, Metzger D, Chambon P, et al. (2002) Germ cell expression of the transcriptional co-repressor TIF1beta is required for the maintenance of spermatogenesis in the mouse. Development 129: 2329-2337.

26. McRory JE, Hamid J, Doering CJ, Garcia E, Parker R, et al. (2004) The CACNA1F Gene Encodes an L-Type Calcium Channel with Unique Biophysical Properties and Tissue Distribution. The Journal of Neuroscience 24: 1707-1718.

27. Strom T, M., Nyakatura G, Apfelstedt-Sylla E, Hellebrand H, Lorenz B, et al. (1998) An L-type calcium-channel gene mutated in incomplete X-linked congenital stationary night blindness. Nature Genetics 19: 260-263.

28. Catterall WA (2000) STRUCTURE AND REGULATION OF VOLTAGE-GATED Ca2+ CHANNELS. Annual Review of Cell and Developmental Biology 16: 521-555.

29. Hansen N, T, B., Naylor M, J., Maybaum T, A., Pearce W, G., Koop B, et al. (1998) Loss-of-function mutations in a calcium-channel alpha-1-subunit gene in Xp11.23 cause incomplete X-linked congenital stationary night blindness. Nature Genetics 19.

30. Chen L, Tanriover G, Yano H, Friedlander R, Louvi A, et al. (2009) Apoptotic Functions of PDCD10/CCM3, the Gene Mutated in Cerebral Cavernous Malformation 3. Stroke 40: 1474-1481.

31. Fidalgo M, Fraile M, Pires A, Force T, Pombo C, et al. (2010) CCM3/PDCD10 stabilizes GCKIII proteins to promote Golgi assembly and cell orientation. Journal of Cell Science 123: 1274-1284.

32. Lauenborg B, Kopp K, Krejsgaard T, Eriksen KW, Geisler C, et al. (2010) Programmed cell death-10 enhances proliferation and protects malignant T cells from apoptosis. APMIS 118: 719-728.

33. Pagenstecher A, Stahl S, Sure U, Felbor U (2009) A two-hit mechanism causes cerebral cavernous malformations: complete inactivation of CCM1, CCM2 or CCM3 in affected endothelial cells. Human Molecular Genetics 18: 911-918.

34. He Y, Zhang H, Yu L, Gunel M, Goggon JT, et al. (2011) Cerebral cavernous malformation gene CCM3 is critical for vascular development by regulating VEGFR2 signalling. Science Signaling 3.

35. Pagliarini DJ, Calvo SE, Chang B, Sheth SA, Vafai SB, et al. (2008) A Mitochondrial Protein Compendium Elucidates Complex I Disease Biology. Cell 134: 112-123.

36. Das K, Lewis RY, Combatsiaris TP, Lin Y, Shapiro L, et al. (1999) Predominant expression of the mitochondrial dicarboxylate carrier in white adipose tissue. Biochem J 344: 313-320.

37. Mizuarai S, Miki S, Araki H, Takahashi K, Kotani H (2005) Identification of Dicarboxylate Carrier Slc25a10 as Malate Transporter in de Novo Fatty Acid Synthesis. Journal of Biological Chemistry 280: 32434-32441.

38. Saffin J-M, Venoux M, Prigent C, Espeut J, Poulat F, et al. (2005) ASAP, a human microtubule-associated protein required for bipolar spindle assembly and cytokinesis. Proceedings of the National Academy of Sciences of the United States of America 102: 11302-11307.

39. Venoux M, Delmouly K, Milhavet O, Vidal-Eychenie S, Giorgi D, et al. (2008) Gene organization, evolution and expression of the microtubule-associated protein ASAP (MAP9). BMC Genomics 9: 406.

40. Grandinetti KB, David G (2008) Sin3B: An essential regulator of chromatin modifications at E2F target promoters during cell cycle withdrawal. Cell Cycle 7: 1550-1554.

41. David G, Grandinetti KB, Finnerty PM, Simpson N, Chu GC, et al. (2008) Specific requirement of the chromatin modifier mSin3B in cell cycle exit and cellular differentiation. Proceedings of the National Academy of Sciences 105: 4168-4172.

42. Aboulaich N, Vainonen JP, Stralfors P, Vener AV (2004) Vectorial proteomics reveal targeting, phosphorylation and specific fragmentation of polymerase I and transcript release factor (PTRF) at the surface of caveolae in human adipocytes. Biochem J 383: 237-248.

43. Vinten J, Johnsen AH, Roepstorff P, Harpoth J, Tranum-Jensen J (2005) Identification of a major protein on the cytosolic face of caveolae. Biochimica et Biophysica Acta (BBA) - Biomembranes 1717: 34-40.

44. Hayashi YK, Matsuda C, Ogawa M, Goto K, Tominaga K, et al. (2009) Human PTRF mutations cause secondary deficiency of caveolins resulting in muscular dystrophy with generalized lipodystrophy. The Journal of Clinical Investigation 119: 2623-2633.

45. Zhu H, Lin P, De G, Choi K-h, Takeshima H, et al. (2011) Polymerase Transcriptase Release Factor (PTRF) Anchors MG53 Protein to Cell Injury Site for Initiation of Membrane Repair. Journal of Biological Chemistry 286: 12820-12824.

46. Hasegawa T, Takeuchi A, Miyaishi O, Xiao H, Mao J, et al. (2000) PTRF (polymerase I and transcript-release factor) is tissue-specific and interacts with the BFCOL1 (binding factor of a type-I collagen promoter) zinc-finger transcription factor which binds to the two mouse type-I collagen gene promoters. Biochem J 347: 55-59.

47. Jansa P, Mason SW, Hoffmann-Rohrer U, Grummt I (1998) Cloning and functional characterization of PTRF, a novel protein which induces dissociation of paused ternary transcription complexes. EMBO J 17: 2855-2864.

48. Hill MM, Bastiani M, Luetterforst R, Kirkham M, Kirkham A, et al. (2008) PTRF-Cavin, a Conserved Cytoplasmic Protein Required for Caveola Formation and Function. Cell 132: 113-124.

49. Liu L, Brown D, McKee M, LeBrasseur NK, Yang D, et al. (2008) Deletion of Cavin/PTRF Causes Global Loss of Caveolae, Dyslipidemia, and Glucose Intolerance. Cell Metabolism 8: 310-317.

50. Pietrobon D (2002) Calcium channels and channelopathies of the central nervous system. Molecular Neurobiology 25: 31-50.

51. Fletcher CF, Lutz CM, O'Sullivan TN, Shaughnessy JD, Hawkes R, et al. (1996) Absence Epilepsy in Tottering Mutant Mice Is Associated with Calcium Channel Defects. Cell 87: 607-617.

52. Zwingman TA, Neumann PE, Noebels JL, Herrup K (2001) Rocker Is a New Variant of the Voltage-Dependent Calcium Channel Gene Cacna1a. The Journal of Neuroscience 21: 1169-1178.

53. Gotoh M, Sato T, Kiyohara K, Kameyama A, Kikuchi N, et al. (2004) Molecular cloning and characterization of [beta]1,4-N-acetylgalactosaminyltransferases IV synthesizing N,N'-diacetyllactosediamine. FEBS Letters 562: 134-140.

54. Shen L, Black ED, Witkowski ED, Lencer WI, Guerriero V, et al. (2006) Myosin light chain phosphorylation regulates barrier function by remodeling tight junction structure. Journal of Cell Science 119: 2095-2106.

55. Yu D, Marchiando AM, Weber CR, Raleigh DR, Wang Y, et al. (2010) MLCK-dependent exchange and actin binding region-dependent anchoring of ZO-1 regulate tight junction barrier function. Proceedings of the National Academy of Sciences 107: 8237-8241.

56. He W-Q, Peng Y-J, Zhang W-C, Lv N, Tang J, et al. (2008) Myosin Light Chain Kinase Is Central to Smooth Muscle Contraction and Required for Gastrointestinal Motility in Mice. Gastroenterology 135: 610-620.e612.

57. Subramaniam M, Hefferan TE, Tau K, Peus D, Pittelkow M, et al. (1998) Tissue, cell type, and breast cancer stage-specific expression of a TGF-β inducible early transcription factor gene. Journal of Cellular Biochemistry 68: 226-236.

58. Yajima S, Lammers C-H, Lee S-H, Hara Y, Mizuno K, et al. (1997) Cloning and Characterization of Murine Glial Cell-Derived Neurotrophic Factor Inducible Transcription Factor (MGIF). The Journal of Neuroscience 17: 8657-8666.

59. Subramaniam M, Hawse JR, Rajamannan NM, Ingle JN, Spelsberg TC (2010) Functional role of KLF10 in multiple disease processes. BioFactors 36: 8-18.

60. Hirota T, Kon N, Itagaki T, Hoshina N, Okano T, et al. (2010) Transcriptional repressor TIEG1 regulates Bmal1 gene through GC box and controls circadian clockwork. Genes to Cells 15: 111-121.

61. Subramaniam M, Hawse JR, Bruinsma ES, Grygo SB, Cicek M, et al. (2010) TGF beta inducible early gene-1 directly binds to, and represses, the OPG promoter in osteoblasts. Biochemical and Biophysical Research Communications 392: 72-76.

62. Johnsen SA, Subramaniam M, Effenberger KE, Spelsberg TC (2004) The TGFβ inducible early gene plays a central role in the anti-proliferative response to TGFβ. Signal Transduction 4: 29-35.

63. Subramaniam M, Gorny G, Johnsen SA, Monroe DG, Evans GL, et al. (2005) TIEG1 Null Mouse-Derived Osteoblasts Are Defective in Mineralization and in Support of Osteoclast Differentiation In Vitro. Mol Cell Biol 25: 1191-1199.

64. Rajamannan NM, Subramaniam M, Abraham TP, Vasile VC, Ackerman MJ, et al. (2007) TGFβ inducible early gene-1 (TIEG1) and cardiac hypertrophy: Discovery and characterization of a novel signaling pathway. Journal of Cellular Biochemistry 100: 315-325.

65. Meissner M, Dechat T, Gerner C, Grimm R, Foisner R, et al. (2000) Differential nuclear localization and nuclear matrix association of the splicing factors PSF and PTB. Journal of Cellular Biochemistry 76: 559-566.

66. Kuwahara S, Ikei A, Taguchi Y, Tabuchi Y, Fujimoto N, et al. (2006) PSPC1, NONO, and SFPQ Are Expressed in Mouse Sertoli Cells and May Function as Coregulators of Androgen Receptor-Mediated Transcription. Biology of Reproduction 75: 352-359.

67. Figueroa Al, Fujita Y, Gorospe M (2009) Hacking RNA: Hakai promotes tumorigenesis by enhancing the RNA-binding function of PSF. Cell Cycle 8: 3648-3651.

68. Wang G, Cui Y, Zhang G, Garen A, Song X (2009) Regulation of proto-oncogene transcription, cell proliferation, and tumorigenesis in mice by PSF protein and a VL30 noncoding RNA. Proceedings of the National Academy of Sciences 106: 16794-16798.

69. Rajesh C, Baker DK, Pierce AJ, Pittman DL (2011) The splicing-factor related protein SFPQ/PSF interacts with RAD51D and is necessary for homology-directed repair and sister chromatid cohesion. Nucleic Acids Research 39: 132-145.

70. Buxade M, Morrice N, Krebs DL, Proud CG (2008) The PSF·p54nrb Complex Is a Novel Mnk Substrate That Binds the mRNA for Tumor Necrosis Factor alpha. Journal of Biological Chemistry 283: 57-65.

71. Dong X, Sweet J, Challis JRG, Brown T, Lye SJ (2007) Transcriptional Activity of Androgen Receptor Is Modulated by Two RNA Splicing Factors, PSF and p54nrb. Mol Cell Biol 27: 4863-4875.

72. Patton SM, Pinero DJ, Surguladze N, Beard J, Connor JR (2005) Subcellular localization of iron regulatory proteins to Golgi and ER membranes. Journal of Cell Science 118: 4365-4373.

73. Pinero DJ, Li N, Hu J, Beard JL, Connor JR (2001) The Intracellular Location of Iron Regulatory Proteins Is Altered as a Function of Iron Status in Cell Cultures and Rat Brain. The Journal of Nutrition 131: 2831-2836.

74. Samaniego F, Chin J, Iwai K, Rouault TA, Klausner RD (1994) Molecular characterization of a second iron-responsive element binding protein, iron regulatory protein 2. Structure, function, and post-translational regulation. Journal of Biological Chemistry 269: 30904-30910.

75. Crichton RR, Wilmet S, Legssyer R, Ward RJ (2002) Molecular and cellular mechanisms of iron homeostasis and toxicity in mammalian cells. Journal of Inorganic Biochemistry 91: 9-18.

76. LaVaute T, Smith S, Cooperman S, Iwai K, Land W, et al. (2001) Targeted deletion of the gene encoding iron regulatory protein-2 causes misregulation of iron metabolism and neurodegenerative disease in mice. Nat Genet 27: 209-214.

4.12 Concluding remarks

This chapter presents the results of two independent attempts in which recombinant importin α proteins were used as bait to pull-down their binding partners from lysates of spermatocytes and spermatids of adult rat testes, followed by mass spectrometric identification. In the first attempt, only 20 candidates were identified after mass spectrometric analysis on pull-down of importin α2, the importin α2-ED mutant, and importins α3 and α4 from both spermatocytes and spermatids (Section 4.11). Due to the limited number of candidates identified in the first attempt, and the likelihood that technical issues prevented robust data collection, the potential to draw conclusions from categorization of these candidates into cohorts based on importin α- or cell-specific interactions was deemed inappropriate. All of these candidates however, are listed in Table 4.4, each with information regarding the presence of a putative cNLS, known or predicted subcellular localization, proposed function and any association with disease. In the second attempt, 101 proteins were identified as putative binding partners of importin α2, α2-ED mutant and importin α4 from these two testicular cell types. These candidates included two known binding partners of importin α, namely, importin β1 and Nup50, as well as four candidates (Hnrnpa2b1, Npm1, Trim 28, and Mylk) that were also identified in the first pull-down experiment attempt.

Several approaches were taken to assess the validity of the second experimental outcome. These were: (1) searching the protein sequence of each candidate with the cNLS Mapper algorithm to identify putative cNLSs, (2) evaluating the likely subcellular localization of each candidate through PSORT II analysis and (3) examining the transcript profile of each candidate in the developing mouse testis and in isolated germ cells from mouse testes through a GEO profile search. The results of cNLS Mapper analysis showed that the binding partners of different importin α family members in different cell types have distinct NLS motif composition. Thus, 39% (11 candidates) of importin α2 putative binding proteins had strong cNLSs in spermatocytes compared to 52% (13 candidates) in spermatids. On the other hand, amongst the importin α4 binding candidates in spermatocytes, 52% (10 candidates) contained strong cNLSs compared to 30% (8 candidates) in spermatids. The result of PSORT II analysis on different cohorts of candidates produced very similar patterns

for all. Not surprisingly, the nucleus was the most probable site of localization for the majority of candidates in every cohort, followed by the cytoplasm, while in every cohort some candidates were allocated to mitochondria. The GEO profile analysis of candidates showed that with few exceptions, the majority of the candidates exhibit regulated synthesis at mRNA level throughout spermatogenesis and are present at distinct levels in different germ cell subtypes. The cohort of candidates produced by importin α2 and importin α4 from each cell type were also submitted to WebGestalt program to identify the molecular pathways that are most represented by each cohort of candidates. From this analysis, distinct terms were enriched by cohorts of candidates linked to different importin αs from each cell type. RNA stability and differentiation were the most enriched Biological Processes terms within the group of importin α2 binding candidates in spermatocytes, while many nuclear and chromatin assembly terms were enriched in the importin α2 binding candidate cohort in spermatids. The most enriched Biological Processes term for importin α4 binding candidates in spermatocytes was mitochondrial organization, followed by many terms related to protein localization and transport. The cohort of importin α4 binding candidates in spermatids however, enriched many terms related to chromosomal conformation and nuclear organization.

These data collectively demonstrate that, (1) importin binding partners can be reproducibly identified using this pull-down and mass spectrometry approach, (2) novel candidate binding partners linked to non-nuclear functions bind to importin α proteins, (3) binding to importin α proteins may require sequences distinct from the canonical cNLSs and (4) each importin α protein recognizes distinct binding partners in a developmentally regulated manner. These topics are discussed further in Chapter 6 (Section 6.2), the General Discussion for this thesis.

Appendix I

The transcript expression pattern of 40 importin α binding candidates were examined in GDS3142 datasets, since no detectable expression for these candidates were found in mouse testis age series or isolated murine germ cells from testes (Section 4.10). Of these candidates, 22 had detectable expression pattern in the testis and other tissues (graphs), while 18 candidates had no detection values due to lack of an mRNA probe (listed below). The bar corresponding to the transcript for each candidate in the testis is highlighted with red colour.

Agbl2

Arhgap40

Cyp2c7

LRRGT00108

mt-Co2

Psgb1

RGD1309291

Setl1

Tubb4b

ULF-250

Wdr96

LOC100360057

LOC100364059

LOC100364838

LOC10036554

LOC500118

LOC680417

LOC687024

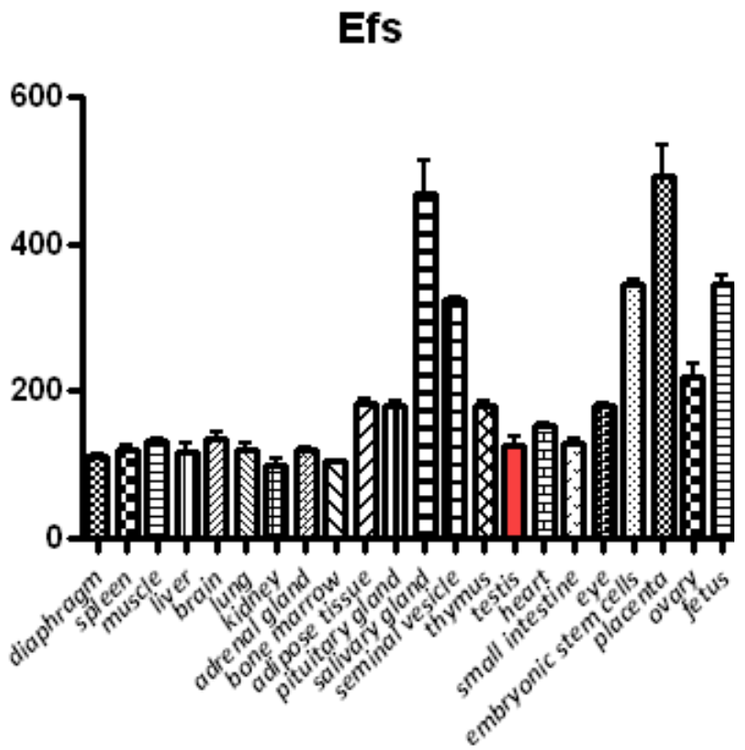
Efs
600
400
200
0
diaphragm
spleen
muscle
liver
brain
lung
kidney
adrenal gland
bone marrow
adipose tissue
pituitary gland
salivary gland
seminal vesicle
thymus
testis
heart
small intestine
eye
embryonic stem cells
placenta
ovary
fetus

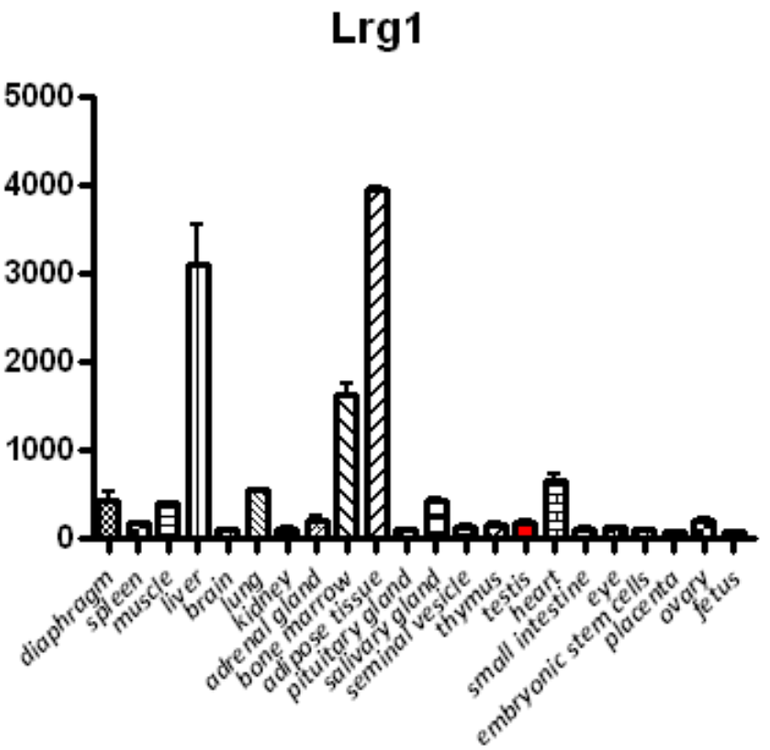
Lrg1
5000
4000
3000
2000
1000
0
diaphragm
spleen
muscle
liver
brain
lung
kidney
adrenal gland
bone marrow
adipose tissue
pituitary gland
salivary gland
seminal vesicle
thymus
testis
heart
small intestine
eye
embryonic stem cells
placenta
ovary
fetus

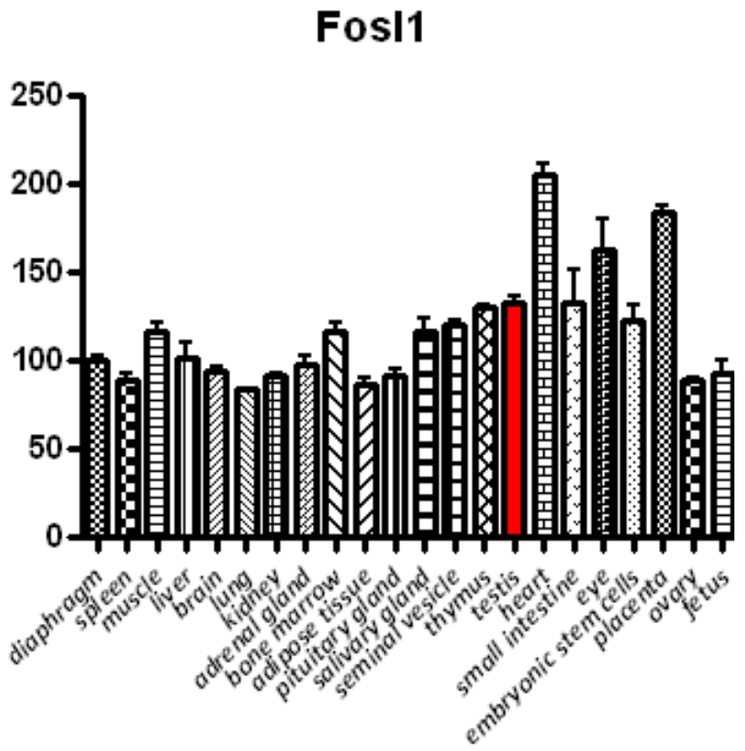
Fosl1
250
200
150
100
50
0
diaphragm
spleen
muscle
liver
brain
lung
kidney
adrenal gland
bone marrow
adipose tissue
pituitary gland
salivary gland
seminal vesicle
thymus
testis
heart
small intestine
eye
embryonic stem cells
placenta
ovary
fetus

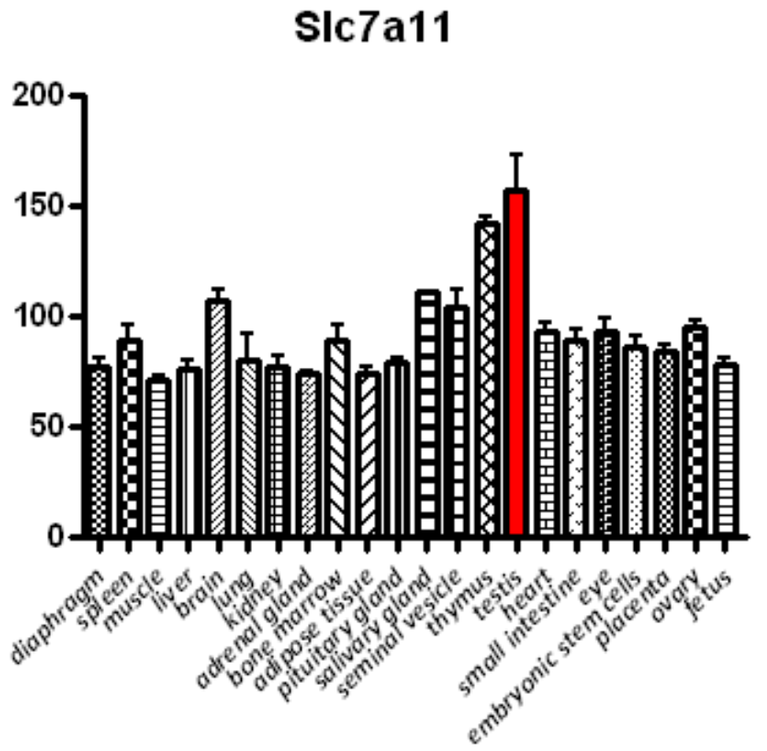
Slc7a11
200
150
100
50
0
diaphragm
spleen
muscle
liver
brain
lung
kidney
adrenal gland
bone marrow
adipose tissue
pituitary gland
salivary gland
seminal vesicle
thymus
testis
heart
small intestine
eye
embryonic stem cells
placenta
ovary
fetus

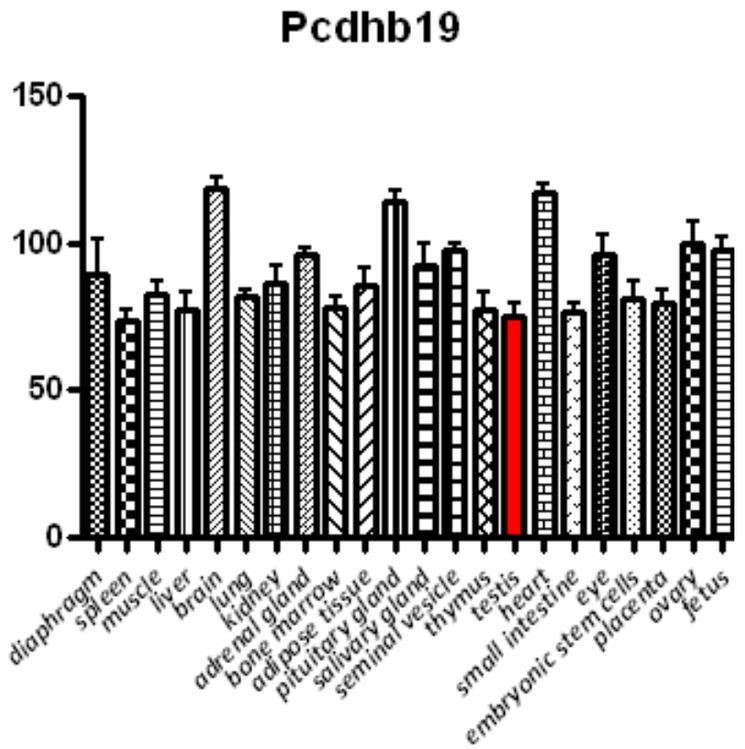
Pcdhb19
150
100
50
0
diaphragm
spleen
muscle
liver
brain
lung
kidney
adrenal gland
bone marrow
adipose tissue
pituitary gland
salivary gland
seminal vesicle
thymus
testis
heart
small intestine
eye
embryonic stem cells
placenta
ovary
fetus

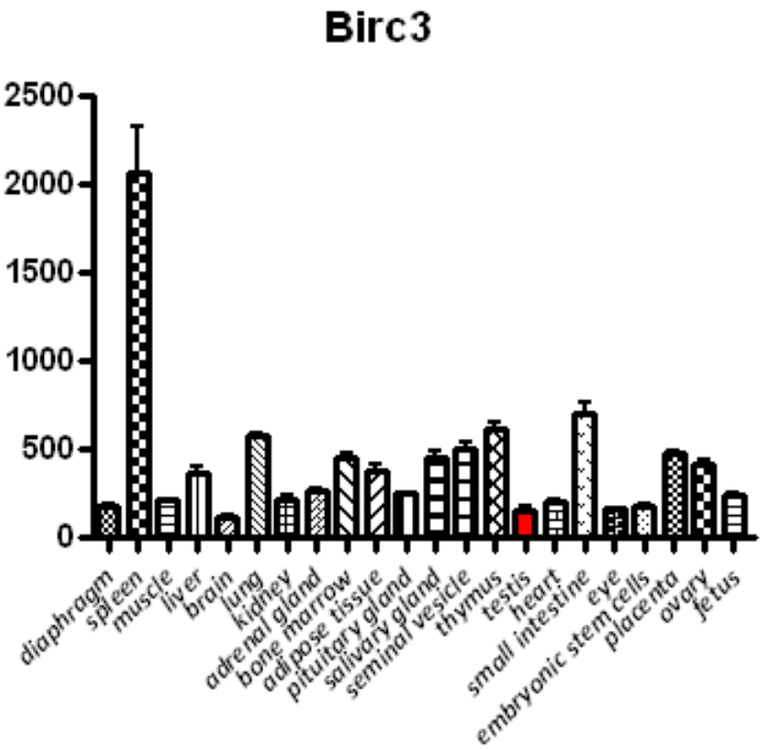
Birc3
2500
2000
1500
1000
500
0
diaphragm
spleen
muscle
liver
brain
lung
kidney
adrenal gland
bone marrow
adipose tissue
pituitary gland
salivary gland
seminal vesicle
thymus
testis
heart
small intestine
eye
embryonic stem cells
placenta
ovary
fetus

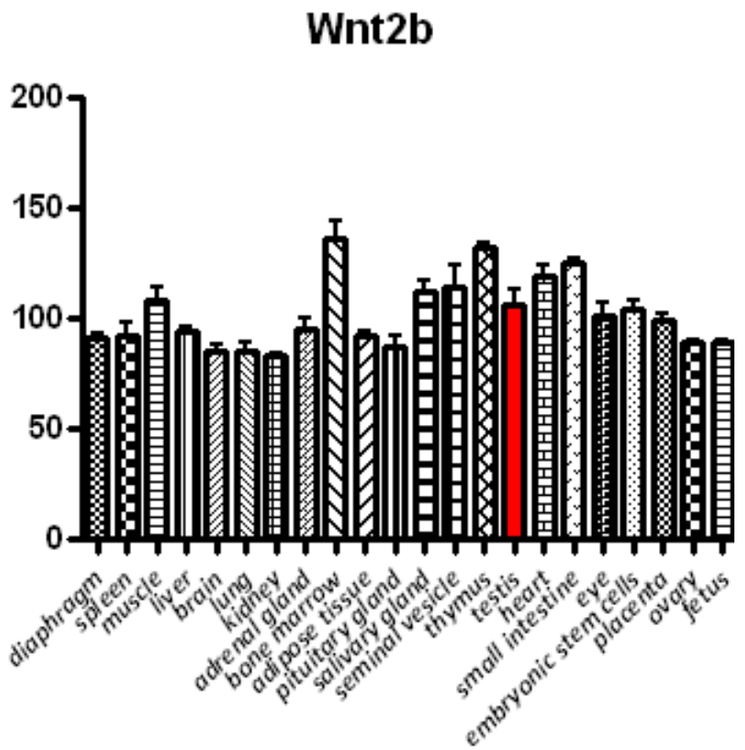
Wnt2b
200
150
100
50
0
diaphragm
spleen
muscle
liver
brain
lung
kidney
adrenal gland
bone marrow
adipose tissue
pituitary gland
salivary gland
seminal vesicle
thymus
testis
heart
small intestine
eye
embryonic stem cells
placenta
ovary
fetus

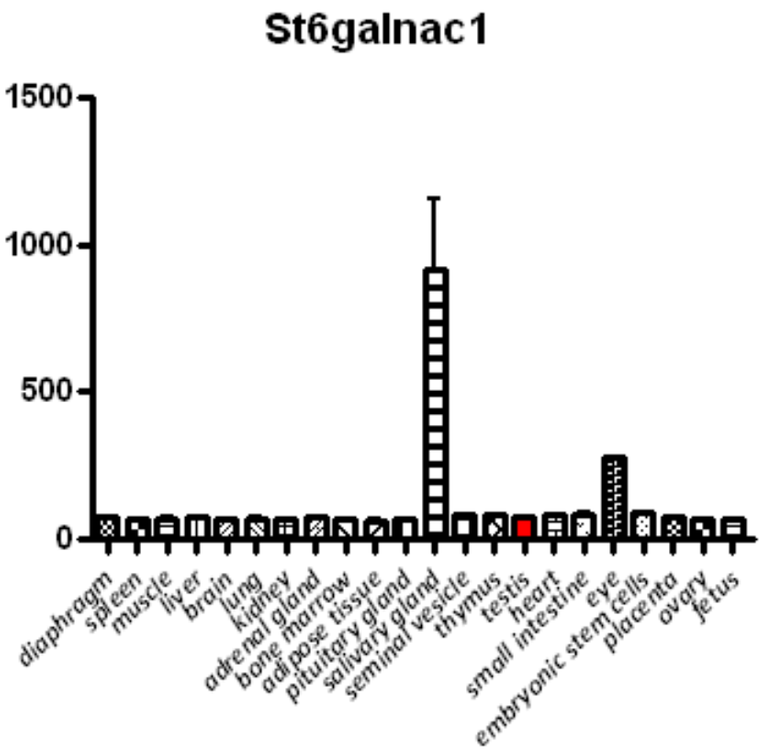
St6galnac1
1500
1000
500
0
diaphragm
spleen
muscle
liver
brain
lung
kidney
adrenal gland
bone marrow
adipose tissue
pituitary gland
salivary gland
seminal vesicle
thymus
testis
heart
small intestine
eye
embryonic stem cells
placenta
ovary
fetus

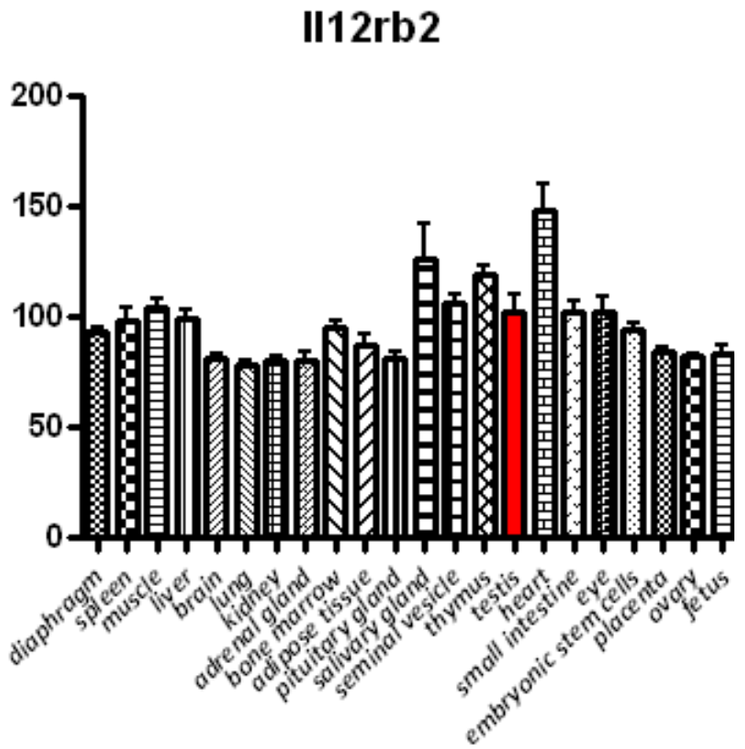
Il12rb2
200
150
100
50
0
diaphragm
spleen
muscle
liver
brain
lung
kidney
adrenal gland
bone marrow
adipose tissue
pituitary gland
salivary gland
seminal vesicle
thymus
testis
heart
small intestine
eye
embryonic stem cells
placenta
ovary
fetus

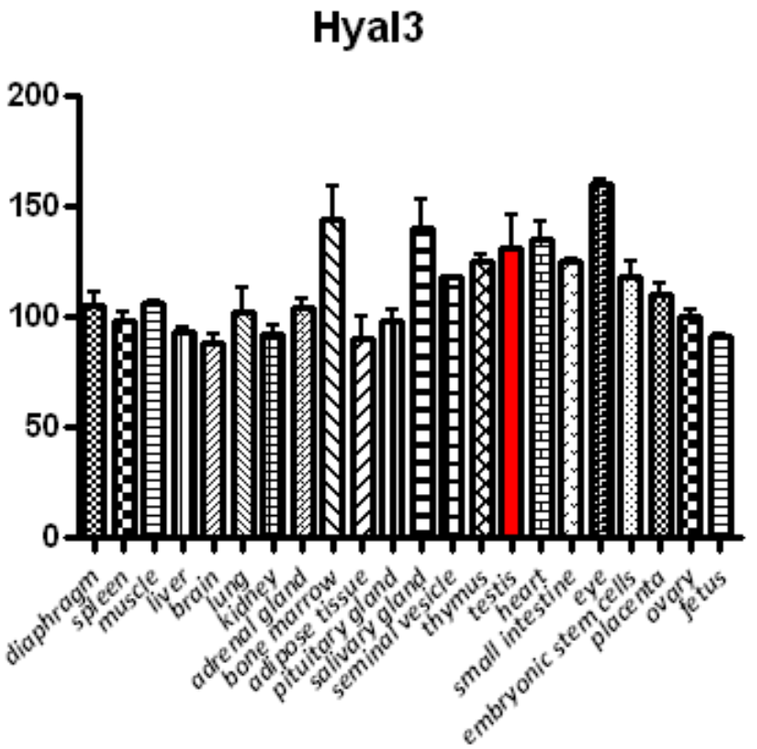
Hyal3
200
150
100
50
0
diaphragm
spleen
muscle
liver
brain
lung
kidney
adrenal gland
bone marrow
adipose tissue
pituitary gland
salivary gland
seminal vesicle
thymus
testis
heart
small intestine
eye
embryonic stem cells
placenta
ovary
fetus

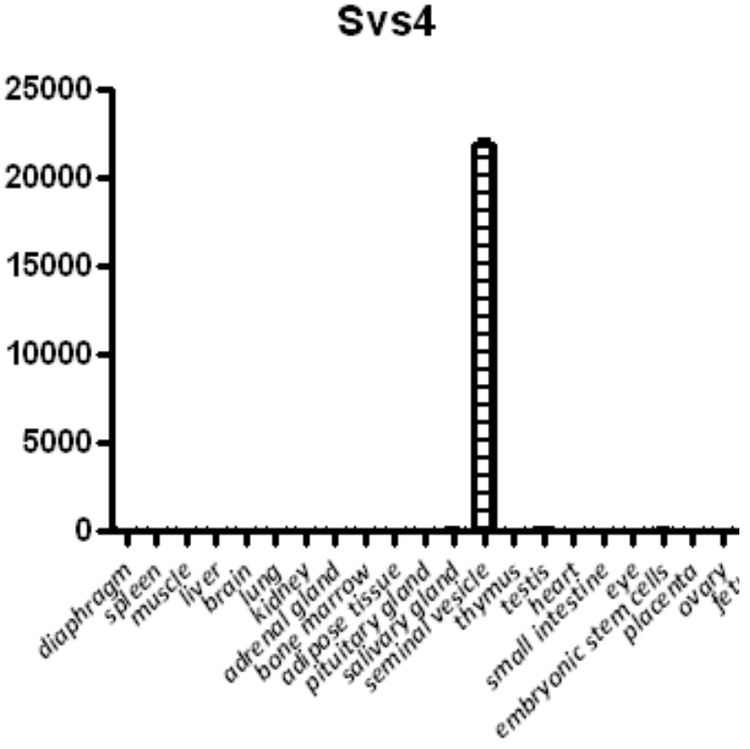
Svs4
25000
20000
15000
10000
5000
0
diaphragm
spleen
muscle
liver
brain
lung
kidney
adrenal gland
bone marrow
adipose tissue
pituitary gland
salivary gland
seminal vesicle
thymus
testis
heart
small intestine
eye
embryonic stem cells
placenta
ovary
fet

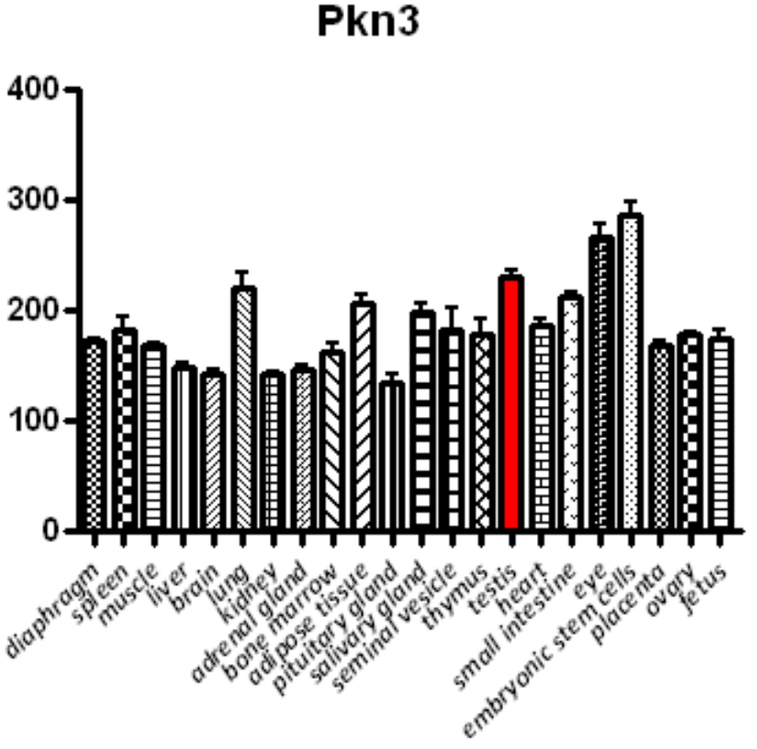
Pkn3
400
300
200
100
0
diaphragm
spleen
muscle
liver
brain
lung
kidney
adrenal gland
bone marrow
adipose tissue
pituitary gland
salivary gland
seminal vesicle
thymus
testis
heart
small intestine
eye
embryonic stem cells
placenta
ovary
fetus

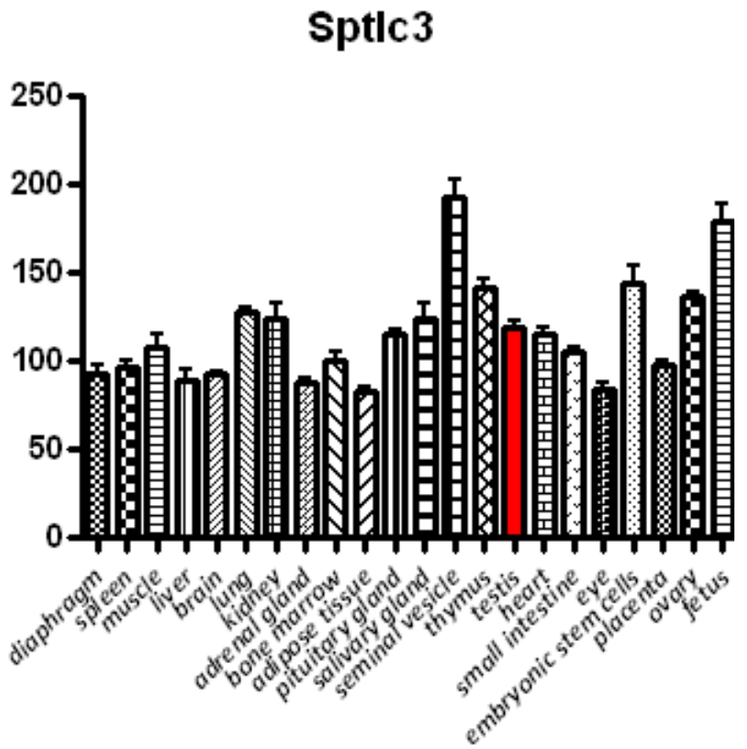
Sptlc3
250
200
150
100
50
0
diaphragm
spleen
muscle
liver
brain
lung
kidney
adrenal gland
bone marrow
adipose tissue
pituitary gland
salivary gland
seminal vesicle
thymus
testis
heart
small intestine
eye
embryonic stem cells
placenta
ovary
fetus

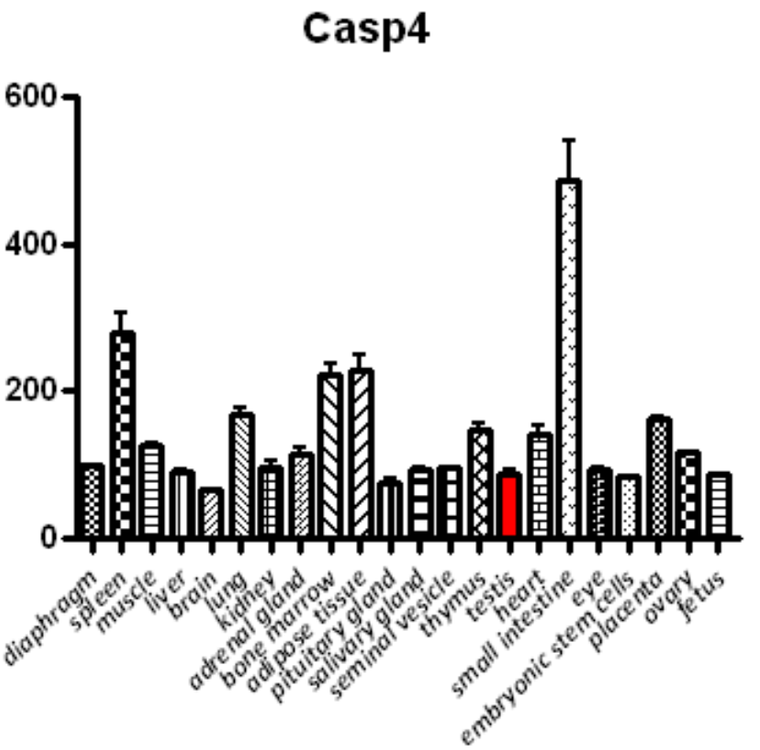
Casp4
600
400
200
0
diaphragm
spleen
muscle
liver
brain
lung
kidney
adrenal gland
bone marrow
adipose tissue
pituitary gland
salivary gland
seminal vesicle
thymus
testis
heart
small intestine
eye
embryonic stem cells
placenta
ovary
fetus

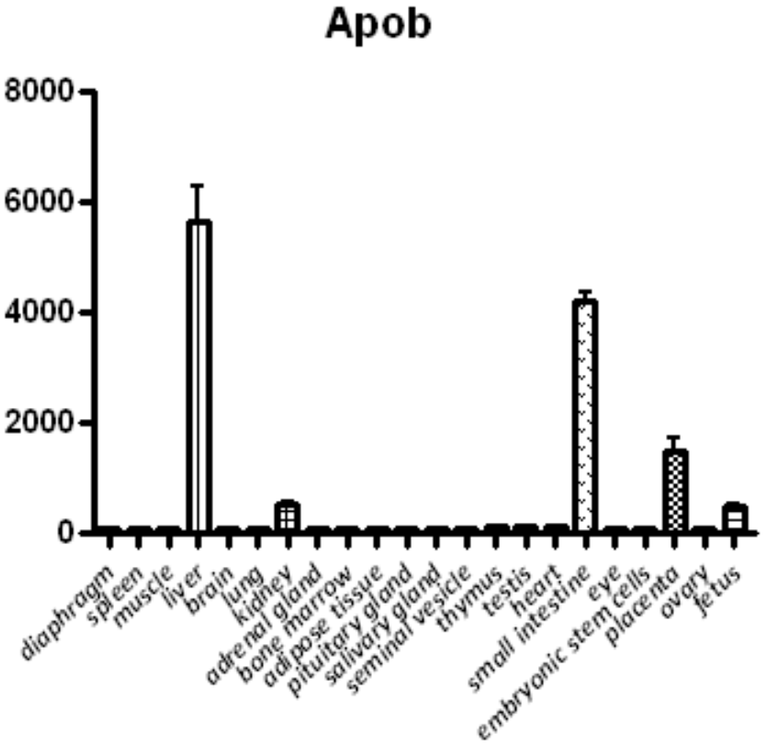
Apob
8000
6000
4000
2000
0
diaphragm
spleen
muscle
liver
brain
lung
kidney
adrenal gland
bone marrow
adipose tissue
pituitary gland
salivary gland
seminal vesicle
thymus
testis
heart
small intestine
eye
embryonic stem cells
placenta
ovary
fetus

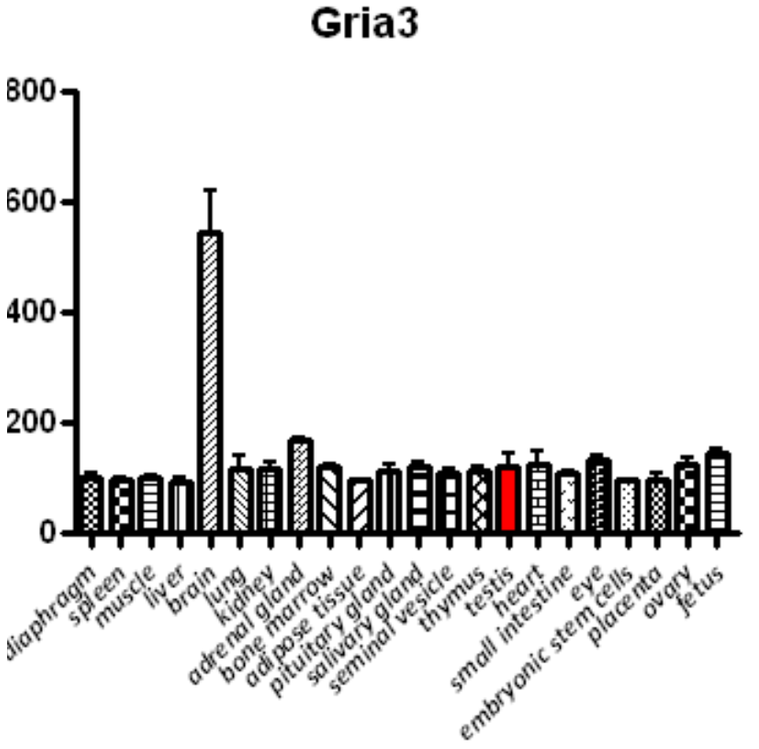
Gria3
800
600
400
200
0
diaphragm
spleen
muscle
liver
brain
lung
kidney
adrenal gland
bone marrow
adipose tissue
pituitary gland
salivary gland
seminal vesicle
thymus
testis
heart
small intestine
eye
embryonic stem cells
placenta
ovary
fetus

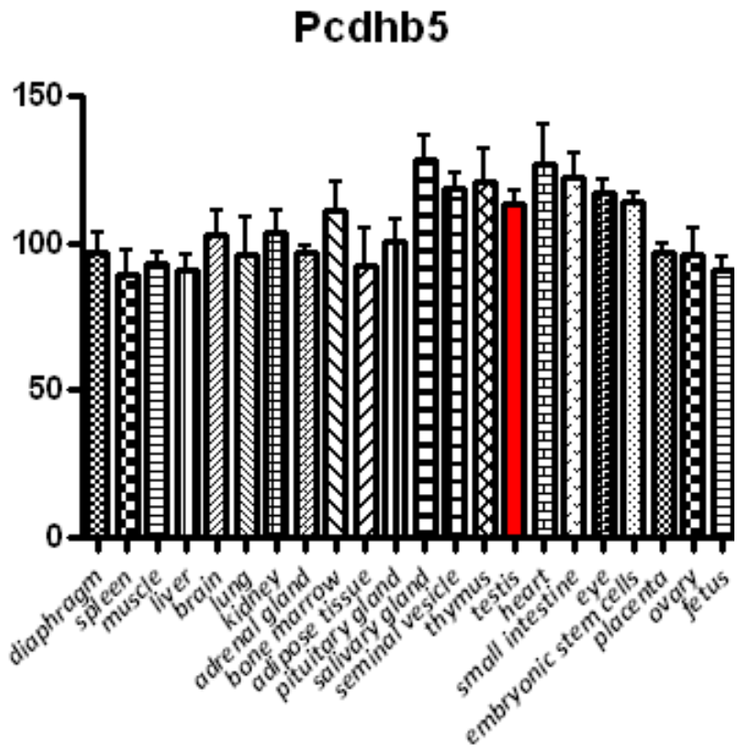
Pcdhb5
150
100
50
0
diaphragm
spleen
muscle
liver
brain
lung
kidney
adrenal gland
bone marrow
adipose tissue
pituitary gland
salivary gland
seminal vesicle
thymus
testis
heart
small intestine
eye
embryonic stem cells
placenta
ovary
fetus

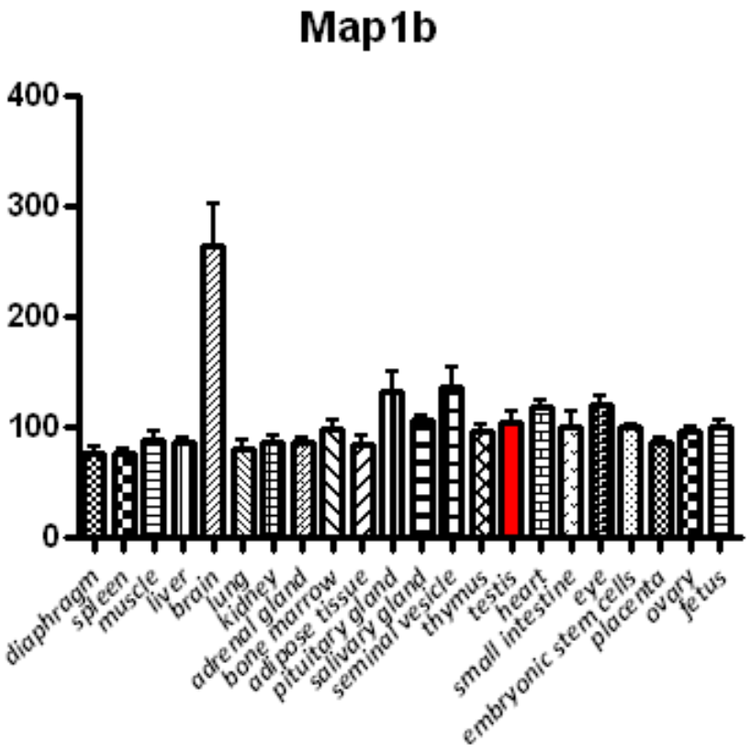
Map1b
400
300
200
100
0
diaphragm
spleen
muscle
liver
brain
lung
kidney
adrenal gland
bone marrow
adipose tissue
pituitary gland
salivary gland
seminal vesicle
thymus
testis
heart
small intestine
eye
embryonic stem cells
placenta
ovary
fetus

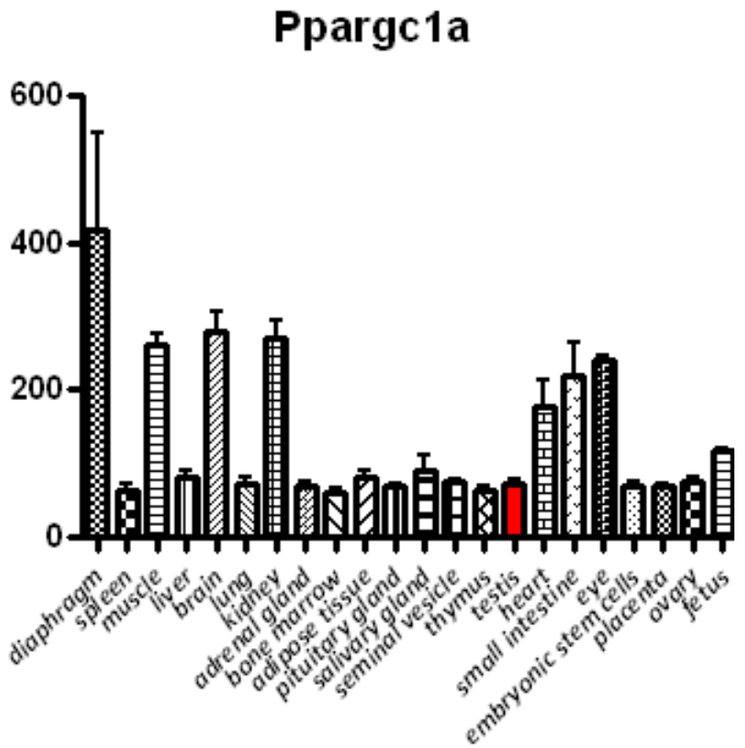
Ppargc1a
600
400
200
0
diaphragm
spleen
muscle
liver
brain
lung
kidney
adrenal gland
bone marrow
adipose tissue
pituitary gland
salivary gland
seminal vesicle
thymus
testis
heart
small intestine
eye
embryonic stem cells
placenta
ovary
fetus

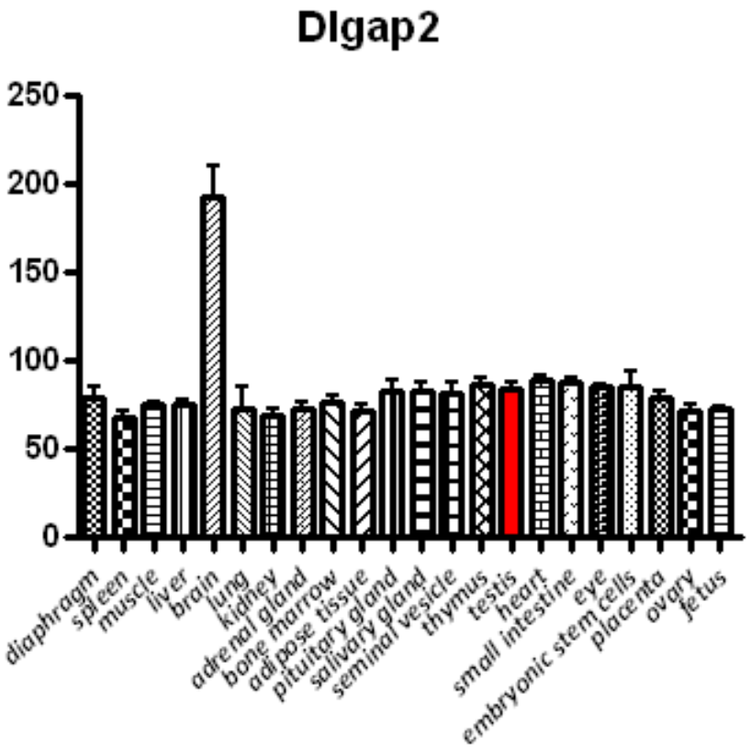
Dlgap2
250
200
150
100
50
0
diaphragm
spleen
muscle
liver
brain
lung
kidney
adrenal gland
bone marrow
adipose tissue
pituitary gland
salivary gland
seminal vesicle
thymus
testis
heart
small intestine
eye
embryonic stem cells
placenta
ovary
fetus

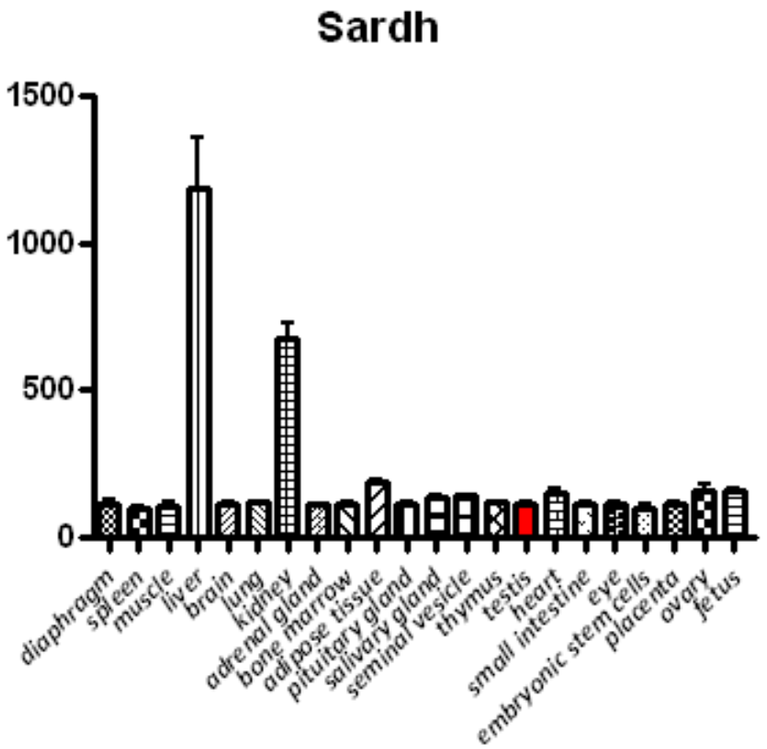
Sardh
1500
1000
500
0
diaphragm
spleen
muscle
liver
brain
lung
kidney
adrenal gland
bone marrow
adipose tissue
pituitary gland
salivary gland
seminal vesicle
thymus
testis
heart
small intestine
eye
embryonic stem cells
placenta
ovary
fetus

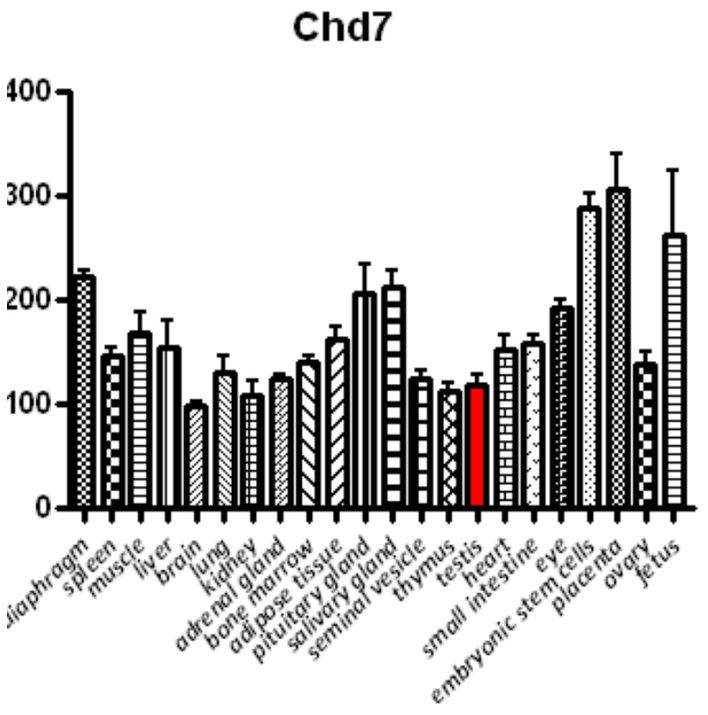
Chd7
400
300
200
100
0
diaphragm
spleen
muscle
liver
brain
lung
kidney
adrenal gland
bone marrow
adipose tissue
pituitary gland
salivary gland
seminal vesicle
thymus
testis
heart
small intestine
eye
embryonic stem cells
placenta
ovary
fetus

Chapter 5-
Characterization of the putative association between importin α and Mtmr4

CHAPTER 5 CHARACTERIZATION OF THE PUTATIVE INTERACTION BETWEEN IMPORTIN A AND MTMR4

5.1 General introduction

In a previous study, multiple binding candidates of three importin α family members, α2, α3, and α4 were identified by immunoprecipitation with lysates of purified adult rat pachytene spermatocytes and round spermatids (Miyamoto et al., 2013). Amongst the candidates, myotubularin related family member 4 (Mtmr4) was identified as a potential interacting partner of importin α4 from spermatocytes lysates. Mtmr4 belongs to a large family of dual specificity phosphatases which utilize phospholipids as their preferred substrate. Myotubularins (Mtmrs) are best known for regulating multiple steps in the endocytic pathway by modulating the lipid composition of intracellular vesicles. Among these, a role for Mtmr2 (a related Mtmr4 family member) in spermatogenesis has been demonstrated by observation of spermatogenic defects in KO mice. Because members of this family may co-associate and function together, it is logical to propose that Mtmr4 may also affect male germline development.

This chapter includes an overview of the myotubularin family of proteins, their substrates, subcellular localization, cellular roles and association with disease. Results, which elucidate the potential association between Mtmr4 and importin α are presented to address the hypothesis that importin α proteins bind and transport cargoes required for particular cellular developmental processes.

5.2 Endocytic pathway

Endocytosis is the process by which intracellular membrane-bound vesicles are generated through invagination of the plasma membrane. The process leads to cellular uptake of fluid, signalling and receptor molecules that reside on the plasma membrane or extracellular space. In general, endocytosis can occur in either a clathrin-dependent or clathrin-independent manner (Doherty and McMahon, 2009). Regardless of the formation route, the contents of all internalized vesicles are part of the endosomal pathway that are destined for degradation in lysosomes, transport to the trans-Golgi network or return to the plasma membrane through the recycling pathway (Figure 5.1, A, Maxfield and McGraw, 2004; van der Goot and Gruenberg, 2006).

The endosomal pathway includes a series of morphological changes in endocytosed vesicles accompanied by alterations in the lipid and protein composition of their outer surface as they mature from early to late endosomes, and during the fusion of late endosomes with lysosomes. The identity of these maturating vesicles is primarily imparted by switching of Rab GTPase family members, in particular Rab5 and Rab7 (Huotari and Helenius, 2011). In addition to Rab family members, different phosphoinositide species play major roles in transition and fusion events of the endocytic pathway (Takenawa and Itoh, 2001). In the following section, a brief overview of these lipids is given with a focus on two species that are the substrates of myotubularins in relationship to their regulation of endocytic pathway.

5.3 Phosphoinositides

The core component of phosphoinositides is a myo-inositol which is composed of six carbons, each containing a hydroxyl group that can be phosphorylated singly or in combination with other hydroxyl groups. Only three of the hydroxyl residues (D3, D4, and D5), however, have been shown to be phosphorylated *in vivo*, and thus seven distinct family members can occur (Figure 5.1, B, Cullen, 2011).

The parent molecule in the family is termed phosphatidylinositol (PtdIns or PIs) in which the first head-group (D1) is attached to diacylglycerol and embedded in the membrane. The outcome of phosphorylation on only one of the possible head-groups are three monophosphate products namely, PtdIns(3)P, PtdIns(4)P, and PtdIns(5)P (the number in the parenthesis indicates the phosphorylated head-group). Phosphorylation on two residues produces three biphosphates termed PtdIns(3,4)P_2, PtdIns(3,5)P_2, and PtdIns(4,5)P_2. The last isoform of this family is the PtdIns(3,4,5)P_3 which is the product of phosphorylation on all three head-groups (Cullen, 2011; Takenawa and Itoh, 2001). The members of this phospholipid family are found in multiple cellular locations, including vesicles of endosomal pathway, in the trans-Golgi system and in the nucleus, and they take part in a wide range of processes such as membrane trafficking, establishment of cell polarity and tumorigenesis (Sasaki et al., 2007).

Phosphatidylinositols constitute a very small proportion of the total cellular phospholipids. Within the cellular phospholipids pool, the most abundant of all is the PtdIns (<10%) and its derivatives make up between 0.0001% and 0.05% of phospholipids (Cullen, 2011). Among these PtdIns, PtdIns(3)P and PtdIns(3,5)P_2 are both localized on the membranes of endocytic pathway (Gillooly et al., 2000; Rusten and Stenmark, 2006) where they are substrates for the myotubularin family of phosphatases (Liu and Bankaitis, 2010). A balance in the composition of different PtdIns is kept in place through the activity of PtdIns kinases and phosphatases (Vanhaesebroeck et al., 2001). Through phosphorylation and dephosphorylation of specific head-groups in a temporally and spatially controlled manner, these enzymes regulate the distribution and concentration of specific pools of PtdIns on different intracellular membrane-bound vesicles. The modulated distribution and segregation of PtdIns allows selective targeting of effector proteins through distinct PtdIns binding motifs to various membrane compartments (Lemmon, 2008); the recruited effector proteins provide the membrane enclosed compartments with the capacity for either fusion or movement. The PtdIns binding domains are diverse, are found in numerous proteins and they possess disparate specificity and affinity for different PtdIns isoforms. These motifs include, but are not limited to, PH and FYVE domains, both of which occur in myotubularin family of PtdIns phosphatases.

Figure 5.1 Summary of the endocytic pathway and PtdIns family of phospholipids

A. Schematic representation of the endocytic pathway. Endocytosis begins by invagination of plasma membrane, either in a clathrin-dependent or clathrin-independent manner leading to generation of intracellular membrane-bound vesicles. The internalized vesicles enter early endosomes from which the contents are sorted to different compartments of the endocytic pathway. These compartments include recycling endosomes which take cargos such as cell surface receptors back to the plasma membrane, and late endosomes from where the cargo is either delivered to the trans-Golgi apparatus or enters the degradative pathway through fusion with lysosomes**.**

B. Phosphatidylinositol (PtdIns) family of phospholipids. The parent molecule of this family of phospholipids is termed phosphatidylinositol (PtdIns) which is composed of a D-myo-inositol in which every carbon head-group (termed D1 to D6) contains a hydroxyl residue. The D1 head-group of PtdIns and all of its derivatives contain diacylglycerol which facilitates membrane anchoring in all the family members. Of the five remaining head-groups (D2-D6) only D3, D4, and D5 can be phosphorylated either alone or in combination with any of other residues. This allows the generation of the seven phosphatidylinositol family members as depicted here (Figure adapted from Cullen, 2011).

A

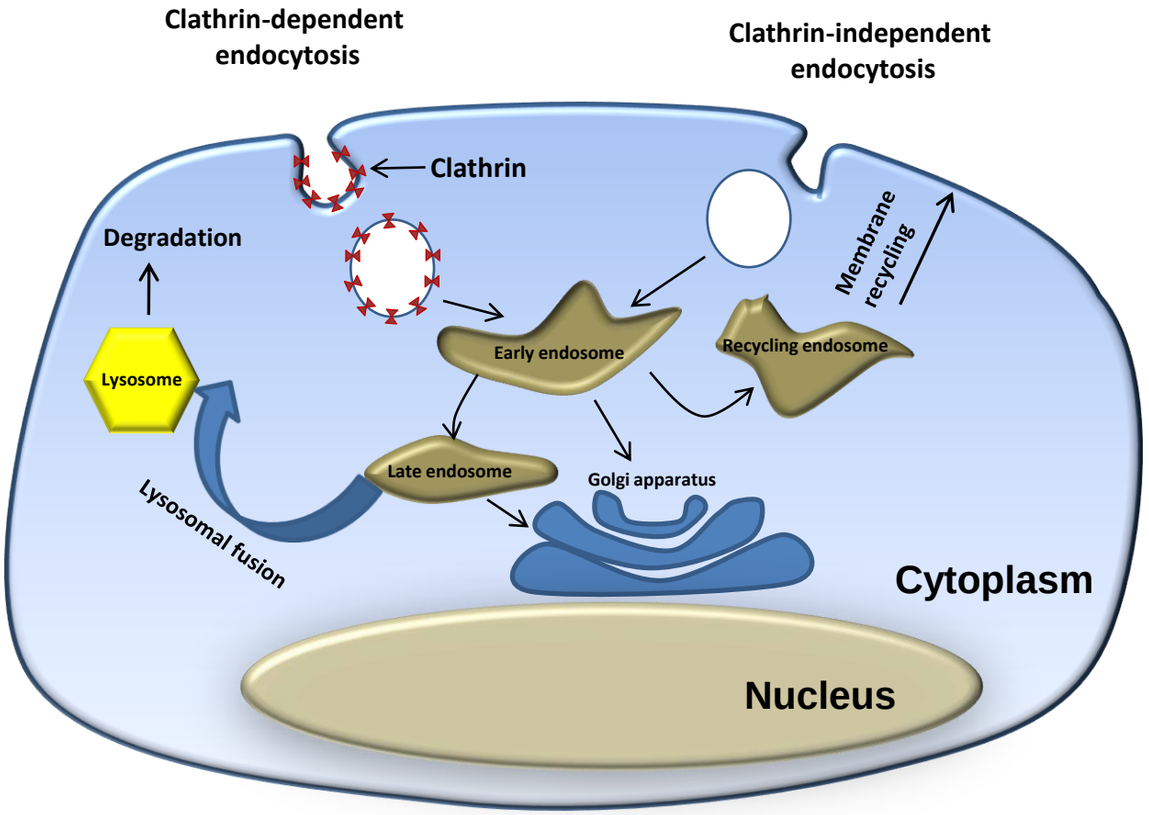
Clathrin-dependent endocytosis
Clathrin-independent endocytosis
Clathrin
Degradation
Membrane recycling
Lysosome
Early endosome
Recycling endosome
Late endosome
Golgi apparatus
Lysosomal fusion
Cytoplasm
Nucleus

B

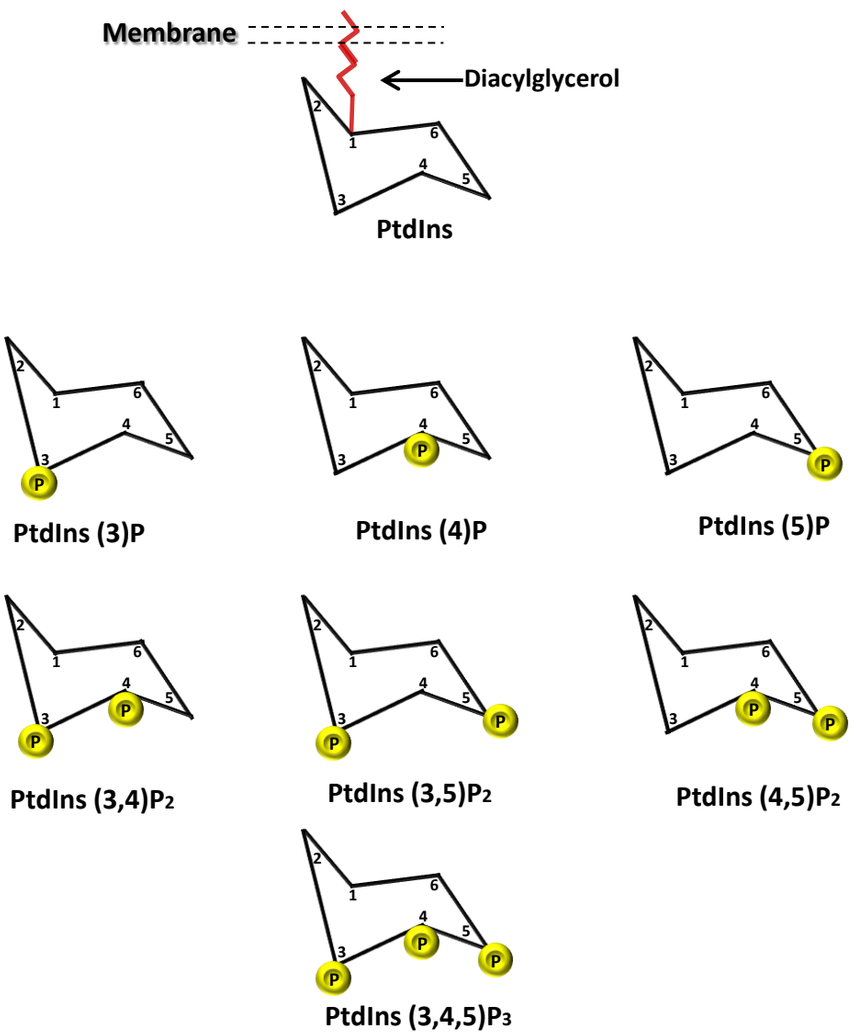
Membrane
Diacylglycerol
PtdIns
PtdIns (3)P
PtdIns (4)P
PtdIns (5)P
PtdIns (3,4)P2
PtdIns (3,5)P2
PtdIns (4,5)P2
PtdIns (3,4,5)P3

5.4 Myotubularins (Mtmrs)

Myotubularins constitute a large subfamily within the superfamily of dual specificity protein tyrosine phosphatases (PTP/DSP) which are defined by the signature motif of CX_5R (in which X can be any residue) within their catalytic domain (Laporte et al., 2003). Besides the catalytic domain, several other domains are found in all or most of the myotubularin family members. These domains include the PH-GRAM (pleckstrin homology, glucosyltransferase, Rab-like GTPase activator and myotubularin) domain, which mediates protein-PtdIns binding (Doerks et al., 2000), and the coiled-coil domain, involved in dimerization of myotubularin family members (discussed briefly below)-(Mruk and Cheng, 2011). In addition, specific to a limited number of family members is the FYVE (Fab1, YOTB, Vps27 and EEA1) domain, involved in PtdIns targeting of host proteins (Kutateladze, 2006; Robinson and Dixon, 2006) and the DENN (differentially expressed in normal versus neoplastic) domain, (Robinson and Dixon, 2006) with an unknown function.

Despite the initial expectation that myotubularins are protein phosphatases, these proteins preferentially dephosphorylate PtdIns, with strong substrate specificity towards PtdIns(3)P and PtdIns(3,5)P2 (Robinson and Dixon, 2006). Given the crucial role of PtdIns in endocytic trafficking, elevation or decrease in expression levels of Mtmrs can lead to defective endosomal morphology and sorting, caused by perturbations to the endosomal PtdIns pool. Overexpression of human Mtmr3 in yeast led to production of enlarged vacuoles concurrent with a drop in the level of endogenous PtdIns(3,5)P2 (Walker et al., 2001); exogenous expression of human Mtmr3 and MTM1 caused formation of large vacuolar structures in COS-7 cells accompanied by a block in the endocytic degradative pathway (Tsujita et al., 2004). Furthermore, genetic and *in vivo* studies in *C.elegans*, through transgenic expression of mutant Mtmrs (mtm-6 and mtm-9) or RNAi down-regulation of endogenous proteins, abrogated endocytosis by the affected worm coelomocytes (Dang et al., 2004).

To date, 16 mammalian myotubularins have been described. The prototype of this family, myotubularin (*MTM1*) was identified as the gene defective in the X-linked

myotubular myopathy (Laporte et al., 1996), a severe congenital muscular dystrophy. Other members are termed myotubularin-related proteins (Mtmr) 1 to 15. In Figure 5.2, human Mtmr protein family members are represented schematically with an emphasis on the conservation in their domain organization. An interesting observation regarding this family of phosphatases is that almost half of the members are catalytically inactive as a result of amino acid substitutions in the cysteine and arginine residues of the catalytic site (Clague and Lorenzo, 2005). The proposed view of negative regulation exerted by inactive members, through protective binding to PtdIns substrates, has been mislaid by observations that show mutations in inactive members of the family lead to conditions indistinguishable from those of the active members (discussed further in Section 5.5). Furthermore, there exist many examples of dimerizations (both homo and hetero) within the family. Through yeast two-hybrid analysis and immunoprecipitation studies, Lorenzo and colleges confirmed all of the previously identified interactions and reported several novel intra-family associations (Lorenzo et al., 2006, and refrences therein). These interactions are functionally significant, since they lead to both enhanced enzymatic activity of the active members (i.e. PtdIns dephosphorylation), and redistribution of associating partners (Kim et al., 2003; Lorenzo et al., 2006; Mochizuki and Majerus, 2003).

5.5 Myotubularins in disease

The first myotubularin implicated in disease is MTM1, in which a mutation was shown to be responsible for a syndrome known as myotubular myopathy (Laporte et al., 1996). The condition is caused by loss of function in MTM1 and is characterized by hypotonia and skeletal muscle weakness, the severity of which is dependent on the nature of the mutation. In general, truncations and splice site mutations lead to more severe conditions than do missense mutations outside the functional domains of MTM1 (Mruk and Cheng, 2011).

Another condition in which myotubularins have been implicated in is Charcot-Marie-Tooth disease (CMT). Mutations in Mtmr2 causes CMT type 4B1 (Bolino et al., 2000), an autosomal recessive condition characterized by progressive sensory loss in

Figure 5.2 Schematic presentation of human myotubularin family members

The figure depicts the domain organization of human myotubularins. The amino acid length of each protein is indicated in the right side of each schematic. Common to all family members are the GRAM domain and catalytic site, the latter of which is inactive in 6 family members. A coiled-coil domain is predicted in all members with the exception of Mtmr 10. The DENN domain is only present in the N-terminus of Mtmr5 and Mtmr13. Specific to Mtmr3 and Mtmr4 is a C-terminal FYVE domain. Mtmr4 is the only family member in which a PY ubiquitination domain has been identified (discussed further in Section 5.6). Overall the occurrence and order of domains is highly conserved within this family of proteins (Figure adapted from Laporte et al., 2003, and David Adam Sheffield PhD thesis, Monash University).

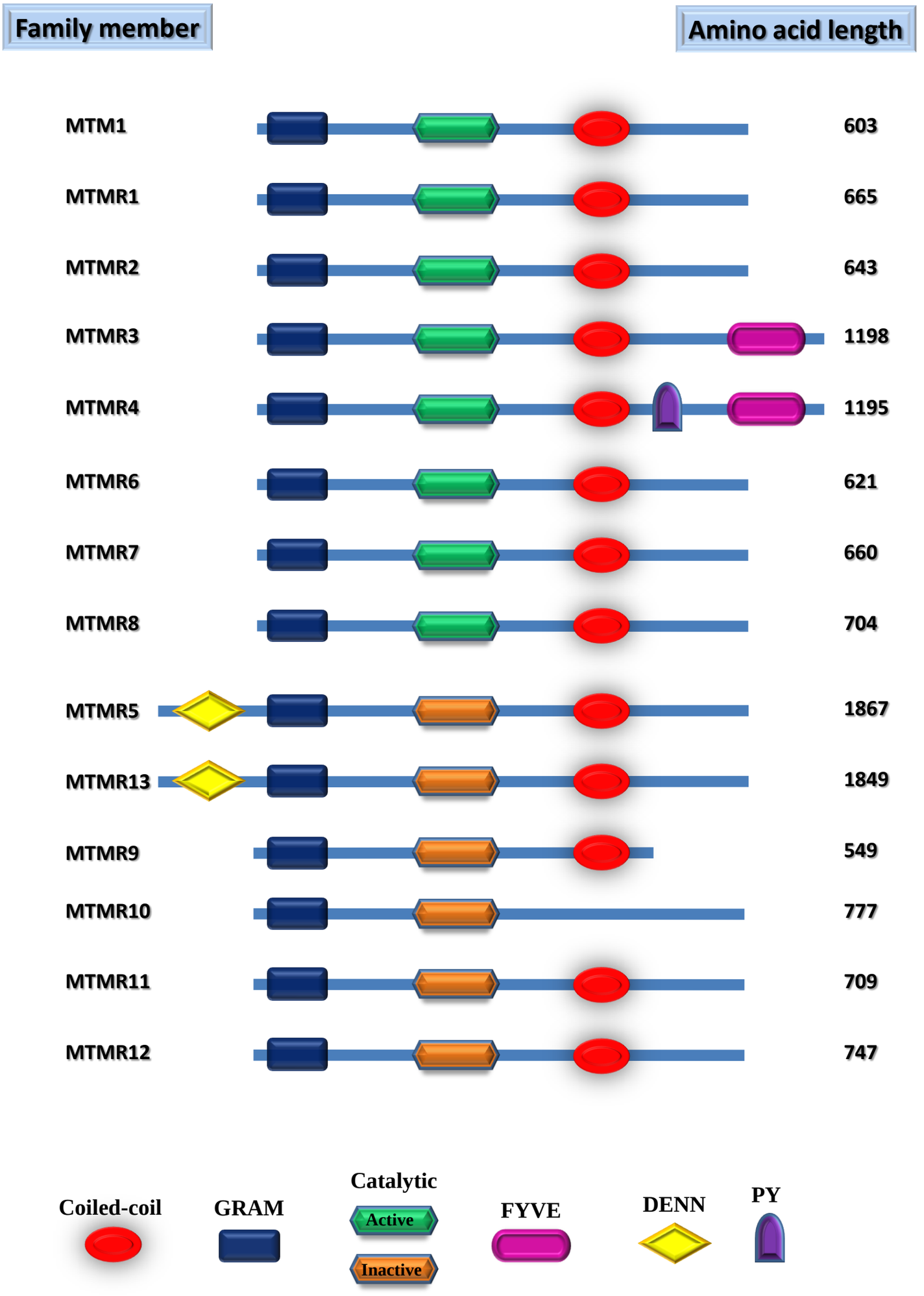
Family member
Amino acid length
MTM1
603
MTMR1
665
MTMR2
643
MTMR3
1198
MTMR4
1195
MTMR6
621
MTMR7
660
MTMR8
704
MTMR5
1867
MTMR13
1849
MTMR9
549
MTMR10
777
MTMR11
709
MTMR12
747
Coiled-coil
GRAM
Catalytic
Active
Inactive
FYVE
DENN
PY

extremities caused by axon demyelination (Previtali et al., 2007). Knock out of the mouse Mtmr2 homolog recapitulated the neuropathy observed in humans (Bolino et al., 2004). In addition, these mice showed defective spermatogenesis, characterized by pre-mature release of developing germ cells (pachytene spermatocytes, round and elongating spermatids) into the lumen of seminiferous tubules (Bolino et al., 2004).

Interestingly, mutations in phosphatase-inactive family members also cause genetic disorders. Mutations in Mtmr13 lead to CMT 4B2, a condition with almost identical pathology to CMT 4B1 both in man and in mice (Azzedine et al., 2003; Robinson et al., 2008). Furthermore, some CMT 4B2 patients suffer from glaucoma, a progressive loss of vision (Azzedine et al., 2003). Homozygous null mice lacking Mtmr5, another phosphatase inactive myotubularin, are infertile due to the loss of post-meiotic gem cells in the seminiferous tubules, within which enlarged vacuoles in Sertoli cells are observed (Firestein et al., 2002). Although not yet clear, defects caused by mutations in myotubularin family members are most likely the result of deficient membrane trafficking and fusion as a result of inadequate dephosphorylation of PtdIns (Robinson and Dixon, 2006). Given the conserved structure and function, distinct conditions caused by mutations in different family members is indicative of differential regulation at subcellular localization, interaction and expression levels.

5.6 Myotubularin-related protein 4 (MTMR4)

Mtmr4 was first isolated from a human brain cDNA library and, based on its sequence similarity to Mtmr3 (47%) and possession of a protein tyrosine phosphatase (PTP) domain, was proposed to belong to the myotubularin dual specificity phosphatase (PTP/DSP) family (Zhao et al., 2001). Examination of *Mtmr4* transcripts across 24 human tissues and 4 cell lines by reverse transcriptase PCR (RT-PCR) demonstrated the ubiquitous expression of *Mtmr4* mRNA. The transcript was readily detectable in 18 tissues with the highest expression in testis, placenta and prostate, and all of the examined cell lines (Zhao et al., 2001). Consistent with the functions of other myotubularin family members, Mtmr4 effectively dephosphorylates PtdIns, with its strongest activity towards PtdIns(3)P and PtdIns(3,5)P2, both *in vivo* and *in vitro*

(Naughtin et al., 2010; Zhao et al., 2001), while its overexpression depletes the host cells of these phospholipid species (Lorenzo et al., 2006; Naughtin et al., 2010).

Mtmr4 is the only family member that has been unequivocally localized on the early and recycling endosomes (Lorenzo et al., 2006; Naughtin et al., 2010), the site of PtdIns(3)P and PtdIns(3,5)P2 substrate accumulation. Intriguingly, Mtmr3, the closest family member to Mtmr4 which shares the substrate specificity and the FYVE and the coiled-coil domains with Mtmr4, is cytosolic (Lorenzo et al., 2005). This observation may point towards further regulatory mechanisms in endosomal targeting of Mtmr4. The observed hetero-dimerization between Mtmr4 and Mtmr3 is the first, and to date, the only reported association between two catalytically active family members, with possible functional significance; when co-expressed in HeLa cells, modest redistribution of Mtmr4 to the cytoplasm and Mtmr3 to the endosomal compartment is observed (Lorenzo et al., 2006).

Recently, two protein-protein interactions have been reported for Mtmr4. Through bioinformatics analysis, Plant and colleagues discerned a PY ubiquitination motif specific to Mtmr4 within the myotubularin family. By immunoprecipitation, co-localization and mutagenesis studies, the PY domain of Mtmr4 was shown to mediate a direct interaction between Mtmr4 and the Nedd4 ubiquitin ligase, leading to degradation of Mtmr4 (Plant et al., 2009). In a more recent study and for the first time, a protein dephosphorylation event was attributed to *in vivo* activity of Mtmr4. Upon TGFβ stimulation, Smad proteins typically accumulate in the nucleus in a phosphorylation-dependent manner (Xu and Massague, 2004). RNAi-mediated down-regulation of Mtmr4 led to reduced dephosphorylation of Smad3, concordant with increased nuclear entry of Smad3 in porcine aortic endothelial (PAE) cells. In a complementary assay, Smad3 was shown to co-localize with over-expressed Mtmr4 in early endosomes of PAE cells, concurrent with enhanced dephosphorylation and reduced nuclear accumulation of Smad3. That Mtmr4 is responsible for Smad3 dephosphorylation was inferred from inadequacy of phosphatase-inactive Mtmr4 in exerting either of these effects (Yu et al., 2010b).

5.7 Expression profiles of Mtmr4

To gain an insight into the developmental regulation of Mtmr4 in various tissues and in the maturing testis, GEO profile data sets were searched. Figure 5.3 presents the *Mtmr4* transcript levels across mouse tissues (A), in the postnatal developing testis (B), and in purified testicular germ cell populations (C). Despite its widespread expression, the transcript of *Mtmr4* is present at a relatively high level in testis compared to many other examined tissues (Figure 5.3, A), being noticeable higher in testis than in 17 out of 22 tissues; the transcript level is roughly equivalent in embryonic stem cells and whole adult testis. The tissues in which *Mtmr4* mRNA levels are higher than testis are liver, small intestine and placenta (Figure 5.3, A). During early postnatal testis development, there is a minimal change in the *Mtmr4* mRNA level between day 0 and day 18 postpartum (Figure 5.3, B). The slow and steady rise between day 8 and 20 is followed by a sharp drop between the day 20 and day 30 timepoints, with the lower transcript level persisting into adulthood (Figure 5.3, B). Examination of the isolated germ cell preparations shows that the *Mtmr4* mRNA is most abundant in pachytene spermatocytes, the cell type in which the interaction of Mtmr4 with importin α4 was originally detected. The transcript is detectable, however, in both type A and type B spermatogonia, and in round spermatids (Figure 5.3, C).

5.8 Examination of Mtmr4 transcript expression in testis

We set out to examine the expression profile of the *Mtmr4* mRNA in several mouse tissues. The *Mtmr4* gene produces a transcript of 5754 bp which includes a 5' UTR of 131 bp, a coding sequence of 3575 bp and a 3' UTR of 2051 bp (Figure 5.4, A). Total RNA from adult mouse testis, brain, liver and kidney in addition to total RNA from the testis of a 21 day old mouse was examined by Northern blot. Inclusion of the 21 day old testis RNA enabled assessment of the *Mtmr4* mRNA in a testis devoid of elongating spermatids. The Northern blot was probed with a DIG-labelled antisense cRNA corresponding to nucleotides 2379 to 2568 of the *Mtmr4* transcript (Figure 5.4, B). As a negative control, a sense probe generated to the same region of *Mtmr4* was used in parallel.

Figure 5.3 Expression profile of *Mtmr4* mRNA across mouse tissues and in developing testis and germ cells

Graphs depict mouse *Mtmr4* transcript levels in different tissues of adult wild type mouse (A), developing mouse testes from birth to adulthood (B) and in isolated germ cells from mouse testes (C). Data were obtained from publicly available GEO profile data sets in the NCBI website and graphed using GraphPad Prism v5.03. The error bars indicate the standard deviation in duplicate experiments. Table 5.1 includes the GDS data sets and the probe ID numbers that were used to extract the data. A sp'gonia: Type A spermatogonia, B sp'gonia: Type B spermatogonia, S'cyte: pachytene spermatocyte, S'tid: round spermatids. Spermatogonia was isolated from day 6-8 mouse testes; spermatocytes and spermatids were purified from adult mouse testes.

Examined biological context	GDS data set	Probe ID number
Various mouse organs	3142	1418151_at
Post-natal testis development time-course	607	130988_f_at
Isolated germ cells of the testis	2390	1418150_at

Table5.1 GDS data sets used for *Mtmr4* transcript level examination

A

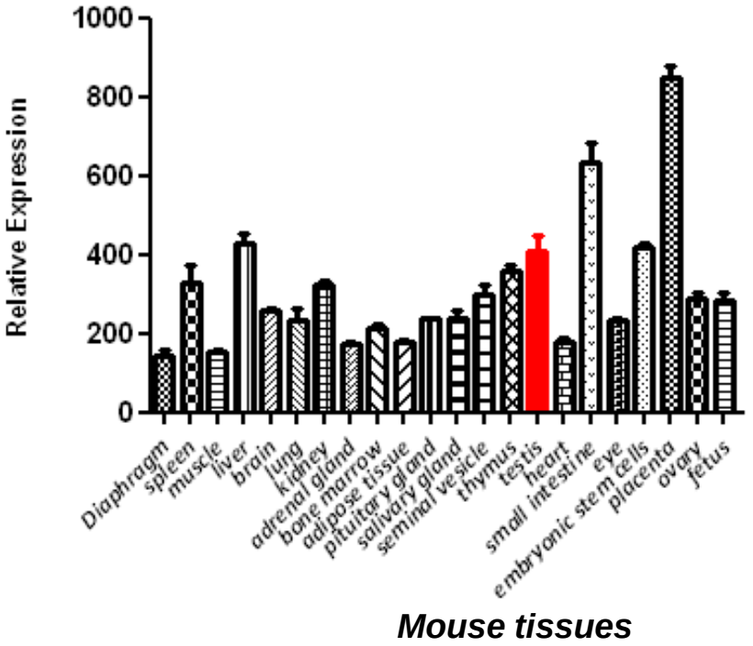

Mouse tissues

B

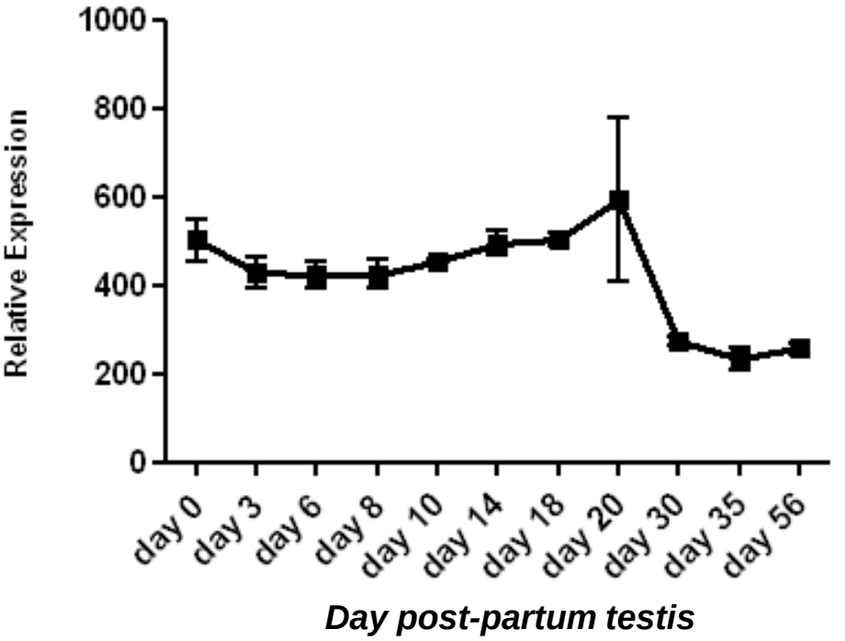

Day post-partum testis

C

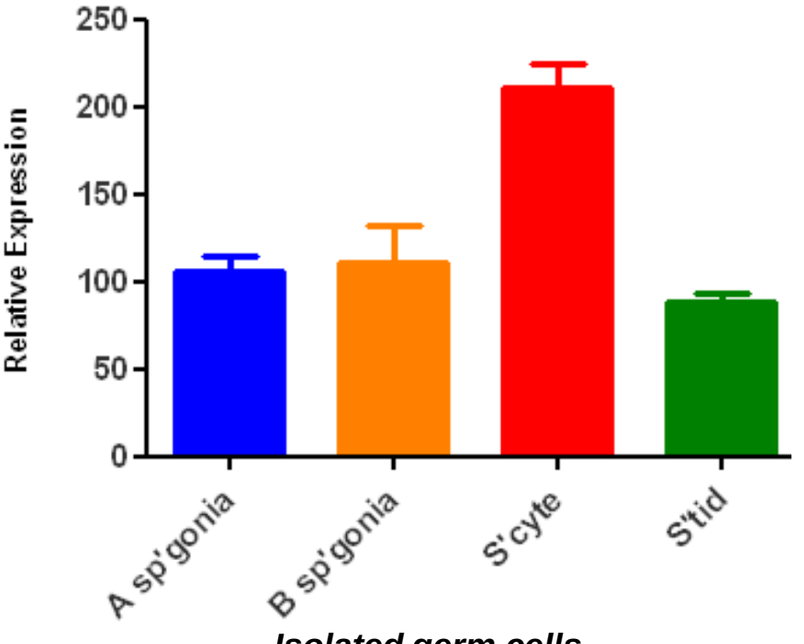

Isolated germ cells

Detection of the labelled probe on the membrane revealed that *Mtmr4* is expressed in all of the examined tissues, as evident by the presence of a band of the expected size (5.7 kb). The abundance of the transcript however, appeared to differ between tissues. Low level signals were detected in kidney and brain (Figure 5.4, B left panel lanes 1 and 3), consistent with the GEO profile data (Figure 5.3, A) in which testicular *Mtmr4* is in higher abundance than in either kidney or brain. The *Mtmr4* mRNA was detected with relatively similar intensity in liver, adult testis and in testis of a 21 day old mouse (Figure 5.4, B, left panel lanes 2, 4 and 5). Notably, several Northern blots consistently produced a signal suggestive of a splice variant specific to adult testis (Figure 5.4, B, left panel, red arrow). A potential splice variant of *Mtmr4* has been reported previously in human kidney (Zhao et al., 2001). The significance of this observation and potential functional implications will be discussed in the general discussion section (Section 6.5). The sense probe did not produce any signal in kidney, brain and adult testis; however, a signal corresponding to a species of approximately 3 kb of unknown origin was present in the liver sample (Figure 5.4, B, right panel, yellow arrow).

In situ hybridization (ISH) was performed to detect the cellular expression profile of *Mtmr4* in adult mouse testis sections. The probes that were validated for specificity by Northern blot were used here. The *Mtmr4* signal appeared most intense in pachytene spermatocytes and round spermatids (Figure 5.4, C), in accordance with previously obtained data in the context of this study. The interaction of Mtmr4 with importin α4 was identified in pachytene spermatocytes in which importin α4 is highly expressed (Section 3.6), indicating a correlation between the expression of these two potential binding partners. It should be noted however, that mRNA expression does not necessarily reflect the presence of protein, especially in post-meiotic germ cells which feature translational arrest and transcript storage (Steger, 2001). Due to the time and resource limitations however, the immunohistochemical detection of Mtmr4 protein in testis sections was not performed in this study.

Figure 5.4 Northern blot and *in situ* hybridization analysis of Mtmr4

A. Schematic representation of the mouse *Mtmr4* mRNA transcript. The region to which an RNA probe was generated is indicated by the green box. UTR: untranslated region, bp: base pair.

B. Total RNA isolated from adult mouse kidney, liver, brain, testis and from 21 day old mouse testis was resolved on a denaturing agarose gel and transferred onto a nylon membrane. The membrane was then incubated with either the antisense (left) or sense (right) DIG-labelled cRNA *Mtmr4* probes. The red arrow points to a potential *Mtmr4* splice variant in adult testis. The yellow arrow indicates the signal of unknown origin produced by sense probe in liver sample. The panel on the bottom of each membrane corresponds to the 28S ribosomal RNA to illustrate the RNA loading for each lane. 28S and 18S band positions are indicated to the left.

C. Adult mouse testis sections were probed with DIG-labelled cRNA probes generated against *Mtmr4* mRNA (A, above). Hybridization of the probe with the target sequence was detected by anti-DIG antibody followed by Harris haematoxylin counterstaining of the nucleus. In each experiment the sense probe (inset) served as a negative control. Two images from two independent experiments are presented. Yellow arrows point towards pachytene spermatocytes and red arrows indicate round spermatids.

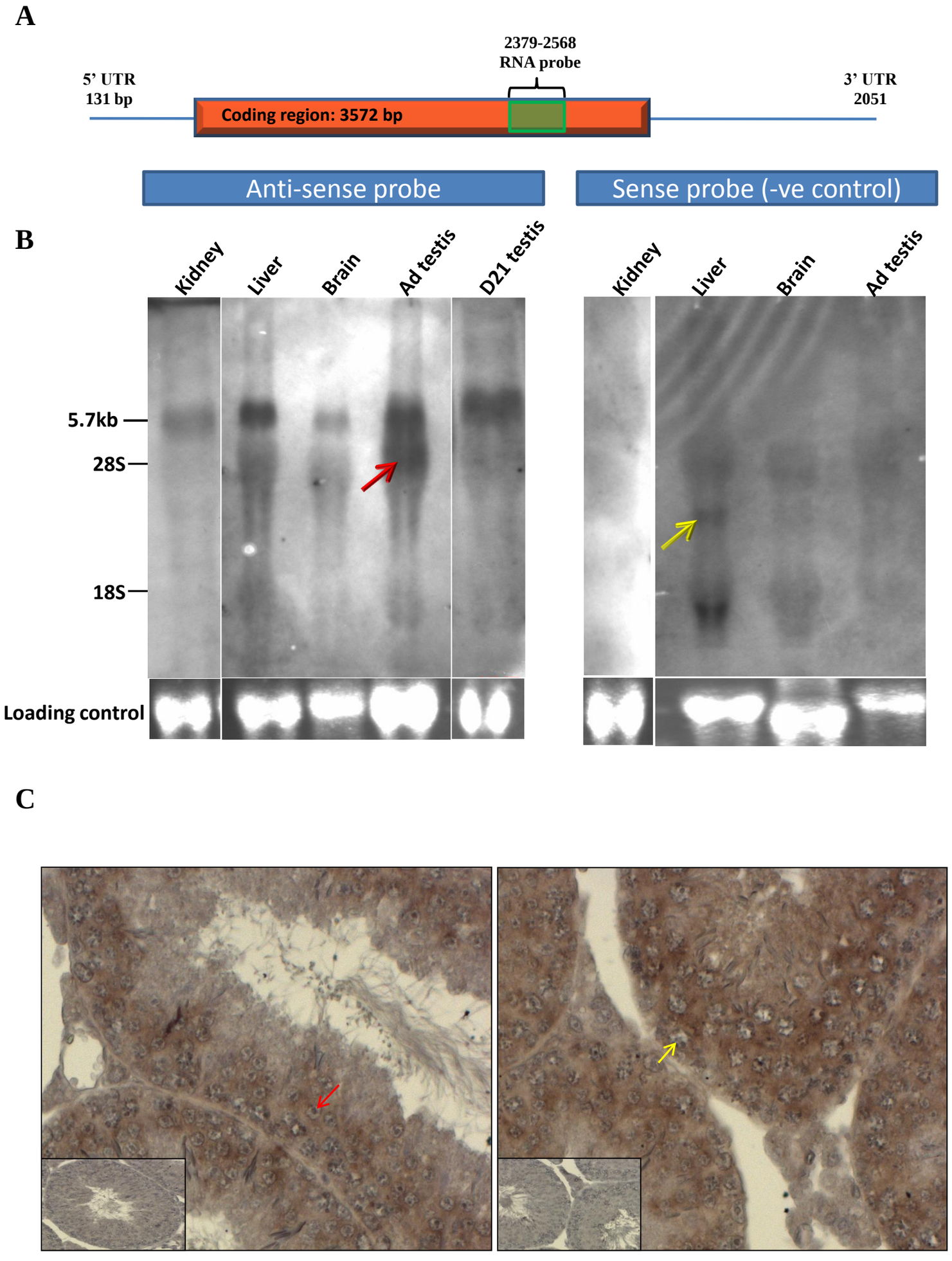
A
2379-2568
RNA probe
5' UTR
131 bp
Coding region: 3572 bp
3' UTR
2051
Anti-sense probe
Sense probe (-ve control)
B
Kidney
Liver
Brain
Ad testis
D21 testis
Kidney
Liver
Brain
Ad testis
5.7kb
28S
18S
Loading control
C

5.9 Identification of a putative cNLS in Mtmr4 protein sequence

To search for an importin α binding region within the Mtmr4 protein, the mouse Mtmr4 protein sequence (NCBI accession number: NP_573478.1) was submitted to the cNLS mapper program (introduced in Section 1.1.3.2) with the cut-off score set at 6. A putative monopartite NLS was identified with the score of 6, referred herein as Mtmr4-NLS. To test its capacity to interact with importin α, a cDNA encoding the amino acid residues 1123 to 1132, representing the mouse Mtmr4-NLS or a mutant form in which the basic residues were replaced by alanine (referred herein as Mtmr4-M-NLS) were cloned into the pGEX-2T bacterial expression vector, fused at the N-terminus with GST and at the C-terminus with GFP tags (Figure 5.5, A, top schematic). The two NLSs were purified as both GST-GFP fusion proteins and as C-terminally GFP-tagged proteins after cleavage of the N-terminal GST (Figure 5.5, A, bottom image).

In pilot experiments the binding of Mtmr4 putative cNLS with importin α2 was examined due to the relative ease in importin α2 recombinant protein purification. Thus, GST-Mtmr4-NLS-GFP, alongside its mutant form, were used as baits in an *in vitro* solution binding assay to pull-down soluble importin α2 recombinant protein. In parallel reactions, GST-T-ag-NLS-GFP and GST-GFP recombinant proteins were used as positive and negative controls, respectively. In addition to this, a set of identical reactions were performed in presence of 0.1% NP-40 detergent to assess its capacity to reduce non-specific binding. The eluate from the pull-down reactions were analysed by Western blotting to detect importin α2 (Figure 5.5, B). These results demonstrated that only GST-T-ag-NLS-GFP was able to bind importin α2 to a higher level than GST-GFP bait in both absence and presence of detergent. Notably, the amount of importin α2 pulled-down by GST-GFP was clearly higher than that pulled-down by GST-Mtmr4-NLS-GFP in absence of detergent. Addition of detergent however, caused a more drastic drop in the amount of pulled-down importin α2 by GST-GFP compared to GST-Mtmr4-NLS-GFP. This observation suggested a degree of specificity, however low, in binding of Mtmr4-NLS to importin α2. Furthermore, it should be noted that the mutations incorporated in Mtmr4-NLS did not cause a reduction in binding to importin α2 in this assay.

Figure 5.5 Binding of the putative Mtmr4 NLS to importin α

A. Two cDNAs encoding either the putative mouse Mtmr4 NLS (Mtmr4-NLS) or its mutant, in which the basic residues at positions 4, 5, 6, and 10 were replaced by alanine (Mtmr4-M-NLS), were cloned into the pGEX-2T bacterial expression vector fused at N-terminus with GST and at the C-terminus with GFP (top). Both polypeptides were purified as either GST-GFP fusion proteins or as C-terminus GFP fusion proteins after cleavage of the N-terminal GST tag with thrombin. Two hundred pmol of each protein was run on a 12% SDS-PAGE and stained with coomassie blue (bottom).

B. Two hundred pmol of each GST-Mtmr4-NLS-GFP, GST-Mtmr4-M-NLS-GFP, GST-T-ag-NLS-GFP and GST-GFP fusion proteins were immobilized on GSH sepharose beads in transport buffer lacking or containing 0.1% NP-40 detergent. Subsequently 200 pmol of importin α2 recombinant protein was added to each reaction. After 2 hours of incubation, the pull-down products were eluted from the beads and analysed by Western blotting to detect importin α2 (left). Half the volume of each recombinant protein used in binding reactions was separated by 12% SDS-PAGE and stained with coomassie blue as an indication of protein loading equivalence (right).

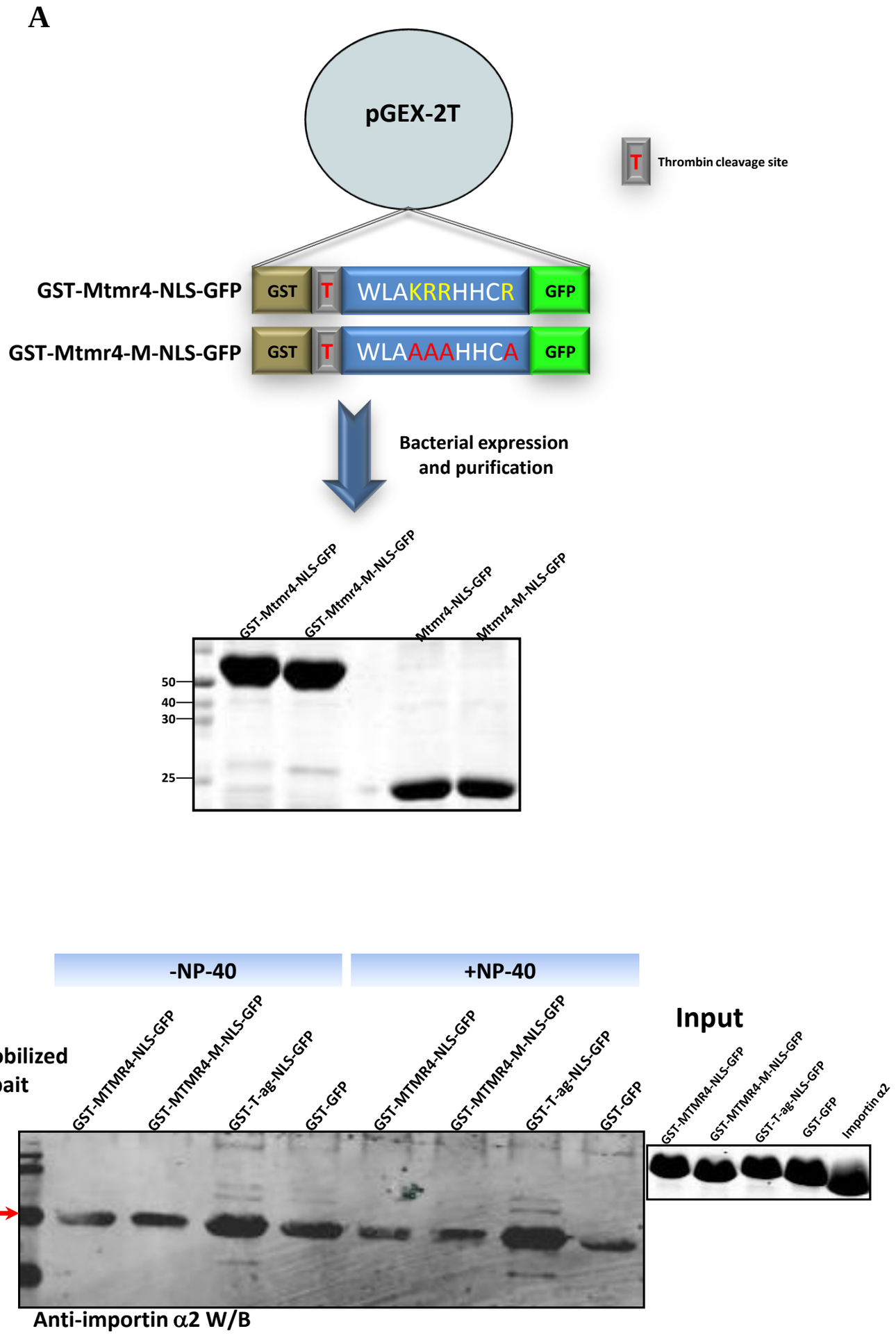
A
pGEX-2T
T
Thrombin cleavage site
GST-Mtmr4-NLS-GFP
GST
T
WLAKRRHHCR
GFP
GST-Mtmr4-M-NLS-GFP
GST
T
WLAAAAHHCA
GFP
Bacterial expression
and purification
GST-Mtmr4-NLS-GFP
GST-Mtmr4-M-NLS-GFP
Mtmr4-NLS-GFP
Mtmr4-M-NLS-GFP
50
40
30
25
B
-NP-40
+NP-40
Immobilized
bait
GST-MTMR4-NLS-GFP
GST-MTMR4-M-NLS-GFP
GST-T-ag-NLS-GFP
GST-GFP
GST-MTMR4-NLS-GFP
GST-MTMR4-M-NLS-GFP
GST-T-ag-NLS-GFP
GST-GFP
55 kDa
Anti-importin α2 W/B
Input
GST-MTMR4-NLS-GFP
GST-MTMR4-M-NLS-GFP
GST-T-ag-NLS-GFP
GST-GFP
Importin α2

In further experiments, GST-importin α2 and GST-importin α4 were each immobilized as bait for *in vitro* solution binding assays to test their capacity to bind soluble Mtmr4-NLS-GFP and its mutant form, alongside with T-ag-NLS-GFP and GFP alone as positive and negative controls, respectively. The pull-down products were analysed by Western blotting for GFP. As expected, T-ag-NLS-GFP bound very strongly to both importin α2 and α4, but not to GST alone (Figure 5.5, C, compare lanes 3 and 7 with lane 11). Using this approach a very small, nevertheless measurable difference in the binding of Mtmr4-NLS and Mtmr4-M-NLS to each importin α2 and α4 was observed (Figure 5.5, C, compare lane 1 with lane 2 and lane 5 with lane 6). Both Mtmr4-NLS-GFP and Mtmr4-M-NLS-GFP bound much more weakly to GST alone (Figure 5.5, C, lanes 9 and 10). To analyse this data in a quantitative manner, the signal intensities of protein bands in the anti-GFP antibody Western blot were measured using the Odyssey V3.0 system. This measurement of signal intensities revealed that the T-ag-NLS-GFP has approximately 10-fold higher binding to both GST-importin α2 and to GST-importin α4 compared to GFP alone. This difference for the Mtmr4-NLS-GFP and the Mtmr4-M-NLS-GFP was reduced to ~4-fold and ~3-fold, respectively (analysis results not shown). To interrogate this further, the drop in the signal intensity of each NLS-GFP fusion protein between pull-downs by each recombinant importin α (i.e. GST-importin α2 and GST-importin α4) and GST-only bait was measured. An 8-fold reduction was observed for the binding of T-ag-NLS-GFP to either GST-fused importin αs compared to GST alone. This decrease was reduced to 4 fold for the Mtmr4-NLS-GFP, and was only 2 fold for Mtmr4-M-NLS-GFP (Figure 5.5, C, bottom panels). Thus, this analysis indicates that binding of Mtmr4-NLS to importin αs is due to an activity that is diminished by the introduced mutations, providing evidence that the sequence identified by cNLS Mapper is functional for importin α binding.

5.10 Anti Mtmr4 antibody validation

An anti-Mtmr4 monoclonal antibody raised in mouse, against the amino acids 665 to 981 of human Mtmr4 (NP_004678.3) was provided by colleagues in the laboratory of Professor Christina Mitchell (Department of Biochemistry and Molecular Biology, Monash University, Victoria). The peptide sequence used to generate this antibody has 73% and 68% identity with the corresponding Mtmr4 sequences from mouse

Figure 5.5 (Continue) Binding of the putative Mtmr4 NLS to importin α

C. Two hundred pmol of GST-importin α2, GST-importin α4 or GST alone were immobilized on GSH sepharose beads in transport buffer containing 0.1% NP-40. Subsequently, 200 pmol of Mtmr4-NLS-GFP, Mtmr4-M-NLS-GFP, T-ag-NLS-GFP or GFP alone were added to the reactions. After 2 hours of incubation, bound material was eluted from GSH beads and the eluate was analysed by Western blotting with an anti-GST antibody to demonstrate the loading equivalence of bait proteins or with an anti-GFP antibody for analysis of the pulled-down targets (Top). The signal intensities produced by anti-GFP antibody (corresponding to the pulled-down targets) in all reactions were measured (Table 5.2, below) and the proportion of the reduction in GFP signals between GST-importin α pull-down samples compared to those obtained with GST alone pull-down was graphed using GraphPad V.5. The combined results of two independent experiments for importin α2 (average shown with the error bars representing the standard deviation) and one experiment for importin α4 is shown.

Reaction number	1	2	3	4	5	6	7	8	9	10	11	12
Signal intensity	23.34	18.43	57.72	5.59	23.7	16.63	48.24	7.98	5.65	11.24	7	0.28

Table 5.2 Signal intensities of protein bands produced by anti-GFP antibody.

C

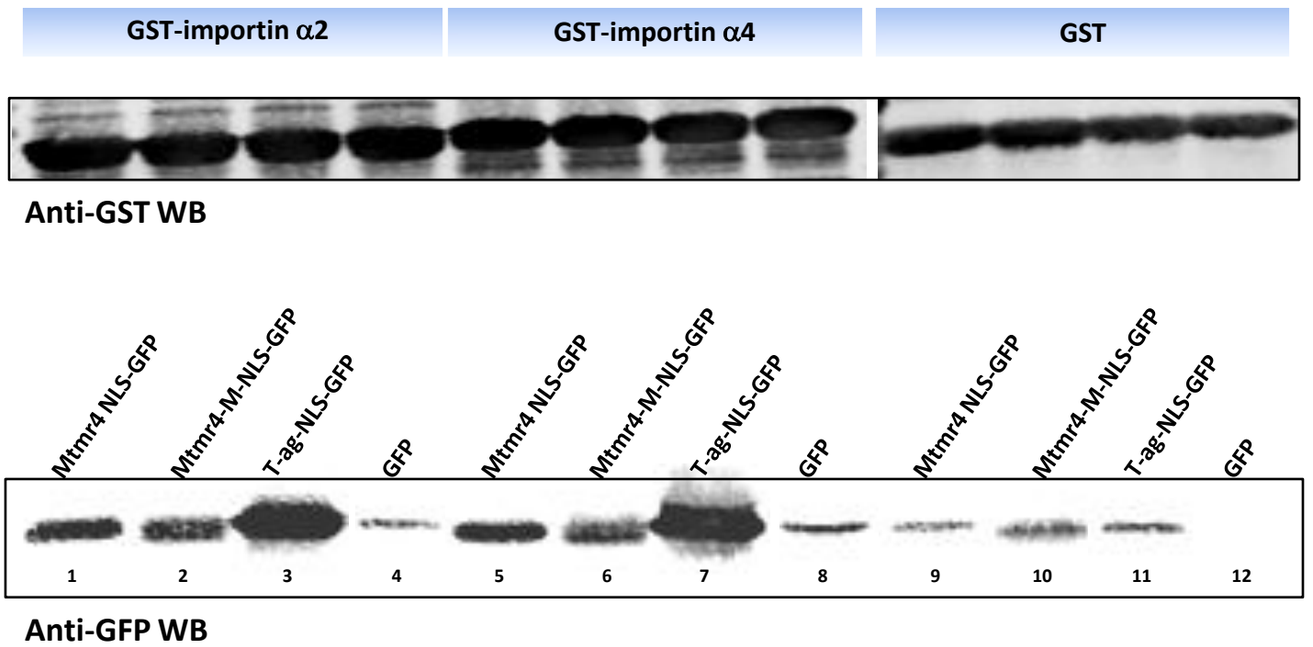

Fold change in NLS-GFP signal intensity between the pull down with GST-α2 and GST

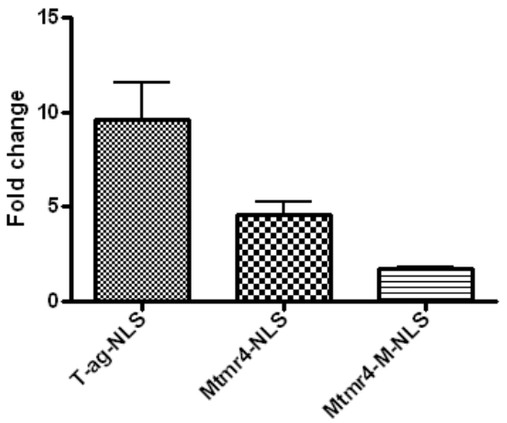

Fold change in NLS-GFP signal intensity between the pull down with GST-α4 and GST

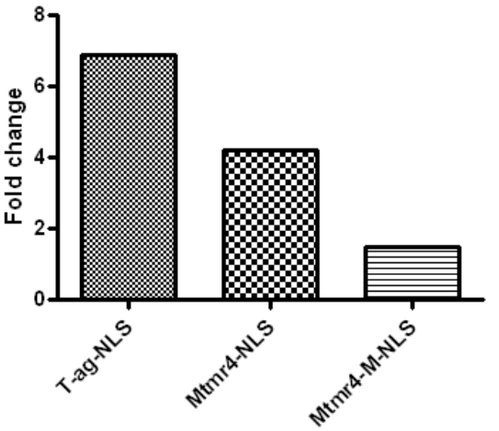

(NP_573478.1) and rat (NP_001099297.3), respectively. Several Western blot experiments were performed to assess this antibody's activity and specificity in recognizing Mtmr4 (Figure 5.6). Sixty µg of lysate from adult rat testis, pachytene spermatocytes and round spermatids, along with lysates prepared from HEK cells and HEK cells transfected with pCGN vector expressing HA-tagged human Mtmr4 or HA only (M.W 4 kDa) were separated by SDS-PAGE and examined by Western blot using anti-Mtmr4 antibody, anti HA antibody, and no primary antibody in separate experiments.

The anti-Mtmr4 monoclonal antibody produced several bands (M.W ~160, 130, 100, 80 and 75 kDa) of identical pattern in all examined lysates (Figure 5.6, left). Despite equal loading of the lysate on each lane, all of these bands were present at much higher levels in lysates prepared from HA-Mtmr4 transfected cells; this observation suggested that these bands are of Mtmr4 origin. The correspondence of these bands to Mtmr4 and its degraded products was inferred by examining of the membrane probed with the anti-HA antibody. The anti-HA antibody recognized all of the bands that were observed on a membrane probed with the anti-Mtmr4 antibody in addition to two bands that were only detected by the anti-HA antibody (Figure 5.6, middle panel, yellow arrows). Lanes loaded with HA-transfected or untransfected HEK cells, produced no bands with the anti-HA antibody (Figure 5.6, middle, lanes 3 and 4). The membrane that was probed with secondary antibody only as a negative control produced no bands, despite detection of equal amounts of α-tubulin as a loading control. Thus, the anti Mtmr4 antibody is specific in detecting the Mtmr4 protein product. The expected molecular mass of Mtmr4 is ~130 kDa; however, the band of ~160 kDa appears to be of Mtmr4 origin, based on its detection by both anti-Mtmr4 and anti-HA antibodies. This 160 kDa species could represent a modified version of Mtmr4 protein. Validation of this antibody with a knock-out tissue was not performed in this study due to time and resource limitation.

An interesting observation was that the endogenous band of ~130 kDa was distinctly more intense in the spermatocyte lysate lane, compared to the lane loaded with round spermatid lysate, and it was absent from the adult rat testis lysate lane (Figure 5.6, left, compare lane 3 with lanes 4 and 2). Given the similar intensity of all other bands

Figure 5.6 Validation of anti-Mtmr4 antibody

Every lane in each membrane contains 60 µg of the lysate prepared from the indicated source. The membranes were probed with the anti-Mtmr4 antibody, the anti-HA antibody, or without primary antibody as negative control. The red arrow in the left hand side membrane points towards the band that appears more strongly in spermatocyte lysate than in spermatid or other lysates (see text). The yellow arrows in the middle membrane point towards the two bands that are detected in the lysate of HA-Mtmr4 transfected HEK cells, only when probed with anti-HA antibody. The α-tubulin detection, shown under each membrane serves as the control for equal loading of proteins on each lane.

Labelling key: AdRT (adult rat testis), S'Cyte (purified rat spermatocyte), S'Tid (purified rat spermatid), HEK/HA-Mtmr4 (HEK cells transfected with HA-Mtmr4 fusion expression vector), HEK/HA (HEK cells transfected with HA-only expression vector), and HEK (HEK cells, not transfected).

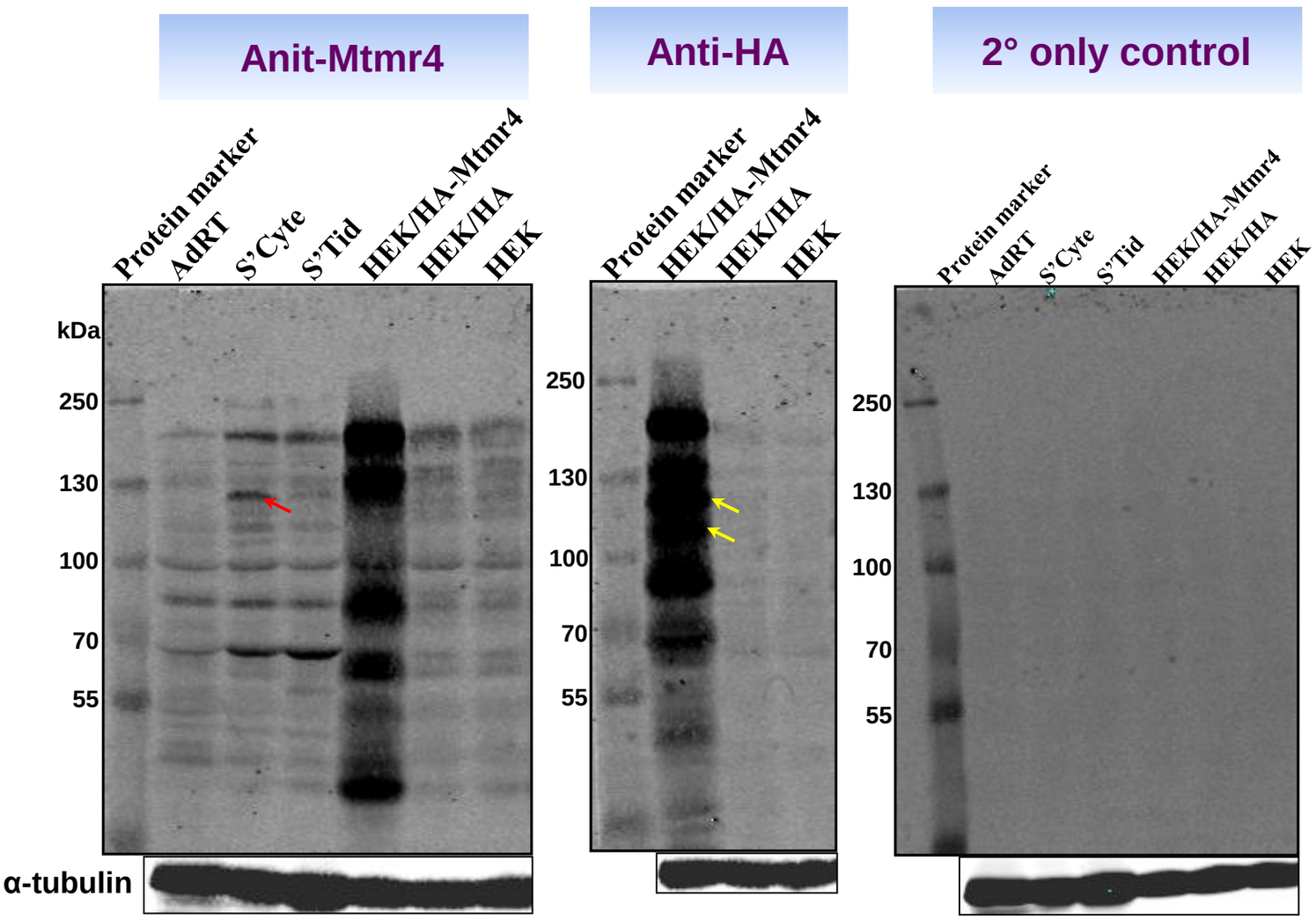
Anit-Mtmr4
Anti-HA
2° only control
Protein marker
AdRT
S'Cyte
S'Tid
HEK/HA-Mtmr4
HEK/HA
HEK
kDa
250
130
100
70
55
α-tubulin

across these three lysates, this band of ~130 kDa is an excellent indication that Mtmr4 is detected in the spermatocyte lysate.

5.11 Pull-down and immunoprecipitation of endogenous Mtmr4 with importin α2 and importin α4

To further examine the potential interaction between importin α and Mtmr4, pull-down and immunoprecipitation assays were performed using lysates from testes of 28 day old mice (Figure 5.7). In parallel reactions recombinant importin α2 and α4 proteins or antibodies to importin α2 and α4 were immobilized on GSH and protein A/G sepharose beads, respectively, followed by addition of 1 mg of protein in a 28 day old mouse testes lysate. The bound fractions were eluted and analysed by Western blotting for detection of the Mtmr4 protein. In pull-down experiments, two variants of importin α2 were utilized for a more in depth investigation of the nature of the potential interaction. One of the variants was the importin α2-ED mutant, defective in NLS binding (introduced in Section 4.2); the second variant was a truncation of importin α2 devoid of its importin β1 binding (IBB) domain (Importin α2-ΔIBB). This variant of importin α has a higher affinity to NLS cargo, since the autoinhibitory effect of IBB has been removed. Thus, the pattern of Mtmr4 interaction with these importin α isoforms should be informative regarding the region of interaction.

When the pull-down products were analysed by Western blotting against Mtmr4, the protein band of ~130 kDa (i.e. the spermatocyte-specific Mtmr4 species, Section 5.10) was enriched in some reactions (Figure 5.7). The Mtmr4 band was readily detected in the pull-down products of both GST-α2 and GST-α4 (Figure 5.7, A, middle panel, lanes 2 and 5, respectively), but was completely absent from the GST-only pull-down reaction (Figure 5.7, A, middle panel lane 1). Intriguingly, the GST-fused importin α2-ΔIBB pull-down appeared to bind higher amounts of Mtmr4 compared to the wild type importin α2 fusion protein (Figre 5.7, A middle panel, compare lane 3 to lane 2), while a much reduced level of Mtmr4 was detected in the pull-down product of GST-fused importin α2-ED mutant (Figure 5.7, A, middle panel compare lane 4 to lane 2). This pattern of Mtmr4 detection in the pull-down products suggests that Mtmr4 may

bind to the NLS binding groove of importin α. Detection of importin β1 in the pull-down products by Western blotting served as the positive control for the assay. As expected, importin β1 was readily detectable in the pull-down products of GST-importin α2, α2-ED and α4, while it was barely detectable in the pull-down products of GST-α2-ΔIBB, and absent from the GST only pull-down (Figure 5.7, A, bottom panel).

The immunoprecipitation product with the importin α2 antibody contained a very faint band of ~130 kDa which was not observed in the negative control sample (Figure 5.7, B, top left panel, yellow arrow); immunoprecipitation with the anti-importin α4 antibody, however, did not produce this band (Figure 5.7, B, top right). Further importin α4 immunoprecipitations to assess the interaction of Mtmr4 with endogenous importin α4 was not performed due to time limitations. As a positive control, importin β1 was readily detected in the immunoprecipitated products from reactions with either importin α2 or importin α4 antibodies, but not in the negative control reactions lacking primary antibody (Figure 5.7, B, bottom panels).

Figure 5.7 pull-down and immunoprecipitation of Mtmr4 with importin α2 and α4

A. Three hundred pmol of each GST, GST-importin α2, GST-importin α2-ΔIBB, GST-importin α2-ED mutant and GST-importin α4 were immobilized on GSH sepharose beads followed by addition of 1 mg of lysate from 28 day old mouse testes. The bound fractions were eluted and analysed by Western blotting for detection of GST (top panel), Mtmr4 (middle panel) and importin β1 (bottom panel). The lane labelled as input (lane 1 from right) contains 10% of the lysate volume used for each pull-down reaction.

B. Three μg of either importin α2 or importin α4 antibodies were immobilized on protein A/G sepharose beads followed by addition of 1mg of lysate from 28 day old mouse testes. The bound fractions were eluted and analysed by Western blotting for detection of Mtmr4 (top panel) or importin β1 (bottom panel). The yellow arrow in the top left panel points towards the expected signal of endogenous Mtmr4.

A

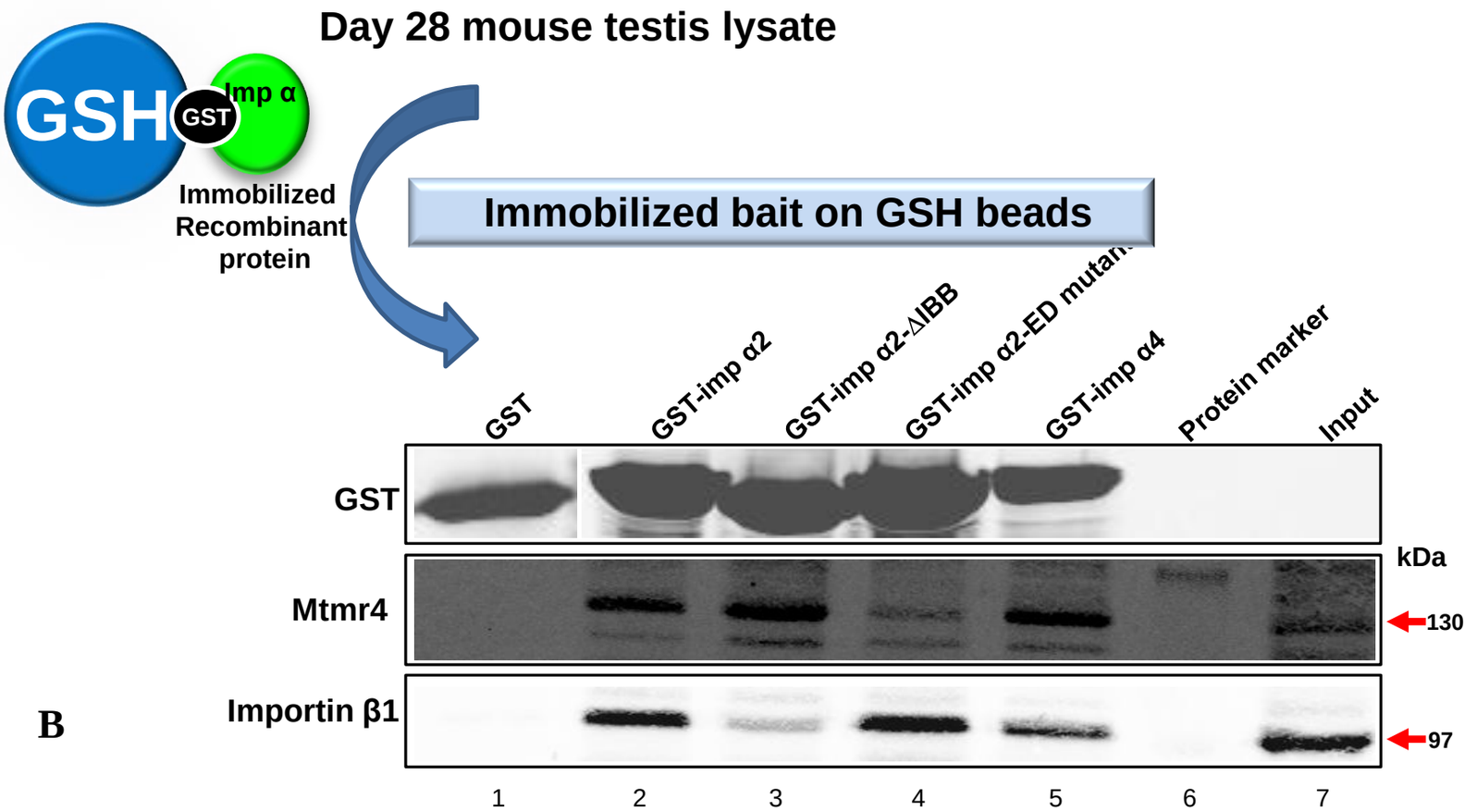
Day 28 mouse testis lysate
GSH
GST
Imp α
Immobilized Recombinant protein
Immobilized bait on GSH beads
GST
GST-imp α2
GST-imp α2-ΔIBB
GST-imp α2-ED mutant
GST-imp α4
Protein marker
Input
GST
Mtmr4
Importin β1
kDa
130
97
1
2
3
4
5
6
7

B

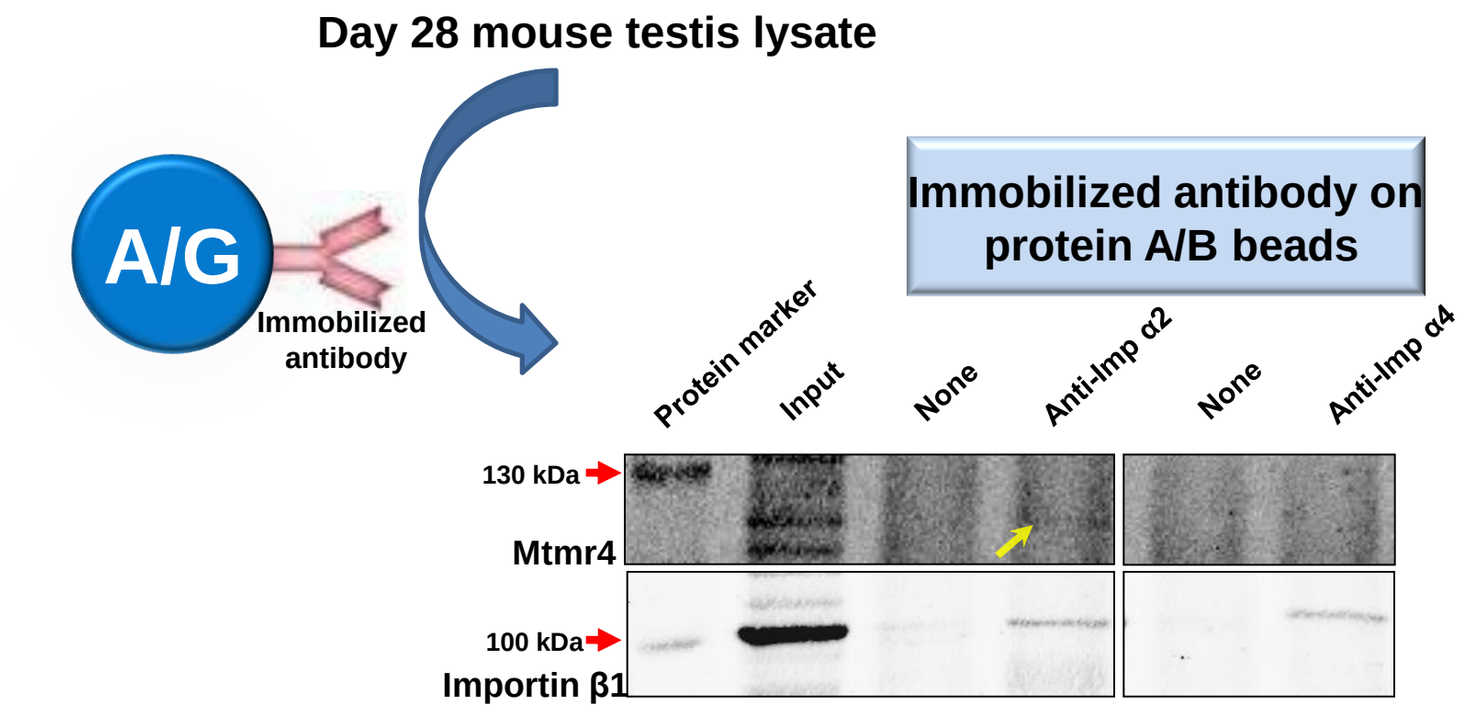
Day 28 mouse testis lysate
A/G
Immobilized antibody
Immobilized antibody on protein A/B beads
Protein marker
Input
None
Anti-Imp α2
None
Anti-Imp α4
130 kDa
Mtmr4
100 kDa
Importin β1

5.12 Concluding remarks

In this chapter the results of several experiments designed to validate the interaction of importin α family members with Mtmr4 are presented, based on the intriguing prospect of linking importin α proteins to another non-nuclear function. Mtmr4 is a lipid and protein phosphatase, and it was identified as a putative binding partner of importin α4 from lysates of pachytene spermatocytes in a previous study (Miyamoto et al., 2013). Northern blot analysis of *Mtmr4* demonstrated that its transcript is ubiquitously synthesized in several tissues (liver, brain, testis and kidney), while a potential splice variant was persistently detected in adult, but not 21 day old, mouse testis total RNA. *In situ* hybridization revealed that the *Mtmr4* transcript is most readily detected in pachytene spermatocytes, the cell type in which the interaction with importin α4 was originally identified. The cNLS Mapper analysis predicted a monopartite cNLS with the score of 6 (i.e. strong) within the Mtmr4 primary amino acid sequence. This sequence, and a mutant isoform, in which all the basic residues were replaced by alanine, were purified as recombinant proteins. Several assays were performed to assess the capacity of this putative cNLS to bind importin α2 and α4; the results revealed that the Mtmr4 putative cNLS binds to importin α with a degree of specificity, and that the binding is diminished as a result of introduced mutations. Subsequent pull-down experiments with recombinant importin α proteins and immunoprecipitations with anti-importin α antibodies revealed that endogenous Mtmr4 binds to both recombinant importin α2 and α4 proteins, but it is immunoprecipitated only with anti-importin α2 antibody, not that of α4. The pattern of Mtmr4 pull-down with recombinant importin α2 isoforms indicated that Mtmr4 may be a part of a nuclear import complex with importin αs. The pull-down of Mtmr4 was more efficient with importin α2 ΔIBB and less efficient with importin α2-ED mutant, compared to wild type importin α2. Thus there appears to be a bona fide interaction between importin α proteins and Mtmr4. The outcome of this interaction in the context of germ cell maturation is not clear currently and awaits further research.

Chapter 6-
General discussion

CHAPTER 6 GENERAL DISCUSSION

6.1 Opening remarks

Classical nucleocytoplasmic transport is an evolutionarily conserved pathway which facilitates the transport of cargo molecules between the nucleus and cytoplasm in all eukaryotic cells. This pathway has many interacting components including nuclear pore complexes, cargo receptors and the Ran system. The focus of this thesis has been on the cargo receptors of the classical nuclear import pathway, the importin α family of proteins. Based on the distinctive expression profiles of importin α family members across tissues, and evidence of their individual NLS binding capacities, we hypothesised that each importin α protein serves unique roles in developmental processes. Postnatal spermatogenesis provides an ideal model for studying development; meiotic cell division of spermatocytes and extensive transformation of spermatids are among the developmental events that occur continuously during adult spermatogenesis. Thus we aimed to delineate the protein levels of several importin proteins in pachytene spermatocytes and round spermatids of adult rat testis, followed by identification of binding partners for selected importin α family members in these two testicular cell types. The original hypothesis was that each importin α would bind distinct cargo within each cell type, and that the functional nature of importin cargoes would change as germ cells differentiate.

6.2 Dynamic importin protein levels in germ cell maturation

The results of the quantitative Western blots presented in Chapter 3 of this thesis have uncovered a novel case of selective importin protein production in rat spermatocytes and spermatids. This is the first example of stoichiometry measurements for different importin α family members in two cell types at distinct stages of a developmental process. The expression pattern and estimated concentration of each importin in pachytene spermatocytes and round spermatids of adult rat testis are presented diagrammatically in Figure 6.1, A (see Table 3.3). The protein level data in Figure 6.1 are shown in combination with the best understood subcellular localization of each

importin in germ cells as revealed by immunohistochemical detection in adult rodent testes (discussed in Section 1.2.6). Several important observations can be made from interrogating these data. Firstly, the levels of importin α proteins change more markedly than importin β1 levels do between lysates of pachytene spermatocytes and round spermatids. Among importins examined here, importin α2 has the highest variation between the two samples, followed by importin α3, and both of these are present at higher concentrations in spermatocytes than in spermatids. On the other hand, importin α4 and importin β1 levels are relatively constant between these two cell types. In line with the NLS-binding role of importin α proteins, this result indicates that the dynamic population of importin αs is the primary determinants of the repertoire of cargo that enters the nucleus via the classical import pathway in germ cells. Furthermore, that the concentrations of both importin α2 and α3 are approximately two-fold higher in spermatocytes than in spermatids is suggestive of meiosis-specific roles for these family members. GEO profiles datasets corresponding to *importin α3* mRNAs in both postnatal mouse testis development and in purified germ cells from mouse testis provide transcript data that are consistent with this proposal (Figure 3.1). The levels of the *importin α2* transcript however, are not consistent with the protein levels and this may provide an excellent example of a highly dynamic, yet tightly regulated gene expression within a developmental context. GEO profiles of *importin α2* in both developing testis and purified germ cells indicate that higher levels of this transcript are present in spermatids (Figure 3.1). The result of the Western blot analysis performed in this study, however, clearly demonstrated that importin α2 protein is much more abundant in pachytene spermatocytes than in round spermatids. Why does the synthesis of the *importin α2* mRNA increase constantly in developing testis, and why is there a lower level of importin α2 protein in round spermatids in which a high transcript level is detected? Consideration of posttranslational regulation of gene expression can provide clues and partial answers to these questions. In a recent study, immunohistochemical detection of importin α2 on adult mouse testis sections indicated that elongating spermatids contain relatively high levels of importin α2 protein (Ly-Huynh et al., 2011). Thus importin α2 protein levels may be controlled by the timely translation of a dormant cellular mRNA pool, according to the requirement of developing germ cells.

The consistent concentration of importin β1 protein detected in spermatocytes and round spermatids suggests that the rate of classical nuclear import is similar between these cell types. This hypothesis is strengthened by the result of stoichiometric analysis (Chapter 3) which indicated that importin β1 is the limiting factor for classical nuclear import in both cell types, since it is lower in abundance than importin αs. To test this hypothesis *in vitro* nuclear import assays could be performed, with the aim of comparing the capacity of lysates from spermatocytes and spermatids to confer nuclear accumulation on an exogenous cargo; thus the expected outcome is that the rate of classical nuclear import is the same in these two cell types. Observation of a difference in nuclear import efficiency conferred by these two cell lysates, however, would be considered as a strong indication that not every importin β1 molecule is involved in the classical nuclear import pathway. This view is consistent with the newly discovered role of importin β1 in mediating protein dislocation from the endoplasmic reticulum into the cytoplasm (Zhong and Fang, 2012) in addition to its previously described roles in nuclear pore complex formation (Section 1.1.7.2; Zhang et al., 2002b). The latter is of particular interest in the context of post-meiotic germ cell maturation. During spermiogenesis, nuclear pore complexes redistribute from being rather uniformly spread throughout the spermatid nucleus to becoming more concentrated at the caudal region of the nucleus (Ho, 2010). Since importin β1 is present at the same concentration in spermatocytes and spermatids, it could be involved in movement or genesis of these pore complexes.

It is of interest that all of the examined importins are present at higher levels in pachytene spermatocytes and round spermatids compared to the lysates from total adult rat testis. This difference is much more evident for all of the importin α family members examined here than for importin β1 (Figure 6.1). Given that an adult mammalian testis contains many developmentally mature cells (i.e. cells that do not divide or differentiate), including Sertoli cells (Sharpe et al., 2003) and Leydig cells (Benton et al., 1995), this observation indicates that importin α family members may have more roles in cell division and differentiation events required during spermatogenesis than those performed in association with importin β1. In support of this hypothesis, several examples of direct roles for importin α family members in

cellular differentiation and proliferation have been documented. These include the alteration in importin α cellular repertoire during neural differentiation (Section 1.1.8.3; Yasuhara et al., 2007) and the increased rate of proliferation and apoptosis by the MCF7 human breast cancer cell line that results from overexpression and knock-down, respectively, of importin α2 (Noetzel et al., 2012). Contrary to this proposition however, are observations from reducing importin protein levels in HeLa cells using RNAi. Reduction of importin β1 levels alone, reduced HeLa cell proliferation to the same magnitude that reduction in importin αs did (Quensel et al., 2004). Given that down-regulation of importin β1 leads to a general reduction in nuclear import, the observed proliferation defect in Quensel study cannot be attributed to the unique role of importin β1 in cell division.

Another intriguing observation regarding the importin proteins concerns their stoichiometry in testicular cells. Interestingly, importin α proteins collectively are more abundant than importin β1 in every examined lysate in this study. This phenomenon has not been examined in any other developmental system or cell type previously. The classical nuclear import complex is composed of an importin α family member with an importin β1 molecule in a 1:1 molar ratio. Therefore, the relatively higher number of importin α proteins compared to importin β1 in a given cellular context provides strong evidence of non-import roles served by importin α family members in spermatogenesis. Consistent with this hypothesis, importin α family members have been found in a wide range of cellular compartments including in association with internal cellular membranes (Hachet et al., 2004), cytoskeletal elements (Smith and Raikhel, 1998) and the plasma membrane (Andrade et al., 2003). Given that few of these non-import roles have already been defined (Section 1.1.7.2; reviewed in Miyamoto et al., 2012a), it is important to explore the possibility that importin α family members are extensively involved in a broad range of cellular functions. Figure 6.1, B is a representation of the proposed importin α compartmentalization and diversity of functions, based on the literature cited above combined with the result of stoichiometry analysis in this study. Subsequent Sections of this General Discussion Chapter contain elaboration on putative non-import functions of importin α based on the results obtained in this study.

Figure 6.1 Schematic representation of importin α protein levels and proposed diversity in localization

A. The measured cellular abundance of importins α2, α3, α4 and β1 is depicted for both pachytene spermatocytes (top row) and round spermatids (bottom row). The numbers at the bottom of each cell refer to the concentration (ng/mg) of each importin estimated to be present in the respective cell types. The brown colouring is reflective of the relative level of each protein, with the intensity being directly correlated to the measured concentration and used to depict the best known subcellular localization within each cell type (see Section 1.2.6). In the case of importin β1, no subcellular localization within spermatids has been described previously. Thus, in this figure, importin β1 in spermatids is depicted as only cytoplasmic.

B. Proposed subcellular compartmentalization of importin α proteins. Since importin α proteins outnumber importin β1 in both cellular contexts that were examined in this study (i.e. spermatocytes and spermatids) we suggest that excess importin α proteins are localized on a wide range of locations within these germ cells. This diagram presents a few examples of these localizations which were previously described (see text for information and references), to which the findings in this thesis will contribute.

A

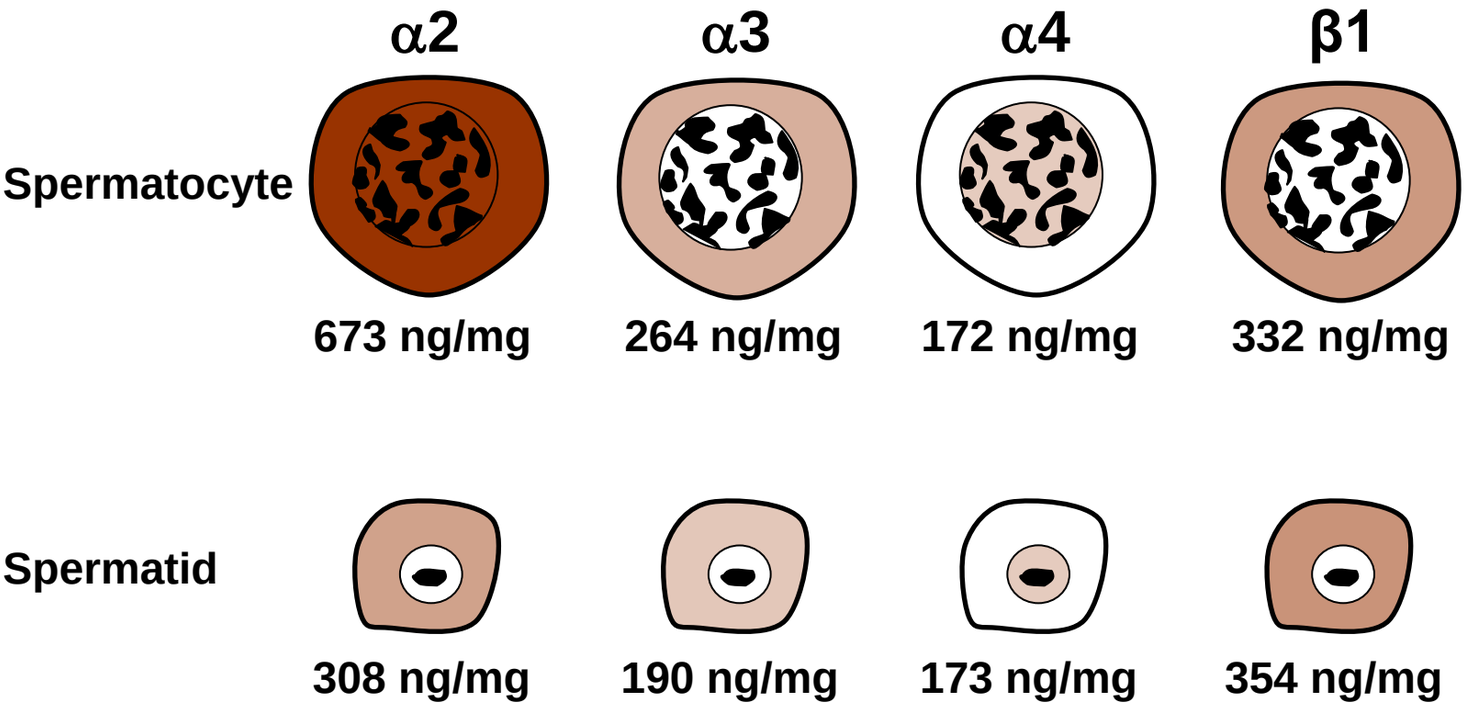
α2
α3
α4
β1
Spermatocyte
673 ng/mg
264 ng/mg
172 ng/mg
332 ng/mg
Spermatid
308 ng/mg
190 ng/mg
173 ng/mg
354 ng/mg

B

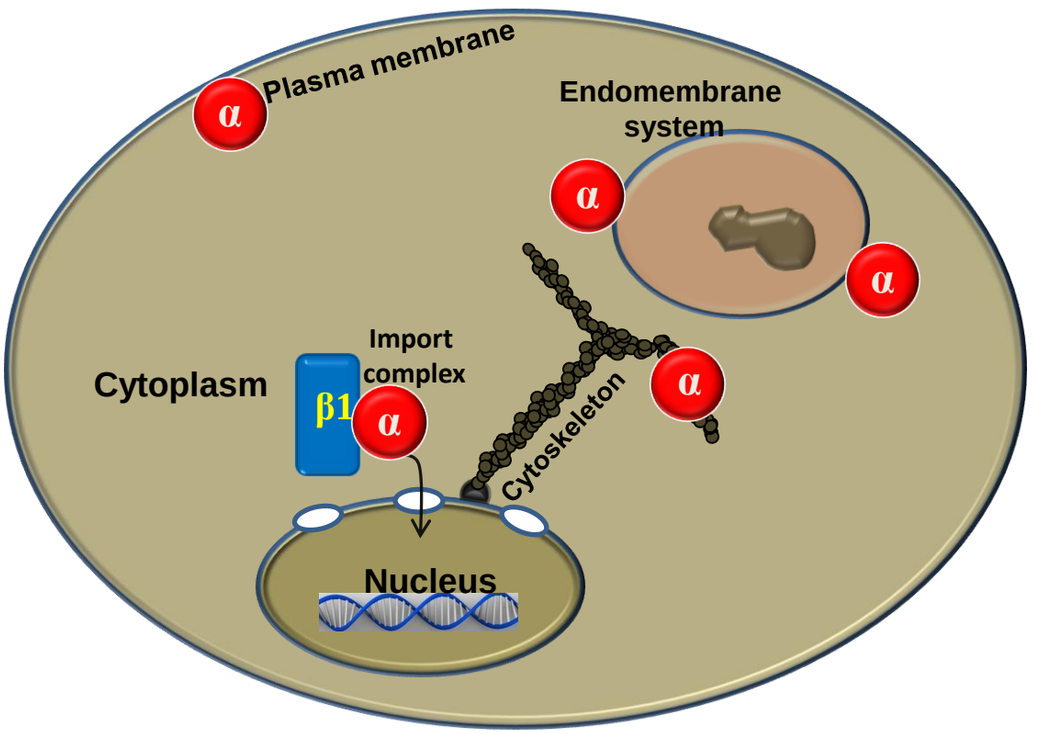
Plasma membrane
α
Endomembrane system
α
α
Import complex
Cytoplasm
β1
α
α
Cytoskeleton
Nucleus

6.3 Differential cargo binding by importin α family members in spermatogenesis; implications in germ cell maturation

In broad terms, a protein's function can be regulated by several factors including its level of expression, interactions with other proteins and subcellular localization. Based on the differential expression of importin α family members in pachytene spermatocytes and round spermatids, we next tested the hypothesis that these family members each bind a distinct cohort of proteins in these two germ cell subtypes.

Pull-down of importin α2 and α4 using lysates of spermatocytes and spermatids facilitated identification of numerous binding candidates for each. As hypothesized, distinct candidate cohorts were identified by each importin and from each lysate source. Many of these identified proteins had not been previously shown to be present in testicular cells, thus this list could provide many avenues for future testis cell biology analyses. Since experimental validation of all or most of the putative interactions is not feasible in the context of this thesis study, we selected several bioinformatics approaches to assess the likely validity of these interactions.

The initial approach applied to validating the experimental outcomes included searching the protein sequence of identified candidates for presence of putative cNLSs. Many putative cNLSs, both monopartite and bipartite, and with varying strengths (i.e. weak, moderate and strong) were identified by cNLS Mapper analysis (Kosugi et al., 2009). Each of these represents good candidates for experimental validation, and the identified cNLSs in this study could contribute to refinement of a cNLS sequence consensus, an outcome that would facilitate the identification of other importin binding proteins with higher accuracy.

The cNLS Mapper analysis showed that, of the importin α2 binding candidates in spermatocytes, 39% (11 candidates) contained strong cNLSs, while 17% (5 candidates) contained moderate cNLSs and a high proportion, 42% (12 candidates) contained weak cNLSs. Stoichiometric analyses showed that importin α2 protein is in higher abundance than importin β1 in lysates prepared from spermatocytes (Figure 3.6). Thus it is conceivable that a large proportion of importin α2 binding proteins in

spermatocytes are not nuclear import cargos. Despite the relatively lower level of importin α2 protein in spermatids compared to spermatocytes (Figure 6.1), the recombinant importin α2 pull-down identified 25 candidates from the spermatids lysate. Interestingly, 52% (13) of these have a strong putative cNLS (Figure 4.8, B). Thus, down-regulation of importin α2 in spermatids may reduce the nuclear access of a wide range of proteins which could otherwise bind to importin α and enter into the nucleus. This might indicate that a shift in transcriptional requirement of the germ cells during their maturation is accompanied by a change in the repertoire of importin αs, a phenomenon already delineated for neural cells (Yasuhara et al., 2007). Given that none of the importin αs examined in this thesis study had higher levels in spermatids than in spermatocytes, examination of the remaining family members may reveal another case of subtype switching of importin αs in a developmental context (i.e. spermatogenesis), in which a particular nuclear transport factor is required to effect a differentiation switch.

The pattern produced by classification of the cNLS motif composition of importin α4 binding candidates indicates a potential shift in the cellular roles for importin α4 as spermatocytes transform into spermatids. Fifty two percent of importin α4 binding candidates in spermatocytes (10 candidates) possessed a strong cNLS compared to only 30% of candidates in spermatids (8 candidates). In view of the consistent importin α4 protein levels between these two cell types (Figure 6.1), the difference in cNLS binding activity may indicate that importin α4 switches its role from a general nuclear import receptor in spermatocytes to serve another or additional functions in spermatids. Although the result of protein localization prediction is not consistent with this view (because majority of proteins in every cohort of candidates are predicted to be nuclear), bioinformatics analyses used to uncover pathways in which importin αs participate supports this proposition (both discussed below). Furthermore, it must be considered that importin α4 appears as predominantly nuclear in both spermatocytes and spermatids (Section 1.2.6, Figure 6.1). The implications of this observation are that either importin α4 stays in the spermatocyte nucleus after carrying its cargo, or that importin α4 does not take part in nuclear import, since it is

confined to the nucleus. The later possibility would mean that there is no competition between importin α2 and α4 in spermatocytes for binding to NLS-bearing cargoes.

The use of PSORT II analysis to predict the subcellular localization of candidates produced a uniform pattern between all cohorts. As expected, the nucleus was the primary predicted site of localization for the vast majority, followed by the cytoplasm, while the mitochondrial and endoplasmic reticulum compartments both had several allocated proteins. There is a good correlation between putative cNLS motif composition and the predicted subcellular localization of the candidates, in that the majority of the proteins containing strong or moderate cNLSs were also predicted to localize in the nucleus (Table 4.2). That many candidates were allocated to locations other than nucleus is not surprising. Two recent reports, in which an approach similar to that used in the present study was employed to identify importin α binding partners, have identified candidates with predicted or known localizations in cellular compartments including the cytoplasm, cytoskeleton and to plasma membrane (Fukumoto et al., 2011; Park et al., 2012).

Of note, there are several candidates that did not possess a discernible cNLS based on the cNLS Mapper algorithm, yet they were predicted to be nuclear (Table 4.2). The widely held belief regarding the classical NLSs is that they occur within the primary sequence of a nuclear protein (Lange et al., 2007). If one or some of the above mentioned proteins enter the nucleus in an *in vitro* nuclear import assay facilitated by an importin α/β1 heterodimer, then it could be argued that some cNLSs will form within a secondary conformation of the cargo protein. Furthermore, the belief that inactivation of a cNLS should abrogate nuclear accumulation of the host protein is challenged by the identification of multiple putative cNLSs in many candidates (see the CD attached to this thesis for the complete cNLS Mapper output for all the candidates).

Bioinformatics analyses performed on the candidate lists indicated that the protein networks of different importin αs in germ cells may be part of distinct functional associations. Caution should be taken, however, not to over interpret the result of this analysis for several reasons. Firstly, the result of an analysis of this nature is limited

by the available knowledge regarding each candidate in the list. Inevitably, not all proteins in an organism have been studied in terms of their function, localization and interactions to the same extent. Thus, some terms may have been enriched because of the dominant effect exerted by a better-characterized candidate or a more thoroughly studied biological process. The accuracy of the output could also be heavily compromised by the presence of false candidates in the list. It must also be conceded that the enriched terms do not necessarily refer to the functional attributes of importin αs themselves; rather they are processes that are most represented by a network of proteins that importin αs are part of. Despite the caveats mentioned above, the results obtained by bioinformatics analysis can provide valuable hints regarding functional association of a protein list. Figure 6.2 summarises the most highly enriched Biological Processes that are affected by importin α2 and α4 interacting partners in spermatocytes and spermatids, as discussed below.

Biological annotations pertinent to RNA stability and differentiation were of highest enrichment in importin α2 binding candidates cohort from spermatocytes (Figure 4.10, E). Regulation of RNA stability is a critical aspect of germ cell development. A large proportion of mRNAs in testicular germ cells including spermatocytes are part of messenger ribonucleoprotein (mRNP) complexes (Moussa et al., 1994). Within these complexes, mRNAs are translationally silenced until their protein product is required, usually during spermiogenesis when transcription has ceased (Steger, 2001). Thus, importin α2 interacting partners may be directly involved in keeping mRNA dormant for protein synthesis at a later stage, when spermatids are elongating. Validation of this hypothesis is feasible through several approaches that have been developed for identifying protein-RNA interactions (Ascano et al., 2012). Differentiation is a prominent feature of round spermatids, as these germ cells transform into spermatozoa. That this term was enriched by importin α2 cohorts of candidates in spermatocytes may reflect on the involvement of these proteins in meiotic processes or may indicate involvement in activities that anticipate the upcoming differentiation events of spermiogenesis. Many terms relating to chromatin conformation were enriched in the cohort of spermatid importin α2 binding candidates (Figure 4.10, F); given that importin α2 protein level is relatively lower in spermatids (Figure 3.4 and 3.5), and that many terms related to these functions were enriched by importin α4

binding candidates (see below), these activities may primarily be regulated by importin α4 in haploid germ cells.

Some of the most highly enriched terms in the Biological Processes category within the cohorts of importin α4 binding candidates in spermatocytes are related to nucleocytoplasmic transport (Figure 4.10, G). This observation correlates well with the result of cNLS Mapper analysis which showed a high proportion (52%) of importin α4 binding candidates in spermatocytes contain strong cNLSs (Figure 4.8, B). The highest enriched term in this cohort, however, was mitochondrial organization. Although no clear explanation could be given at this stage, this may be a novel cellular process in which importin αs participate, a proposition that awaits future research and examination. The importin α4 candidate cohort from spermatids generated enrichment of many terms related to chromosomal dynamics (Figure 4.10, H). Given that chromatin modification is an essential part of haploid germ cell maturation (Govin et al., 2004), and in view of the unchanged level of importin α4 in spermatids compared to spermatocytes, it is reasonable to propose that this family member exerts a strong effect on the processes required for DNA packaging during spermiogenesis. This effect is likely to be direct, since a low proportion of importin α4 candidates in round spermatids contained strong cNLSs (Figure 4.8, B). To address the hypothesis that importin α4 may directly bind to chromatin and regulate its dynamics, a chromatin immunoprecipitation (ChIP) assay could be performed using spermatid lysates to detect proteins bound to importin α4 in chromatin.

To draw further correlations between importin αs and the identified binding partners, the GEO profiles of all candidates in postnatal testis development and in isolated germ cells from mouse testis were examined. In agreement with the concept of a developmental switch in which the presence of all factors is required to exert an effect, transcript levels of most candidates exhibited fluctuations in both germ cell subtypes, showing their production is regulated throughout germline differentiation (Figure 4.11). An interesting observation is that, in many instances, the RNA level of a candidate is high in both spermatocytes and spermatids. If these candidate proteins are also present at high levels in both cell types, then the low degree of overlap in binding

partners identified for importin α2 and α4 in these two cell types is a clear indication of regulated binding in different cellular contexts. The results of the GEO profiles search in combination with previous analyses can be a useful guide for selecting candidates for further validation and characterization. For instance, Smarca4 with well-established roles in chromatin remodelling (Roux-Rouquie et al., 1999), was identified as an importin α2 binding candidate from the spermatocyte lysate. The GEO profile of *Smarca4* indicates that its transcript level is highest in spermatocytes. Furthermore, the result of cNLS Mapper analysis of Smarca4 protein sequence identified a putative monopartite cNLS with the score of 14 and a bipartite cNLS with the score of 9.7, while the nucleus is the most probable site of localization of this protein based on PSORT II analysis (Table 4.2). Thus, Smarca4 is most likely to be an import cargo for importin α2, and this strategy could be employed to identify candidates that are probable import cargoes for each importin α. A feasible way of validating such a list would be immunohistochemical detection of candidates in testis sections comparing wild type and an importin α (α2 and α4) knockout mouse, with the hypothesis being a shift in localization from predominantly nuclear to cytoplasmic compartment. The absence of a change would reveal the potential for functional redundancy between importin α family members, particularly if appropriate nuclear localization of the candidate occurred in the absence of the predicted or known importin α carrier.

In summary, the result of proteomic analyses of importin α binding partners showed that importin αs bind different proteins in various cellular contexts, indicating that they take on different cellular roles through these selective interactions. This outcome, combined with the observation of differential expression of importin αs in purified germ cells, is strong evidence of distinct roles played by importin α family members during spermatogenesis.

Figure 6.2 Summary of bioinformatics analyses on importin α binding candidate lists

The schematics depict the result of bioinformatics analyses on the importin α2 and importin α4 binding partner cohorts in pachytene spermatocytes (top) and round spermatids (bottom). These diagrams are not a comprehensive summary of the analysis presented in Figure 4.10, rather they represent the two most enriched Biological Processes terms for each cohort of candidates. Table 6.1 lists these terms for each importin α in both spermatocytes and spermatids. RBP: RNA binding protein, TF: Transcription Factor, DBP: DNA Binding Protein, CRF: Chromatin Remodelling Factor.

	Spermatocytes	**Spermatids**
Importin α2	1. Regulation of mRNA stability 2. Embryonic hindlimb morphogenesis	1. Nucleosome organization 2. Chromatin assembly
Importin α4	1. Mitochondrial organization 2. Protein import	1. Chromosome condensation 2. Nucleus organization

Table 6.1 The two most enriched terms within the Biological Process category for importins α2 and α4 candidate binding partners in spermatocytes and spermatids, as identified in Chapter 4.

Pachytene spermatocyte

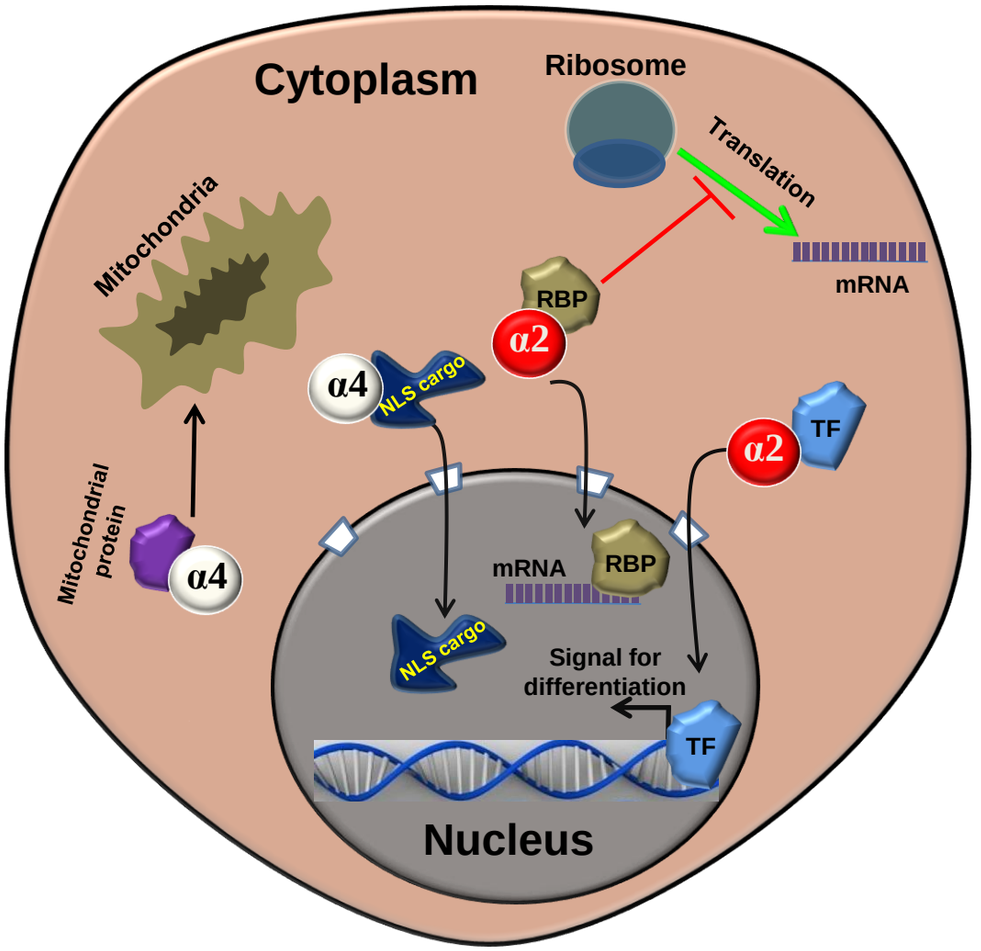

Round spermatid

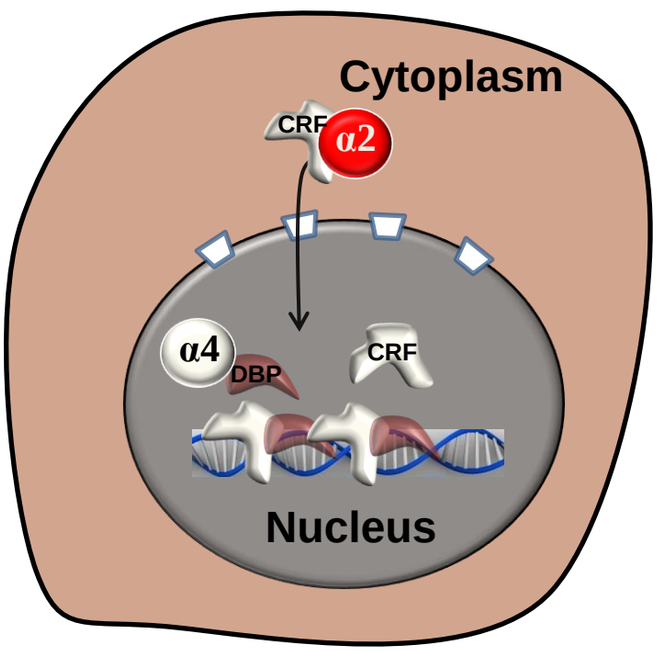

6.4 The common candidates identified in both pull-down and mass spectrometry experiments

As mentioned described in Section 4.11, four importin α binding candidates were identified in two independent pull-down and mass spectrometry experiments. These four candidates constitute 20% of the total candidates (i.e. 20) that were identified in the first experiments. This is an encouraging indication of outcome reproducibility. Several attributes of these candidates are presented in Table 6.2. There is an overall consistency regarding the importin α and cell types from which these putative interactions were reported. In this section a brief overview of the functional attributes of these candidates is given with the aim of elucidating a potential link between each candidate and importin α in the context of spermatogenesis.

Candidate	First experiment	Second experiment	cNLS score	Subcellular localization
Mylk	α2-ED,mutant, spermatids	α2, spermatids	5.6	Cytoplasm
Npm1	α2 and α3, spermatocytes	α2 and α4, spermatocytes α2, spermatids	9.6	Nucleus
Trim 28	α2, spermatocytes	α2, spermatocytes and spermatids	6.1	Nucleus
Hnrnpa2b1	α2, spermatocytes	α2-ED mutant, spermatids	6	Nucleus

Table 6.2 Candidates identified in two independent analyses as importin α binding partners. Importins and cell types from which the interactions were identified are indicated. cNLS score was determined by cNLS Mapper and subcellular localization is based on available literature (see text below).

6.4.1 Myosin light chain kinase (Mylk)

Myosin light chain kinase (Mylk) is found as long (220 kDa) and short (130 kDa; lacks the N-terminal 922 amino acids) isoforms arising from alternative promoter activity (Martin Watterson et al., 1995). The long Mylk isoform has restricted tissue expression, with the highest protein level detectable in lung, and none detectable in testis, colon and heart. The short isoform (130 kDa), however, is ubiquitously expressed, with testis having intermediate protein levels amongst 15 tissues examined by Western blotting (Blue et al., 2002). It is of note that the putative cNLS of Mylk

(Table 6.2) occurs in both isoforms. The best understood function of Mylk is phosphorylation of the regulatory light chain (RLC) of myosin II, which induces cell contraction leading to cellular responses such as cell migration, division and adhesion (Kamm and Stull, 2001). Mylk expression is regulated during development and is perturbed in several diseases (Herring et al., 2006). Examples of these includes fluctuations in level of both protein and mRNA during chicken embryogenesis (Fisher and Ikebe, 1995), and up-regulation of Mylk during epithelial barrier dysfunction of intestine (Wang et al., 2005a). Despite having the same substrate specificity (i.e. phosphorylation of myosin II RLC), the two Mylk isoforms are differentially localized within cells. The long isoform is known to colocalize with actin and stress bundles in REF-52 and HeLa cells, respectively, while the short isoform (detectable in testis) has been shown to have mainly a diffuse cytoplasmic localization with a small pool detectable in cell periphery (Blue et al., 2002; Poperechnaya et al., 2000).

Although as yet untested, an interesting germ cell related-role that could be envisaged for Mylk is in regulation of germ cell movement within the seminiferous tubules. As briefly described in Section 1.2.4, germ cell movement from the basal to the adluminal compartment and their release into the lumen of the seminiferous tubules is facilitated by constant cell-cell junction (e.g. tight junctions) restructuring between Sertoli and germ cells (Yan et al., 2007). Zonula occludens 1 (ZO-1) is a component of the blood-testis barrier (Wong et al., 2005) which exists in both non-exchangeable and exchangeable tight junction pools in addition to in cytosolic exchangeable pool (Shen et al., 2008). Yu and colleagues showed that treatment of confluent Caco-2 cells (which contain tight junctions) with peptide inhibitor of Mylk, leads to stabilization of ZO-1 in the tight junctions, by reducing the fraction which exists in the exchangeable tight junction pool (Yu et al., 2010a). Thus, Mylk may exert a significant effect on regulation of tight junction dynamics during germ cell passage from the base of seminiferous tubules towards the lumen. Identification of Mylk as an importin α binding candidate raises the intriguing possibility of a novel trafficking role served by this family of proteins. Based on the localization and cellular role of Mylk, this trafficking is not likely to relate to canonical nuclear import; rather it seems to be concerned with carrying a cargo towards the cell periphery. This proposition is supported by several discoveries in recent years which have revealed that importin β2

protein is the transport factor for human retinitis pigmentosa 2 (Hurd et al., 2011) and kinesin-like protein KIF17 (Dishinger et al., 2010) from the cytoplasm into the ciliary compartment through interactions with NLS-like motifs in both cargoes. Furthermore this trafficking has been shown to occur across a barrier known as ciliary pore complex which is composed of nucleoporins, and dependent on a Ran gradient identical to that which exists across the nuclear pore complex (Kee et al., 2012). Thus importin αs may also serve as cargo receptors for transport of proteins towards the cell periphery and mediate association of cargo with importin β proteins in contexts previously not recognized.

6.4.2 Nucleophosmin (NPM1)

Nucleophosmin (Npm1), also known as B23, numatrin and NO38, belongs to nucleoplasmin family of nuclear chaperons (Frehlick et al., 2007). Npm1 is an abundant phosphoprotein that constantly shuttles between nucleus and cytoplasm (Borer et al., 1989; Brady et al., 2004), an activity mediated by a putative NLS (see below and Table 6.2) and a CREM1-dependent nuclear export signal (NES) (Wang et al., 2005b). Many cellular processes have been attributed to nucleophosmin function including cell division, chromosome condensation and transcriptional regulation (Okuwaki, 2008), while the best understood roles of Npm1are regulation of centrosome duplication (Okuda, 2002; Wang et al., 2005b) and ribosomal RNA biogenesis and transport (Maggi et al., 2008; Yu et al., 2006). Knockout of *Npm1* leads to embryonic lethality between day 11.5 and 16.5 of gestation in mouse (Grisendi et al., 2005), and elevated levels of its mRNA and protein have been detected in a wide range of tumors (Lim and Wang, 2006; Yung, 2007). Both mRNA and protein of Npm1have been detected in purified germ cell fractions including pachytene spermatocytes and round spermatids from adult mouse testis, while immunoelectron microscopy has revealed the nuclear/nucleolar localization of Npm1 in spermatogonia, leptotene and pachytene spermatocytes and early steps spermatids (Biggiogera et al., 1991).

Npm1 possesses a partially characterized bipartite cNLS. This cNLS correspond to residues 141 to 157 of rat Npm1 protein (^{141}KRSAPGGGSKVPQKKVK^{157}), the

inactivation of which through mutations prevents nuclear accumulation of Npm1(Wang et al., 2005b). Of note, cNLS Mapper analysis in this thesis study has identified the same core sequence as the putative cNLS of Npm1with an extra single amino acid residue at the N-terminus and two amino acid residues at the C-terminus (see the CD attached to this thesis) with the score of 9.6 (Table 6.2). Although the functionality of importin α in directing the nuclear accumulation of Npm1 has not yet been directly tested, we propose that this sequence constitutes a bona fide cNLS in the Npm1protein.

An interesting aspect of Npm1 cellular roles which has remained relatively uncharacterized is its association with other cNLSs, including that of T-ag, HIV-Rev protein and protein p120 (Szebeni et al., 1995; Valdez et al., 1994). This interaction has been shown to stimulate the nuclear accumulation of the target proteins by 2-fold, and if Npm1 is phosphorylated the nuclear import of the target protein is increased by 4-fold. Additionally, this stimulatory effect seems to be exerted on the classical import pathway, since incubation of the reaction with an antibody to importin β1 (p97 in that study) eliminates the Npm1 effect on nuclear import (Szebeni et al., 1997). Thus Npm1 appears to be an interacting partner of importin α (either direct or as part of a complex) with potential regulatory roles in rate of nuclear import of other cargoes.

6.4.3 Tripartite motif containing 28 (Trim28)

Tripartite motif containing 28 (Trim 28), also widely known as KAP-1 and TIF1β, was first isolated in a yeast two-hybrid screen as an interacting partner of KRAB (Kruppel-associated box) domain from human zinc finger factor KOX1 (Moosmann et al., 1996). The first attributed function of Trim28 is repression of transcription (Friedman et al., 1996; Kim et al., 1996; Moosmann et al., 1996) and to date this function remains its best understood role (Iyengar and Farnham, 2011). A well-studied aspect of Trim28 cellular localization is its subnuclear redistribution in response to differentiation cues. When treated with retinoic acid, F9 embryonal carcinoma cells differentiate into primitive endoderm-like cells (Strickland and Mahdavi, 1978). Concordant with this differentiation, Trim28 relocates from being

diffusely distributed within the nucleoplasm to heterochromatic foci (Cammas et al., 2004; Cammas et al., 2007; Cammas et al., 2002). This relocation is shown to bring about chromatin modifications including reduced histone acetylation, in addition to decreased RNA polymerase II recruitment to chromatin, which collectively culminate in gene silencing (Sripathy et al., 2006). Alterations in Trim28 expression lead to a range of phenotypes. Homozygous mice deficient in Trim28 ($Trim28^{-/-}$) are arrested at embryonic day 5.5, demonstrating the importance of this protein function during early embryonic development (Cammas et al., 2000). Tissue-specific deletion of Trim28 in the adult forebrain causes behavioural phenotypes including increased stress level and loss of memory (Jakobsson et al., 2008), while germ cell-specific deletion of Trim28 leads to testicular degeneration (discussed below);(Weber et al., 2002). Furthermore, higher levels of the *Trim28* transcript have been detected in gastric cancer tissues compared to normal tissues (Yokoe et al., 2010).

Northern blot analysis has shown that the *Trim28* transcript is widely expressed, with adult testis having relatively higher levels compared to seven other examined tissues (Kim et al., 1996). Immunohistochemical detection in adult mouse testis revealed Trim28 protein in a subset of testicular cells, including Sertoli cells, late pachytene spermatocytes and steps 1 to 9 spermatids, in all of which Trim28 was associated with heterochromatin. In contrast, spermatogonia, early stage spermatocytes and late stage spermatids were devoid of detectable Trim28 (Weber et al., 2002). Germ cell-specific deletion of Trim28 in adult mice caused germ cell depletion and vacuole formation in half of the seminiferous tubules; interestingly many of these tubule were devoid of spermatogonia which do not contain detectable Trim28 (see above) indicating that Trim28 may facilitate paracrine roles in seminiferous tubules (Weber et al., 2002).

The mechanism of Trim28 nuclear accumulation has not yet been examined. Given its well-established nuclear localization and possession of a putative cNLS (Table 6.2), it is feasible that this protein could be a canonical import cargo for importin αs in germ cells. On the other hand, bioinformatics analyses identified chromosomal dynamics as biological processes that are strongly affected by importin α binding candidates, especially in spermatids (Section 4.9). Thus nuclear importin α proteins could be part of gene regulatory complexes with proteins such as Trim28.

6.4.4 Heterogeneous nuclear ribonucleoprotein A2/B1 (hnRNP A2/B1)

Heterogeneous nuclear ribonucleoprotein A2/B1 (hnRNP A2/B1) belongs to a large family of proteins, hnRNP, first discovered based on their RNA binding capacities (Dreyfuss et al., 1993). Currently, this protein family is known to have roles in cellular processes such as DNA repair and chromatin remodelling, regulation of RNA metabolism and cellular proliferation and tumorigenesis (Carpenter et al., 2006). The two hnRNP A2/B1 isoforms (i.e. hnRNP A2 and B1), are formed through alternative splicing of the same precursor RNA with the B1 isoform having 12 more amino acids in the N-terminus than A2 isoform (Kozu et al., 1995). At the protein level hnRNP A2/B1 is known to be present in a wide range of tissues including testis, with few examples of selective isoform detection in some tissues; for example, in heart, B1, but not the A2 isoform, is detectable, while in brain, A2 but not the B1 isoform is detectable by Western blotting (Kamma et al., 1999). Immunohistochemistry in rat testes sections has revealed that hnRNP A2/B1 is most readily detected in the spermatocytes nucleus, while Western blot and Northern blot analyses have identified a novel testis-specific splice variant of the protein (hnRNP $B0^{a/b}$) in which exon 9 is spliced out and the encoded protein lacks 40 amino acids in a central glycine rich region (Kamma et al., 1999). Down-regulation of hnRNP A2/B1through RNAi experiments led to reduced cellular proliferation in HaCaT and Colo16 (immortalized keratinocyte cells) cell lines (He et al., 2005), indicating the general importance of this protein in cell division. An increase in hnRNP A2/B1 levels has been observed in a wide range of carcinoma cells. These includes the up-regulation of the *hnRNP A2/B1* transcript in pancreatic tumor cell lines (HPAF-11 and SU 88.86) compared to the normal pancreatic cell line (HP-8);(Yan-Sanders et al., 2002), over-expression of hnRNP A2/B1 protein as detected by immunohistochemistry in lung bronchial lavage tumors (Fielding et al., 1999), and Western blot detection of up-regulated hnRNP A2/B1 in gastric cancer tissue (Lee et al., 2005). Cui and co-workers reported that, in addition to protein level up-regulation, there is a shift in hnRNP A2/B1 protein localization from being strictly nuclear in poorly differentiated hepatocellular carcinoma (HCC) to being progressively cytoplasmic in moderately and highly differentiated HCC (Cui et al., 2010). Perhaps the most interesting attribute of hnRNP A2/B1 pertinent to germ cell biology is its association with telomeres. Similar to

cancer cells, germ cells have high telomerase activity (Liu and Li, 2010). hnRNP A2/B1 has been experimentally shown to interact with telomeric single stranded DNA (ssDNA) *in vitro* (Kamma et al., 2001) and to colocalize with components of telomeric DNA such as promyelocytic leukemia protein (PML) and telomere repeat binding factor 2 (TRF2) *in vivo* (Moran-Jones et al., 2005). Thus a protein with potentially unique roles in germ cell maturation which is known to localize in the nucleus and also possesses a putative cNLS (Table 6.2) could be a valuable tool for validation of this study outcome. This could be tested by colocalization of hnRNP A2/B1 with importin α family members *in vivo*, and validation of interaction between importin α and hnRNP A2/B1 through further *in vitro* assays (e.g immunoprecipitation, and *in vitro* solution binding assay).

6.5 Association of Mtmr4 with importin α highlights the contribution of importin α proteins to a wide range of functions

Chapter 5 of this thesis provides the results of several experiments that were designed to elucidate the nature of the association between importin α4 and Mtmr4. This relationship provides an intriguing example of an interaction between a nuclear import receptor and a known cytoplasmic protein, and it could provide a new example of a non-import function for importin α. By the same token, Mtmr4 may be a newly defined nuclear import cargo for importin α in germ cells.

Analysis of *Mtmr4* mRNA expression by *in situ* hybridization revealed that the transcript is most readily detected in pachytene spermatocytes, the same cell type in which the interaction with importin α4 was identified. In addition to an expected mRNA band of 5.7 kb, a ~4 kb band was consistently detected in adult rat testis total RNA by Northern blot analysis. Splice variants are of significant interest in multi-domain proteins. In case of Mtmr4, for instance, if this splice variant translates into an isoform that lacks a lipid binding domain or an endosomal targeting motif, then other signal sequences may have a higher chance of exerting an effect. A small portion of exogenous Mtmr4 has been found in the nucleus through Western blot detection of the overexpressed Mtmr4 after nucleocytoplasmic fractionation of transfected human

HEK 293 cells (Zhao et al., 2001). This nuclear entry may have been subsequent to saturation of Mtmr4 cytoplasmic docking sites in an overexpression situation. However, this observation indicates that Mtmr4 has the potential to enter the nucleus under certain conditions. Could spermatocytes or other germ cells provide the conditions permissible for the interaction of Mtmr4 and importin α required for nuclear entry? This proposition is feasible since the Mtmr4 protein contains a strong putative cNLS (i.e. score of 6; Section 4.9). The *in vitro* binding experiments in this thesis indicated that the Mtmr4 putative cNLS can bind both importin α2 and α4 recombinant proteins with specificity (Figure 5.7). This binding however, does not appear to be strong compared to that of the T-ag-NLS that was used as the positive control, although binding affinity was not directly measured. Two important facts have to be considered in interpreting this observation. Firstly, the activity of a cNLS is modulated within the cellular context (Section 1.1.8.1) and that of the host protein (Friedrich et al., 2006). Thus, the binding of a putative cNLS in isolation and *in vitro* may not necessarily represent the *in vivo* capacity of the cNLS to bind an importin α protein. Secondly, there is a direct correlation between the binding strength of a cNLS to importin α and its rate of nuclear import (Section 1.1.3.2). Thus, if the Mtmr4 putative cNLS has low binding affinity for importin α, then Mtmr4 may not be an import cargo, and the interaction between the two may serve another purpose.

The pull-down of endogenous Mtmr4 with importin α recombinant proteins produced intriguing results, in that the pattern of Mtmr4 pull-down with full length and mutant importin αs suggested that Mtmr4 is part of an import complex with importin αs. The Western blot signal corresponding to Mtmr4 was stronger in the pull-down product of GST-importin α2 ΔIBB, and weaker in GST-importin α2-ED mutant, compared to wild type GST-importin α2 and α4. To test this observation further, several biochemical approaches could be applied. If Mtmr4 binds in the NLS binding groove of importin α and is indeed part of an import complex, then addition of an exogenous NLS (e.g. T-ag-NLS-GFP) should compete with Mtmr4-NLS in binding to importin α and its ΔIBB truncated isoform. Recapitulation of the nuclear environment by incubation of the pull-down reaction with excess Ran-GTP, should also severely

impair the binding of Mtmr4 with importin αs if the interaction occurs in the NLS binding groove of importins.

Resource constraints prevented further characterization of Mtmr4 expression in the testis and scrutiny of its interaction with importin α in the present study. However the data obtained in this study points towards a bona fide interaction and provide several leads from which to pursue the association of importin α and Mtmr4. It is of prime importance to delineate the localization of Mtmr4 in germ cells, in particular within pachytene spermatocytes in which the interaction with importin α4 was identified. Immunolocalization on purified cells, Western blot detection after fractionation of cells into nuclear and cytoplasmic compartments, and immunohistochemical detection on murine testis section could all be employed for verifying the localization of Mtmr4. Unfortunately the currently available antibodies do not appear to be appropriate for recognition of Mtmr4 in fixed cells or tissues. If Mtmr4 or a fraction of it is found in the nucleus, the experiments described above could be performed on an importin α4 knock-out mouse testis or using cell lines in which importin α family members are knocked-down, with the aim of discerning a difference in the subcellular localization of Mtmr4.

Another intriguing possibility is that importin α could co-localize with Mtmr4 on endosomal membranes. Importin α proteins are described as being predominantly localized in the cytoplasm and nucleus under most physiological conditions. Despite being devoid of any identifiable membrane binding domains, a fraction of importin αs have been shown to localize to, and associate with internal cellular membranes, and participate in formation of the nuclear envelope *in vitro* (Hachet et al., 2004; Section 1.1.7.2). In these circumstances, importin αs may have membrane anchoring partners. An interesting observation in the study of Hachet and colleagues was that importin α association with the extracted intracellular membranes of the *X. laevis* oocyte was regulated by phosphorylation and sensitive to the presence of NLS-containing proteins. Their work showed that importin α can be released from the membranes by incubation of the membranes with casein kinase II (CKII) and this occurs only in presence of exogenous NLS-containing proteins (i.e. T-ag-NLS-BSA). Mtmr4 possesses a protein phosphatase activity which can counteract a kinase function in

addition to the putative cNLS (Section 5.10) that could compete with an exogenous NLS. Thus Mtmr4 may sequester importin α molecules on membranes and regulate their activities in membrane formation and fusion events. This hypothesis is supported by another previously described molecular mechanism in which importin α takes part. As described in Section 1.1.7.2, binding of importin α to TPX2 through an NLS-like motif contributes to regulation of microtubule formation (Gruss et al., 2001; Section 1.1.7.2). It has recently been shown that the NLS-like motif of TPX2 binds to importin α in an "atypical" manner (Giesecke and Stewart, 2010). Despite resembling a monopartite sequence, the TPX2 NLS binds preferentially to the minor NLS groove of importin α, while monopartite cNLSs normally occupy the major binding groove (Fontes et al., 2000; Leung et al., 2003). Thus it is important to uncover the specific nature of how and where the putative NLS in Mtmr4 binds to importin α in order to fully understand the association between these two proteins.

6.6 Summary of thesis outcome and future directions; applying new knowledge regarding importin α to understanding spermatogenesis

The experiments in this thesis were designed to test the hypothesis that importin αs have distinct roles in mammalian spermatogenesis through regulated expression and selective cargo binding in different germ cells. Overall, the results obtained have uncovered a novel case of differential importin protein levels in spermatogenesis and provide evidence that individual importin α family members serve distinct roles that are unique to each germ cell subtype. Importin α2 and importin α3 are present at distinctly higher levels in spermatocytes than in spermatids of the adult rat testis. The protein levels of importin α4 and importin β1 on the other hand, remain constant between these two testicular cell types. In the light of known subcellular localization of several importins in testicular cells, the perturbed synthesis level or mislocalization of these proteins could become a diagnostic tool for some cases of infertility. Both of these phenomena have been reported in several types of carcinoma, including breast, lung, bladder and prostate cancer cells and in a case of diabetics (Christiansen and Dyrskjot, 2013; reviewed in Miyamoto et al., 2012b)

The pull-down of importin α2 and α4 from spermatocytes and spermatids followed by mass spectrometric analysis have identified numerous candidate binding partners for each. The majority of these candidates were identified specifically by a given importin α and from a given cell type. Thus it would be of significant interest to conduct further comparative proteomic analyses to define additional comprehensive α-importomes in different developmental systems or disease conditions. The cNLS Mapper analysis on the candidates identified many novel putative cNLSs; this is an indication of the enormity in repertoire of nuclear localization signals. As briefly mentioned in the previous section, the outcome of this analysis could lead to a refinement of the cNLS consensus and facilitate their computational discovery. Thus another attractive avenue for further research would be refinement of the cNLS consensus based on selective importin α binding. An enhanced capacity to discern importin α specific cNLSs, combined with the knowledge of their differential expression, could facilitate the creation of a repository for binding candidates of each importin α in different biological contexts through bioinformatics approaches. Molecular pathway analysis indicated that the binding partners of different importin αs from different cell types take part in distinct molecular processes, consistent with the hypothesis that importins serve many developmentally regulated roles in spermatogenesis.

The work presented in this thesis has also provided evidence for a bona fide association between importin α proteins and Mtmr4, identified recently as a binding candidate of importin α4 in spermatocytes (Miyamoto et al., 2013). Although it is possible that Mtmr4 is a novel nuclear cargo for importin α, the intriguing prospect that this interaction contributes to some other functions cannot be ignored. In addition to the previously described role of importin α in nuclear envelope formation both *in vitro* and *in vivo* (Section 1.1.7.2), there have been recent findings that link importin α proteins or some of their putative interacting partners to membrane trafficking and fusion events. These include the specific interaction of bovine and murine importin α6 with a histone variant (SubH2Bv) which is localized on the acrosome during spermiogenesis (Tran et al., 2012). The interaction of SubH2Bv and importin α6 occurs through a bipartite NLS motif that is sufficient for nuclear accumulation of

overexpressed SubH2Bv in somatic cells but does not result in nuclear entry of SubH2Bv in germ cells. By immunolocalization in murine and bovine testes sections, Tran and co-workers showed that importin α6 is localized on the outer surface of acrosomal vesicles in early steps of spermiogenesis, but progressively moves to the region between the inner acrosomal membranes and nuclear envelope. As a result, these authors have proposed a role for importin α family members in directing the trafficking of acrosomal vesicles from the Golgi to the nuclear envelope during spermiogenesis (Tran et al., 2012).

Members of the poorly characterized Dpy19l protein family provide further evidence of membrane-related functions of importin α family members. One of the candidates identified from spermatid lysates in this study was Dpy19l1. Interestingly, Dpy19l1 was identified only by the importin α2-ED mutant, and it contains a putative cNLS with the score of 4.9 (i.e. moderate). In a recent study, a Dpy19l1 family member, Dpy19l2 (with 55% identity at amino acid sequence level), which contains a putative cNLS with the low to moderate score of 4.3, was demonstrated to be essential for proper acrosomal formation during spermiogenesis via its involvement in anchoring of the acrosome to the nuclear envelope (Pierre et al., 2012). These two examples provide strong evidence that importin α family members are critically involved in cellular homeostasis through their functions in membrane or organelle trafficking in developing sperm and in other cell types.

These observations highlight the essential contributions of importin α proteins to male fertility. Many molecular defects during spermatogenesis lead to infertility in men, and some of the most prominent malfunctions are of processes that regulate post-meiotic germ cell maturation. These include DNA packaging and acrosome formation (Yan, 2009). Given the strong possibility that importin αs are involved in regulation of both of these processes, it is important to uncover the specific roles that importin α family members may play during acrosome biogenesis and nuclear remodelling. Detailed examination of acrosomal and nuclear morphology in different steps of spermatid maturation in importin α knockout animals could provide clues to whether or not there are any phenotypes caused by absence of importin αs. Another cause of infertility relates to abnormal development and functioning of sperm midpiece and tail,

which in some instances is caused by mitochondrial malfunction (Chemes and Alvarez Sedo, 2012). Based on the unpublished data from our laboratory which clearly demonstrates the presence of importin α proteins in these regions of spermatozoa, and the enrichment of the "mitochondrial organization" term by importin α binding candidates through bioinformatics analysis, it is logical to propose that importin α proteins serve roles that culminate in a functional sperm midpiece and a motile tail.

Specific knowledge of the roles that importin α family members play in these processes may ultimately lead to therapeutic approaches to correct or compensate for the lack of these functions in infertile men. For example, if some causes of defective acrosome formation are consequences of impaired vesicle trafficking from Golgi to the nuclear surface as a result of perturbation in importin α levels, then cell-type specific, transgenic overexpression or knock-down of importin α may provide a solution. Furthermore, an area of immense interest which benefits from reproductive biology research is advent of contraceptives. In this case, development of a drug or a therapeutic approach that strictly targets a post-meiotic aspect of sperm development could be used as a safe and reversible male contraceptive. Thus, a better understanding of the roles of importin α family of proteins in developmental systems could facilitate development of novel and effective cures and therapeutics.

Overall, the findings of this thesis have shed light on potential new functions of importin α family of proteins in mammalian spermatogenesis and created new research avenues for further exciting discoveries.

Bibliography

BIBLIOGRAPHY

Adam, E.J., and Adam, S.A. (1994). Identification of cytosolic factors required for nuclear location sequence-mediated binding to the nuclear envelope. J Cell Biol *125*, 547-555.

Adam, S.A., Marr, R.S., and Gerace, L. (1990). Nuclear protein import in permeabilized mammalian cells requires soluble cytoplasmic factors. J Cell Biol *111*, 807-816.

Akey, C., and Radermacher, M. (1993). Architecture of the Xenopus nuclear pore complex revealed by three-dimensional cryo-electron microscopy. The Journal of Cell Biology *122*, 1-19.

Alber, F., Dokudovskaya, S., Veenhoff, L.M., Zhang, W., Kipper, J., Devos, D., Suprapto, A., Karni-Schmidt, O., Williams, R., Chait, B.T., *et al.* (2007). Determining the architectures of macromolecular assemblies. Nature *450*, 683-694.

Alberts, B., Johnson, A., Lewis, J., Raff, M., Roberts, K., and Walter, P. (2002). Molecular biology of the cell. *Fourth edition*.

Alvisi, G., Jans, D.A., Guo, J., Pinna, L.A., and Ripalti, A. (2005). A Protein Kinase CK2 Site Flanking the Nuclear Targeting Signal Enhances Nuclear Transport of Human Cytomegalovirus ppUL44. Traffic *6*, 1002-1013.

Andrade, R., Alonso, R., Peña, R., Arlucea, J., and Aréchaga, J. (2003). Localization of importin a (Rch1) at the plasma membrane and subcellular redistribution during lymphocyte activation. Chromosoma *112*, 87-95.

Angeline, M., Merle, E., and Moroianu, J. (2003). The E7 oncoprotein of high-risk human papillomavirus type 16 enters the nucleus via a nonclassical Ran-dependent pathway. Virology *317*, 13-23.

Arnold, M., Nath, A., Hauber, J., and Kehlenbach, R.H. (2006). Multiple Importins Function as Nuclear Transport Receptors for the Rev Protein of Human Immunodeficiency Virus Type 1. Journal of Biological Chemistry *281*, 20883-20890.

Ascano, M., Hafner, M., Cekan, P., Gerstberger, S., and Tuschl, T. (2012). Identification of RNA–protein interaction networks using PAR-CLIP. Wiley Interdisciplinary Reviews: RNA *3*, 159-177.

Askjaer, P., Galy, V., Hannak, E., and Mattaj, I.W. (2002). Ran GTPase Cycle and Importins alpha and beta Are Essential for Spindle Formation and Nuclear Envelope Assembly in Living Caenorhabditis elegans Embryos. Mol Biol Cell *13*, 4355-4370.

Azzedine, H., Bolino, A., Taieb, T., Birouk, N., Di Duca, M., Bouhouche, A., Benamou, S., Mrabet, A., Hammadouche, T., Chkili, T., *et al.* (2003). Mutations in MTMR13, a New Pseudophosphatase Homologue of MTMR2 and Sbf1, in Two Families with an Autosomal Recessive Demyelinating Form of Charcot-Marie-Tooth Disease Associated with Early-Onset Glaucoma. The American Journal of Human Genetics *72*, 1141-1153.

Baba, T., Niida, Y., Michikawa, Y., Kashiwabara, S.-i., Kodaira, K., Takenaka, M., Kohno, N., Gerton, L., George., and Arai, Y. (1994). An Acrosomal Protein, sp32 in Mammalian Sperm Is a Binding Protein Specific for Two Proacrosins and an Acrosin intermediate. The Journal of Biological Chemistry *269*, 10133-10140.

Baker, M.A., Hetherington, L., Reeves, G., Müller, J., and Aitken, R.J. (2008a). The rat sperm proteome characterized via IPG strip prefractionation and LC-MS/MS identification. PROTEOMICS *8*, 2312-2321.

Baker, M.A., Hetherington, L., Reeves, G.M., and Aitken, R.J. (2008b). The mouse sperm proteome characterized via IPG strip prefractionation and LC-MS/MS identification. PROTEOMICS *8*, 1720-1730.

Baudat, F., Manova, K., Yuen, J.P., Jasin, M., and Keeney, S. (2000). Chromosome Synapsis Defects and Sexually Dimorphic Meiotic Progression in Mice Lacking Spo11. Molecular Cell *6*, 989-998.

Beck, M., Forster, F., Ecke, M., Plitzko, J.M., Melchior, F., Gerisch, G., Baumeister, W., and Medalia, O. (2004). Nuclear pore complex structure and dynamics revealed by cryoelectron tomography. Science *306*, 1387-1390.

Beg, A.A., Finco, T.S., Nantermet, P.V., and Baldwin, A.S., Jr (1993). Tumor necrosis factor and interleukin-1 lead to phosphorylation and loss of I kappa B alpha: a mechanism for NF-kappa B activation. Mol Cell Biol *13*, 3301-3310.

Beg, A.A., Ruben, S.M., Scheinman, R.I., Haskill, S., Rosen, C.A., and Baldwin, A.S. (1992). I kappa B interacts with the nuclear localization sequences of the subunits of NF-kappa B: a mechanism for cytoplasmic retention. Genes & Development *6*, 1899-1913.

Behrens, J. (2000). Control of β-Catenin Signaling in Tumor Development. Annals of the New York Academy of Sciences *910*, 21-35.

Ben-Efraim, I., and Gerace, L. (2001). Gradient of Increasing Affinity of Importin beta for Nucleoporins along the Pathway of Nuclear Import. The Journal of Cell Biology *152*, 411-418.

Benton, L., Shan, L.-X., and Hardy, M.P. (1995). Differentiation of adult Leydig cells. The Journal of Steroid Biochemistry and Molecular Biology *53*, 61-68.

Bian, X.-L., Rosas-Acosta, G., Wu, Y.-C., and Wilson, V.G. (2007). Nuclear Import of Bovine Papillomavirus Type 1 E1 Protein Is Mediated by Multiple Alpha Importins and Is Negatively Regulated by Phosphorylation near a Nuclear Localization Signal. J Virol *81*, 2899-2908.

Bian, X.-L., and Wilson, V.G. (2010). Common importin alpha specificity for papillomavirus E2 proteins. Virus Research *150*, 135-137.

Biggiogera, M., Kaufmann, S.H., Shaper, J.H., Gas, N., Amalric, F., and Fakan, S. (1991). Distribution of nucleolar proteins B23 and nucleolin during mouse spermatogenesis. Chromosoma *100*, 162-172.

Bischoff, F.R., Klebe, C., Kretschmer, J., Wittinghofer, A., and Ponstingl, H. (1994). RanGAP1 induces GTPase activity of nuclear Ras-related Ran. Proc Natl Acad Sci U S A *91*, 2587-2591.

Bischoff, F.R., Krebber, H., Smirnova, E., Dong, W., and Ponstingl, H. (1995). Co-activation of RanGTPase and inhibition of GTP dissociation by Ran-GTP binding protein RanBP1. EMBO J *14*, 705-715.

Bischoff, R., F, and Ponstingl, H. (1991). Mitotic regulator protein RCC1 is complexed with a nuclear ras-related polypeptide. Proceedings of the National Academy of Sciences *88*, 10830-10834.

Blue, E.K., Goeckeler, Z.M., Jin, Y., Hou, L., Dixon, S.A., Herring, B.P., Wysolmerski, R.B., and Gallagher, P.J. (2002). 220- and 130-kDa MLCKs have distinct tissue distributions and intracellular localization patterns. American Journal of Physiology - Cell Physiology *282*, C451-C460.

Bolino, A., Bolis, A., Previtali, S.C., Dina, G., Bussini, S., Dati, G., Amadio, S., Del Carro, U., Mruk, D.D., Feltri, M.L., *et al.* (2004). Disruption of Mtmr2 produces CMT4B1-like neuropathy with myelin outfolding and impaired spermatogenesis. The Journal of Cell Biology *167*, 711-721.

Bolino, A., Muglia, M., Conforti, F.L., LeGuern, E., Salih, M.A.M., Georgiou, D.-M., Christodoulou, K., Hausmanowa-Petrusewicz, I., Mandich, P., Schenone, A., *et al.* (2000). Charcot-Marie-Tooth type 4B is caused by mutations in the gene encoding myotubularin-related protein-2. Nat Genet *25*, 17-19.

Bonner, W.M. (1975). Protein migration into nuclei. II. Frog oocyte nuclei accumulate a class of microinjected oocyte nuclear proteins and exclude a class of microinjected oocyte cytoplasmic proteins. J Cell Biol *64*, 431-437.

Borer, R.A., Lehner, C.F., Eppenberger, H.M., and Nigg, E.A. (1989). Major nucleolar proteins shuttle between nucleus and cytoplasm. Cell *56*, 379-390.

Bourne, H.R., Sanders, D.A., and McCormick, F. (1991). The GTPase superfamily: conserved structure and molecular mechanism. Nature *349*, 117-127.

Brady, S.N., Yu, Y., Maggi, L.B., and Weber, J.D. (2004). ARF Impedes NPM/B23 Shuttling in an Mdm2-Sensitive Tumor Suppressor Pathway. Molecular and Cellular Biology *24*, 9327-9338.

Caires, K., Broady, J., and McLean, D. (2010). Maintaining the male germline: regulation of spermatogonial stem cells. Journal of Endocrinology *205*, 133-145.

Cammas, F., Herzog, M., Lerouge, T., Chambon, P., and Losson, R. (2004). Association of the transcriptional corepressor TIF1β with heterochromatin protein 1 (HP1): an essential role for progression through differentiation. Genes & Development *18*, 2147-2160.

Cammas, F., Janoshazi, A., Lerouge, T., and Losson, R. (2007). Dynamic and selective interactions of the transcriptional corepressor TIF1β with the heterochromatin protein HP1 isotypes during cell differentiation. Differentiation *75*, 627-637.

Cammas, F., Mark, M., Dolle, P., Dierich, A., Chambon, P., and Losson, R. (2000). Mice lacking the transcriptional corepressor TIF1beta are defective in early postimplantation development. Development *127*, 2955-2963.

Cammas, F., Oulad-Abdelghani, M., Vonesch, J.-L., Huss-Garcia, Y., Chambon, P., and Losson, R. (2002). Cell differentiation induces TIF1β association with centromeric heterochromatin via an HP1 interaction. Journal of Cell Science *115*, 3439-3448.

Capelson, M., and Hetzer, M.W. (2009). The role of nuclear pores in gene regulation, development and disease. EMBO Rep *10*, 697-705.

Carpenter, B., MacKay, C., Alnabulsi, A., MacKay, M., Telfer, C., Melvin, W.T., and Murray, G.I. (2006). The roles of heterogeneous nuclear ribonucleoproteins in tumour development and progression. Biochimica et Biophysica Acta (BBA) - Reviews on Cancer *1765*, 85-100.

Casolari, J.M., Brown, C.R., Komili, S., West, J., Hieronymus, H., and Silver, P.A. (2004). Genome-Wide Localization of the Nuclear Transport Machinery Couples Transcriptional Status and Nuclear Organization. Cell *117*, 427-439.

Cassimeris, L., and Skibbens, R.V. (2003). Regulated Assembly of the Mitotic Spindle: A Perspective from Two Ends. Curr Issues Mol Biol *5*, 99-112.

Chemes, H.E., and Alvarez Sedo, C. (2012). Tales of the Tail and Sperm Head AchesChanging concepts on the prognostic significance of sperm pathologies affecting the head, neck and tail. Asian J Androl *14*, 14-23.

Chen, C.-F., Li, S., Chen, Y., Chen, P.-L., Sharp, Z.D., and Lee, W.-H. (1996). The Nuclear Localization Sequences of the BRCA1 Protein Interact with the Importin-alpha Subunit of the Nuclear Transport Signal Receptor. Journal of Biological Chemistry *271*, 32863-32868.

Chen, J., Liu, M.Y., Parish, C.R., Chong, B.H., and Khachigian, L.M. (2011). Nuclear import of early growth response-1 involves importin-7 and the novel nuclear localization signal serine-proline-serine. The International Journal of Biochemistry & Cell Biology *43*, 905-912.

Chiarini-Garcia, H., Hornick, J.R., Griswold, M.D., and Russell, L.D. (2001). Distribution of Type A Spermatogonia in the Mouse Is Not Random. Biology of Reproduction *65*, 1179-1185.

Chiarini-Garcia, H., Raymer, A., and Russell, L. (2003). Non-random distribution of spermatogonia in rats: evidence of niches in the seminiferous tubules. Reproduction *126*, 669-680.

Christiansen, A., and Dyrskjot, L. (2013). The functional role of the novel biomarker karyopherin α 2 (KPNA2) in cancer. Cancer Letters *331*, 18-23.

Chuderland, D., Konson, A., and Seger, R. (2008). Identification and Characterization of a General Nuclear Translocation Signal in Signaling Proteins. Molecular Cell *31*, 850-861.

Clague, M.J., and Lorenzo, Ó. (2005). The Myotubularin Family of Lipid Phosphatases. Traffic *6*, 1063-1069.

Coates, J.C. (2003). Armadillo repeat proteins: beyond the animal kingdom. Trends in Cell Biology *13*, 463-471.

Cobb, J., and Handel, M.A. (1998). Dynamics of meiotic prophase I during spermatogenesis: from pairing to division. Seminars in Cell & Developmental Biology *9*, 445-450.

Cokol, M., Nair, R., and Rost, B. (2000). Finding nuclear localization signals. European Molecular biology organization Journal *1*, 411-415.

Cole, F., Keeney, S., and Jasin, M. (2010). Evolutionary conservation of meiotic DSB proteins: more than just Spo11. Genes & Development *24*, 1201-1207.

Com, E., Evrard, B., Roepstorff, P., Aubry, F., and Pineau, C. (2003). New Insights into the Rat Spermatogonial Proteome. Molecular & Cellular Proteomics *2*, 248-261.

Conti, E., and Kuriyan, J. (2000). Crystallographic analysis of the specific yet versatile recognition of distinct nuclear localization signals by karyopherin alpha. Structure *8*, 329-338.

Conti, E., Uy, M., Leighton, L., Blobel, G., and Kuriyan, J. (1998). Crystallographic Analysis of the Recognition of a Nuclear Localization Signal by the Nuclear Import Factor Karyopherin alpha. Cell *94*, 193-204.

Cooke, H.J., and Saunders, P.T.K. (2002). Mouse models of male infertility. Nat Rev Genet *3*, 790-801.

Cortes, P., Ye, Z.S., and Baltimore, D. (1994). RAG-1 interacts with the repeated amino acid motif of the human homologue of the yeast protein SRP1. Proc Natl Acad Sci U S A *91*, 7633-7637.

Costoya, J.A., Hobbs, R.M., Barna, M., Gattoretti, G., Manova, K., Sukhwani, M., Orwig, K.E., Wolgemuth, D.J., and Pandolfi, P.P. (2004). Essential role of plzf in Mainteance of spermatogonial stem cells. Nature Genetics *36*, 653-659.

Cronshaw, J.M., Krutchinsky, A.N., Zhang, W., Chait, B.T., and Matunis, M.J. (2002). Proteomic analysis of the mammalian nuclear pore complex. The Journal of Cell Biology *158*, 915-927.

Cui, H., Wu, F., Sun, Y., Fan, G., and Wang, Q. (2010). Up-regulation and subcellular localization of hnRNP A2/B1 in the development of hepatocellular carcinoma. BMC Cancer *10*, 356.

Cullen, P.J. (2011). Phosphoinositides and the regulation of tubular-based endosomal sorting. Biochemical society transactions *39*, 839-850.

Dadoune, J.-P. (2003). Expression of mammalian spermatozoal nucleoproteins. Microscopy Research and Technique *61*, 56-75.

Dadoune, J.-P. (2007). New insights into male gametogenesis: what about the spermatogonial stem cell niche? FOLIA HISTOCHEMICA ET CYTOBIOLOGICA *45*, 141-147.

Daigle, N., Beaudouin, J.l., Hartnell, L., Imreh, G., Hallberg, E., Lippincott-Schwartz, J., and Ellenberg, J. (2001). Nuclear pore complexes form immobile networks and have a very low turnover in live mammalian cells. The Journal of Cell Biology *154*, 71-84.

Dang, C.V., and Lee, W.M. (1988). Identification of the human c-myc protein nuclear translocation signal. Mol Cell Biol *8*, 4048-4054.

Dang, H., Li, Z., Skolnik, E.Y., and Fares, H. (2004). Disease-related Myotubularins Function in Endocytic Traffic in Caenorhabditis elegans. Molecular Biology of the Cell *15*, 189-196.

de Kretser, D.M. (1995). Morphology and physiology of the testis. Endocronology of the male *111*, 1032-1042.

de Kretser, D.M., and Kerr, J.B. (1994). The Cytology of the Testis. The Physiology of Reproduction *Second edition*, 1177-1290.

de Rooij, D. (2001). Proliferation and differentiation of spermatogonial stem cells. Reproduction *121*, 347-354.

de Rooij, D.G. (2009). The spermatogonial stem cell niche. Microscopy Research and Technique *72*, 580-585.

de Rooij, D.G., and Russell, L.D. (2000). All you wanted to know about spermatogonia but were afraid to ask. J Androl *21*, 776-798.

DeGrasse, J.A., DuBois, K.N., Devos, D., Siegel, T.N., Sali, A., Field, M.C., Rout, M.P., and Chait, B.T. (2009). Evidence for a shared nuclear pore complex architecture that is conserved from the last common eukaryotic ancestor. Mol Cell Proteomics *8*, 2119-2130.

Dingwall, C., Robbins, J., Dilworth, S.M., Roberts, B., and Richardson, W.D. (1988). The nucleoplasmin nuclear location sequence is larger and more complex than that of SV-40 large T antigen. The Journal of Cell Biology *107*, 841-849.

Dingwall, C., Sharnick, S.V., and Laskey, R.A. (1982). A polypeptide domain that specifies migration of nucleoplasmin into the nucleus. Cell *30*, 449-458.

Dishinger, J.F., Kee, H.L., Jenkins, P.M., Fan, S., Hurd, T.W., Hammond, J.W., Truong, Y.N.-T., Margolis, B., Martens, J.R., and Verhey, K.J. (2010). Ciliary entry of the kinesin-2 motor KIF17 is regulated by importin-[beta]2 and RanGTP. Nat Cell Biol *12*, 703-710.

Doerks, T., Strauss, M., Brendel, M., and Bork, P. (2000). GRAM, a novel domain in glucosyltransferases, myotubularins and other putative membrane-associated proteins. Trends in Biochemical Sciences *25*, 483-485.

Doherty, G.J., and McMahon, H.T. (2009). Mechanisms of Endocytosis. Annual Review of Biochemistry *78*, 857-902.

Dreyfuss, G., Matunis, M.J., Pinol-Roma, S., and Burd, C.G. (1993). hnRNP Proteins and the Biogenesis of mRNA. Annual Review of Biochemistry *62*, 289-321.

Efthymiadis, A., Shao, H., Hubner, S., and Jans, D.A. (1997). Kinetic Characterization of the Human Retinoblastoma Protein Bipartite Nuclear Localization Sequence (NLS) in Vivo andin Vitro. Journal of Biological Chemistry *272*, 22134-22139.

Elad, N., Maimon, T., Frenkiel-Krispin, D., Lim, R.Y.H., and Medalia, O. (2009). Structural analysis of the nuclear pore complex by integrated approaches. Current Opinion in Structural Biology *19*, 226-232.

Fagerlund, R., Melen, K., Kinnunen, L., and Julkunen, I. (2002). Arginine/Lysine-rich Nuclear Localization Signals Mediate Interactions between Dimeric STATs and Importin alpha 5. Journal of Biological Chemistry *277*, 30072-30078.

Fagotto, F., Glück, U., and Gumbiner, B.M. (1998). Nuclear localization signal-independent and importin/karyopherin-independent nuclear import of beta-catenin. Current Biology *8*, 181-190.

Fahrenkrog, B., Hurt, E.C., Aebi, U., and Pante, N. (1998). Molecular Architecture of the Yeast Nuclear Pore Complex: Localization of Nsp1p Subcomplexes. The Journal of Cell Biology *143*, 577-588.

Fang, X.-d., Chen, T., Tran, K., and Parker, C.S. (2001). Developmental regulation of the heat shock response by nuclear transport factor karyopherin alpha 3. Development *128*, 3349-3358.

Fernandez-Martinez, J., and Rout, M.P. (2009). Nuclear pore complex biogenesis. Current Opinion in Cell Biology *21*, 603-612.

Fielding, P., Turnbull, L., Prime, W., Walshaw, M., and Field, J.K. (1999). Heterogeneous Nuclear Ribonucleoprotein A2/B1 Up-Regulation in Bronchial Lavage Specimens: A Clinical Marker of Early Lung Cancer Detection. Clinical Cancer Research *5*, 4048-4052.

Fijak, M., and Meinhardt, A. (2006). The testis in immune privilege. Immunological Reviews *213*, 66-81.

Finlay, D.R., Newmeyer, D.D., Price, T.M., and Forbes, D.J. (1987). Inhibition of in vitro nuclear transport by a lectin that binds to nuclear pores. The Journal of Cell Biology *104*, 189-200.

Firestein, R., Nagy, P.L., Daly, M., Huie, P., Conti, M., and Cleary, M.L. (2002). Male infertility, impaired spermatogenesis, and azoospermia in mice deficient for the pseudophosphatase Sbf1. The Journal of Clinical Investigation *109*, 1165-1172.

Firooznia, A., Revenkova, E., and Jessberger, R. (2005). From the XXVII North American Testis Workshop: The Function of SMC and Other Cohesin Proteins in Meiosis. J Androl *26*, 1-10.

Fisher, S.A., and Ikebe, M. (1995). Developmental and Tissue Distribution of Expression of Nonmuscle and Smooth Muscle Isoforms of Myosin Light Chain Kinase. Biochemical and Biophysical Research Communications *217*, 696-703.

Fleckenstein, D., Rohde, M., Klionsky, D.J., and Rudiger, M. (1998). Yel013p (Vac8p), an armadillo repeat protein related to plakoglobin and importin alpha is associated with the yeast vacuole membrane. Journal of Cell Science *111*, 3109-3118.

Fontes, M.R.M., Teh, T., and Kobe, B. (2000). Structural basis of recognition of monopartite and bipartite nuclear localization sequences by mammalian importin-[alpha]. Journal of Molecular Biology *297*, 1183-1194.

Forwood, J.K., Harley, V., and Jans, D.A. (2001). The C-terminal Nuclear Localization Signal of the Sex-determining Region Y (SRY) High Mobility Group Domain Mediates Nuclear Import through Importin beta1. Journal of Biological Chemistry *276*, 46575-46582.

Frehlick, L.J., Eirín-López, J.M., and Ausió, J. (2007). New insights into the nucleophosmin/nucleoplasmin family of nuclear chaperones. BioEssays *29*, 49-59.

Friedman, J.R., Fredericks, W.J., Jensen, D.E., Speicher, D.W., Huang, X.P., Neilson, E.G., and Rauscher, F.J. (1996). KAP-1, a novel corepressor for the highly conserved KRAB repression domain. Genes & Development *10*, 2067-2078.

Friedrich, B., Quensel, C., Sommer, T., Hartmann, E., and Kohler, M. (2006). Nuclear Localization Signal and Protein Context both Mediate Importin {alpha} Specificity of Nuclear Import Substrates. Mol Cell Biol *26*, 8697-8709.

Fukumoto, M., Sekimoto, T., and Yoneda, Y. (2011). Proteomic Analysis of Importin α-interacting Proteins in Adult Mouse Brain. Cell Structure and Function *36*, 57-67.

Furuta, M., Kose, S., Koike, M., Shimi, T., Hiraoka, Y., Yoneda, Y., Haraguchi, T., and Imamoto, N. (2004). Heat-shock induced nuclear retention and recycling inhibition of importin α. Genes to Cells *9*, 429-441.

Gashler, A.L., Swaminathan, S., and Sukhatme, V.P. (1993). A novel repression module, an extensive activation domain, and a bipartite nuclear localization signal defined in the immediate-early transcription factor Egr-1. Mol Cell Biol *13*, 4556-4571.

Geles, K.G., and Adam, S.A. (2001). Germline and developmental roles of the nuclear transport factor importin alpha3 in C. elegans. Development *128*, 1817-1830.

Geles, K.G., Johnson, J.J., Jong, S., and Adam, S.A. (2002). A Role for Caenorhabditis elegans Importin IMA-2 in Germ Line and Embryonic Mitosis. Mol Biol Cell *13*, 3138-3147.

Gen, K., Yamaguchi, S., Okuzawa, K., Kagawa, H., and Alam, M.S. (2008). Novel expression of importin alpha homologue in marine teleost, Pagrus major. Comparative Biochemistry and Physiology Part B: Biochemistry and Molecular Biology *151*, 420-427.

Giarrè, M., Török, I., Schmitt, R., Gorjánácz, M., Kiss, I., and Mechler, B.M. (2002). Patterns of importin-alpha expression during Drosophila spermatogenesis. Journal of Structural Biology *140*, 279-290.

Giesecke, A., and Stewart, M. (2010). Novel Binding of the Mitotic Regulator TPX2 (Target Protein for Xenopus Kinesin-like Protein 2) to Importin-α. Journal of Biological Chemistry *285*, 17628-17635.

Gilchrist, D., Mykytka, B., and Rexach, M. (2002). Accelerating the Rate of Disassembly of Karyopherin·Cargo Complexes. Journal of Biological Chemistry *277*, 18161-18172.

Gillooly, D.J., Morrow, I.C., Lindsay, M., Gould, R., Bryant, N.J., Gaullier, J.-M., Parton, R.G., and Stenmark, H. (2000). Localization of phosphatidylinositol 3-phosphate in yeast and mammalian cells. EMBO J *19*, 4577-4588.

Goldfarb, D.S., Corbett, A.H., Mason, D.A., Harreman, M.T., and Adam, S.A. (2004). Importin alpha: a multipurpose nuclear-transport receptor. Trends in Cell Biology *14*, 505-514.

Goldfarb, D.S., Gariepy, J., Schoolnik, G., and Kornberg, R.D. (1986). Synthetic peptides as nuclear localization signals. Nature *322*, 641-644.

Gorjánácz, M., Ádám, G., Török, I., Mechler, B.M., Szlanka, T., and Kiss, I. (2002). Importin-alpha2 Is Critically Required for the Assembly of Ring Canals during Drosophila Oogenesis. Developmental Biology *251*, 271-282.

Gorlich, D., Dabrowski, M., Bischoff, F.R., Kutay, U., Bork, P., Hartmann, E., Prehn, S., and Izaurralde, E. (1997). A novel class of RanGTP binding proteins. J Cell Biol *138*, 65-80.

Gorlich, D., Henklein, P., Laskey, R.A., and Hartmann, E. (1996a). A 41 amino acid motif in importin-alpha confers binding to importin-beta and hence transit into the nucleus. EMBO J *15*, 1810-1817.

Görlich, D., Kostka, S., Kraft, R., Dingwall, C., Laskey, R.A., Hartmann, E., and Prehn, S. (1995). Two different subunits of importin cooperate to recognize nuclear localization signals and bind them to the nuclear envelope. Current Biology *5*, 383-392.

Gorlich, D., and Kutay, U. (1999). TRANSPORT BETWEEN THE CELL NUCLEUS AND THE CYTOPLASM. Annual Review of Cell and Developmental Biology *15*, 607-660.

Gorlich, D., Pante, N., Kutay, U., Aebi, U., and Bischoff, F.R. (1996b). Identification of different roles for RanGDP and RanGTP in nuclear protein import. EMBO J *15*, 5584-5594.

Govin, J., Caron, C., Lestrat, C., Rousseaux, S., and Khochbin, S. (2004). The role of histones in chromatin remodelling during mammalian spermiogenesis. European Journal of Biochemistry *271*, 3459-3469.

Grisendi, S., Bernardi, R., Rossi, M., Cheng, K., Khandker, L., Manova, K., and Pandolfi, P.P. (2005). Role of nucleophosmin in embryonic development and tumorigenesis. Nature *437*, 147-153.

Gruss, O.J., Carazo-Salas, R.E., Schatz, C.A., Guarguaglini, G., Kast, J., Wilm, M., Le Bot, N., Vernos, I., Karsenti, E., and Mattaj, I.W. (2001). Ran Induces Spindle Assembly by Reversing the Inhibitory Effect of Importin alpha on TPX2 Activity. Cell *104*, 83-93.

Gu, L., Tsuji, T., Jarboui, M., Yeo, G., Sheehy, N., Hall, W., and Gautier, V. (2011). Intermolecular masking of the HIV-1 Rev NLS by the cellular protein HIC: Novel insights into the regulation of Rev nuclear import. Retrovirology *8*, 17.

Guo, X., Shen, J., Xia, Z., Zhang, R., Zhang, P., Zhao, C., Xing, J., Chen, L., Chen, W., Lin, M., *et al.* (2010). Proteomic Analysis of Proteins Involved in Spermiogenesis in Mouse. Journal of Proteome Research *9*, 1246-1256.

Hachet, V., Kocher, T., Wilm, M., and Mattaj, I.W. (2004). Importin alpha associates with membranes and participates in nuclear envelope assembly in vitro. EMBO J *23*, 1526-1535.

Hanover, J.A., Love, D.C., DeAngelis, N., O'Kane, M.E., Lima-Miranda, R., Schulz, T., Yen, Y.-M., Johnson, R.C., and Prinz, W.A. (2007). The High Mobility Group Box Transcription Factor Nhp6Ap Enters the Nucleus by a Calmodulin-dependent, Ran-independent Pathway. Journal of Biological Chemistry *282*, 33743-33751.

Harel, A., Chan, R.C., Lachish-Zalait, A., Zimmerman, E., Elbaum, M., and Forbes, D.J. (2003). Importin beta Negatively Regulates Nuclear Membrane Fusion and Nuclear Pore Complex Assembly. Mol Biol Cell *14*, 4387-4396.

Hawryluk-Gara, L.A., Shibuya, E.K., and Wozniak, R.W. (2005). Vertebrate Nup53 Interacts with the Nuclear Lamina and Is Required for the Assembly of a Nup93-containing Complex. Mol Biol Cell *16*, 2382-2394.

Hay, R.T., Vuillard, L., Desterro, J.M., and Rodrigues, M.S. (1999). Control of NF-kB transcriptional activation by signal induced proteolysis of IkBalpha. Philosophical transactions of the Royal Society of London
354, 1601-1609.

He, Y., Brown, M.A., Rothnagel, J.A., Saunders, N.A., and Smith, R. (2005). Roles of heterogeneous nuclear ribonucleoproteins A and B in cell proliferation. Journal of Cell Science *118*, 3173-3183.

Hecht, N.B. (1995). The making of a spermatozoon: A molecular perspective. Developmental Genetics *16*, 95-103.

Hecht, N.B. (1998). Molecular mechanisms of male germ cell differentiation. BioEssays *20*, 555-561.

Henkel, T., Machleidt, T., Alkalay, I., Kronke, M., Ben-Neriah, Y., and Baeuerle, P.A. (1993). Rapid proteolysis of I kappa B-alpha is necessary for activation of transcription factor NF-kappa B. Nature *365*, 182-185.

Hermo, L., Pelletier, R.M., Cyr, D.G., and Smith, C.E. (2009a). Surfing the wave, cycle, life history, and genes/proteins expressed by testicular germ cells. Part 1: Background to spermatogenesis, spermatogonia, and spermatocytes. Microscopy Research and Technique *73*, 241-278.

Hermo, L., Pelletier, R.M., Cyr, D.G., and Smith, C.E. (2009b). Surfing the wave, cycle, life history, and genes/proteins expressed by testicular germ cells. Part 2: Changes in spermatid organelles associated with development of spermatozoa. Microscopy Research and Technique *73*, 279-319.

Hermo, L., Pelletier, R.M., Cyr, D.G., and Smith, C.E. (2009c). Surfing the wave, cycle, life history, and genes/proteins expressed by testicular germ cells. Part 3: Developmental changes in spermatid flagellum and cytoplasmic droplet and interaction of sperm with the zona pellucida and egg plasma membrane. Microscopy Research and Technique *73*, 320-363.

Herold, A., Truant, R., Wiegand, H., and Cullen, B.R. (1998). Determination of the functional domain organization of the importin alpha nuclear import factor. J Cell Biol *143*, 309-318.

Herring, B.P., El-Mounayri, O., Gallagher, P.J., Yin, F., and Zhou, J. (2006). Regulation of myosin light chain kinase and telokin expression in smooth muscle tissues. American Journal of Physiology - Cell Physiology *291*, C817-C827.

Hess, R.A., and Franca, L.R. (2009). Spermatogenesis and Cycle of the Seminiferous Epithelium. In Molecular Mechanisms in Spermatogenesis, pp. 1-15.

Hetzer, M., Bilbao-Cortés, D., Walther, T.C., Gruss, O.J., and Mattaj, I.W. (2000). GTP Hydrolysis by Ran Is Required for Nuclear Envelope Assembly. Molecular Cell *5*, 1013-1024.

Hieda, M., Tachibana, T., Yokoya, F., Kose, S., Imamoto, N., and Yoneda, Y. (1999). A Monoclonal Antibody to the COOH-terminal Acidic Portion of Ran Inhibits Both the Recycling of Ran and Nuclear Protein Import in Living Cells. The Journal of Cell Biology *144*, 645-655.

Ho, H.-C. (2010). Redistribution of nuclear pores during formation of the redundant nuclear envelope in mouse spermatids. Journal of Anatomy *216*, 525-532.

Hodel, A.E., Harreman, M.T., Pulliam, K.F., Harben, M.E., Holmes, J.S., Hodel, M.R., Berland, K.M., and Corbett, A.H. (2006). Nuclear Localization Signal Receptor Affinity Correlates with in Vivo Localization in Saccharomyces cerevisiae. Journal of Biological Chemistry *281*, 23545-23556.

Hodel, M.R., Corbett, A.H., and Hodel, A.E. (2001). Dissection of a Nuclear Localization Signal. Journal of Biological Chemistry *276*, 1317-1325.

Hoelz, A., Debler, E.W., and Blobel, G.n. (2011). The Structure of the Nuclear Pore Complex. Annual Review of Biochemistry.

Hogarth, C., Itman, C., Jans, D.A., and Loveland, K.L. (2005). Regulated nucleocytoplasmic transport in spermatogenesis: a driver of cellular differentiation? BioEssays *27*, 1011-1025.

Hogarth, C.A., Calanni, S., Jans, D.A., and Loveland, K.L. (2006). Importin α mRNAs have distinct expression profiles during spermatogenesis. Developmental Dynamics *235*, 253-262.

Hogarth, C.A., Jans, D.A., and Loveland, K.L. (2007). Subcellular distribution of importins correlates with germ cell maturation. Developmental Dynamics *236*, 2311-2320.

Hood, J.K., and Silver, P.A. (1998). Cse1p is required for export of Srp1p/importin-alpha from the nucleus in Saccharomyces cerevisiae. J Biol Chem *273*, 35142-35146.

Höppener, C., Siebrasse, J.P., Peters, R., Kubitscheck, U., and Naber, A. (2005). High-Resolution Near-Field Optical Imaging of Single Nuclear Pore Complexes under Physiological Conditions. Biophysical Journal *88*, 3681-3688.

Hosokawa, K., Nishi, M., Sakamoto, H., Tanaka, Y., and Kawata, M. (2008). Regional distribution of importin subtype mRNA expression in the nervous system: Study of early postnatal and adult mouse. Neuroscience *157*, 864-877.

Hu, J., Wang, F., Yuan, Y., Zhu, X., Wang, Y., Zhang, Y., Kou, Z., Wang, S., and Gao, S. (2010). Novel Importin alpha Family Member Kpna7 Is Required for Normal Fertility and Fecundity in the Mouse. Journal of Biological Chemistry *285*, 33113-33122.

Hu, W., and Jans, D.A. (1999). Efficiency of Importin alpha /beta -Mediated Nuclear Localization Sequence Recognition and Nuclear Import. DIFFERENTIAL ROLE OF NTF2. J Biol Chem *274*, 15820-15827.

Huber, A.H., Nelson, W.J., and Weis, W.I. (1997). Three-Dimensional Structure of the Armadillo Repeat Region of beta-Catenin. Cell *90*, 871-882.

Hubner, S., Xiao, C.-Y., and Jans, D.A. (1997). The Protein Kinase CK2 Site (Ser111/112) Enhances Recognition of the Simian Virus 40 Large T-antigen Nuclear Localization Sequence by Importin. Journal of Biological Chemistry *272*, 17191-17195.

Huckins, C. (1978). Spermatogonial intercellular bridges in whole-mounted seminiferous tubules from normal and irradiated rodent testes. American Journal of Anatomy *153*, 97-122.

Huh, W.-K., Falvo, J.V., Gerke, L.C., Carroll, A.S., Howson, R.W., Weissman, J.S., and O'Shea, E.K. (2003). Global analysis of protein localization in budding yeast. Nature *425*, 686-691.

Huotari, J., and Helenius, A. (2011). Endosome maturation. EMBO J *30*, 3481-3500.
Hurd, T.W., Fan, S., and Margolis, B.L. (2011). Localization of retinitis pigmentosa 2 to cilia is regulated by Importin β2. Journal of Cell Science *124*, 718-726.

Imamoto, N., Shimamoto, T., Kose, S., Takao, T., Tachibana, T., Matsubae, M., Sekimoto, T., Shimonishi, Y., and Yoneda, Y. (1995). The nuclear pore-targeting complex binds to nuclear pores after association with a karyophile. FEBS Lett *368*, 415-419.

Inagaki, A., Schoenmakers, S., and Baarends, W.M. (2010). DNA double strand break repair, chromosome synapsis and transcriptional silencing in meiosis. Epigenetics *5*, 255-266.

Iyengar, S., and Farnham, P.J. (2011). KAP1 Protein: An Enigmatic Master Regulator of the Genome. Journal of Biological Chemistry *286*, 26267-26276.

Izaurralde, E., Kutay, U., von Kobbe, C., Mattaj, I.W., and Gorlich, D. (1997). The asymmetric distribution of the constituents of the Ran system is essential for transport into and out of the nucleus. EMBO J *16*, 6535-6547.

Jakobsson, J., Cordero, M.I., Bisaz, R., Groner, A.C., Busskamp, V., Bensadoun, J.-C., Cammas, F., Losson, R., Mansuy, I.M., Sandi, C., *et al.* (2008). KAP1-Mediated Epigenetic Repression in the Forebrain Modulates Behavioral Vulnerability to Stress. Neuron *60*, 818-831.

Jans, D.A., Ackermann, M.J., Bischoff, J.R., Beach, D.H., and Peters, R. (1991). p34cdc2-mediated phosphorylation at T124 inhibits nuclear import of SV-40 T antigen proteins. The Journal of Cell Biology *115*, 1203-1212.

Jans, D.A., Xiao, C.-Y., and Lam, M.H.C. (2000). Nuclear targeting signal recognition: a key control point in nuclear transport? BioEssays *22*, 532-544.

Jarnik, M., and Aebi, U. (1991). Toward a more complete 3-D structure of the nuclear pore complex. Journal of Structural Biology *107*, 291-308.

Kalderon, D., Richardson, W.D., Markham, A.F., and Smith, A.E. (1984). Sequence requirements for nuclear location of simian virus 40 large-T antigen. Nature *311*, 33-38.

Kalverda, B., Pickersgill, H., Shloma, V.V., and Fornerod, M. (2010). Nucleoporins Directly Stimulate Expression of Developmental and Cell-Cycle Genes Inside the Nucleoplasm. Cell *140*, 360-371.

Kamei, Y., Yuba, S., Nakayama, T., and Yoneda, Y. (1999). Three Distinct Classes of the alpha-Subunit of the Nuclear Pore-targeting Complex (Importin-alpha) Are Differentially Expressed in Adult Mouse Tissues. J Histochem Cytochem *47*, 363-372.

Kamm, K.E., and Stull, J.T. (2001). Dedicated Myosin Light Chain Kinases with Diverse Cellular Functions. Journal of Biological Chemistry *276*, 4527-4530.

Kamma, H., Fujimoto, M., Fujiwara, M., Matsui, M., Horiguchi, H., Hamasaki, M., and Satoh, H. (2001). Interaction of hnRNP A2/B1 Isoforms with Telomeric ssDNA and the in Vitro Function. Biochemical and Biophysical Research Communications *280*, 625-630.

Kamma, H., Horiguchi, H., Wan, L., Matsui, M., Fujiwara, M., Fujimoto, M., Yazawa, T., and Dreyfuss, G. (1999). Molecular Characterization of the hnRNP A2/B1 Proteins: Tissue-Specific Expression and Novel Isoforms. Experimental Cell Research *246*, 399-411.

Kaur, G., Delluc-Clavieres, A., Poon, I.K.H., Forwood, J.K., Glover, D.J., and Jans, D.A. (2010). Calmodulin-dependent nuclear import of HMG-box family nuclear factors: importance of the role of SRY in sex reversal. Biochemical Journal *430*, 39-48.

Kee, H.L., Dishinger, J.F., Lynne Blasius, T., Liu, C.-J., Margolis, B., and Verhey, K.J. (2012). A size-exclusion permeability barrier and nucleoporins characterize a ciliary pore complex that regulates transport into cilia. Nat Cell Biol *14*, 431-437.

Kerr, J.B., Loveland, K.L., O'Bryan, M.K., and de Kretser, D.M. (2006). Cytology of the Testis and Intrinsic Control Mechanisms. In: Knobil and Neill's Physiology of Reproduction Amsterdam Boston *Third Edition*, 827-947.

Kim, Kanbe, Akashi, Mizuguchi, and Kikuchi (2002). Identification of a single nuclear localization signal in the C-terminal domain of an Aspergillus DNA topoisomerase II. Molecular Genetics and Genomics *268*, 287-297.

Kim, S.-A., Vacratsis, P.O., Firestein, R., Cleary, M.L., and Dixon, J.E. (2003). Regulation of myotubularin-related (MTMR)2 phosphatidylinositol phosphatase by MTMR5, a catalytically inactive phosphatase. Proceedings of the National Academy of Sciences *100*, 4492-4497.

Kim, S.-S., Chen, Y.-M., O'Leary, E., Witzgall, R., Vidal, M., and Bonventre, J.V. (1996). A novel member of the RING finger family, KRIP-1, associates with the KRAB-A transcriptional repressor domain of zinc finger proteins. Proceedings of the National Academy of Sciences *93*, 15299-15304.

Kitamura, R., Sekimoto, T., Ito, S., Harada, S., Yamagata, H., Masai, H., Yoneda, Y., and Yanagi, K. (2006). Nuclear Import of Epstein-Barr Virus Nuclear Antigen 1 Mediated by NPI-1 (Importin alpha 5) Is Up- and Down-Regulated by Phosphorylation of the Nuclear Localization Signal for Which Lys379 and Arg380 Are Essential. J Virol *80*, 1979-1991.

Knapp, A.A., McManus, P.M., Bockstall, K., and Moroianu, J. (2009). Identification of the nuclear localization and export signals of high risk HPV16 E7 oncoprotein. Virology *383*, 60-68.

Kobe, B. (1999). Autoinhibition by an internal nuclear localization signal revealed by the crystal structure of mammalian importin alpha. Nature structural biology *6*, 388-397.

Kodiha, M., Bański, P., Ho-Wo-Cheong, D., and Stochaj, U. (2008a). Dissection of the molecular mechanisms that control the nuclear accumulation of transport factors importin-α and CAS in stressed cells. Cellular and Molecular Life Sciences *65*, 1756-1767.

Kodiha, M., Tran, D., Qian, C., Morogan, A., Presley, J.F., Brown, C.M., and Stochaj, U. (2008b). Oxidative stress mislocalizes and retains transport factor importin-alpha and nucleoporins Nup153 and Nup88 in nuclei where they generate high molecular mass complexes. Biochimica et Biophysica Acta (BBA) - Molecular Cell Research *1783*, 405-418.

Koehler, M., Fiebeler, A., Hartwig, M., Thiel, S., Prehn, S., Kettritz, R., Luft, F.C., and Hartmann, E. (2002). Differential Expression of Classical Nuclear Transport Factors During Cellular Proliferation and Differentiation. Cellular Physiology and Biochemistry *12*, 335-344.

Kohler, M., Speck, C., Christiansen, M., Bischoff, F.R., Prehn, S., Haller, H., Gorlich, D., and Hartmann, E. (1999). Evidence for Distinct Substrate Specificities of Importin alpha Family Members in Nuclear Protein Import. Mol Cell Biol *19*, 7782-7791.

Kose, S., Imamoto, N., Tachibana, T., Yoshida, M., and Yoneda, Y. (1999). Beta-Subunit of Nuclear Pore-targeting Complex (Importin-Beta) Can Be Exported from the Nucleus in a Ran-independent Manner. Journal of Biological Chemistry *274*, 3946-3952.

Kosugi, S., Hasebe, M., Tomita, M., and Yanagawa, H. (2009). Systematic identification of cell cycle-dependent yeast nucleocytoplasmic shuttling proteins by prediction of composite motifs. Proceedings of the National Academy of Sciences *106*, 10171-10176.

Kotera, I., Sekimoto, T., Miyamoto, Y., Saiwaki, T., Nagoshi, E., Sakagami, H., Kondo, H., and Yoneda, Y. (2005). Importin alpha transports CaMKIV to the nucleus without utilizing importin beta. EMBO J *24*, 942-951.

Kozu, T., Henrich, B., and Schäfer, K.P. (1995). Structure and expression of the gene (HNRPA2B1) encoding the human hnRNP protein A2/B1. Genomics *25*, 365-371.

Kubitscheck, U., Wedekind, P., Zeidler, O., Grote, M., and Peters, R. (1996). Single nuclear pores visualized by confocal microscopy and image processing. Biophysical Journal *70*, 2067-2077.

Kumar, R., Bourbon, H.-M., and de Massy, B. (2010). Functional conservation of Mei4 for meiotic DNA double-strand break formation from yeasts to mice. Genes & Development *24*, 1266-1280.

Kussel, P., and Frasch, M. (1995). Pendulin, a Drosophila protein with cell cycle-dependent nuclear localization, is required for normal cell proliferation. The Journal of Cell Biology *129*, 1491-1507.

Kutateladze, T.G. (2006). Phosphatidylinositol 3-phosphate recognition and membrane docking by the FYVE domain. Biochimica et Biophysica Acta (BBA) - Molecular and Cell Biology of Lipids *1761*, 868-877.

Kutay, U., Bischoff, F.R., Kostka, S., Kraft, R., and Gorlich, D. (1997). Export of importin alpha from the nucleus is mediated by a specific nuclear transport factor. Cell *90*, 1061-1071.

Lange, A., McLane, L.M., Mills, R.E., Devine, S.E., and Corbett, A.H. (2010). Expanding the Definition of the Classical Bipartite Nuclear Localization Signal. Traffic *11*, 311-323.

Lange, A., Mills, R.E., Lange, C.J., Stewart, M., Devine, S.E., and Corbett, A.H. (2007). Classical Nuclear Localization Signals: Definition, Function, and Interaction with Importin alpha. Journal of Biological Chemistry *282*, 5101-5105.

Laporte, J., Bedez, F., Bolino, A., and Mandel, J.-L. (2003). Myotubularins, a large disease-associated family of cooperating catalytically active and inactive phosphoinositides phosphatases. Human Molecular Genetics *12*, R285-R292.

Laporte, J., Hu, L.J., Kretz, C., Mandel, J.L., Kioschis, P., Coy, J.F., Klauck, S.M., Poustka, A., and Dahl, N. (1996). A gene mutated in X-linked myotubular myopathy defines a new putative tyrosine phosphatase family conserved in yeast. Nature Genetics *13*, 175-182.

Laskey, R.A., and Leno, G.H. (1990). Assembly of the cell nucleus. Trends in Genetics *6*, 406-410.

Lee, Jin, Chang, Lin, and Su (1999). Immunolocalization of BRCA1 protein in normal breast tissue and sporadic invasive ductal carcinomas: a correlation with other biological parameters. Histopathology *34*, 106-112.

Lee, C.-h., Lum, J.H.-k., Cheung, B.P.-y., Wong, M.-s., Butt, Y.K.-c., Tam, M.F., Chan, W.Y., Chow, C., Hui, P.-k., Kwok, F.S.L., *et al.* (2005). Identification of the heterogeneous nuclear ribonucleoprotein A2/B1 as the antigen for the gastrointestinal cancer specific monoclonal antibody MG7. PROTEOMICS *5*, 1160-1166.

Leight, E.R., and Sugden, B. (2000). EBNA-1: a protein pivotal to latent infection by Epstein-Barr virus. Reviews in Medical Virology *10*, 83-100.

Lemmon, M.A. (2008). Membrane recognition by phospholipid-binding domains. Nat Rev Mol Cell Biol *9*, 99-111.

Leung, S.W., Harreman, M.T., Hodel, M.R., Hodel, A.E., and Corbett, A.H. (2003). Dissection of the Karyopherin alpha Nuclear Localization Signal (NLS)-binding Groove. Journal of Biological Chemistry *278*, 41947-41953.

Li, S., Ehrhardt, W.D., and Rhee, Y.S. (2006). Systemic Analysis of Arabidopsis Organelles and a Protein Localization Database for Facilitating Fluorescent Tagging of Full-Lenght Arabidopsis Proteins. Plant Physiology *141*, 527-539.

Li, S., Ku, C.-Y., Farmer, A.A., Cong, Y.-S., Chen, C.-F., and Lee, W.-H. (1998). Identification of a Novel Cytoplasmic Protein That Specifically Binds to Nuclear Localization Signal Motifs. Journal of Biological Chemistry *273*, 6183-6189.

Lie, P.P.Y., Cheng, C.Y., and Mruk, D.D. (2009). Coordinating cellular events during spermatogenesis: a biochemical model. Trends in Biochemical Sciences *34*, 366-373.

Lim, M.J., and Wang, X.W. (2006). Nucleophosmin and human cancer. Cancer Detection and Prevention *30*, 481-490.

Lindsay, M.E., Plafker, K., Smith, A.E., Clurman, B.E., and Macara, I.G. (2002). Npap60/Nup50 Is a Tri-Stable Switch that Stimulates Importin alpha Mediated Nuclear Protein Import. Cell *110*, 349-360.

Liu, J.-P., and Li, H. (2010). Telomerase in the ovary. Reproduction *140*, 215-222.

Liu, L., McBride, K.M., and Reich, N.C. (2005). STAT3 nuclear import is independent of tyrosine phosphorylation and mediated by importin-alpha 3. Proceedings of the National Academy of Sciences of the United States of America *102*, 8150-8155.

Liu, Y., and Bankaitis, V.A. (2010). Phosphoinositide phosphatases in cell biology and disease. Progress in Lipid Research *49*, 201-217.

Lo, H.-W., Ali-Seyed, M., Wu, Y., Bartholomeusz, G., Hsu, S.-C., and Hung, M.-C. (2006). Nuclear-cytoplasmic transport of EGFR involves receptor endocytosis, importin β1 and CRM1. Journal of Cellular Biochemistry *98*, 1570-1583.

Loeb, J.D., Schlenstedt, G., Pellman, D., Kornitzer, D., Silver, P.A., and Fink, G.R. (1995). The yeast nuclear import receptor is required for mitosis. Proceedings of the National Academy of Sciences *92*, 7647-7651.

Lorenzo, O., Urbe, S., and Clague, M.J. (2005). Analysis of phosphoinositide binding domain properties within the myotubularin-related protein MTMR3. Journal of Cell Science *118*, 2005-2012.

Lorenzo, O., Urbe, S., and Clague, M.J. (2006). Systematic analysis of myotubularins: heteromeric interactions, subcellular localisation and endosomerelated functions. Journal of Cell Science *119*, 2953-2959.

Losada, A., and Hirano, T. (2005). Dynamic molecular linkers of the genome: the first decade of SMC proteins. Genes & Development *19*, 1269-1287.

Lott, K., Bhardwaj, A., Mitrousis, G., Pante, N., and Cingolani, G. (2010). The Importin beta Binding Domain Modulates the Avidity of Importin beta for the Nuclear Pore Complex. Journal of Biological Chemistry *285*, 13769-13780.

Lott, K., and Cingolani, G. (2011). The importin β binding domain as a master regulator of nucleocytoplasmic transport. Biochimica et Biophysica Acta (BBA) - Molecular Cell Research *1813*, 1578-1592.

Loveland, K.L., Hedger, M.P., Risbridger, G., Herszfeld, D., and de Kretser, D.M. (1993). Identification of Receptor Tyrosine kinase in the rat testis. Molecular reproduction and development *36*, 440-447.

Loveland, K.L., Hogarth, C., Szczepny, A., Prabhu, S.M., and Jans, D.A. (2006). Expression of Nuclear Transport Importins beta 1 and beta 3 Is Regulated During Rodent Spermatogenesis. Biology of Reproduction *74*, 67-74.

Ly-Huynh, J.D., Lieu, K.G., Major, A.T., Whiley, P.A.F., Holt, J.E., Loveland, K.L., and Jans, D.A. (2011). Importin Alpha2-Interacting Proteins with Nuclear Roles During Mammalian Spermatogenesis. Biology of Reproduction *85*, 1191-1202.

Maas, S., and Gommans, W.M. (2009). Identification of a selective nuclear import signal in adenosine deaminases acting on RNA. Nucleic Acids Research *37*, 5822-5829.

MacDonald, T., Bryan, Tamai, K., and He, X. (2009). Wnt/beta-catenin signaling: components, mechanisms, and diseases. Developmenal cell *17*, 9-26.

Maeshima, K., Yahata, K., Sasaki, Y., Nakatomi, R., Tachibana, T., Hashikawa, T., Imamoto, F., and Imamoto, N. (2006). Cell-cycle-dependent dynamics of nuclear pores: pore-free islands and lamins. J Cell Sci *119*, 4442-4451.

Maggi, L.B., Jr., Kuchenruether, M., Dadey, D.Y.A., Schwope, R.M., Grisendi, S., Townsend, R.R., Pandolfi, P.P., and Weber, J.D. (2008). Nucleophosmin Serves as a Rate-Limiting Nuclear Export Chaperone for the Mammalian Ribosome. Mol Cell Biol *28*, 7050-7065.

Major, A.T., Whiley, P.A.F., and Loveland, K.L. (2011). Expression of nucleocytoplasmic transport machinery: Clues to regulation of spermatogenic development. Biochimica et Biophysica Acta (BBA) - Molecular Cell Research *1813*, 1668-1688.

Malik, H.S., Eickbush, T.H., and Goldfarb, D.S. (1997). Evolutionary specialization of the nuclear targeting apparatus. Proceedings of the National Academy of Sciences *94*, 13738-13742.

Marchenko, N.D., Hanel, W., Li, D., Becker, K., Reich, N., and Moll, U.M. (2010). Stress-mediated nuclear stabilization of p53 is regulated by ubiquitination and importin-alpha 3 binding. Cell Death Differ *17*, 255-267.

Martin Watterson, D., Collinge, M., Lukas, T.J., Van Eldik, L.J., Birukov, K.G., Stepanova, O.V., and Shirinsky, V.P. (1995). Multiple gene products are produced from a novel protein kinase transcription region. FEBS Letters *373*, 217-220.

Mason, D.A., Fleming, R.J., and Goldfarb, D.S. (2002). Drosophila melanogaster Importin alpha1 and alpha3 Can Replace Importin alpha2 During Spermatogenesis but Not Oogenesis. Genetics *161*, 157-170.

Mason, D.A., Mathe, E., Fleming, R.J., and Goldfarb, D.S. (2003). The Drosophila melanogaster importin alpha 3 Locus Encodes an Essential Gene Required for the Development of Both Larval and Adult Tissues. Genetics *165*, 1943-1958.

Máthé, E., Bates, H., Huikeshoven, H., Deák, P., Glover, D.M., and Cotterill, S. (2000). Importin-alpha 3 Is Required at Multiple Stages of Drosophila Development and Has a Role in the Completion of Oogenesis. Developmental Biology *223*, 307-322.

Matsuura, Y., and Stewart, M. (2005). Nup50/Npap60 function in nuclear protein import complex disassembly and importin recycling. EMBO J *24*, 3681-3689.

Matunis, M.J., Coutavas, E., and Blobel, G. (1996). A novel ubiquitin-like modification modulates the partitioning of the Ran-GTPase-activating protein RanGAP1 between the cytosol and the nuclear pore complex. J Cell Biol *135*, 1457-1470.

Maxfield, F.R., and McGraw, T.E. (2004). Endocytic recycling. Nat Rev Mol Cell Biol *5*, 121-132.

McCarrey, J. (1993). CELL AND MOLECULAR BIOLOGY OF THE TESTIS, C. Desjardins, and E.L. L., eds. (New York: Oxford University Press), pp. 58-90.

Meistrich, M.L., Longtin, J., Brock, W.A., Grimes, S.R.J., and Mace, M.L. (1981). Purification of Rat Spermatogenic Cells and Preliminary Biochemical Analysis of These Cells. Biol Reprod *25*, 1065-1077.

Melchior, F., Paschal, B., Evans, J., and Gerace, L. (1993). Inhibition of nuclear protein import by nonhydrolyzable analogues of GTP and identification of the small GTPase Ran/TC4 as an essential transport factor [published erratum appears in J Cell Biol 1994 Jan;124(1-2):217]. J Cell Biol *123*, 1649-1659.

Meng, X., Lindahl, M., Hyvonen, M.E., Parvinen, M., de Rooij, D.G., Hess, M.W., Raatikainen-Ahokas, A., Sainio, K., Rauvala, H., Lakso, M., *et al.* (2000). Regulation of Cell Fate Decision of Undifferentiated Spermatogonia by GDNF. Science *287*, 1489-1493.

Meyer, T., Begitt, A., Lodige, I., van Rossum, M., and Vinkemeier, U. (2002). Constitutive and IFN-[gamma]-induced nuclear import of STAT1 proceed through independent pathways. EMBO J *21*, 344-354.

Miyamoto, Y., Baker, M.A., Whiley, P.A., Arjomand, A., Ludeman, J., Wong, C., Jans, D.A., and Loveland, K.L. (2013). Towards delineation of a developmental α-importome in the mammalian male germline. Biochimica et Biophysica Acta (BBA) - Molecular Cell Research *1833*, 731-742.

Miyamoto, Y., Boag, P.R., Hime, G.R., and Loveland, K.L. (2012a). Regulated nucleocytoplasmic transport during gametogenesis. Biochimica et Biophysica Acta (BBA) - Gene Regulatory Mechanisms *1819*, 616-630.

Miyamoto, Y., Hieda, M., Harreman, M.T., Fukumoto, M., Saiwaki, T., Hodel, A.E., Corbett, A.H., and Yoneda, Y. (2002). Importin alpha can migrate into the nucleus in an importin beta- and Ran-independent manner. EMBO J *21*, 5833-5842.

Miyamoto, Y., Imamoto, N., Sekimoto, T., Tachibana, T., Seki, T., Tada, S., Enomoto, T., and Yoneda, Y. (1997). Differential Modes of Nuclear Localization Signal (NLS) Recognition by Three Distinct Classes of NLS Receptors. The Journal of Biological Chemistry *272*, 26375-26381.

Miyamoto, Y., Loveland, K.L., and Yoneda, Y. (2012b). Nuclear importin alpha and its physiological importance. Communicative and Integrative Biology *5*, 220-222.

Miyamoto, Y., Saiwaki, T., Yamashita, J., Yasuda, Y., Kotera, I., Shibata, S., Shigeta, M., Hiraoka, Y., Haraguchi, T., and Yoneda, Y. (2004). Cellular stresses induce the nuclear accumulation of importin alpha and cause a conventional nuclear import block. The Journal of Cell Biology *165*, 617-623.

Mochizuki, Y., and Majerus, P.W. (2003). Characterization of myotubularin-related protein 7 and its binding partner, myotubularin-related protein 9. Proceedings of the National Academy of Sciences *100*, 9768-9773.

Monesi, V. (1965). Synthetic activities during spermatogenesis in the mouse : RNA and protein. Experimental Cell Research *39*, 197-224.

Moore, M.S., and Blobel, G. (1992). The two steps of nuclear import, targeting to the nuclear envelope and translocation through the nuclear pore, require different cytosolic factors. Cell *69*, 939-950.

Moore, M.S., and Blobel, G. (1993). The GTP-binding protein Ran/TC4 is required for protein import into the nucleus. Nature *365*, 661-663.

Moosmann, P., Georgiev, O., Le Douarin, B., Bourquin, J.-P., and Schaffner, W. (1996). Transcriptional Repression by RING Finger Protein TIF1β That Interacts with the KRAB Repressor Domain of KOX1. Nucleic Acids Research *24*, 4859-4867.

Moran-Jones, K., Wayman, L., Kennedy, D.D., Reddel, R.R., Sara, S., Snee, M.J., and Smith, R. (2005). hnRNP A2, a potential ssDNA/RNA molecular adapter at the telomere. Nucleic Acids Research *33*, 486-496.

Moroianu, J., Blobel, G., and Radu, A. (1995a). Previously identified protein of uncertain function is karyopherin alpha and together with karyopherin beta docks import substrate at nuclear pore complexes. Proc Natl Acad Sci U S A *92*, 2008-2011.

Moroianu, J., Blobel, G., and Radu, A. (1996a). The binding site of karyopherin alpha for karyopherin beta overlaps with a nuclear localization sequence. Proc Natl Acad Sci U S A *93*, 6572-6576.

Moroianu, J., Blobel, G., and Radu, A. (1996b). Nuclear protein import: Ran-GTP dissociates the karyopherin alphabeta heterodimer by displacing alpha from an overlapping binding site on beta. Proc Natl Acad Sci U S A *93*, 7059-7062.

Moroianu, J., Hijikata, M., Blobel, G., and Radu, A. (1995b). Mammalian karyopherin alpha 1 beta and alpha 2 beta heterodimers: alpha 1 or alpha 2 subunit binds nuclear localization signal and beta subunit interacts with peptide repeat-containing nucleoporins. Proc Natl Acad Sci U S A *92*, 6532-6536.

Moussa, F., Oko, R., and Hermo, L. (1994). The immunolocalization of small nuclear ribonucleoprotein particles in testicular cells during the cycle of the seminiferous epithelium of the adult rat. Cell and Tissue Research *278*, 363-378.

Mruk, D.D., and Cheng, C.Y. (2011). The myotubularin family of lipid phosphatases in disease and in spermatogenesis. Biochemical Journal *433*, 253-262.

Nadler, S.G., Tritschler, D., Haffar, O.K., Blake, J., Bruce, A.G., and Cleaveland, J.S. (1997). Differential Expression and Sequence-specific Interaction of Karyopherin alpha with Nuclear Localization Sequences. J Biol Chem *272*, 4310-4315.

Nagata, Y., and Burger, M.M. (1974). Wheat Germ Agglutinin. Journal of Biological Chemistry *249*, 3116-3122.

Nakai, K., and Horton, P. (1999). PSORT: a program for detecting sorting signals in proteins and predicting their subcellular localization. Trends in Biochemical Sciences *24*, 34-35.

Nardozzi, J., Lott, K., and Cingolani, G. (2010). Phosphorylation meets nuclear import: a review. Cell Communication and signaling *8*.

Naughtin, M.J., Sheffield, D.A., Rahman, P., Hughes, W.E., Gurung, R., Stow, J.L., Nandurkar, H.H., Dyson, J.M., and Mitchell, C.A. (2010). The myotubularin phosphatase MTMR4 regulates sorting from early endosomes. Journal of Cell Science *123*, 3071-3083.

Nebel, B.R., Amarose, A.P., and Hackett, E.M. (1961). Calendar of Gametogenic Development in the Prepuberal Male Mouse. Science *134*, 832-833.

Nelson, J.W. (2008). Regulation of cell-cell adhesion by the cadherin-catenin complex. Biochemical society transactions *36*, 146-155.

Newmeyer, D.D., and Forbes, D.J. (1988). Nuclear import can be separated into distinct steps in vitro: nuclear pore binding and translocation. Cell *52*, 641-653.

Newmeyer, D.D., Lucocq, J.M., Burglin, T.R., and De Robertis, E.D. (1986b). Assembly in vitro of nuclei active in nuclear protein transport: ATP is required for nucleoplasmin accumulation. European Molecular biology organization Journal *5*, 501-510.

Noetzel, E., Rose, M., Bornemann, J., Gajewski, M., Knuchel, R., and Dahl, E. (2012). Nuclear transport receptor karyopherin-alpha 2 promotes malignant breast cancer phenotype *in vitro*. Oncogene *31*, 2101-2114.

Ogawa, T., Ohmura, M., and Ohbo, K. (2005). The Niche for Spermatogonial Stem Cells in the Mammalian Testis. International journal of HEMATOLOGY *82*, 381-388.

Okada, N., Ishigami, Y., Suzuki, T., Kaneko, A., Yasui, K., Fukutomi, R., and Isemura, M. (2008). Importins and exportins in cellular differentiation. Journal of Cellular and Molecular Medicine *12*, 1863-1871.

Okuda, M. (2002). The role of nucleophosmin in centrosome duplication. Oncogene *21*, 6170-6174.

Okuwaki, M. (2008). The Structure and Functions of NPM1/Nucleophsmin/B23, a Multifunctional Nucleolar Acidic Protein. Journal of Biochemistry *143*, 441-448.

Paine, P.L. (1975). Nucleocytoplasmic movement of fluorescent tracers microinjected into living salivary gland cells. The Journal of Cell Biology *66*, 652-657.

Pan, X., Roberts, P., Chen, Y., Kvam, E., Shulga, N., Huang, K., Lemmon, S., and Goldfarb, D.S. (2000). Nucleus-Vacuole Junctions in Saccharomyces cerevisiae Are Formed Through the Direct Interaction of Vac8p with Nvj1p. Mol Biol Cell *11*, 2445-2457.

Pante, N., and Kann, M. (2002). Nuclear Pore Complex Is Able to Transport Macromolecules with Diameters of ~39 nm. Mol Biol Cell *13*, 425-434.

Park, K.-E., Inerowicz, H.D., Wang, X., Li, Y., Koser, S., and Cabot, R.A. (2012). Identification of Karyopherin α1 and α7 Interacting Proteins in Porcine Tissue. PLoS ONE *7*, e38990.

Pemberton, L.F., and Paschal, B.M. (2005). Mechanisms of Receptor-Mediated Nuclear Import and Nuclear Export. Traffic *6*, 187-198.

Pierre, V., Martinez, G., Coutton, C., Delaroche, J., Yassine, S., Novella, C., Pernet-Gallay, K., Hennebicq, S., Ray, P.F., and Arnoult, C. (2012). Absence of Dpy19l2, a new inner nuclear membrane protein, causes globozoospermia in mice by preventing the anchoring of the acrosome to the nucleus. Development *139*, 2955-2965.

Plant, P.J., Correa, J., Goldenberg, N., Bain, J., and Batt, J. (2009). The inositol phosphatase MTMR4 is a novel target of the ubiquitin ligase Nedd4. Biochem J *419*, 57-63.

Poon, I.K.H., and Jans, D.A. (2005). Regulation of Nuclear Transport: Central Role in Development and Transformation? Traffic *6*, 173-186.

Poperechnaya, A., Varlamova, O., Lin, P.-j., Stull, J.T., and Bresnick, A.R. (2000). Localization and Activity of Myosin Light Chain Kinase Isoforms during the Cell Cycle. The Journal of Cell Biology *151*, 697-708.

Previtali, S.C., Quattrini, A., and Bolino, A. (2007). Charcot-Marie-Tooth type 4B demyelinating neuropathy: deciphering the role of MTMR phosphatases. Expert Reviews in Molecular Medicine *9*, 1-16.

Prieve, M.G., Guttridge, K.L., Munguia, J.E., and Waterman, M.L. (1996). The Nuclear Localization Signal of Lymphoid Enhancer Factor-1 Is Recognized by Two Differentially Expressed Srp1-Nuclear Localization Sequence Receptor Proteins. The Journal of Biological Chemistry *271*, 7654-7658.

Pyhtila, B., and Rexach, M. (2003). A Gradient of Affinity for the Karyopherin Kap95p along the Yeast Nuclear Pore Complex. Journal of Biological Chemistry *278*, 42699-42709.

Quensel, C., Friedrich, B., Sommer, T., Hartmann, E., and Kohler, M. (2004). In Vivo Analysis of Importin alpha Proteins Reveals Cellular Proliferation Inhibition and Substrate Specificity. Mol Cell Biol *24*, 10246-10255.

Radu, A., Blobel, G., and Moore, M.S. (1995a). Identification of a protein complex that is required for nuclear protein import and mediates docking of import substrate to distinct nucleoporins. Proc Natl Acad Sci U S A *92*, 1769-1773.

Radu, A., Moore, M.S., and Blobel, G. (1995b). The peptide repeat domain of nucleoporin Nup98 functions as a docking site in transport across the nuclear pore complex. Cell *81*, 215-222.

Ramalho-Santos, J.o., Schatten, G., and Moreno, R.D. (2002). Control of Membrane Fusion During Spermiogenesis and the Acrosome Reaction. Biology of Reproduction *67*, 1043-1051.

Rexach, M., and Blobel, G. (1995). Protein import into nuclei: association and dissociation reactions involving transport substrate, transport factors, and nucleoporins. Cell *83*, 683-692.

Ribbeck, K., and Gorlich, D. (2001). Kinetic analysis of translocation through nuclear pore complexes. EMBO J *20*, 1320-1330.

Richards, S.A., Lounsbury, K.M., Carey, K.L., and Macara, I.G. (1996). A nuclear export signal is essential for the cytosolic localization of the Ran binding protein, RanBP1. J Cell Biol *134*, 1157-1168.

Richardson, W.D., Mills, A.D., Dilworth, S.M., Laskey, R.A., and Dingwall, C. (1988). Nuclear protein migration involves two steps: rapid binding at the nuclear envelope followed by slower translocation through nuclear pores. Cell *52*, 655-664.

Riggleman, B., Wieschaus, E., and Schedl, P. (1989). Molecular analysis of the armadillo locus: uniformly distributed transcripts and a protein with novel internal repeats are associated with a Drosophila segment polarity gene. Genes Dev *3*, 96-113.

Rihs, H.P., Jans, D.A., Fan, H., and Peters, A. (1991). The rate of nuclear cytoplasmic protein transport is determined by the casein kinase II site flanking the nuclear localization sequence of the SV40 T-antigen. The EMBO journal *10*, 633-639.

Rihs, H.P., and Peters, R. (1989). Nuclear transport kinetics depend on phosphorylation-site-containing sequences flanking the karyophilic signal of the Simian virus 40 T-antigen. The EMBO journal *8*, 1479-1484.

Robbins, J., Dilwortht, S.M., Laskey, R.A., and Dingwall, C. (1991). Two interdependent basic domains in nucleoplasmin nuclear targeting sequence: Identification of a class of bipartite nuclear targeting sequence. Cell *64*, 615-623.

Robinson, F.L., and Dixon, J.E. (2006). Myotubularin phosphatases: policing 3-phosphoinositides. Trends in Cell Biology *16*, 403-412.

Robinson, F.L., Niesman, I.R., Beiswenger, K.K., and Dixon, J.E. (2008). Loss of the inactive myotubularin-related phosphatase Mtmr13 leads to a Charcot-Marie-Tooth 4B2-like peripheral neuropathy in mice. Proceedings of the National Academy of Sciences *105*, 4916-4921.

Rooij, D.G.D., Dissel-Emiliani, F.M.F.V., and Pelt, A.M.M.V. (1989). Regulation of Spermatogonial Proliferation. Annals of the New York Academy of Sciences *564*, 140-153.

Ross, S., and Hill, C.S. (2008). How the Smads regulate transcription. The International Journal of Biochemistry & Cell Biology *40*, 383-408.

Rother, F., Shmidt, T., Popova, E., Krivokharchenko, A., Hugel, S., Vilianovich, L., Ridders, M., Tenner, K., Alenina, N., Kohler, M., *et al.* (2011). Importin alpha7 Is Essential for Zygotic Genome Activation and Early Mouse Development. PLoS ONE *6*, e18310.

Rout, M.P., Aitchison, J.D., Suprapto, A., Hjertaas, K., Zhao, Y., and Chait, B.T. (2000). The yeast nuclear pore complex: composition, architecture, and transport mechanism. J Cell Biol *148*, 635-651.

Roux-Rouquie, M., Chauvet, M.-L., Munnich, A., and Frezal, J. (1999). Human Genes Involved in Chromatin Remodeling in Transcription Initiation, and Associated Diseases: An Overview Using the GENATLAS Database. Molecular Genetics and Metabolism *67*, 261-277.

Russell, L.D., Ettlin, R.A., Sinha Hikim, A.P., and Glegg, E.D. (1999). Histological and Histopathological EVALUATION OF THE TESTIS. Cache River Press *First edition*, 4-28.

Russell, L.D., and Frank, B. (1978). Characterization of rat spermatocytes after plastic embedding. Archives of Andrology *1*, 5-18.

Rusten, T.E., and Stenmark, H. (2006). Analyzing phosphoinositides and their interacting proteins. Nat Meth *3*, 251-258.

Sanderson, M.L., Hassold, T.J., and Carrell, D.T. (2008). Proteins Involved in Meiotic Recombination: A Role in Male Infertility? Systems Biology in Reproductive Medicine *54*, 57-74.

Sasaki, T., Sasaki, J., Sakai, T., Takasuga, S., and Suzuki, A. (2007). The Physiology of Phosphoinositides. Biological and Pharmaceutical Bulletin *30*, 1599-1604.

Schatz, C.A., Santarella, R., Hoenger, A., Karsenti, E., Mattaj, I.W., Gruss, O.J., and Carazo-Salas, R.E. (2003). Importin alpha-regulated nucleation of microtubules by TPX2. EMBO J *22*, 2060-2070.

Schaub, M., and Keller, W. (2002). RNA editing by adenosine deaminases generates RNA and protein diversity. Biochimie *84*, 791-803.

Scheidtmann, K.H., Echle, B., and Gernot, W. (1982). Simian Virus 40 Large T Antigen Is Phosphorylated at Multiple Sites Clustered in Two Separate Regions. Journal of Virology *44*, 116-133.

Schmid, M., Arib, G., Laemmli, C., Nishikawa, J., Durussel, T., and Laemmli, U.K. (2006). Nup-PI: The Nucleopore-Promoter Interaction of Genes in Yeast. Molecular Cell *21*, 379-391.

Schmid, M., Durussel, T., and Laemmli, U.K. (2004). ChIC and ChEC: Genomic Mapping of Chromatin Proteins. Molecular Cell *16*, 147-157.

Scott, S.V., Nice, D.C., Nau, J.J., Weisman, L.S., Kamada, Y., Keizer-Gunnink, I., Funakoshi, T., Veenhuis, M., Ohsumi, Y., and Klionsky, D.J. (2000). Apg13p and Vac8p Are Part of a Complex of Phosphoproteins That Are Required for Cytoplasm to Vacuole Targeting. Journal of Biological Chemistry *275*, 25840-25849.

Sehorn, M.G., Sigurdsson, S., Bussen, W., Unger, V.M., and Sung, P. (2004). Human meiotic recombinase Dmc1 promotes ATP-dependent homologous DNA strand exchange. Nature *429*, 433-437.

Sekimoto, T., Imamoto, N., Nakajima, K., Hirano, T., and Yoneda, Y. (1997). Extracellular signal-dependent nuclear import of Stat1 is mediated by nuclear pore-targeting complex formation with NPI-1, but not Rch1. EMBO J *16*, 7067-7077.

Shah, S., Tugendreich, S., and Forbes, D.J. (1998). Major binding sites for the nuclear import receptor are the internal nucleoporin Nup153 and the adjacent nuclear filament protein Tpr. J Cell Biol *141*, 31-49.

Sharpe, R., McKinnell, C., Kivlin, C., and Fisher, J. (2003). Proliferation and functional maturation of Sertoli cells, and their relevance to disorders of testis function in adulthood. Reproduction *125*, 769-784.

Shen, L., Weber, C.R., and Turner, J.R. (2008). The tight junction protein complex undergoes rapid and continuous molecular remodeling at steady state. The Journal of Cell Biology *181*, 683-695.

Shinohara, A., and Shinohara, M. (2004). Roles of RecA homologues Rad51 and Dmc1 during meiotic recombination. Cytogent Genome research *107*, 201-207.

Shmidt, T., Hampich, F., Ridders, M., Schultrich, S., Hans, V.H., Tenner, K., Vilianovich, L., Qadri, F., Alenina, N., Hartmann, E., *et al.* (2007). Normal brain development in importin-[alpha]5 deficient-mice. Nat Cell Biol *9*, 1337-1338.

Shuai, K., Stark, G.R., Kerr, I.M., and Jr, J.E.D. (1993a). A Single Phosphotyrosine Residue of Stat91 Required for Gene Activation by Interferon-gamma. Science *261*, 1744-1746.

Shuai, K., Ziemiecki, A., Wilks, A.F., Harpur, A.G., Sadowski, H.B., Gilman, M.Z., and Darnell, J.E. (1993b). Polypeptide signalling to the nucleus through tyrosine phosphorylation of Jak and Stat proteins. Nature *366*, 580-583.

Simpson, C.J., and Pepperkok, R. (2003). Localizing the proteome. Genome Biology *4*.

Smith, A., Brownawell, A., and Macara, I.G. (1998). Nuclear import of Ran is mediated by the transport factor NTF2. Current Biology *8*, 1403-1406, S1401.

Smith, H.M.S., and Raikhel, N.V. (1998). Nuclear Localization Signal Receptor Importin {alpha} Associates with the Cytoskeleton. Plant Cell *10*, 1791-1800.

Smith, J.M., and Koopman, P.A. (2004). The ins and outs of transcriptional control: nucleocytoplasmic shuttling in development and disease. Trends in Genetics *20*, 4-8.

Solsbacher, J., Maurer, P., Bischoff, F.R., and Schlenstedt, G. (1998). Cse1p Is Involved in Export of Yeast Importin alpha from the Nucleus. Mol Cell Biol *18*, 6805-6815.

Sorokin, V.A., Kim, R.E., and Ovchinnikov, P.L. (2007). Nucleocytoplasmic Transport of Proteins. Biochemistry (Moscow) *72*, 1439-1457.

Sripathy, S.P., Stevens, J., and Schultz, D.C. (2006). The KAP1 Corepressor Functions To Coordinate the Assembly of De Novo HP1-Demarcated Microenvironments of Heterochromatin Required for KRAB Zinc Finger Protein-Mediated Transcriptional Repression. Molecular and Cellular Biology *26*, 8623-8638.

Steger, K. (1999). Transcriptional and translational regulation of gene expression in haploid spermatids. Anatomy and Embryology *199*, 471-487.

Steger, K. (2001). Haploid spermatids exhibit translationally repressed mRNAs. Anatomy and Embryology *203*, 323-334.

Stoffler, D., Fahrenkrog, B., and Aebi, U. (1999). The nuclear pore complex: from molecular architecture to functional dynamics. Current Opinion in Cell Biology *11*, 391-401.

Strickland, S., and Mahdavi, V. (1978). The induction of differentiation in teratocarcinoma stem cells by retinoic acid. Cell *15*, 393-403.

Svetlanov, A., and Cohen, P.E. (2004). Mismatch repair proteins, meiosis, and mice: understanding the complexities of mammalian meiosis. Experimental Cell Research *296*, 71-79.

Szebeni, A., Herrera, J., and Oslon, M. (1995). Interaction of nucleolar protein B23 with peptides related to nuclear localization signals. Biochemistry *34*, 8037-8042.

Szebeni, A., Mehrotra, B., Baumann, A., Adam, S.A., Wingfield, P.T., and Olson, M.O.J. (1997). Nucleolar Protein B23 Stimulates Nuclear Import of the HIV-1 Rev Protein and NLS-Conjugated Albumin†. Biochemistry *36*, 3941-3949.

Tabb, M.M., Tongaonkar, P., Vu, L., and Nomura, M. (2000). Evidence for Separable Functions of Srp1p, the Yeast Homolog of Importin alpha (Karyopherin alpha): Role for Srp1p and Sts1p in Protein Degradation. Mol Cell Biol *20*, 6062-6073.

Taddei, A., Van Houwe, G., Hediger, F., Kalck, V., Cubizolles, F., Schober, H., and Gasser, S.M. (2006). Nuclear pore association confers optimal expression levels for an inducible yeast gene. Nature *441*, 774-778.

Takenawa, T., and Itoh, T. (2001). Phosphoinositides, key molecules for regulation of actin cytoskeletal organization and membrane traffic from the plasma membrane. Biochimica et Biophysica Acta (BBA) - Molecular and Cell Biology of Lipids *1533*, 190-206.

Tewari, R., Bailes, E., Bunting, K.A., and Coates, J.C. (2010). Armadillo-repeat protein functions: questions for little creatures. Trends in Cell Biology *20*, 470-481.

Thompson, M.E. (2010). BRCA1 16 years later: an overview. FEBS Journal *277*, 3071-3071.

Tran, M.H., Aul, R.B., Xu, W., van der Hoorn, F.A., and Oko, R. (2012). Involvement of Classical Bipartite/Karyopherin Nuclear Import Pathway Components in Acrosomal Trafficking and Assembly During Bovine and Murid Spermiogenesis. Biology of Reproduction *86*, 84, 81-11.

Truant, R., and Cullen, B.R. (1999). The Arginine-Rich Domains Present in Human Immunodeficiency Virus Type 1 Tat and Rev Function as Direct Importin beta - Dependent Nuclear Localization Signals. Mol Cell Biol *19*, 1210-1217.

Tsuji, L., Takumi, T., Imamoto, N., and Yoneda, Y. (1997). Identification of novel homologues of mouse importin alpha, the alpha subunit of the nuclear pore-targeting complex, and their tissue-specific expression. FEBS Lett *416*, 30-34.

Tsujita, K., Itoh, T., Ijuin, T., Yamamoto, A., Shisheva, A., Laporte, J., and Takenawa, T. (2004). Myotubularin Regulates the Function of the Late Endosome through the GRAM Domain-Phosphatidylinositol 3,5-Bisphosphate Interaction. Journal of Biological Chemistry *279*, 13817-13824.

Valdez, B.C., Perlaky, L., Henning, D., Saijo, Y., Chan, P.K., and Busch, H. (1994). Identification of the nuclear and nucleolar localization signals of the protein p120. Interaction with translocation protein B23. Journal of Biological Chemistry *269*, 23776-23783.

van der Goot, F.G., and Gruenberg, J. (2006). Intra-endosomal membrane traffic. Trends in Cell Biology *16*, 514-521.

Vanhaesebroeck, B., Leevers, S.J., Ahmadi, K., Timms, J., Katso, R., Driscoll, P.C., Woscholski, R., Parker, P.J., and Waterfield, M.D. (2001). SYNTHESIS AND FUNCTION OF 3-PHOSPHORYLATED INOSITOL LIPIDS. Annual Review of Biochemistry *70*, 535-602.

Walker, D.M., Urbe, S., Dove, S.K., Tenza, D., Raposo, G., and Clague, M.J. (2001). Characterization of MTMR3: an inositol lipid 3-phosphatase with novel substrate specificity. Current Biology *11*, 1600-1605.

Wang, F., Graham, W.V., Wang, Y., Witkowski, E.D., Schwarz, B.T., and Turner, J.R. (2005a). Interferon-γ and Tumor Necrosis Factor-α Synergize to Induce Intestinal Epithelial Barrier Dysfunction by Up-Regulating Myosin Light Chain Kinase Expression. The American Journal of Pathology *166*, 409-419.

Wang, W., Budhu, A., Forgues, M., and Wang, X.W. (2005b). Temporal and spatial control of nucleophosmin by the Ran-Crm1 complex in centrosome duplication. Nat Cell Biol *7*, 823-830.

Wang, Y.-X., Catlett, N.L., and Weisman, L.S. (1998). Vac8p, a Vacuolar Protein with Armadillo Repeats, Functions in both Vacuole Inheritance and Protein Targeting from the Cytoplasm to Vacuole. The Journal of Cell Biology *140*, 1063-1074.

Wang, Y.-X., Kauffman, E.J., Duex, J.E., and Weisman, L.S. (2001). Fusion of Docked Membranes Requires the Armadillo Repeat Protein Vac8p. Journal of Biological Chemistry *276*, 35133-35140.

Ward, W.S., and Coffey, D.S. (1991). DNA packaging and organization in mammalian spermatozoa: comparison with somatic cells. Biology of Reproduction *44*, 569-574.

Weber, P., Cammas, F., Gerard, C., Metzger, D., Chambon, P., Losson, R., and Mark, M. (2002). Germ cell expression of the transcriptional co-repressor TIF1beta is required for the maintenance of spermatogenesis in the mouse. Development *129*, 2329-2337.

Weis, K., Ryder, U., and Lamond, A.I. (1996). The conserved amino-terminal domain of hSRP1alpha is essential for nuclear protein import. European Molecular biology organization Journal *15*, 1818-1825.

Whiley, P.A.F., Miyamoto, Y., McLachlan, R.I., Jans, D.A., and Loveland, K.L. (2011). Changing subcellular localization of nuclear transport factors during human spermatogenesis. International Journal of Andrology, no-no.

Whitehurst, A.W., Wilsbacher, J.L., You, Y., Luby-Phelps, K., Moore, M.S., and Cobb, M.H. (2002). ERK2 enters the nucleus by a carrier-independent mechanism. Proceedings of the National Academy of Sciences *99*, 7496-7501.

Wilde, A., and Zheng, Y. (1999). Stimulation of Microtubule Aster Formation and Spindle Assembly by the Small GTPase Ran. Science *284*, 1359-1362.

Williams, M.A., and Smith, D.C. (1996). RNA and protein synthesis in the nonspermatozoal cells of normal human semen. Journal of Anatomy *188*, 137-147.

Winey, M., Yarar, D., Giddings, T.H., Jr., and Mastronarde, D.N. (1997). Nuclear Pore Complex Number and Distribution throughout the Saccharomyces cerevisiae Cell Cycle by Three-Dimensional Reconstruction from Electron Micrographs of Nuclear Envelopes. Mol Biol Cell *8*, 2119-2132.

Wittmann, T., Wilm, M., Karsenti, E., and Vernos, I. (2000). Tpx2, a Novel Xenopus Map Involved in Spindle Pole Organization. The Journal of Cell Biology *149*, 1405-1418.

Wong, C., Cheng, C.Y., and Gerald, P.S. (2005). The Blood-Testis Barrier: Its Biology, Regulation, and Physiological Role in Spermatogenesis. In Current Topics in Developmental Biology (Academic Press), pp. 263-296.

Xiao, Z., Latek, R., and Lodish, H.F. (2003). An extended bipartite nuclear localization signal in Smad4 is required for its nuclear import and transcriptional activity. Oncogene *22*, 1057-1069.

Xu, L., and Massague, J. (2004). Nucleocytoplasmic shuttling of signal transducers. Nat Rev Mol Cell Biol *5*, 209-219.

Yan-Sanders, Y., Hammons, G.J., and Lyn-Cook, B.D. (2002). Increased expression of heterogeneous nuclear ribonucleoprotein A2/B1 (hnRNP) in pancreatic tissue from smokers and pancreatic tumor cells. Cancer Letters *183*, 215-220.

Yan, H.H.N., Mruk, D.D., and Cheng, C.Y. (2007). Junction Restructuring and Spermatogenesis: The Biology, Regulation, and Implication in Male Contraceptive Development. In Current Topics in Developmental Biology, P.S. Gerald, ed. (Academic Press), pp. 57-92.

Yan, W. (2009). Male infertility caused by spermiogenic defects: Lessons from gene knockouts. Molecular and Cellular Endocrinology *306*, 24-32.

Yang, Q., Rout, M.P., and Akey, C.W. (1998). Three-Dimensional Architecture of the Isolated Yeast Nuclear Pore Complex: Functional and Evolutionary Implications. Molecular Cell *1*, 223-234.

Yang, W., Gelles, J., and Musser, S.M. (2004). Imaging of single-molecule translocation through nuclear pore complexes. Proceedings of the National Academy of Sciences of the United States of America *101*, 12887-12892.

Yano, R., Oakes, M., Yamaghishi, M., Dodd, J.A., and Nomura, M. (1992). Cloning and characterization of SRP1, a suppressor of temperature-sensitive RNA polymerase I mutations, in Saccharomyces cerevisiae. Mol Cell Biol *12*, 5640-5651.

Yasuda, Y., Miyamoto, Y., Saiwaki, T., and Yoneda, Y. (2006). Mechanism of the stress-induced collapse of the Ran distribution. Experimental Cell Research *312*, 512-520.

Yasuda, Y., Miyamoto, Y., Yamashiro, T., Asally, M., Masui, A., Wong, C., Loveland, K.L., and Yoneda, Y. (2012). Nuclear retention of importin alpha coordinates cell fate through changes in gene expression. EMBO J *31*, 83-94.

Yasuhara, N., Oka, M., and Yoneda, Y. (2009). The role of the nuclear transport system in cell differentiation. Seminars in Cell & Developmental Biology *20*, 590-599.

Yasuhara, N., Shibazaki, N., Tanaka, S., Nagai, M., Kamikawa, Y., Oe, S., Asally, M., Kamachi, Y., Kondoh, H., and Yoneda, Y. (2007). Triggering neural differentiation of ES cells by subtype switching of importin-[alpha]. Nat Cell Biol *9*, 72-79.

Yokoe, T., Toiyama, Y., Okugawa, Y., Tanaka, K., Ohi, M., Inoue, Y., Mohri, Y., Miki, C., and Kusunoki, M. (2010). KAP1 Is Associated With Peritoneal Carcinomatosis in Gastric Cancer. Ann Surg Oncol *17*, 821-828.

Yokoya, F., Imamoto, N., Tachibana, T., and Yoneda, Y. (1999). beta -Catenin Can Be Transported into the Nucleus in a Ran-unassisted Manner. Mol Biol Cell *10*, 1119-1131.

Yoon, S., and Seger, R. (2006). The extracellular signal-regulated kinase: Multiple substrates regulate diverse cellular functions. Growth Factors *24*, 21-44.

Yu, D., Marchiando, A.M., Weber, C.R., Raleigh, D.R., Wang, Y., Shen, L., and Turner, J.R. (2010a). MLCK-dependent exchange and actin binding region-dependent anchoring of ZO-1 regulate tight junction barrier function. Proceedings of the National Academy of Sciences *107*, 8237-8241.

Yu, J., Pan, L., Qin, X., Chen, H., Xu, Y., Chen, Y., and Tang, H. (2010b). MTMR4 Attenuates Transforming Growth Factor beta (TGFbeta) Signaling by Dephosphorylating R-Smads in Endosomes. Journal of Biological Chemistry *285*, 8454-8462.

Yu, Y., Maggi, L.B., Jr., Brady, S.N., Apicelli, A.J., Dai, M.-S., Lu, H., and Weber, J.D. (2006). Nucleophosmin Is Essential for Ribosomal Protein L5 Nuclear Export. Mol Cell Biol *26*, 3798-3809.

Yung, b.Y.M. (2007). Oncogenic role of nucleophosmin/B23. Chang Gung Med J *30*, 285-293.

Zacksenhaus, E., Bremner, R., Phillips, R.A., and Gallie, B.L. (1993). A bipartite nuclear localization signal in the retinoblastoma gene product and its importance for biological activity. Mol Cell Biol *13*, 4588-4599.

Zhang, B., Kirov, S., and Snoddy, J. (2005). WebGestalt: an integrated system for exploring gene sets in various biological contexts. Nucleic Acids Research *33*, W741-W748.

Zhang, C., Hughes, M., and Clarke, P.R. (1999). Ran-GTP stabilises microtubule asters and inhibits nuclear assembly in Xenopus egg extracts. Journal of Cell Science *112*, 2453-2461.

Zhang, C., Hutchins, J.R.A., Mühlhäusser, P., Kutay, U., and Clarke, P.R. (2002a). Role of Importin-[beta] in the Control of Nuclear Envelope Assembly by Ran. Current Biology *12*, 498-502.

Zhang, C., Hutchins, J.R.A., Mühlhäusser, P., Kutay, U., and Clarke, P.R. (2002b). Role of Importin-beta in the Control of Nuclear Envelope Assembly by Ran. Current Biology *12*, 498-502.

Zhao, R., Qi, Y., Chen, J., and Zhao, Z.J. (2001). FYVE-DSP2, a FYVE Domain-Containing Dual Specificity Protein Phosphatase That Dephosphorylates Phosphotidylinositol 3-Phosphate. Experimental Cell Research *265*, 329-338.

Zhong, Y., and Fang, S. (2012). Live Cell Imaging of Protein Dislocation from the Endoplasmic Reticulum. Journal of Biological Chemistry *287*, 28057-28066.

Papers published during the course of candidature

Biochimica et Biophysica Acta 1833 (2013) 731–742

Contents lists available at SciVerse ScienceDirect

Biochimica et Biophysica Acta

journal homepage: www.elsevier.com/locate/bbamcr

Towards delineation of a developmental α-importome in the mammalian male germline

Yoichi Miyamoto [a], Mark A. Baker [b,c], Penny A. Whiley [a,c], Arash Arjomand [a,c], Justin Ludeman [a], Chin Wong [a,c], David A. Jans [a,c,1], Kate L. Loveland [a,c,d,*,1]

[a] Department of Biochemistry and Molecular Biology, School of Biomedical Sciences, Monash University, Wellington Road, Clayton, VIC 3800, Australia
[b] Priority Research Centre in Reproductive Biology, School of Environmental and Life Sciences, University of Newcastle, Callaghan, NSW, 2308, Australia
[c] ARC Centre of Excellence in Biotechnology and Development, Australia
[d] Department of Anatomy and Developmental Biology, School of Biomedical Sciences, Monash University, Wellington Road, Clayton, VIC 3800, Australia

ARTICLE INFO

Article history:
Received 12 September 2012
Received in revised form 3 November 2012
Accepted 6 November 2012
Available online 13 November 2012

Keywords:
Nuclear transport
Importin α
NLS
SMC6
Testis
Spermatogenesis

ABSTRACT

Nucleocytoplasmic transport mediated by importin proteins is central to many developmental processes, such as precisely regulated germ cell differentiation during spermatogenesis. Here we examine for the first time the dynamic association of importins with cargo during two successive spermatogenic stages: meiotic pachytene spermatocytes and haploid round spermatids of the adult rat testis. Immunoprecipitation followed by mass spectrometry yielded the first non-biased identification of proteins selectively interacting with importin α2, α3 and α4 in each of these cell types. Amongst the 22 novel importin binding proteins identified, 11 contain a predicted classical nuclear localization signal (cNLS) for importin α binding using a new algorithm (Kosugi et al. [22]), although only 6 of these have known nuclear functions. An importin α2-immunoprecipitated protein with a key nuclear role in meiosis, structural maintenance of chromosomes 6 (SMC6), contained a predicted bipartite NLS that was shown to be preferentially recognized by importin α together with importin β1. In contrast, the predicted cNLS of synovial sarcoma, X breakpoint 2 interacting protein (SSX2IP) was found not to confer either nuclear accumulation or direct binding to importin αs, implying that NLS prediction algorithms may identify cryptic importin binding sites or require additional refinement to increase their accuracy. Unbiased identification of importin α binding proteins in cellular differentiation represents a powerful tool to help identify the functional roles of importin αs.

1. Introduction

Spermatogenesis is the highly specialized process of male germ cell differentiation that occurs in three phases: mitotic proliferation of spermatogonial stem cells and spermatogonia, meiosis by spermatocytes and differentiation of haploid spermatids during spermiogenesis [1]. Pertinent for the regulation of spermatogenesis is the precise delivery of appropriate cargo proteins from the cytosol into the nucleus of differentiated cells such that proteins including transcription factors and chromatin remodelling proteins coordinate synthesis of the new gene products needed for each developmental stage. Trafficking between the nucleus and the cytoplasm occurs through the nuclear pore complexes (NPC) embedded in the nuclear envelope [2]. The process of protein import into the nucleus commonly involves recognition by the importin α/β1 heterodimer of a nuclear localization signal (NLS), typically comprising one or two short stretches of basic amino acids such as that found in the simian virus 40 (SV40) large tumor-antigen [3]. The trimeric complex docks at the NPC and translocates through it via interactions of importin β1 with specific components of the NPC. Once inside the nucleus, the monomeric guanine nucleotide-binding protein, Ran, in its activated, GTP-bound form, binds to importin β1 to promote complex disassembly and release of the NLS-containing protein to perform its nuclear functions [4].

Six importin α proteins have been identified in mouse: importin α1/KPNA1/S1, α2/KPNA2/P1, α3/KPNA3/Q2, α4/KPNA4/Q1, α6/KPNA6/S2 and α8/KPNA7 [4–6]. Each belongs to one of three conserved subfamilies based on their sequence similarity, referred to here as the α1 clade (α1/α6), α2 clade (α2/α8) or α3 clade (α3/α4). Each importin α protein exhibits distinct NLS-binding specificities and selective expression in various tissues at both the RNA and protein levels, suggesting that the different importin α subtypes have specialized cellular roles. Moreover, it was recently demonstrated that nuclear-localized importin α2 can directly affect transcription of specific genes, including *Serine/threonine kinase 35* (*STK35*), in HeLa

Abbreviations: IMPα, importin α; KPNA, karypherin α; cNLS, classical nuclear localization signal; SMC6, structural maintenance of chromosomes 6; SSX2IP, synovial sarcoma, X breakpoint 2 interacting protein

* Corresponding author at: Department of Biochemistry & Molecular Biology, Department of Anatomy & Developmental Biology, Building 77, School of Biomedical Sciences, Monash University, Wellington Road, Clayton VIC 3800, Australia. Tel.: [redacted]
E-mail address: [redacted] (K.L. Loveland).

[1] Both authors contributed equally to this manuscript.

0167-4889/$ – see front matter.
http://dx.doi.org/10.1016/j.bbamcr.2012.11.005

cells [7]. This finding added depth to the growing understanding that each importin α is a multi-functional molecule [4,5]. Switching the expression of importin α family members, for example, can directly trigger formation of neuronal cells from ES cells [8], whilst importin α2 and α4 differentially contribute to the modulation of ES cell pluripotency [9]. In the case of mammalian spermatogenesis, we previously demonstrated that importin α proteins display stage- and cell-specific patterns of mRNA expression and protein subcellular localization [10]. This is consistent with the idea that regulated synthesis of importin α proteins with particular substrate specificity could play crucial roles in guiding cellular differentiation [4,11].

Although a number of importin α binding partners have been identified (eg. using yeast 2-hybrid screening [12]), there has been no comprehensive, unbiased approach to document the full complement of proteins recognized by an individual importin α in a developmental context. In this study, we employ for the first time a proteomic analysis to define molecules that bind each of three importin α proteins, importin α2, α3 and α4, in enriched primary isolates of spermatocytes or spermatids from rat testis. We identify both nuclear and non-nuclear importin α binding partners and use a new predictive search tool to identify classical NLSs in each of them. The results demonstrate the utility of combining unbiased proteomic approaches together with tools to probe protein function in the context of cellular development in the germline. Our outcomes highlight the potentially dynamic involvement of importin α proteins in roles distinct from nuclear transport in testicular germ cells.

2. Materials and methods

2.1. Animals and tissue preparation

Adult Sprague Dawley rats (60–90 days) were obtained from the Monash University Central Animal Services. Animals were killed by CO_2 inhalation immediately before tissue removal. All investigations conformed to the NHMRC/CSIRO/AAC Code of Practice for the Care and Use of Animals for Experimental Purposes and were approved by the Monash University Standing Committee on Ethics in Animal Experimentation and the Monash Medical Centre Animal Ethics Committee.

Testes for immunohistochemical analyses were immersion-fixed in Bouins fixative for 5 h and then washed in 70% ethanol for storage and subsequent paraffin embedding. Testes for RNA extraction were snap-frozen in dry ice at collection and stored at −80 °C until use.

2.2. Germ cell isolation

Germ cells were isolated from testes of adult rats using previously established methods [13]. Animals were sacrificed by CO_2 inhalation and the testes immediately removed and finely chopped. Interstitial cells were removed by collagenase treatment (25 min, 32 °C, 80 rpm on an orbital shaker), and germ cells were released from the epithelium with subsequent 0.062% trypsin treatment (20 min, 32 °C, 80 rpm on an orbital shaker). To achieve a single cell suspension, the preparation was filtered (70 μm cell strainer, BD Biosciences, CA, USA) and isolated by elutriation (Beckman JE 5.0 elutriation rotor, Palo Alto, CA, USA) as described [14].

2.3. Purity of isolated germ cell fractions

Approximately 10 million cells from the isolated germ cell fractions were fixed in Bouins for 30 min, then washed in 70% ethanol, suspended in 2% warm agar, and then pelleted at 15,500 ×*g* for 5 min and embedded in paraffin. To distinguish cell types, 5 μm sections were stained with haematoxylin and viewed under brightfield microscopy. Based on chromatin morphology and size, cells were designated as spermatocytes or spermatids or counted as impurities. The final purity for each fraction was 92% for spermatocytes and 80% for round spermatids.

2.4. Antibodies

The antibodies used were: anti-importin α2 (karypherin α2, C-20, Santa Cruz Biotechnology, Inc, CA, USA), anti-importin α3 (KPNA3, Abcam, Cambridge, UK), importin α4 (KPNA4, Abcam), anti-α-tubulin (B-5-1-2 mAb, Sigma, MO, USA), anti-GFP (Roche, Mannheim, Germany) and anti-GST (GE Healthcare, Buckinghamshire, UK).

2.5. Immunohistochemistry and western blot

Immunohistochemistry with anti-importin α antibodies was performed as previously described [15] using Bouins-fixed adult rat testis tissue. The experiments were repeated at least two times on two different samples, with qualitatively identical results obtained. Western blotting in Fig. 1E was performed with 30 μg of protein separated on an 8% sodium dodecylsulfate-polyacrylamide gel electrophoresis (SDS-PAGE) gel. Following transfer, the nitrocellulose membrane was blocked with 3% skim milk in TBS (20 mM Tris–HCl [pH7.5], 150 mM NaCl) for 1 h and probed with primary antibody in 3% skim milk in 0.1% Tween-20 in TBS (TTBS). The final concentration of each antibody was: anti-importin α2 (0.2 μg/ml), anti-importin α3 (0.5 μg/ml), anti-importin α4 (1 μg/ml) and anti-α-tubulin (0.03 μg/ml). Anti-goat IgG-Alkaline Phosphatase (AP) conjugated secondary antibody (Sigma-Aldrich, Sigma, MO, USA; 1:1000 dilution) and anti-mouse IgG-AP antibody (Silenus, VIC, Australia; 1:1000 dilution) in 3% skim milk in TTBS were incubated for 1 h at room temperature, and the bands were detected with NBT-BCIP (One-Step; Thermo Scientifc, Rockford, IL, USA).

2.6. Immunoprecipitation

Ten million purified spermatocytes or spermatids were placed in 4 ml Lysis buffer (50 mM Tris–HCl [pH7.3], 150 mM NaCl, 1% NP-40, 0.5% Tween-20, 0.1% SDS, 1 mM EDTA, protease inhibitor (used at 1:100, Protease Inhibitor Cocktail Set III, Calbiochem/EMD Chemicals Inc., La Jolla, CA, USA)) on ice and sonicated for 2 cycles (30 s on/30 s off, high-energy settings) using an Ultrasonics homogenizer 4710 series (Cole Palmer Instrument, Chicago, IL, USA). Insoluble material was removed by centrifugation at 10,000 ×*g* at 4 °C for 10 min, and the supernatant precleared using Protein A/G PLUS-Agarose (4 ml the lysate with 60 μl beads; Santa Cruz) at 4 °C overnight. After centrifugation to collect beads at 1000 ×*g*, at 4 °C for 5 min, the pre-cleared cell lysates were incubated with 10 μl Protein A/G PLUS-Agarose beads and 1–1.5 μg of each primary antibody specific for importin α2, α3 and α4 at 4 °C for 12 h. The beads were washed 5 times with 1 ml Lysis buffer (1 min each) and bound proteins eluted by addition of SDS-PAGE loading buffer (50 mM Tris–HCl [pH 6.8], 10% glycerol, 2% SDS, 2% β-mercaptoethanol and 0.1% Bromophenol Blue). Samples were denatured by boiling and separated in 10% SDS-PAGE gels. Gels were silver stained using Dodeca Silver Stain kit (Bio-Rad) and regions of the gel excised and analyzed by mass spectrometry (MS).

2.7. In-gel tryptic digest, peptide separation by nano-flow liquid chromatography and mass spectrometry

Protein spots of interest were excised manually and tryptic digests and LC-MS were performed as previously described [16].

2.8. Analysis of MS/MS data

For protein identification the derived mass spectrometric data were converted to TurboSequest™ (Thermo-Scientific) generic format (*.dat)

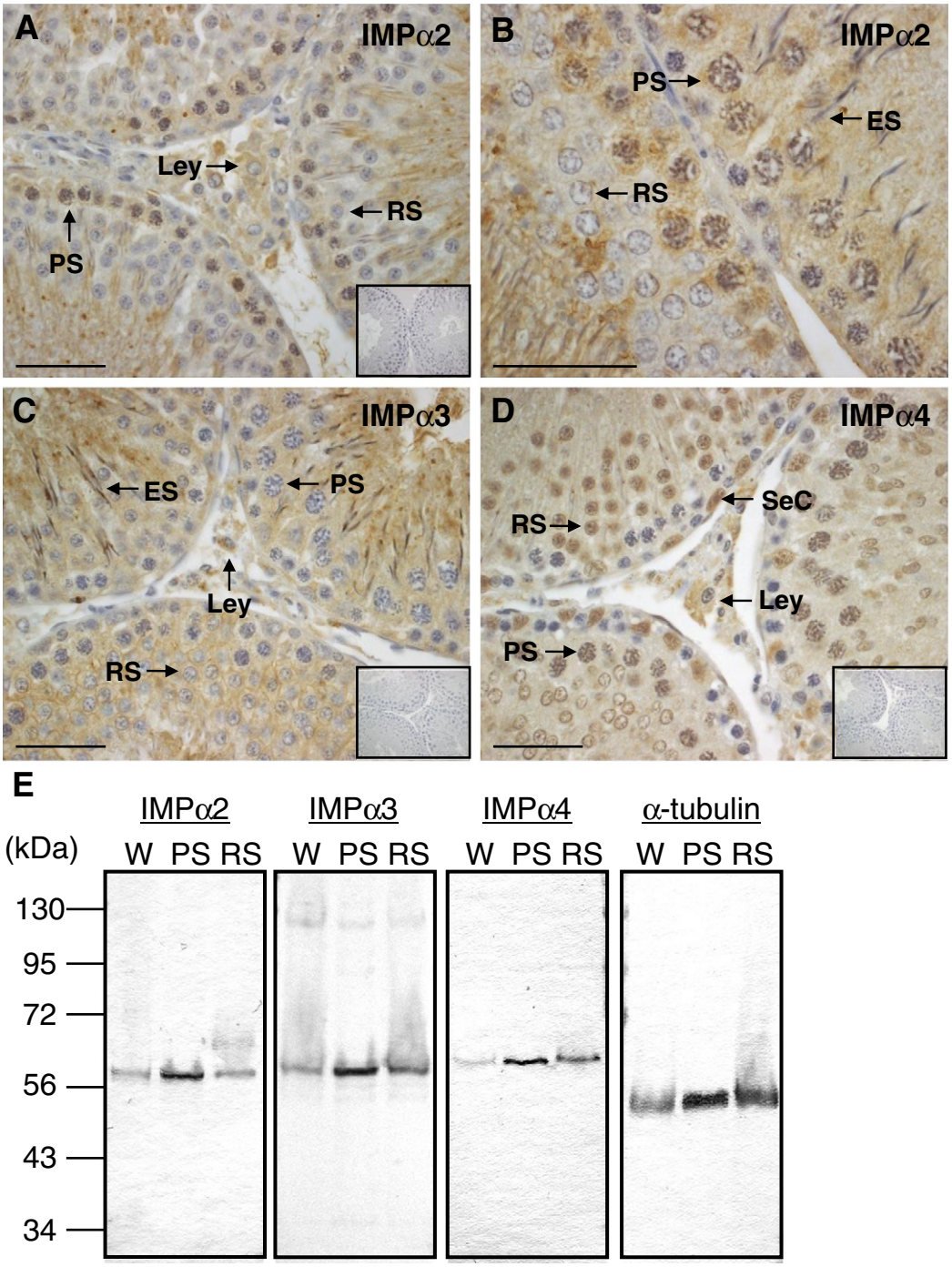

Fig. 1. Cellular localization of importin (IMP) α2, α3 and α4 in adult rat testis. Results for immunohistochemical detection in adult rat testes sections. (A, B) importin α2, (C) importin α3, and (D) importin α4. Insets show control sections using no primary antibody. PS, pachytene spermatocyte; RS, round spermatid; ES, elongating spermatid; SeC, Sertoli cell; Ley, Leydig cell. Bar = 40 μm. (E) Western blot analysis using specific antibodies to detect importin α2, α3, α4 and α-tubulin (loading control) in extracts of whole adult rat testis (W), purified pachytene spermatocytes (PS) and round spermatids (RS).

files using the Bioworks Browser (version 3.2). The files were then searched against the International Protein Index (IPI; Ref. [17]) *Rattus* database (version 3.33, released 12/06/2006, European Bioinformatics Institute, www.ebi.ac.uk/IPI/) containing the forward sequence of all 51,252 proteins in the data set using the TurboSequest™ search algorithm (version 3.2). Search parameters were specified as follows: oxidized methionine was set to differential modification, the number of allowed missed cleavages to 1.0, peptide tolerance to 1.0, intensity threshold to 100, parent ion selection to 1.4 Da and fragment ion tolerance to 0.7 Da. Protein identifications were based on single peptide hits using the following rigorous filtering standards: a minimum cross-correlation score (Xcorr) of 2.9 was required for peptides with a charge state of +1 or +2, and 3.2 for peptides with a charge state of +3. In addition, collision-induced dissociation (CID) spectra were all manually validated on a residue by residue basis to ensure correct assignment of the *y* and *b* ion series.

2.9. Cell culture and transfection

HeLa cells were cultured in Dulbecco's modified Eagle's medium (DMEM; Invitrogen, Carlsbad, CA, USA) supplemented with 10%

heat-inactivated fetal calf serum (FCS; PAA Laboratories, Morningside, QLD, Australia) at 37 °C in a 5% CO_2 atmosphere.

HeLa cells were plated onto 18×18 mm coverslips (Menzel-Glaser, Braunschweig, Germany) in 6-well plates 1 day prior to transfection, which was performed using the TransIT-LT1 Transfection Reagent (Mirus, Madison, WI, USA). Cells were fixed 24 h post-transfection using 3.7% formaldehyde in PBS, and the EGFP-tagged proteins detected using a Leica DC200 fluorescence microscope (Leica Microsystems, Heerbrugg, Germany).

2.10. Cloning and plasmid construction

RNA was isolated from adult mouse testis samples using TRIzol (Invitrogen) or the Qiagen RNeasy Mini kit (Qiagen, Hilden, Germany). Reverse transcription was performed using Superscript III (Invitrogen). *Smc6* and *Ssx2ip* cDNAs were amplified using the specific primers listed in Table S2. The full-length *Smc6* or *Ssx2ip* coding sequences were cloned into the pEGFPC1 or the pEGFPC2 vector, respectively (Clontech, Palo Alto, CA). Truncation derivatives of *Smc6* encoding a.a. 1–642 or 642–1097 were amplified using the primers shown in Table S2 and ligated into the pEGFPC1 vector subsequent to *BglII–HindIII* or *HindIII–KpnI*-digestion. The pEGFPC1-*Smc6* truncation derivatives encoding a.a. 1–262, 1–124 and 264–642 were generated from pEGFPC1-*Smc6* (1–642 a.a.) by digestion with *XmnI–HindIII*, *EcoRV–SmaI* or *BglII–XnmI*, respectively. To produce pEGFPC1-*Smc6* (48–1907 a.a.), pEGFPC1-*Smc6* full-length was digested with *BspEI* and ligated with PstI linker (5′-GGCTGCAGCC-3′), prior to deletion of the sequences encoding the N-terminal 47 a.a. of *Smc6* by digestion with *PstI*. The pEGFPC2-*Ssx2ip* truncation derivatives encoding a.a. 1–495 and 165–615 were generated from pEGFPC2-*Ssx2ip* (1–615 a.a.) by digestion with *XmnI–BamHI* or *EcoRI–PstI*, respectively. To produce pEGFPC2-*Ssx2ip* (165–495 a.a.), pEGFPC2-*Ssx2ip* (1–495 a.a.) was digested with *EcoRI* and *PstI*.

For constructs encoding SV40 large T antigen NLS (PPKKKRKVED), SMC6 NLS Wild-type (Wt: MAKRKEENFCSPENAKRPRQE), SMC6 NLS N-terminal mutant (Nm: MAAAAEENFCSPENAKRPRQE), SMC6 NLS C-terminal mutant (Cm: MAKRKEENFCSPENAAAPAQE), and SSX2IP's bipartite NLS-like sequence (biNLS: KKEMISLLSPQKKKPRERAE) and the predicted NLS (pNLS: HPRPRQKKPHSVAN), the relevant oligonucleotides (see Table S2) were ligated into the *Bam*HI–*SmaI* sites of pGEX2T (GE Healthcare) carrying the *GFP* gene at the C-terminus of the multi-cloning site [18].

Full length cDNAs encoding mouse importin α1, α2, α3, α4 or α6 were inserted into the *BamHI–XhoI* sites of pGEX6P1 (*imp a1*, *a3*, *a4*, and *a6*; GE Healthcare) or *BamHI-EcoRI* sites of pGEX6P2 (*imp a2*). Construct integrity in all cases was confirmed by DNA sequencing (Sequencing Centre at Monash Health Translation Precinct).

2.11. Purification of recombinant proteins

All five mouse importin α proteins, importin β1 and GST-GFP fused proteins which encode NLSs were purified as previously described [19]. Importin α proteins, β1 and Ran proteins lacking GST were prepared by cleavage with PreScission protease (20 units/mg of fusion protein; GE Healthcare) for 12 h at 4 °C.

Cleavage of GST from the GST-GFP fused protein of each NLS protein described in Fig. 6 was performed using Thrombin Protease (10 units/mg of fusion protein; GE Healthcare) in 50 mM Tris–HCl [pH 8.0], 150 mM NaCl, 2.5 mM $CaCl_2$. Ran protein without GST was equilibrated with buffer (50 mM HEPES [pH 7.3], 75 mM NaCl, 1 mM $MgCl_2$, 1 mM DTT, 0.1 mM PMSF) and incubated with GDP (Sigma-Aldrich, St. Louis, MO, USA) to a final concentration of 2 mM on ice for 1 h. After incubation, the protein was equilibrated with buffer (20 mM HEPES [pH 7.3], 100 mM CH_3COOK, 2 mM DTT and protease inhibitor (Protease Inhibitor Cocktail Set III, Calbiochem) using an Amicon Ultra (10K; Millipore, Billerica, MA, USA).

2.12. Solution binding assay

GST-importin α proteins (100 pmol) immobilized on glutathione-Sepharose were mixed with 100 pmol each of the GFP-fused NLS proteins (purified as described above) and the total reaction volume adjusted to 200 μl with Transport buffer (TB; 20 mM HEPES [pH 7.3], 110 mM CH_3COOK, 5 mM CH_3COONa, 2 mM $(CH3COO)_2$ Mg, 0.5 mM EGTA, 2 mM DTT, protease inhibitor (Protease Inhibitor Cocktail Set III, Calbiochem) containing 0.1% Triton X-100). After incubation for 1 h at 4 °C, the beads were washed 5 times with TB containing 0.1% Triton X-100 and then resuspended in SDS-PAGE loading buffer. Binding proteins were detected by western blot using anti-GFP mAb.

2.13. ELISA

ELISA was performed as described previously [20]. One hundred microliters containing 0.5 μg of each NLS recombinant protein (SV40TNLS-GFP or SMC6NLS-GFP) in coating solution (50 mM $NaHCO_3$ [pH 9.6]) was applied to each well of a 96 well plate that was then incubated at 4 °C for 16 h. After shaking, 300 μl Hybridization Buffer (HB: 80 mM HEPES [pH7.4], 440 mM KCl, 20 mM $NaHCO_3$, 20 mM $MgCl_2$, 4 mM EGTA, 0.4 mM $CaCl_2$, 1 mM DTT) with 1% BSA (HB + BSA) was added to each well and incubated at room temperature for 1 h, then the plate washed with 300 μl HB/well 3 times. For mixtures of GST-importin α and importin β1 recombinant proteins, α:β1 at a 1:1.2 molar ratio in HB + BSA were pre-incubated at room temperature for 30 min before dilution of GST-importin α to a final concentration of 230 nM. The protein mixtures were added to the plate (100 μl/well) in duplicates in serial 2-fold dilutions starting from 230 nM. The plate was incubated for 16 h at 4 °C with shaking. After washing, 100 μl of an anti-GST primary antibody (GE Healthcare) was added to each well at a 1:1000 dilution in Antibody Binding Buffer (ABB; 1× PBS, 0.3% Tween-20, 1% BSA) and incubated at room temperature for 3 h. The plate was washed 9 times with ABB, followed by addition to each well of 100 μl of anti-goat IgG alkaline phosphatase conjugated antibody (Sigma-Aldrich, St. Louis, MO, USA; 1:25,000 in ABB) and incubated for 1 h at room temperature. Finally 100 μl substrate solution (Phosphatase substrate tablets, Sigma-Aldrich final concentration of 1 mg/ml, 10% diethanolamine, 0.5 mM $MgCl_2$ [pH 9.6]) was added prior to reading the absorbance kinetics at 405 nm on a FLUOstar OPTIMA (BMG Labtech, Germany) every 5 min up to 90 min. Rates (mOD/s) were fitted against [GST-importin α] to obtain a hyperbolic saturation curve. The curve was fitted to a single site binding hyperbolic equation $[Y = B_{max} \times X/(B_{max} + X)]$ to yield K_d values. Duplicate samples were measured in at least three independent experiments.

2.14. Microinjection

HeLa cells were grown to semi-confluence in 60 mm plates prior to microinjection using an Eppendorf FemtoJet injection system (Eppendorf, Hamburg, Germany). Samples of 1 mg/ml GST-GFP or GST-GFP fusion proteins encoding NLS sequences in TB containing 1 mg/ml Alexa546-conjugated antibody as an injection marker were filtered prior to injection through a Nanosep MF centrifugal device with a GH Polypro (GHP) membrane (0.45 um; Pall Life Sciences, Ann Arbor, MI, USA) and then injected into the cell cytoplasm using Femtotips II (Eppendorf). After incubation for 30 min at 37 °C, injected fluorescent proteins were visualized by fluorescence microscopy (Olympus IX71, Tokyo, Japan).

2.15. In vitro nuclear import assay

Digitonin-permeabilized HeLa cells were prepared as described previously [18]. The reaction solution contained 20 pmol of GFP-tagged protein, 10 pmol each of importin α2 or α4, importin β1 and NTF2/

p10 (Sigma-Aldrich), 40 pmol of Ran-GDP and an ATP regenerating system (1 mM ATP, 20 U/ml of creatine kinase, 5 mM phosphocreatine) in TB containing 2% BSA in a total volume of 10 μl. After 30 min, the GFP-tagged proteins were visualized by fluorescence microscopy (Olympus IX71).

3. Results

3.1. Cellular expression profiles and localization of three importin α proteins in adult rat testes

We set out to use an unbiased approach to identify binding partners of importin α2, α3 and α4. As a first step, the cellular expression and localization profiles for each importin α were determined in adult rat testis by immunohistochemistry. As observed previously in mouse testis [12], the importin α2 protein was detected in the cytoplasm of pachytene spermatocytes, round spermatids, elongating spermatids and Leydig cells (Fig. 1A, B). A signal was also uniquely evident in the nucleus of pachytene spermatocytes, the staining clearly overlapping with chromatin staining (Fig. 1B). Importin α3 was broadly distributed in the cytoplasm of pachytene spermatocytes, round spermatids and elongating spermatids (Fig. 1C). In contrast, importin α4 was predominantly detected in the nucleus of pachytene spermatocytes, round spermatids and Sertoli cells, whilst weak cytoplasmic signals were detected in meiotic and post-meiotic germ cells (Fig. 1D). Antibody specificity was demonstrated by western blot analysis (Fig. 1E), with a single band of the expected size identified in lysates of whole testis and purified spermatocytes and spermatids; additionally, a faint band of a higher molecular weight (~130 kDa) was recognized by the anti-importin α3 antibody in the whole testis sample.

3.2. Identification of importin α binding proteins in rat spermatocytes and spermatids

To search for molecules with the capacity to bind individual importin α proteins, highly enriched preparations of both spermatocytes and spermatids were generated by elutriation. These cells were then solubilized in 1% Triton X-100 and used as the basis for co-immunoprecipitation with specific importin α antibodies. Fig. 2 illustrates the candidate binding proteins pulled down by each importin-α antibody. Individual bands were excised and analyzed by liquid chromatography mass spectrometry. A total of 22 proteins were identified unequivocally [17], reflecting the fact that some of the excised bands contained multiple proteins (Table 1). Fig. 3A shows the specific gene products identified by immunoprecipitation with each importin α in each spermatocytes and spermatids. There was no overlap in binding partners identified for any of the distinct importin αs, with the almost complete absence of overlap in importin α binding partners between these two cell types. The exceptions were ZFP386 and VPS8, which were uniquely bound by importin α3 and importin α4, respectively, in spermatocytes and spermatids (Fig. 3A).

Broad molecular functions were assigned for each protein according to the PANTHER classification system (Fig. 3B; Table 1; [21]). The majority of candidate binding proteins fall into one of four main categories, with the largest proportion (27%) listed under "Metabolic process", including DNA repair, replication and protein synthesis. The other categories were "Transport", including protein transport, vesicle-mediated transport and lysosomal transport, "Cellular processes" including cell communication, cell-cell signalling and signal transduction, and "Developmental processes" including reproduction and gamete formation. Whilst limited in precision, these classifications show the potential for importin α binding partners to function in both nuclear and cytoplasmic compartments, highlighting the value of understanding the physiological or developmental significance of their interactions with importin α proteins.

3.3. Prediction of classical nuclear localization signals

Kosugi and colleagues recently defined new algorithms to identify classical importin α/β1 pathway-specific NLSs in creating the cNLS Mapper computer program (http://nls-mapper.iab.keio.ac.jp/cgi-bin/NLS_Mapper_form.cgi [22]). To test the capacity for cNLS Mapper to find putative NLS sequences recognized by importin α proteins in our list of binding partners, we first independently assessed the program's prediction accuracy by surveying 15 known nuclear proteins using a cut-off of scores above 6 to indicate the presence of a cNLS (Table S1). The well-characterized NLS of SV40 large T-antigen, ^{125}PPKKKRKVED^{134} [3,19], was identified (the ^{125}PPKKKRKVEDPKDF^{138} sequence) with the highest score of 16.0. For the other 14 proteins, almost all of the predicted NLSs overlapped with, or were close to, experimentally validated NLSs. We found only two exceptions: one of the two BRCA1 NLSs, ^{606}PKKNRLRRKS^{615} [3,23], was not predicted, and for DAXX,

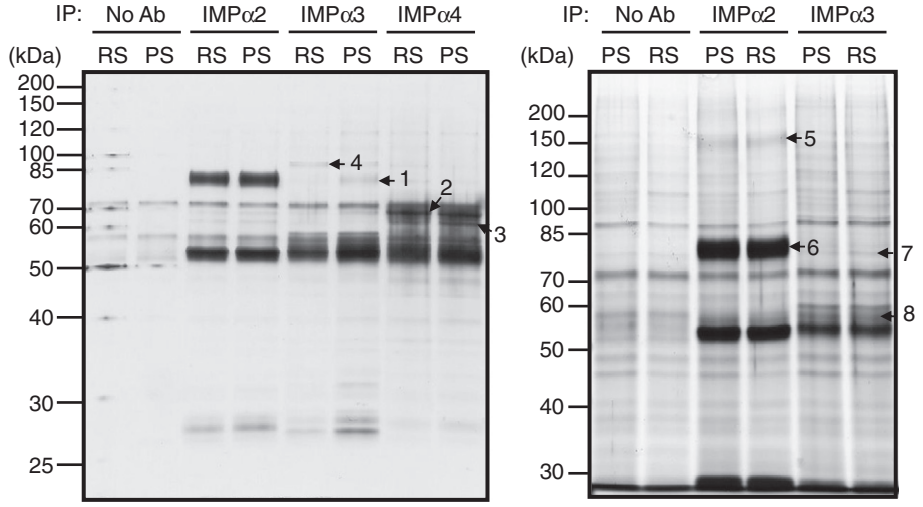

Fig. 2. Importin α binding proteins identified by SDS-PAGE and used for MS analysis. Immunoprecipitation was performed using antibodies specific for importin (IMP) α2, α3 or α4 with each isolated rat pachytene spermatocytes (PS) or round spermatids (RS) or in the absence of an antibody. SDS-PAGE was performed and bands were visualized by silver staining. Specific regions of the gels containing bands that were analyzed by mass spectrometry are indicated (#1–8). Size markers are indicated on the left.

Table 1
IMPαs binding proteins identified by mass spectrometry.

Band no	Germ cells	IP: IMPα antibodies	IPI acc. no	Gene name	Abbreviation‡	Length¶ a.a.	Xcorr	Molecular functions†
1	PS	IMPα3:	IPI00200926	Regulating synaptic membrane exocytosis 2	RIMS2	1557	10.12	Small GTPase regulator activity
			IPI00189783	KRAB-zinc finger protein KZF-1	ZFP386‡	589	30.19	Transcription factor activity
			IPI00201112	Dynein cytoplasmic 2 heavy chain 1	DYNC2H1	4306	26.15	Microtubule motor activity
			IPI00363995	Pseudouridylate synthase 7	PUS7	660	6.14	Catalytic activity
			IPI00366805	Small nuclear ribonucleoprotein 40 (U5)	SNRNP40	358	16.17	RNA splicing factor activity
			IPI00203214	Eukaryotic translation elongation factor 2	EEF2	858	48.16	Translation regulator activity
			IPI00363762	Enolase 4	ENO4	602	10.14	Lyase activity
			IPI00192609	Synovial sarcoma, X breakpoint 2 interacting protein	SSX2IP	613	20.16	Cell adhesion molecule
2	RS	IMPα4:	IPI00372956	Structural maintenance of chromosomes 1 beta	SMC1β	1247	10.15	Chromatin-binding protein
			IPI00470280	Olfactory receptor 614	OLR614	316	10.16	G-protein coupled receptor activity
			IPI00765101	LOC686590	LOC686590	961	22.19	Small GTPase regulator activity
			IPI00362062	Vacuolar protein sorting 8 homolog	VPS8‡	1430	28.16	Protein transport
3	PS	IMPα4:	IPI00558967	Myotubularin related protein 4	MTMR4	1191	8.13	Protein tyrosine phosphatase
			IPI00362062	Vacuolar protein sorting 8 homolog	VPS8‡	1430	10.17	Protein transport
			IPI00371105	Neurobeachin-like 2	NBEAL2	2745	24.16	Protein binding
4	RS	IMPα3:	IPI00189783	KRAB-zinc finger protein KZF-1	ZFP386‡	589	18.16	Transcription factor activity
			IPI00766161	RGD1307722	RGD1307722	476	18.19	Unknown
			IPI00210566	Heat shock protein 90 kDa alpha	HSP90α	733	16.18	Molecular chaperones
			IPI00369217	TNF receptor-associated protein 1	TRAP1	706	16.18	Molecular chaperones
5	RS	IMPα2:	IPI00208152	Meningioma expressed antigen 5	MGEA5	916	18.17	Histone acetyltransferase
6	RS	IMPα2:	IPI00360352	Structural maintenance of chromosomes 6-like 1	SMC6L1	1097	14.16	Chromatin-binding protein
			IPI00357941	Protein tyrosine phosphatase, receptor type, D	PTPRD	1801	30.18	Protein tyrosine phosphatase
7	RS	IMPα3:	IPI00207361	Centrosomal protein 350 kDa	CEP350	3079	60.15	Centrosomal protein
8	RS	IMPα3:	IPI00230937	Phosphatidylethanolamine binding protein 1	PEBP1	187	28.26	Kinase regulator activity

PS: pachytene spermatocyte, RS: round spermatid.
‡ Peptides for ZFP386 or VPS8 were identified in >1 sample.
¶ In some cases the molecular weight identified does not correspond with the predicted molecular weight from the primary sequence, which may be attributed to protein degradation, post-translational modification, or aberrant electrophoretic mobility in SDS gels (Shirai et al., 2008, JBC;283(16):10745–10752).
† Molecular functions were assigned for each protein according to the PANTHER classification system.

an unvalidated NLS (^{390}ERKKRRARLQ^{399}) was predicted with a score of 6.0, and the validated cNLS ^{218}PDSAYLQEARLKRKLIR^{234} [24] was identified (^{225}EARLKRKLIRL^{235}) with a score of only 3.0.

Since the program performance was generally robust, we used it to search for putative cNLSs in the candidate importin α binding proteins in Table 1. Eleven of the proteins exhibited one to three cNLS or NLS-like sequences with a score of 6.0 or greater (Table 2). Interestingly, some of these, DYNC2H1 [25], SSX2IP [26], MTMR4 [27], PTPRD [28] and PEBP1 [29], have been reported to be exclusively cytoplasmic, although the human orthologue of SSX2IP was observed to have nuclear distribution in NRK [30] and HeLa cells [31], as described below. These observations raise the distinct possibilities that these proteins may have undiscovered functions in the nucleus or that their interaction with importin α proteins relates to functions unrelated to nucleocytoplasmic transport.

3.4. A bipartite nuclear localization signal identified in the N-terminus of SMC6

To assess the NLSs prediction capacity of cNLS Mapper to identify importin α binding proteins, we selected two of the candidates identified in this study. One of these, structural maintenance of chromosomes 6 (SMC6; original name SMC6L1 in rat, IPI00360352 in Table 1), was identified in the round spermatid lysate precipitated with an anti-importin α2 antibody. The other, synovial sarcoma, X breakpoint 2 interacting protein (SSX2IP: IPI00192609), known also as afadin- and α-actinin binding protein (ADIP), was identified in the spermatocyte lysate, and was precipitated by the anti-importin α3 antibody (Table 1). The human SMC6 transcript level is known to be especially high in the testis relative to other organs. The protein forms a heterodimer with SMC5 to function in various DNA repair responses, including DNA double-strand break repair [32,33]. The mechanism of SMC6 nuclear localization has not been previously examined directly, although an unvalidated NLS has been predicted within the N-terminus of the human orthologue [32]. Table 2 shows that cNLS Mapper identified a bipartite-like NLS within the N-terminus (1–21 a.a.) with a relatively high score of 8.4, overlapping with the region speculated to be an NLS in human, as well as in yeast, SMC6 [32,34].

As a first step for assessing potential NLSs in the rodent SMC6 protein, we constructed a series of truncation derivatives of mouse SMC6 fused to GFP for transient transfection into HeLa cells. As shown in Fig. 4A and B, the N-terminal domain, composed of amino acids 1–124, exhibited nuclear localization, as did the full-length SMC6. Mutants lacking the N-terminus corresponding to residue numbers 264–642, 642–1097 or 48–1097 displayed cytoplasmic localization. Together, the results imply strongly that the first 48 residues of SMC6 are essential for nuclear accumulation.

To further test the capacity of the predicted N-terminal 21 amino acids of SMC6 to function as an NLS, constructs encoding chimeric proteins with a.a. 1–21 inserted between GST at the N-terminus and GFP at the C-terminus were generated. These were expressed in bacteria, purified and microinjected into the cytoplasm of HeLa cells. In addition, to test the bipartite nature of the predicted NLS, we also generated constructs encoding fusion proteins with mutations within N- (Nm) and C- (Cm) terminal basic amino acid clusters of the NLS (Fig. 4C) and expressed and assayed them in the same way. At 30 min after microinjection, GST-SMC6 (1–21 a.a.)-GFP exhibited strong nuclear localization, in contrast to both mutant derivatives, which showed exclusively cytoplasmic localization (Fig. 4C; fluorescence images). This demonstrates that the N-terminal 21 residues of SMC6 represent a bipartite NLS sufficient to mediate nuclear localization of a heterologous protein.

3.5. The predicted NLS sequence in SSX2IP is insufficient to direct its nuclear accumulation

The subcellular distribution of SSX2IP has previously been recorded at cell–cell adherence junctions and in perinuclear regions, such as the Golgi complex [26,30]. In addition, its nuclear localization has been reported in NRK cells [30] and in HeLa cells when the protein included the predicted bipartite NLS-like sequence (^{285}KKEMISLLSPQKKKPR^{300}, referred to as biNLS in this study) [31], which is conserved in the human, mouse and rat orthologues. The

A

	PROTEINS IDENTIFIED BY IP/MS		
	IMPα2	IMPα3	IMPα4
Spermatocytes	ND	RIM2 ZFP386 DYNC2H1 PUS7 SNRNP40 EEF2 ENO4 SSX2IP	MTMR4 VPS8 NBEAL2
Spermatids	MGEA5 SMC6 PTPRD	ZFP386 RGD1307722 HSP90α TRAP1 CEP350 PEBP1	SMC1β OLR614 OC686590 VPS8

B

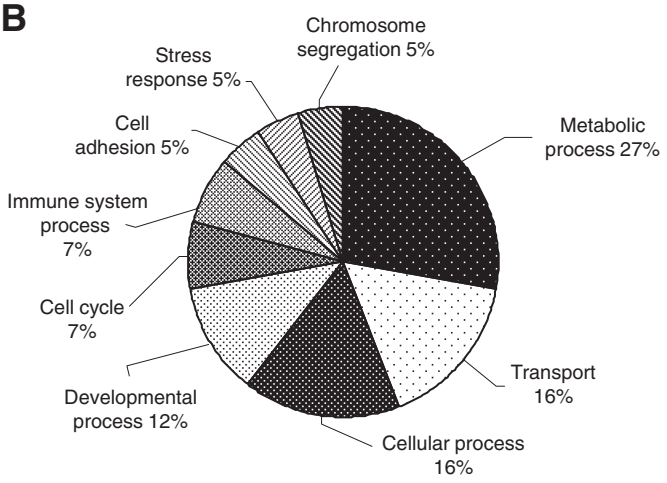

Fig. 3. Summary of importin α binding proteins identified by mass spectroscopy. (A) List of importin (IMP) α binding proteins identified in spermatocytes and spermatids by mass spectroscopy; see Table 1 for definition of abbreviated names of proteins. ND: no proteins specifically identified. (B) Pie chart illustration of the biological functions for all proteins according to the PANTHER classification system.

cNLS Mapper algorithm identified a putative monopartite NLS between 514 and 523 (RPRQKKPHSV, referred to as pNLS) in rat SSX2IP (Table 2). However, the full-length mouse SSX2IP EGFP-tagged fusion protein and its derivatives did not exhibit nuclear localization in HeLa cells (Fig. 5A, B). Moreover, we assessed the nuclear import activity of both biNLS and pNLS with GST-GFP fusion recombinant proteins by cytoplasmic microinjection in HeLa cells and in the mouse germ cell line, GC-2 (data not shown), and neither construct exhibited nuclear localization (Fig. 5C).

3.6. Validation of importin α binding and nuclear transport activity

Since SMC6 and SSX2IP were identified in this study as interacting with importin α2 and α3, respectively, a pull-down assay was used to assess the extent to which the NLS sequences are selectively recognized by each importin α *in vitro*. All 5 mouse importin α proteins were purified as GST fusion proteins, immobilized on glutathione-Sepharose beads and then incubated with SMC6NLS-GFP, SSX2IPbiNLS-GFP, SSX2IPpNLS-GFP or SV40TNLS-GFP. Proteins bound to importin αs were subsequently eluted and detected by western analysis using a specific anti-GFP antibody. SMC6NLS-GFP interacted with all importin αs and to the same extent as SV40TNLS-GFP under conditions in which GFP alone did not bind (Fig. 6A). To confirm that the interactions with importin α were dependent on the SMC6 NLS, two mutant derivatives, SMC6NLSNm-GFP and SMC6NLSCm-GFP, were also assessed with respect to GST-importin α2 and α4. Both showed a markedly reduced interaction (Fig. 6B), clearly indicating that the bipartite NLS of SMC6 is recognized by all importin αs tested. On the other hand, both predicted NLSs in SSX2IP did not show binding with the importin α proteins tested, including importin α3 with which it had been originally identified as a binding candidate in spermatocytes (Fig. 6A). This indicates its binding site is either cryptic or relies on a co-factor.

We determined the binding affinity between importin αs and the SMC6 NLS using an ELISA assay in the presence and absence of recombinant importin β1 protein, as previously [20,35], using SV40TNLS-GFP as a positive control. Importin α2/β1 and importin α4/β1 bound SMC6NLS-GFP with high affinity (Table 3; apparent dissociation constants, Kds, of approximately 9 and 15 nM, respectively, compared to lower binding/binding affinity in its absence, see also Fig. 6C), consistent with previous reports indicating that importin α binds NLSs with significantly higher affinity in the presence of importin β1 [36]. Neither importin α showed appreciable binding to the SMC6 NLSNm-GFP or to the Cm-GFP fusion proteins (Fig. 6C).

To determine the functional capacity of the SMC6 NLS, we reconstituted nuclear transport in digitonin-permeabilized, semi-intact HeLa cells. In the presence of Ran, GST-SMC6NLS-GFP accumulated efficiently in the nucleus in the presence of importin α2 or α4 together with importin β1, but not in the presence of importin β1 alone (Fig. 6D). The fusion protein was also transported into the

Table 2
Prediction of IMPα binding sequences in proteins identified using cNLS Mapper.

Name	Score (≥6)	Predicted NLS-like sequences	Subcellular localization*	Ref.	Anti-IMPα antibodies†
SNRNP40	14.4	^{4}QQKRKGPELPLVPVKRPRHE^{23}	Nu	[40]	IMPα3
	7.0	^{15}KKSKRRNCHC^{23}			
CEP350	7.0	^{578}PVISKKRHYD^{587}	Cen/Glg/MT/Nu	[43]	IMPα3
	11.0	^{1724}MPPLRKKQRGL^{1734}			
	7.8	^{2041}RALKGELRKRKSVVEQLKKEQRKRQKER^{2068}			
SMC1β	8.5	^{1055}EQVKRRRYDAF^{1065}	Nu	[41]	IMPα4
SMC6	8.4	^{1}MAKRKEENFCSPENAKRPRQE^{21}	Nu	[32]	IMPα2
MGEA5	7.5	^{786}VTPFIKKCKISWIPF^{800}	Cyt/Nu	[42]	IMPα2
DYNC2H1	7.0	^{3123}EDRKRKLEDL^{3132}	Cyt/Glg/MT/PM	[25]	IMPα3
PUS7	6.8	^{8}LKRGCLVVEDNDSVTPHEETKKQKVSEG^{35}	Un	–	IMPα3
SSX2IP	6.5	^{514}RPRQKKPHSV^{523}	CJ/Glg/Nu	[26,30,31]	IMPα3
MTMR4	6.0	^{1124}WLAKRRHHCR^{1133}	ER	[27]	IMPα4
PTPRD	6.0	^{1177}LLYKRKRAES^{1186}	PM	[28]	IMPα2
PEBP1	6.0	^{151}VESFRKKYHLG^{161}	Cyt/PM	[29]	IMPα3

Cen: Centrosome, CJ: Cell junction, Cyt: Cytoplasm, ER: Endoplasmic Reticulem, Glg: Golgi complex.
MT: Microtuble, Mit: Mitochondoria, Nu: Nucleus, PM: Plasma Membrane, Un: Unknown.
* Subcellular localization deduced from references in the column (Ref.).
† Antibodies used for immunoprecipitation.

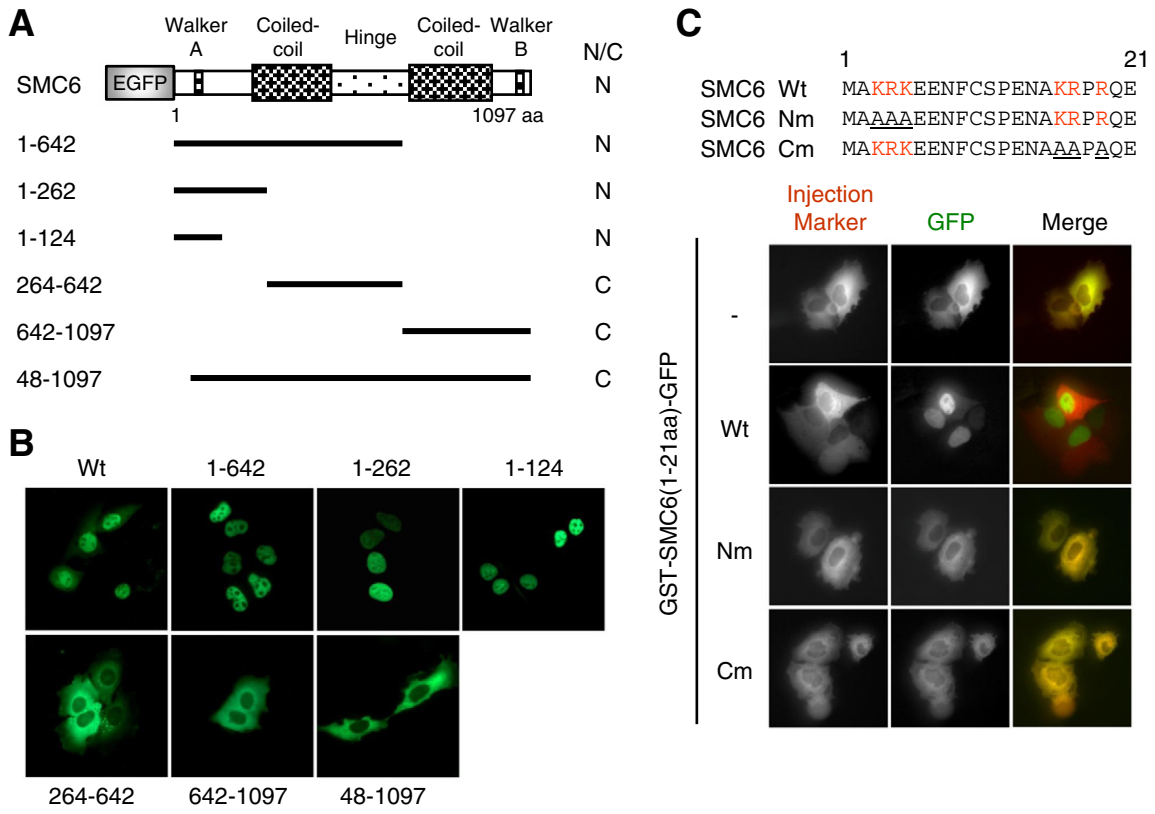

Fig. 4. Identification of an N-terminal bipartite NLS in SMC6. (A) Schematic representation of EGFP-tagged SMC6 fusion constructs. Numbers refer to amino acid positions in the truncation constructs. Nuclear–cytoplasmic (N/C) distributions of these SMC6 domains upon expression in HeLa cells are summarized (right) and shown below in (B). (C) SMC6 amino acids 1 to 21, with the basic amino acid clusters indicated in red and introduced alanine mutations (single letter amino acid code) underlined for N-terminal (Nm) and C-terminal (Cm) mutants. Bacterially expressed GST-GFP-fused SMC6 1–21 Wt and mutant derivatives were microinjected into the cytoplasm of HeLa cells along with Alexa546-conjugated antibody as an injection marker. Yellow color identifies colocalization of GFP-tagged protein (green) with the cytoplasmic injection marker (red).

nucleus in the presence of importin α1, α3 or α6 when importin β1 was present (data not shown). No nuclear localization was conferred by the SMC6 NLS in the presence of importin α alone (data not shown). We conclude that the SMC6 NLS confers nuclear transport, generally via importin α/β1, with recognition by all the different importin αs potentially functional for nuclear import in cells.

3. Discussion

This is the first study to reveal the α-importome for several different importin αs (α2, α3 and α4) from spermatogenic cells of the mammalian testis in which they are expressed in a stage- and cellular localization-specific manner (Fig. 1). In this study, highly purified spermatocytes and spermatids were used as the material for an unbiased proteomic screening approach incorporating, for the first time, the use of immunoprecipitation to preserve native interactions during the capture of binding partners [37,38]. Our study was designed specifically to identify all bands which represent selective interactions for individual importin α proteins occurring in two developmentally distinct germ cell types. It is our prediction that rare, specific interactions are likely to represent key developmental switches in these and other cellular transitions. Of the proteins identified by mass spectrometry, ZFP386 [39], SNRNP40 [40], SSX2IP [30,31], SMC1β [41], SMC6 [32], MGEA5 [42] and CEP350 [43] are all known to localize in the nucleus, with application of the cNLS Mapper algorithm implying that several reported cytoplasmic proteins that bind to importin α proteins may do so through cNLSs (Table 2); only ZFP386 of these proteins was not predicted to contain an cNLS by cNLS Mapper.

We selected SMC6 to validate both the recognition by importin α and the capabilities of cNLS Mapper. This program predicted a bipartite NLS within SMC6's N-terminal 21 residues with a score of 8.4 (Table 2), a sequence which overlapped with a previously predicted NLS in yeast and human SMC6 [32,34]. Transient transfection experiments using SMC6 truncation derivatives indeed confirmed that SMC6 nuclear localization was dependent on this sequence, and together with microinjection experiments, established that the NLS is sufficient to target a GST-GFP recombinant fusion protein to the nucleus (Fig. 4). In addition, interactions with importin α were confirmed directly, and the predicted bipartite NLS shown to be functional for importin α binding and importin α/β1-dependent nuclear import *in vitro* (Fig. 6). These results demonstrate the power of using our non-biased, proteomic approach to identify importin α binding proteins in combination with the cNLS Mapper to assist validation.

In contrast, the other candidate, SSX2IP, did not exhibit nuclear localization in HeLa cells (Fig. 5) and its predicted NLS sequences were not recognized by importin αs, unlike SMC6 (Fig. 6A), although SSX2IP has been previously identified in the nucleus of NRK cells and HeLa cells [30,31]. Whilst we cannot exclude the possibility that SSX2IP can distribute in the nucleus of cells and tissues in the presence of a binding partner such as SSX2 [31], our result provides an important challenge for improvement of current NLS prediction algorithms, as discussed below.

There are a growing number of tools available for the prediction of nuclear localization signals or importin α binding sequences (see review [3]). Kosugi and colleagues developed cNLS Mapper using amino acid replacement analysis in budding yeast [22], and we suggest this

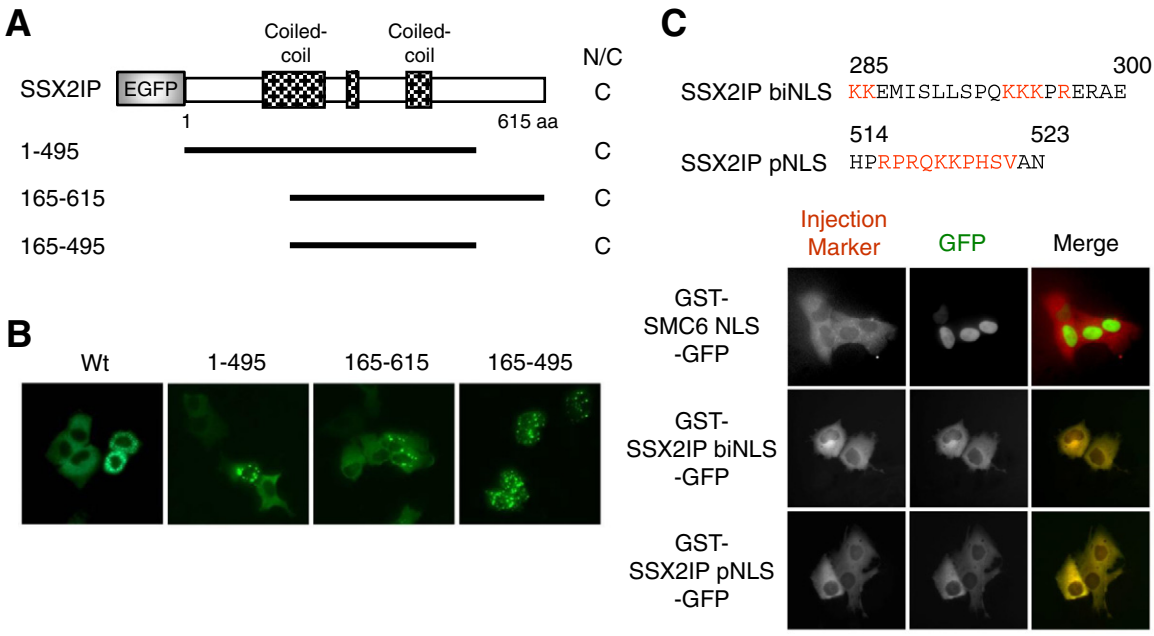

Fig. 5. Evidence for failure to direct nuclear migration by SSX2IP bipartite-like NLS and predicted NLS sequences. (A) Ectopically expressed mouse SSX2IP protein in HeLa cells. Schematic representation of EGFP-tagged SSX2IP fusion constructs. Numbers refer to amino acid positions in the mutants. Nuclear–cytoplasmic (N/C) distributions of these SSX2IP domains are summarized (right) and shown in (B). (C) GST–GFP-fusion proteins containing the SSX2IP bipartite NLS-like sequence (285 to 300 a.a., biNLS), with the basic amino acid clusters indicated in red or the cNLS Mapper predicted sequence (514 to 523 a.a. with cNLS Mapper predicted sequences indicated in red, pNLS) were microinjected into the cytoplasm of HeLa cells along with Alexa546-conjugated antibody as an injection marker. The GST-SMC6NLS-GFP fusion proteins were used as a positive control to illustrate migration into the nucleus after cytoplasmic injection in the same experiment.

would result in a tendency for this program to preferentially locate sequences suited for the structural features of the budding yeast importin α, Kap60p/Srp1p. As shown in Table S1, cNLS Mapper displayed high specificity for many known NLSs which were originally described in mammalian cells, demonstrating the efficacy of this new algorithm for mammalian NLS identification. However, we observed that proteins demonstrated to bind to members of the importin α1 subfamily α1 clade or α2 clade [CBP80 (score: 15.4), Nucleoplasmin (12.0), LEF1 (12.0), mCRY2 (11.4), DNA helicaseQ1 (8.5) and HHV-6 U69 (7.5)] showed higher relative scores than those known to bind specifically to the clade α3 proteins [RCC1 (8.7), RNA helicaseA (7.5), NF-κB p50 (7.0), RAC3 (6.8), RANBP3 (6.5), p53 (6.2) and DAXX (3.0, 6.0 and 7.5); summarized in Table S1].

With regard to the candidate proteins identified in this study, all 3 of the importin α2-binding proteins were found to contain an NLS recognized by cNLS Mapper, but only 6 out of 13 importin α3-binding proteins and 2 out of 6 importin α4-binding proteins were predicted to contain an NLS (Table 2). This implies that cNLS Mapper more efficiently identifies NLSs in importin α2-recognized cargoes than in those recognized by α3 or α4. Since Kap60p is evolutionarily close to the α1 clade [6], the apparent bias of cNLS Mapper to predict NLS sequences for clade α1 or α2- rather than the clade α3-recognized cargoes may reflect subtle structural differences between the cNLS motifs for the respective importin αs. Alternatively, this outcome may more likely reflect the disproportionately greater availability of cNLS data amongst the different importin α family members. To understand the highly complex features relating to NLS-recognition and its closely-related cargo transport mechanisms, further development of NLS prediction algorithms is required to accommodate not only characterization of NLS sequence specificity, but also the unique structural features of each importin α clade and protein [44].

An intriguing observation from this study was the identification of RIM2 as an importin α binding partner. A role for RIM in mediating acrosomal exocytosis in mature sperm due to its function as a Rab3A effector protein was recently demonstrated [45]. The protein appears localized to the perinuclear theca of spermatozoa, a region recently identified to be the site of KPNA1/6 association with a unique histone variant, SubH2Bv, in bovine sperm [46]. These exciting results highlight the need to further interrogate the potential for importin α proteins to serve roles distinct from classical nucleocytoplasmic transport but in alignment with their original discovery as molecular scaffolds. We anticipate that such roles will be extremely revealing with regard to nature of assembly of cell-specific structures in many developmental processes.

Through this study, our combined utilization of (a) unbiased identification of importin α binding proteins through immunoprecipitation/mass spectrometry, (b) prediction of potential cNLSs and/or importin α-recognized sequences and (c) experimental validation has demonstrated the need to evaluate the potential for importin α proteins to serve multiple roles in highly specialized developmental processes such as male germ cell differentiation. Future work in this laboratory is focussed on evaluating the functions of individual importin αs in testis development in relationship to their interactions with their various binding partners.

Supplementary data to this article can be found online at http://dx.doi.org/10.1016/j.bbamcr.2012.11.005.

Acknowledgements

We thank Marilyn Bakker and Elizabeth Richards for many technical contributions to this study. This work was supported in part by Grants from the Australian Research Council (Discovery Project; DP0878102 to Y. M. and K. L.) and from the Australian Research Council Centre of Excellence in Biotechnology and Development (CE0348239 to K. L. and D. J.). K. L. and D. J. were supported by the Australian National Health and Medical Research Council Fellowships (ID545916 and APP1002486) and Y. M. by a Japan Society for the Promotion of Science Postdoctoral Fellowship for Research Abroad and an Australian Research Council Fellowship.

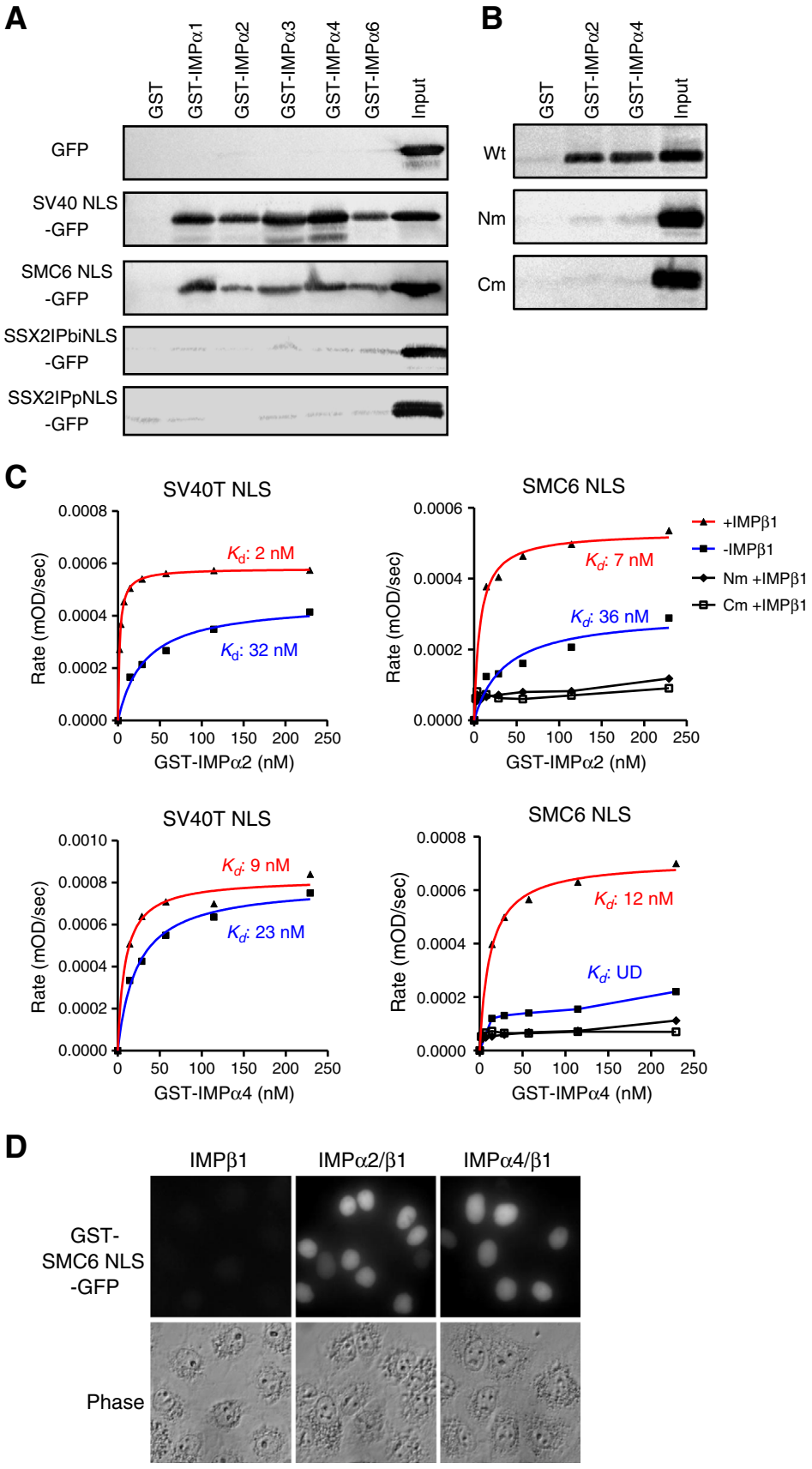
A
GST
GST-IMPα1
GST-IMPα2
GST-IMPα3
GST-IMPα4
GST-IMPα6
Input
GFP
SV40 NLS -GFP
SMC6 NLS -GFP
SSX2IPbiNLS -GFP
SSX2IPpNLS -GFP
B
GST
GST-IMPα2
GST-IMPα4
Input
Wt
Nm
Cm
C
SV40T NLS
Rate (mOD/sec)
GST-IMPα2 (nM)
Kd: 2 nM
Kd: 32 nM
SMC6 NLS
Kd: 7 nM
Kd: 36 nM
+IMPβ1
-IMPβ1
Nm +IMPβ1
Cm +IMPβ1
SV40T NLS
GST-IMPα4 (nM)
Kd: 9 nM
Kd: 23 nM
SMC6 NLS
Kd: 12 nM
Kd: UD
D
IMPβ1
IMPα2/β1
IMPα4/β1
GST-SMC6 NLS -GFP
Phase

Table 3
Importin binding parameters for the SMC6 NLS as determined using an ELISA-based assay.

	IMPα2		IMPα2/β1		IMPα4		IMPα4/β1	
	Kd (nM)	B_{max} (% α2/β1)	Kd (nM)	B_{max} (% α2/β1)	Kd (nM)	B_{max} (% α2/β1)	Kd (nM)	B_{max} (% α2/β1)
SV40T NLS[a]	56.2 ± 14.0	51.2 ± 8.3	15.7 ± 1.6	100.0	47.8 ± 7.4	105.7 ± 5.2	19.8 ± 4.1	107.5 ± 5.1
SMC6 NLS[b]	29.0 ± 10.3	45.6 ± 10.4	9.4 ± 1.2	95.6 ± 2.3	UD*	22.8 ± 9.2	14.9 ± 2.8	90.0 ± 4.5

Data represent the mean ± S. E. (n = 3) for the apparent dissociation constant (Kd) and maximal binding determined by ELISA-based assay.
Bmax expressed as percent increase in signal due to IMPα2/β1 binding to SV40T NLS-GFP.
[a] Significant differences (t-test) were observed between Kd values for IMPα2 in the absence or presence of IMPβ1 (SV40TNLS: $p = 0.0154$ and SMC6NLS: $p = 0.0427$).
[b] Significant differences (t-test) were observed between Kd values for IMPα4 in the absence or presence of IMPβ1 (SMC6NLS: $p = 0.0211$).
* Unable to be determined due to low binding; R2 values 0.74-0.87.

References

[1] J.B. Kerr, K.L. Loveland, O.B. MK, d.K. DM, Cytology of the testis and intrinsic control mechanisms, in: Neill JD (Ed.), Knobil and Neill's Physiology of Reproduction, vol. 1, Elsevier, 2006, pp. 827–947.
[2] A. Hoelz, E.W. Debler, G. Blobel, The structure of the nuclear pore complex, Annu Rev Biochem 80 (2011) 613–643.
[3] M. Marfori, A. Mynott, J.J. Ellis, A.M. Mehdi, N.F. Saunders, P.M. Curmi, et al., Molecular basis for specificity of nuclear import and prediction of nuclear localization, Biochim Biophys Acta 1813 (2011) 1562–1577.
[4] Y. Miyamoto, P.R. Boag, G.R. Hime, K.L. Loveland, Regulated nucleocytoplasmic transport during gametogenesis, Biochim Biophys Acta 1819 (2012) 616–630.
[5] D.S. Goldfarb, A.H. Corbett, D.A. Mason, M.T. Harreman, S.A. Adam, Importin α: a multipurpose nuclear-transport receptor, Trends Cell Biol 14 (2004) 505–514.
[6] D.A. Mason, D.E. Stage, D.S. Goldfarb, Evolution of the metazoan-specific importin alpha gene family, J Mol Evol 68 (2009) 351–365.
[7] Y. Yasuda, Y. Miyamoto, T. Yamashiro, M. Asally, A. Masui, C. Wong, et al., Nuclear retention of importin α coordinates cell fate through changes in gene expression, EMBO J 31 (2012) 83–94.
[8] N. Yasuhara, N. Shibazaki, S. Tanaka, M. Nagai, Y. Kamikawa, S. Oe, et al., Triggering neural differentiation of ES cells by subtype switching of importin-α, Nat Cell Biol 9 (2007) 72–79.
[9] J.C. Young, A.T. Major, Y. Miyamoto, K.L. Loveland, D.A. Jans, Distinct effects of importin α2 and α4 on Oct3/4 localization and expression in mouse embryonic stem cells, FASEB J 25 (2011) 3958–3965.
[10] A.T. Major, P.A. Whiley, K.L. Loveland, Expression of nucleocytoplasmic transport machinery: clues to regulation of spermatogenic development, Biochim Biophys Acta 1813 (2011) 1668–1688.
[11] C. Itman, Y. Miyamoto, J. Young, D.A. Jans, K.L. Loveland, Nucleocytoplasmic transport as a driver of mammalian gametogenesis, Semin Cell Dev Biol 20 (2009) 607–619.
[12] J.D. Ly-Huynh, K.G. Lieu, A.T. Major, P.A. Whiley, J.E. Holt, K.L. Loveland, et al., Importin alpha2-interacting proteins with nuclear roles during mammalian spermatogenesis, Biol Reprod 85 (2011) 1191–1202.
[13] M.L. Meistrich, J. Longtin, W.A. Brock, S.R. Grimes Jr., M.L. Mace, Purification of rat spermatogenic cells and preliminary biochemical analysis of these cells, Biol Reprod 25 (1981) 1065–1077.
[14] K.L. Loveland, M.P. Hedger, G. Risbridger, D. Herszfeld, D.M. De Kretser, Identification of receptor tyrosine kinases in the rat testis, Mol Reprod Dev 36 (1993) 440–447.
[15] C.A. Hogarth, D.A. Jans, K.L. Loveland, Subcellular distribution of importins correlates with germ cell maturation, Dev Dyn 236 (2007) 2311–2320.
[16] M.A. Baker, L. Hetherington, G. Reeves, J. Muller, R.J. Aitken, The rat sperm proteome characterized via IPG strip prefractionation and LC-MS/MS identification, Proteomics 8 (2008) 2312–2321.
[17] P.J. Kersey, J. Duarte, A. Williams, Y. Karavidopoulou, E. Birney, R. Apweiler, The International Protein Index: an integrated database for proteomics experiments, Proteomics 4 (2004) 1985–1988.
[18] Y. Miyamoto, M. Hieda, M.T. Harreman, M. Fukumoto, T. Saiwaki, A.E. Hodel, et al., Importin α can migrate into the nucleus in an importin β- and Ran-independent manner, EMBO J 21 (2002) 5833–5842.
[19] Y. Miyamoto, N. Imamoto, T. Sekimoto, T. Tachibana, T. Seki, S. Tada, et al., Differential modes of nuclear localization signal (NLS) recognition by three distinct classes of NLS receptors, J Biol Chem 272 (1997) 26375–26381.
[20] A.J. Brooks, M. Johansson, A.V. John, Y. Xu, D.A. Jans, S.G. Vasudevan, The interdomain region of dengue NS5 protein that binds to the viral helicase NS3 contains independently functional importin β1 and importin α/β-recognized nuclear localization signals, J Biol Chem 277 (2002) 36399–36407.
[21] H. Mi, B. Lazareva-Ulitsky, R. Loo, A. Kejariwal, J. Vandergriff, S. Rabkin, et al., The PANTHER database of protein families, subfamilies, functions and pathways, Nucleic Acids Res 33 (2005) D284–D288.
[22] S. Kosugi, M. Hasebe, M. Tomita, H. Yanagawa, Systematic identification of cell cycle-dependent yeast nucleocytoplasmic shuttling proteins by prediction of composite motifs, Proc Natl Acad Sci U S A 106 (2009) 10171–10176.
[23] C.F. Chen, S. Li, Y. Chen, P.L. Chen, Z.D. Sharp, W.H. Lee, The nuclear localization sequences of the BRCA1 protein interact with the importin-α subunit of the nuclear transport signal receptor, J Biol Chem 271 (1996) 32863–32868.
[24] P.L. Yeung, L.Y. Chen, S.C. Tsai, A. Zhang, J.D. Chen, Daxx contains two nuclear localization signals and interacts with importin α3, J Cell Biochem 103 (2008) 456–470.
[25] E.A. Vaisberg, P.M. Grissom, J.R. McIntosh, Mammalian cells express three distinct dynein heavy chains that are localized to different cytoplasmic organelles, J Cell Biol 133 (1996) 831–842.
[26] M. Asada, K. Irie, K. Morimoto, A. Yamada, W. Ikeda, M. Takeuchi, et al., ADIP, a novel Afadin- and α-actinin-binding protein localized at cell-cell adherens junctions, J Biol Chem 278 (2003) 4103–4111.
[27] O. Lorenzo, S. Urbe, M.J. Clague, Systematic analysis of myotubularins: heteromeric interactions, subcellular localisation and endosome related functions, J Cell Sci 119 (2006) 2953–2959.
[28] N.K. Tonks, Protein tyrosine phosphatases: from genes, to function, to disease, Nat Rev Mol Cell Biol 7 (2006) 833–846.
[29] S. Sperandio, K.S. Poksay, B. Schilling, D. Crippen, B.W. Gibson, D.E. Bredesen, Identification of new modulators and protein alterations in non-apoptotic programmed cell death, J Cell Biochem 111 (2010) 1401–1412.
[30] M. Asada, K. Irie, A. Yamada, Y. Takai, Afadin- and α-actinin-binding protein ADIP directly binds β'-COP, a subunit of the coatomer complex, Biochem Biophys Res Commun 321 (2004) 350–354.
[31] D.R. de Bruijn, N.R. dos Santos, E. Kater-Baats, J. Thijssen, L. van den Berk, J. Stap, et al., The cancer-related protein SSX2 interacts with the human homologue of a Ras-like GTPase interactor, RAB3IP, and a novel nuclear protein, SSX2IP, Genes Chromosomes Cancer 34 (2002) 285–298.
[32] E.M. Taylor, J.S. Moghraby, J.H. Lees, B. Smit, P.B. Moens, A.R. Lehmann, Characterization of a novel human SMC heterodimer homologous to the Schizosaccharomyces pombe Rad18/Spr18 complex, Mol Biol Cell 12 (2001) 1583–1594.
[33] G. De Piccoli, J. Torres-Rosell, L. Aragon, The unnamed complex: what do we know about Smc5-Smc6? Chromosome Res 17 (2009) 251–263.
[34] A.R. Lehmann, M. Walicka, D.J. Griffiths, J.M. Murray, F.Z. Watts, S. McCready, et al., The rad18 gene of Schizosaccharomyces pombe defines a new subgroup of the SMC superfamily involved in DNA repair, Mol Cell Biol 15 (1995) 7067–7080.
[35] J.K. Forwood, D.A. Jans, Nuclear import pathway of the telomere elongation suppressor TRF1: inhibition by importin α, Biochemistry 41 (2002) 9333–9340.
[36] B. Catimel, T. Teh, M.R. Fontes, I.G. Jennings, D.A. Jans, G.J. Howlett, et al., Biophysical characterization of interactions involving importin-α during nuclear import, J Biol Chem 276 (2001) 34189–34198.
[37] E. Blazek, M. Meisterernst, A functional proteomics approach for the detection of nuclear proteins based on derepressed importin alpha, Proteomics 6 (2006) 2070–2078.
[38] M. Fukumoto, T. Sekimoto, Y. Yoneda, Proteomic Analysis of Importin α-interacting Proteins in Adult Mouse Brain, Cell Struct Funct 36 (2011) 57–67.
[39] R. Urrutia, KRAB-containing zinc-finger repressor proteins, Genome Biol 4 (2003) 231.

Fig. 6. Nuclear transport of the SMC6 NLS mediated by importin α/β1. (A) GST alone or each of the five GST-importin αs were immobilized on glutathione-Sepharose and incubated with either SV40TNLS-GFP, SMC6NLS-GFP, SSX2IPbiNLS-GFP or SSX2IPpNLS-GFP recombinant proteins. Subsequent to gel electrophoresis of samples, bound proteins were detected by western blot analysis using an anti-GFP-specific antibody, with 3 pmol of GFP fusion protein loaded on each gel as input. (B) GST and GST-importin α2 or α4 were immobilized on glutathione-Sepharose and incubated with the indicated recombinant proteins SMC6NLS-GFP fusion proteins (Wt, Nm, and Cm). Subsequent to gel electrophoresis of samples, bound proteins were detected as in A. (C) Microtiter plates were coated with GFP-fused NLS proteins containing either the SV40T NLS or the wild type NLS or the mutant NLSs (Nm or Cm) of SMC6, as indicated, and incubated with increasing concentrations of importin α2 or α4 fused to GST. Rates (mOD/s) were fitted against GST-importin αs to obtain a hyperbolic saturation curve (see "Materials and methods"). The results are from a single typical experiment performed in triplicate with pooled data shown in Table 3. UD, Kd was unable to be determined due to low binding. Apparent Kds are indicated where R^2 values for the curve fit were >0.92. (D) Digitonin-permeabilized HeLa cells were incubated with importin β1, RanGDP, p10/NTF2 and an ATP regenerating system, together with GST-SMC6NLSWt-GFP recombinant protein with either importin α2 or α4, and after 30 min at 30 °C, GFP-tagged proteins were visualized by fluorescence microscopy.

[40] I.A. Turner, C.M. Norman, M.J. Churcher, A.J. Newman, Roles of the U5 snRNP in spliceosome dynamics and catalysis, Biochem Soc Trans 32 (2004) 928–931.
[41] E. Revenkova, M. Eijpe, C. Heyting, B. Gross, R. Jessberger, Novel meiosis-specific isoform of mammalian SMC1, Mol Cell Biol 21 (2001) 6984–6998.
[42] N. Comtesse, E. Maldener, E. Meese, Identification of a nuclear variant of MGEA5, a cytoplasmic hyaluronidase and a β-N-acetylglucosaminidase, Biochem Biophys Res Commun 283 (2001) 634–640.
[43] H. Patel, R. Truant, R.A. Rachubinski, J.P. Capone, Activity and subcellular compartmentalization of peroxisome proliferator-activated receptor α are altered by the centrosome-associated protein CAP350, J Cell Sci 118 (2005) 175–186.
[44] S.N. Yang, A.A. Takeda, M.R. Fontes, J.M. Harris, D.A. Jans, B. Kobe, Probing the specificity of binding to the major nuclear localization sequence-binding site of importin-alpha using oriented peptide library screening, J Biol Chem 285 (2010) 19935–19946.
[45] O.D. Bello, M.N. Zanetti, L.S. Mayorga, M.A. Michaut, RIM, Munc13, and Rab3A interplay in acrosomal exocytosis, Exp Cell Res 318 (2012) 478–488.
[46] M.H. Tran, R.B. Aul, W. Xu, F.A. van der Hoorn, R. Oko, Involvement of classical bipartite/karyopherin nuclear import pathway components in acrosomal trafficking and assembly during bovine and murid spermiogenesis, Biol Reprod 86 (2012) 84.